UNIVERSIDAD COMPLUTENSE DE MADRID

FACULTAD DE CIENCIAS FÍSICAS

TESIS DOCTORAL

Study of the properties and nature of the lightest scalar mesons and their relation to spontaneous chiral symmetry breaking

Estudio de las propiedades y naturaleza de las resonancias escalares más ligeras y su relación con la ruptura espontánea de la simetría quiral

MEMORIA PARA OPTAR AL GRADO DE DOCTOR

PRESENTADA POR

Jacobo Ruiz de Elvira Carrascal

Director

José R. Peláez

Madrid, 2013

Study of the properties and nature of the lightest scalar mesons and their relation to spontaneous chiral symmetry breaking

Estudio de las propiedades y naturaleza de las resonancias escalares más ligeras y su relación con la ruptura espontánea de la simetría quiral.

by

Jacobo Ruiz de Elvira Carrascal

under the supervision of

Dr. José R. Peláez

TESIS DOCTORAL

Universidad Complutense de Madrid

Contents

Acknowledgments

De alguna forma, el camino hacía un doctorado es un camino hacía la ignorancia, a medida que pasan los días, que acaban convirtiéndose en años, es imposible evitar darse cuenta de la magnitud de nuestra ignorancia, y junta a ella, de lo pequeños que somos nosotros. A la hora de afrontar este hecho y también de recorrer este camino, el apoyo de mucha gente ha sido, sin duda, imprescindible.

En primer lugar quiero agradecer a Jose Ramón la oportunidad que me ha dado de comenzar esta tesis a su lado. Su esfuerzo y confianza me han hecho llegar hoy hasta aquí, pero ante todo, quiero agradecerle esa contagiosa forma que tiene de ver y vivir la ciencia, pues son en gran medida, las que hoy me hacen seguir adelante por este arduo camino. También quiero acordarme de todos aquellos con las que he tenido la oportunidad y fortuna de trabajar y aprender. A Ángel, porque trabajar con él siempre ha sido muy fácil, a Felipe, porque ha sido larga y muy dura la "lucha" que hemos afrontado juntos contra el "polyquark de Jaffe", a Mike Pennington por la inexplicable confianza que siempre ha tenido en mí, a Guo, por todo su tiempo y paciencia, a Jose Antonio, por haberme invitado a Murcia, a Robert, porque ha sido un colaborador pero también un amigo, y a Rubén, porque sin su tiempo y esfuerzo nunca podría haberme incorporado al proyecto del scattering de piones.

Nada habría sido igual sin la compañía y apoyo de mis "hermanos de tesis", Rubén, con el que he compartido interminables charlas y del que he aprendido tanto, Guillermo, por todas esas dudas sobre física que en todo momento he podido compartir con él, Jeni, porque ha sido muy parecida a una hermana durante estos cuatro años. Con todos ellos he pasado muchas horas dentro y fuera del despacho, y son, sin duda, uno de los mejores regalos que me llevo de esta tesis. Tampoco puedo olvidar a todos los que han sido mis compañeros de despacho: Ricardo y Miguel por tantas risas y buenos momentos, Daniel Cabrera y Daniel Fernández por su ayuda en los comienzos de mi tesis, a Jose Carlos, Jose luis y Giovanni. También quiero expresar mi agradecimiento a mis compañeros teóricos, a Jose Alberto, un verdadero amigo y mejor persona, a Alejando, pues conocerle ha sido una verdadera suerte, a Bea, porque sin su ayuda, apoyo y dedicación al comienzo de esta tesis, y aún antes, ésta no habría sido posible. A David, nuestro informático, porque sin su apoyo técnico, todo habría sido, sin duda, mucho más difícil, a Domingo, Markus, Diego, Álvaro, Carlos, Javi, Juan, Marco, Ángela, Édgar, Luis, David, por todas las cosas que hemos vivido.

Tampoco podría olvidarme de Pablo, porque hemos compartido muchos años y mucha cafeína juntos, y su apoyo ha sido realmente importante, de Edu, por todas esas interminables discusiones sobre física, de todos mis compañeros y amigos de Hypatia, porque compartimos

juntos un sueño que seguirá siempre en mi recuerdo. De muchos y buenos amigos que han conseguido mantenerme cuerdo durante todos estos años, Natasha, Laura, María, Vero, Diego, Christian, Javi, Tabas, Isra, Carmen, Patricia, Miguel, Juan, Sonia, Eva, Daniel y muchos otros que ahora olvido.

Tampoco podría olvidarme de Jose, al que no sé cómo agradecer todo lo que me ha dado. Conocerle ha sido una de las mejores cosas que me han pasado, y sin su apoyo y compañia nada habría sido igual. De Nan, por hacerme sentir tan especial a su lado, por la ilusión con la que compartimos tantas cosas, que me ha hecho mantener las fuerzas para seguir hacía adelante, porque luchar juntos me ha permitido darme cuenta de lo que importa, y de lo que soy a su lado, y porque sin ella, esta tesis habría acabado terminando conmigo.

También quiero agradecer a mi hermana, Laura, que siempre me haya apoyado cuando lo he necesitado, y por último, a mis padres, el que me lo hayan dado todo. Su esfuerzo y sacrificio, su dedicación, cariño y confianza me han hecho llegar hoy hasta aquí, y sin ellos, nada habría sido posible.

List of publications

The research activity performed in this thesis has given rise to the following list of publications:

1. *Chiral dynamics in form factors, spectral-function sum rules, meson-meson scattering and semi-local duality*. Zhi-Hui Guo, J.A. Oller, J. Ruiz de Elvira, ***Phys. Rev.*** **D86 054006 (2012)**

2. *Chiral dynamics in U(3) unitary chiral perturbation theory*. Zhi-Hui Guo, J.A. Oller, J. Ruiz de Elvira, **Phys. Lett. B712 (2012)**

3. *Chiral Perturbation Theory, the 1/Nc expansion and Regge behaviour determine the structure of the lightest scalar meson*. J.R. Pelaez, M.R. Pennington, J. Ruiz de Elvira, D.J. Wilson, ***Phys. Rev.*** **D84 096006 (2011)**

4. *Precise determination of the f0(600) and f0(980) pole parameters from a dispersive data analysis*. R. Garcia-Martin, R. Kaminski, J.R. Pelaez, J. Ruiz de Elvira, ***Phys. Rev. Lett.*** **107 072001 (2011)**.

5. *The Pion-pion scattering amplitude. IV: Improved analysis with once subtracted Roy-like equations up to 1100 MeV*. R. Garcia-Martin, R. Kaminski, J.R. Pelaez, J. Ruiz de Elvira, F.J. Yndurain, ***Phys. Rev.*** **D83 074004 (2011)**.

6. *Fock space expansion of sigma meson in leading-Nc.*. F. J. LLanes-Estrada, J.R. Pelaez, J. Ruiz de Elvira, **Nucl. Phys. Proc. Supp. 207-208 (2010)**.

7. *Non-factorization of four-quark condensates at low energies within Chiral Perturbation Theory*. A. Gomez Nicola, J.R. Pelaez, J. Ruiz de Elvira, ***Phys. Rev.*** **D82 074012 (2010)**,

which have been included in different sections of this volume, and to the preprint:

1. *Scalar susceptibilities and four-quark condensates in the meson gas within Chiral Perturbation Theory* A. Gomez Nicola, J.R. Pelaez, J. Ruiz de Elvira, **arXiv:1210.7977**,

already submitted for publication and also included in this thesis.

The work developed in the thesis has been presented in a series of workshops with the following contributions to the corresponding Proceedings:

1. *f0(600) and f0(980) pole positions from a dispersive pi pi scattering data analysis.* J. Ruiz de Elvira, R. Garcia-Martin, R. Kaminski, J. R. Peláez, Proceedings of the Conference on Quark Confinement and the Hadron Spectrum IX, August 31 - 24 2010, Madrid (Spain). AIP Conf. Proc. **1343**, 632 (2011).

2. *Precise dispersive analysis of the f0(600) and f0(980) resonances from pi pi scattering.* J. Ruiz de Elvira, R. Garcia-Martin, R. Kaminski, J.R. Pelaez, Proceedings of the QCD 10: 15th International QCD Conference (25th anniversary), Montpellier, France, 8 Jun - 3 Jul 2010, **Nucl. Phys. Proc.Suppl. 207-208** (2010).

3. *Structure of the Lightest Scalar Meson from the 1/Nc expansion of Unitarized Chiral Perturbation Theory and Regge Theory.* J. Ruiz de Elvira, J. R. Peláez, M. Pennington, D. J. Wilsson, Proceedings of the Hadron 2009: 13th International Conference on Hadron Spectroscopy, Tallahassee, Florida, USA, 29 Nov - 4 Dec 2009. AIP Conf. Proc. **1257**, 141 (2010).

4. *The Nature of the Lightest Scalar Meson, Its Nc Behaviour and Semi-local Duality.* J. R. Peláez, M. Pennington, J. Ruiz de Elvira, D. J. Wilsson, to appear in the Proceedings of the XIV International Conference on Hadron Spectroscopy (hadron2011), 13-17 June 2011, Munich, Germany.

5. *Recent developments in U(3) ChPT: meson-meson scattering and finite energy sum rules.* Zhi-Hui Guo, J.A. Oller, J. Ruiz de Elvira, Proceedings of the VI International Conference on Quarks and Nuclear Physics (QNP2012), Palaiseau, Paris, France, 16-20 April. PoS QNP2012 **066** (2012)

6. *Precise dispersive determination of the f0(600) and f0(980) resonances.* J. R. Peláez, R. Garcia-Martin, R. Kaminski, J. Ruiz de Elvira, Proceedings of the VI International Conference on Quarks and Nuclear Physics (QNP2012), Palaiseau, Paris, France, 16-20 April. PoS QNP2012 **066** (2012)

Preface

Light scalar mesons play a key role in Hadron and Nuclear Physics. In particular, the lightest of this states, the $f_0(500)$ or σ meson, is largely responsible of the attractive part of the nucleon-nucleon interaction [1]. In addition, the scalar-isoscalar mesons have the vacuum quantum numbers, so they are also important for the realization of the spontaneous chiral symmetry breaking in Quantum Chromodynamics (QCD). Moreover, this breaking, although with relevant differences, is relatively similar to the Higgs mechanism in the Electroweak Symmetry Breaking Sector in the Standard Model [2, 3, 4]. Another relevant aspect for this discussion is that a characteristic feature of the non-abelian nature of QCD is the prediction of glueballs. Since the lightest glueball has the quantum numbers of the light scalars, it is expected to mix with them. Finally, it is also of interest to understand why light scalars contribute so little to the saturation of the parameters of the low energy effective theory of QCD in contrast to the role of vector mesons [5, 6].

In spite of their importance in many different fields of nuclear and hadron physics, the nature of the lightest scalar mesons is still a subject of intense debate, see for instance the "Note on scalar mesons" in [10, 11]. There are many scalar states in the region below 2 GeV, some of them are so wide that lead to overlaps, which makes difficult their experimental identification. Furthermore, they are distorted by a large destructive background, and by crossed channels exchanges, and their spectroscopic classification is still not clear. Besides, it is believed that the lightest scalars do not have an ordinary $\bar{q}q$ nature, and several possibilities have been discussed in the literature, such as molecules, tetraquarks, glueball, or mixtures of some of them [12, 13, 14, 15, 16, 17, 18, 19, 20, 21, 22, 23, 24].

In particular the properties and even the existence of the σ meson have been, for many years, a long standing problem. This is illustrated by the fact that the Particle Data Group (PDG) only included the σ in the 1996 edition of their Review of Particle Physics (RPP), almost 40 years after being proposed first in [1]. Furthermore, in the period from 1996 to 2010 its mass was estimated in the region between 400-1200 MeV, whereas its width estimate was 600-1200 MeV [10]. However, recent and precise dispersive analyses have triggered a substantial revision of this resonance in the last PDG edition [11]: the σ estimate has changed to 400-550 MeV for its mass, and 400-700 MeV for its width.

Hence, in this thesis we will study the properties and nature of the lightest scalar mesons appearing in $\pi\pi$-scattering. Despite QCD is well-established as the theory of strong interactions, at low energies the running coupling constant of the theory is very large, and we cannot use it to study the interaction of light mesons. Therefore, in this thesis we use other

methods to analyze this problem. In the first place, we will use dispersion relations, which relate the scattering amplitude at any energy with an integral over the whole energy range, given precise results and providing information even where there are not experimental data available. In the second place, we will use Chiral Perturbation Theory (ChPT) [7, 8, 9], which is the low energy effective theory of QCD. ChPT is consequence of the spontaneous chiral symmetry breaking and its relevant degrees of freedom are the lightest pseudoscalar mesons, whose masses are separated from the rest of resonances by a gap of hundred of MeV.

We can divide our results in three different blocks. In a first block, we use dispersive techniques to parametrize in a precise and model independent way the $\pi\pi$-scattering amplitude. Through this approach, we have been able to obtain the pole position and coupling to two pions of the $f_0(500)$ and $f_0(980)$ resonances. In a second block, we will use Chiral Perturbation Theory, unitarized with the Inverse Amplitude Method and the N/D method, to generate poles associated to the lightest resonances. As we will see, we use the former approach because, following from a dispersion relation, it does not introduce any spurious parameter, which makes it very suit in order to study the nature of the generated resonances. The latter is used because it is a straightforward way to incorporate resonances. We will use both methods combined with the $1/N_c$ expansion of QCD, and some phenomenological features of hadron physics, like semi-local duality and spectral sum rules. These approaches will allow us to study and constrain the nature of these resonances. Finally in the third block, we will analyze the role and influence of the σ meson in the chiral symmetry restoration of QCD by combining ChPT with the finite temperature formalism and the virial approach.

This thesis is presented in an "article" format, which means that the original publications originating from the work carried out in this thesis are presented after a brief summary and discussion of the main results. Nevertheless, we also include some recent and not published results which are presented here for first time. This thesis is organized as follows: In Chapter 1, we present an introduction to the basic concepts and main tools. In Chapter 2 we collect our results, after a brief motivation and outlook of the main contributions. In Section 2.1, we introduce our results about $\pi\pi$-scattering, and the dispersive determination of the lightest scalar-isoscalar resonances. The analysis about their nature is given in Section 2.2. In Section 2.3, we study the relation and role of the σ meson in the chiral symmetry restoration. Finally, in the third Chapter, we present the conclusions.

Introduction

There are four known fundamental interactions in nature: the Electromagnetic force, the Weak force, the Strong force and Gravity. The first three interactions are described by the Standard Model of Particle Physics, constructed as a relativistic quantum field theory that satisfies both special relativity and quantum mechanics. The building blocks of the Standard Model are quarks and leptons, which combined are known as fermions, interacting via the exchange of force-mediating particles called bosons. Both matter units, quarks and leptons, have spin 1/2 and are structureless at the smallest distances currently proved by the highest-energy accelerators. The simplest of these forces is the electromagnetic interaction, which is well described by Quantum Electrodynamics (QED). QED describes the interactions between charged particles as electrons, muons and nucleons, interacting with the quantum of the electromagnetic field, known as photon. QED is constructed by simple symmetry considerations, electrons are invariant respect to changes in an absolute phase. This symmetry is known as a gauge symmetry, which is one of the main ingredients of the Standard Model. The strong and weak forces act only at very short distances, and are responsible for the interactions between subatomic particles including nucleons and compound nuclei. The weak force is due to the exchange of the W and Z bosons, and it is responsible for the nuclear disintegration, the alpha and beta decays, and for radioactivity. The adjective accompanying its name, "weak", derives from the fact that the coupling is thousands of times less than that of the strong interactions. The strong force is described by Quantum Chromodynamics (QCD), and characterizes the interactions between coloured particles, quarks and anti-quarks mediated by gluons, which also interact between themselves. As it happens with QED, QCD also comes from symmetry principles, and particularly from a non abelian gauge symmetry. The strong interaction acts directly upon quarks, resulting in compound objects called hadrons, that interact among themselves through a residual part of the strong force, which, on a first approximation is mediated by mesons.

The purpose of this thesis is the study of certain aspects of Hadronic Physics, in particular, mesons at low energies and temperatures. In this section, we are going to review the main phenomenological and theoretical properties of hadrons, and particularly, of the lightest mesons.

1.1 Hadrons and quarks

The discovery of hadrons was made during the earliest experiments that exposed photographic plates to cosmic rays. Before long, a whole spectrum of states were discovered that could be classified in a similar manner to atomic systems with total angular momentum (J), parity (P) and charge conjugation (C) quantum numbers, J^{PC}. In the early studies of nuclear reactions, it was found that, in a very good approximation, the nuclear forces were independent of the charge of the interacting particles, i.e. the strong interactions are invariant to the interchange of protons and neutrons. This property lead to assume that the strong interactions have a SU(2) symmetry called isospin (I), in which protons and neutrons form an isospin doublet. This concept was easily extended to other hadrons; for example the pions, the lightest pseudoscalar meson states with $J^P = 0^-$, form an isotriplet of SU(2). The discovery of kaons (K) and Lambdas (Λ), which have very long lifetimes, lead to postulate a new quantum number for these particles: the strangeness (S). The strangeness, like the electric charge (Q), is associated with a U(1) symmetry. In fact, it was noted that there is a linear relation, the Gell-Mann-Nishijima relation, between both quantities and the diagonal generator T_3 of the SU(2) isospin group,

$$\begin{aligned} Q &= T_3 + \frac{Y}{2} \\ Y &= B + S, \end{aligned} \tag{1.1}$$

where B is the baryon number, (+1 for a baryon, -1 for an anti-baryon and 0 for mesons) and Y is called hypercharge.

1.1.1 The naive Quark model

In 1961 Gell-Mann and Ne'eman suggested a classification for hadrons [25, 26], sometimes referred to as the Eightfold Way. According to this method, it was possible to group all mesons and baryons with the same spin and parity in a (T_3, Y) plot, which corresponded to representations of the SU(3) group, which contains $SU(2)_I \times U(1)_Y$ as a subgroup. In 1964 Gell-Mann and Zweig proposed independently the (naive)[1] quark model [27, 28], in which all hadrons are built out of spin-1/2 quarks transforming as members of the fundamental representations of SU(3). There were three different types of flavours of quarks, "up", "down" and "strange" in the fundamental representation **3** of SU(3), whereas their antiparticles, antiquarks, were in the conjugate representations $\mathbf{3}^*$. Therefore, the mesons, which within the quark model are defined as $\bar{q}q$ states, come from the product of both representations:

$$\mathbf{3} \times \mathbf{3}^* = \mathbf{1} + \mathbf{8}, \tag{1.2}$$

i.e. the quark model predicts mesons in singlets and octets, while the baryons, qqq states, come from the product:

$$\mathbf{3} \times \mathbf{3} \times \mathbf{3} = \mathbf{1} + \mathbf{8} + \mathbf{8} + \mathbf{10}, \tag{1.3}$$

An example of this classification is depicted in fig. 1.1, where we plot the particle position in the (I_3, Y) plane of the **3**, $\mathbf{3}^*$ and **8** representations of SU(3).

[1] Many other models based in the quark model were proposed later, therefore, the initial one proposed by Gell-Mann and Zweig is called naive quark model

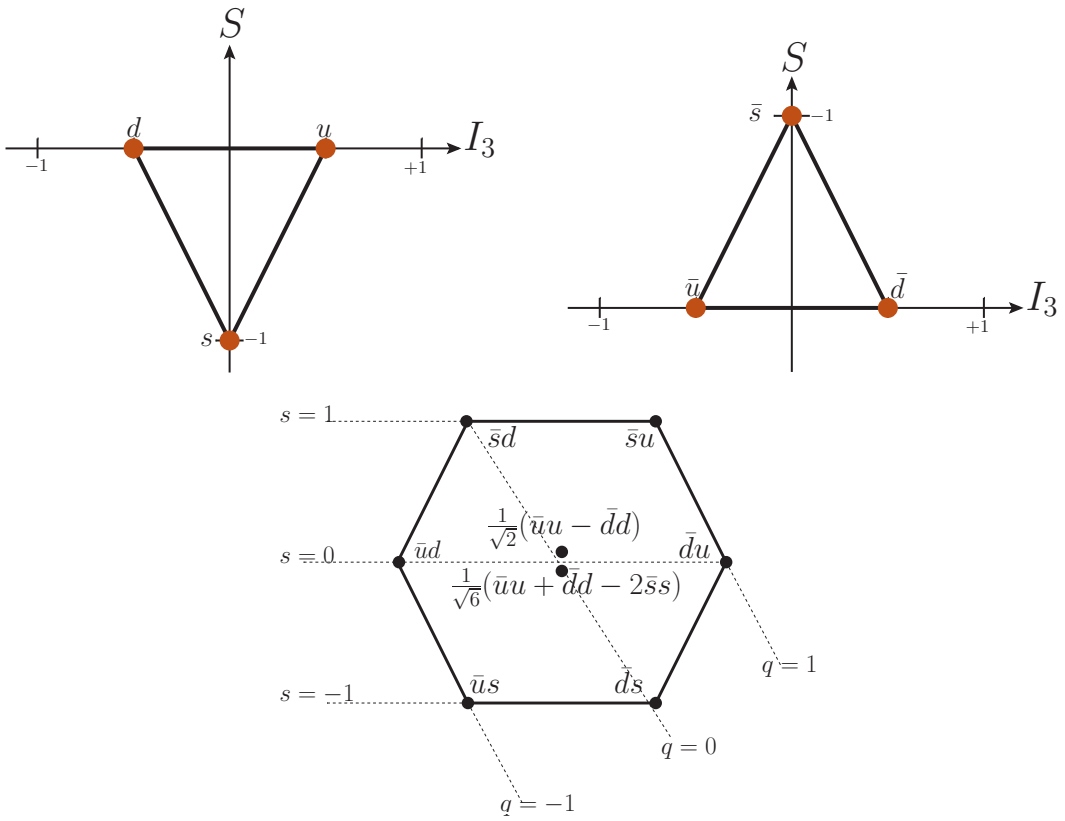

Figure 1.1: Top Left: The fundamental representation of SU(3): the quark representation. Right: The anti-quark representation. Bottom: the $\bar{q}q$ octet obtained by combining the quark and anti-quark representation above. Note that the convention states that the strange quark has strangeness, s=-1

The naive quark model was a successful tool to predict and classify hadrons, the Ω^-, for example, was discovered in 1964 [29] after being predicted by Gell-Mann in 1962 [26]. Despite its advantages, it had also several difficulties. For example, it could not explain the absence of hadron states different than the experimentally observed $\bar{q}q$ and qqq configurations. The detection of the Δ^{++}, belonging to the $3/2^+$ baryon decuplet, also highlighted a problem between the quark model and the spin–statistics. The quark model classified the Δ^{++} as a state of three u-quarks with a spatial wave–function of zero total angular momentum, and therefore, totally symmetric. But, since the Δ^{++} has spin-3/2, the spin of all u-quaks must be lined up in the same direction, the spin wave–function is also totally symmetric, and so does the total wave-function, which means it is symmetric in respect to the interchange of any pair of quarks. Therefore, the naive quark model predicts a state which violates the Fermi-Dirac statistics, unless some other ingredient was taken into account.

Actually, in order to solve this problem, a new degree of freedom for the quarks was postulated: the colour, which was introduced as an exact gauge symmetry of the strong interactions (unlike flavor symmetry, which is only approximate). Color can take three possible values: red, green or blue, and it is postulated that all hadrons are colorless (singlets of color), in order to account for the absence of coloured configurations.

Flavour	u (up)	d (down)	s (strange)	c (charm)	b (botton)	t (top)
Charge	2/3	-1/3	-1/3	2/3	-1/3	2/3
Mass	1.5-3.3 MeV	3.5-6.0 MeV	104^{+26}_{-24} MeV	$1.27^{+0.07}_{-0.11}$ GeV	$4.20^{+0.17}_{-0.07}$ GeV	171.2 ± 2.1 GeV
I_3	1/2	-1/2	0	0	0	0
S	0	0	-1	0	0	0
C	0	0	0	1	0	0
B	0	0	0	0	-1	0
T	0	0	0	0	0	1

Table 1.1: Quark properties. Charges are given in units of the electron charge, e. Values for the masses correspond to the ones given in [10]. I_3 is the third component of isospin, S is strangeness, C is charmness, B denotes bottomness, and T is topness. All quarks have positive parity.

Later on, three more quarks were discovered: the quark charm (observed in 1974 [30]), the quark bottom (observed in 1977 [31]), and the quark top (observed in 1995 [32]). Consequently, three new quantum numbers were introduced: charmness, bottomness and topness respectively, and the symmetry group enhanced. However, as we see in Table 1.1.1, where the quark properties are summarized, these three new quarks are much heavier than the , u, d and s, and therefore, less important in the low energy interactions of hadrons, which are precisely those in which we are interesting in this thesis.

1.1.2 Spectroscopy of light mesons

Since in this thesis we analyze light mesons, we are going to review in this Section their main spectroscopic properties. As mentioned above, mesons are states with $B = 0$ and in the quark model picture, they are $\bar{q}q'$ bound states of quarks (q) and anti-quarks ($\bar{q}'$), which may have different flavour. Mesons are classified by its parity P, total angular momentum J and charge conjugations C. If l is the orbital angular momentum of the $\bar{q}q'$ pair, then, its parity is $P = (-1)^{l+1}$. The total angular momentum J is given by the usual relation $|l + s| \leq J \leq |l - s|$ which comes from the product of SU(2) representations, and where s is the spin of the $\bar{q}q'$ pair, whose value is 0 (anti-parallel quark spins) or 1 (parallel quarks spins). The charge conjugation or C-parity describes the behaviour of the state under the symmetry of substituting each particle by its anti-particle and it is given by $C = (-1)^{l+s}$. In this way, mesons are organized in J^{PC} multiplets.

States with $l = 0$ are known as pseudocalars 0^{-+} and vectors 1^{--}. The orbital excitations $l = 1$, are the scalars 0^{++}, the axial-vectors 1^{++} and 1^{+-} and the tensors 2^{++}. States with $s = 1$ imply that $P = C = (-1)^J$ so then $CP = 1$. Therefore, states of spin one with $CP = -1$ as for example 0^{+-}, $1^{-+} \cdots$ are forbidden within the quark model. Of course the state 0^{--} is also forbidden. If states with such exotic quantum numbers were exist, they would lie outside the naive quark model.

As we have said above, following SU(3) flavour, i.e. a three flavour quark model, the nine possible $\bar{q}q'$ combinations of u, d and s quarks are grouped in an octet and a singlet of light quark mesons. Furthermore, isoscalar states with the same J^{PC} quantum numbers will mix with an angle that should be determined from experiment. It is common to use the generic name of a for the $I = 1$, K for the $I = 1/2$ and f and f' for the $I = 0$ states of the light quark

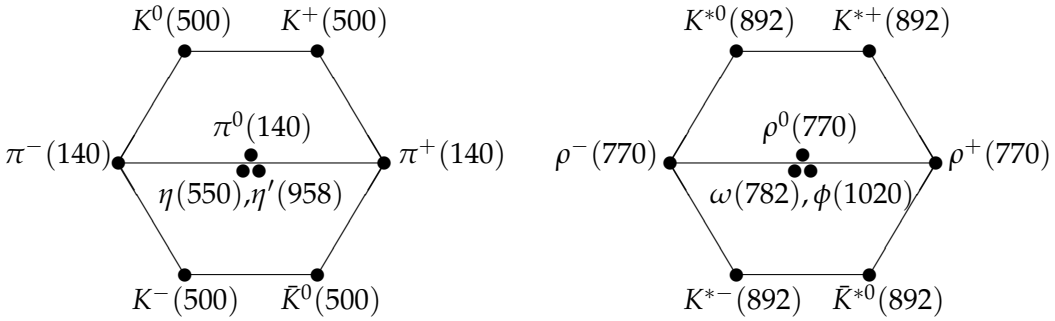

Figure 1.2: Left: The nonet of pseudoscalars. Right: The nonet of vectors.

Meson	Mass (MeV)	Width (MeV)	Isospin, Strangeness
$f_0(500)$, σ	400 — 550	400 — 700	$I = 0$, $S = 0$
$K_0^*(800)$, κ	682 ± 29	547 ± 24	$I = 1/2$, $S = \pm 1$
$f_0(980)$	990 ± 20	40 — 100	$I = 0$, $S = 0$
$a_0(980)$	980 ± 20	50 — 100	$I = 1$, $S = 0$
$f_0(1370)$	1200 — 1500	200 — 500	$I = 0$, $S = 0$
$K_0^*(1430)$	1425 ± 50	270 ± 80	$I = 1/2$, $S = \pm 1$
$a_0(1450)$	1474 ± 19	265 ± 13	$I = 1$, $S = 0$
$f_0(1500)$	1505 ± 6	109 ± 7	$I = 0$, $S = 0$
$f_0(1710)$	1720 ± 6	135 ± 8	$I = 0$, $S = 0$

Table 1.2: Scalar mesons below 2 GeV. Values for the masses and widths correspond to the ones given in [11].

nonets.

The $\bar{q}q$ quark model classification fits very well for pseudoscalar and vector mesons. In Fig. 1.2 we show the pseudoscalar and vector nonet. Resonances without strangeness are nearly degenerate in mass, however, due to the fact that the strange quark is much heavier than the up and down quarks, resonances with strange quarks have a mass increment of about 150-300 MeV for each additional strange valence quark or anti-quark.

In contrast to pseudoscalar, vector and tensor mesons, the identification of scalars, which are the main object of interest in this thesis, is a longstanding puzzle. In Tab. 1.2 we show the properties of the scalars below 2 GeV from [11], where we can see that they do not show the expected mass hierarchy. Furthermore, some of them have large decay widths which cause overlap between resonances and background, and makes their analysis a really complicated task.

As previously mentioned, using the $n^{2s+1}l_J$ classification, where n is the principal value quantum number and denotes radial excitations, the naive quark model predicts the lightest scalar $\bar{q}q$ nonet of mesons in a 1^3P_0 configuration. It is expected that P-wave states will be

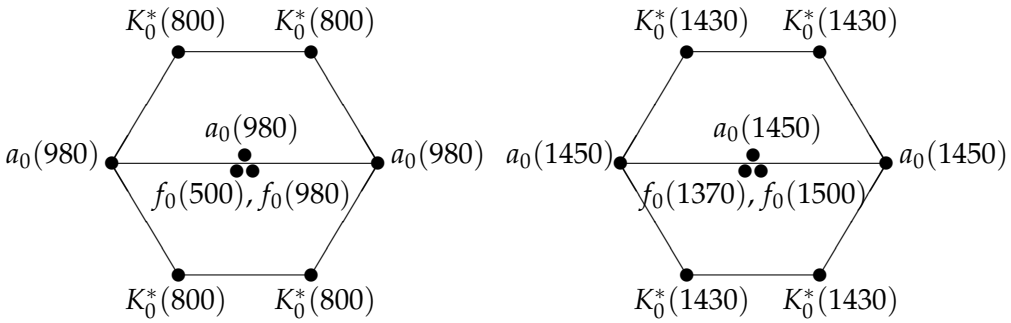

Figure 1.3: Left: Nonet of scalar mesons below 1 GeV. Right: Nonet of scalar mesons above 1 GeV

heavier than those in S-wave. In particular, models based in the naive quark model predict a mass above 1 GeV for those states [12, 33]. However, from Tab. 1.2, we can see that there are many of them with a mass below this energy. Furthermore, as we can see in the left panel of Fig. 1.3, these lightest scalar mesons show an inverted hierarchy, i.e. mesons with strangeness are lighter that some without. These arguments suggests that light scalars might have a non-$\bar{q}q$ nature [12, 13, 14, 15, 16, 17, 18, 19, 20, 21, 22, 23, 24]. The presence of two a_0 states with $I = 1$ and two strange K^{*0} resonances with $I = 1/2$ hints to the presence of two octets, which should be accompanied by the respective singlets, forming two mesons nonets, one of them corresponding to ordinary mesons with a mass above 1 GeV, and another with an exotic nature below [34], as we show in Fig. 1.3. There is, however, no agreement on this issue, which is still a subject of intense debate.

Furthermore, as we will see in the next section, QCD predicts the existence of isoscalar mesons, which, in the pure gauge theory, only contain gluons and are called glueballs. The ground state glueball is predicted by lattice gauge theories to be a 0^{++} state with a mass around 1500 MeV [35, 36, 37]. Although some states have been claimed to be good glueball candidates [38, 39, 40, 41, 24], there is no agreement on the issue, which is still a subject of intense debate. However, both glue and $\bar{q}q$ states will couple to singlet scalar mesons. Therefore, glueballs will mix with nearby $\bar{q}q$ states of the same quantum numbers. For example, the two isoscalar 0^{++} mesons around 1500 MeV will mix with the pure ground state glueball to generate the observed physical states $f_0(1370)$, $f_0(1500)$, and $f_0(1710)$.

1.1.3 The σ or $f_0(500)$ resonance

The $f_0(500)$ or σ is the lightest scalar meson and the main object of study in this thesis. It has been know for long that an interaction with these quantum numbers plays a key role in the nucleon-nucleon attractive interaction [1]. Furthermore, since it is the lightest hadronic resonance with the vacuum quantum numbers, it also plays a relevant role in the realization of the QCD spontaneous symmetry breaking in many models [63, 64]. In addition, as we have commented above, it is also expected that the lightest glueball show up with these quantum numbers, but its identification is hindered by its mixing with all other f_0 mesons and, possibly,

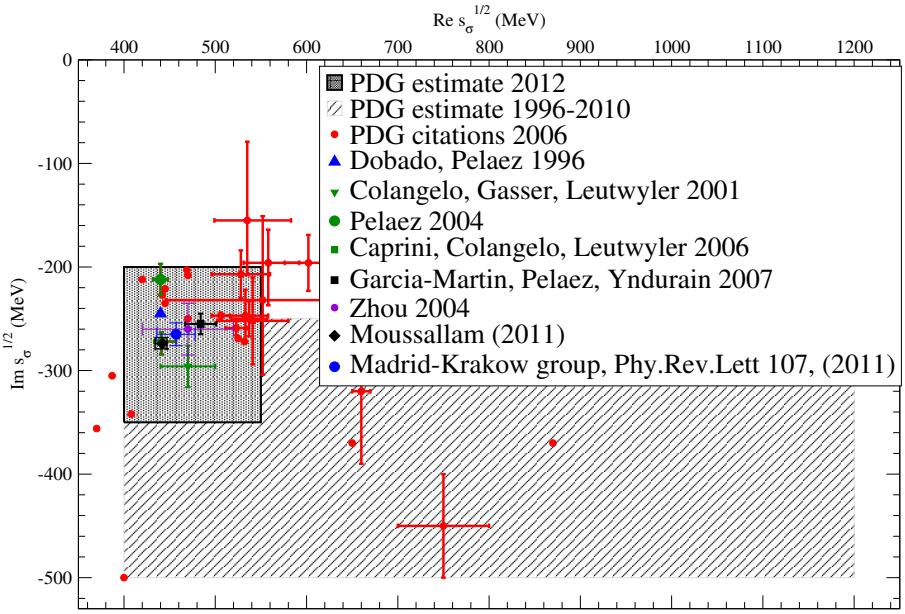

Figure 1.4: Location of the $f_0(500)$ or σ poles in the complex energy plane. We can particularly see, how the PDG estimation in the period from 1996 to 2010 has been substantially revised in the 2012 edition [11].

the $f_0(500)$ itself. Finally, as we will study in Section 1.3.5, it is interesting for ChPT since, despite being so light and strongly coupled to pions, it plays a very small role in the saturation values of the LECs of ChPT [5, 6].

In spite of its great interest for many different fields of physics, the existence and properties of the σ have been controversial since its very proposal. Just for illustration, until 1974 [44] , the PDG listed a O^+ isoscalar state as not well established", which was removed from 1976 [45] until 1994 [46]. In 1996 [47], it came back, listed now as $f_0(600)$, but with a too conservative estimation: a mass between 400 and 1200 MeV and a width between 600 and 1200 MeV. The reason of this is that the σ is extremely wide: its width is comparable to (or even greater than) its mass, and for many authors this could not be considered a particle or a resonance, since it barely propagates. Moreover, it can be distorted by a large background required by chiral symmetry, and from crossed channel exchanges [11], so it is very hard to see experimentally. In 2002, the PDG considered the $f_0(600)$ as "a well established state" [48], although the too conservative range for its mass and width was kept.

However, in the last years, new very precise data and the use of effective theories combined with dispersion theory have shed some light in this longstanding problem. In the last PDG edition of 2012 [11], the PDG has quoted a new estimation for the σ, with a mass between 400 and 550 MeV, and a width between 400 and 700 MeV, whereas its name has changed to $f_0(500)$. In their "Note on scalar mesons below 2 GeV" the PDG argues that it is due to: *the sensitivity of the extracted $f_0(500)$ pole position on the high accuracy low energy $\pi\pi$ scattering data, as well as to the advanced dispersion analyses.* Among these "advanced dispersion analyses", the PDG includes the one presented in this thesis in Section 2.1.4, which is one of our main results.

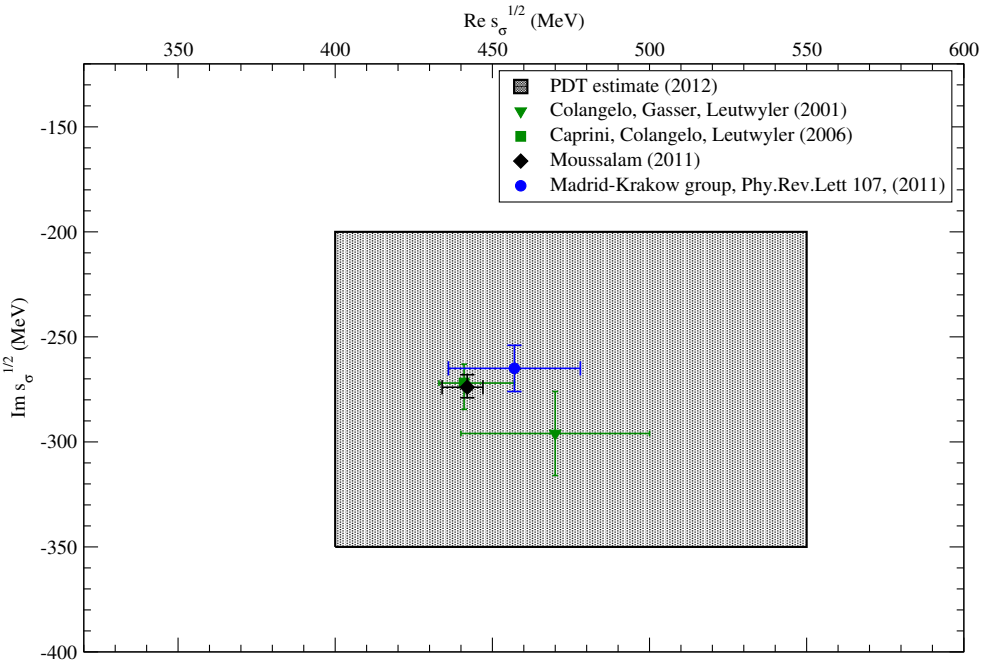

Figure 1.5: Location of the $f_0(500)$ or σ poles in the complex energy plane, and the results of the dispersive analyses cited in [11], given in [49, 50, 51] and in Section 2.1 of this thesis.

1.2 QCD

QCD has been shown to be the correct theory to describe the strong interactions, providing precise predictions in its perturbative regime and describing the general features of Hadronic Physics, which is the main object of study in this thesis. It is a non-abelian gauge field theory based around a SU(3) colour symmetry, whose basic degrees of freedom are quarks, fermions with spin 1/2, and gluons, massless gauge bosons with spin 1. In order to introduce QCD, we are going to review briefly the main properties of the non-abelian gauge symmetries, and then we will continue analyzing the QCD Lagrangian and its symmetries.

1.2.1 Gauge Symmetries

Gauge theories are based on the feature that the existence and some of the properties of the gauge fields follow from a principle of invariance under local gauge transformations, i.e. given a matter complex-valued field $\psi(x)$, invariance under the transformation

$$\psi(x) \to e^{i\epsilon^a(x)t_a}\psi(x), \tag{1.4}$$

where t_a is a set of independent constant matrices, and ϵ^a infinitesimal real parameters, which are allowed to depend on position and time. We assume now that these symmetry transformations are the infinitesimal part of a Lie group. In the case of QCD, which is the one interesting for this thesis, this invariance is under a non abelian-group, which requires that

the t_a matrices obey the commutation relations,

$$[t_a, t_b] = i f^c_{ab} t_c, \tag{1.5}$$

where the f^c_{ab} are the structure constants of the corresponding group. In the particular case of QCD, $a, b = 1 \cdots N_c$, where as we will see in the next section, N_c is the number of colours. Any set of these structure constants define a set of matrices t^A_a, defined as $(t^A_a)_c{}^b \equiv -i f^b_{ca}$, that satisfy the commutation relation:

$$[t^A_a, t^A_b] = i f^c_{ab} t^A_c, \tag{1.6}$$

known as the adjoint representation of the Lie algebra, and in the case QCD, $a, b = 1 \cdots N_c^2 - 1$.

Now, we should wonder what is needed to make a Lagrangian invariant under the transformations (1.4). Any term with non derivatives, as the fermion mass term

$$m\bar{\psi}\psi \tag{1.7}$$

will be invariant. However, this will not be the case if the Lagrangian includes derivatives of the fields; because of the position dependent parameter $\epsilon^a(x)$, the derivatives of the fields do not transform like the fields themselves, the infinitesimal transformation of the matter field $\psi_l(x)$ is given by

$$\delta\psi_l(x) = i\epsilon^\alpha(x)(t_\alpha)_l{}^m \psi_m(x), \tag{1.8}$$

whereas the infinitesimal transformation of its derivative is

$$\delta\left(\partial_\mu\psi_l(x)\right) = i\epsilon^a(x)(t_a)_l{}^m\left(\partial_\mu\psi_m(x)\right) + i\left(\partial_\mu\epsilon^a(x)\right)(t_a)_l{}^m\psi_m(x). \tag{1.9}$$

In order to make the Lagrangian invariant, we need another field whose transformation cancels the second term in eq. (1.9), i.e. a field A^a_μ which undergoes a matrix transformation like eq. (1.8) but involving a term $\partial_\mu\epsilon^a(x)$. However, since it carries an a-index, t_a should be replaced by the adjoint representation of the corresponding gauge group. Therefore, the transformation relation of the field A^a_μ will be given by

$$\delta A^a_\mu(x) = \partial_\mu\epsilon^a(x) + f^a_{bc}\epsilon^b(x)A^c_\mu. \tag{1.10}$$

This new field allows us to construct the covariant derivative

$$D_\mu\psi_l(x) = \partial_\mu\psi_l(x) - iA^a_\mu(x)(t_a)_l{}^m\psi_m(x), \tag{1.11}$$

whose variation is given by

$$\delta\left(D_\mu\psi_l(x)\right) = i\epsilon^a(t_a)_l{}^m D_\mu\psi_m(x), \tag{1.12}$$

so that the covariant derivative of the fields transforms just like the fields themselves. However, we also need to take into account the derivatives of the gauge fields. Proceeding in the same way, it is possible to construct a covariant curl defined as

$$F^a_{\mu\nu}(x) \equiv \partial_\mu A^a_\nu(x) - \partial_\nu A^a_\mu(x) + f^a_{bc}A^b_\mu(x)A^c_\nu(x), \tag{1.13}$$

which transforms in the same way as a matter field but under the adjoint representation of the group,

$$\delta F^a_{\mu\nu}(x) = \epsilon^b f^a_{cb} F^c_{\mu\nu}. \tag{1.14}$$

The transformation rules of the matter fields $\psi(x)$, their covariant derivatives and the gauge-field tensor $F^\alpha_{\mu\nu}$, do not introduce any derivative of the transformation parameter $\epsilon^a(x)$, so if we construct a Lagrangian with these ingredients, then it will be invariant under gauge transformations and we will be able to obtain a gauge invariance theory from it.

1.2.2 The QCD Lagrangian

As we have commented above, QCD is built upon non-abelian gauge invariance, and its Lagrangian is constructed from the gauge invariant terms we have just seen. Neglecting gauge fixing terms and ghosts (required to prevent unitarity violation in perturbation theory), which are not of interest in this thesis, the QCD Lagrangian has the form:

$$\begin{aligned} \mathcal{L}_{QCD} &= \sum_{j=1}^{N_f} \bar{q}_j(x) \left(i\not{D} - m_j \right) q_j(x) - \frac{1}{4} \sum_{a=1}^{8} F^a_{\mu\nu}(x) F^{\mu\nu}_a(x) \\ F^a_{\mu\nu}(x) &= \partial_\mu A^a_\nu - \partial_\nu A^a_\mu + g f^a_{bc} A^b_\mu A^c_\nu, \\ D_\mu &= \partial_\mu - ig\lambda_a A^a_\mu, \end{aligned} \tag{1.15}$$

where g is the bare coupling constant, q denotes the quark fields, A_μ the gluon field, λ_a the Gell-Mann matrices associated to the generator of the SU(3) group, and f^a_{bc} denotes the structure constants of SU(3). As we have mentioned before, the quarks have another degree of freedom: the colour. This means that a quark with a given flavour is also a colour triplet. It is important to note from eq. (1.15), that the covariant derivative is independent of the flavour of quarks, so it is the gluon-quark interaction. The non-abelian gauge invariance of the Lagrangian implies that, as we can see from the gauge field term of eq. (1.15), there are self-interactions between gauge bosons with vertices involving 2, 3 and 4 gluons.

As it is usual in quantum field theories, in order to quantize and renormalize the theory, an scale has to be introduced explicitly. This scale dependence must be canceled in all observable quantities, but leads to the running of the QCD coupling constant. Up to one-loop, it is given by:

$$\beta(\nu) = \mu \frac{dg(\mu)}{d\mu} = -\frac{g^3}{(4\pi)^2} \left(\frac{11}{3} N_c - \frac{2}{3} N_f \right) + \mathcal{O}(g^5), \tag{1.16}$$

where N_c and N_f denote the number of colours and flavour respectively. The solution of eq. (1.16) is:

$$\alpha_s(\mu) \equiv \frac{g^2(\mu)}{4\pi} = \frac{12\pi}{\left(11N_c - 2N_f\right) \log\left(\frac{\mu^2}{\Lambda^2_{QCD}} \right)}, \tag{1.17}$$

which implies that the dimensionless coupling constant g depend on a free dimensional parameter, the integration constant Λ_{QCD}, which can be understand as the scale where g,

diverges to one loop. It has been found in [52] that the strong coupling extrapolated to $\mu = m_Z = 91.2$ GeV, where m_z is the mass of the weak Z boson, is $\alpha_s(m_Z) = 0.119 \pm 0.005$, corresponding to $\Lambda_{QCD} = 251^{+130}_{-96}$.

For $N_c = 3$ and $N_f \leq 16$, the β function is negative, which means that the coupling constant decreases with increasing μ. The consequence of this fact is the celebrated property of *asymptotic freedom* of QCD, first discussed by Gross, Wilczek and Politzer in 1973 [53, 54, 55], which means that strong interactions are weaker at large momentum transfer, as observed experimentally for the constituents of hadrons. Therefore, for high energies, QCD behaves as a free theory and it is successfully described using perturbation theory. On the contrary, at low energies, quark and gluons interact strongly, consistently with the fact that quarks are observed confined in hadrons, which are the relevant degrees of freedom in this regime and the object of interest in this thesis.

1.2.3 QCD and Chiral symmetry

As we have said before, there is a large mass difference between the lightest three quarks (u, d, s) and the heaviest three (c, b, t). For this reason, the dynamics of heavy quarks are decoupled from the low energy interactions, and it makes sense to consider the case N_f = 2,3. In addition, since the masses of the light quarks are small in comparison to the typical QCD scale Λ_{QCD}, we can consider these physical masses as perturbations around $m_q = 0$. This case, when considering N_f = 2 or 3 the quark masses are taken as zero is known as *chiral limit* , and the QCD Lagrangian simplifies to:

$$\mathcal{L}^0_{QCD} = \sum_{f=u,d,s} \bar{q}_f(x) i \not{D} q_f(x) - \frac{1}{4} \sum_{a=1}^{8} F^a_{\mu\nu}(x) F^{\mu\nu}_a(x). \tag{1.18}$$

The chiral Lagrangian is invariant under the global *chiral transformations* in flavour space of the left and right handed projections of the quark fields:

$$q_L \longrightarrow L q_L = \exp\left(-i\theta^L_a \frac{t^a}{2}\right) q_L, \tag{1.19}$$

$$q_R \longrightarrow R q_R = \exp\left(-i\theta^R_a \frac{t^a}{2}\right) q_R, \tag{1.20}$$

where t^a are the generators of the corresponding $SU(N_f)$ algebra, q and $q_{L,R}$ denote flavour vectors and their spatial dependence is assumed, and the left and right handed projections are given by:

$$q_L = P_L q = \left(\frac{1-\gamma_5}{2}\right) q, \tag{1.21}$$

$$q_R = P_R q = \left(\frac{1+\gamma_5}{2}\right) q. \tag{1.22}$$

Therefore, the Lagrangian of eq. (1.18) is invariant under the group $SU(N_f)_L \times SU(N_f)_R$, which is known as chiral symmetry and gives rise to the Noether conserved currents:

$$J_\mu^{L,a} = \bar{q}_L \gamma_\mu \frac{t^a}{2} q_L \quad \text{and} \quad J_\mu^{R,a} = \bar{q}_R \gamma_\mu \frac{t^a}{2} q_R, \tag{1.23}$$

From them, it is possible to define the vector and axial currents as:

$$J_\mu^{V,a} = J_\mu^{L,a} + J_\mu^{R,a} = \bar{q}\gamma_\mu \frac{t^a}{2} q \quad \text{and} \quad J_\mu^{5,a} = J_\mu^{L,a} - J_\mu^{R,a} = \bar{q}\gamma_\mu\gamma_5 \frac{t^a}{2} q, \tag{1.24}$$

which means that it also has to be invariant under the $SU(N_f)_V \times SU(N_f)_A$ group and consequently:

$$\partial^\mu J_\mu^{V,a} = 0 \quad \text{and} \quad \partial^\mu J_\mu^{5,a} = 0. \tag{1.25}$$

The associated charges to these currents are the generator of the vector and axial symmetries and are given by:

$$Q^{V,a} = \int d^3x J_0^{V,a} \quad \text{and} \quad Q^{5,a} = \int d^3x J_0^{5,a}, \tag{1.26}$$

which satisfy the commutation relations:

$$\begin{aligned} [Q^{V,a}, Q^{V,b}] &= i f_c^{ab} Q_V^c, \\ [Q^{V,a}, Q^{A,b}] &= i f_c^{ab} Q_A^c, \\ [Q^{A,a}, Q^{A,b}] &= i f_c^{ab} Q_V^c, \end{aligned} \tag{1.27}$$

where again, f_c^{ab} denotes the structure constants of the $SU(N_f)$ group. Acting on the quark fields, these charge operators induce the chiral transformation of eq. (1.19) since:

$$\begin{aligned} [Q^{V,a}, q] &= -\frac{t^a}{2} q, \\ [Q^{A,a}, q] &= -\gamma_5 \frac{t^a}{2} q. \end{aligned} \tag{1.28}$$

The QCD chiral Lagrangian of eq. (1.18), is also invariant under the global U(1) transformation:

$$q \to q^{'} = \mathrm{e}^{i\alpha_Y} q. \tag{1.29}$$

By performing this transformations to each chiral projection with the same and opposite phases, it is possible to obtain a singlet conserved vector and a singlet axial-vector current respectively:

$$J_\mu^V = \bar{q}\gamma_\mu q \quad \text{and} \quad J_\mu^5 = \bar{q}\gamma_\mu\gamma_5 q, \tag{1.30}$$

which implies that the QCD Lagrangian is also invariant under the global $U(1)_B \times U(1)_A$ group, where B refers to the baryon number, and A to the axial transformation. The $U(1)_B$ symmetry, associated to the baryon number conservation, is observed in nature, but the $U(1)_A$ is an anomalous symmetry, broken by quantum corrections [56, 57, 58].

1.2.4 Spontaneous chiral symmetry breaking

Nevertheless, as we have shown in Table 1.1.1, the masses of the lightest quarks are not zero, which means that the chiral symmetry is explicitly broken. However, given their small value, the invariance under the $SU(N_f)_L \times SU(N_f)_R$ group should still be an approximate symmetry in QCD. It is clear that there should be a better symmetry for the $N_f = 2$ case, but even considering the strange quark, the particle spectrum of the theory should reflect this symmetry. In consequence, the Q_V^a and Q_A^a charge operators commute with the QCD Hamiltonian, and since they have different parity, for each state of positive parity, one would expect the existence of a degenerate state of negative parity. Therefore, vector and axial particles, which have the same quantum numbers but opposite parity, should show a chiral degeneracy, i.e. should be organized in multiplets, with approximately the same mass transforming under irreducible representations of $SU(2)_L \times SU(2)_R$, and also multiplets transforming under irreducible representations of $SU(3)_L \times SU(3)_R$ with a bigger mass difference, but still approximately degenerated.

However, this is not the case; vector and axial mesons are not even nearly degenerated. For example, in the vector multiplet, Fig. 1.2, we find the $\rho(770)$, with a mass of 770 MeV, whereas its axial partner, the $a_1(1260)$, is 490 MeV heavier. This difference, which is also found in the rest of multiplets, is too big to be accounted for by the explicit breaking of the symmetry due to the quarks masses, which are just a few MeV. Furthermore, if it is a true physical symmetry, the vacuum expectations values of the axial and vector currents should be equal up to the corrections expected by the explicit symmetry breaking due to the non-zero quark masses. But it is not the case as it has been shown in experiments of semileptonic weak decays [59, 60].

These arguments suggest that the chiral symmetry is not realized in the Wigner-Weyl mode, but in the Goldstone mode, which means that chiral symmetry is spontaneously broken with the breaking pattern:

$$SU(N_f)_L \times SU(N_f)_R \equiv SU(N_f)_V \times SU(N_f)_A \longrightarrow SU(N_f)_V. \tag{1.31}$$

The fact that the vector part of the chiral group should remain unbroken was proved by Vafa and Witten in [61], but the reason for the breaking of the axial part remains unknown. In addition, the vector isospin symmetry shows up very well in the particle spectrum, since we observe particles of approximately equal masses within the isospin multiplet, the pions for example Fig. 1.2, form a isospin triplet with $m_{\pi^\pm} \sim m_{\pi^0}$ as a consequence of $m_u \sim m_d$.

Therefore, according to the Goldstone theorem [62, 63, 64, 65, 66], there will appear as many Nambu Goldstone bosons (NGB) as the number of broken generators, which will behave with the transformation properties induced by the broken group. In the case of the group of axial transformations, $(N_f^2 - 1)$ massless psedoscalar bosons with spin 0 will appear, which of course will also be invariant under the vector group. This picture is consistent with the experimental observation, for $N_f = 2$ the 3 NGB are easily identified with the pions, which are not massless and, in strict sense, should be considered as pseudo-NGB. However, their masses are small compared to other hadron masses, and they can be explained by the small quark masses that explicitly break chiral symmetry. For $N_f = 3$, the eight pseudo-NGB are now the three pions together with the four kaons and the eta. In this case, however, since the mass of the s quark is much heavier that the mass of the u and d quarks, the explicit symmetry

breaking of the $SU(3)_V$ group is larger, which explains that the mass of the kaons and eta are about 350 to 400 MeV larger the pion mass.

The eight NGB of the three flavour case have the necessary quantum numbers to form the pseudoscalar octet of Fig. (1.2). However, the quark model, Section 1.1, predicts together with the pseudoscalar octet, an isospin singlet with the same parity and spin quantum numbers. The lightest candidate is the η'; however, with a mass of 960 MeV. it is too heavy. The cause for this high mass is the axial $U(1)_A$ anomaly [56, 57, 58], which appears when quantizing QCD and implies that the axial J^5_μ current of eq. (1.30), is not conserved and consequently, the $U(1)_A$ group is not dynamically broken. Therefore, the $\eta'(960)$ has a mass higher than the octet of pseudoscalars, which does not vanish in the chiral limit, and it is not a Goldstone boson.

Via the Goldstone theorem, the spontaneously symmetry breaking (SSB) implies that the axial charges of eq. (1.26), do not annihilate the vacuum. As a consequence:

$$\langle 0|\partial^\mu J^{5\,a}_\mu(0)|\phi^b(p)\rangle = \delta^{ab} F_b M_b^2, \tag{1.32}$$

which is known as the partial conservation of the axial current (PCAC), ϕ^b are NGB fields, M_b their corresponding masses and F_b their decays constants.

An important object in order to study the SSB is the quark or chiral condensate $\langle 0|\bar{q}q|0\rangle$. It is easy to check from eq. (1.19), that the infinitesimal transformation of the scalar operator $\bar{q}q$ under the $SU(N_f)_L \times SU(N_f)_R$ group is:

$$\bar{q}q \to \bar{q}q - i\left(\theta^L_a - \theta^R_a\right)\bar{q}\gamma_5\frac{t^a}{2}q, \tag{1.33}$$

whereas the transformation of the pseudoscalar operator $\bar{q}\gamma_5 q$ reads:

$$\bar{q}\gamma_5 q \to \bar{q}\gamma_5 q - i\left(\theta^L_a - \theta^R_a\right)\bar{q}\frac{t^a}{2}q. \tag{1.34}$$

From eq. (1.28), it is simple to show that:

$$\langle 0|[Q^{A,a}, \bar{q}\gamma_5 t^b q]|0\rangle = -\frac{1}{2}\langle 0|\bar{q}\{t^a, t^b\}q|0\rangle = -\frac{2}{3}\delta_{ab}\langle 0|\bar{q}q|0\rangle. \tag{1.35}$$

Therefore, the SSB implies that the quark condensate $\langle 0|\bar{q}q|0\rangle$, develops a vacuum expectation value, which has been estimated as [67, 68]:

$$\langle 0|\bar{q}q|0\rangle \sim (-240\,\text{MeV})^3, \tag{1.36}$$

and makes for a good candidate to be the order parameter of the spontaneous chiral symmetry breaking, since it vanishes when the chiral symmetry of the vacuum is restored.

1.3 Chiral Perturbation Theory

Effective field theories (EFT) provide the proper framework to perform detailed calculations in a systematic manner and in a restricted energy region, describing an underlying theory that

is valid on a wider energy scale. The basic premise of EFT is that dynamics at low energies (or large distances) do not depend on the details of the dynamics at high energies (or short distances). As a result, low energy physics can be described using an effective Lagrangian that contains only a few degrees of freedom, ignoring those present at higher energies.

EFT are particularly useful when a full calculation is not yet possible, as is the case with QCD at low energies. On the one hand, QCD interactions are non-perturbative at energies below the breaking scale of chiral symmetry, which makes very difficult any description of the low-energy hadronic interactions in terms of QCD degrees of freedom. On the other hand, the spectrum of the theory only contains at low energies the octet of light pseudoscalar mesons: π's, K's and η. Furthermore, it is known from experiment that in this regime, these pseudoscalar mesons interact weakly. Therefore, it is reasonable to expect that QCD can be treated perturbatively within a low energy Effective Formalism, when a suitable transformation of degrees of freedom is performed. This is exactly the goal of Chiral Perturbation Theory (ChPT) [7, 8, 9], where the pseudoscalar mesons are assumed to be the fundamental degrees of freedom. Since in this thesis we are interested in the study of the low energy meson interactions, ChPT is one of the main theoretical approaches we use. In this section, we briefly review some aspects of ChPT, along the lines of [69, 70], but further detailed reviews can be found in [71, 72, 73, 74].

1.3.1 Transformation properties of the Goldstone bosons

The Goldstone nature of the lightest pseudoscalar mesons implies strong constraints on their interactions, which can be most easily analyzed on the basis of an effective Lagrangian. Since there is a large mass gap between the pseudoscalar octet and the rest of the hadronic spectrum, we can build an EFT containing only Goldstone modes.

In order to construct the effective Lagrangian, it is necessary to obtain the transformation rules of the Goldstone bosons under the original chiral group [75, 76, 77]. It can be shown that an isomorphic mapping exists between the quotient group G/H and the Goldstone bosons fields ϕ_i [78], where $G \equiv SU(N_f)_L \times SU(N_f)_R$ and $H \equiv SU(N_f)_V$, so to each Goldstone field ϕ_i corresponds a coset $g_i H$, where g_i is an appropriate element of G. Therefore, the transformation of the Goldstone fields under the chiral group, is given by the transformation of the left coset gH up to an appropriate choice of variables parametrizing the elements of the quotient G/H. Let $\tilde{g} = (\tilde{L}, \tilde{R}) \in G$ where $\tilde{L} \in SU(N_f)_L$ and $\tilde{R} \in SU(N_f)_R$, and let $V \in H$, then the left coset of $\tilde{g}$, $\tilde{g}H$, can be expressed as:

$$\tilde{g}V = (\tilde{L}V, \tilde{R}V) = (\tilde{L}V, \tilde{R}\tilde{L}^\dagger \tilde{L}\tilde{V}) = (1, \tilde{R}\tilde{L}^\dagger)\tilde{L}V. \tag{1.37}$$

since $\tilde{L}V \in H$, we have that:

$$\tilde{g}H = (1, \tilde{R}\tilde{L}^\dagger)H. \tag{1.38}$$

which implies that we can uniquely characterized the left coset $\tilde{g}H$ through the $SU(N_f)$ matrix $U(x) = \tilde{R}\tilde{L}^\dagger$, if we follow the convention that the representative of the coset is chosen such that the unit matrix stands in its first argument. In addition, we introduce the dependence on x due to the fact that the Goldstone bosons are a function in the Minkowski space.

The transformation behaviour of $U(x)$ under G can be obtained by multiplying the left coset by an element $g = (L, R) \in G$, that is:

$$g\tilde{g}H = (L, R\tilde{R}\tilde{L}^\dagger)H = (L, R\tilde{R}\tilde{L}^\dagger L^\dagger L)H = (1, R\tilde{R}\tilde{L}^\dagger L^\dagger)(L, L)H = (1, R\tilde{R}\tilde{L}^\dagger L^\dagger)H, \tag{1.39}$$

which implies that under a G transformation:

$$U(x) = \tilde{R}\tilde{L}^\dagger \xrightarrow{G} U(x)' = R\tilde{R}\tilde{L}^\dagger L^\dagger = RU(x)L^\dagger. \tag{1.40}$$

Let us then construct a matrix, out of Goldstone bosons, with similar transformation properties. In particular, the matrices:

$$\Phi(x) = \sum_a t^a \phi(x)_a, \tag{1.41}$$

which belong to the set of all Hermitian and traceless $N \times N$ matrices and generate a real vector space, are a convenient way to collect the Goldstone bosons fields, which are given by:

$$\phi_a(x) = \frac{1}{2}\mathrm{Tr}(t_a \Phi(x)), \tag{1.42}$$

where again t_a denotes the generators of the corresponding $SU(N_f)$ algebra.

For the two-flavour case, $\Phi(x)$ is given by;

$$\Phi(x) \;=\; \begin{pmatrix} \pi^0(x) & \sqrt{2}\pi^+(x) \\ \sqrt{2}\pi^-(x) & -\pi^0(x) \end{pmatrix},$$

while for the three-flavour case

$$\Phi(x) \;=\; \begin{pmatrix} \pi^0(x) + \frac{1}{\sqrt{3}}\eta(x) & \sqrt{2}\pi^+(x) & \sqrt{2}K^+(x) \\ \sqrt{2}\pi^-(x) & -\pi^0(x) + \frac{1}{\sqrt{3}}\eta(x) & \sqrt{2}K^0(x) \\ \sqrt{2}K^-(x) & \sqrt{2}\bar{K}^0(x) & -\frac{2}{\sqrt{3}}\eta(x) \end{pmatrix},$$

Finally, the set matrices:

$$U(x) = \exp\frac{i\Phi(x)}{f}, \tag{1.43}$$

where f is a constant with mass dimension introduced to make a dimensionless quotient, belong to the corresponding $SU(N_f)$ group and are an exponential parametrization of the Goldstone bosons, transforming under G as:

$$U(x) \xrightarrow{G} U(x)' = (L, R)U(x) = RU(x)L^\dagger \tag{1.44}$$

The set of $U(x)$ matrices does not define a vector space, since the sum of two $SU(N)$ matrices is not a $SU(N)$ matrix, and the action of G on the space of these matrices is a non-linear realization of the group. Expanding $U(x)$ in powers of $\Phi(x)$, it can be immediately seen that the transformation behaviour of $\Phi(x)$ under the unbroken subgroup H is:

$$\Phi(x) \xrightarrow{H} \Phi(x)' = V\Phi(x)V^\dagger, \tag{1.45}$$

where V denotes an element of H. It means that $\Phi(x)$ transforms linearly under H. Furthermore, from eq. (1.26), it can be seen, that this non-linear transformation on $U(x)$ implies the following transformations for the Goldstone bosons separately under the vector and axial charges:

$$[Q^{V,a}, \phi^b(x)] = i f_c^{ab} \phi(x)^c \qquad [Q^{V,a}, \phi^b(x)] = g^{ab}(\Phi) \tag{1.46}$$

where $g^{ab}(\Phi)$ is some non-linear function of Φ. So we see that under the unbroken group the Goldstone bosons transform linearly, but they do it non-linearly under the axial charges corresponding to the broken generators, i.e. the Goldstone bosons transform as a triplet and octet in SU(2) and SU(3) respectively.

1.3.2 The effective chiral Lagrangian

Once the transformation rules for the Goldstone bosons associated to the SSB of QCD are known, we will construct the most general Lagrangian describing their dynamics. This Lagrangian should be compatible with the QCD symmetries, and in the chiral limit it should be invariant under the $SU(N_f)_L \times SU(N_f)_R \times U(I)_V$ group, but the ground state should only be invariant under the $SU(N_f)_V \times U(1)_V$ group. It should contain exactly $N_f^2 - 1$ pseudoscalars as degrees of freedom transforming in the adjoint representation of the group $SU(N_f)$, which we can collect in the matrix $U(x)$ defined in eq. (1.43). The Lagrangian can be organized in terms of increasing powers of momentum or, equivalently, in terms of an increasing number of derivatives of $U(x)$ (parity conservation requires an even number of derivatives):

$$\mathcal{L}_{\text{ChPT}} = \sum_n \mathcal{L}_{2n}. \tag{1.47}$$

Due to the unitarity of the U matrix, $U(x)U(x)^\dagger = \mathbb{I}$, at least two derivatives are required to generate a non-trivial interaction, so the most general chirally invariant Lagrangian with only two derivatives reads

$$\mathcal{L}_2^0 = \frac{f^2}{4} \langle \partial_\mu U(x)^\dagger \partial^\mu U(x) \rangle, \tag{1.48}$$

where $\langle \cdot \rangle$ denotes the trace in flavour space. The global coefficient $f^2/4$ is fixed from the requirement that the kinetic term is properly normalized, since expanding eq. (1.48) in powers of Φ:

$$\begin{aligned} \mathcal{L}_2^0 \;=\; & \frac{1}{2} \partial_\mu \phi(x)_a \partial^\mu \phi(x)^a + \\ & \frac{1}{12 f^2} (\phi(x)_a \partial^\mu \phi(x)^a)(\phi(x)^b \partial_\mu \phi(x)_b) + \mathcal{O}(\frac{\phi^6}{f^4}), \end{aligned} \tag{1.49}$$

one obtains the standard kinetic term plus a tower of interactions involving an increasing number of fields.

An important technique that we will thoroughly use in Section 2.3 and which allows us to compute different quark current Green functions in a straightforward way is the external field method, i.e. the addition of external sources to the Lagrangian. The extended chiral QCD Lagrangian of eq. (1.18) with quarks coupling to external fields reads:

$$\mathcal{L}_{QCD} = \mathcal{L}_{QCD}^0 + \bar{q}(x) \left[\gamma_\mu \left(v^\mu(x) + \gamma_5 a^\mu(x) \right) - \left(s(x) - i\gamma_5 p(x) \right) \right] q(x) \tag{1.50}$$

where $\mathcal{L}^0_{QCD}$ is the QCD Lagrangian with massless quarks and v_μ, a_μ, s, and p are some external (and color-neutral) iso-vector, axial vector, scalar and pseudo-scalar fields respectively. The usual QCD Lagrangian of eq. (1.15) with massive quarks is recovered by setting $v_\mu = a_\mu = p = 0$ and $s = \text{diag}(m_{f_1}, \ldots, m_{f_{N_f}})$. These external fields have also a matrix structure. For instance, in the $N_f = 3$ case:

$$v^\mu = \sum_{a=1}^{8} \lambda^a 2 v_a^\mu, \qquad a^\mu = \sum_{a=1}^{8} \lambda^a 2 a_a^\mu, \qquad s = \sum_{a=0}^{8} \lambda^a s_a, \qquad p = \sum_{a=0}^{8} \lambda^a p_a, \tag{1.51}$$

where $\{\lambda^a\}_{a=1}^8$ are the Gell-Mann matrices and $\lambda_0 = 2/3\,\text{diag}(1,1,1)$.

The extended QCD Lagrangian of eq. (1.50) is also invariant under the local $SU(N_f)_L \times SU(N_f)_R$ transformations:

$$\begin{aligned} q_L &\to L q_L, \qquad q_R \to R q_R, \qquad s + ip \to R(s+ip)L^\dagger, \\ l_\mu &\to L l_\mu L^\dagger + iL\partial_\mu L^\dagger, \qquad r_\mu \to R r_\mu R^\dagger + iR\partial_\mu R^\dagger, \end{aligned} \tag{1.52}$$

where: $l_\mu = \frac{1}{2}(v_\mu + a_\mu)$ and $r_\mu = \frac{1}{2}(v_\mu - a_\mu)$.

It is possible to use this symmetry to generalize the effective Lagrangian in the presence of external fields. Since the transformation of v_μ and a_μ involves their derivatives, we know from Section 1.2.1, that to preserve local symmetry, these external fields can only appear through the covariant derivatives:

$$D_\mu U(x) = \left[\partial_\mu - i(r_\mu - l_\mu)\right] U(x), \tag{1.53}$$

and through the field tensor:

$$F_L^{\mu\nu} = \partial^\mu l^\nu - \partial^\nu l^\mu - i[l^\mu, l^\nu] \qquad F_R^{\mu\nu} = \partial^\mu r^\nu - \partial^\nu r^\mu - i[r^\mu, r^\nu]. \tag{1.54}$$

However, the scalar and pseudoscalar sources can appear coupled to the $U(x)$ fields directly. Therefore, the generalized version of the lowest order effective Lagrangian of eq. (1.48) reads:

$$\mathcal{L}_2 = \frac{f^2}{4} \langle D_\mu U(x)^\dagger D^\mu U(x) + U(x)^\dagger \chi(x) + \chi(x)^\dagger U(x) \rangle, \tag{1.55}$$

where:

$$\chi = 2B_0(s + ip) \tag{1.56}$$

and $2B_0$ is a constant that we will relate below to a physical quantity.

So far, we have assumed massless quarks and an exact $SU(N_f)_L \times SU(N_f)_R$ symmetry. However, we have seen in Section 1.2.4 that it is explicitly broken by the non-zero quark masses, leading to massive pseudo-Goldstone bosons. The external field method represents an excellent way to incorporate this explicit breaking of chiral symmetry. If one wants to recover at leading order the Gell-Mann-Okubo relation [79, 80]:

$$4m_K^2 + m_\pi^2 + 3m_\eta^2, \tag{1.57}$$

which is well satisfied experimentally, then one can set in eq. (1.55) $l_\mu = r_\mu = p = 0$ and $s = \mathcal{M} = \text{diag}(m_{f_1}, \cdots, m_{f_{N_f}})$, to obtain:

$$\mathcal{L}_2 = \frac{f^2}{4} \langle \partial_\mu U(x) \partial^\mu U(x) \rangle + \frac{B_0 f^2}{2} \langle \mathcal{M} U(x)^\dagger + \mathcal{M}^\dagger U(x) \rangle, \tag{1.58}$$

which is the lowest order effective Lagrangian of eq. (1.48) plus a mass term, thus ensuring that chiral symmetry is broken in the same way as it is in QCD, and that, as we will see below, meson masses squared are proportional to the quark masses, consistently with lattice results [81] [2].

The external field method becomes particularly useful in order to compute the chiral Noether currents. We can obtain Green functions with vector, axial-vector, scalar and pseudoscalar currents simply by taking functional derivatives of the action with respect to their corresponding external sources. Actually, this is the method we will follow in Section 2.3 in order to obtain the four-quark condensate. For example, at leading order, the left and right currents will be given by:

$$J_\mu^{L,a} = \frac{\delta \mathcal{L}_2}{\delta l_a^\mu} = i\frac{f^2}{4}\mathrm{Tr}\left[\lambda^a D_\mu U(x)^\dagger U(x)\right] \tag{1.59}$$

$$J_\mu^{R,a} = \frac{\delta \mathcal{L}_2}{\delta r_a^\mu} = -i\frac{f^2}{4}\mathrm{Tr}\left[\lambda^a D_\mu U(x) U(x)^\dagger\right]. \tag{1.60}$$

Combining both equations, we obtain again the vector and axial currents:

$$\begin{aligned} J_\mu^{V,a} &= -i\frac{f^2}{4}\mathrm{Tr}\left[\lambda^a\left(D^\mu U(x)U(x)^\dagger - D^\mu U(x)^\dagger U(x)\right)\right] = \mathcal{O}\left(\frac{\phi^2}{f^2}\right) \\ J_\mu^{5,a} &= -i\frac{f^2}{4}\mathrm{Tr}\left[\lambda^a\left(D^\mu U(x)U(x)^\dagger + D^\mu U(x)^\dagger U(x)\right)\right] = -f\partial_\mu\phi^a + \mathcal{O}\left(\frac{\phi^2}{f^2}\right), \end{aligned} \tag{1.61}$$

where we can see that the vector current is even in the number of Goldstone bosons whereas the axial one is odd. We can conclude from this result, that the axial current has a non-vanishing matrix element when evaluating between a single Goldstone boson state and the vacuum, i.e.

$$\langle 0|J_\mu^{5,a}|\phi^b\rangle = ip_\mu\delta^{ab}f. \tag{1.62}$$

Comparing this result with the PCAC given in eq. (1.32), we can see that chiral coupling f is related to the pion decay constant F_π. At leading order: $f = F_\pi$=92.4 MeV.

In the same way, taking the functional derivative respect to the scalar field:

$$\bar{q}^i q^j = -\frac{\delta \mathcal{L}_2}{\delta s^{ij}} = -\frac{f^2 B_0}{2}\left(U(x)^{ij} + U(x)^{\dagger\, ij}\right), \tag{1.63}$$

which implies that its vacuum expectation value is:

$$\langle 0|\bar{q}^i q^j|0\rangle = -f^2 B_0\delta^{ij} + \mathcal{O}(\mathcal{M}/f^2), \tag{1.64}$$

so the constant B_0 is related to the quark condensate, which, as we saw in eq. (1.36), is related to the chiral symmetry breaking, and it will play a key role in Section 2.3, when we analyze the role of higher quark-condensate configurations and scalar susceptibilities in the spontaneous chiral symmetry breaking.

[2] An alternative scenario where the squared Goldstone boson masses were not linear on the quark mass was studied in [82, 83, 84, 85]

Finally, we can obtain the pseudo-Goldstone boson masses by expanding the effective Lagrangian in powers of f and reading the resulting mass terms for the fields. At leading order and in the isospin limit, $\hat{m} = m_u = m_d$:

$$m_\pi^2 = 2B_0\hat{m}, \quad m_K^2 = B_0(\hat{m} + m_s), \quad m_\eta^2 = \frac{2}{3}B_0(\hat{m} + 2m_s), \tag{1.65}$$

which implies the Gell–Mann–Okubo formula [79, 80] for meson masses

$$4m_K^2 = m_\pi^2 + 3m_\eta^2, \tag{1.66}$$

which is satisfied phenomenologically. Furthermore, from eq. (1.64), in the chiral limit, we can relate the meson and quark masses to the size of the quark condensate:

$$F_\pi^2 m_\pi^2 = \hat{m}\langle 0|\bar{u}u + \bar{d}d|0\rangle, \tag{1.67}$$

which is known as Gell-Mann-Oakes-Renner formula [86].

1.3.3 Chiral Perturbation Theory at higher orders

In several chapters of this thesis we will have to deal with higher order calculations, i.e. loop diagrams based on the effective Lagrangian of eq. (1.47), which contains an infinitive number of terms and free parameters. In order to address this problem we need a systematic method of assessing the importance of diagrams generated by the interaction terms. The Weinberg's power counting scheme [7] tells us that the order D of a given diagram contributing to the chiral expansion is given by:

$$D = 2 + 2L + \sum_{K=1}^{\infty} V_{2K}(2k - 2), \tag{1.68}$$

where V_{2k} denotes the number of vertices from $\mathcal{L}_{2k}$ in the diagram and L denotes the number of loops. The right–hand–side of eq. (1.68) is a sum of positive terms, which implies that for a given value of D, only a finite number of V_{2k} and L combinations contribute, and hence, there is a finite number of diagrams. It is also important to note that each loop adds two powers of momenta so they are suppressed in the chiral counting. At leading order, $\mathcal{O}(p^2)$, $L = 0$ and $V_{d>2} = 0$ so $D = 2$. However at $\mathcal{O}(p^4)$ $D = 4$, there are two possibilities: one-loop graphs composed of only lowest order vertices ($L = 1$,$V_{d>2} = 0$), or tree-level graphs with a $\mathcal{L}_4$ vertex contribution ($L = 0$, $V_4 = 1$ and $V_{d>4} = 0$).

Higher order Lagrangians, organized in a momentum and quark mass expansion, include all terms compatible with the QCD symmetries, parity and charge conjugation, and the chiral transformation defined in eq. (1.52). Each term comes multiplied by a coupling constant, which all togeher are known as Low Energy Constants (LECs) and take account of the effects of heavier particles and higher scales. They cannot be determined perturbatively from QCD and have to be obtained phenomenologically [87, 88, 89, 49, 90, 91, 81]. However, as we will see below, they can be estimated by including explicitly heavier states [5, 6]. In fact, the resonance saturation hypothesis (RES) states that, the contribution of only the first high energy nonets saturates the value of the LECs. Furthermore, we can also obtain their dependence on the QCD number of colours, which we will use thoroughly in this thesis.

The renormalization of the LECs absorbs the divergences coming from previous orders, so the theory can be renormalized order by order. The number of independent terms and hence, low energy constants, increases rapidly at higher orders, which makes the theory to loose its predictive power. In practice, only $\mathcal{L}_2$, $\mathcal{L}_4$ and $\mathcal{L}_6$ are used. As we have seen $\mathcal{L}_2$ contains only two constants, f and B_0, whereas $\mathcal{L}_4$ and $\mathcal{L}_6$ contain 7 and 53 constants respectively in the $SU(2)$ case [92], and 10 and 90 in $SU(3)$ [93].

Finally, for completeness, we give the SU(3) $\mathcal{L}_4$ Lagrangian [9]:

$$\begin{aligned}\mathcal{L}_4 &= L_1 Tr\left(D^\mu U^\dagger D_\mu U\right)^2 + L_2 Tr\left(D^\mu U^\dagger D^\nu U\right) Tr\left(D_\mu U^\dagger D_\nu U\right) \\ &+ L_3 Tr\left(D^\mu U^\dagger D_\mu D^\nu U^\dagger D_\nu\right) + L_4 Tr\left(D^\mu U^\dagger D_\mu U\right) Tr\left(\chi^\dagger U + \chi U^\dagger\right) \\ &+ L_5 Tr\left(D^\mu U^\dagger D_\mu U(\chi^\dagger U + U^\dagger \chi)\right) + L_6 Tr^2\left(\chi^\dagger U + \chi U^\dagger\right) \\ &+ L_7 Tr^2\left(\chi^\dagger U - \chi U^\dagger\right) + L_8 Tr\left(\chi^\dagger U \chi^\dagger U + \chi U^\dagger \chi U^\dagger\right) \\ &- i L_9 Tr\left(F^R_{\mu\nu} D^\mu U D^\nu U^\dagger + F^L_{\mu\nu} D^\mu U D^\nu U^\dagger\right) + L_{10} Tr\left(U^\dagger F^R_{\mu\nu} U F^{L\ \mu\nu}\right) \\ &+ H_1 Tr\left(F^R_{\mu\nu} F^{R\ \mu\nu} + F^L_{\mu\nu} F^{L\ \mu\nu}\right) + H_2 Tr\left(\chi^\dagger \chi\right),\end{aligned} \tag{1.69}$$

where χ is given in eq. (1.56) and, in the physical case, is proportional to the quark mass matrix $\mathcal{M} = \text{diag}(m_{f_1}, \cdots, m_{f_{N_f}})$. We will use this Lagrangian in the Sections 2.2 and 2.3 of this thesis. The LECs L_1, L_2 and L_3 multiply massless terms that do not vanish in the chiral limit. L_4 and L_5 multiply terms which depend linearly on the quark masses and contribute to the renormalization of the NGB wave functions and decay constants. L_7 will be important when studying the $U_A(1)$ anomaly, Section 1.4.3. L_6 and L_8 come also multiplying mass terms and contribute to the renormalization of the NGB masses. As we will see, they play a key role in the renormalization of the quark condensate and the scalar susceptibility, Section 2.3. L_9 and L_{10} are coupled to other fields and are not of interest in this thesis. Finally, H_1 and H_2 do not appear multiplying any field, but the latter will be important in Section 2.3.

1.3.4 $U(3)$ Chiral perturbation theory

As we have seen in Section 1.2.3, the QCD Lagrangian is invariant under the exact $U(1)_B$ symmetry and under the broken $SU(N_f)_L \times SU(N_f)_R$ as a natural consequence of the smallness of the lightest quarks. But the chiral QCD Lagrangian of eq. (1.18) has also another chiral symmetry, the $U(1)_A$ symmetry under the transformation:

$$q \to q' = e^{i\gamma_5\theta} q \tag{1.70}$$

which leads to the conserved J^5_μ current of eq. (1.30). On the one hand, this symmetry, if unbroken, would impose a parity doubling in the hadron spectrum, which, however, is not observed. On the other hand, a spontaneously broken $U(1)_A$ symmetry would imply, together with the η meson, the existence of another isoscalar 0^{-+} meson with a mass comparable to the other NGB. However, it is not the case. The best candidate, the η', which has a mass of 960 MeV, is too heavy. The $U(1)_A$ chiral symmetry in QCD is broken because of quantum effects that violate the conservation of the singlet axial vector current, which is known as the $U_A(1)$

anomaly [56, 57, 58]. As a result, the singlet pseudoscalar η' is not a pseudo-Goldstone boson [94, 95]. If this anomaly was not present, an almost conserved current for the $U_A(1)$ symmetry would exist and it could be dynamically broken, so that the η' would also be an NGB.

However, as we will see in Section 1.4.3, from a large N_c QCD point of view, the η' mass is $1/\sqrt{N_c}$ suppresed [57], thus indicating that the η' meson becomes the ninth pseudo-Goldstone boson in the large N_c and chiral limits [96, 97, 98, 99]. Therefore at $N_c = \infty$, the chiral QCD Lagrangian of eq. (1.18) possesses a $U(3)_L \times U(3)_R$ chiral symmetry. If we assume that this symmetry is spontaneously broken down to the $U(3)_V$, there is a nonet of Goldstone bosons: the π's, K's, η, and η'.

In this thesis we will study the effect of the η' in the low energy meson dynamics when increasing the numbers of colors. Therefore, in this section, we are going to describe briefly the U(3) chiral Lagrangian, which we will use in Section 2.2. In order to do that, we should proceed as we did in Sections 1.3.1 and 1.3.2, i.e. reproduce the transformation properties of the Goldstone bosons under the original $U(3)_R \times U(3)_L$ group, and then construct the most general Lagrangian compatible with the QCD symmetries and the chiral $U(3)_L \times U(3)_R$ symmetry, which describes their dynamics.

As we did in Section 1.3.1, we can now parametrize the nonet of NGB in the exponential parametrization:

$$U_3(x) = \exp \frac{i\Phi_3(x)}{f}, \tag{1.71}$$

with

$$\Phi_3(x) = \sum_{a=1}^{9} t^a \phi_a(x) = \begin{pmatrix} \pi^0 + \frac{1}{\sqrt{3}}\eta + \sqrt{\frac{2}{3}}\eta' & \sqrt{2}\pi^+ & \sqrt{2}K^+ \\ \sqrt{2}\pi^- & -\pi^0 + \frac{1}{\sqrt{3}}\eta + \sqrt{\frac{2}{3}}\eta' & \sqrt{2}K^0 \\ \sqrt{2}\bar{K}^- & \sqrt{2}\bar{K}^0 & -\frac{2}{\sqrt{3}}\eta + \sqrt{\frac{2}{3}}\eta' \end{pmatrix} \tag{1.72}$$

where t^a are the generators of the U(3) algebra, so $\mathrm{Tr}(t^a t^b) = \delta^{ab}$. The $U(3)_L \times U(3)_R$ group acting on the Goldstone bosons fields induces the transformation:

$$U_3(x) \to U_3(x)' = R_3 U_3(x) L_3^\dagger, \tag{1.73}$$

where R_3 and L_3 are respectively elements of the $U(3)_R$ and $U(3)_L$ group.

Therefore, the lowest order U(3) effective Lagrangian is then given by [100, 101, 102]:

$$\mathcal{L}_{U(3)} = \frac{f^2}{4}\langle \partial_\mu U_3(x) \partial^\mu U_3(x)^\dagger \rangle + \frac{B_0 f^2}{2}\langle \mathcal{M} U_3(x)^\dagger + \mathcal{M}^\dagger U_3(x) \rangle. \tag{1.74}$$

However, if we want to obtain a realistic description of the $U(3)$ nonet dynamics, we have to incorporate a $U(3)_L \times U(3)_R$ breaking term induced by the $U(1)_A$ anomaly. To lowest order in the $1/N_c$ expansion and in the quark masses, we must simply add a new operator to the effective Lagrangian of eq. (1.74) which breaks $U(3)_L \times U(3)_R$ down to $SU(3)_L \times SU(3)_R$. It

can be shown that, without derivatives, such an operator must be a function of $\det U_3(x)$ and its complex conjugate [100, 101]. Furthermore, as we will see in Section 1.4.3, it is known from the $1/N_c$ expansion counting rules, that the anomaly-induced interaction is, to leading order in $1/N_c$, quadratic in the mass of the η' only [103]. The interaction that satisfies these conditions is [100, 101, 102]:

$$\mathcal{L}_{\text{anomaly}} = \frac{f^2}{2N_c} M_0^2 \log^2(\det U_3(x)), \tag{1.75}$$

where M_0 is $\mathcal{O}(1)$ in the N_c counting.

Therefore, the effective Lagrangian of eq. (1.74) with the anomaly breaking term of eq. (1.75) can be used to calculate soft meson amplitudes including the η' effects, to lowest order in $1/N_c$ and in quark masses. As we have said above, we will use just this leading order Lagrangian in Section 2.2, in order to study the role of the η' in the low energy meson dynamics at large N_c.

1.3.5 Resonance saturation

As we have seen in Section 1.3.3, the chiral Lagrangian depends on a number of coupling constants called LECs, which cannot be determined from the symmetries of the theory. These constants are fixed by the dynamics of the underlying theory through the renormalization scale and the heavy quark masses. However, it is not possible to calculate them directly from perturbative QCD, and they are obtained from experimental low-energy information and by using large-N_c arguments. In principle, they receive contributions from different sources, in particular, from mesons resonances, but also from other hadronic states. In [8], it was shown that the observed values of the LECs are quite well reproduced if one assumes that they are due to the interchange of the $\rho(770)$, which is known as vector dominance. Nevertheless, all low-lying resonances contribute to the LECs, and therefore, to the chiral Lagrangian [5, 6].

In the results presented in Section 2.2 of this thesis, we will make use of the resonances saturation hypothesis, which as we have said above, states that the LECs are saturated by the lightest resonances. Therefore in this section we are going to study how they can be included in the chiral Lagrangian and estimate their contributions to the LECs. In order to do that, we write the renormalized LECs as:

$$L_i^r(\mu) = \sum_{R=V,A,S,P} L_i^R + \hat{L}_i(\mu), \tag{1.76}$$

where μ is renormalized scale, V, A, S and P refer to the vector, axial-vector, scalar and pseudoscalar resonances, L_i^R are the resonance contributions to the renormalized LEC $L_i^r(\mu)$, and $\hat{L}_i(\mu)$ is the remaining part. It is natural to expect that if low-energy resonances dominate the $L_i^r(\mu)$, μ has to be taken not too far from this resonance region.

If we want to find which resonances contribute to the low-energy meson interactions, we should include them explicitly in the ChPT Lagrangian, and calculate then the chiral couplings of vector, axial-vector, scalar and pseudo-scalar resonances to the NGB, in a way that respects the invariance under the chiral group $G \equiv SU(3)_L \times SU(3)_R$, and, as we studied in Section 1.3.1, the non-linear transformation of the NGB.

We will consider octet and singlet resonances, denoted respectively as $R(x)$ and $R_1(x)$, and as we did for the NGB. We collect the first ones in the matrix:

$$R(x) = \sum_{i=1}^{8} \lambda_i R^i(x), \tag{1.77}$$

where λ_i denotes the Gell-Mann matrices.

In [5, 6], it was shown that the lowest order couplings in the chiral expansion, which are linear in the resonance fields and transform correctly, are obtained by including all resonance couplings in the Lagrangian:

$$\mathcal{L}_{Res} = \sum_{R=V,A,S,P} \mathcal{L}_{\rm Kin}(R) + \mathcal{L}_2(2), \tag{1.78}$$

where the kinetic term is given by:

$$\begin{aligned} \mathcal{L}_{\rm Kin}(R) &= -\frac{1}{2}\left\langle \nabla^\mu R_{\mu\nu}\nabla_\rho R^{\rho\nu} - \frac{1}{2}M_R^2 R_{\mu\nu}R^{\mu\nu}\right\rangle \\ &\quad -\frac{1}{2}\partial^\mu R_{1,\mu\nu}\partial_\rho R_1^{\rho,\nu} + \frac{1}{4}M_{R_1}^2 R_{1,\mu\nu}R_1^{\mu\nu}, \quad \text{for} \quad R = V, A, \\ \mathcal{L}_{\rm Kin}(R) &= -\frac{1}{2}\left\langle \nabla^\mu R\nabla_\mu R - M_R^2 R^2\right\rangle - \frac{1}{2}\left(\partial^\mu R_1\partial_\mu R_1 - M_{R_1}^2 R_1^2\right), \quad \text{for} \quad R = S, P, \end{aligned} \tag{1.79}$$

where M_R and M_{R_1} are the corresponding octet and singlet resonance masses in the chiral limit, and the dependence in x is assumed. The interaction terms $\mathcal{L}_2(R)$ read:

$$\begin{aligned} \mathcal{L}(V) &= \frac{F_V}{2\sqrt{2}}\left\langle V_{\mu\nu}f_+^{\mu\nu}\right\rangle + \frac{G_V}{\sqrt{2}}\left\langle V_{\mu\nu}u^\mu u^\nu\right\rangle, \\ \mathcal{L}(A) &= \frac{F_A}{2\sqrt{2}}\left\langle A_{\mu\nu}f_-^{\mu\nu}\right\rangle, \\ \mathcal{L}(S) &= c_d\left\langle S u_\mu u^\mu\right\rangle + c_m\left\langle S\chi_+\right\rangle + \tilde{c}_d S_1\left\langle u_\mu u^\mu\right\rangle + \tilde{c}_m S_1\left\langle\chi_+\right\rangle, \\ \mathcal{L}(P) &= id_m\left\langle P\chi_-\right\rangle + i\tilde{d}_m\left\langle P_1\chi_-\right\rangle, \end{aligned} \tag{1.80}$$

where:

$$\begin{aligned} u &= U^{1/2} = \exp\left(\frac{i\Phi(x)}{2f}\right), \\ u_\mu &= iu^\dagger D_\mu U u^\dagger = u_\mu^\dagger, \\ \chi_\pm &= u^\dagger\chi u^\dagger \pm u\chi^\dagger u, \\ f_\pm^{\mu\nu} &= uF_L^{\mu\nu}u^\dagger \pm u^\dagger F_R^{\mu\nu}u, \\ \nabla_\mu R &= \partial_\mu + \left[\Gamma_\mu, R\right], \\ \Gamma_\mu &= \frac{1}{2}u^\dagger\left[\partial_\mu - i(v_\mu + a_\mu)\right]u + \frac{1}{2}u^\dagger\left[\partial_\mu - i(v_\mu - a_\mu)\right]u. \end{aligned} \tag{1.81}$$

All the coupling constants are real and $\mathcal{O}(p^2)$, and their numerical value have to be obtained from experiment or by theoretical considerations [5].

Given the chiral couplings of eq. (1.80), it has been possible to determine the resonance contributions to the LECs [5] by comparing with the $\mathcal{L}_4$ Lagrangian given in eq. (1.69). Since

the couplings are $\mathcal{O}(p^2)$, resonance exchange produces $\mathcal{O}(p^4)$ contributions, which implies that only the non derivative parts of the resonance propagators are relevant for the LECs. In this way the contributions of the vector resonances to the LECs are given by [5, 6]:

$$\begin{aligned} L_1^V &= \tfrac{G_V^2}{8M_V^2}, \quad L_2^V = 2L_1^V, \quad L_3^V = -6L_1^V \\ L_9^V &= \tfrac{G_V F_V}{2M_V^2}, \quad L_{10}^V = -\tfrac{F_V^2}{4M_V^2}, \quad H_1^V = -\tfrac{F_V^2}{8M_V^2}. \end{aligned}$$

The axial resonances contribute to:

$$L_{10}^A = \frac{F_A^2}{4M_A^2}, \quad H_1^A = -\frac{F_A^2}{8M_A^2}. \tag{1.82}$$

The scalar octet and singlet resonances contribution is:

$$\begin{aligned} L_1^S &= -\tfrac{c_d^2}{6M_S^2}, \quad L_3^S = -3L_1^S, \quad L_4^S = -\tfrac{c_d c_m}{3M_S^2}, \quad L_5^S = -3L_4^S \\ L_6^S &= -\tfrac{c_m^2}{2M_S^2}, \quad L_8^S = -L_6^S, \quad H_2^S = 2L_8^S, \\ L_1^{S_1} &= -\tfrac{\tilde{c}_d^2}{2M_{S_1}^2}, \quad L_4^{S_1} = \tfrac{\tilde{c}_d \tilde{c}_m}{M_{S_1}^2}, \quad L_6^{S_1} = -\tfrac{\tilde{c}_m^2}{2M_{S_1}^2}, \end{aligned} \tag{1.83}$$

Finally the pseudoscalar octet and singlet contribute to the LECs as:

$$\begin{aligned} L_7^P &= \tfrac{d_m^2}{6M_P^2}, \quad L_8^P = -3L_7^P, \quad H_2^P = -6L_7^P \\ L_1^{P_1} &= -\tfrac{\tilde{d}_m^2}{2M_{\eta_1}^2}. \end{aligned} \tag{1.84}$$

Using the coupling constant determinations given in [5], it is possible to obtain the resonance contributions to the LECs. On the one hand, whenever vector and axial contribute, they strongly dominate the low-energy coupling constants, leaving very little room for additional contributions. On the other hand, the scalars only give an important contribution to $L_5^r(\mu)$, $L_8^r(\mu)$ and $H_2^r(\mu)$, whereas the pseudoscalar singlet dominate L_7. Since H_2^r cannot be estimated phenomenologically but appears explicitly in the expressions of the quark condensates and scalar susceptibilities, which we will study in Section 2.3, in this thesis we will assume scalar dominance to estimate $H_2^2 \sim 2L_8^r$. In Table 1.3 we show the results obtained in [5] compared with the phenomenological LECs determination from [9].

1.4 The QCD $1/N_c$ expansion

As we have seen in Section 1.2, at low energy, the running coupling constant of QCD is large, and the colored quarks and gluons are confined into colorless mesons and baryons. It is not known how to calculate the structure and interactions of hadrons directly in terms of the underlying quark-gluon dynamics because the theory is strongly coupled at low energies. It was 't Hooft the first who pointed out, that the large N_c formulation of QCD provides a framework for studying the nonperturbative dynamics of hadrons in a systematic expansion in the parameter $1/N_c$, [96]. Although QCD is still not solvable in this limit, the theory simplifies, making it possible to explain qualitatively several hadron properties [96, 102].

	$L_i^r(M_\rho)$	V	A	S	S_1	η_1	Total
L_1^r	0.7 ± 0.3	0.6	0	-0.2	0.2	0	0.6
L_2^r	1.3 ± 0.7	1.2	0	0	0	0	1.2
L_3^r	-4.4 ± 2.5	-3.6	0	0.6	0	0	-3.0
L_4^r	-0.3 ± 0.5	0.0	0	-0.5	0.5	0	0.0
L_5^r	1.4 ± 0.5	0.0	0	1.4	0	0	1.4
L_6^r	-0.2 ± 0.3	0.0	0	-0.3	0.3	0	0-0
L_7^r	-0.4 ± 0.2	0.0	0	0	0.5	0	-0.3
L_8^r	0.9 ± 0.3	0.0	0	0.9	0	0	0.9
L_9^r	6.9 ± 0.7	6.9	0	0	0	0	6.9
L_{10}^r	-5.2 ± 0.3	-10.0	4.0	0	0	0	-6.0

Table 1.3: V, A, S, S_1 and η_1 contribution to the LECs in units of 10^{-3}, renormalized at the $\rho(770)$ mass scale. The entries in the second column are from [9]. The entries from the last six columns are from [5].

Therefore, we define large N_c QCD as the $SU(N_c)$ gauge theory of quarks and gluons, where the number of colours is taken as expansion parameter [96]. Despite the fact that we are looking for simplifications in the theory, at larger N_c, many more intermediate states can contribute to Feynmann diagrams, so that the sum over them gives rise to large combinatorial factors. These combinatorial factors are, however, responsible for the Large N_c nature of QCD. The spectroscopic nature of light resonances, particularly the scalars, is studied in this thesis through its leading behavior in the $1/N_c$ expansion, Section 2.2. Thus we review here some aspects of this expansion. Further details can be found in [104, 105].

1.4.1 Feynmann diagrams for large N_c

At large N_c the number of gluons is $N_c^2 - 1 = \mathcal{O}(N_c^2)$, since as we have seen in Section 1.2, they transform into the adjoint representation of the group $SU(N_c)$. However, the number of quarks is $\mathcal{O}(N_c)$, so gluons are much more prevalent than quarks. In order to define the large-N_c limit of the theory, we have to know the leading N_c dependence of the quark-gluon diagrams. We can do that if we replace the gluon field $\mathcal{A}^A$ in the adjoint color representation by a tensor $(A^\mu)^i_j$ with a lower and upper index in the fundamental representation. From this point of view, gluons can be considered as a quark-antiquark combination, so if quarks and antiquarks are represented in Feynmann diagrams with a single-line with and arrow whose direction distinguishes them, gluons are represented by a double line, made up of a quark and an anti-quark line respectively. This representation is known as "double line notation" and is depicted if Fig. 1.6, where we show a quark, antiquark and gluon propagator, panel a; a quark–gluon vertex $\bar{q}^j \gamma_\mu A^{\mu\, i}_j q_i$, panel b, and a three and four–gluon vertex, panel c and d respectively.

As we will see below, when Feynmann diagrams are drawn using the double line notation, the power of N_c of a diagram is obtained by counting the number of closed quark loops, since each quark loop implies an unconstrained summation over the color index of the quark, which produces a factor of N_c. In [96], 't Hooft analyzed the N_c-counting of Feynman diagrams in

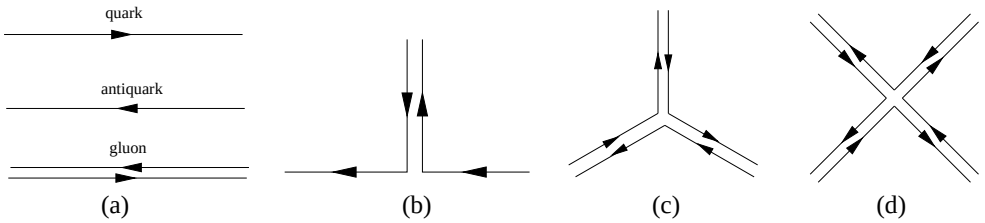

Figure 1.6: Double line notation for the gluon field. a) quark, antiquark and gluon lines. b) quark–gluon vertex. c) three–gluon vertex. d) four–gluon vertex.

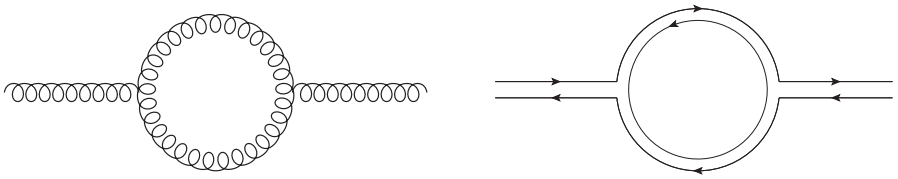

Figure 1.7: One–loop gluon contribution to the gluon vacuum polarization. Left: standard notation. Right: double line notation.

the double line notation, and found that the graphs are proportional to:

$$(g^2 N_c)^{\frac{1}{2}V_3+V_4} N_c^{\chi}, \tag{1.85}$$

where V_n is the number of n-point quark and gluon vertices in a given diagram, and χ is the Euler topological invariant, which depends on the number of holes and quark loops in the diagram. Therefore, diagrams with an arbitrary number of vertices grow with large powers of N_c unless $g^2 N_c$ is taken as fixed with N_c, which implies that the coupling constant of QCD must be rescaling as:

$$g \to \frac{g}{\sqrt{N_c}}, \tag{1.86}$$

This result is actually the behaviour demanded by the running of the coupling constant:

$$\beta(\nu) = \mu \frac{dg(\mu)}{d\mu} = -\frac{g^3}{(4\pi)^2}\left(\frac{11}{3}N_c - \frac{2}{3}N_f\right) + \mathcal{O}(g^5). \tag{1.87}$$

It can be shown [96, 102], that the dominant diagrams in the $1/N_c$ expansion are planar diagrams, those that can be drawn in a plane without lines crossing each other, with a minimum number of quark loops. Non planar diagrams are $1/N_c^2$ suppressed, whereas each quark-loop is suppressed by a factor $1/N_c$.

This N_c behaviour can be illustrated by studying the one-loop gluon and quark corrections to the gluon vacuum polarization depicted in Figs. 1.7 and 1.8.

In the case of the one-loop gluon correction Fig. 1.7, the external lines are fixed by the initial and final gluon state, but the colour of the internal lines is unspecified, contributing with a combinatorial factor of N_c. The two vertices contribute with a factor $1/N_c$, so the diagram is $\mathcal{O}(1)$ and has a smooth limit for large N_c. The one–quark–loop correction to the gluon propagator is, however, $1/N_c$ suppressed, Fig. 1.8. In this case, the quark propagator corresponds to a single color line, not two, so there are not unconstrained color indices, and

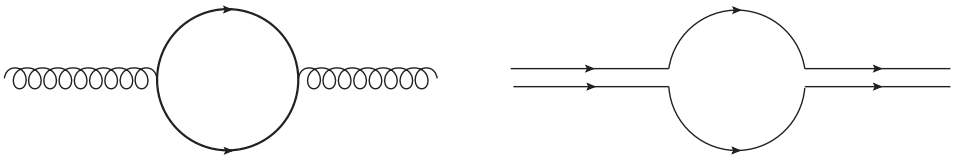

Figure 1.8: One–loop quark contribution to the gluon vacuum polarization. Left: standard notation. Right: double line notation.

the only N_c dependence comes from factors of $1/\sqrt{N_c}$ at each of the two vertices. The fact that the coupling constant behaves as $1/\sqrt{N_c}$, makes that many diagrams vanish for large N_c, and only those with large combinatorial factors survive in the large N_c limit. These techniques will be thoroughly applied in Section 2.2 of this thesis.

1.4.2 Ordinary $\bar{q}q$ mesons at large N_c

As we have commented above, we will use in this thesis the $1/N_c$ expansion in order to distinguish the nature of the lightest scalar resonances, Section 2.2. In this section we are going to review the usual case, the study of the ordinary $\bar{q}q$ mesons, which is well known from long [96, 102]. However in Section 2.2.6, we will address this problem with different non-ordinary configurations.

Large-N_c mesons are color singlet bound states of a quark and an antiquark,

$$\sum_{i}^{N_c} \bar{q}^i q_i, \tag{1.88}$$

where the color summation is given explicitly. It implies that we have to include an extra $1/\sqrt{N_c}$ factor in the meson wave function to normalize it properly.

Again, the N_c-dependence of meson amplitudes can be determined by studying quark-gluon diagrams. In this case, the leading order graphs have a single quark loop and no holes, so they can be written in a plane in double line notation. Arbitrary numbers of planar gluons can be exchanged inside the single quark loop without affecting the N_c-counting of the diagram, but, as we have seen, additional quark loops or non-planar gluons are systematically suppressed in $1/N_c$. In this way the dominant diagrams contributing to the meson propagator, the simplest one is depicted in panel *a* of Fig. 1.9, is $\mathcal{O}(1)$ in N_c, since it includes a factor N_c from the close quark-loop and a factor $1/N_c$ from the initial and final meson states. Consequently, the mass of a $\bar{q}q$ meson is also $\mathcal{O}(1)$. The coupling of n-mesons is given by the planar diagrams with n meson insertions on the quark loop. There is a single factor of N_c from the single quark loop of the diagram and n factors of $1/\sqrt{N_c}$, so the n-meson coupling is $\mathcal{O}(N_c^{1-n/2})$. From this N_c counting, one concludes that a meson decay constant is $\mathcal{O}(\sqrt{N_c})$, panel *b* of Fig. 1.9; the self-coupling of three mesons is $\mathcal{O}(1/\sqrt{N_c})$; the self-coupling of four mesons is $\mathcal{O}(1/N_c)$, panel *c* of Fig. 1.9, etc. The amplitude for a meson to decay to two other mesons is $\mathcal{O}(1/\sqrt{N_c})$, so the decay width is $1/N_c$. Thus, large-N_c $\bar{q}q$ mesons are narrow states which are weakly coupled to each other. Of course in the $N_c \to \infty$ limit, they are stable and non-interacting. In Section 2.2, we will use this scaling properties to identify

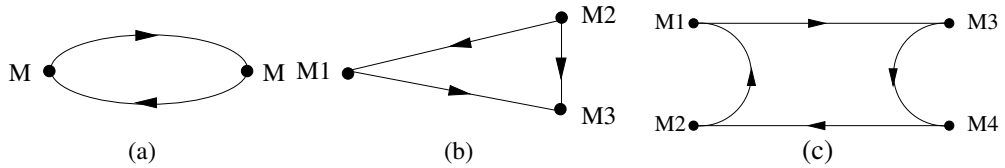

Figure 1.9: Propagator (a), decay (b), and scattering (c) of $\bar{s}qq$ mesons in double line notation.

$\bar{q}q$ components inside resonances even if quarks and antiquarks are not explicit in the meson interaction formalism.

1.4.3 The axial anomaly at N_c

The spontaneous chiral symmetry breaking implies the partial conservation of the axial current of eq. (1.62), which can be expressed as:

$$\langle 0|\partial^\mu J_\mu^{5,a}|\phi(p)^v\rangle = f_\pi m_i^2 \delta^{ab}. \tag{1.89}$$

For the octet of currents, this divergence vanishes for zero quark masses, and as we have seen, leads to the identification of the π, K and η as NGB. However, for the singlet current, the $U(1)_A$ anomaly is present, because of the gluonic corrections, and even in the chiral limit eq. (1.91) does not vanish [56, 57, 58]:

$$\langle 0|\partial^\mu J_\mu^{5,0}|\eta'(p)\rangle = f_\pi m_{\eta'}^2 = \langle 0|\frac{3g^2}{32\pi^2}F^{a\mu\nu}F^a_{\mu\nu}|\eta'(p)\rangle \sim \mathcal{O}(1/\sqrt{N_c}). \tag{1.90}$$

However, the gluonic contribution to the axial anomaly vanishes in the large N_c limit, so taking into account that the pion decay constant is $f_\pi \sim \mathcal{O}(\sqrt{N_c})$, we conclude that in the chiral limit $m_{\eta'}^2 \sim 1/N_c$. Therefore, in the N_c limit the anomaly contribution to the η' vanishes and it becomes the ninth NGB.

1.4.4 $1/N_c$ expansion in Chiral Perturbation Theory

The beauty of the chiral Lagrangian is that the dependence on the number of colours is determined and implemented through the chiral parameters.

As we have seen in Section 1.3.2, the chiral parameters that appear in the $\mathcal{L}_2$ effective Lagrangian are the NGB masses and the pion decay constant, f_π. The NGB are assumed to scale as $\bar{q}q$ states [98], and from the previous counting rules, their mass is $\mathcal{O}(1)$ in the $1/N_c$ expansion. Regarding the pion decay constant, we have seen, using the same counting rules, that it is $\mathcal{O}(\sqrt{N_c})$. Furthermore, we can see from the partial conservation of the axial current given in eq. (1.62):

$$\langle 0|\bar{q}^i\gamma_5\gamma^\mu\lambda^a q_i|\phi^b\rangle = ip_\mu\delta^{ab}f_\pi, \tag{1.91}$$

that this is the right behaviour, since the left hand side of eq. (1.91) involves a factor N_c from the sum over the colour index i, and a factor $1/\sqrt{N_c}$, from the insertion of the meson ϕ.

At higher orders, the dependence on N_c is also carried by the LECs. Each LEC multiplies a certain term in the Lagrangian. These terms involve the product of one or more traces of some operators, which are functions of the $U(x)$ matrix given in eq.(1.43), its derivative and the quark masses. So the LEC dependence on N_c is dictated by the operator it multiplies. These traces are taken over flavour indices and amount to a sum over the quark flavours, which in turn can arise only in a quark loop. For example, operators with one flavour trace will require one-quark loop, while those with two flavour traces will require two quark loops. However, as we have seen in the previous section, every quark loop leads to a $1/N_c$ suppression, so the chiral contribution with two traces will be suppressed with a factor $1/N_c$ relative to those with just one trace.

In particular, in the $\mathcal{L}_4$ Lagrangian given in eq. (1.69), there are terms multiplying operators with one trace:

$$\begin{aligned}\sim\ & L_3 Tr\left(D^\mu U^\dagger D_\mu D^\nu U^\dagger D_\nu\right) + L_5 Tr\left(D^\mu U^\dagger D_\mu U(\chi^\dagger U + U^\dagger \chi)\right) \\ & + L_8 Tr\left(\chi^\dagger U \chi^\dagger U + \chi U^\dagger \chi U^\dagger\right) - iL_9 Tr\left(F^R_{\mu\nu} D^\mu U D^\nu U^\dagger + F^L_{\mu\nu} D^\mu U D^\nu U^\dagger\right) \\ & + L_{10} Tr\left(U^\dagger F^R_{\mu\nu} U F^{L\ \mu\nu}\right) + H_1 Tr\left(F^R_{\mu\nu} F^{R\ \mu\nu} + F^L_{\mu\nu} F^{L\ \mu\nu}\right) + H_2 Tr\left(\chi^\dagger \chi\right),\end{aligned} \tag{1.92}$$

and others that multiply operators with two traces:

$$\begin{aligned}\sim\ & L_1 Tr\left(D^\mu U^\dagger D_\mu U\right)^2 + L_2 Tr\left(D^\mu U^\dagger D^\nu U\right) Tr\left(D_\mu U^\dagger D_\nu U\right) \\ & + L_4 Tr\left(D^\mu U^\dagger D_\mu U\right) Tr\left(\chi^\dagger U + \chi U^\dagger\right) \\ & + L_6 Tr^2\left(\chi^\dagger U + \chi U^\dagger\right) + L_7 Tr^2\left(\chi^\dagger U - \chi U^\dagger\right),\end{aligned} \tag{1.93}$$

which will be subdominant respect the previous ones.

Finally, the dominant N_c behaviour of the LECs can be obtained by studying the contribution of the effective Lagrangian to a NGB scattering process, whose amplitude is $1/N_c$ suppressed:

$$\langle \phi^c(k_1)\phi^d(k_2)|e^{i\int dx^4 \mathcal{L}_{\text{ChPT}}(x)}|\phi^a(p_1)\phi^b(p_2)\rangle \sim \mathcal{O}\left(\frac{1}{N_c}\right). \tag{1.94}$$

Since scattering amplitudes are $\mathcal{O}(1/N_c)$, and the $SU(3)$ LECs of the $\mathcal{L}_4$ Lagrangian appear in scattering amplitudes multiplied by a factor $1/f_\pi^4 \sim 1/N_c^2$, we conclude that the dominant LECs are $\mathcal{O}(N_c)$. In summary, L_3, L_5, L_8, L_9, L_{10}, H_1 and H_2 LECs are $\mathcal{O}(N_c)$, whereas the others are $\mathcal{O}(1)$.

There are, however, some subtleties related to the identification of the independent terms of $\mathcal{L}_4$. For arbitrary 3×3 traceless matrices, A and B, the following identity holds:

$$\langle ABAB\rangle = -2\langle A^2B^2\rangle + \frac{1}{2}\langle A^2\rangle\langle B^2\rangle + \langle AB\rangle^2. \tag{1.95}$$

Then, applying this identity to the operators $A = D_\mu U U^\dagger$ and $B = D_\nu U U^\dagger$ we get:

$$\begin{aligned}\langle D_\mu U \partial_\nu U^\dagger D^\mu U \partial^\nu U^\dagger\rangle =& -2\langle D_\mu U D^\mu U^\dagger D_\nu U D^\nu U^\dagger\rangle + \tfrac{1}{2}\langle D_\mu U D^\mu U^\dagger\rangle^2 \\ & + \langle D_\mu U D_\nu U^\dagger\rangle\langle D^\mu U D^\nu U^\dagger\rangle.\end{aligned} \tag{1.96}$$

$\langle D_\mu U D_\nu U^\dagger D^\mu U D^\nu U^\dagger \rangle$ is a single trace operator that could have appeared in the Lagrangian with a coefficient $c = O(N_c)$. However, applying eq. (1.96), this operator is expressed in terms of those with L_1, L_2 and L_3, so these LECs receive a $\mathcal{O}(N_c)$ contribution $\delta L_1 = c/2$, $\delta L_2 = c$ and $\delta L_3 = -2c$. Therefore L_1 and L_2 should also be taken as $\mathcal{O}(N_c)$, but the combination $2L_1 - L_2$, which cancels this $\mathcal{O}(N_c)$ contribution, should be imposed as $\mathcal{O}(1)$. This N_c behaviour of the LECs will be used thoroughly in Section 2.2 of this thesis, when studying the N_c dependence of the lightest scalar resonances.

1.5 Analytic properties of scattering amplitudes

Scattering is one of the most important methods in the experimental investigation of particle properties, and consequently, one of the best tools to study low energy meson dynamics, which is the objective of analysis of this thesis. Therefore in this section we are going to review the general properties of scattering amplitudes, focusing on their unitarity and analyticity properties. Further details on these topics can be found [106, 73, 107].

The main idea is quite simple; two beams of particles with well-defined momenta are made to collide, and then we can observe the outcome. In a typical scattering setup, a well defined initial state of two or more particles interact, giving rise to a final state of two or more non-interacting particles, which are experimentally measured. In case of strong interactions, since they have a very short range, we can regard all particles as free, except when they are very close together. Therefore, the asymptotic states corresponding to the states before and after the collision in a scattering experiment consist only of free particles. This implies neglecting all long-range interactions such as electromagnetism or gravity, which are nevertheless much weaker.

In practice, however, meson-meson scattering is not that simple. In particular, for the scattering of NGB, which is the case of interest in this thesis, it is impossible to arrange collisions of real pions, kaons and etas, so these scattering processes are measured in two different ways, colliding NGB with protons or from the decay of heavier particles. In Section 1.7, we will review the available data on $\pi\pi$-scattering, since it is the process we will mainly use in this thesis.

It is common to classify scattering events into two different types: elastic and inelastic. On the one hand, an elastic scattering process is one in which the final state particles are the same than the initial ones. On the other hand, in an inelastic process the initial and final state particles are different.

One-particle states are determined by their 4-momentum p. Since $p^2 = p_\mu p^\mu = m^2$, they are also determined by the particle mass, m, and its 3-momentum, $\vec{p}$. Other quantum numbers needed to describe the particle, such as spin or isospin for instance, will be denoted generically as λ. Therefore, we will write one-particle states as $|p\rangle = |m, \vec{p}, \lambda\rangle$. They are normalized as

$$\langle p|p'\rangle = \langle m, \vec{p}, \lambda | m', \vec{p}', \lambda'\rangle = (2\pi)^3 \, 2E_{\vec{p}} \, \delta^{(3)}(\vec{p} - \vec{p}')\delta_{mm'}\delta_{\lambda\lambda'}, \tag{1.97}$$

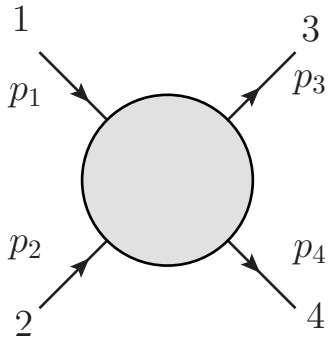

Figure 1.10: Scattering process $12 \to 34$

where the factor $2E_{\vec{p}}$ is chosen so that the normalization is Lorentz invariant and

$$E_{\vec{p}} = \sqrt{\vec{p}^2 + m^2} \tag{1.98}$$

is the free particle energy, also denoted as p^0, since it is the 0-th component of the particle 4-momentum $p^\mu = (p^0, \vec{p})$. Multiparticle states are constructed as the direct product of one-particle states,

$$|p_1, \cdots, p_n\rangle = |p_1\rangle \otimes |p_2\rangle \otimes \cdots \otimes |p_n\rangle. \tag{1.99}$$

The set of all multiparticle states is called Fock space.

Let us consider now the two-body scattering process of spinless particles $1 + 2 \to 3 + 4$ of Fig. (1.10), as for example, the one which involves Goldstone bosons. The particles have masses m_i and four-momentum $p_i = (E_i, \vec{p}_i)$, with $i = 1, \ldots, 4$. The Lorentz invariant Mandelstam variables, s, t and u are defined by:

$$\begin{aligned} s &= (p_1 + p_2)^2, \\ t &= (p_1 - p_3)^2, \\ u &= (p_1 - p_4)^2, \end{aligned} \tag{1.100}$$

with the relation:

$$s + t + u = \sum_{i=1} m_i^2. \tag{1.101}$$

Since a scattering process is a Lorentz scalar, and the final and initial states are only a function of the four-momentum p_i, with $i = 1, \ldots, 4$, a two-body scattering process can only be a function of the invariants that can be constructed with them. Apart for the particles' masses, there are only two more invariants, which are usually chosen to be two of the Mandelstam variables. In this way, any scattering process can be written as a function of these variables. We have assumed that Fig. (1.10) describes the process $1 + 2 \to 3 + 4$ in the s-channel but, by reversing the signs of some of the four-momenta, it can also represent the process $1 + \bar{3} \to \bar{2} + 4$ in the t-channel, and $1 + \bar{4} \to 3 + \bar{2}$ in the u-channel, where the bar denotes the corresponding antiparticle. Depending on how we look at Fig. (1.10), a particular choice of these two Mandelstam variables will be more convenient.

Particularly, in the s-channel centre-of-mass of the initial particles, where $p_1 = (E_1, \vec{p})$, $p_2 = (E_2, -\vec{p})$, $p_3 = (E_3, \vec{p}')$ and $p_4 = (E_2, -\vec{p}')$, the Mandelstam variables are given by:

$$\begin{aligned} s &= m_1^2 + m_2^2 + 2(E_1E_2 + |\vec{p}|^2), \\ t &= m_1^2 + m_3^2 + 2(E_1E_3 - |\vec{p}||\vec{p}'|\cos\theta_s), \\ u &= m_1^2 + m_4^2 + 2(E_1E_4 + |\vec{p}||\vec{p}'|\cos\theta_s), \end{aligned} \tag{1.102}$$

where θ_s is the angle between the three momenta of particles 1 and 3 in the s-channel centre-of-mass frame.

However, the particle energies and momenta can also be expressed as a function of s and the particle's masses:

$$\begin{aligned} E_1 &= \frac{1}{\sqrt{2}}(s + m_1^2 - m_2^2), \qquad E_2 = \frac{1}{\sqrt{2}}(s + m_2^2 - m_1^2), \\ E_3 &= \frac{1}{\sqrt{2}}(s + m_1^2 - m_2^2), \qquad E_4 = \frac{1}{\sqrt{2}}(s + m_2^2 - m_1^2), \end{aligned} \tag{1.103}$$

$$\begin{aligned} p &= \frac{1}{2\sqrt{s}}\sqrt{(s - (m_1 + m_2)^2)(s - (m_1 - m_2)^2)}, \\ p' &= \frac{1}{2\sqrt{s}}\sqrt{(s - (m_3 + m_4)^2)(s - (m_3 - m_4)^2)}. \end{aligned} \tag{1.104}$$

We can see from eq. (1.102) that a physical process implies then that $s \geq (m_1 + m_2)^2$ and $-1 \leq \cos\theta_s \leq +1$.

For equal masses $m_i = m$, $i = 1, \ldots, 4$, so that $\vec{p} = \vec{p}'$, eq. (1.102) simplifies to:

$$\begin{aligned} s &= 4(m^2 + |\vec{p}|^2), \\ t &= -2|\vec{p}|^2(1 - \cos\theta_s), \\ u &= -2|\vec{p}|^2(1 + \cos\theta_s). \end{aligned} \tag{1.105}$$

In this simpler case, the physical region for a s-channel scattering process is given by the condition: $s \geq 4m^2$, $t \leq 0$ and $u \leq 0$. Therefore, in this channel, s is an energy squared and each of t and u is a momentum transfer squared. In the same way, for t-channel processes the physical region is given by the condition: $t \geq 4m^2$, $s \leq 0$ and $u \leq 0$ and for a u-channel $u \geq 4m^2$, $s \leq 0$ and $t \leq 0$. This property implies a clear symmetry between s, t and u, as we can see in Fig. 1.11, where we have plotted the physical regions in the $s - t$ plane with the s and t axes inclined at 60°. For arbitrary masses, the boundary of the physical region in the s–t plane is rather complicated, but still, they do not overlap, and most of the physical region lies in $t, u < 0$.

We define the S-matrix as the operator which relates the incoming and outgoing Fock spaces of a scattering process. That is, suppose we have an initial state $|i\rangle_{\text{in}}$ belonging to the incoming Fock space, and a final state $|f\rangle_{\text{out}}$ in the outgoing one, then the S-matrix is defined such that:

$$P_{fi} = |_{out}\langle f|i\rangle_{in}|^2 = |S_{fi}|^2 = |\langle f|S|i\rangle|^2 = \langle i|S^\dagger|f\rangle\langle f|S|i\rangle \tag{1.106}$$

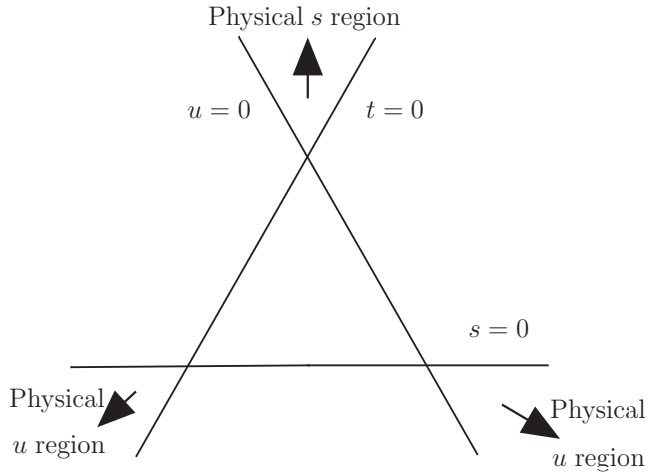

Figure 1.11: Physical regions for equal-mass scattering

is the probability of $|f\rangle$ being the final state, given $|i\rangle$ as the initial state, and where $|i\rangle$ and $|f\rangle$ belong to the common Fock Space. Therefore, the matrix element S_{fi} represents the amplitude for an initially observed free particle state $|i\rangle$ to be observed as a final free particle state $|f\rangle$.

It is clear that starting from a initial state $|i\rangle$, the probability of ending up in some final state must be unity so:

$$1 = \sum_f |\langle f|S|i\rangle|^2 = \sum_f \langle i|S^\dagger|f\rangle\langle f|S|i\rangle = \langle i|S^\dagger S|i\rangle, \tag{1.107}$$

where we have assumed that $|f\rangle$ is a complete set of orthonormal states so: $\sum_f |f\rangle\langle f| = \mathbb{1}$.

Since eq. (1.107) must hold for any $|i\rangle$, it follows that the diagonal terms of $S^\dagger S$ are 1. Similarly, using $\sum_i |i\rangle\langle i| = \mathbb{1}$ yields $\langle f|SS^\dagger|f\rangle = 1$ for any final state $|f\rangle$, so the diagonal terms of $SS^\dagger$ are also 1. If we choose now for the initial state a linear combination of two orthonormal states, $|i\rangle = (|\alpha|^2 + |\beta|^2)^{-1/2}(\alpha|a\rangle + \beta|b\rangle)$, we obtain from eq. (1.107)

$$1 = \frac{1}{|\alpha|^2 + |\beta|^2}\left(|\alpha|^2 + |\beta|^2 + \alpha^*\beta\langle a|S^\dagger S|b\rangle + \alpha\beta^*\langle b|S^\dagger S|a\rangle\right). \tag{1.108}$$

Since α and β are arbitrary complex numbers and $|a\rangle$ and $|b\rangle$ are arbitrary states, the off-diagonal matrix elements of $S^\dagger S$ and $SS^\dagger$ are 0. Consequently:

$$SS^\dagger = S^\dagger S = \mathbb{1} \tag{1.109}$$

and S is unitary.

The process $|i\rangle \to |f\rangle$ can occur in two different scenarios. It is possible that the two particles do not interact at all, so the amplitude for this is simply δ_{if}. The other possibility is that the two particles do interact and such interaction is given by the so-called T-matrix:

$$\langle f|S|i\rangle = \delta_{if} + i\langle f|T|i\rangle \longrightarrow \mathbf{S} = \mathbb{1} + i\mathbf{T}. \tag{1.110}$$

To take into account the four-momentum conservation we usually express the transition amplitude $\langle f|T|i\rangle$ as:

$$S_{fi} = \delta_{fi} + i(2\pi)^4\delta^4(p^f - p^i)T_{fi}, \tag{1.111}$$

where p^i and p^f are respectively the sum of the initial and final four-momentum.

The unitarity of the S-matrix implies that:

$$\delta_{ij} = \langle j|SS^\dagger|i\rangle = \sum_f \langle j|S|f\rangle\langle f|S^\dagger|i\rangle, \tag{1.112}$$

where $|i\rangle$, $|j\rangle$ and $|f\rangle$ are arbitrary orthonormal states. Including in eq. (1.112) the transition amplitude definition of eq. (1.111), we have:

$$\langle j|T|i\rangle - \langle j|T^\dagger|i\rangle = (2\pi)^4 i\sum_f \delta^4(p^f - p^i)\langle j|T^\dagger|f\rangle\langle f|T|i\rangle. \tag{1.113}$$

For the particular case $j = i$, and taking into account that the strong interactions are invariant under time reversal, so $T_{if} = T_{fi}$, we have:

$$2\mathrm{Im}\langle j|T|i\rangle = (2\pi)^4\sum_f \delta^4(p^f - p^i)|\langle f|T|i\rangle|^2. \tag{1.114}$$

In a scattering experiment, the likelihood of any particular final state can be expressed in terms of the cross section. It is an intrinsic quantity to the colliding particles and allows comparison of experiments with different conditions. The total cross section, denoted by σ, is defined as the total number of events of a scattering experiment divided by the density of incoming particles, the length of the bunches of particles and the cross area common to the bunches. A cross section is therefore a measure of the effective surface area seen by the scattering particles, and as such is expressed in units of area.

In the case of a continuum of states, the total cross section for the reaction $1 + 2 \to$ any final state is given by:

$$\sigma_{12} = \frac{1}{4|p_1|\sqrt{s}}\sum_f (2\pi)^4\delta^4\left(p^f - p^i\right)|\langle f|T|i\rangle|^2, \tag{1.115}$$

where p_1 is the initial momentum in the s-channel centre-of-mass frame and it is given by:

$$|p_1|^2 = \frac{1}{4s}\left[s - (m_1 + m_2)^2\right]\left[s - (m_1 - m_2)^2\right]. \tag{1.116}$$

However, using the transition amplitude unitarity condition of eq. (1.114), we can express eq. (1.115) as:

$$\sigma_{12} = \frac{1}{2|p_1|\sqrt{s}}\mathrm{Im}\langle i|T|i\rangle = \frac{1}{2|p_1|\sqrt{s}}\mathrm{Im}T(s, t = 0), \tag{1.117}$$

i.e. the total cross section of a $1 + 2 \to$ n-particles process is proportional to the scattering amplitude of $1 + 2 \to 1 + 2$, with the direction of motion of the particles unchanged, this is the so-called forward scattering amplitude corresponding to a scattering angle $\theta = 0$. This relation is known as the optical theorem, and we will use it in Section 1.8, when discussing the high energy behaviour of scattering amplitudes.

1.5.1 Crossing and analyticity

The basic principle of crossing is the Mandelstam hypothesis [108, 109], which states that the transition amplitude in the t and u regions is the analytic continuation of $\langle p_3; p_4|T|p_1; p_2\rangle = T(s,t,u)$ in the s-region. However, in order to continue analytically from one physical region to another, it is necessary to make some assumptions about the analytic structure of $T(s,t,u)$.

The assumption generally made is that any singularity of the transition amplitude has a dynamical origin. In this way, it is assumed that poles are associated with bound states and threshold give rise to cuts. A bound state of the s-plane with a mass $m_B = \sqrt{s_B}$ will lead to a pole at $s = s_B$ in the real axis. Cuts arise because of the unitarity condition of eq. (1.114). In this equation, $(p^f)^2 = s$ is the invariant mass of the final state f, so n-particle states contribute to the imaginary part if $\sqrt{s}$ is greater than the n-particle threshold energy. The threshold for producing a state in which the particles have masses $m_1, m_2, \ldots, m_n$ is at $s = (m_1 + \cdots + m_n)^2$. For example, in a process where there is only a single-particle state of mass m with the right quantum numbers, the thresholds are $s = 4m^2, 9m^2, \ldots$

Let us now take the amplitude $T(s,t,u)$ for a fixed value of t. We know that $\mathrm{Im}T(s,t,u)$ is non-zero along the part of the real s-axis from the first particle threshold to ∞. If it is a scattering process of particles with the same mass, it will be from $4m^2$ to ∞. Furthermore, for a physical value of t in the s-channel, $t < 0$, $T(s,t,u)$ will also have non-vanishing imaginary part when imposing the u-channel unitarity condition, i.e. for a physical threshold in the u-channel. That threshold will occur when s takes the value given by eq. (1.101). For simplicity, if we assume that the energy spectrum in the u-channel is the same than in s, then, $\mathrm{Im}T(s,t,u)$ will be non-zero for the part of the u-axis from $4m^2$ to ∞, or in terms of s, from $-\infty$ to $-t$. Thus, there is a region below threshold where $\mathrm{Im}T(s,t,u) = 0$, then the Schwarz reflection principle states that:

$$T(s^*,t,u) = T(s,t,u)^* \tag{1.118}$$

for any s and s^* belonging to a domain D of the s-complex plane whose intersection with the real axis is such that the amplitude has no imaginary part.

The consequence of eq. (1.118) is that the domain of analyticity of $T(s,t,u)$ cannot extend to the whole s-plane. In that case, eq. (1.118) would be valid in the whole real axis and $\mathrm{Im}T(s,t,u)$ would be zero for real values of s. However, we know from unitarity that it is not the case, which implies that the amplitude must have a cut along the real s-axis, where unitarity demands its imaginary part to be non-zero, i.e. from each threshold to infinity. The discontinuity across the cut is:

$$\begin{aligned}\lim_{\epsilon\to 0^+}\Big[T(s+i\epsilon,t,u) - T(s-i\epsilon,t,u)\Big] &= \lim_{\epsilon\to 0^+}\Big[T(s+i\epsilon,t,u) - T(s+i\epsilon,t,u)^*\Big] \\ = 2i\lim_{\epsilon\to 0^+}\Big[\mathrm{Im}\,T(s+i\epsilon,t,u)\Big] &= 2i\,\mathrm{Im}\,T(s,t,u),\end{aligned} \tag{1.119}$$

where we have defined the physical value of the amplitude to be taken above the cut. Similar arguments can be applied to the physical t and u-channels. There must be cuts along the real positive t and u axes, with branch points at the appropriate physical thresholds in these channels, and possibly poles associated to bound states.

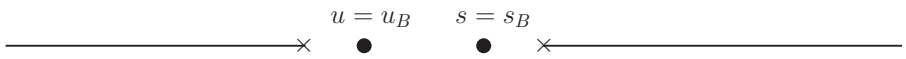

Figure 1.12: Analytical structure of T(s,t,u) in the s-plane for an equal mass process case at fixed t.

To summarize, in the equal mass case, we can conclude that the analytic structure in the s-complex plane of the transition amplitude is that shown in Fig. 1.12. The right hand cut, from $s = 4m^2$ to ∞, arises from the physical threshold in the s-channel. The pole at $s = s_B$ assumes that there is a bound state in the s-channel with a mass $m_B = \sqrt{s_B}$. The left hand cut along the negative real axis, with a branch point at $s = 4m^2 - t - u_0$, arises from the physical threshold u_0 in the u-channel. The left hand pole, at $s = 4m^2 - t - u_B$, arises from an assumed u-channel bound state at $u = u_B$. Both left hand poles and cuts move as t varies and, for sufficiently large physical values of $t < 0$, the u-channel pole moves to the right hand of the s-channel and the right and left cuts overlap.

A consequence of the assumption of analyticity is crossing symmetry. As we have mentioned above, Fig. 1.10 represents the process:

$$1 + 2 \to 3 + 4 \tag{1.120}$$

in the s-channel, i.e. when we look the picture from left to right. Let us denote its amplitude as $T_{1+2\to3+4}(s,t,u)$. The physical region for the process of eq. (1.120) is:

$$s > \max\left[(m_a + m_b)^2, (m_c + m_d)^2\right]. \tag{1.121}$$

In the equal–mass case $t, u < 0$; in the unequal-mass case the constraints on t and u are more complicated, but most of the physical region lies in the $t, u < 0$ region.

The Mandelstam hypothesis implies that the amplitude can be continued analytically to the physical region $t > \max\left[(m_a + m_b)^2, (m_c + m_d)^2\right]$ and $s, u < 0$. Therefore Fig. 1.10 can also represent the t-channel process:

$$1 + \bar{3} \to \bar{2} + 4, \tag{1.122}$$

That is, looking Fig. 1.10 from top to bottom, we find:

$$T_{1+\bar{3}\to\bar{2}+4}(t,s,u) = T_{1+2\to3+4}(s,t,u) \tag{1.123}$$

Similarly, for the the u-channel process:

$$1 + \bar{4} \to \bar{2} + 3, \tag{1.124}$$

we have $T_{1+\bar{4}\to3+\bar{2}}(u,t,s) = T_{1+2\to3+4}(s,t,u)$. In conclusion, the Mandelstam hypothesis assumes that the scattering amplitudes for the s, t and u-channels, which describes the processes of eqs. (1.120), (1.122) and (1.124) are the boundary of the same analytic function:

$$T(s,t,u) = \begin{cases} T_{12\to34}(s,t,u), & s \geq 4m^2, \quad t \leq 0, \quad u \leq 0, \\ T_{1\bar{3}\to\bar{2}4}(t,s,u), & t \geq 4m^2, \quad s \leq 0, \quad u \leq 0, \\ T_{1\bar{4}\to3\bar{2}}(u,t,s), & u \geq 4m^2, \quad s \leq 0, \quad t \leq 0, \end{cases}.$$

The Mandelstam hypothesis is generally accepted and proved order by order for Feynmann diagrams, although no general proof is known.

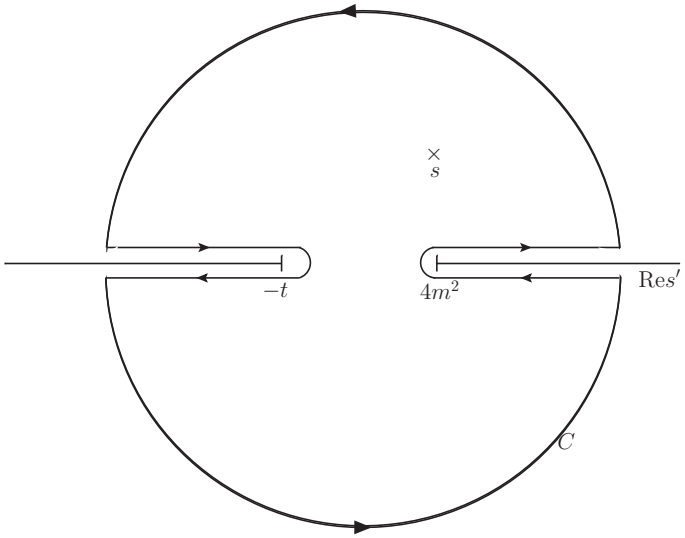

Figure 1.13: Contour of integration in the complex s-plane

1.5.2 Dispersion relations

Once we know the analytic structure of a transition amplitude, we can use the Cauchy Theorem to derive a dispersion relation. In the cases of interest for this thesis there are no bound states, therefore, we will assume that there are no poles in the real axis. Furthermore, since we are going to work mainly with $\pi\pi$-scattering, we consider in advance scattering processes of particles with the same mass. We will comment briefly at the end of Section 1.5.3 the most significant differences of the different mass case.

Hence, fixing t, the contour C shown in Fig. 1.13, encloses a domain in which $T(s,t,u)$ is analytic. Therefore, for any value of s within C different than those for which there is a pole, the transition amplitude can be written as:

$$T(s,t,u) = \frac{1}{2\pi i}\oint ds' \frac{T(s',t,u)}{s'-s}. \tag{1.125}$$

The Contour C can be separated into two parts: a circle of radius R with centre at $s'=0$, and the remainder, which is made up of lines parallel to the left and right cuts on the real axis. On the one hand, if we assume now that $T(s,t,u)$ goes to zero faster than $1/s$ as $|s|\to\infty$, then the contribution coming from the circular part of the contour should tend to zero if we take $R\to\infty$. On the other hand, the contribution along the cuts is given by eq. (1.119). Therefore, eq. (1.125) simplifies to:

$$\begin{aligned} T(s,t,u) &= \frac{1}{\pi}\int_{4m^2}^{\infty} ds' \frac{\mathrm{Im}T(s',t,u)}{s'-(s+i\epsilon)} + \frac{1}{\pi}\int_{4m^2}^{\infty} du' \frac{\mathrm{Im}T(s,t,u')}{u'-(u-i\epsilon)} \\ &= \frac{1}{\pi}\int_{4m^2}^{\infty} ds' \frac{\mathrm{Im}T(s',t,u)}{s'-(s+i\epsilon)} + \frac{1}{\pi}\int_{-\infty}^{-t} ds' \frac{\mathrm{Im}T(s',t,u)}{s'-(s+i\epsilon)}, \end{aligned} \tag{1.126}$$

where we have given s a small imaginary part $i\epsilon$ since s is only defined above and below the

axis. For physical values of s we may use the relation:

$$\frac{1}{s'-s-i\epsilon} = P\frac{1}{s'-s} + i\pi\delta(s'-s). \tag{1.127}$$

where P denotes principal value, so we can write the real part of the amplitude as:

$$\mathrm{Re}T(s,t,u) = \frac{1}{\pi}P\int_{4m^2}^{\infty} ds' \frac{\mathrm{Im}T(s',t,u)}{s'-s} + \frac{1}{\pi}\int_{-\infty}^{-t} ds' \frac{\mathrm{Im}T(s',t,u)}{s'-s}, \tag{1.128}$$

If the transition amplitude $T(s,t,u)$ does not go to zero fast enough as $s \to \infty$, the circle contribution of Fig. 1.13 to the integral of eq. (1.125) will not vanish. However, choosing a value s_1 of s where the transition amplitude value is known, we can write:

$$T(s,t,u) - T(s_1,t,u) = \frac{1}{2\pi i}(s-s_1)\oint ds' \frac{T(s',t,u)}{(s'-s)(s'-s_1)}. \tag{1.129}$$

Then, if $s^{-1}T(s,t,u)$ goes to zero faster than $1/s$, the integral over the infinite-circular part of the contour of Fig. 1.13 vanishes again, and we can obtain the expression:

$$T(s,t,u) = T(s_1,t,u) + \frac{s-s_1}{\pi}\int_{4m^2}^{\infty} ds' \frac{T(s',t,u)}{(s'-s)(s'-s_1)} + \frac{s-s_1}{\pi}\int_{-\infty}^{-t} ds' \frac{T(s',t,u)}{(s'-s)(s'-s_1)}. \tag{1.130}$$

This kind of dispersion relations are called once-subtracted dispersion relations, and the point s_1 is known as subtraction point.

If one subtraction is not enough to be able to discard the contribution from the circular part of the contour of Fig. 1.13, we can make another one, so:

$$\begin{aligned} T(s,t,u) &= T(s_1,t,u) + (s-s_1)\frac{\partial}{\partial s_1}T(s_1,t,u) \\ &\quad + \frac{1}{2\pi i}(s-s_1)^2\oint ds' \frac{T(s',t,u)}{(s'-s)(s'-s_1)^2} \end{aligned} \tag{1.131}$$

which will lead to twice-subtracted dispersion relationsm etc ... Dispersion relations are one of the main techniques that we use in this thesis, as we will see in Sections 1.7 and 1.6. In our results, we will use dispersion relations to constrain the $\pi\pi$-scattering amplitude in Section 2.1 and to unitarize ChPT in Section 2.2.

1.5.3 Partial-wave expansion

The conservation of angular momentum implies that the scattering amplitude can be expanded in a series of partial-wave amplitudes with defined angular momentum, which are functions of only one of the Mandelstam variables. Partial-wave amplitudes are really useful in order to identify the resonances which appear in a given scattering process, and they are used thoroughly in this thesis. Therefore, in this section we are going to review the main properties of partial-wave amplitudes.

For a fixed value of s, according to eqs. (1.102), (1.103) and (1.104), the momenta transfer t and u are only function of $z_s = \cos\theta_s$, i.e. the cosine of the s-channel scattering angle in the centre-of mass frame. Therefore, instead of t or u, we can use z_s together with s as the independent variables of the transition amplitude. For the scattering of spin-zero particles, it can then be expanded as a series in Legendre Polynomials:

$$T(s,t,u) = 16\pi N \sum_{J=0}^{\infty} (2J+1) t_J(s) P_J(z_s), \tag{1.132}$$

where $N = 1$ except in the case of the scattering of identical particles, where $N = 2$. $P_J(z_s)$ is the Legendre Polynomials of the first kind, of order J. The s dependent coefficients of the expansion are called partial-waves, and represent the transition amplitudes between states with well defined angular momentum J. The factor 16π is included so that in the nonrelativistic limit the partial-wave amplitude has the conventional normalization.

The Legendre Polynomial are normalized so that:

$$\int_{-1}^{1} P_J(x) P'_J(x) dx = \frac{2}{2J+1} \delta_{JJ'}. \tag{1.133}$$

Thus, multiplying eq (1.132) by $P'_l(x)$ and integrating between $z_s = -1$ and $+1$, we find that the explicit expression of a partial-wave amplitude is:

$$t_J(s) = \frac{1}{32\pi N} \int_{-1}^{1} dz_s \, P_J(x) T(s, t(z_s), u(z_s)). \tag{1.134}$$

One of the main advantages of using partial-wave amplitudes is the simple form of the constraints imposed by unitarity. Let us consider the $1+2 \to 3+4$ process of spinless particles of Fig. 1.10. We have seen that in the s-channel centre of mass, the initial and final states are respectively $|i\rangle = |p_1, p_2\rangle$ and $|f\rangle = |p_3, p_4\rangle$, with $\vec{p}_2 = -\vec{p}_1$ and $\vec{p}_4 = -\vec{p}_3$. Therefore, the total momentum and energy are respectively zero and $\sqrt{s}$ for both states. If we consider only two-particle intermediate states $|n\rangle = |k_n, k'_n\rangle$, we find that the transition amplitude unitarity condition of eq. (1.114) reads:

$$\begin{aligned} 2\mathrm{Im}T(s,t,u) &= (2\pi)^4 \sum_n \int\int \frac{d^3k_n}{2E_{k_n}(2\pi)^3} \frac{d^3k'_n}{2E_{k'_n}(2\pi)^3} \\ &\quad \times \delta(E_{k_n} + E_{k'_n} - \sqrt{s}) \delta^3(\vec{k}_n + \vec{k}'_n) T_{fn} T^*_{ni}, \end{aligned} \tag{1.135}$$

where, in this case, the index n refers only to the type of intermediate state since the sum over the momenta is done explicitly. Operating with the Dirac's delta functions, we can perform all integrals except the angular one, so:

$$\mathrm{Im}T(s,t,u) = \frac{1}{64\pi^2} \sum_n \frac{2k_f}{\sqrt{s}} \int d\Omega_{\vec{k}_n} \, T_{fn} T^*_{ni}, \tag{1.136}$$

where the intermediate momentum k_n satisfies now eq. (1.116). Inserting now the partial-wave expansion of the transition amplitude given in eq. (1.132), we obtain on the one hand, that the right hand side of eq. (1.136) is:

$$4 \sum_n \frac{2k_n}{\sqrt{s}} \sum_{J,J'} (2J+1)(2J'+1) t_J^{fn}(s) t_{J'}^{ni}(s)^* \int d\Omega_{\vec{k}_n} P_J(\hat{k}_n \cdot \hat{p}') P_{J'}(\hat{p} \cdot \hat{k}_n), \tag{1.137}$$

where the scattering angles for the amplitudes $i \to n$ and $n \to f$ are the ones formed by the initial and final particles momenta, $\vec{p}$ and $\vec{p}'$, and the momentum of the intermediate particles $\vec{k}_n$, i.e. $\cos\theta_{in} = \hat{p} \cdot \hat{k}_n$ and $\cos\theta_{fn} = \hat{k}_n \cdot \hat{p}'$, where $\hat{v}$ denotes the unit vector in the direction of $\vec{v}$. Taking now into account the spherical harmonics expansion of the Legendre polynomials:

$$P_J(\hat{p} \cdot \hat{k}) = \frac{4\pi}{2J+1} \sum_{M=-J}^{J} Y^*_{JM}(\hat{p}) Y_{JM}(\hat{k}), \tag{1.138}$$

and the orthonormal condition for the former:

$$\int d\Omega_{\vec{k}} Y^*_{JM}(\hat{k}) Y_{J'M'}(\hat{k}) = \delta_{JJ'}\delta_{MM'}, \tag{1.139}$$

we obtain:

$$16\pi \sum_J (2J+1) P_J(\hat{p} \cdot \hat{p}') \sum_n \frac{2k_n}{\sqrt{s}} t_J^{fn}(s) t_J^{ni}(s)^*. \tag{1.140}$$

On the other hand, the left hand side of eq. (1.136) reads:

$$16\pi \sum_J (2J+1) P_J(\hat{p} \cdot \hat{p}') \mathrm{Im} t_J^{fi}(s), \tag{1.141}$$

which implies that the unitarity condition for partial-waves amplitudes is given by:

$$\mathrm{Im} t_J^{fi}(s) = \sum_n \sigma_n(s) t_J^{fn}(s) t_J^{ni}(s)^*, \tag{1.142}$$

where $\sigma_n(s) = 2k_n/\sqrt{s}$ is the two body phase-space of the process. For elastic processes, i.e. below the first inelastic threshold, eq. (1.142) simplifies to:

$$\mathrm{Im} t_J(s) = \sigma(s) |t_J(s)|^2. \tag{1.143}$$

As we will see in Section (1.6), eq. (1.143) plays a key role in this thesis, since this elastic unitarity condition is violated in ChPT, which leads to the different unitarization techniques we will use in Section (2.2).

As in the non-relativistic case, partial-waves amplitudes can be written in terms of a real phase shift $\delta_J(s)$ and an inelasticity $\eta_J(s)$:

$$t_J(s) = \frac{\eta_J(s) e^{2i\delta_J(s)} - 1}{2i\sigma(s)}. \tag{1.144}$$

Below the first inelastic threshold $\eta_J(s) = 1$ and eq. (1.144) can be written as:

$$t_J(s) = \frac{e^{i\delta_J(s)} \sin\delta_J(s)}{\sigma(s)}, \tag{1.145}$$

where, the unitarity condition given in eq. (1.142) requires that $0 \leq \eta_J(s) \leq 1$. Equations (1.144) and (1.145) are used intensively in Section (2.1), where we parametrize the phase shifts and inelasticities of several $\pi\pi$-scattering partial-waves.

As we have commented above, eq. (1.143) is only valid for elastic processes, i.e. when there is only one state available and the partial-wave amplitude can be parametrized in terms of a single observable, the phase-shift. However, it can be easily generalized to scattering processes with multiple coupled channels by employing a matrix notation. Therefore, in the coupled channel formalism eq. (1.143) reads:

$$\mathrm{Im}T_J(s) = T_J(s)\Sigma(s)T_J(s)^*, \tag{1.146}$$

where $T_J(s)$ is now a matrix, which incorporates all the physically available states and $\Sigma(s)$ is the diagonal matrix whose elements are the phase-spaces of the corresponding processes. For example, in the case of the scalar iso-scalar channel $I = J = 0$, when considering just π's, K's and η's, the partial-wave amplitude will be given by the matrix:

$$T_{00}(s) = \begin{pmatrix} t_{\pi\pi\to\pi\pi} & t_{\pi\pi\to K\bar{K}} & t_{\pi\pi\to\eta\eta} \\ t_{K\bar{K}\to\pi\pi} & t_{K\bar{K}\to K\bar{K}} & t_{K\bar{K}\to\eta\eta} \\ t_{\eta\eta\to\pi\pi} & t_{\eta\eta\to K\bar{K}} & t_{\eta\eta\to\eta\eta} \end{pmatrix}, \tag{1.147}$$

and

$$\Sigma_{00}(s) = \begin{pmatrix} \sigma_{\pi\pi} & 0 & 0 \\ 0 & \sigma_{K\bar{K}} & 0 \\ 0 & 0 & \sigma_{\eta\eta} \end{pmatrix}. \tag{1.148}$$

In the case of U(3) ChPT, which we will use in Section 2.2, also the $\eta\eta'$ and $\eta'\eta'$ processes contribute to the amplitude, so (1.147) would be a 5×5 matrix.

Let us finally study the analytic structure of partial-wave amplitudes. From eq. (1.134), we can see that there are two possible sources of singularities. The first one is when $T(s,t,u)$ has singularities in the s-plane whose positions are independent of the values of t or u. Therefore, the right hand cut in $T(s,t,u)$ from the s-channel physical threshold up to ∞ will also occur in $t_J(s)$. In the same way, if $T(s,t,u)$ has a pole in the real axis below threshold associated to a bound state, this pole will also appear in $t_J(s)$, unless the residue happens to be zero as a result of the integration over z_s.

There is also a second possible source of singularities in $t_J(s)$. If the partial-wave series for $T(s,t,u)$ given in eq. (1.132) converge for all t or u, then, since $P_J(z_s)$ for $J \geq 0$ is an entire function of z_s, $T(s,t,u)$ would have no singularities in t or u, but we have previously discussed in Section 1.5 that this is not the case. The series must diverge at the nearest t or u singularity. It can be shown [106], that these singularities occur at the points $z_s = \pm 1$.

In the case of elastic scattering of particles with equal masses m, the kinematics are given by eq. (1.105), so $t_J(s)$ will be singular at those values of s for which:

$$1 + \frac{\hat{t}}{2p^2} = \pm 1, \qquad -1 - \frac{\hat{u}}{2p^2} = \pm 1, \tag{1.149}$$

where $4m^2 \leq \hat{t}, \hat{u} \leq \infty$ and $p^2 = s^2/4 - m^2$. Namely, along the negative axis from $s = 0$ to -∞. Therefore, in this case, the partial-wave amplitude $t_J(s)$, has a right hand cut from threshold to ∞ and a left hand cut from 0 to $-\infty$.

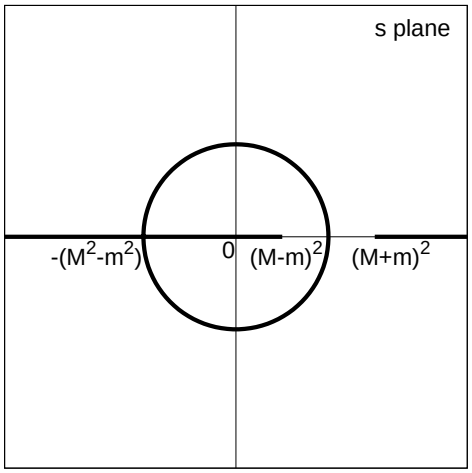

Figure 1.14: Analytic structure on the complex s-plane of $t_J(s)$ for the elastic scattering of two particles with masses M and m, $M > m$.

When the kinematics are more complicated, more singularities may appear. For example, for the elastic scattering process: $a + b \to a + b$ where m and M are respectively the masses of a and b and $M > m$, together to the right and left hand cut of the equal mass case, a cut off the real axis on the circumference $|s| = M^2 - m^2$, appears from the t-channel, and a cut in the real axis for $s \leq (M - m)^2$ from the u-channel, Fig. 1.14.

1.5.4 Resonances

One of the most remarkable features of scattering is the occurrence of peaks or bumps when different cross-section or amplitudes are displayed as a function of energy. Very frequently, such peaks can be related to resonances, interpreted as quasi-bound states, where the phase shift δ_J increases dramatically. But this is not always the case, and as we will see bellow, it is more rigorous to study them in terms of poles in the Second Riemann sheet of the amplitude.

In particular, the Mandelstam hypothesis states that a bound state of mass M_B appears as a simple pole at $s = M_B^2$ on the real axis below threshold in a partial-wave with the angular momentum of the particle. In the same way, resonances are also associated to poles in each of the channels to which it couples, namely those channels with its same quantum numbers. Intuitively, a resonance can be regarded as a quasi-bound state, but with a mass higher than the physical threshold of at least one of the channels it couples to, so it can decay into that channel. This implies that its rest mass must have a non-zero imaginary part. However, the only poles that are allowed on the s-plane are bound state poles, since poles on the real axis above threshold violate unitarity, and those off the real axis violate causality, therefore resonances poles may occur in unphysical sheets.

Rigorously, the amplitude for physical values of s, which lie on the right hand cut, is defined as the limit $s + i\epsilon$ when ϵ goes to zero of the analytic amplitude $T(s, t, u)$. If we cross

continously the physical right cut from the upper half plane to the lower half plane, we will reach an unphysical Riemann sheet. In the case when there is only one open channel, there are only two Riemann sheets, the physical one is called first sheet, and the unphysical one is called second sheet. In case there are more channels opened there will be more unphysical Riemann sheets, which can be reached by continuing the square momenta of the intermediate states in different ways.

Therefore, for s values on the cut, the S matrix on the unphysical sheet is defined as:

$$S^{II}(s - i\epsilon, t, u) = S^{I}(s + i\epsilon, t, u). \tag{1.150}$$

Applying now the Schwatz reflection principle, $S(s + i\epsilon) = S^*(s - i\epsilon)$, and the unitarity condition for the S-matrix, $SS^* = \mathbb{1}$, we can express eq. (1.150) as:

$$S^{II}(s - i\epsilon, t, u) = S^{-1}(s - i\epsilon, t, u). \tag{1.151}$$

Since both sides of eq. (1.151) are analytic, we can analytically extend this relation to the whole complex s-plane, so a pole on the second Riemann sheet translates into a zero in the physical one.

For a partial-wave of angular momentum J, taking account that $S_J(s) = \mathbb{1} + 2i\sigma(s)t_J(s)$, this relation reads:

$$t_J^{II}(s) = \frac{t_J(s)}{1 + 2i\sigma(s)t_J(s)}, \tag{1.152}$$

where the determination of $\sigma(s)$ is chosen so that: $\sigma(s^*) = -\sigma(s)^*$.

1.6 Unitarized Chiral Perturbation Theory

1.6.1 Unitarity in Chiral Perturbation Theory

As we have seen in section 1.3, ChPT provides an excellent and model independent theoretical description of the interaction of pions, kaons and etas at low energies. Using ChPT, a partial-wave amplitude involving NGB interactions t_{IJ}, is obtained as a low energy expansion on even powers of momenta and meson masses, dropping for simplicity the IJ indices:

$$t(s) = t_2(s) + t_4(s) + t_6(s) + \dots \tag{1.153}$$

where $t_n(s) = \mathcal{O}(p^n)$. However, the ChPT series is only valid at low energies compared with the chiral symmetry breaking scale $4\pi f_\pi \sim 1.2$ GeV, and in practice it is limited to scattering momenta of the order of 200-300 MeV above threshold. At larger momenta, several partial-waves become resonant, a behaviour that cannot be reproduced with a power expansion in energy, since, as we have studied in Section 1.5.4, resonances are associated with poles on the second Riemann sheet. Furthermore, they cannot satisfy exactly the unitarity condition given in eq. (1.142). Nevertheless, at each order, they do satisfy perturbative unitarity conditions

given by:

$$\begin{aligned}
&\mathrm{Im}\, t_2(s) = 0,\\
&\mathrm{Im}\, t_4(s) = \sigma(s) t_2^2(s),\\
&\mathrm{Im}\, t_6(s) = 2\sigma(s) t_2(s) \mathrm{Re}\, t_4(s) = \frac{\mathrm{Im}\, \left(t_4^2(s)\right)}{t_2(s)},\\
&\quad \text{etc}\ldots
\end{aligned} \tag{1.154}$$

The deviations between the exact unitarity condition of eq. (1.142) and the perturbative unitarity conditions of eq. (1.154) grow bigger at high energies and at the resonance region, which means that the chiral expansion cannot reproduce the enhancements and bounds on partial-waves required by unitarity. Note that the unitarity condition given in eq. (1.142) implies a upper bound on the size of the modulus of the partial-wave:

$$|t(s)| \leq \frac{1}{\sigma(s)}, \tag{1.155}$$

which clearly is violated by the ChPT series expansion for large s. In order to study the influence of unitarity and to make poles appear in the complex plane, many unitarization techniques have been developed to construct chiral amplitudes that satisfy unitarity exactly. For instance, the explicit introduction of resonances [5, 6, 110, 111, 112, 113, 114], the K matrix [115], the resummation of diagrams in a Lippmann- Schwinger or Bethe-Salpeter approach [116, 117, 118, 119, 120, 121, 122, 123], the Chiral Unitary approach [118, 120], the N/D method [113] and the Inverse Amplitude Method (IAM) [124, 125, 126, 127, 128]. Although the results provided by all these methods are in general consistent with one another, they differ in their simplicity or the kind of approximations used in their derivation. Therefore, depending on the subject of the study, some of them are more suitable than others. In Section 2.2 of thesis we make use of the elastic IAM and the N/D method. The former it is only consequence of unitarity, analyticity and ChPT, and does not introduce on any spurious parameter, which makes it very suitable to study the N_c dependence of the resonances it generates. The latter is a simple and useful method to incorporate explicitly resonances, and can be easily extended to the case of multiple coupled channels. Thus, in this Section, we will review both methods.

1.6.2 The N/D method

As we have said above, we will use the N/D method in Section 2.2. Therefore, we will review here the main properties of the N/D description of meson meson amplitudes as derived in [113].

As we have seen in Section 1.5.3, unitarity imposes in partial waves amplitudes the conditions:

$$\begin{aligned}
\mathrm{Im} t_{IJ}(s)^{-1} = &\quad -\sigma(s) &&\text{for } s > s_{th}\\
t_{IJ}(s+i\epsilon) - t_{IJ}(s-i\epsilon) = &\quad 2i\mathrm{Im} t_{IJ}(s) &&\text{for } s < s_L,
\end{aligned} \tag{1.156}$$

where s_L denote the left hand cut threshold, which in the equal mass case is zero. In order to solve the system given in eq. (1.156), in the N/D method, $t_{IJ}(s)$ is expressed as a quotient of

two functions:

$$t_{IJ}(s) = \frac{N_{IJ}(s)}{D_{IJ}(s)}, \tag{1.157}$$

in such a way that $D_{IJ}(s)$ only contains the right hand cut, and N_{IJ} only the left hand cut of $t_{IJ}(s)$. In addition, both functions may contain poles, although we can remove them from either one of these by introducing zeros at the appropriate points in the other. We are also free to multiply both quantities by any factor without affecting $t_{IJ}(s)$. Because of that, in order to take explicitly into account the behaviour of the amplitude near threshold, which vanish like p^{2J}, we consider the new quantity:

$$\hat{t}_{IJ}(s) = \frac{t_{IJ}(s)}{p^{2J}}, \tag{1.158}$$

which also satisfies a eq. like eq. (1.156), so:

$$\hat{t}_{IJ}(s) = \frac{\hat{N}_{IJ}(s)}{\hat{D}_{IJ}(s)}, \tag{1.159}$$

where $\hat{N}_{IJ}$ and $\hat{D}_{IJ}$ satisfy:

$$\begin{aligned}
&\mathrm{Im}\hat{D}_{IJ}(s) = \quad \mathrm{Im}\hat{t}_{IJ}\hat{N}_{IJ}(s) = -\sigma(s)\hat{N}_{IJ}(s)p^{2J}, && \text{for} \quad s > s_{th},\\
&\mathrm{Im}\hat{D}_{IJ}(s) = \quad 0, && \text{for} \quad s < s_{th},\\
&\mathrm{Im}\hat{N}_{IJ}(s) = \quad \mathrm{Im}\hat{t}_{IJ}\hat{D}_{IJ}(s), && \text{for} \quad s < s_L,\\
&\mathrm{Im}\hat{N}_{IJ}(s) = \quad 0, && \text{for} \quad s > s_L.
\end{aligned} \tag{1.160}$$

Taking into account eq. (1.160), we can write dispersion relations for $\hat{D}_{IJ}(s)$ and $\hat{N}_{IJ}(s)$ as:

$$\hat{D}_{IJ}(s) = \sum_{m=0}^{n-1} \hat{a}_m s^m - \frac{(s-s_0)^n}{\pi} \int_{s_{th}}^{\infty} ds' \frac{p^{2J}(s')\sigma(s')\hat{N}_{IJ}(s')}{(s'-s)(s'-s_0)^n}, \tag{1.161}$$

$$\hat{N}_{IJ}(s) = \sum_{m=0}^{n-J-1} a'_m s^m + \frac{(s-s_0)^{n-J}}{\pi} \int_{-\infty}^{s_J} ds' \frac{\mathrm{Im}\hat{T}_L(s')\hat{D}_{IJ}(s')}{p^{2J}(s')(s'-s)(s'-s_0)^{n-J}}, \tag{1.162}$$

where n is the number of subtractions needed so that: $p^{2J}\hat{N}_{IJ}/s^n \to 0$ as $s \to \infty$. Eqs. (1.161) and (1.162) are a pair of coupled equations for $\hat{N}_{IJ}(s)$ and $\hat{D}_{IJ}(s)$, usually referred as N/D equations. The input into these equations consists of $\mathrm{Im}t_{IJ}(s)$ in the left hand cut, together with the subtractions constants of $\hat{D}_{IJ}(s)$ and $\hat{N}_{IJ}(s)$. However, since the poles of $\hat{N}_{IJ}(s)$ and $\hat{D}_{IJ}(s)$ can be removed arbitrarily, possible zeros of $t_{IJ}(s)$ may exist, which are not originated when solving eqs. (1.161) and (1.162). These zeros can be included as poles in $\hat{D}_{IJ}(s)$ and they are known as Castillejo-Dalitz-Dyson (CDD) poles. Including them, we rewrite $\hat{D}_{IJ}(s)$ as:

$$\hat{D}_{IJ}(s) = \sum_{m=0}^{n-1} \hat{a}_m s^m - \frac{(s-s_0)^n}{\pi} \int_{s_{th}}^{\infty} ds' \frac{p^{2J}(s')\sigma(s')\hat{N}_{IJ}(s')}{(s'-s)(s'-s_0)^n} + \sum_i \frac{\gamma}{(s-s_i)}. \tag{1.163}$$

In order to solve eqs. (1.163) and (1.162), we neglect here the left-hand cut, i.e. we set $\mathrm{Im}t_{IJ} = 0$ for $s < s_L$, which is a crude estimate. In Section 1.6.3, we will see that in deriving the IAM, the left cut is not set to zero, but approximated by using ChPT. In Section 1.7, we will see how, for $\pi\pi$-scattering, the left-hand cut is treated exactly.

If we neglect the left hand cut, it is always possible to take $\hat{N}_{IJ}(s) = 1$, by including all the possible zeros of the polynomial $\sum_{m=0}^{n-J-1} a'_m s^m$ as CDD poles in $\hat{D}_{IJ}(s)$. In this way we have:

$$\begin{aligned} \hat{t}_{IJ}(s) &= \frac{1}{\hat{D}_{IJ}(s)}, \\ \hat{N}_{IJ}(s) &= 1, \\ \hat{D}_{IJ}(s) &= \sum_{m=0}^{J} a_m s^m + \sum_{i}^{M_J} \frac{R_i}{s - s_i} - \frac{(s-s_0)^{J+1}}{\pi} \int_{s_{th}}^{\infty} ds' \frac{p^{2J}(s')\sigma(s')}{(s'-s)(s'-s_0)^{J+1}}, \end{aligned} \tag{1.164}$$

where we have taken into account that $n = J + 1$, and we have redefined the subtraction constants a_m and the CDD pole residues. Eq. (1.164) is the most general structure of an elastic partial wave of angular momentum J when the left hand cut is neglected [113].

Let us now split the subtraction constants of eq. (1.164) in two different pieces, which have a different dependence on the QCD number of colours:

$$a_m = a_m^L + a_m^{SL}, \tag{1.165}$$

where the term a_m^L is $\mathcal{O}(N_c)$ and a_m^{SL} is $\mathcal{O}(1)$ in N_c. This is so because in the $N_c \to \infty$ limit, as we will see in Section 1.4, the meson-meson amplitude goes with $1/N_c$. In addition, the integral of eq. (1.164) is $\mathcal{O}(1)$ in this counting. Therefore when $N_c \to \infty$, eq. (1.164) becomes:

$$\hat{D}_{IJ}^{\infty}(s) = \sum_{m=0}^{J} a_m^L s^m + \sum_{i}^{M_J^{\infty}} \frac{R_i^{\infty}}{s - s_i}, \tag{1.166}$$

where R^{∞} is the N_c leading part of R_i and M_J^{∞} the number of leading CDD poles.

In order to determine eq. (1.166), we will make use of ChPT and the resonance exchange saturation hypothesis studied in Section 1.3.5, to state that, at large N_c, the contact terms in the inverse of eq. (1.166) come from the lowest order ChPT Lagrangian and the poles from the exchange of resonances in the s-channel. It implies that we are neglecting the exchange of resonances in crossed channels and higher orders contact terms. Thus, at large N_c, we assume that the lowest partial-waves have the structure [113]:

$$\begin{aligned} \hat{t}_{I0}^{\infty}(s) &= as + a'\hat{m}^2 \sum_{i=1}^{R_0} \frac{c_i s + c'_i m^2}{M_i^2 - s}, \\ \hat{t}_{I1}^{\infty}(s) &= b + \sum_{i=1}^{R_1} \frac{d_i s}{M_i^2 - s}, \end{aligned} \tag{1.167}$$

where M_i is the mass of the i^{th} resonance, m^2 and $\hat{m}^2$ are some combination of squared masses of the NGB, c_i, c'_i and d_i are arbitrary constants, and a, a' and b are the coefficients of the lowest order ChPT partial waves expansion. Furthermore, it can be shown [113], that the number of poles of $t_{IJ}^{\infty}(s)$ is equal to the number of zeros of $D_{IJ}^{\infty}(s)$, and that the number of CDD poles of $D_{IJ}^{\infty}(s)$ is equal to the number of zeros $t_{IJ}^{\infty}(s)$. As a consequence, the previous statement is correct, and eq. (1.167) can always be cast in the form of eq. (1.166), so that:

$$D_{IJ}^{\infty}(s) = \frac{1}{t_{IJ}^{\infty}(s)}. \tag{1.168}$$

Finally, defining the function $g_J(s)$ by:

$$g_J(s)p^{2J} = \sum_{m=0}^{J} a_m^{SL} s^m - \frac{(s-s_0)^{J+1}}{\pi} \int_{s_{th}}^{\infty} ds' \frac{p^{2J}\sigma s'}{(s'-s)(s'-s_0)^{L+1}}, \tag{1.169}$$

which in the case of equal mass particles has the form:

$$g_J(s)p^{2J} = \sum_{m=0}^{J} a_m^{SL} s^m + \log\frac{m^2}{\mu^2} - \sigma(s)\log\frac{\sigma(s)-1}{\sigma(s)+1}, \tag{1.170}$$

we have that:

$$t_{IJ}(s) = \left[1/t_{IJ}^{\infty}(s) + g_J(s)\right]^{-1}, \tag{1.171}$$

which is the N/D expression for a partial wave amplitude. As we have commented, $t_{IJ}^{\infty}(s)$ corresponds to the three level contributions before the unitarization, i.e. lowest order ChPT partial waves and s-channel resonances exchanges:

$$t_{IJ}^{\infty} = t_{IJ}^{(2)}(s) + t_{IJ}^{\mathrm{RES}}.$$

The unitarization is accomplished through the function $g_J(s)$, since:

$$\mathrm{Im}\frac{1}{t_{IJ}(s)} = \mathrm{Im}g_J(s) = -\sigma(s). \tag{1.172}$$

This formalism can be easily generalized to scattering processes with multiple coupled channels by employing a matrix notation. In this way, t_{IJ}, t_{IJ}^{∞} and g_J are now matrices and eq. (1.171) still holds. Since phase space $\sigma(s)$ is diagonal then the matrix $g_J(s)$ is also diagonal, with its matrix elements given by eq. (1.169), evaluated with the appropriate masses for the corresponding channel. As we have said, we will use this formalism in Section 2.2 to analyze different meson-meson amplitudes by including explicitly the exchange of resonance.

1.6.3 The Inverse Amplitude Method

The elastic IAM [124, 125, 126, 127, 128] consists in using elastic partial-wave unitarity and ChPT to evaluate a dispersion relation for the inverse of the partial-wave. In this section we will follow the derivation given in [128]. The elastic unitarity condition of eq. (1.143) can be written as:

$$\mathrm{Im}\,\frac{1}{t(s)} = \sigma(s), \quad \text{for } s \geq s_{th}, \tag{1.173}$$

so writing a dispersion relation for $1/t(s)$, we will know exactly its right hand cut contribution. In practice, we will write it for:

$$G(s) = \frac{t_2(s)^2}{t(s)}.$$

Since $t_2(s)$ is a real polynomial, it does not change the analytical structure of t^{-1}, which is the same as the one of $t(s)$, so $t(s)$ and $G(s)$ have both the same analytical properties. Therefore, as we studied in Section 1.5.3, in the equal mass case $G(s)$ has a right hand cut (RC) from $s = s_{th}$ to ∞, a left hand cut (LC) from 0 to $-\infty$, and possible poles coming from possible zeros of t(s) (PC).

At $\mathcal{O}(p^4)$, the ChPT amplitudes grow as s^2 when $s \to \infty$, and we should write a dispersion relation with three subtractions, so in the equal mass case, we have: If we write now a three-times subtracted dispersion for $t_2(s)$ and $t_4(s)$:

$$\begin{aligned} t_2(s) &= t_2(0) + t_2'(0)s, \\ t_4(s) &= t_4(0) + t_4'(0)s + t_4''(0)s^2 + \frac{s^3}{\pi}\int_{s_{th}}^{\infty} ds' \frac{\mathrm{Im}t_4(s)}{s'^3(s'-s-i\epsilon)} + LC(t_4(s)), \end{aligned} \tag{1.174}$$

where we have taken into account that $t_2(s)$ is just a real first order polynomial in s. Similarly:

$$G(s) = G_0 + G_1 s + G_2 s^2 + \frac{s^3}{\pi}\int_{s_th}^{\infty} ds' \frac{\mathrm{Im}G(s')}{s'^3(s'-s-i\epsilon)} + LC(G) + PC. \tag{1.175}$$

However, using eq. (1.173), in the right cut we have:

$$\mathrm{Im}G(s) = t_2(s)^2 \mathrm{Im}\frac{1}{t(s)} = -\sigma(s)t_2(s)^2 = -\mathrm{Im}t_4(s), \tag{1.176}$$

which can be exactly calculated in ChPT. For the LC we can still use the ChPT $\mathcal{O}(p^2)$ expansion, so that:

$$\mathrm{Im}G(s) = t_2(s)^2 \mathrm{Im}\frac{1}{t(s)} \simeq t_2(s)^2 \mathrm{Im}\frac{1}{t_2(s)+t_4(s)} \simeq -\mathrm{Im}t_4(s). \tag{1.177}$$

Thus $LC(G(s)) \simeq -LC(t_4(s))$. The pole contribution PC, for those waves where it is present, starts contributing at $\mathcal{O}(p^6)$, and is numerically very small, except in the region near the pole of $1/t(s)$, and we will neglect it. However, in so doing, there appears a spurious pole near the zero of t, which has been studied in [129] and shown to have a negligible numerical influence both in the physical region and in the part of the complex plane where the resonance poles appear.

Therefore, only the subtraction coefficients G_0, G_1 and G_2 are still unknown in eq. (1.179). However, these constants involve the amplitude and its derivatives evaluated at $s = 0$, where ChPT should give a very good approximation, so, up to $\mathcal{O}(p^4)$, we have:

$$\begin{aligned} &G(0) \simeq t_2(0) - t_4(0), \\ &G'(0) \simeq t_2'(0) - t_4'(0) \\ &G''(0) \simeq -t_4''(0). \end{aligned} \tag{1.178}$$

Finally, we can write:

$$\begin{aligned} G(s) &= t_2(0) + t_2'(0)s - t_4(0) - t_4'(0)s - t_4''(0)s^2 \\ &\quad -\frac{s^3}{\pi}\int_{s_{th}}^{\infty} ds' \frac{\mathrm{Im}t_4(s)}{s'^3(s'-s-i\epsilon)} - LC(t_4(s)), \end{aligned} \tag{1.179}$$

and we see that:

$$G(s) = \frac{t_2(s)^2}{t(s)} = t_2(s) - t_4(s) \Longrightarrow t^{IAM}(s) = \frac{t_2(s)^2}{t_2(s) - t_4(s)}, \tag{1.180}$$

which is the IAM formula for the $\mathcal{O}(p^4)$ elastic partial-wave amplitude. On the one hand, the IAM amplitude satisfies elastic unitarity exactly, since:

$$\mathrm{Im}t^{IAM}(s) = \frac{t_2^2(s)\mathrm{Im}t_4(s)^*}{|t_2(s)-t_4(s)|^2} = \frac{\sigma t_2^4(s)}{|t_2(s)-t_4(s)|^2} = \sigma|t^{IAM}|^2, \tag{1.181}$$

where we have used the perturbative unitarity of ChPT amplitudes given in eq. (1.154). On the other hand, expanding a low energy when $|t_2(s)| \sim \mathcal{O}(s)$ is much bigger than $|t_4(s)| \sim \mathcal{O}(s^2)$:

$$t^{IAM}(s) = \frac{t_2(s)}{1-t_4(s)/t_2(s)} \sim t_2(s)\left(1+\frac{t_4(s)}{t_2(s)}+\dots\right) = t_2(s)+t_4(s)+\dots, \tag{1.182}$$

so we recover the chiral expansion at low energies.

For the unequal mass case, the derivation is almost the same. As we saw in Section 1.5.3 and as it is shown in Fig. 1.14, for different masses new cuts are presented. However, they appear at low energies and can be again evaluated using ChPT.

The IAM formula can also be extended at higher orders [128, 130] just by evaluating the subtraction constants, the left hand cut, and the pole contributions to that order in the chiral expansion. For example, at order $\mathcal{O}(p^6)$ it is given by:

$$t^{IAM}(s) = \frac{t_2(s)^2}{t_2(s)-t_4(s)-t_6(s)+t_4(s)^2/t_2(s)}, \tag{1.183}$$

In spite of its simplicity, the IAM amplitude fits very well different scattering processes of NGB, up to energies around 1 GeV, with LECs compatible with those of ChPT within errors [124, 125, 126, 127], In Fig. 1.15, we plot the $I=J=0$, $I=J=1$ and $I=2, J=0$ $\pi\pi$-scattering partial waves.

Furthermore, since it has the correct analytic structure, it can be analytically continued to the complex s-plane. Thus as we explained in Section 1.5.4, it is possible to use the IAM amplitude to study resonances associated to poles on the second Riemann sheet. For example, in the I=J=0, I=J=1 and I=1/2=1 channels, the IAM amplitude present poles on the second Riemann sheet associated to the $f_0(500)$, $\rho(770)$ and $K^*(892)$ resonances respectively, whose pole positions are in good agreement with the PDG estimates [11]. Therefore the IAM generates poles that are not initially present in the Lagrangian, without any assumption about their nature or properties. These resonances are only consequence of unitarity, analyticity and ChPT, and they do not depend on any spurious parameter.

It is important to note that, despite its success, we have made several approximations in order to derive eq. (1.180). First of all, we have neglected eventual pole contributions for G(s), which correspond to zeros of the partial-wave amplitude. Such zeros, which are called Adler zeros and are consequence of chiral symmetry, indeed appear for some channels but are located below threshold at $\mathcal{O}(p^6)$. Actually, in [129], the IAM was modified taking into account the Adler zeros, showing that they are numerically irrelevant, so that neglecting them is justified. Second, we have approximated the left cut using the chiral expansion, which breaks crossing symmetry, since we have dealt differently with the right hand cut required by unitarity and the left cuts coming from crossing. However, on the one hand, these two

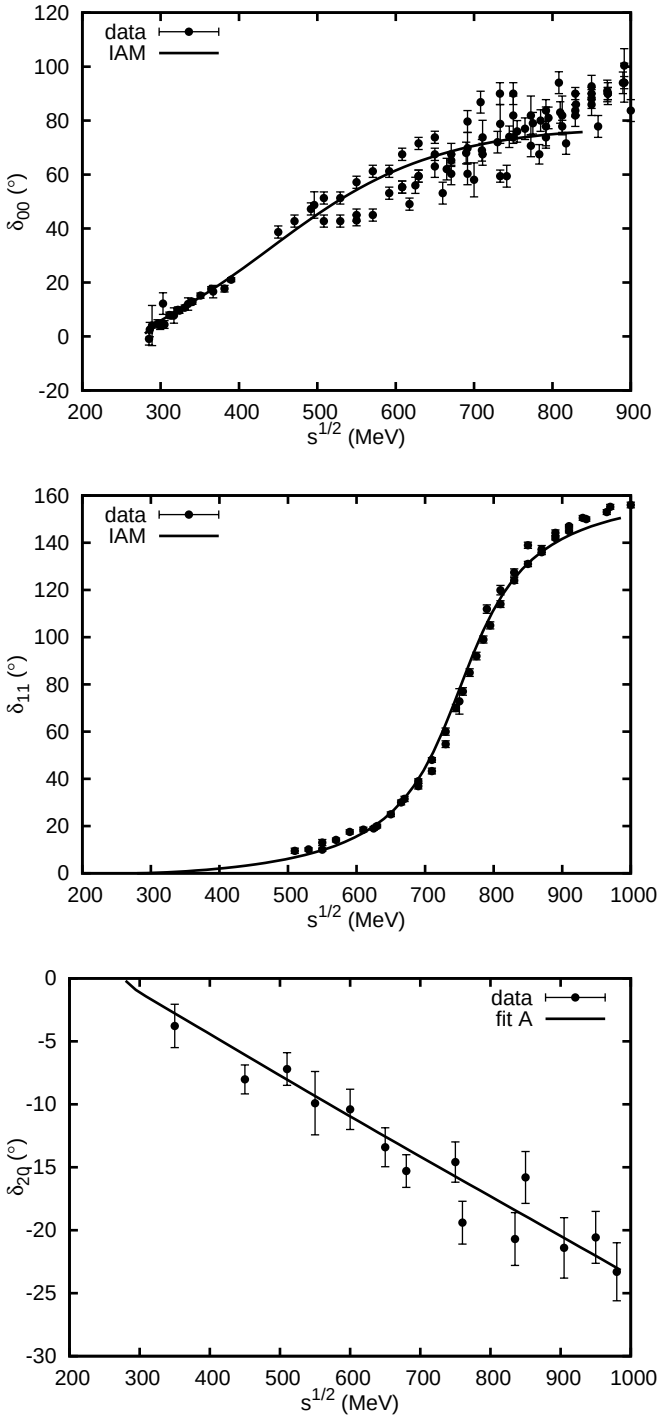

Figure 1.15: IAM fit to $\pi\pi$ scattering phase shift data obtained in [132]. Phase shift data come from [133, 134, 135, 136, 137, 138, 139, 140, 141].

approximations seem justified at high energies since the denominator $s'(s'-s)$ ensures that the integrals are suppressed at this regime. On the other hand, at low energies, the IAM amplitude matches exactly ChPT at a given order, so the pole and left hand cut contributions are subdominant, which has been numerically shown in [129].

In addition, $t_2(s)$ vanishes for partial-waves amplitudes with $J \geq 2$, so the IAM can only be used for S and P waves. Therefore, in Section 2.2, where we will study the role of the $f_2(1270)$ in the fulfillment of local duality, we will not use the IAM to introduce the $I = 0, J = 2$ $\pi\pi$-scattering partial-wave.

Furthermore, the IAM amplitude above has been derived for elastic processes. The first inelastic channels are the four pion state for $\pi\pi$ scattering, and the $\pi K \pi\pi$ state in the πK channel, but their contributions are suppressed by the four particle phase space, so we expect that the IAM still provides a good approximation in that region. However, there are other intermediate states of two particles, whose contributions cannot be neglected, as for example, the $\bar{K}K$ in the $I = J = 0$ channel at 988 MeV. Above that threshold, the unitarity condition involves two channels and a new, non-negligible integral appears, so that the IAM cannot be trusted anymore. Nevertheless, the IAM can also be extended to account for unitarity in coupled channels [118, 120, 142, 143], also generating the poles of the $f_0(980)$ and $a_0(980)$ resonances. In this case, however, the IAM formula cannot be obtained from a dispersion relation, and its derivation is, of course, less rigorous. Also, it can be extended to finite temperature [144], in order to study thermal effects.

1.7 $\pi\pi$-scattering and dispersion theory

As we have seen in Section 1.2.3, pions are the NGB of the $N_f = 2$ spontaneous chiral symmetry breaking and thus the relevant degrees of freedom at low energies. A precise and unbiased knowledge of $\pi\pi$-scattering has become increasingly important in the last years. Since it is one of the few places where there are more observables than unknown constants in a ChPT 1-loop analysis, it provides an important test of ChPT. Furthermore, it is a way to study the mechanism of the spontaneous chiral symmetry breaking and provides essential information about light scalars spectroscopy, a subject of intensive investigation at present. In this thesis $\pi\pi$-scattering plays a key role. In Section 2.1 we will parametrize the $\pi\pi$-scattering amplitude, by combining the analysis of experimental data with theoretical constraints in the form of dispersion relations. In Section 2.2, we will use the ChPT description of the $\pi\pi$-scattering amplitude to study the nature of the lightest resonances. For this reason in this section we are going to review the main properties of $\pi\pi$-scattering.

If we assume that isospin is exactly conserved, although this is only approximately true, typically just within a 3% accuracy, $\pi\pi$-scattering is a case of two-particle scattering in which the two particles involved have the same mass, which leads to many simplifications in the formulas studied in previous sections.

There are three pion states with different charges: π^+, π^0 and π^-. However, it is more convenient when dealing with strong interactions, which conserve isospin, to use the isospin basis, where the three pions are classified by their third isospin isospin component, $m =$

$\{1, 0, -1\}$, i.e. $\pi^1(p) = |1, 1\rangle$, $\pi^0(p) = |1, 0\rangle$ and $\pi^{-1}(p) = |1, -1\rangle$, where the first number is the isospin and the second one the third isospin component. The relation between the charged and the isospin states is given by:

$$\pi^1 = \frac{1}{\sqrt{2}}(\pi^+ + \pi^-), \quad \pi^0 = \pi^0, \quad \pi^{-1} = \frac{i}{\sqrt{2}}(\pi^+ - \pi^-). \tag{1.184}$$

Therefore, we label a pion state by its four-momenta p_i, and its isospin denoted by a Latin letter, namely: a, b, and d.

The conservation of isospin enables us to express the amplitudes describing a given process in terms of an amplitude $T^I(s, t, u)$ of definite total isospin in that channel. For example in a s-channel process: $a + b \to c + d$, we have the following isospin decomposition:

$$\langle I_c, m_c; I_d, m_d | T^s | I_a, m_a; I_b, m_b \rangle = \sum_I \langle m_c m_d | Im \rangle \langle m_a m_b | Im \rangle T^{I_s = I}(s, t, u), \tag{1.185}$$

where again I_i is the isospin of the i-particle and m_i its third component. $T^{I_s}(s, t, u)$ is the transition amplitude of the s-channel process with definite isospin, and $\langle m_i m_j | Im \rangle$ are the tabulated Clebsch-Gordan coefficients, which are real numbers. For the t-channel process: $\bar{d} + b \to c + \bar{a}$ the decomposition is given by:

$$\langle I_c, m_c; \overline{I_a, m_a} | T^t | \overline{I_d, m_d}; p_b, I_b, m_b \rangle = \sum_I \langle m_c m_a | Im \rangle \langle m_d m_b | Im \rangle T^{I_t = I}(s, t, u), \tag{1.186}$$

where we denote an antiparticle isospin state as $\overline{|p_i, I_i, m_i\rangle}$. However, crossing symmetry implies that the left hand sides of eqs. (1.185) and (1.186) are equal, so that:

$$T^{I_t}(s, t, u) = \sum_{I_s} C_{st} T^{I_s}(s, t, u), \tag{1.187}$$

where the matrix C_{st} is known as isospin crossing matrix.

In the case of $\pi\pi$-scattering, the amplitude for any process can be written in terms of three well-defined isospin amplitudes, $T^I(s, t)$, with I=0, 1 and 2 while the crossed-channel amplitudes

$$\begin{aligned} \pi^a(k_1)\, \pi^b(k_2) &\to \pi^c(p_1)\, \pi^d(p_2), && (s\text{-channel}) \\ \pi^a(k_1)\, \pi^c(-p_1) &\to \pi^b(-k_2)\, \pi^d(p_2), && (t\text{-channel}) \\ \pi^a(k_1)\, \pi^d(-p_2) &\to \pi^c(p_1)\, \pi^b(-k_2), && (u\text{-channel}) \end{aligned}$$

are related by means of the three following crossing matrices:

$$C_{st} = \begin{pmatrix} \frac{1}{3} & 1 & \frac{5}{3} \\ \frac{1}{3} & \frac{1}{2} & -\frac{5}{6} \\ \frac{1}{3} & -\frac{1}{2} & \frac{1}{6} \end{pmatrix}, \; C_{su} = \begin{pmatrix} \frac{1}{3} & -1 & \frac{5}{3} \\ -\frac{1}{3} & \frac{1}{2} & \frac{5}{6} \\ \frac{1}{3} & \frac{1}{2} & \frac{1}{6} \end{pmatrix}, \; C_{tu} = \begin{pmatrix} 1 & 0 & 0 \\ 0 & -1 & 0 \\ 0 & 0 & 1 \end{pmatrix}. \tag{1.188}$$

Note that the products of these crossing matrices have the following properties:

$$\begin{aligned} &C_{st}^2 = 1, \quad C_{su}^2 = 1, \quad C_{tu}^2 = 1, \\ &C_{st} C_{tu} = C_{tu} C_{us} = C_{us} C_{st} \quad C_{su} C_{ut} = C_{ts} C_{su} = C_{ut} C_{tu}. \end{aligned} \tag{1.189}$$

Furthermore, $(1 \pm C_{tu})/2 = (1 \pm C_{tu})^\dagger/2$, which implies that these are a orthogonal projectors. We will use this property when deriving the once and twice-subtracted Roy equations, Section 2.1.

Furthermore, using crossing and isospin, $\pi\pi$-scattering amplitudes with definite isospin can be described through the scattering amplitude of the process $A(s,t,u) = T(\pi^+\pi^- \to \pi^0\pi^0)$ as:

$$\begin{aligned} T^{I_s=0}(s,t,u) &= 3A(s,t,u) + A(t,s,u) + A(u,t,s), \\ T^{I_s=I}(s,t,u) &= A(t,s,u) - A(u,t,s), \\ T^{I_s=2}(s,t,u) &= A(t,s,u) + A(u,t,s). \end{aligned} \tag{1.190}$$

Using eq. (1.134), we can write the $\pi\pi$-partial-wave amplitudes with definite isospin I and angular momentum J as:

$$t_J^I(s) = \frac{1}{64\pi}\int_{-1}^{1} dz_s P_J(z_s) T^I(s,t,u). \tag{1.191}$$

Since we are assuming exact isospin symmetry, pions are considered identical particles, so Bose-Einstein statistics imply that the partial-wave amplitude must be symmetric, and, consequently, $I + J$ must be an even number.

As we have seen in Section 1.5.3, $\pi\pi$ partial-waves can be expressed as a function of the phase-shifts and inelasticities of definite isospin:

$$t_J^I(s) = \frac{\eta_J^I(s) e^{2i\delta_J^I(s)} - 1}{2i\sigma(s)}. \tag{1.192}$$

Actually, in Section 2.1, we will parametrize the $J = 0, 1, 2, 3$ phase-shifts and inelasticities to characterize the different $\pi\pi$ partial-waves. Note that in that Section and in what follows we will also make use of the traditional spectroscopic notation: where S, P, D, F $\cdots$ stand for $J = 0, 1, 2, 3 \cdots$.

Let us also remark that partial waves behave near threshold as p^{2J}, which means that the scalar ones do not have to vanish at threshold. However, in the chiral limit, the chiral Lagrangian involves derivative couplings only, which implies that scalar partial waves can be expressed as a polynomial in s, which indeed vanishes at $s = 0$. Nevertheless, the non-zero quark masses introduce a small correction and scalar partial waves do not vanish exactly at zero but for nearby $s = 0$ values, which are known as Adler zeros [145]. In Section 2.1, we will study the exact position of the Adler zeros in the $I = 0$ and $I = 2$ S waves, also called S0 and S2 respectively.

Finally, the real part of the partial-wave amplitude can be expanded near the threshold as:

$$\mathrm{Re}\, t_J^I(s) \sim m_\pi \left(a_J^I + b_J^I k^2 + \mathcal{O}(k^4) \right), \qquad s \to 4m_\pi^2, \tag{1.193}$$

where $k = \sqrt{s/4 - m_\pi^2}$. The coefficients a_J^I, b_J^I,... of the expansion are collectively known as threshold parameters. The first one as the scattering length and the second as the scattering slope. We will calculate the $\pi\pi$ scattering lengths and slopes of the S, P and D waves in Section 2.1.

1.7.1 $\pi\pi$-scattering experimental data

As we have commented above, in Section 2.1 we will parametrize the $\pi\pi$-scattering amplitude by fitting experimental data. In particular, in this thesis we pay special attention to the S0 wave, which we improve upon previous works [146, 147, 148, 149] and is where we look for the poles associated to the $f_0(500)$ and $f_0(980)$ resonances. For this reason, in this section we are going to review in some more detail the available experimental data for the S0 phase-shift and inelasticity. The other waves will be just shown for completeness because we use them as input, but we have not modified their functional form. As we have said in the beginning of Section 1.5, it is impossible to arrange collisions of real pions. So experimental data are obtained from two different ways, namely, from pion-proton scattering and from kaon decays. The former are more numerous and extend through a larger energy range, but they are sometimes imprecise and inconsistent between different experiments. The latter give information just in the low energy region, but provide a precise information close to threshold. This is the interesting region for the determination of the scattering lengths, which, as we will see in Section 1.7.2, play an important role in the precision of the dispersive techniques that we will use.

For the phase-shift experimental data, the pion-proton collision produces two pions and either a nucleon or a Δ resonance:

$$\pi p \to \pi\pi N, \qquad \pi p \to \pi\pi\Delta. \tag{1.194}$$

In order to obtain $\pi\pi$-scattering data, on the one hand, only those processes where the momentum transferred by the incoming pion to the proton is small are selected, assuming that they are mediated by the exchange of a virtual pion. On the other hand, it is assumed that the scattering amplitude for the full process factorizes into the $\pi\pi$-scattering amplitude, with one virtual pion joined to the proton-nucleon or proton-Δ matrix element. In different analyses further complications are added to this simple model, giving rise to large systematic uncertainties, which lead in many cases to inconsistent experimental sets of data.

S0 wave

In Fig. 1.16, we plot different phase-shift sets of data coming from pion-proton scattering [133, 136, 137, 138, 150]. References [136, 137] are all analysis from the same CERN-Munich collaboration. In particular [137] contains five different sets of data, some of which are incompatible with each other. Reference [138] is a theoretical reanalysis of the same experiment and reference [150] is a more recent analysis, which eliminates some phase ambiguities. In [147], dispersion relations were used to check the consistency of each individual data set. Those sets satisfying these conditions, were very consistent with each other and also with an averaged "global fit" obtained from a data selection in the region where the sets agree, once the uncertainties in the data were enlarged to cover the difference between them. In Section 2.1 of this thesis we will improve the "global fit" by imposing continuity and differentiability of the parametrization and updating the experimental data. Later on it will be constrained to satisfy, to a very good accuracy, a whole set of dispersion relations, including the new ones derived in Section 2.1. This will be one of the main results of this thesis.

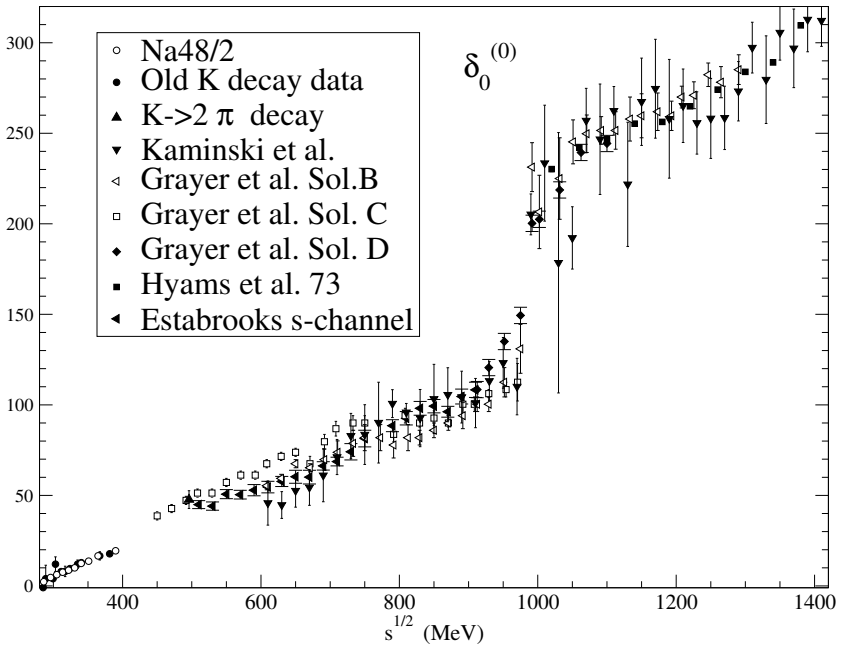

Figure 1.16: $\pi\pi$ S0 phase-shift. The experimental data above the m_K is obtained from the pion-proton analysis from [133, 136, 137, 138, 150]. The low energy data are obtained from the K_{l4} data from [153, 140, 154].

The phase-shift experimental data coming from the so called K_{l4} decays, are obtained from two different processes:

$$K^- \to e\bar{\nu}_e\pi^+\pi^-, \qquad K^+ \to e^+\nu_e\pi^+\pi^-, \tag{1.195}$$

where e denotes an electron, e^+ a positron, ν_e an electron neutrino and $\bar{\nu}_e$ an electron anti-neutrino. Following the analysis of [152], from these measurements one can extract the $\pi\pi$-scattering phase-shift combination $\delta_0^0 - \delta_1^1$. Since, as we will see below, the P wave is much better known than the S0 wave, these experiments provide information on δ_0^0. In this thesis together with the old results on K_{l4} decays [153, 140], we will also use the very recent results from NA48/2 published in [154], all them plotted in Fig. 1.16. Finally, in [155], it was shown that due to threshold effects, the isospin correction to the K_{l4} data might be larger than naively expected. For this reason, in this thesis we will apply the isospin correction suggested in [155] to the K_{l4} data of [154]. These very recent K_{l4} data are very relevant to achieve the remarkable final precision in our results.

Finally, the experimental data for the S0 inelasticity η_0^0 come from two different pion-proton scattering processes:

$$\pi p \to \pi\pi N, \qquad \pi p \to KKN. \tag{1.196}$$

Thus, using the factorization hypothesis of the full scattering matrix, as commented above, the first one gives information about $\pi\pi \to \pi\pi$ and the second one about $\pi\pi \to KK$. In the left panel of Fig. 1.17 we plot experimental data from [156, 137, 157, 158] obtained from $\pi\pi \to KK$, whereas in the right panel we plot data from [133, 136, 150] obtained from $\pi\pi \to \pi\pi$. We can

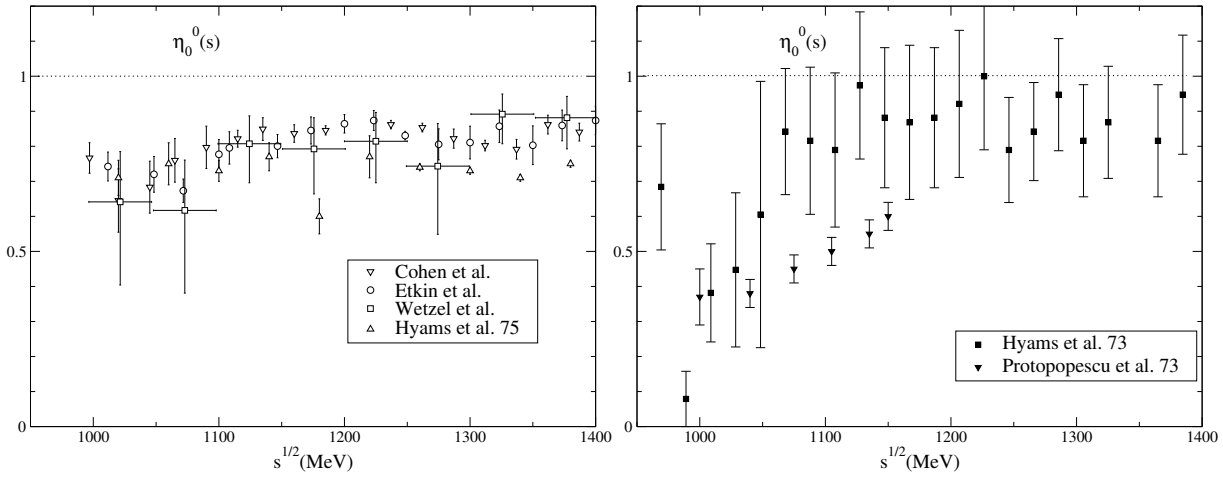

Figure 1.17: Data on $\pi\pi$ S0 inelasticity. Left panel: "no-dip scenario". Experimental data obtained from $\pi\pi - KK$ scattering [156, 137, 157, 158]. Right panel: "dip scenario". Experimental data obtained from $\pi\pi \to \pi\pi$ [133, 136]. In order to highlight the differences between both scenarios, we have omitted the points from [150], which have very large uncertainties and are nevertheless plotted in the figures given in Section 2.1.

see from this figure, that both sets of data are quite incompatible. On the one hand, the former favor a inelasticity greater than 0.6, which is known as "non-dip" solution, On the other hand, the latter favor a big dip in the elasticity between 1000 and 1100 MeV and is therefore called "dip solution". We will see in Section 2.1 that our analysis on dispersion relations clearly prefer the solution with a dip. This settles a long standing debate [159, 160, 161, 162] and is, therefore, one of the most relevant results of this thesis.

Other waves and high energy data

As commented above, in this thesis we use partial wave parametrizations for the S2, P, D, F partial waves up to 1420 MeV, and Regge fits to data above that energy. The parametrizations and fits we used are taken from [146, 147, 148, 149]. The functional form of these parametrizations is given in the appendix inside publication 2.1.3, that we include in Section 2.1. We just show the fits and the data in Figs. 1.18 and 1.19 for completeness. Note that for these partial waves the available data are, in general, more consistent with each other that in the S0 wave case.

1.7.2 Dispersive techniques in $\pi\pi$-scattering

The analytic properties of the $\pi\pi$ transition amplitude imply that we can write a Cauchy representation for it, and use the dispersion relations derived in Section 1.5.2. However, from a theoretical point of view, $\pi\pi$-scattering is also constrained from isospin, crossing and chiral symmetries, which implies further relations between the left and right hand cuts and simpler expressions. As we have seen, dispersive techniques relate the $\pi\pi$ amplitude at any energy

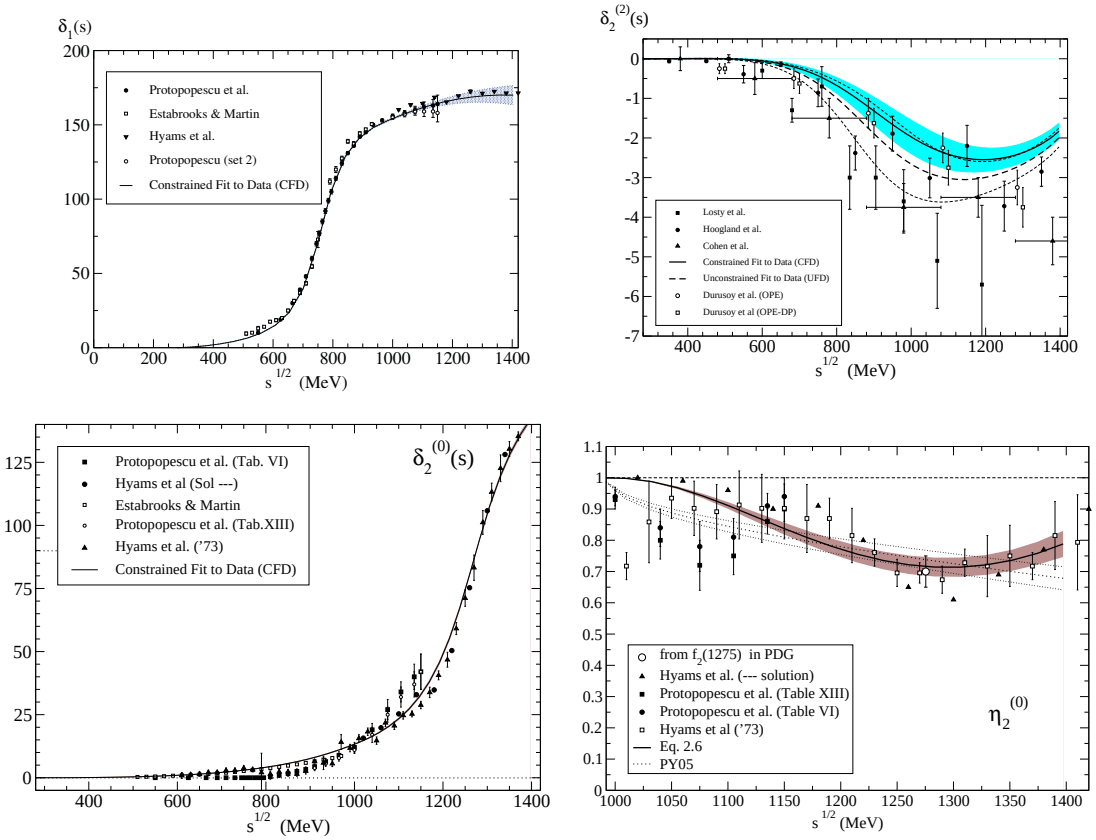

Figure 1.18: P, D0 and D2 waves, and D0 inelasticities from [149]. Experimental data are from [133, 136]. The Unconstrained Fit to Data (solid lines) are the starting point of our data analysis.

with an integral over the whole energy range, which provides information on the amplitude at energies where experimental data can be poor, or in the complex plane. As we saw in Section 1.5.4, the latter is specially important in order to study resonance properties whose poles are located in the complex plane on the second Riemann sheet.

Forward dispersion relations

The dispersion relations studied in Section 1.5.2, written for $t = 0$ (this corresponds to the *forward* or $z_s = 1$ direction), are known as Forward Dispersion Relations (FDR) [146, 147, 148, 149]. They can be written in a basis of $s \leftrightarrow u$ symmetric or antisymmetric amplitudes describing the processes $\pi^0\pi^0 \to \pi^0\pi^0$, $\pi^0\pi^+ \to \pi^0\pi^+$, and the amplitude corresponding to the process with isospin one in the t-channel T^{I_t}. In terms of the usual s-channel isospin states, this basis is written as:

$$T^{00} = \frac{1}{3}(T^0 + 2T^2), \quad T^{0+} = \frac{1}{2}(T^1 + T^2), \quad T^{I_t=1} = \frac{1}{3}T^0 + \frac{1}{2}T^1 - \frac{5}{6}T^2. \tag{1.197}$$

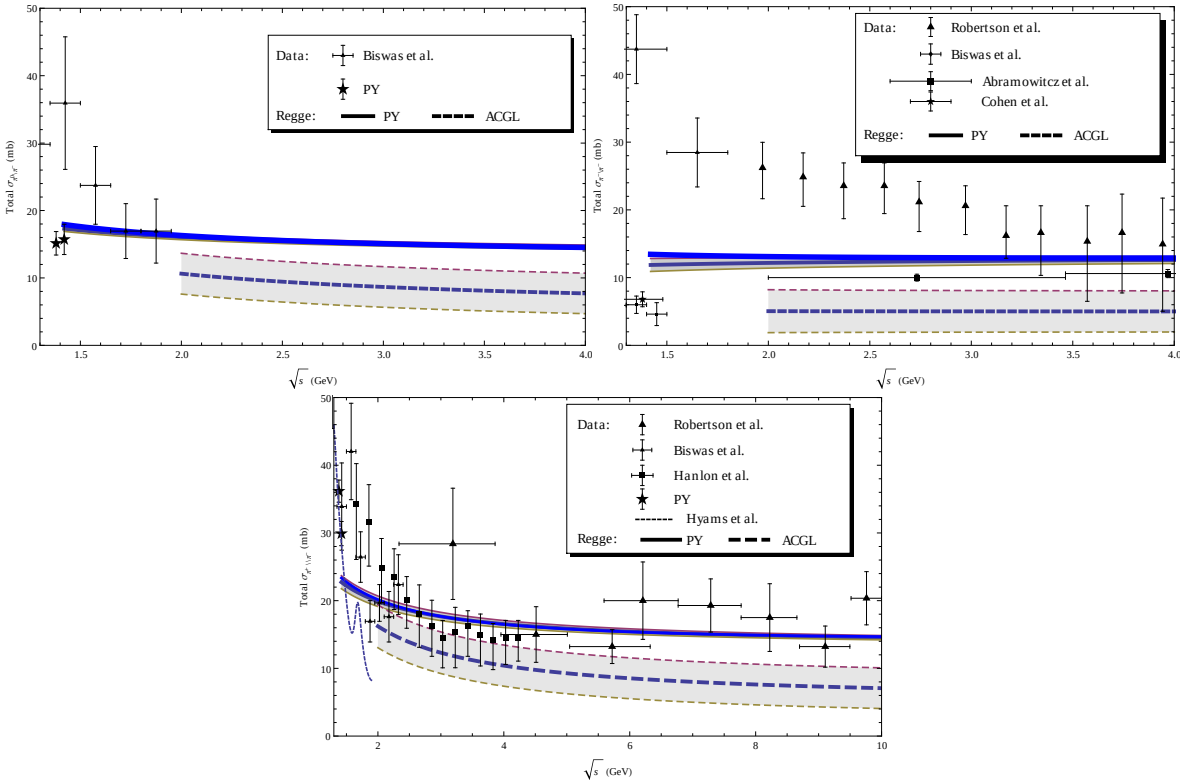

Figure 1.19: Total cross sections $\sigma_{\pi^0\pi^-}$, $\sigma_{\pi^-\pi^-}$, and $\sigma_{\pi^+\pi^-}$ from [163]. Black dots, triangles, and squares: experimental points from [164, 156, 165, 166, 139]. The stars at 1.38 and 1.42 GeV are from the phase shift analysis of experimental data given in [146]. Solid lines, from 1.42 GeV Regge formula from [146]. Dashed lines, above 2 GeV from [179]. Below 2 GeV, the dotted line corresponds to the $\pi^+\pi^-$ cross section from the Cern-Munich analysis.

Let us start with the $T^{00}(s,t,u)$ amplitude, which is symmetric under $s \leftrightarrow u$ crossing. Performing one subtraction at threshold in order to ensure convergence, at t=0, eq. (1.130) reads:

$$\begin{aligned} \mathrm{Re}T^{00}(s,0,u) - T^{00}(4m^2,0,0) &= \frac{(s-4m^2)}{\pi}\left[P\int_{4m^2}^{\infty} ds' \frac{\mathrm{Im}T^{00}(s',0,u)}{(s'-s)(s'-4m^2)}\right. \\ &\left. + \int_{4m^2}^{\infty} du' \frac{\mathrm{Im}T^{00}(s,0,u')}{(u'-u)u'}\right], \end{aligned} \tag{1.198}$$

Using the fact that the amplitude is even under crossing, so that: $T^{00}(s,t,u) = T^{00}(u,s,t)$, and that $u = 4m^2 - s$ at $t = 0$, we have:

$$\mathrm{Re}T^{00}(s) = T^{00}(4m_\pi^2) + \frac{(s-4m_\pi^2)}{\pi} P\int_{4m_\pi^2}^{\infty} ds' \frac{(2s'-4m_\pi^2)\mathrm{Im}T^{00}(s')}{s'(s'-s)(s'-4m_\pi^2)(s'+s-4m_\pi^2)}, \tag{1.199}$$

where we have specified that it is just a function of s.

For $\pi^0\pi^+ \to \pi^0\pi^+$ scattering, whose amplitude, $T^{0+}(s,t,u)$, is also symmetric under $s \leftrightarrow u$ crossing, we can obtain exactly the same result:

$$\mathrm{Re}T^{0+}(s) = T^{0+}(4m_\pi^2) + \frac{(s-4m_\pi^2)}{\pi} P\int_{4m_\pi^2}^{\infty} ds' \frac{(2s'-4m_\pi^2)\mathrm{Im}T^{0+}(s')}{s'(s'-s)(s'-4m_\pi^2)(s'+s-4m_\pi^2)}. \tag{1.200}$$

The reason for choosing these two amplitudes, which we will use in Section 2.1, is that as we can see from eq. (1.197), the amplitudes for $\pi^0\pi^0$ and $\pi^0\pi^+$ depend only on two isospin states, and have positivity properties, i.e. their imaginary parts are sums of positive terms. Because of this, the errors are much reduced for them.

For the antisymmetric $I_t = 1$ amplitude no subtractions are needed. Using the same procedure, we obtain:

$$\mathrm{Re}T^{I_t=1}(s) = \frac{2s-4m_\pi^2}{\pi}\, P\int_{4m_\pi^2}^{\infty} ds' \,\frac{\mathrm{Im}F^{I_t=1}(s',0)}{(s'-s)(s'+s-4m_\pi^2)}. \tag{1.201}$$

1.7.3 Sum rules

Other interesting dispersive techniques, that we will use in this thesis, are the so called sum rules, which relate the amplitude at some energy point with an integral over the whole energy region [146, 147, 148, 149]. They are particularly interesting when studied at threshold, so the amplitude can be expressed in term of the threshold parameters given in eq. (1.193).

For illustration, let us derive some of the sum rules used in Section 2.1. Writing an unsubtracted FDR for the quantity $\mathrm{Re}T^{I_s=1}(s)/(s-4m^2)$ we have:

$$\frac{\mathrm{Re}T^{I_s=1}(s)}{s-4m_\pi^2} = \frac{1}{\pi}\int_{4m^2}^{\infty}\frac{ds'\mathrm{Im}T^{I_s=1}(s')}{(s'-s)(s-4m_\pi^2)} + \frac{1}{\pi}\sum_{I_s} C_{su}^{1I_s}\int_{4m^2}^{\infty}\frac{ds'\mathrm{Im}T^{I_s}(s')}{s'(s'+s-4m_\pi^2)}, \tag{1.202}$$

where we have expressed the amplitude with definite isospin in the u-channel as a function of s-channel amplitudes through the crossing matrices of eq. (1.188). Since, for $s \to 4m_\pi^2$ we have:

$$\mathrm{Re}T^{I_s=1}(s) = 32\pi m_\pi \sum_J (2J+1)P_J(z_s=1)k^{2J}\left(a_J + b_J k^2 + \dots\right), \tag{1.203}$$

where the value $I = 1$ is assumed for the threshold parameters, then, at threshold, eq. (1.202) reads:

$$24\pi m_\pi a_1 = \frac{1}{\pi}\int_{4m^2}^{\infty}\frac{ds'\mathrm{Im}T^{I_s=1}(s')}{(s-4m_\pi^2)^2} + \frac{1}{\pi}\sum_{I_s} C_{su}^{1I_s}\int_{4m^2}^{\infty}\frac{ds'\mathrm{Im}T^{I_s}(s')}{s'^2},$$

which is known as Olsson sum-rule. Canceling a_1 with the Froissart-Gribov sum rule for this quantity [168, 146], and substituting the values of $C_{su}^{1I_s}$, we find the result:

$$\begin{aligned} I \;=\; & \int_{4m^2}^{\infty} ds \frac{\left(\mathrm{Im}T^{I_t=1}(s,4m_\pi^2,-s) - \mathrm{Im}T^{I_t=1}(s,0,4m_\pi^2-s)\right)}{s^2} \\ & - \int_{4m^2}^{\infty} ds \frac{8m_\pi^2(s-2m_\pi^2)\mathrm{Im}T^{I_s=1}(s,0,4m_\pi^2-s)}{s^2(s-4m_\pi^2)} = 0 \end{aligned} \tag{1.204}$$

Proceeding in the same way, it is possible to derive a second $\pi\pi$ sum-rule:

$$J = \int_{4m_\pi^2}^{\infty} ds \left(\frac{4\mathrm{Im}T'^{(0)}(s) - 10\mathrm{Im}T'^{(2)}(s)}{s^2(s-4m_\pi^2)^2} - 6(3s-4m_\pi^2)\frac{\mathrm{Im}T'^{(1)}(s) - \mathrm{Im}T^{(1)}(s)}{s^2(s-4m_\pi^2)^3}\right) = 0. \tag{1.205}$$

where $T'^{(I)}(s,t,u) \equiv \partial T^{(I)}(s,t,y)/\partial\cos\theta$, and the upper indices refer to isospin in the s-channel. These I and J sum rules will be used in Section 2.1 as additional constraints on the $\pi\pi$ parametrization, in addition to the Roy-like dispersion relations that we explain next.

Roy equations

Let us finally study the standard twice subtracted Roy equations [169]. They are an infinite set of coupled integral equations, which are equivalent to non-forward dispersion relations plus $s \leftrightarrow t$ crossing symmetry. They are written in terms of partial-waves amplitudes t_J^I of definite isospin and angular momentum, with the left-hand cut contribution rewritten as a series of integrals over the physical region. In this way, the left-hand cut, which cannot be obtained directly from data, is treated exactly. It is an important difference with the other dispersive methods that we use in this thesis, in particular, the N/D method, Section 1.6.2, neglects the left hand cut whereas the IAM, Section 1.6.3, approximates it by using ChPT. As we will see, Roy equations provide very precise results in the low-energy region and, since they include correctly the analytic structure of the partial-wave amplitudes, they can be analytically continued to the complex plane and used to find poles associated to resonances on the second Riemann sheet.

After the original article of Roy [169], they were used extensively by many authors in the seventies [170, 171, 172, 173, 174, 175, 176]. However, in the last decade, they have regained notoriety motivated by the success of ChPT and the recent and precise available $\pi\pi$-scattering data at very low energies [141, 154]. In particular, they have been used to improve the precision of scattering data and to discard spurious solutions [177], to test ChPT [83, 178], or to study the $\pi\pi$-scattering amplitude [179, 49, 50, 149].

The general structure of Roy equations is given by:

$$\mathrm{Re}\, t_J^I(s) = ST_J^I(s) + \sum_{J'=0}^{\infty}(2J'+1)\sum_{I'=0,1,2} P\int_{4m_\pi^2}^{\infty} ds' K_{JJ'}^{II'}(s',s)\mathrm{Im}\, t_{J'}^{I'}(s'),$$

where the subtraction terms $ST_J^I(s)$ and the kernels $K_{JJ'}^{II'}(s',s)$ are known functions. Therefore, Roy equations are expressed as a sum over all partial-waves and an integral over the physical cut. In practice, however, for the calculation that we will use in this thesis, they are truncated at $J < 2$ and at some energy cutoff s_0, treating the higher partial-waves and the high energy contributions as input, gathered in the so called driving terms. In [179], it has been proved that Roy equations are valid up to $\sqrt{s} \leq 8m_\pi \simeq 1120$ MeV.

In this thesis we have used the S0, S2 and P waves, which are given by:

$$\begin{aligned}\mathrm{Re}\, t_0^0(s) = a_0^0 + (2a_0^0 - 5a_0^2)\frac{s-4m_\pi^2}{12m_\pi^2} \\ + \sum_{J'=0,1}(2J'+1)\sum_{I'=0,1,2} P\int_{4m_\pi^2}^{s_0} ds' K_{0J'}^{0I'}(s',s)\mathrm{Im}\, t_{J'}^{I'}(s') + DT_0^0(s),\end{aligned} \tag{1.206}$$

$$\begin{aligned}\mathrm{Re}\, t_0^2(s) = a_0^2 - (2a_0^0 - 5a_0^2)\frac{s-4m_\pi^2}{24m_\pi^2} \\ + \sum_{J'=0,1}(2J'+1)\sum_{I'=0,1,2} P\int_{4m_\pi^2}^{s_0} ds' K_{0J'}^{2I'}(s',s)\mathrm{Im}\, t_{J'}^{I'}(s') + DT_0^2(s),\end{aligned} \tag{1.207}$$

$$\mathrm{Re}\, t_1^1(s) = (2a_0^0 - 5a_0^2)\frac{s-4m_\pi^2}{72m_\pi^2} + \sum_{J'=0,1}(2J'+1)\sum_{I'=0,1,2} P\int_{4m_\pi^2}^{s_0} ds' K_{1J'}^{1I'}(s',s)\mathrm{Im}\, t_{J'}^{I'}(s') + DT_1^1(s), \tag{1.208}$$

where we have explicitly separated the contributions from higher partial-waves and higher energy into the driving term $DT_J^I(s)$. Since Roy equations are derived with two-subtractions, the subtraction terms are strong s-dependence (proportional to s), which is the reason why they are very suitable for low energy studies [170, 171, 172, 173, 174, 175, 176], especially when further theoretical predictions are used for the subtraction terms [179, 49, 50]

However, at larger energies, the uncertainties of the scattering lengths, and in particular of the a_0^2, whose experimental knowledge is still poor, propagate proportionally to s becoming larger and larger as the energy increases. One of the main results of this thesis is the derivation of once-subtracted Roy like equation, which we discuss in Section 2.1. As we will see in that section, they have a much smaller uncertainty in the energy region above roughly 450 MeV, which implies that they provide a much more stringent constraint in that region. In appendix A, we give the derivation of Roy equations whereas the derivation of the once-subtracted version, called GKPY equations, is a result of this thesis and it is given in Section 2.1.

1.8 Regge Theory and Local Duality

Regge theory plays a key role in the description of the high energy hadron phenomenology. In this thesis, we will use it to parametrize the high energy contribution of the $\pi\pi$-scattering amplitude, Section 2.1. In addition, it can be used to constrain the dynamics of the low energy meson interactions, through the so-called finite-energy sum-rules. This property is known as duality and we will make use of it in Section 2.2, when studying the nature of the lightest scalars. Therefore, in this section we will give a short motivation to Regge theory, which is used to introduce duality. In appendix B we briefly derive the Regge representation of the scattering amplitude. For further details we refer to the references [180, 181, 106, 107].

1.8.1 Basic Regge pole theory

Experimentally, it has been observed for long an important recurrence property: particles with the same quantum numbers and signature (τ), which for mesons is defined as $\tau = (-1)^J$, can be represented in a common trajectory, known as Regge trajectory, on a plot of angular momentum versus mass square [182, 183]. An extraordinary feature of these trajectories is that for mesons, they can be approximated by straight lines in the Mandelstam variable t,

$$\alpha(t) = a + bt, \tag{1.209}$$

where a and b are constant, which must be determined experimentally, and $\alpha(t)$ is the so-called Regge trajectory, independent of s, which satisfies that at the meson mass M_R, $\alpha(M_R^2) = J_R$, where J_R is the meson angular momentum.

Let us provide a simple and heuristic derivation of the Regge behaviour. For this, we start by studying the t-channel exchange of a single meson of momentum J and mass M_J. Neglecting the widht, the amplitude of such exchange can be written as [180, 181, 106]:

$$T(s,t) \simeq \frac{g_J^2 P_J(z_t)}{M_J^2 - t}. \tag{1.210}$$

For high values of s, $t < 0$ and $P_J(z_t) \sim z_t^J$. Assuming that this exchange is produced in a scattering process of equal mass particles, which is the case used in this thesis, we know from eq. (1.105), that the scattering angle is given by:

$$z_t = 1 + \frac{2s}{t - 4m^2}. \tag{1.211}$$

so $P_J(z_t) \sim (-s)^J$ and eq. (1.212) reads:

$$T(s,t) \sim \frac{g_J^2 (-s)^J}{M_J^2 - t}. \tag{1.212}$$

If we suppose that the exchanged particle is a member of a Regge trajectory, for example with negative signature, i.e. $J = 1, 3, 5, , \cdots$, then, the scattering amplitude due to the contribution of all the meson exchanges on that trajectory can be expressed as:

$$T(s,t) \sim \sum_{J=0}^{\infty} \frac{g_J^2}{M_J^2 - t} \left(\frac{(-1)^J - 1}{2} \right) s^J. \tag{1.213}$$

However, assuming that the coupling constants are equal for all the exchanges, and that the Regge trajectory is given by eq. (1.209), so $M_J^2 = (J - a)/b$, then the series sum can be expressed in closed form as [180]:

$$T(s,t) \sim -\sum_i \frac{g^2 b \pi}{2} \frac{\left(1 - e^{-i\pi\alpha_i(t)}\right)}{\sin \pi\alpha_i(t)} s^{\alpha_i(t)} \sim \sum_{i=1} \beta_i(t) s^{\alpha_i(t)} \tag{1.214}$$

where i denotes the position of each exchange in the Regge trajectory. Eq. (1.214) is the Regge or high energy representation of the scattering amplitude, for odd signature exchanges. The representation for even signature exchanges, can also be expressed like eq. (1.214). The conditions on which the general proof are based can be considerably relaxed and are given in Appendix B. A more rigorous derivation can be found in [180, 181, 106, 107].

1.8.2 Finite-energy sum rules

In this section we are going follow the derivation given in [107] to introduce the concept of finite energy sum rules, which we will use in Section 2.2.

We have seen in Section 1.5 that for the elastic s-channel process: $1 + 2 \to 1 + 2$, the u-channel related process is: $1 + \bar{2} \to 1 + \bar{2}$. For most physical scattering processes, amplitudes are neither symmetric nor antisymmetric under this crossing, but in particular, the

$\pi\pi$-scattering amplitude with well defined isospin in the t-channel, is symmetric for $I_t = 0, 2$ and antisymmetric for $I_t = 1$. This symmetry can be easily reflected by writing the amplitudes as a function of $\nu = (s+u)/2$ since:

$$T^{I_t=0,2}(\nu, t) = T^{I_t=0,2}(-\nu, t), \quad T^{I_t=1}(\nu, t) = -T^{I_t=1}(-\nu, t). \tag{1.215}$$

We can write fixed-t dispersion relations for these amplitudes. In particular for the anti-symmetric one, we have:

$$\begin{aligned} \mathrm{Re}T^A(\nu, t) &= \frac{\nu}{\pi}\left[P\int_{\hat{t}}^{\infty} d\nu' \frac{\mathrm{Im}T^A(\nu'+i\epsilon, t)}{\nu'-\nu} + P\int_{-\infty}^{-\hat{t}} d\nu' \frac{\mathrm{Im}T^A(\nu'+i\epsilon, t)}{\nu'-\nu}\right] \\ &= \frac{2\nu}{\pi} P\int_{\hat{t}}^{\infty} d\nu' \frac{\mathrm{Im}T^A(\nu'+i\epsilon, t)}{\nu'^2-\nu^2}, \end{aligned} \tag{1.216}$$

where $\hat{t} = t/2 + 2m^2$ and, for simplicity, we have omitted the subtractions constants. For values of $t \geq -4m^2$ in the s-channel, $\mathrm{Im}T^A(\nu'+i\epsilon, t)$ is zero for values of ν' below the physical threshold, so we can set $\hat{t} = 0$.

If $T(\nu, t)$ goes to zero faster than ν^{-1} as $\nu \to \infty$, then multiplying eq. (1.216) by ν and taking the limit $\nu \to \infty$, we have:

$$\lim_{\nu\to+\infty} \nu \mathrm{Re}T^A(\nu, t) = \lim_{\nu\to+\infty} \frac{2}{\pi} P\int_0^{\infty} d\nu' \frac{\nu^2\, \mathrm{Im}T^A(\nu'+i\epsilon, t)}{\nu'^2-\nu^2} = 0 \tag{1.217}$$

which leads to the super-convergence relation:

$$\int_0^{\infty} d\nu' \mathrm{Im}T^A(\nu', t) = 0. \tag{1.218}$$

However, this is just the limit where Regge Theory provides information on the behaviour of $T^A(\nu, t)$. Therefore, assuming that the large-ν behaviour of $T^A(\nu, t)$ is dominated by the sums of Regge poles given in eq. (1.214), we have that:

$$T^A(\nu, t) \sim T^A_{\mathrm{Regge}}(\nu, t) = \sum_i \beta_i(t)\nu^{\alpha_i}(t), \tag{1.219}$$

If we define now $\bar{T}(\nu, t)$ as the transition amplitude which only sum over those Regge poles for which $\alpha_i(t) \leq -1$:

$$\bar{T}^A(\nu, t) = T^A(\nu, t) - \sum_j \hat{\beta}_j(t)\nu^{\hat{\alpha}_j}(t), \tag{1.220}$$

where $\hat{\alpha}_j(t) \geq -1$. Then, $\bar{T}^A(\nu, t)$ decreases faster than ν^{-1} as $\nu \to \infty$ and satisfies the superconvergence relation of eq. (1.218), so:

$$\int_0^{\infty} d\nu' \mathrm{Im}\bar{T}^A(\nu', t) = \int_0^{\infty} d\nu' \left(\mathrm{Im}T^A(\nu, t) - \mathrm{Im}T^A_{\mathrm{Regge}}(\nu, t)\right) = 0. \tag{1.221}$$

However, eq. (1.219) is only the asymptotic representation of $T^A(\nu', t)$. If we suppose now that it is a good numerical approximation to $T^A(\nu, t)$ for $\nu > \bar{\nu}$, so that eq. (1.221) receives a

negligible contribution from values of ν greater that $\bar{\nu}$, then we can replace the upper limit of eq. (1.221) by $\bar{\nu}$. Therefore, using in eq. (1.221) the definition of $\bar{T}(\nu,t)$ given in eq. (1.220) and performing the integration over the Regge-pole terms, we obtain that:

$$\int_0^{\bar{\nu}} d\nu \mathrm{Im} T^A(\nu,t) = \sum_j \mathrm{Im}\hat{\beta}_j(t)\bar{\nu}^{\hat{\alpha}_j(t)+1}/(\hat{\alpha}_j(t)+1). \tag{1.222}$$

This relation is known as finite energy sum rule (FESR) [184, 185]. For a amplitude symmetric under $s \leftrightarrow u$, we can apply the same argument to $\nu T^S(\nu,t)$ to obtain a similar finite energy sum rule [107]:

$$\int_0^{\bar{\nu}} d\nu \nu \mathrm{Im} T^S(\nu,t) = \sum_j \mathrm{Im}\hat{\beta}_j(t)\bar{\nu}^{\hat{\alpha}_j(t)+2}/(\hat{\alpha}_j(t)+2). \tag{1.223}$$

If the convergence criteria are not satisfied, we can apply the same arguments to $T^A(\nu,t)/\nu^{2n}$ and $T^S(\nu,t)/\nu^{2n+1}$, where n is an integer number. Finite energy sum rules relate the Regge pole parameters $\alpha_i(t)$ and $\beta_i(t)$ to low energy amplitudes. In the case of amplitudes dominated at low energies by resonances, this leads to a relation between Regge poles and resonances known as duality.

1.8.3 Duality and semi-local Duality

On the one hand, FESRs can be used as phenomenological tools for obtaining information about Regge poles by using low energy amplitudes, since at low energies, phase-shift analyses determine the decomposition into individual amplitudes when assuming that only a few partial-waves contribute to them. On the other hand, they can be used to constraint low energy dynamics.

The role of the upper integration limit $\bar{\nu}$ is crucial in this procedure. Eqs (1.222) and (1.223) are only valid for ν such that the Regge representation of $T(\nu,t)$ is a good approximation for $\nu > \bar{\nu}$. However, phase shift analysis is only possible for energies lower than those, and in practice $\bar{\nu}$ has as taken to be the upper limit of the phase-shift analysis, corresponding to values of $\sqrt{s}$ between 1 and 2 GeV. This effect can be seen by writing eq. (1.222) as:

$$\int_0^{\bar{\nu}} d\nu \mathrm{Im}(T^A(\nu,t) - T^A_{\mathrm{Regge}}(\nu,t)) = 0, \tag{1.224}$$

which states that Regge theory describes on the average the amplitude at low energies. Nevertheless, if we cut off the integral at low energies, then we are assuming that this property takes place even for smaller intervals, which is known as semi-local duality. In Section 2.2, where we will show for $\pi\pi$-scattering that eq. (1.224) holds for $\sqrt{\nu} \sim \sqrt{1}$ GeV, indeed.

As we will see in Section 2.2, we will use this phenomenological feature to study the nature of the lightest scalar resonances. The $I_t = 2$ $\pi\pi$-scattering amplitude is an exotic one, where there are no resonances to contribute. This can be understood from the small value of the Regge trajectory in that channel, due to a cancellation between the $I_s = 0$ and $I_s = 1$ amplitudes, which are dominated by the $f_0(500)$ and $\rho(770)$ respectively. However, as we will see in Section 2.2, the different nature with N_c of the $\rho(770)$ and $f_0(500)$ might spoil in principle such cancellation at large N_c, which has to be checked explicitly. This is a general

problem for all models that predict a different N_c behaviour for these two resonances. In Section 2.2, we will show how unitarized ChPT avoids this conflict.

1.9 Chiral symmetry restoration and Finite-Temperature Field Theory

Despite chiral symmetry being broken at zero temperature (T), it is expected that in a hot and dense medium chiral symmetry gets restored [186]. The chiral symmetry restoration is a milestone in our present understanding of hadronic physics under extreme conditions of temperature and density and has been one of the main motivations for the development of the present program of relativistic heavy ion collisions and reactions in nuclear matter at RHIC, CERN (ALICE) and FAIR.

The main properties of the chiral symmetry transition have been considerably clarified during the last decades, due to the improvement of lattice data at finite temperature [187, 188, 189, 190, 191, 192, 193]. Now is widely believed that the chiral symmetry restoration takes place in the same range as deconfinement, in a crossover-like transition for $N_f = 3$, becoming of second order for $N_f = 2$. The transition temperature lies within the range $T_c \sim$ 150-175 MeV. It is important to remark that since the transition is a crossover for $N_f = 3$, we cannot talk about a critical temperature (T_c) but about a transition range, which can be established by looking at different order-like parameters, which can give different values for T_c.

The parameters used in the analysis of the chiral symmetry restoration are the quark condensate and its corresponding susceptibility. At non-zero temperatures, the correlation between a quark anti-quark pair reduces, and the quark-condensates decrease in absolute value, showing a drastic change as T increases, which makes it an useful tool in order to study the chiral symmetry restoration. The scalar susceptibilities of the QCD vacuum describe its response to any scalar field, and are defined as first derivatives of quark condensates with respect to quark masses. Therefore, susceptibilities measure fluctuations of the associated order parameter and can be expressed in terms of current correlators. Thus, the scalar susceptibility provides direct information about the transition and its nature, since they tend to peak around the transition point reflecting the change of correlations. Another possible way to study chiral restoration is through the degeneration of current correlators which behave as chiral partners. In particular, this would imply that the scalar and pseudoscalar susceptibilities should become approximately degenerate as medium effects, such as temperature and density, are increased. This would be a particular realization of the earlier proposal of the $\pi - \sigma$ meson degeneracy [194] and has been studied in nuclear matter, where it has been found that to leading order the pseudoscalar susceptibility decreases as the quark condensate [260]. Quark condensates and scalar and pseudoscalar susceptibilities will be analyzed in Section 2.3 of this thesis.

A useful approach, which has proven to be quite successful to describe thermodynamic quantities as compared to lattice data [197, 198, 193], is the Hadron Resonance Gas (HRG), Within the HRG approach, the free contribution of all known physical hadron states is considered.

In addition, the low-temperature meson gas can be described by Chiral Perturbation Theory in a model-independent and systematic way, using the imaginary time formalism or the virial approach. In early studies using these descriptions [196], extrapolations of the condensate and other quantities to the transition region gave a qualitatively reasonable description of the relevant physics. Furthermore, in the last few years, there has been an important development of the ChPT-framework description of the meson gas properties, using unitarized techniques [199, 200, 201, 202]. In Section 2.3 of this thesis, we will use these formalisms in order to perform our analysis about the role of scalars in the chiral symmetry restoration. Therefore, in the rest of this Section, we will review the main properties of both formalisms.

1.9.1 Imaginary time formalism

In this section we only give the main ideas of the imaginary time formalism, as well as the formulas we use in order to study the thermal dependence of quark condensate and scalar susceptibilities. In Appendix C we derive this formalism.

The imaginary time formalism is based in performing an analytical continuation from $t \to -i\tau$ [203, 204], i.e. from the Minkowski to the Euclidean space. In this way, the partition function, which describes the statistical properties of a system at temperature T, in thermodynamic equilibrium is defined as:

$$Z_\beta \equiv \mathrm{Tr}[\mathrm{e}^{-\beta\hat{H}}] = \int \mathcal{D}\Phi(x)\mathrm{e}^{-S_E(\beta)}, \tag{1.225}$$

where S_E is the euclidean action, which in the case of interest in this thesis, the analysis of scalar fields $\Phi(x)$, is defined as:

$$S_E(\beta) = \int_0^\beta d^4x \left(\frac{1}{2}\partial^\mu\Phi\partial_\mu\Phi + \frac{1}{2}m^2\Phi(x)^2 + V(\phi(x))\right). \tag{1.226}$$

with $x = (\tau, \mathbf{x})$, $\int_0^\beta d^4x = \int_0^\beta d\tau \int d^3x$ and $\beta = 1/T$.

Thus, the partition function eq. (1.225) can be understood as a generating functional in imaginary time in a finite interval, i.e. with $t \to -i\tau$ and $\tau \in [0, \beta]$. Hence, by means of an analytical continuation, the imaginary time formalism relates quantum field theory and quantum statistics [203, 204]. In this way a propagator in imaginary time is defined as:

$$G(x-y) = \frac{1}{Z(\beta)}\int D_\Phi\Phi(x)\Phi(y)\mathrm{e}^{-S_E(\beta)}. \tag{1.227}$$

In the free case, the Fourier transform of eq. (1.227), $G_0(\tau, k)$, is given by.

$$G_0(\tau, k) = \sum_n \mathrm{e}^{-iw_n\tau}\Delta_0(iw_n, k), \tag{1.228}$$

where $w_n = (2\pi n)/\beta$ are known as Matsubara frequencies and $\Delta_0(iw_n, k)$ is the so-called Matsubara propagator, which is defined as:

$$\Delta_0(iw_n, k) = \left(w_n^2 + w_k^2\right)^{-1}, \tag{1.229}$$

with $w_k = \left(k^2 + m^2\right)^{1/2}$. Therefore, the thermal free-propagator in position space will be given by:

$$G_0(x) = \int \frac{d^3k}{(2\pi)^3} \mathrm{e}^{ik\cdot x} G_0(\tau, k) \tag{1.230}$$

From eq. (1.230), we can see that when obtaining Feynman rules at finite T, we will have to deal with sums over functions of Matsubara frequencies, known as Matsubara sums. A useful technique to compute these sums is based on Cauchy's Theorem by using a convenient contour of integration. If we have a complex function $f(z)$ without any cut, which goes to zero fast enough as $z \to \infty$ then

$$T\sum_n f(iw_n) = -\sum_{i_{\text{poles}}} \frac{\text{Res}(f; z = z_i)}{\mathrm{e}^{\beta k_0} - 1}. \tag{1.231}$$

In Section 2.3, we will have to deal with two different Matsubara sums, which appear in the quark condensate and the scalar susceptibility. The first one is the meson tadpole, which is appears in the quark condensate and is given by:

$$\begin{aligned} G_0(0) &= \int \frac{d^3k}{(2\pi)^3} T\sum_n \Delta_0(iw_n, k) = \int \frac{d^3k}{(2\pi)^3} T\sum_n \frac{1}{w_n^2 + E_K^2} \\ &= \int \frac{d^3k}{(2\pi)^3} \frac{1}{2E_K} + \int \frac{d^3k}{(2\pi)^3} \frac{1}{E_K} \frac{1}{e^{\beta E_k} - 1} = G_0^0(0) + g_1(m, T), \end{aligned} \tag{1.232}$$

where:

$$G_0^0(0) = \int \frac{1}{(2\pi)^4} \frac{1}{k^2 + E_K^2}, \tag{1.233}$$

is the usual $T = 0$ meson divergent tadpole that needs renormalization and we have defined:

$$g_1(m, T) = \int \frac{d^3k}{(2\pi)^3} \frac{1}{E_K} \frac{1}{e^{\beta E_k} - 1} = \frac{1}{2\pi^3} \int_0^\infty dk \frac{k^2}{E_K} \frac{1}{e^{\beta E_k} - 1}, \tag{1.234}$$

which is the temperature dependent contribution to $G_0(0)$, which is a well defined finite quantity. The other thermal quantity that we need because it will appear in the scalar susceptibility in Section 2.3 is:

$$\int_0^\beta d^4x G_0(x)^2 = -\frac{d}{dm^2} G_0(0). \tag{1.235}$$

which implies that we will need the thermal function:

$$g_2(m, T) = -\frac{dg_1(m, T)}{dm^2} = \frac{1}{4\pi^2} \int_0^\infty dk \frac{1}{E_K} \frac{1}{e^{\beta E_k} - 1}. \tag{1.236}$$

1.9.2 Virial expansion

The virial expansion is a simple and successful approach already applied to describe many thermodynamical properties of dilute gases [205]. In particular, it has been applied to a dilute gas made of pions [205, 206, 207] or other hadrons [196, 208], which allows us to parametrize efficiently the effect of interactions in the partition function. States of more energy are weighted by Boltzmann factors and then become more relevant as the system approaches

the transition. Thus, in this approach and at low temperatures, it is more important to include accurately the interaction of the lightest mesons, e.g. via unitarization methods, while the heavier ones can be added as free states.

As we have commented above, the thermodynamics of a system of hadrons is encoded in the free energy density, which is defined as:

$$z = -\lim_{V\to\infty} \frac{1}{\beta V} \log Z = \epsilon_0 - P, \tag{1.237}$$

where ϵ_0 is the free energy density at $T = 0$, and P stands for the thermodynamic pressure $P = z^{T=0} - z$. Since in this thesis we are interested in the low energy dynamics, we will onsider a multi-component interacting relativistic gas made of pions, kaons and etas in thermal and chemical equilibrium, so the pressure only depends on the temperature T. Thus, the second order relativistic virial expansion of the pressure reads [206]:

$$\beta P = \sum_i \left(B_i^{(1)}(T)\xi_i + B_i^{(2)}\xi_i^2 + \sum_{j\geq i} B_{ij}^{\text{int}}\xi_i\xi_j \right), \tag{1.238}$$

where $i = \pi, K, \eta$, the fugacities $\xi_i = e^{-\beta M_i}$, $\beta = 1/T$, M_i is the mass of the i species and $B(T)$ are the virial coefficient for the gas. Expanding up to the second order in ξ_i means that we only consider binary interactions. The coefficients

$$B_i^{(n)} = \frac{g_i}{2\pi^2 n} \int_0^\infty dp\, p^2 e^{-n\beta(\sqrt{p^2+M_i^2}-M_i)}, \tag{1.239}$$

where the degeneracy is $g_i = 3, 4, 1$ for π, K, η respectively, correspond simply to the virial expansion for a free boson gas:

$$\beta P_{\text{free}} = -\sum_i \frac{g_i}{2\pi^2} \int_0^\infty dp\, p^2 \log\left[1 - e^{-\beta(\sqrt{p^2+M_i^2})}\right]. \tag{1.240}$$

The above free result is nothing but the HRG approach mentioned above, for the case of only the lightest hadrons π, K, η. Moreover, the virial expansion provides naturally the corrections to the HRG due to interactions, which appear through the S-matrix. For the meson-meson interactions, relevant for this work, these can be recast in terms of the elastic scattering phase-shifts. In this way, we can write [196]:

$$B_{ij}^{\text{int}} = \frac{\xi_i^{-1}\xi_j^{-1}}{2\pi^3} \int_{M_i+M_j}^\infty dE\, E^2 K_1(E/T) \sum_{I,J,S} (2I+1)(2J+1)\delta_{I,J,S}^{ij}(E), \tag{1.241}$$

where K_1 is the first modified Bessel function and the $\delta_{I,J,K}^{ij}$ are the $ij \to ij$ elastic scattering phase-shifts of a state ij with quantum number I, J, S (isospin, angular momentum and strangeness). The virial expansion breaks down typically where the dilute gas expansion does, for $T \sim 200$ MeV [207], but it provides a reasonable description for the physics below the chiral transition.

Results

In this chapter we present the main results obtained in this thesis divided in three different sections. In the first one, we include our works on $\pi\pi$-scattering, combining the analysis of experimental data with theoretical constraints in the form of dispersion relations. This analysis allows us to obtain a precise and model independent determination of phase shifts, inelasticities and the position of the lightest poles that appear at low energies in the scalar isoscalar wave, i.e. the σ or $f_0(500)$ and the $f_0(980)$, and their coupling to two pions.

In the second section, we analyze the nature of the lightest resonances by using different ChPT unitarization methods, namely the IAM and N/D, together to the $1/N_c$ expansion, and other phenomenological features as semi-local duality and spectral sum rules. All these tools are used to constrain the dynamics of the lightest resonances, and to shed some light about their nature. We also analyze in this Section the $1/N_c$ meson couplings of the most representative states, described in terms of quarks and gluons, with the same quantum numbers than the $f_0(500)$ resonance. Finally, we use these previous studies to describe the σ meson as a mixing of different QCD states, whose proportion we estimate.

In the third and last Section, we study the influence of the $f_0(500)$ in chiral symmetry restoration, by studying the properties of four-quark condensates and scalar susceptibilities within ChPT, both a $T = 0$ and at $T \neq 0$.

2.1 Properties of the lightest scalars from a dispersive $\pi\pi$-scattering analysis.

2.1.1 Motivation

As we have reviewed in Section 1.7, a precise determination of the $\pi\pi$-scattering amplitude at low energies is relevant for the study of Chiral Perturbation Theory, quark masses, the chiral condensate and, at intermediate energies, for the properties of the controversial σ meson as well as those of the $f_0(980)$ resonance, whose analysis is the main object of study in this thesis. Furthermore, their phase-shifts and inelasticities are also relevant for many other hadronic processes where the final state is made of two or more pions. These hadronic processes are

the subject of an intensive experimental and theoretical study. Nevertheless, as we have seen in Section 1.7, the existing experimental information from $\pi\pi$-scattering has many conflicting data sets at intermediate energies and for many years, very few data close to the interesting threshold region. This situation has made it very hard to obtain conclusive results on $\pi\pi$-scattering at low energies or even in the σ region. However, there has been a renewed interest in this process, due to the recent and precise experiments on kaon decays [141, 154] related to $\pi\pi$-scattering at very low energies, but also on the theoretical side due to the use of dispersive techniques, sometimes combined with ChPT [179, 49, 146, 147, 50, 148, 149]. In addition, there is a worldwide experimental effort studying decays of heavier mesons like Φ, D or B into final states with π's.

As we have studied in Sections 1.5.2 and 1.7, the dispersive integral formalism is model independent, just based on analyticity and crossing, and relates the $\pi\pi$ amplitude at a given energy with an integral over the whole energy range, increasing the precision and providing information on the amplitude at energies where data are poor, or in the complex plane. In addition, it makes the parametrization of the data irrelevant once it is included in the integral and relates different scattering channels among themselves.

In a series of works [146, 147, 148, 149], the Madrid-Krakow group has used a dispersive approach, to built a $\pi\pi$-scattering amplitude which incorporates analyticity, unitarity and crossing symmetry, using as a starting point, a set of simple expressions used to parametrize the available experimental data. They shared a common methodology. First, simple parametrizations to data were given, in which each partial wave amplitude was fitted independently to data in that channel only. These parametrizations were then checked against dispersion relations, and in the case they were reasonably well satisfied, these parametrizations were used as a starting point for a Constrained Fit to Data, in which dispersion relations were imposed as an additional constraint to the data fits. Therefore, the set so obtained was a consistent description of the $\pi\pi$-scattering amplitude.

Particularly, in the last of these works, the authors completed and improved the fits to experimental $\pi\pi$-scattering amplitudes obtained in the previous two papers, by including the latest NA48/2 data to that date [154], as well as other reliable data from K_{l4} decays [153, 140, 209]. Then, they repeated the fits including as constraints forward dispersion relations (FDR), Roy equations below $\bar{K}K$ threshold and sum rules. These constrained scattering amplitudes verified very accurately FDR, sum rules and, especially, Roy equations, and changed very little from the one obtained by just fitting data. Therefore, these improved parametrizations provide a reliable representation of pion-pion amplitudes with which one can test various physical relations.

However, since the publication of that work, a calculation has appeared [155] to take into account the fact that the data in K_{l4} decays have a larger than expected isospin correction due to the different thresholds of the charged and neutral two pion channels. Moreover, it was suggested [210] that the matching between low and intermediate energy parametrizations of the Madrid-Krakow S0 wave, with a discontinuity in the phase shift derivative at the matching point, could be a source of important errors.

Finally, as we have explained in Section 1.1.3, the status and properties of the $f_0(500)$ resonance, illustrated in Fig. 1.4, was calling for further model independent data analysis.

2.1.2 Outline of the results

The results of this section have been published in two research articles that we append in the next Sections, 2.1.3 and 2.1.4.

In the publication of Section 2.1.3, we continue the previous analysis in order to update the experimental input in order to include the latest NA48/2 data, which takes into account the isospin violation corrections proposed in [155], and to improve the S0 wave intermediate energy parametrization by imposing a continuous derivative in the phase matching. Furthermore, as we have commented in Section 1.7, we prove that only one subtraction is needed in order to derive a set of dispersion relations similar to Roy's, which we have called GKPY equations. The most relevant feature of the GKPY equations, is the very slow increase of the uncertainty as the energy grows, due to the fact that, contrary to the Roy equation case, the GKPY subtraction terms are constant and the uncertainties they produce do not grow with increasing energy. Therefore, these new one-subtracted dispersion relations are very well suited for constraining our amplitudes in the intermediate energy region, which allows us to improve the S0 wave parametrization in this controversial region. Finally, we also extend the range for which we apply both GKPY and Roy equations. Note that, until now, they had been used as constraints up to $\sqrt{s} \sim 932$ MeV by the Madrid-Krakow group and up to 800 MeV in [49], whereas in our work they are extended up to $\sqrt{s} \sim 1.1$ GeV in order to describe properly the $f_0(980)$ region near the $\bar{K}K$ threshold. The results we obtain can be summarized as follows:

- We present the GKPY equations, providing a detailed account of all the kernels and studying their expected threshold behaviour. In addition, we study and compare the way uncertainties are propagated through Roy and GKPY equations, concluding that Roy Equations are most suitable for studying the low energy region, whereas GKPY equations provide a better precision for $\sqrt{s} > 500$ MeV. We also extend the Roy and GKPY analysis to 1.14 GeV, in order to improve the description of the controversial $f_0(980)$.

- We obtain an Unconstrained Fit to Data (UFD) set of parametrizations for the S0, S2, P, D0, D2, and F waves, as well as for the high energy region, solving the caveats raised in the literature. In particular, we improve the intermediate S0 wave parametrization by imposing a continuous matching with continuous derivative.

- We then impose Roy and GKPY equations, FDR and the sum rules derived in eqs. (1.204) and (1.205) to the previous UFD set. As a result, we obtain very consistent and easy to use parametrizations which satisfy well all dispersion relations within errors, uniformly throughout the whole energy range. This we call the "Constrained Fit to Data" (CFD) set. In order to have this, the intermediate energy S0 wave parameters change about 0.8 standard deviations respect to the UFD.

- We have obtained precise values of S, P, D and F scattering lengths and slopes by means of sum rules, which are compatible with experimental and previous theoretical determinations [179, 49].

- We obtain the position of the S0 and S2 wave Adler zeros by means of Roy and GKPY equations, and find them to be in very good agreement with existing ChPT predictions.
- The use of the GKPY equations allow us to show that the sudden drop around 1050 MeV in the S0 wave inelasticity, or dip solution, is clearly favored with respect to the non-dip solution. Actually, for the non-dip inelasticity scenario to fulfill dispersion relations, it would require a very poor description of the phase-shift data, even when allowing for large systematic uncertainties.

In the publication of Section 2.1.4, we used the dispersive Roy and GKPY equations obtained in publication 2.1.3, to perform an analytic extrapolation to the complex plane of these partial-wave amplitudes in a model independent way. As we have studied in Section 1.5.4, this allows us to look for poles on the second Riemann sheet. The results we obtain can be summarized as follows:

- We determine, in a very precise and model independent way, the $f_0(500)$, $\rho(770)$ and $f_0(980)$ poles from data with no further theoretical inpunt using both Roy and GKPY equations.
- The poles that we obtain from both sets of equations are very compatible. The one obtained with GKPY equations has smaller uncertainties, and is taken to be the most reliable one.
- We also provide for each resonance its coupling to two pions defined from the pole residue.

As we have commented in Section 1.1.3, the $f_0(500)$ pole position determination given in publication 2.1.4, together with other recent dispersive analysis, have trigger the substantial revision of the $f_0(500)$ properties in the last PDG edition [11].

2.1.3 Publication: R. Garcia-Martin, R. Kaminski, J.R. Pelaez, J. Ruiz de Elvira, F.J. Yndurain, *The Pion-pion scattering amplitude. IV: Improved analysis with once subtracted Roy-like equations up to 1100 MeV, Phys. Rev.* D83 (2011) 074012

PHYSICAL REVIEW D **83,** 074004 (2011)

Pion-pion scattering amplitude. IV. Improved analysis with once subtracted Roy-like equations up to 1100 MeV

R. García-Martín,[1] R. Kamiński,[2] J. R. Peláez,[1] J. Ruiz de Elvira,[1] and F. J. Ynduráin[3,*]

[1]*Departamento de Física Teórica II, Universidad Complutense de Madrid, 28040 Madrid, Spain*

[2]*Department of Theoretical Physics, Henryk Niewodniczański Institute of Nuclear Physics, Polish Academy of Sciences, 31-342, Kraków, Poland*

[3]*Departamento de Física Teórica, C-XI Universidad Autónoma de Madrid, Canto Blanco, E-28049, Madrid, Spain*

(Received 26 November 2010; revised manuscript received 7 February 2011; published 4 April 2011)

We improve our description of $\pi\pi$ scattering data by imposing additional requirements on our previous fits, in the form of once-subtracted Roy-like equations, while extending our analysis up to 1100 MeV. We provide simple and ready to use parametrizations of the amplitude. In addition, we present a detailed description and derivation of these once-subtracted dispersion relations that, in the 450 to 1100 MeV region, provide an additional constraint which is much stronger than our previous requirements of forward dispersion relations and standard Roy equations. The ensuing constrained amplitudes describe the existing data with rather small uncertainties in the whole region from threshold up to 1100 MeV, while satisfying very stringent dispersive constraints. For the S0 wave, this requires an improved matching of the low and high energy parametrizations. Also for this wave we have considered the latest low energy $K_{\ell 4}$ decay results, including their isospin violation correction, and we have removed some controversial data points. These changes on the data translate into better determinations of threshold and subthreshold parameters which remove almost all disagreement with previous chiral perturbation theory and Roy equation calculations below 800 MeV. Finally, our results favor the dip structure of the S0 inelasticity around the controversial 1000 MeV region.

DOI: 10.1103/PhysRevD.83.074004 PACS numbers: 12.39.Fe, 11.15.Pg, 12.39.Mk, 13.75.Lb

I. INTRODUCTION

In a series of papers [1–3] that we will denote by PY05, KPY06, and KPY08, respectively, we have provided several sets of precise phenomenological fits to $\pi\pi$ scattering data. The interest in a precise and model-independent description of the data available in this process is twofold: On the one hand, it could be used at low energies to extract information about the parameters of chiral perturbation theory (ChPT) [4], quark masses, and the size of the chiral condensate, pionic atom decays, or CP violation in the kaonic system. On the other hand, in the intermediate energy region, it could provide model-independent information to identify the properties of hadronic resonances, particularly the scalar ones which are related to the spontaneous chiral symmetry breaking of QCD and the possible existence of glueball states.

Pion-pion scattering is very special due to the strong constraints from isospin, crossing, and chiral symmetries, but mostly from analyticity. The latter allows for a very rigorous dispersive integral formalism that relates the amplitude at any energy with an integral over the whole energy range, increasing the precision and providing information on the amplitude even at energies where data are poor. Our aim is to provide reliable and model-independent $\pi\pi$ scattering amplitudes that describe data and are consistent, within uncertainties, with dispersion relations. Note that, since we would like to test ChPT, we are not using it in our analysis, and that, in order to calculate dispersive integrals up to infinity, we have been using Regge parametrizations obtained from a fit to data on nucleon-nucleon, meson-nucleon, and pion-pion total cross sections [5]. In this work we will further improve our data analysis by imposing in the fits an additional set of once-subtracted dispersion relations, that we will also derive and describe in detail, showing that they are much more precise in the intermediate energy region than those we have used up to now.

In general, for each paper of this series (or also in [6]), we have first obtained a set of phenomenological ''unconstrained'' fits to data (UFD), which was fairly consistent with the dispersive requirements. Next, starting from that UFD set, we obtained ''constrained'' fits to data (CFD) by imposing simultaneous fulfillment of dispersion relations. These constrained fits not only describe data, but are remarkably consistent with the strong analyticity requirements. Furthermore, the output of the dispersive integrals is model independent and very precise.

The constraints we imposed in the first two papers of this series were just a complete set of forward dispersion relations (FDR), plus some crossing sum rules. In the third paper, apart from including the most recent and reliable data up to that date on $K_{\ell 4}$ decays [7,8], we also imposed Roy equations [9], because they constrain the $t \neq 0$ behavior of the amplitude, while ensuring $s - t$ crossing symmetry. These equations, which had already been used

*Deceased.

in the 1970s to analyze some of the existing data [10], as derived by S. M. Roy, have two subtractions and provide a strong constraint in the low energy part of the partial waves. For this reason there has recently been a considerable effort to analyze them in relation to ChPT [11]. They have also recently been used to eliminate [12] the long-standing ambiguity about ''up'' or ''down'' type solutions of the S0 wave data analyses. Since Roy equations are written in terms of partial waves, they lead, if supplemented with further theoretical input from ChPT [13], to precise predictions for resonance poles like the much debated $f_0(600)$. Despite being listed with huge uncertainties in the Particle Data Book [14], several analyses using analytic methods or dispersive techniques with chiral constraints [6,15], as well as those using Roy equations [13], are in fair agreement about its pole position, around 450–i250 MeV. However, its nature remains controversial, since it might not be an ordinary meson [16]. A precise analysis of $\pi\pi$ scattering data may help clarify the situation by studying the $f_0(600)$ parameters (like the coupling [17]), and the connection of the pole to QCD parameters [18], although one has to bear in mind [19] the difficulties to interpret the coupling in terms of simple intuitive models. Nevertheless, let us remark that here we only aim at a precise description of data, which could later be used for those purposes among many others, but the interpretation of this resonance and the extension to the complex plane are beyond the scope of this work.

Back to Roy equations, when used only with data, as in our case, the S2 wave scattering length, which is very poorly known experimentally, completely dominates the Roy equation uncertainties, which become very large above roughly 450 MeV, for the S0 and S2 waves. For that reason, Roy equations do not provide a significant additional constraint for the amplitudes beyond that energy, once they are already constrained with FDR. In this work we will overcome that caveat with additional once-subtracted Roy-like equations that have a much weaker dependence on scattering lengths. The fact that these additional equations have a much smaller uncertainty above roughly 450 MeV will force us to refine the matching of our S0 wave parametrizations.

Let us remark, though, that our parametrizations are consistent with those in KPY08 within 1 standard deviation, with the only exception being the S0 wave. However, the new central values satisfy Roy equations and the new once-subtracted dispersion relations better. Moreover, we will now be able to extend the Roy equations analysis, both with one and two subtractions, up to 1115 MeV, instead of just the $K\bar{K}$ threshold.

Once again we remark that the functional form of the amplitude parametrizations becomes irrelevant once the imaginary part of the amplitude is used in the dispersive integrals, whose results are model independent. With the understanding that running the dispersive representation could be tedious for the reader, we provide results in terms of our simple and ready-to-use CFD parametrizations, which are very good approximations to the dispersive result.

The plan of this work goes as follows: In Sec. II we very briefly comment on the simple unconstrained data fits (detailed in Appendix A) of all partial waves obtained in previous works. Only the S0 wave is given in more detail in Sec. III to introduce the new improvements. These are of two kinds: On the one hand, the data have changed, since we are taking into account the final and more precise NA48/2 data [20], including the threshold-enhanced isospin violation correction to all $K_{\ell 4}$ data, and getting rid of the controversial $K \to 2\pi$ datum. On the other hand, we have improved our parametrization, by imposing a continuous derivative matching between the low and intermediate energy regions and allowing for more flexibility in the parametrization around the $f_0(980)$ region.

In Sec. IV, after introducing FDRs and Roy equations very briefly, we present the once-subtracted dispersion relations and compare their structure with the standard Roy equations. Next, in Sec. V we impose these new relations together with the constraints already used in previous works (FDRs, sum rules, standard Roy equations ...) to obtain the final representation for the amplitudes, i.e., the CFD set of amplitudes. In Sec. VI we study the threshold parameters and Adler zero determinations stemming from this constrained fit through the use of additional sum rules and dispersive integrals. Then, in the discussion section, we compare these CFD with our previous results and other works in the literature, and we comment on the effect of considering different choices of data or parametrizations as a starting point to obtain our final result. In particular, we show how our results favor a ''dip'' structure in the S0 wave inelasticity right above 1000 MeV, which has been the subject of a long-standing controversy [21]. Finally, we present our conclusions. In the appendixes we provide a list of all parametrizations and parameters of the UFD and CFD, as well as the detailed derivation of the once-subtracted relations together with all relevant integral kernels. In Appendix D we provide a table with the phase shifts in the elastic region, as obtained from the dispersive representation.

II. THE UNCONSTRAINED FITS TO DATA

A. Our previous works

To explain the motivation for further improvements in our previous amplitudes, we briefly describe next the results of the previous articles.

(i) In PY05 [1] we obtained simple and easy-to-use phenomenological parametrizations of $\pi\pi$ scattering data whose consistency was checked by means of FDR and several crossing sum rules. The P, S2, D0, D2, F, G0, and G2 partial waves were described by simple fits to $\pi\pi$ scattering data up to 1.42 GeV.

In the elastic regime, the P wave was obtained from a fit to the pion form factor. For the S0 wave, given the fact that there are several conflicting sets of data, we first fitted each set separately and then performed another global fit only in the energy regions where different data sets are consistent. Surprisingly, some of the most commonly used data sets failed to pass these consistency tests, although the global fit was in fairly good agreement with FDR. Hence, it could be used as a starting point for a constrained fit to data. This CFD was obtained by imposing FDR and crossing sum rules to be satisfied within errors, in the elastic regime and up to 925 MeV. As a result, a precise description of the data up to 925 MeV was obtained by means of a constrained fit, satisfying the FDR and sum rule requirements remarkably well.

(ii) In KPY06 [2] we refined our parametrizations above $K\bar{K}$ threshold, including more $\pi\pi$ data but, most importantly, $\pi\pi \to K\bar{K}$ data in a coupled channel fit. These reduced uncertainties forced us to slightly refine the UFD parametrizations of our D0, D2, and P waves between 1 and 1.42 GeV as well as the Regge parameters. This led to a remarkable improvement in the consistency of the $\pi^0\pi^0$ FDR.

(iii) In KPY08 [3] we also considered Roy equations [9] for our amplitudes below $K\bar{K}$ threshold. The UFD fits, where we had previously incorporated [6] the most reliable low energy data from $K_{\ell 4}$ decays to that date [8], satisfied Roy equations fairly well and the agreement was remarkably good once they were imposed into a new set of CFD.

Since, in this work, we are going to consider a set of dispersion relations *in addition* to the dispersive constraints we have just described, our starting point will be the UFD set already obtained in KPY08, which we describe only very briefly in the next subsections, but explain in detail in Appendix A. The only exception will be the S0 wave, which we describe in Sec. III. The reasons are the appearance of new data [20], the existence of modifications on the analysis of the old experimental results, and, in addition, the fact that we have found that the new constraints are strong enough to require a better matching, with a continuous derivative, between the low and intermediate energy parametrizations.

B. Notation

For $\pi\pi \to \pi\pi$ scattering amplitudes of definite isospin I in the s channel, we write a partial wave decomposition as follows:

$$F^{(I)}(s,t) = \frac{8}{\pi}\sum_{\ell}(2\ell+1)P_\ell(\cos\theta)t_\ell^{(I)}(s),$$

$$t_\ell^{(I)}(s) = \frac{\sqrt{s}}{2k}\hat{f}_\ell^{(I)}(s), \quad \hat{f}_\ell^{(I)}(s) = \frac{\eta_\ell^{(I)}(s)e^{2i\delta_\ell^{(I)}(s)} - 1}{2i}, \tag{1}$$

where $\delta_\ell^{(I)}(s)$ and $\eta_\ell^{(I)}(s)$ are the phase shift and inelasticity of the I, ℓ partial wave, ℓ is the angular momentum, and k is the center-of-mass momentum. In the elastic case, $\eta = 1$ and

$$\hat{f}_\ell^{(I)}(s) = \sin\delta_\ell^{(I)}(s)e^{i\delta_\ell^{(I)}(s)}. \tag{2}$$

Note that $I = 0, 1, 2$ and that whenever I is even (odd) then ℓ is even (odd), and thus we will omit the isospin index for odd waves. We may refer to partial waves either by their I, ℓ quantum numbers or by the usual spectroscopic notation S0, S2, P, D0, D2, F, G0, G2, etc. ...

In addition, we recall the expressions for the so-called threshold parameters, which are the coefficients of the amplitude expansion in powers of center-of-mass momenta around threshold:

$$\frac{s^{1/2}}{2M_\pi k^{2\ell+1}}\,\mathrm{Re}\hat{f}_\ell^{(I)}(s) \simeq a_\ell^{(I)} + b_\ell^{(I)}k^2 + O(k^4). \tag{3}$$

Note that $a_\ell^{(I)}$ and $b_\ell^{(I)}$ are the usual scattering lengths and slope parameters. Customarily, these are given in M_π units.

C. Parametrizations for S2, P, D, F, and G waves

The S2, P, D0, D2, F, and G waves are described by very simple expressions. For the S2, P, and D0 waves, we use separate parametrizations for the "low energy region," i.e. energies $s^{1/2} < s_M^{1/2} \sim 1$ GeV, and the "intermediate energy region," which extends from the matching energy $s_M^{1/2}$ up to 1.42 GeV. For each wave, $s_M^{1/2}$ is typically the energy where inelastic processes cannot be neglected. Note that, above 1.42 GeV we will assume that $\pi\pi$ amplitudes are given by Regge formulas, which correspond to fits to experimental data (see [5] and KPY06 for details).

In the low energy region, where the elastic approximation is valid, we use a *model-independent* parametrization for each partial wave $t_\ell^{(I)}$, which ensures elastic unitarity:

$$t_\ell^{(I)} = \frac{\sqrt{s}}{2k}\frac{1}{\cot\delta_\ell^{(I)}(s) - i}.$$

To ensure maximal analyticity in the complex plane, $\cot\delta_\ell^{(I)}(s)$ is then expanded in powers of the conformal variable

$$w(s) = \frac{\sqrt{s} - \sqrt{s_i - s}}{\sqrt{s} + \sqrt{s_i - s}},$$

where s_i is a convenient scale for each wave, to be precised later, always larger than the s range where conformal mapping is used. The use of a conformal variable allows for a very rapid convergence—at most, two or three terms are needed in the expansion—so that each wave is represented by only three to five parameters, corresponding to the coefficients of the expansion and the position of the zeros and poles when we have found it convenient to factorize them explicitly [6]. We remark again that the use of a conformal expansion does not imply any model dependence.

In the intermediate energy inelastic region, we have used purely polynomial expansions both for the phase shifts and inelasticities in terms of the typical energy or momenta involved in the process.

All these simple parametrizations have been fitted to a large number of experimental data on $\pi\pi$ phase shifts or, in the case of the P wave, to the vector form factor data, which gives much more precise results. In Appendix A, we provide the detailed parametrizations for each partial wave, together with the resulting parameters and their uncertainties, from now on denoted by $p_i^{\rm exp}$ and δp_i, respectively.

Let us remark that, as a first step, each partial wave has been fitted independently of each other, without imposing any constraint from dispersion relations, and that is why we refer to such initial fits as unconstrained fits to data or UFD. In KPY08 we showed that these UFD provided a good description of data, and a fairly reasonable consistency in terms of dispersion relations. Of course, the consistency is much better, remarkable indeed, once we impose the dispersion relations as constraints to the fit, but then all waves become correlated. The uncorrelated fits, apart from providing the starting point of our calculation, and although they are less reliable than our final constrained results, could be of relevance if new and more precise data become available for a given partial wave, since then only that particular partial wave should be modified, without affecting the others.

III. S0 WAVE PARAMETRIZATION

This is the only wave that changes in the new sets of unconstrained data fits. This is due to three reasons that we will explain in separate subsections.

A. Isospin violation in $K_{\ell 4}$ decays

There has been a recent calculation [22] showing that, due to threshold enhancements, isospin corrections in $K_{\ell 4}$ decays [7,8,20] could be larger than naively expected. A leading order ChPT calculation has been provided to correct the phase-shift determination in the isospin limit, which should be valid within the whole range of $K_{\ell 4}$ decays. Note that the uncertainties in the previous UFD set in [6] were obtained taking into account systematic errors on the data, including possible isospin corrections, but only of natural size. Since the most recent data from $K_{\ell 4}$ decays play a relevant role in the S0 wave of our UFD set, and the suggested isospin breaking effect is unnaturally large, we will modify the S0 wave by correcting the $K_{\ell 4}$ data as suggested in [22], so that it can be used in our isospin limit formalism. Note that this isospin correction was already made available in [8] and again in the final NA48/2 results [20].

B. The $K \to 2\pi$ data

Let us emphasize again that this is a data analysis, and, as such, it depends on whether we include or not certain experimental results that are somewhat controversial. This is, for instance, the case of the phase-shift difference obtained from $K \to 2\pi$ decay [23] that we used in KPY08:

$$\delta_0^{(0)}(M_K^2) - \delta_0^{(2)}(M_K^2) = (57.27 \pm 0.82_{\rm exp} \pm 3_{\rm rad} \pm 1_{\rm ChPT\ appr})^\circ. \quad (4)$$

The extraction of the $\pi\pi$ scattering phase from this decay is affected by large uncertainties that have to be estimated from ChPT. A similar value is obtained if using the Particle Data Group data and the prescription for radiative corrections in [24]. In [6] we took the simple linear sum of the errors quoted in [23], which is larger than the usual quadrature addition. However, the use of the datum above has been questioned in [25], also suggesting that it could be partly responsible for the differences between our approaches in the intermediate energy region. It is true that this data point always lies somewhat above our parametrizations of KPY08, $51.7 \pm 1.2^\circ$ for the UFD and $50.4 \pm 1.1^\circ$ for the CFD, and even more so from those in [11], $47.7 \pm 1.5^\circ$. While preparing this work, a reanalysis has appeared [26] taking into account more precise experimental data and other improvements including an update of the low energy constants, yielding

$$\delta_0^{(0)}(M_K^2) - \delta_0^{(2)}(M_K^2) = (52.5 \pm 0.8_{\rm exp} \pm 2.8_{\rm theor})^\circ. \quad (5)$$

This is still compatible with the value in Eq. (4), but seems in much better agreement with $\pi\pi$ scattering determinations. However, this new extraction uses as an input the S0 phase-shift value from a $\pi\pi$ scattering analysis using Roy equations and ChPT, obtained by the Bern group [11]. Thus it would be somewhat circular to use it as input in our approach. Furthermore, we have studied the alternative scenarios with and without the $K \to 2\pi$ value in our fits, finding that the scenario without it is slightly preferred by dispersion relations. For these reasons, we will present results for fits removing the $K \to 2\pi$ controversial datum. As a consequence, our new unconstrained fits have somewhat smaller errors than those in KPY08, which makes dispersion relations harder to satisfy.

C. Improved parametrization and matching condition between low and intermediate energies

In previous works, only continuity, but not a continuous derivative, was imposed for the S0 phase shift at the matching point, then chosen at $s_M^{1/2} = 932$ MeV. It has been suggested [27] that such a crude matching could explain the roughly 2σ level discrepancies in the S0 wave between the KPY08 analysis and that of the Bern group [11] in the 450–800 MeV region. We have checked that the improved matching by itself only affects the S0 wave sizably in the $f_0(980)$ region, although the effect is rather small below. However, this improved matching adds together with the two effects in kaon decays discussed above, to become a relatively larger effect that certainly improves the agreement with the predicted S0 wave in [11].

In this work we want to keep the same low energy conformal parametrization of KPY08 or [6]. However, to improve the flexibility of the parametrization we will keep one more term in this expansion. Actually, it has been pointed out that the difference between the parametrization in KPY08 and that of [11] could be due to the fact that our conformal parametrization at low energies was not sufficiently flexible [28]. The additional parameter does not improve significantly the fulfillment of dispersion relations nor the data fit, but the *output* of the dispersion relations with one parameter less would violate very slightly the elastic unitarity condition around 500 MeV. For that reason, we keep this additional term, and use

$$\cot\delta_0^{(0)}(s) = \frac{s^{1/2}}{2k}\frac{M_\pi^2}{s-\frac{1}{2}z_0^2}\left\{\frac{z_0^2}{M_\pi\sqrt{s}} + B_0 + B_1 w(s) + B_2 w(s)^2 + B_3 w(s)^3\right\}, \quad (6)$$

$$w(s) = \frac{\sqrt{s}-\sqrt{s_0-s}}{\sqrt{s}+\sqrt{s_0-s}}, \qquad s_0 = 4M_K^2, \quad (7)$$

where the new values for the UFD parameters are

$$B_0 = 7.26 \pm 0.23, \quad B_1 = -25.3 \pm 0.5,$$
$$B_2 = -33.1 \pm 1.2, \quad B_3 = -26.6 \pm 2.3, \quad z_0 = M_\pi, \quad (8)$$

which are obtained with the same procedure as in [6] but now including the additional B_3 and the isospin corrections, and getting rid of the $K \to 2\pi$ data, as already commented in Secs. III A and III B above. Namely, in this fit we have considered the data on $K_{\ell 4}$ decays [7], including the final $K_{\ell 4}$ decay data from NA48/2 [20] (which supersedes [8]), and a selection of all the existing and often conflicting $\pi\pi$ scattering data [29,30]. This selection corresponds to an average of the different experimental solutions that passed a consistency test with forward dispersion relations and other sum rules in the initial work PY05. To this average, we assigned a large uncertainty to cover the difference between the initial data sets. For the sake of brevity, we simply refer to that work, or the Appendix of Ref. [6], for a complete and detailed description of the data selection.

Uncertainties in Eq. (8) come from data only. In order to use the UFD by itself, a systematic uncertainty due to parametrization dependence [32] should be taken into account. But as we have seen, possible parametrizations are strongly restricted by imposing dispersion relations and unitarity in their output, thus reducing dramatically this source of systematic uncertainty. Hence, we will only quote the data uncertainty for the CFD. Of course, since dispersion relations are imposed within uncertainties, the residual parametrization dependence is reflected in the error bars from the result of the dispersive representation, which we give in Table XII of Appendix D.

Despite this amplitude being used only in the physical region, we have explicitly factorized a zero at $s_A = z_0^2/2 = M_\pi^2/2 \simeq (98.7\ \mathrm{MeV})^2$ for these unconstrained fits. This corresponds to the position of the so-called Adler zero, required by chiral symmetry [31], at leading order in ChPT. Note, however, that this zero lies very close to the border of the convergence region of the conformal expansion (see Fig. 16 in KPY08), which is therefore not very well described by the expression above. Hence, z_0 should not really be interpreted as the exact position of the Adler zero, but just as another parameter of our parametrization. Of course, the physical low energy region, which is the only one relevant for the dispersive representation, lies well inside the convergence region of the conformal expansion, and is very well described by Eq. (6). Actually, we will show in Sec. VI below that, when this parametrization is used inside the dispersive representation, one finds an Adler zero in the correct position.

Let us now turn to the intermediate energy region. In previous works, a two-channel K-matrix formalism, following the experimental reference in [30], was used to describe the region around the $K\bar{K}$ threshold. This is a rather popular formalism to describe multichannel scattering of two-body states, but has several disadvantages for our purposes. One, of course, is the use of only two channels, $\pi\pi$ and $K\bar{K}$, neglecting possible inelasticity contributions from 4π or other channels. These are rather small, but since we aim at a precision determination, we should allow for more flexibility on the inelasticity, whereas the two-channel K matrix yields a strong relation between phase and inelasticity. The second caveat is the huge correlation between K-matrix parameters, which makes it very hard to improve by means of constrained fits, as we will do later on. Finally, a very strong disadvantage is that the phase dependence on the K-matrix parameters is so complicated that it is not possible to make an analytic matching with the low energy parametrization, and a numerical matching is much more ineffective and harder to implement. Let us note that some of these caveats were already removed when using some very naive polynomial parametrizations considered in Appendix B of KPY06. We will use those same parametrizations here but with additional terms in the expansion to compensate the loss of flexibility due to the improved matching conditions. In particular, between the matching point and 1.42 GeV, we will use

$$\delta_0^{(0)}(s) = \begin{cases} d_0 + a\frac{|k_2|}{M_K} + b\frac{|k_2|^2}{M_K^2} + c\frac{|k_2|^3}{M_K^3} & (0.85\ \mathrm{GeV})^2 < s < 4M_K^2 \\ d_0 + B\frac{k_2^2}{M_K^2} + C\frac{k_2^4}{M_K^4} + D\theta(s-4M_\eta^2)\frac{k_3^2}{M_\eta^2} & 4M_K^2 < s < (1.42\ \mathrm{GeV})^2, \end{cases} \quad (9)$$

where $k_2 = \sqrt{s/4 - M_K^2}$, $k_3 = \sqrt{s/4 - M_\eta^2}$, and d_0 is the phase shift at the two-kaon threshold. Note, however, that we have lowered the matching point to $s_M^{1/2} = 850$ MeV, since we have found empirically that this helps improve the dispersion relation fulfillment, as the slope is somewhat smaller there. As a final remark, we have added a term proportional to the η momentum, to reflect the opening of the $\eta\eta$ channel, which is shown to have some relevance in the description of the data [33]. In this respect, we want to clarify a common source of confusion about Roy (or GKPY) equations: These relations include all possible coupled channel contributions, or at least are consistent with them, as long as they are in agreement with the experimental inelasticity. This simple term is purely phenomenological, and given the size of the experimental errors, this additional term is more than enough to just describe the cusp due to the presence of this channel. However, it yields very slightly, but favorable, differences in the fulfillment of dispersion relations.

By defining $\delta_M = \delta(s_M)$ and $\delta'_M = d\delta(s_M)/ds$, which are obtained from Eq. (6), and $k_M = |k_2(s_M)|$, it is rather straightforward to impose continuity and a continuous derivative for the phase shift at s_M, to find

$$\delta_0^{(0)}(s) = \begin{cases} d_0\left(1 - \frac{|k_2|}{k_M}\right)^2 + \delta_M \frac{|k_2|}{k_M}\left(2 - \frac{|k_2|}{k_M}\right) + |k_2|(k_M - |k_2|)\left(8\delta'_M + c\frac{(k_M - |k_2|)}{M_K^3}\right) & (0.85\ \text{GeV})^2 < s < 4M_K^2 \\ d_0 + B\frac{k_2^2}{M_K^2} + C\frac{k_2^4}{M_K^4} + D\theta(s - 4M_\eta^2)\frac{k_3^2}{M_\eta^2} & 4M_K^2 < s < (1.42\ \text{GeV})^2. \end{cases} \tag{10}$$

As previously commented, with the exception of the $K \to 2\pi$ datum, the inclusion of isospin corrections to $K_{\ell 4}$ data explained above, and our use of the final NA48/2 results [20], our treatment and selection of data for the phase are exactly the same as followed in the previous works [2,6], so we will not repeat them here. In Table V of Appendix A, we provide the values for the d_0, c, B, C, and D parameters resulting from the unconstrained fit to those data. In Fig. 1 we show the resulting phase from the unconstrained data fit to the S0 wave phase shift up to 1420 MeV, and in Fig. 2 we show the low energy region in detail, including the isospin violation correction [22] that we have subtracted from all the $K_{\ell 4}$ data. Note that this correction amounts to slightly less than 1° in the region from threshold to 400 MeV, which is not much at high energies, but very relevant close to threshold.

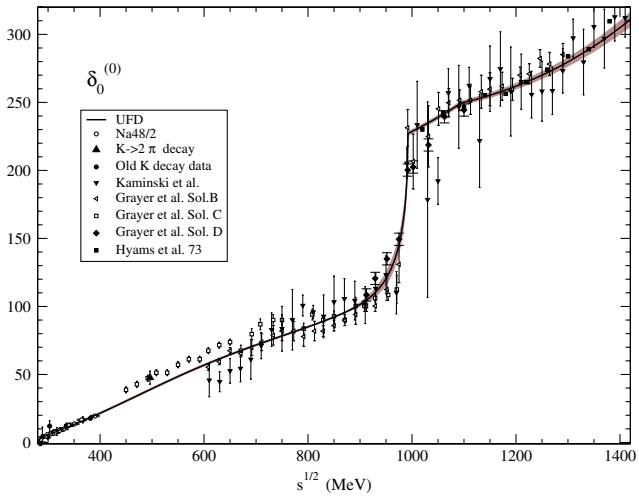

FIG. 1 (color online). The new S0 wave UFD, where the dark band covers the uncertainties, versus the existing phase-shift data from [29,30]. Note that the $K \to 2\pi$ point has been excluded from the fit as explained in the text.

In Fig. 3 we show a comparison of the phase shift resulting from the new UFD with the improved matching versus the one obtained in KPY08. The changes at low energy are due to the update on the $K_{\ell 4}$ data and their isospin corrections, together with the fact that we now discard the $K \to 2\pi$ datum. The bump in the 500 to 800 MeV region observed in KPY08 has almost disappeared. Thus, the improvement on the data and its corrections almost completely reduces the disagreement of our UFD description with the phases in [11]—the line labeled CGL in the plot—although our central values are still

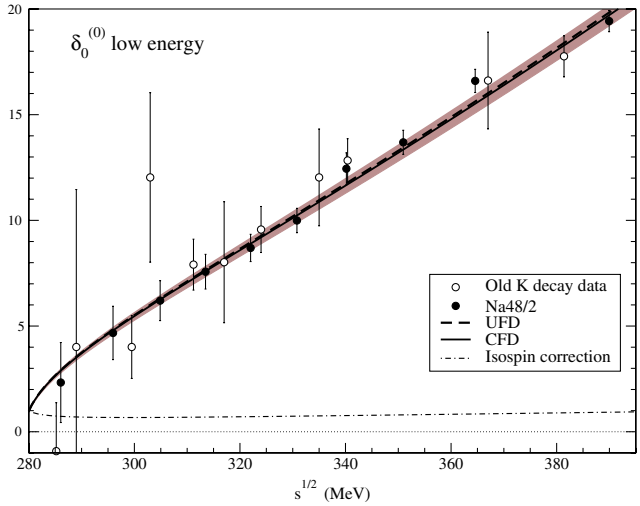

FIG. 2 (color online). The new S0 wave UFD, where the dark band covers the uncertainties, versus the "old" phase-shift data from $K_{\ell 4}$ decays [7] together with the final NA48/2 results, which supersede the data from the same experiment [8] that we used in KPY08. We are also showing the isospin violation correction [22], which has been included in the data shown here. Finally, we show the results of the CFD parametrization to be explained in Sec. V, which are almost indistinguishable from the UFD curve.

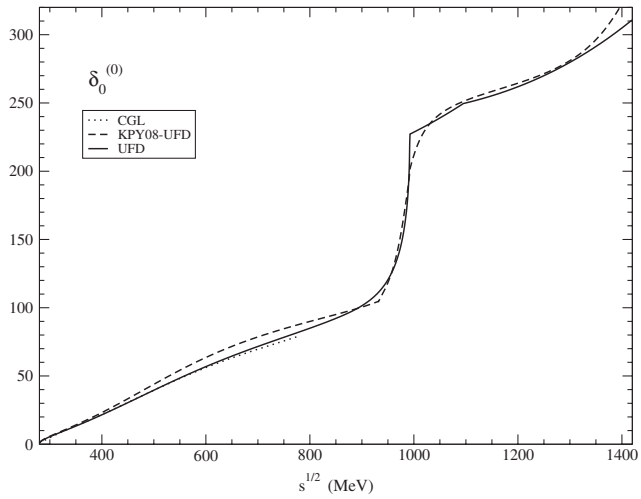

FIG. 3. Fit to the S0 wave phase shift, with the improved continuous derivative matching (UFD, continuous line) versus the simpler one used in KPY08. We also show the phase predicted in [11] (CGL).

larger in the 550–800 MeV region. Furthermore, as we will see later, for the constrained fits we are in even better agreement with [11]. The changes above the matching point are sizable for the phase, mostly around the sharp phase increase usually associated with the $f_0(980)$ resonances, as can be seen in Fig. 3, where the central value for the new phase is compared with that in KPY08. Note the much smoother behavior in the matching region for the new UFD parametrization and the more dramatic $\bar{K}K$ threshold effect.

Concerning the S0 wave inelasticity, we approximate it to 1 up to the two-kaon threshold, and use the following parametrization above that energy:

$$\eta_0^{(0)}(s) = \exp\left[\frac{-k_2(s)}{s^{1/2}}\left(\tilde{\epsilon}_1 + \tilde{\epsilon}_2\frac{k_2}{s^{1/2}} + \tilde{\epsilon}_3\frac{k_2^2}{s}\right)^2 - \tilde{\epsilon}_4\theta(s-4M_\eta^2)\frac{k_3(s)}{s^{1/2}}\right], \quad (11)$$

for $4M_K^2 < s < (1.42\ \text{GeV})^2$. By neglecting the term proportional to the η momentum, which is numerically very small as seen in Appendix A, and by reexpanding the above equation in powers of $k_2/s^{1/2}$ up to third order, we recover the polynomial expression in KPY06, but the definition above ensures the $0 \le \eta_0^{(0)} \le 1$ physical condition, whereas the simple polynomial in KPY06 did not.

For the inelasticity data, we follow again the same selection as in previous works of this series, but now we do not include the data from Kamiński *et al.* [29] in the χ^2 calculation; we only consider the 1973 data of Hyams *et al.* [29] and Protopopescu *et al.* [29]. The reason is that the main source of uncertainty is systematic, and if we include the large number of points of Kamiński *et al.* with their huge statistical errors, the outcome of the fit has much smaller errors than the original systematic uncertainties. By keeping only the other two sets, which are incompatible, we obtain a fit with a large χ^2/d.o.f., and by rescaling the uncertainties in the inelasticity parameters, we mimic the dominant systematic uncertainties much better. Of course, our results are still in very good agreement with Kamiński *et al.* Was the systematic uncertainty not dominant, this would not be necessary. In Table V of Appendix A, we provide the values for the $\tilde{\epsilon}_i$ parameters, and in Fig. 4 we show the results of the unconstrained fit to the S0 wave inelasticity data up to 1420 MeV.

Finally, let us remark that the inelasticity is the scattering parameter that suffers the biggest change with respect to the KPY08-KPY06 parametrization, as can be seen in Fig. 5. The new parametrization shows a big dip in the inelasticity between 1 and 1.1 GeV, whereas the KPY08 one does not. As already commented in PY05, this is a long-standing controversy (see, for instance, [21] and references therein) between different sets of data coming from pure $\pi\pi \to \pi\pi$ scattering versus those coming from $\pi\pi \to \bar{K}K$ analysis. Actually, in PY05 (see Fig. 6 there) we considered both possibilities: We found that forward dispersion relations favored the "nondip solution" very slightly, but we kept the "dip-solution" in order to use the phase and inelasticity coming from the same experiment. In KPY06 we found a similar situation, but since the K matrix slightly preferred again the nondip solution, this time we decided to use it. However, in terms of fulfillment, the difference is minute for FDRs, and even more so for standard Roy equations, since, as we have already commented and we will see in detail below, the uncertainties in the subtraction constants become so large above 500 MeV

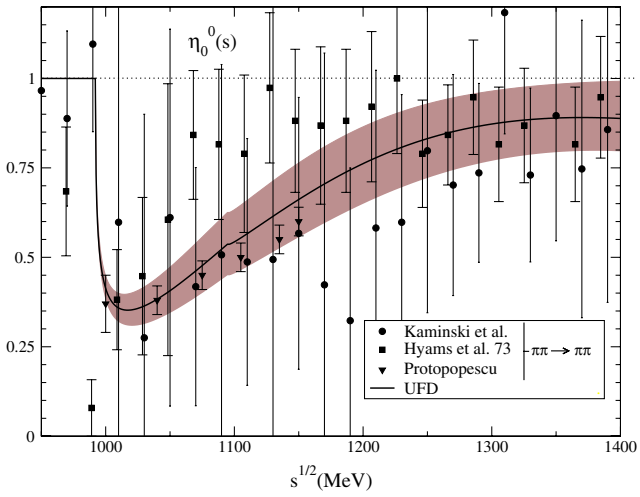

FIG. 4 (color online). The new S0 inelasticity fit (UFD set) to the $\pi\pi \to \pi\pi$ scattering data of Hyams *et al.* (1973) and Protopopescu *et al.* As explained in the text, we do not fit the Kamiński *et al.* data [29], although our fit is compatible with them. The dark band covers our uncertainties. For all data sets, see Fig. 18.

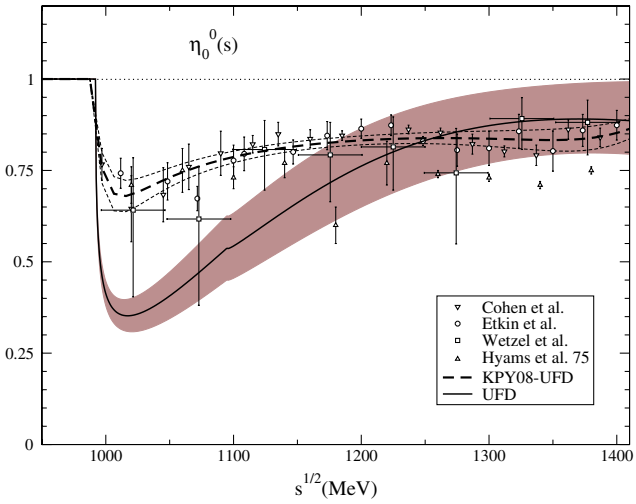

FIG. 5 (color online). Fit to the S0 wave inelasticity (UFD) with the improved continuous derivative matching (continuous line) versus the simpler one used in KPY08 (dashed line). The dark band covers the uncertainties of the former, whereas the dotted curves enclose the uncertainties of the latter. Note that the drop in the inelasticity right above 1 GeV has become much deeper. In contrast to Fig. 4, we only show the data coming from $\pi\pi \to K\bar{K}$ and the $\pi\pi \to \pi\pi$ on which the KPY08 fit is based. For all data sets, see Fig. 18.

that we cannot use them to discard either of the two scenarios. The existing set of dispersion relations did not allow us to make a really conclusive statement about the inelasticity in the 1 GeV region.

One of the main results of this work is the derivation and use of once-subtracted Roy-like dispersion relations, the GKPY equations presented in Sec. IV D below, which are more precise in the 1 GeV region and clearly favor the solution with a dip, thus helping to settle this dip versus nondip controversy.

IV. DISPERSION RELATIONS AND SUM RULES

From the theoretical side, $\pi\pi$ scattering is very special due to the strong constraints from isospin, crossing, and chiral symmetries, but mostly from analyticity. The latter allows for a very rigorous dispersive integral formalism that relates the $\pi\pi$ amplitude at any energy with an integral over the whole energy range, increasing precision and providing information on the amplitude even at energies where data are poor, or in the complex plane.

Let us emphasize once more that the dispersive approach is model independent, since it makes the data parametrization irrelevant once it is included in the integral. The previous works [3,6] of this series made use of two complementary dispersive approaches, forward dispersion relations and Roy equations, that we briefly review next, before introducing the new set of once-subtracted Roy-like equations.

A. Forward dispersion relations

They are calculated at $t = 0$, so that the unknown large-t behavior of the amplitude is not needed. There are two symmetric and one antisymmetric isospin combinations to cover the isospin basis. For further convenience, we will write them as a difference $\Delta_i(s)$ that should vanish if the dispersion relation is satisfied exactly. In particular, the two symmetric ones, for $\pi^0\pi^+$ and $\pi^0\pi^0$, have *one subtraction* and imply the vanishing of

$$\Delta_i(s) \equiv \mathrm{Re}F_i(s,0) - F_i(4M_\pi^2,0) - \frac{s(s-4M_\pi^2)}{\pi} \times \mathrm{P.P.}\int_{4M_\pi^2}^{\infty} \frac{(2s'-4M_\pi^2)\,\mathrm{Im}F_i(s',0)ds'}{s'(s'-s)(s'-4M_\pi^2)(s'+s-4M_\pi^2)}, \tag{12}$$

where F_i stands for the $F_{0+}(s,t)$ or $F_{00}(s,t)$ amplitudes, and "P.P." stands for the principal part of the integral. They are very precise, since all the integrand contributions are positive. The antisymmetric isospin combination $I_t = 1$ does not require subtractions and implies the vanishing of the following difference:

$$\Delta_{(I_t=1)}(s) \equiv F^{(I_t=1)}(s,0) - \frac{2s-4M_\pi^2}{\pi} \times \mathrm{P.P.}\int_{4M_\pi^2}^{\infty} ds' \frac{\mathrm{Im}F^{(I_t=1)}(s',0)}{(s'-s)(s'+s-4M_\pi^2)}. \tag{13}$$

All FDRs are calculated up to $\sqrt{s} = 1420$ MeV.

B. Roy equations

These are an infinite set of coupled equations [9], equivalent to nonforward dispersion relations plus $t-s$ crossing symmetry. They are well suited to study poles of resonances and scattering data, since they are written directly in terms of partial waves $t_\ell^{(I)}$ of definite isospin I and angular momentum ℓ. Remarkably, S. M. Roy managed to rewrite the complicated left cut contribution as a series of integrals over the physical region. In the original work of Roy and all applications until now, the convergence of the integrals was ensured by making two subtractions.

As we did with FDR, we will recast each one of the Roy equations as the difference

$$\Delta_\ell^{(I)}(s) \equiv \mathrm{Re}t_\ell^{(I)}(s) - ST_\ell^I(s) - DT_\ell^I(s) - \sum_{I'=0}^{2}\sum_{\ell'=0}^{1} \mathrm{P.P.}\int_{4M_\pi^2}^{s_{\max}} ds' K_{\ell\ell'}^{II'}(s,s')\,\mathrm{Im}t_{\ell'}^{I'}(s'), \tag{14}$$

that should vanish when the equation is exactly satisfied. Roy equations provide as output the real part of partial waves below 1115 MeV. Although, in principle, one could consider output for waves up to higher ℓ, in this work we are interested in results for $\ell = 0, 1$ only. Hence, we have separated those waves explicitly below $s_{\max}$.

As it was done in KPY08, below $s_{\rm max}^{1/2} = 1420$ MeV, we consider the imaginary parts from all our $\ell \leq 4$ partial wave parametrizations as input. Above that energy, we take into account all waves together, parametrized with Regge theory—see Appendix A 8. The $K^{II'}_{\ell\ell'}(s,s')$ are known kernels, and thus we will refer to the integral terms as "kernel terms" or $KT(s)$. The "driving terms" $DT^I_\ell(s)$ have the same structure as the kernel terms, but their input contains both the contribution from $\ell = 2$, 3 partial waves up to $s_{\rm max}^{1/2} = 1420$ MeV, and the Regge parametrizations above. We have explicitly checked that the $\ell = 4$ contribution below $s_{\rm max}$ is irrelevant, so that we will refer just to waves up to $\ell = 3$. Finally, the so-called subtraction terms are given by

$$ST^I_\ell(s) = a_0^0\delta_{I0}\delta_{\ell 0} + a_0^2\delta_{I2}\delta_{\ell 0} + \frac{s-4M_\pi^2}{12M_\pi^2}(2a_0^0 - 5a_0^2) \times\left(\delta_{I0}\delta_{\ell 0} + \frac{1}{6}\delta_{I1}\delta_{\ell 1} - \frac{1}{2}\delta_{I2}\delta_{\ell 0}\right). \quad (15)$$

It is very relevant to remark once more that these equations have two subtractions, as can be seen by the presence of the term proportional to $(s-4M_\pi^2)(2a_0^0 - 5a_0^2)$. This strong energy dependence of $ST(s)$ makes these twice-subtracted Roy equations very suitable for low energy studies, and even more so when complemented with theoretical predictions of the scattering lengths coming from ChPT [11].

Roy equations are valid up to $\sqrt{s} \leq 8M_\pi \simeq 1120$ MeV. However, we will see that the uncertainties in the scattering lengths, when propagated to high energies, become too large above roughly 450 MeV, due to the term proportional to s. For this reason, in KPY08 it did not make sense to deal with the complications of a precise description around $\bar{K}K$ threshold, and thus we implemented them up to $2M_K$. One of the main novelties of the present work is that, since the once-subtracted Roy-like equations explained below will have much smaller uncertainties in the $\bar{K}K$ threshold region, we have now implemented these new equations, together with the standard Roy equations, up to 1115 MeV.

C. Two sum rules

Apart from FDRs and Roy equations, two sum rules that relate high energy (Regge) parameters for $t \neq 0$ to low energy P and D waves have been considered throughout previous works. In Table XII in Appendix D we provide the S0, P, and S2 phase shifts that result from using the CFD set inside the dispersive representation.

The first sum rule (PY05) is nothing but the vanishing of the following difference:

$$I \equiv \int_{4M_\pi^2}^\infty ds\frac{{\rm Im}F^{(I_t=1)}(s,4M_\pi^2) - {\rm Im}F^{(I_t=1)}(s,0)}{s^2} - \int_{4M_\pi^2}^\infty ds\frac{8M_\pi^2[s-2M_\pi^2]{\rm Im}F^{(I_s=1)}(s,0)}{s^2(s-4M_\pi^2)^2}, \quad (16)$$

where the contributions of the S waves cancel and only the P and D waves contribute (we also include F and G waves, but they are negligible). At high energy, the integrals are dominated by the rho Reggeon exchange.

The second sum rule we consider is given in Eqs. (B.6) and (B.7) of the second reference in [11], which requires the vanishing of

$$J \equiv \int_{4M_\pi^2}^\infty ds\left\{\frac{4{\rm Im}F'^{(0)}(s,0) - 10{\rm Im}F'^{(2)}(s,0)}{s^2(s-4M_\pi^2)^2} - 6(3s-4m_\pi^2)\frac{{\rm Im}F'^{(1)}(s,0) - {\rm Im}F^{(1)}(s,0)}{s^2(s-4M_\pi^2)^3}\right\}. \quad (17)$$

Here, $F'^{(I)}(s,t) \equiv \partial F^{(I)}(s,t)/\partial\cos\theta$. At high energy, the integral is dominated by isospin zero Regge trajectories.

D. GKPY equations

The main novelty of this work is that we present and use a new set of Roy-like dispersion relations for $\pi\pi$ scattering amplitudes. For brevity, we will call them GKPY equations, as we have already done when presenting some partial and preliminary results in several references [34,35]. In brief, their derivation follows the same steps as for Roy equations, starting from fixed t dispersion relations for a complete isospin basis, which S. M. Roy subtracted twice to ensure that the integrals converged when extended to infinity. However, by using the complete set of isospin amplitudes F_{00}, F_{0+}, and $F^{(I_t=1)}$, it is easy to see that one subtraction is enough. Actually, the first two amplitudes are $s-u$ symmetric, and the contributions from the s and u channels, which would be divergent by themselves alone, cancel when considered simultaneously. The $F^{(I_t=1)}$ amplitude is dominated by the rho Regge exchange, and neither the left nor the right cut is divergent with one subtraction. We provide the detailed derivation in Appendix B, which leads to the vanishing of the following difference:

$$\Delta_\ell^{{\rm GKPY}(I)} \equiv {\rm Re}t_\ell^{(I)}(s) - \overline{ST}^I_\ell - \overline{DT}^I_\ell(s) - \sum_{I'=0}^{2}\sum_{\ell'=0}^{1}{\rm P.P.}\int_{4M_\pi^2}^{s_{\rm max}} ds'\overline{K}^{II'}_{\ell\ell'}(s',s)\,{\rm Im}t^{(I')}_{\ell'}(s'). \quad (18)$$

The subtraction terms $\overline{ST}^I_\ell$ are linear combinations of scattering lengths a_0^I, and can be found in Appendix B. A very relevant observation for this work is that, in contrast to the standard Roy equations, the subtraction terms in GKPY do not depend on s.

The integral and driving terms $\overline{DT}^I_\ell(s)$ in Eq. (18) are analogous to the kernel and driving terms in Roy equations, but the integrals contain the $\overline{K}^{II'}_{\ell\ell'}$ kernels, instead of the $K^{II'}_{\ell\ell'}$. The explicit expressions for $\overline{K}^{II'}_{\ell\ell'}$ are lengthy, and we provide them in Appendix C. Note that, as the once-subtracted GKPY equations have kernel terms that behave

as $\sim 1/s^2$ at higher energies, instead of the $\sim 1/s^3$ behavior in Roy equations, the weight of the high energy region is larger. Nevertheless, the contribution to the driving terms coming from energies above 1.42 GeV is generically smaller than the contribution coming from the D and F waves below 1.42 GeV, which means that their influence is still under control.

E. Roy versus GKPY equations

Figure 6 presents a decomposition of Roy equations for the S0, P, and S2 waves into four parts: the "in" part that represents what our parametrizations give for $\mathrm{Re}t_\ell^{(I)}$, the subtracting terms $ST(s)$, the kernel terms $KT(s)$, and the driving terms $DT(s)$. Note that, for these equations to be satisfied exactly, the first contribution should equal the sum of the other three. The numerical calculations have been performed by taking the UFD amplitudes described in the previous sections as input. For illustration, we have drawn as a gray area the region that violates the unitarity bound $|\mathrm{Re}t| \leq \eta s^{1/2}/4k$ (note that $\eta = 1$ in the elastic region). For comparison, we present in Fig. 7 the same decompositions for the GKPY equations. Note the very different scales on both sets of figures.

As can be seen in Fig. 6, the $ST(s)$ and $KT(s)$ terms in Roy equations become huge at higher energies and suffer a large cancellation against each other. This cancellation is particularly strong for the S0 wave, where, for a sufficiently large energy, both terms are much larger than the unitarity bound. For instance, they are larger by roughly a factor of 4 at 750 MeV, and of 8 at 1100 MeV.

In contrast, as seen in Fig. 7 for the GKPY equations, Eq. (18), the $\overline{ST}$ terms are constant and, in fact, much smaller than the $\overline{KT}(s)$ terms, which are clearly the dominant ones. Therefore, no big cancellations between any two terms are needed in order to reconstruct the total real part of the amplitude. Moreover, we have checked that the high energy part, which has been parametrized by means of Regge theory, corresponds to somewhat less than half of the total $\overline{DT}(s)$ contribution. Therefore, although the $\overline{DT}(s)$ terms in the GKPY equations are larger than in Roy equations due to the fact that there is one subtraction less, the contribution coming from the amplitudes above 1420 MeV is still small compared with the dominant term $KT(s)$. Thus, the high energy behavior is still well under control.

Note that, to keep the plots clear, we have only provided central values for the moment. In the next section we will provide the total uncertainties (the uncertainties of each separated contribution were presented in an article [35] using a very preliminary UFD set). For our purposes it is enough to remark that uncertainties follow a similar pattern to these central values. In particular, the $ST(s)$ term in Roy equations for scalar waves has a large uncertainty due to the poor experimental knowledge of the a_0^2 scattering length, which becomes larger and larger, proportionally

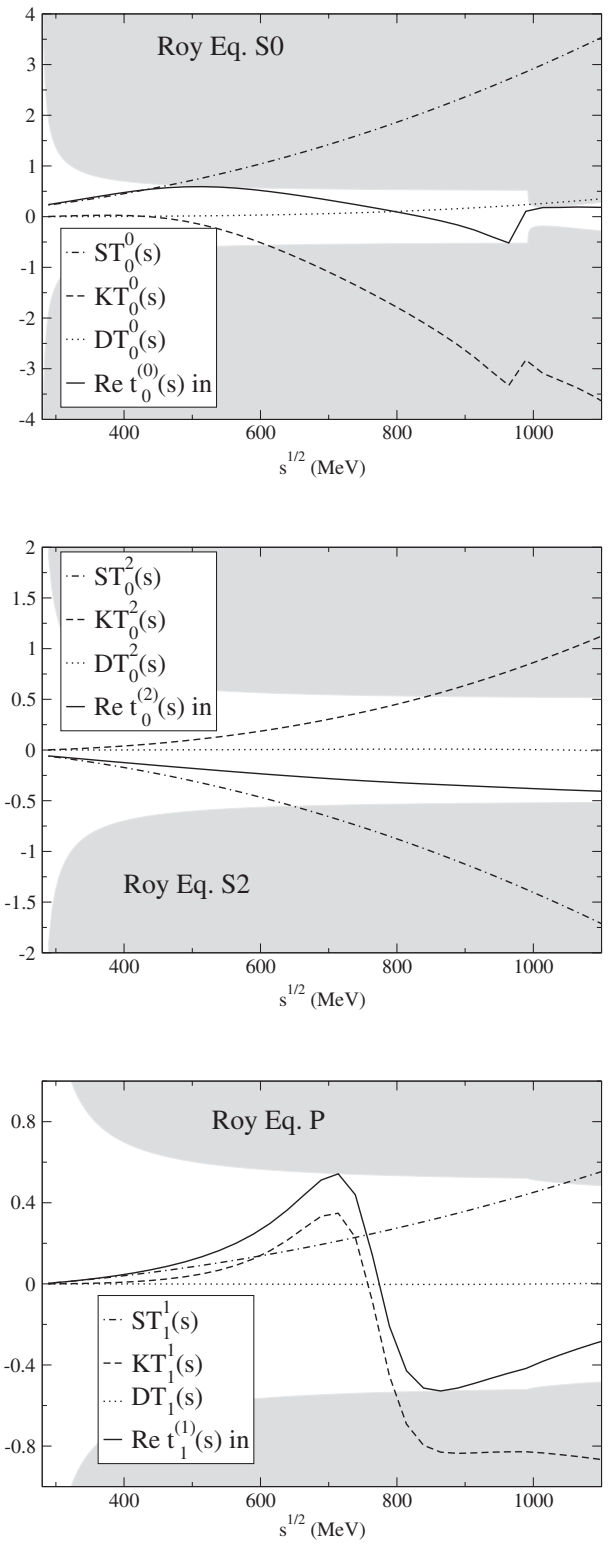

FIG. 6. Using the UFD set as input, we show the decomposition of Roy equations into the subtracting term ST, the kernel term KT, and the driving term DT for the S0, P, and S2 waves. Note the different scales used on each plot. The gray areas lie beyond the unitarity bound.

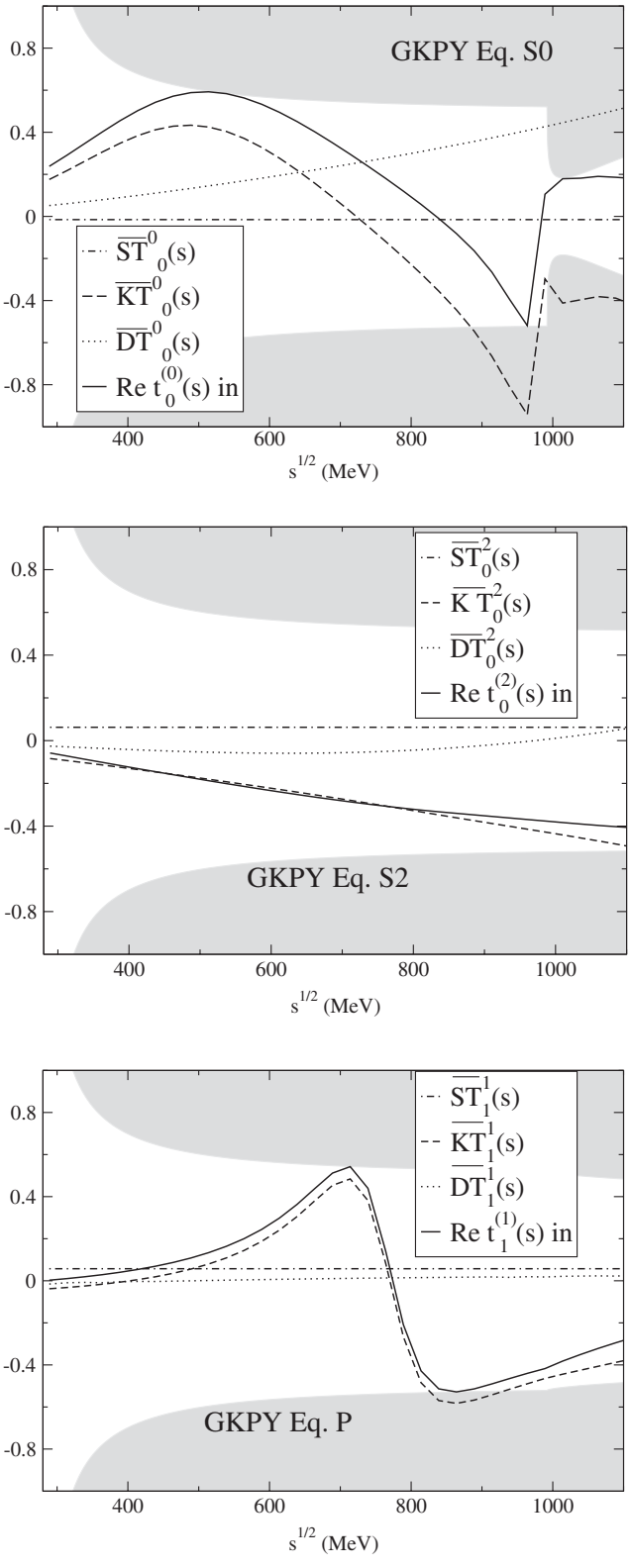

FIG. 7. Using the UFD set as input, we show the decomposition of GKPY equations into the subtracting term $\overline{ST}$, the kernel term $\overline{KT}$, and the driving term $\overline{DT}$ for the S0, P, and S2 waves. Note the different scales used here and in Fig. 6. The gray areas lie beyond the unitarity bound.

to s, as the energy grows, becoming dominant above roughly 450 MeV. In contrast, since the GKPY $\overline{ST}$ term is constant and there are no large cancellations, the resulting GKPY equations have a much smaller uncertainty in that region. Actually, the errors for the GKPY equations in the three waves come almost completely from the $\overline{KT}(s)$ terms. At low energies, the effect is reversed and Roy equations provide a much more stringent constraint than GKPY. Therefore, and as we will show next, they become complementary ways of checking our data parametrizations at different energies.

F. Consistency check of unconstrained fits

In order to provide a consistency measure for our parametrizations with respect to the dispersive relations and sum rules presented in the previous sections, we will make use (as we did in previous works) of a quantity similar to an averaged $\chi^2/(\text{d.o.f.})$ distribution. In particular, we can consider that a dispersion relation i is well satisfied at a point s_n if the difference Δ_i, defined in Eqs. (12)–(14) and (18), is smaller than its uncertainty $\delta\Delta_i$. Thus, when the average discrepancy verifies

$$\bar{d}_i^2 \equiv \frac{1}{\text{number of points}} \sum_n \left(\frac{\Delta_i(s_n)}{\delta\Delta_i(s_n)}\right)^2 \leq 1, \qquad (19)$$

we consider that the corresponding dispersion relation is well satisfied within uncertainties in the energy region spanned by the points s_n. In practice, the values of $s_n^{1/2}$ are taken at intervals of 25 MeV between threshold and the maximum energy, where we study each dispersion relation (1420 MeV for FDR and 1115 MeV for Roy and GKPY equations). In addition, we have added a point below threshold at $s = 2M_\pi^2$ for the F_{00} and F_{0+} FDRs.

Similarly, we define discrepancies for the sum rules in Eqs. (16) and (17), as follows:

$$\bar{d}_I^2 = \left(\frac{I}{\delta I}\right)^2, \qquad \bar{d}_J^2 = \left(\frac{J}{\delta J}\right)^2. \qquad (20)$$

In order to calculate the uncertainties $\delta\Delta_i(s_n)$, δI, δJ, we have followed two approaches: On the one hand, we have simply added in quadrature the effect of varying each parameter independently in our parametrizations from p_i to $p_i \pm \delta p_i$. The errors are symmetric since, in order to be conservative, we have always taken the largest variation as the final error when changing the sign of δp_i. This is rather simple but does not take their correlations into account. On the other hand, we have also estimated the uncertainties using a Monte Carlo Gaussian sampling [34] of all CFD parameters (within 6 standard deviations). The uncertainties are then slightly asymmetric, corresponding to the independent left and right widths of the generated distribution for 10^5 events. This is, of course, much more time consuming, although in this way we can keep part of the correlations in the results. However, we have checked that

both methods yield very similar results, because the errors coming from each individual parameter are small and the number of parameters is large. The difference between using one method or another is almost negligible [34] and thus, for simplicity, we are providing numbers and figures with the first one, which would be much easier to reproduce should someone use our parametrizations.

In Table I we show the averaged squared discrepancies $\bar{d}_i^2$ that result when we use the UFD set described in Secs. II and III. We are showing these discrepancies up to two different energy regions, 932 MeV and 1420 MeV for FDRs, and up to 992 MeV and 11115 MeV for both Roy and GKPY equations (note that we have kept the same definition of energy regions as in KPY08, so that we can compare easily with the results obtained there). Let us remark that these discrepancies are ''squared distances,'' similar to a χ^2, and so we will abuse the language and talk about average ''standard deviations,'' which correspond to the *square root* of $\bar{d}_i^2$. Still, one has to keep in mind that these dispersion relations have not been fitted yet.

Let us first concentrate in the low energy part below 932 MeV or 992 MeV. We can observe that FDRs are reasonably well satisfied: Discrepancies are never beyond 1.3 standard deviations. Roy equations are also well satisfied, with a discrepancy below 1.2 standard deviations. However, the GKPY equations are much more demanding: The UFD set satisfies the S2 wave equation fairly well, but it does not satisfy the S0 and P wave relations so well. Still, no dispersion relation lies beyond 1.6 standard deviations. This is not too bad, given the fact that we have not fitted the dispersion relations, but there is clear room for improvement. Let us recall that this is just how experimental data satisfy these constraints; there is no theory on the UFD set.

If we now also include the region above 932 MeV for FDRs or above 992 MeV for Roy and GKPY equations, we find that the agreement deteriorates considerably: Four relations lie between 1.4 and 1.65 average standard deviations, but not beyond that. Fortunately, we will get much better fulfillment of dispersion relations in all regions by allowing for a small variation of the parameters in the constrained fits to be discussed below.

Let us also remark that the two sum rules, Eqs. (16) and (17), are satisfied within 1.9 and 0.3 standard deviations. Even for the first one, this is still a fair agreement, because, in practice, both of them correspond to a 1 order of magnitude cancellation between the low and high energy contributions to the sum rules, which, in these UFD sets, are determined from uncorrelated data fits.

Also in Table I we show the average discrepancies for the old UFD set in KPY08. With regard to FDRs and Roy equations, it is evident that the new UFD fit is doing worse than the one in KPY08. Nevertheless, one should keep in mind that the new S0 wave has reduced its uncertainty at low energies by somewhat more than 10%, because the published NA48/2 data are more precise and also because we are discarding the controversial $K \to 2\pi$ datum. For that reason, one would have expected the averaged squared discrepancies to now look bigger by as much as 20% or 30% whenever the S0 wave contributes significantly to the dispersion relation. With this correction in mind, the deterioration is not so significant. Nevertheless, we want to insist that this is basically due to the new results of NA48/2 and our getting rid of the $K \to 2\pi$ datum. The data have changed.

Why do we then claim to have improved the S0 wave in this work? The answer comes from GKPY equations, which, as we already explained, are much more precise than Roy

TABLE I. Average discrepancies $\bar{d}_i^2$ of the unconstrained data fits (UFD set) for each dispersion relation. We compare the results of the parametrization obtained in this work (new UFD) with those in KPY08 (old UFD set). The huge discrepancies seen in KPY08 for GKPY equations all come from energies above ~500 MeV. This is the main reason to improve our unconstrained S0 fit, as explained in Sec. III C.

$\bar{d}_i^2$	New UFD	Old UFD	New UFD	Old UFD
FDRs	$s^{1/2} \leq 932$ MeV		$s^{1/2} \leq 1420$ MeV	
$\pi^0\pi^0$	0.31	0.12	2.13	0.29
$\pi^+\pi^0$	1.03	0.84	1.11	0.86
$I_{t=1}$	1.62	0.66	2.69	1.87
Roy equations	$s^{1/2} \leq 992$ MeV		$s^{1/2} \leq 1100$ MeV	
S0	0.64	0.54	0.56	0.47
S2	1.35	1.63	1.37	1.68
P	0.79	0.74	0.69	0.65
GKPY equations	$s^{1/2} \leq 992$ MeV		$s^{1/2} \leq 1100$ MeV	
S0	1.78	5.0	2.42	8.6
S2	1.19	0.49	1.14	0.58
P	2.44	3.1	2.13	2.7
Average	1.24	1.46	1.58	1.97

equations above roughly 450 MeV for the S0 wave, given the present experimental input. It is clear that the KPY08 UFD parametrization satisfies the S0 GKPY equation very poorly at any energy and is not satisfying the low energy P GKPY equation very well. For that reason, we have improved the matching and the data selection, so that our new UFD parametrization, which will be our starting point for the constrained fits, satisfies GKPY equations much better without spoiling FDR and Roy equations. The improvement due to the new unconstrained S0 wave fit is obvious from Table I, particularly in the S0 GKPY equation. Up to 1100 MeV, the old UFD set from KPY08 had an averaged squared discrepancy of 8.6, whereas the new UFD set has 2.42. This huge improvement on the S0 wave has been compensated by some deterioration in other relations at high energy, so that the averaged discrepancy up to high energies is reduced only from 1.97 to 1.58. Note that the change in the inelasticity parameter, that now shows a much bigger dip in the 1000 to 1100 MeV region, as shown in Fig. 5, plays a relevant role in this dramatic improvement. This dip structure is thus favored by the GKPY equations, something that could not be seen with standard Roy equations since their uncertainties in that region are huge. We will discuss this in detail in Sec. VII B. At low energies, the average squared discrepancy has been reduced very little, from 1.46 down to 1.24. Of course, let us remark once again that our uncertainties are now 10%–15% smaller in the S0 wave at low energies, so that the improvement is actually bigger than it seems just from the numbers in the table.

Let us mention here that the inclusion of the new terms parametrizing a crude dependence on the η momentum above $\eta\eta$ threshold help reduce the average squared distances by 6%, namely, from 1.68 to 1.58. In particular, the average squared discrepancies $\bar{d}_i^2$ for the S0 GKPY equation decrease from 3.02 to 2.42 and for the F_{00} FDR equation from 2.35 to 2.13.

Up to now, we have studied the overall uncertainties, but in Fig. 8 we show to what extent FDRs are satisfied by the UFD set, as a function of energy. Of course, the best fulfillment is found at lower energies. In Fig. 9 we show how the usual, twice-subtracted Roy equations are satisfied by the UFD set. Here, as we did in Sec. IV E, we denote by "in" what our parametrizations give for $\mathrm{Re}t_\ell^{(I)}$, whereas we denote by "out" the result of the dispersive representation from Roy equations, namely, the subtraction constant terms, plus the kernel terms, plus the driving terms in Eq. (14). Finally, in Fig. 10 we show how the new, once-subtracted, GKPY equations are satisfied by the UFD set. We follow the same in and out notation as for Roy equations.

Comparing Fig. 9 with Fig. 10, it is clear that, given the present experimental input, the uncertainty band for GKPY equations is much smaller than that for Roy equations above 450 MeV, whereas the opposite occurs at lower energies. Therefore, as we have emphasized repeatedly, the new GKPY equations represent a much stronger

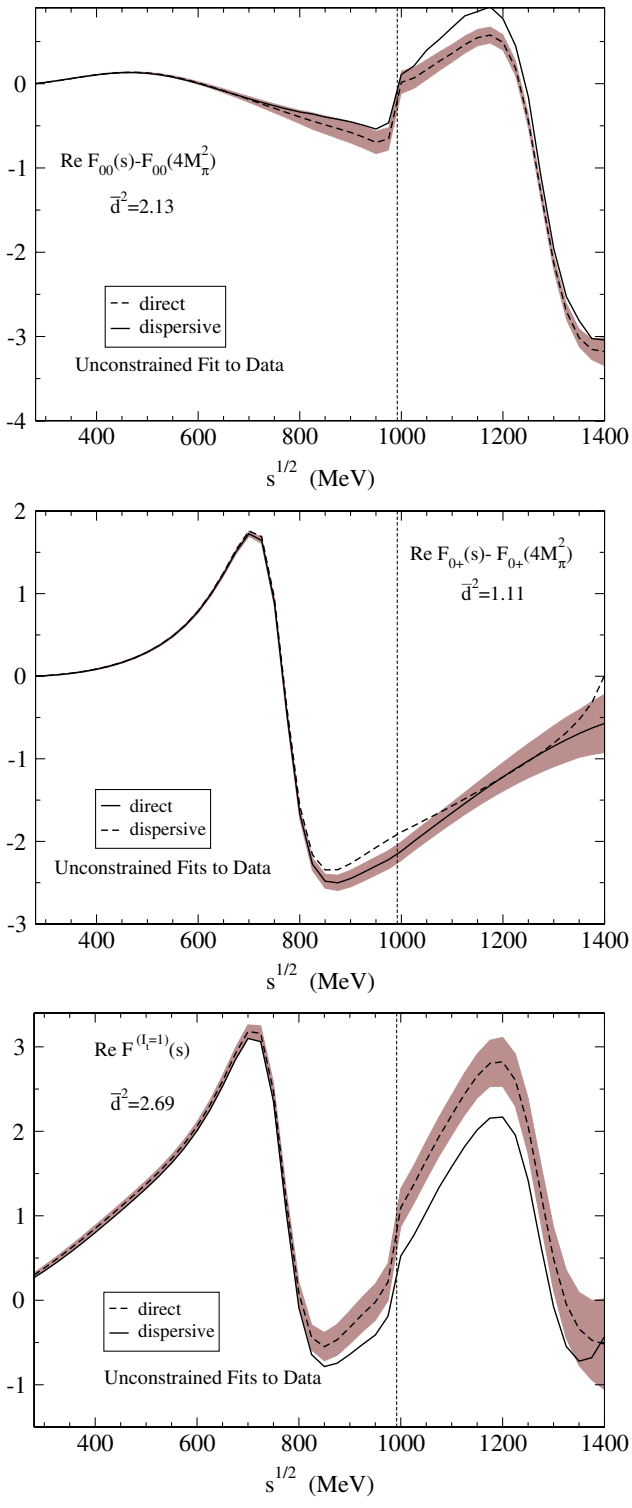

FIG. 8 (color online). Results for forward dispersion relations. Dashed lines: real part, evaluated directly with the UFD parametrizations. Continuous lines: the result of the dispersive integrals. The dark bands cover the uncertainties in the difference between both. From top to bottom: (a) the $\pi^0\pi^0$ FDR, (b) the $\pi^0\pi^+$ FDR, and (c) the FDR for $I_t = 1$ scattering. The dotted vertical line stands at the $\bar{K}K$ threshold.

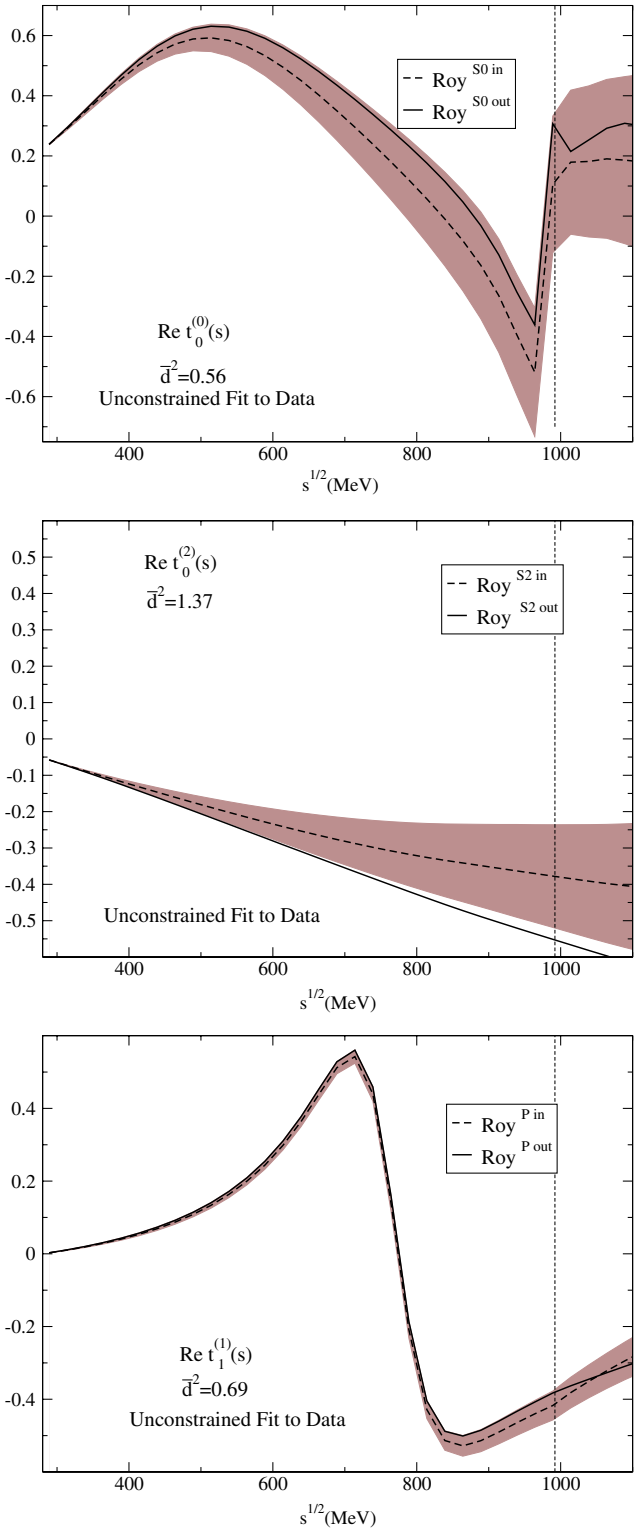

FIG. 9 (color online). Results for Roy equations. Dashed lines (in): real part, evaluated directly with the UFD parametrizations. Continuous lines (out): the result of the dispersive representation. The gray bands cover the uncertainties in the difference between both. From top to bottom: (a) S0 wave, (b) S2 wave, and (c) P wave. The dotted vertical line stands at the $\bar{K}K$ threshold.

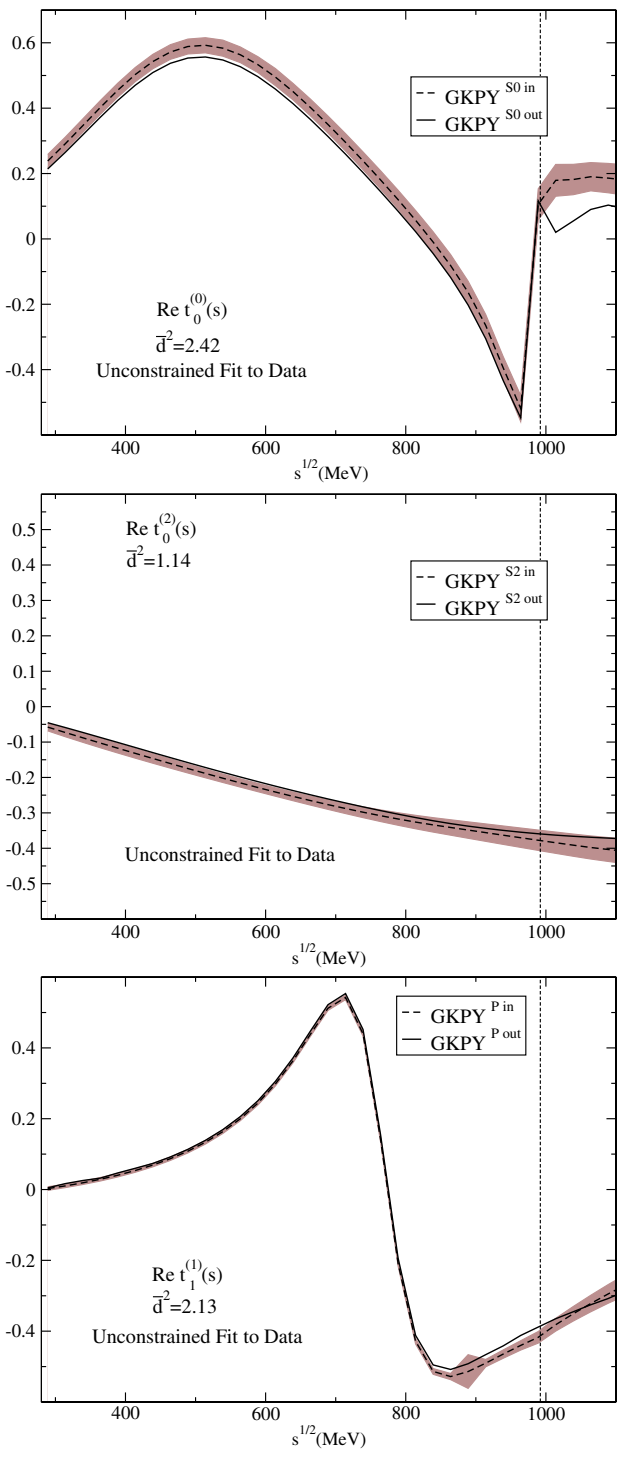

FIG. 10 (color online). Results for GKPY equations. Dashed lines (in): real part, evaluated directly with the UFD parametrizations. Continuous lines (out): the result of the dispersive representation. The gray bands cover the uncertainties in the difference between both. From top to bottom: (a) S0 wave, (b) S2 wave, and (c) P wave. Note how these uncertainties are much smaller above 450 MeV than those from the standard Roy equations shown in Fig. 9. The dotted vertical line stands at the $\bar{K}K$ threshold.

constraint in the intermediate energy region than standard Roy equations.

In summary, with the new S0 unconstrained fit, all dispersion relations are satisfied in the different energy regions within less than 1.6 standard deviations in the low energy regime, and 1.7 including the intermediate energies. This is a fairly reasonable fulfillment, given the fact that the information about analyticity has not been included as a constraint in the UFD description. Nevertheless, it is obvious that there is room for improvement, which is what we will do by obtaining constrained data fits in the next section.

V. FITS TO DATA CONSTRAINED BY DISPERSION RELATIONS

In previous works (PY05, KPY08) we had improved the consistency of our description of $\pi\pi$ scattering amplitudes by imposing FDR and Roy equation fulfillment within uncertainties. As we have just seen in the previous section, the GKPY equations provide a much more stringent constraint in the intermediate energy region than standard Roy equations, and thus it now makes sense to impose the new GKPY equations *as an additional constraint* in a new set of constrained fits to data (CFD set).

A. Minimization procedure

Our goal is then to obtain a fit to data, by changing the UFD parametrizations slightly, that fulfills each dispersion relation within errors. As we did in [3], we will now use the average discrepancies $\bar{d}_i^2$, defined in Eqs. (19) and (20), to obtain these constrained fits, by minimizing

$$\sum_i W_i^2 \bar{d}_i^2 + \bar{d}_I^2 + \bar{d}_J^2 + \sum_k \left(\frac{p_k - p_k^{\rm exp}}{\delta p_k} \right)^2, \qquad (21)$$

where i runs over the three FDRs, as well as the three Roy and the three GKPY equations. Here, we denote by $p_k^{\rm exp}$ all the parameters of the UFD parametrizations for each wave or Regge trajectory. In this way, we force the previous data parametrizations to satisfy dispersion relations and sum rules within uncertainties. In KPY06 and KPY08 a common weight of $W_i^2 \sim 9$ was estimated from the typical number of degrees of freedom needed to describe the shapes of the output. This value ensured that every single dispersion relation was fairly well described by the KPY08 constrained data fits up to the matching energy used in that work, namely, 932 MeV.

However, we are now considering partial waves up to 1115 MeV. For most waves, this extension does not alter significantly their shape, and $W_i = 3$ is still a good weight. Nevertheless, we have less points in the region above 932 MeV, and if we want the fit to give not just a good average $\bar{d}_i^2$, but also a good description for each wave, some of these waves need further weight on the high energy region, in particular, if their UFD $\bar{d}_i^2$ was larger than 2. For this purpose, we have increased W_i up to 3.5 for the high energy parts of the F_{00}, $F^{(I_t=1)}$, as well as 4.2 for the GKPY P wave in the whole energy region. Finally, we have increased W_i up to 7 for the high energy part of the S0 GKPY equation. The latter was to be expected, since in this region there is a lot more structure, both in the phase and inelasticity, due to the presence of the $f_0(980)$. These values are not arbitrary, since they have been obtained by increasing each W_i gradually, starting from 3, until the $\bar{d}_i^2$ are below or very close to 1 *uniformly* throughout the whole energy range, for all dispersion relations obtained from the constrained fit. This uniformity is very relevant to avoid dispersive constraints being badly satisfied in some small energy region despite the averaged $\bar{d}_i^2$ still remaining below 1.

Before proceeding further, let us recall that, strictly speaking, the quantity that we minimize in Eq. (21) is *not* a χ^2, but that each individual $\bar{d}_i^2$ is a measure of how well each dispersion relation is satisfied.

B. Variation of the S2 Adler zero

As we have seen in Sec. III C, in the parametrization of each scalar wave, we explicitly factorized a zero in the subthreshold region. These are the Adler zeros required by chiral symmetry constraints [31]. Actually, we fixed them to $\sqrt{s_A^{\rm S0}} \equiv \sqrt{M_\pi^2/2} \simeq 99$ MeV and $\sqrt{s_A^{\rm S2}} \equiv \sqrt{2M_\pi^2} \simeq 197$ MeV, which are their current algebra values (leading order ChPT). Of course, once these UFD parametrizations are used inside the S0 and S2 Roy or GKPY equations, we can also obtain the *dispersive result* for the S0 and S2 Adler zeros, which we provide in Table II.

In order to determine the positions of Adler zeros better when making constrained fits in KPY08, we allowed them to change within the dispersive uncertainties obtained from the UFD set. However, in this work we will not insist on $z_0/\sqrt{2}$ reproducing the S0 wave Adler zero very precisely. The reason is that, as we see in Table II, the uncertainties in $\sqrt{s_A^{\rm S0}}$ obtained either from Roy or GKPY equations are huge, and setting z_0 free introduces a spurious and

TABLE II. Adler zero positions $\sqrt{s_A}$, in MeV, for the S0 and S2 waves, obtained from Roy or GKPY equations using the parametrizations from either the UFD or CFD set.

	Roy equations with UFD	GKPY equations with UFD	Roy equations with CFD	GKPY equations with CFD
$\sqrt{s_A^{\rm S0}}$	112 ± 24	120 ± 30	83 ± 32	85 ± 34
$\sqrt{s_A^{\rm S2}}$	189 ± 11	200 ± 6	200 ± 10	201 ± 5

extremely correlated source of error. In addition, in KPY08, the z_0 central value moved in the wrong direction [36]. In addition, as already explained in Sec. III C, the S0 wave Adler zero lies close to the border of the conformal circle, i.e., $w(s_A^{S0}) \simeq -1$, where the conformal expansion converges very slowly. We simply have to accept that our S0 wave conformal expansion is not very accurate around the Adler zero. Of course, this is irrelevant for the integrals in the physical region and has a negligible influence on the set of constrained fits we will obtain next.

In contrast, the S2 Adler zero obtained from the dispersive representation moves very little from its current algebra value, and its uncertainty is rather small. The reason for this difference in uncertainties is, for a good part, that the S0 wave Adler zero lies very close to the left cut, whereas the S2 Adler zero is not so far from threshold and is quite well determined when data are used as input of either Roy or, even better, GKPY equations. For that reason, we still allow the S2 Adler zero to vary when making the constrained fits, using as a starting point the weighted average of the values obtained from the UFD set inside Roy and GKPY equations, namely, $\sqrt{s_A^{S2}} = 197.7 \pm 5.1$ MeV.

C. Constrained fits to data

The resulting parameters for the CFD are gathered in the tables of Appendix A. It is reassuring to observe that, except for the S0 wave at intermediate energies, the values of the parameters do not change much from the UFD to the CFD sets, as could be expected, since, as we saw in Table I, the UFD fulfillment of dispersive constraints only needed some improvement, but not a radical change. In particular, the GKPY equation for the S0 wave is very well satisfied in the CFD at the expense of an average change of 0.82 standard deviations in the high energy parameters and almost no change in the low energy ones. Certainly, most of this change is concentrated in the parameters c and $\tilde{\epsilon}_1$ in Eqs. (10) and (11). We will discuss below that the resulting phase after this change still describes the phase shift and inelasticity data fairly well, but tends to make the $f_0(980)$ somewhat wider. The D2 wave is the one that deviates most from its unconstrained parametrization, but its parameters are, on average, within 1.4 standard deviations of their UFD value. This could be expected, as was already commented in our previous works [1,3], since, together with the S0 at high energy, it is probably the one where data have the worst quality. The parameters of the other waves, or those of the Regge parametrizations, do not deviate—on average—beyond 0.6 standard deviations from their UFD values. In Table XII in Appendix D we provide the S0, P, and S2 phase shifts that result from using the CFD set inside the dispersive representation.

In Table III we list the averaged discrepancies that result when we use the CFD inside the dispersion relations. Let us remark that all discrepancies are now below 1, and are very similar both for the low energy region and also when including the high energy region. This shows a remarkable average consistency and homogeneity for this new set of data parametrizations. Let us recall that we only constrain our fits to satisfy dispersion relations up to 1420 MeV for FDR and 1115 MeV for Roy and GKPY equations. Consequently, we expect the dispersive representation to be somewhat worse satisfied in the region near the maximum energy under consideration. This is indeed observed since the average squared discrepancies are somewhat smaller below 1 GeV than up to the maximum energy, where we usually find the point satisfying the dispersion relations worse.

TABLE III. Average discrepancies $\bar{d}_i^2$ of the CFD for each dispersion relation.

FDRs	$s^{1/2} \leq 932$ MeV	$s^{1/2} \leq 1420$ MeV
$\pi^0\pi^0$	0.32	0.51
$\pi^+\pi^0$	0.33	0.43
$I_{t=1}$	0.06	0.25
Roy equations	$s^{1/2} \leq 992$ MeV	$s^{1/2} \leq 1100$ MeV
S0	0.02	0.04
S2	0.21	0.26
P	0.04	0.12
GKPY equations	$s^{1/2} \leq 992$ MeV	$s^{1/2} \leq 1100$ MeV
S0	0.23	0.24
S2	0.12	0.11
P	0.68	0.60
Average	0.22	0.28

Furthermore, as already commented, the updated selection and treatment of the S0 wave data has decreased the S0 wave uncertainties by roughly 10% to 15%. This means that the consistency shown by the average discrepancies in Table III is even better than it looks when comparing with similar results given in KPY08 for FDR and Roy equations, since we are getting a very good consistency with slightly smaller uncertainties.

As we did for the UFD set, we now show in Figs. 11–13 how well the CFD set satisfies FDR, Roy, and GKPY equations, respectively. The improvement in the consistency of the CFD set over the UFD is evident by comparing these plots with their UFD counterparts in Figs. 8–10.

Finally, the two sum rules in Eqs. (16) and (17) are also remarkably well satisfied, within 0.93 and 0.1 standard deviations, respectively. In particular, the 1.9 standard deviations for the sum rule in Eq. (17) using the UFD set are reduced dramatically, and this implies now a 2 orders of magnitude cancellation between the low and high energy contributions.

VI. THRESHOLD PARAMETERS AND ADLER ZEROS

Apart from the additional GKPY equations, the main novelty of this work is the S0 wave improvement, both in

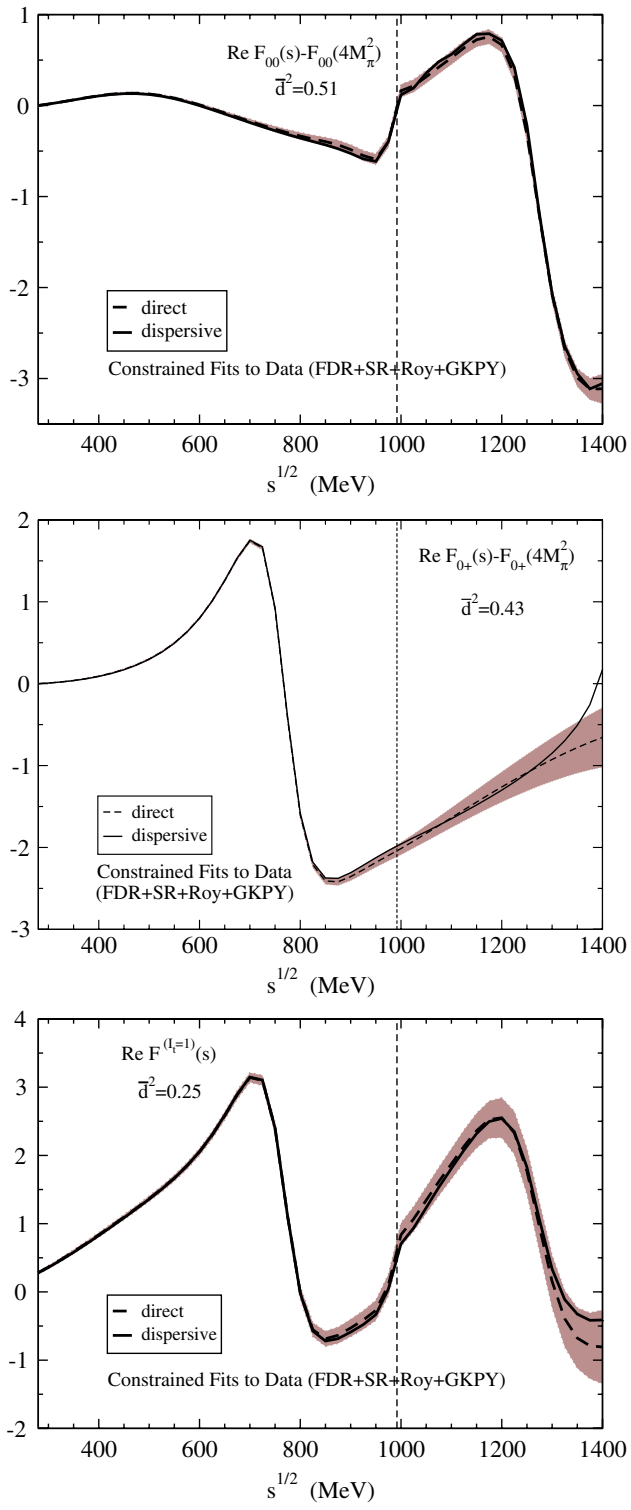

FIG. 11 (color online). Results for forward dispersion relations. Dashed lines: real part, evaluated directly with the CFD parametrizations. Continuous lines: the result of the dispersive integrals. The dark bands cover the uncertainties in the difference between both. From top to bottom: (a) the $\pi^0\pi^0$ FDR, (b) the $\pi^0\pi^+$ FDR, and (c) the FDR for $I_t = 1$ scattering. The dotted vertical line stands at the $\bar{K}K$ threshold.

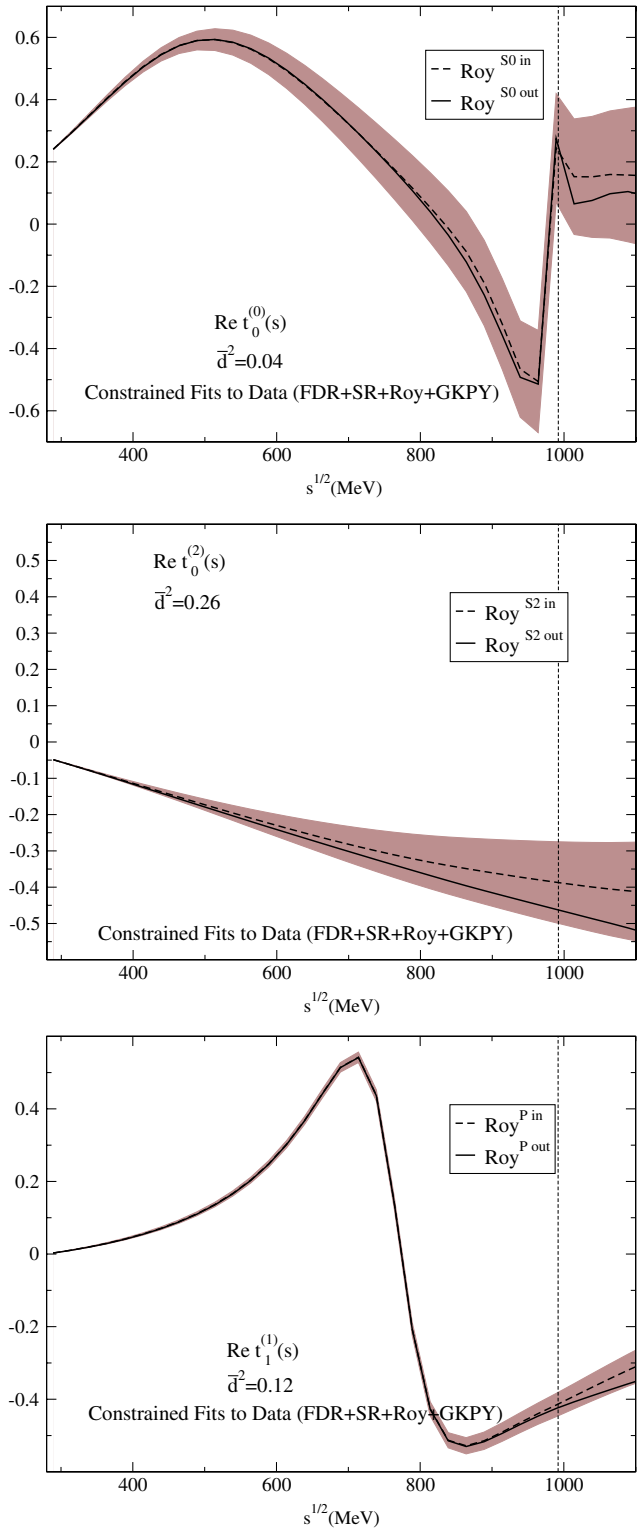

FIG. 12 (color online). Results for Roy equations. Dashed lines (in): real part, evaluated directly with the CFD parametrizations. Continuous lines (out): the result of the dispersive representation. The gray bands cover the uncertainties in the difference between both. From top to bottom: (a) S0 wave, (b) S2 wave, and (c) P wave. The dotted vertical line stands at the $\bar{K}K$ threshold.

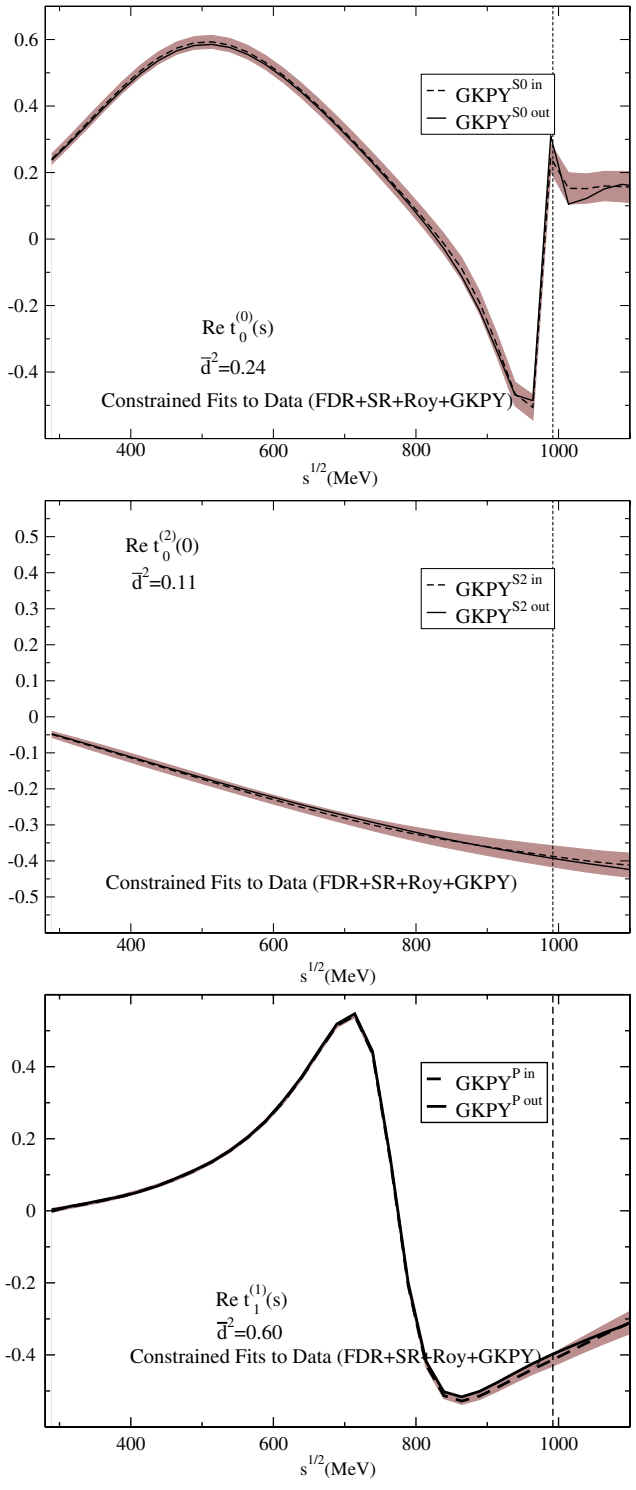

FIG. 13 (color online). Results for GKPY equations. Dashed lines (in): real part, evaluated directly with the CFD parametrizations. Continuous lines (out): the result of the dispersive representation. The gray bands cover the uncertainties in the difference between both. From top to bottom: (a) S0 wave, (b) S2 wave, and (c) P wave. Note how these uncertainties are much smaller above 450 MeV than those from the standard Roy equations shown in Fig. 12. The dotted vertical line stands at the $\bar{K}K$ threshold.

its parametrization and data analysis. Thus, naively, one may not expect a big variation in the low energy part of the other waves with respect to previous works.

However, let us recall that, as we did in KPY08, we calculate most threshold parameters from sum rules. Thus, the changes in the S0 wave can also affect the calculation of these low energy parameters for other waves. In particular, when using sum rules with one subtraction, the intermediate energy part of our parametrizations, now constrained by GKPY equations, also plays a relevant role in our final results. In this section we will thus recalculate all these threshold parameters with the new CFD set. Actually, we will find that not only the S0 wave, but also the D wave threshold parameters suffer sizable modifications.

Finally, in previous works we did not use the dispersive or sum rule techniques to determine, with precision, the position of Adler zeros, which are required by chiral symmetry in the subthreshold region of the S0 and S2 waves, and are therefore of interest for chiral perturbation theory. Also in this section we will determine them using the Roy and GKPY equations with the CFD set as input for the integrals.

A. Sum rules for threshold parameters

We list in Table IV the values of the threshold parameters for all the partial waves we considered in this analysis, namely, S0, S2, P, D0, D2, and F. In addition, we provide values for $a_0^{(0)} - a_0^{(2)}$, $2a_0^{(0)} - 5a_0^{(2)}$, and $\delta_0^{(0)}(M_K^2) - \delta_0^{(2)}(M_K^2)$, since these parameters are of relevance for pion atoms, scalar threshold parameters, and kaonic decays. In the second and third columns, we provide the results from the UFD and CFD sets. We already commented that the CFD parametrizations change only very slightly compared to the UFD, and this is well corroborated by the fact that all the UFD and CFD results in Table IV are compatible with one another within roughly 1 standard deviation.

In the fourth column, we use the very reliable CFD set inside several sum rules, which we detail next only very briefly, since they had already been given in detail in KPY08. First, we use the well-known Olsson sum rule:

$$2a_0^{(0)} - 5a_0^{(2)} = 3M_\pi \int_{4M_\pi^2}^{\infty} ds \frac{\mathrm{Im}F^{(I_t=1)}(s,0)}{s(s-4M_\pi^2)}, \qquad (22)$$

which is dominated at high energies by the ρ-Regge exchange, and can thus have only one subtraction. Apart from the normalization, this is just the FDR in Eq. (13), but evaluated at threshold.

Next, for $\ell \geq 1$, we use the Froissart-Gribov representation:

TABLE IV. Threshold parameters in the customary $M_\pi = 1$ units and the $\delta_0^{(0)}(M_K^2) - \delta_0^{(2)}(M_K^2)$ phase difference. The values in the second and third columns are obtained directly from the UFD and CFD parametrizations, respectively. The fourth column is obtained using the CFD set inside sum rules.

	UFD	CFD	Sum rules with CFD	Best values	KPY08 values
$a_0^{(0)}$	0.218 ± 0.009	0.221 ± 0.009		0.220 ± 0.008[e]	0.223 ± 0.009
$a_0^{(2)}$	-0.052 ± 0.010	-0.043 ± 0.008		-0.042 ± 0.004[e]	-0.044 ± 0.004
$a_0^{(0)} - a_0^{(2)}$	0.270 ± 0.009	0.264 ± 0.009		0.262 ± 0.006[e]	0.267 ± 0.009
$2a_0^{(0)} - 5a_0^{(2)}$	0.696 ± 0.054	0.657 ± 0.043	0.648 ± 0.016[a]	0.650 ± 0.015	0.668 ± 0.017
$\delta_0^{(0)}(M_K^2) - \delta_0^{(2)}(M_K^2)$	$47.4 \pm 0.9°$	$47.3 \pm 0.9°$		$47.3 \pm 0.9°$	$50.9 \pm 1.2°$
$b_0^{(0)}$	0.276 ± 0.007	0.278 ± 0.007	0.278 ± 0.008[d]	0.278 ± 0.005	0.290 ± 0.006
$b_0^{(2)}$	-0.085 ± 0.010	-0.080 ± 0.009	-0.082 ± 0.004[d]	-0.082 ± 0.004	-0.081 ± 0.003
$a_1(\times 10^3)$	37.3 ± 1.2	38.5 ± 1.2	37.7 ± 1.3[b]	38.1 ± 0.9	38.1 ± 0.9
$b_1(\times 10^3)$	5.18 ± 0.23	5.07 ± 0.26	6.0 ± 0.9[b], 5.48 ± 0.17[c]	5.37 ± 0.14	5.12 ± 0.15
$a_2^{(0)}(\times 10^4)$	18.7 ± 0.4	18.8 ± 0.4	17.8 ± 0.3[b]	17.8 ± 0.3	18.33 ± 0.36
$a_2^{(2)}(\times 10^4)$	2.5 ± 1.1	2.8 ± 1.0	1.85 ± 0.18[b]	1.85 ± 0.18	2.46 ± 0.25
$a_2^{(0)}(\times 10^4)$	-4.2 ± 0.3	-4.2 ± 0.3	-3.5 ± 0.2[b]	-3.5 ± 0.2	-3.82 ± 0.25
$b_2^{(2)}(\times 10^4)$	-2.7 ± 1.0	-2.8 ± 0.8	-3.3 ± 0.1[b]	-3.3 ± 0.1	-3.59 ± 0.18
$a_3(\times 10^5)$	5.2 ± 1.3	5.1 ± 1.3	5.65 ± 0.23[b]	5.65 ± 0.21	6.05 ± 0.29
$b_3(\times 10^5)$	-4.7 ± 2.6	-4.6 ± 2.5	-4.06 ± 0.27[b]	-4.06 ± 0.27	-4.41 ± 0.36

[a]From Eq. (22).
[b]From Eq. (23).
[c]From Eq. (24).
[d]From Eqs. (25) and (26).
[e]In addition, for the best values of the S0 and S2 scattering lengths, we have refitted their CFD values constrained to satisfy the Olsson sum rule, Eq. (22), which is also used to obtain the best value for their difference and its uncertainty, Eqs. (27) and (28).

$$a_\ell = \frac{\sqrt{\pi}\Gamma(\ell+1)}{4M_\pi\Gamma(\ell+3/2)}\int_{4M_\pi^2}^{\infty} ds \frac{\mathrm{Im}F(s,4M_\pi^2)}{s^{l+1}},$$

$$b_\ell = \frac{\sqrt{\pi}\Gamma(\ell+1)}{2M_\pi\Gamma(\ell+3/2)}\int_{4M_\pi^2}^{\infty} ds \times\left\{\frac{4\,\mathrm{Im}F'_{\cos\theta}(s,4M_\pi^2)}{(s-4M_\pi^2)s^{\ell+1}} - \frac{(\ell+1)\mathrm{Im}F(s,4M_\pi^2)}{s^{\ell+2}}\right\}, \quad (23)$$

with $\mathrm{Im}F'_{\cos\theta} \equiv (\partial/\partial\cos\theta_s)\mathrm{Im}F$, where $\cos\theta_s$ is the angle between the initial and final pions. For amplitudes with fixed isospin in the t channel, an extra factor of 2 (due to the identity of particles) has to be added to the left-hand side of the equation above.

In addition, we use the following sum rule that we derived in [1]:

$$b_1 = \frac{2}{3M_\pi}\int_{4M_\pi^2}^{\infty} ds\left\{\frac{1}{3}\left[\frac{1}{(s-4M_\pi^2)^3} - \frac{1}{s^3}\right]\mathrm{Im}F^{(I_t=0)}(s,0) + \frac{1}{2}\left[\frac{1}{(s-4M_\pi^2)^3} + \frac{1}{s^3}\right]\mathrm{Im}F^{(I_t=1)}(s,0) - \frac{5}{6}\left[\frac{1}{(s-4M_\pi^2)^3} - \frac{1}{s^3}\right]\mathrm{Im}F^{(I_t=2)}(s,0)\right\}, \quad (24)$$

together with another two sum rules, derived in [3], involving either the S0 and S2 slopes,

$$b_0^{(0)} + 2b_0^{(2)} = \lim_{s\to 4M_\pi^{2+}} \mathrm{P.P.}\int_{4M_\pi^2}^{\infty} ds' \times\frac{6M_\pi(2s'-4M_\pi^2)\mathrm{Im}F_{00}(s')}{s'(s'+s-4M_\pi^2)(s'-4M_\pi^2)(s'-s)}, \quad (25)$$

or the S2 slope parameter and the P wave scattering length:

$$3a_1^{(1)} + b_0^{(2)} = \lim_{s\to 4M_\pi^{2+}} \mathrm{P.P.}\int_{4M_\pi^2}^{\infty} ds' \times\frac{4M_\pi(2s'-4M_\pi^2)\mathrm{Im}F_{0+}(s')}{s'(s'+s-4M_\pi^2)(s'-4M_\pi^2)(s'-s)}. \quad (26)$$

Note that, as explained in [3], the limits above are to be taken for $s > 4M_\pi^2$. In practice, for the value of a_1 we simply use its Froissart-Gribov representation, and we are left with a sum rule representation for both $b_0^{(0)}$ and $b_0^{(2)}$.

The results for all these sum rules are listed in the fourth column of Table IV.

The fifth column, which contains what we consider our best values, is obtained as follows: For $2a_0^{(0)} - 5a_0^{(2)}$, $b_0^{(0)}$, $b_0^{(2)}$, a_1, and b_1, we take the average between the sum rules above and the direct value of the CFD set, since they are basically independent. However, for the D0, D2, and F waves, in order to stabilize the fits, we had already constrained the value of the threshold parameters by means of the Froissart-Gribov representation in the UFD set (see [1]). Hence, in those cases, it makes no sense to average either the UFD or CFD direct result with the Froissart-

Gribov representation for $a_2^{(0)}$, $a_2^{(2)}$, $b_2^{(0)}$, and a_3, which is therefore considered our best result. The only exceptions are $b_2^{(2)}$ and b_3, since those values were not constrained in the initial UFD, but their uncertainty from the CFD is an order of magnitude larger than from the sum rule, which is the value we quote as the best one.

Let us remark that the S0 and S2 scattering lengths, which are of special interest for ChPT, are refined by refitting them again to the CFD direct results and the Olsson sum rule simultaneously. Obviously, the resulting errors are strongly correlated, and the corresponding correlation ellipse is shown in Fig. 14. The uncertainties can be uncorrelated by using two new variables, x, y, defined as

$$\begin{aligned} a_0^{(0)} &= 0.220 + 0.130x + 0.337y, \\ a_0^{(2)} &= -0.042 - 0.337x + 0.130y, \\ a_0^{(0)} - a_0^{(2)} &= 0.262 + 0.467x + 0.206y, \\ x &= 0 \pm 0.076, \qquad y = 0 \pm 0.023, \end{aligned} \tag{27}$$

which give the numbers listed in the tables as our "Best values":

$$\begin{aligned} a_0^{(0)} &= 0.220 \pm 0.008, \\ a_0^{(2)} &= -0.042 \pm 0.004, \\ a_0^{(0)} - a_0^{(2)} &= 0.262 \pm 0.006, \end{aligned} \tag{28}$$

in units of M_π.

For the sake of comparison, we list in the sixth column our results from KPY08, where we did not impose the GKPY equations nor did we add the several improvements to the amplitudes and the data implemented in this work. Note that the low energy parameters are quite consistent with our previous results; i.e. many central values lie within 1 standard deviation of our KPY08 results, and most of them overlap within 1 standard deviation. There are, of course, the expected exceptions: First, the $\delta_0^{(0)}(M_K^2) - \delta_0^{(2)}(M_K^2)$ central value changes by 3 standard deviations, mostly due to the fact that we have discarded here the controversial $K \to \pi\pi$ datum. Next, the S0 slope $b_0^{(0)}$ changes by 2 standard deviations, and this is mostly due to the inclusion of the isospin violation correction in the low energy $K_{\ell 4}$ data. One could have expected that the scattering length $a_0^{(0)}$ may have suffered a large shift for the same reason, but it has only decreased by about a third of a standard deviation. Hence, most of the change due to the $K_{\ell 4}$ isospin correction is concentrated on the slope parameter. In addition, as we already anticipated, both D wave scattering lengths have decreased by roughly 2 standard deviations.

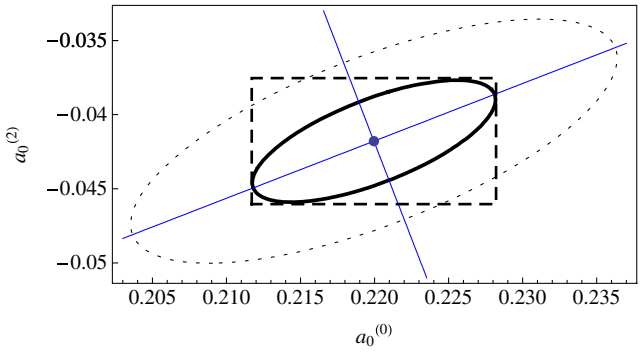

FIG. 14 (color online). The 1 and 2 standard deviation ellipses (thick and dashed lines, respectively) in the $(a_0^{(0)}, a_0^{(2)})$ plane. The rectangle covers the uncertainties of our best results in Eq. (28), obtained from the uncorrelated expressions in Eq. (27).

Although it will be commented in detail in the discussion section, let us note that these new results are in much better agreement with the results in [11] than were those in KPY08.

As commented in Sec. V, we can also check here that the new uncertainties are slightly smaller, but only by 10%–15%, than in KPY08, due to discarding the $K \to \pi\pi$ conflicting input and keeping the S0 Adler zero fixed, and to the more precise NA48/2 published data. The $a_0^{(0)} - a_0^{(2)}$ uncertainty in (28) has decreased by almost 50%, although this is not only due to our improvement of the S0 wave, but mainly to the fact that we are now calculating it differently, using Eqs. (27).

B. Determination of Adler zeros

As already explained, chiral symmetry requires the existence of zeros in the amplitude close to $s = 0$ for the scalar waves S0 and S2 [31]. We have explicitly factorized them in our amplitudes at $s_A^{S0} = z_0^2/2$ and $s_A^{S2} = 2z_2^2$; see Eqs. (6) or (A1) and (A5). As a starting point, we have first fixed them to the ChPT leading order estimate by setting $z_0 = z_2 = M_\pi$ for the UFD parametrizations. We then used these parametrizations inside Roy or GKPY equations to recalculate the position of these Adler zeros, which were listed in the first two columns of Table II.

In previous works, we allowed the z_0 and z_2 parameters to change in the CFD set, expecting them to be accurately fixed by imposing the dispersion relations. Unfortunately, as discussed in Sec. V B, this does not work for the S0 wave. The reason is that its Adler zero is very close to the left cut, in a region where, on the one hand, neither Roy nor GKPY equations provide a precise determination of the zero position (see Table II) and, on the other hand, the conformal expansion converges badly. For that reason, we have simply kept the S0 parameter z_0 fixed to M_π on both the UFD and CFD sets. Being so far from the threshold region, this effect is irrelevant inside the dispersive integrals. Thus, only the S2 Adler zero is allowed to change when obtaining the CFD set, but only within the UFD uncertainties obtained from Roy and GKPY equations.

In this section we go one step further and we finally provide, in the last two columns of Table II, the value of the S0 and S2 wave Adler zeros obtained when the CFD set is

used inside Roy and GKPY equations. The CFD S0 zero is closer to its expected position (around 80 MeV) than the UFD result, but note that the uncertainty gets worse because of this displacement towards the left cut. In summary, we do not have enough precision to pin down the location of this S0 Adler zero accurately.

In contrast, the S2 Adler zero is determined quite precisely by GKPY equations (and to a lesser extent by Roy equations), and the resulting z_2 parameter, if allowed to vary, is almost identical to its UFD determination. Thus, as explained in Sec. V B, we have allowed $\sqrt{2}z_2$ to vary within the weighted average between the GKPY and Roy equation results of the UFD set. The resulting Adler zero, when read directly from the CFD parametrization, is $\sqrt{s_A^{S2}} = \sqrt{2}z_2 = 201 \pm 5$ MeV, which is almost identical to the values obtained by using the CFD set inside Roy or GKPY equations—listed in Table II. This confirms that it is correct to identify the Adler zero with the $\sqrt{2}z_2$ term in our S2 wave conformal parametrization.

VII. DISCUSSION

First of all, we want to remark that ours is just a data analysis, and we are not predicting the value of any observable, just determining them from experiment. In contrast to other approaches [11], we are *not solving* FDR, Roy, or GKPY equations, but just imposing them as constraints on the data analysis. Actually, all these equations have been obtained with several approximations; for instance, they are obtained in the isospin limit, and we only expect them to describe the real world up to some uncertainty of the order of 3%. In addition, all Roy equation studies we are aware of—including this one—neglect any inelasticity to four or more pion states below the two-kaon threshold. This is certainly a very small effect, but is nevertheless an approximation.

Being a data analysis, our parametrizations change when the data change. In particular, in this work we have updated the NA48/2 data [8] with their final results [20], which have smaller uncertainties. In addition, we have incorporated the threshold-enhanced isospin correction in [22] to all $K_{\ell 4}$ data. Moreover, we have discarded the controversial $K \to \pi\pi$ datum [23]. Furthermore, the increased precision provided by the once-subtracted dispersion relations that we have introduced in this work requires an improved parametrization with a continuous derivative matching. This additional constraint and the requirement that the *output* of the dispersion relations should satisfy the elastic unitarity bound—which is automatic in the input parametrizations—have made us also add an additional parameter to the S0 wave parametrization at low energies. As we will see below, the S0 wave parametrization at intermediate energies favors the "dip scenario" for the S0 inelasticity between 1000 and 1100 MeV. In this discussion section we will show in detail the new CFD set, particularly the S0 wave, comparing it to other works, and we will discuss the consequences of these modifications.

A. The new CFD S0 wave

In Fig. 15 we show the resulting CFD S0 wave from threshold up to 1420 MeV, versus the data from different sets in the literature [29,30]. Note the smooth matching at 850 MeV and the kink at $K\bar{K}$ threshold. This is in contrast with our old KPY08 results, already shown in Fig. 3, which have a spurious kink at the matching point (932 MeV in that work), and a much less pronounced kink at $K\bar{K}$ threshold. The difference between the UFD and CFD S0 wave phase shift at low energies, which we showed in Fig. 2, is almost imperceptible.

To ease the comparison of this CFD result with the UFD set for all energies, we have plotted their central values together in Fig. 16. It can be noted that the change above $K\bar{K}$ threshold is again almost imperceptible up to 1200 MeV. The only sizable differences between the phase of the UFD and CFD parametrizations are above 1200 MeV, where our parametrizations are less reliable since Roy and GKPY equations only extend up to 1115 MeV, and on the sharp phase rise in the 900 MeV to $2m_K = 992$ MeV region due to the $f_0(980)$ resonance, which is clearly less steep in the CFD case than in the UFD. The latter is one of the reasons why the CFD solution satisfies GKPY equations well within uncertainties, but the UFD lies somewhere around 2 standard deviations away (see Tables I and III, respectively).

In addition, we also show in Fig. 16 the results from [11], which are in good agreement with ours, but lie slightly lower, only above 550 MeV (see discussion below). Actually, our CFD solution does not show the "hunchback" between 500 and 900 MeV seen in KPY08, as already shown in Fig. 3.

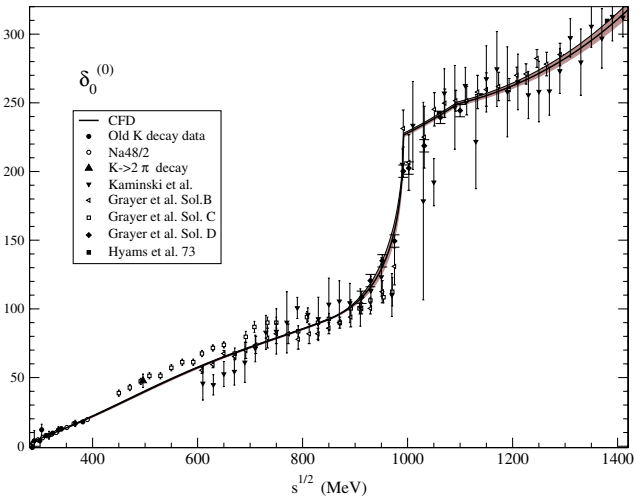

FIG. 15 (color online). The new CFD for the S0 wave versus the existing phase-shift data from [29,30]. The dark band covers the uncertainties.

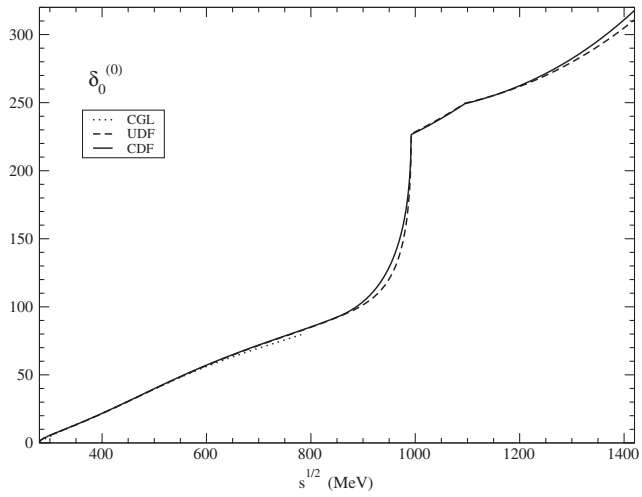

FIG. 16. Comparison between the phase of the CFD and UFD for the S0 wave. We also plot the phase from the Roy equations analysis in [11].

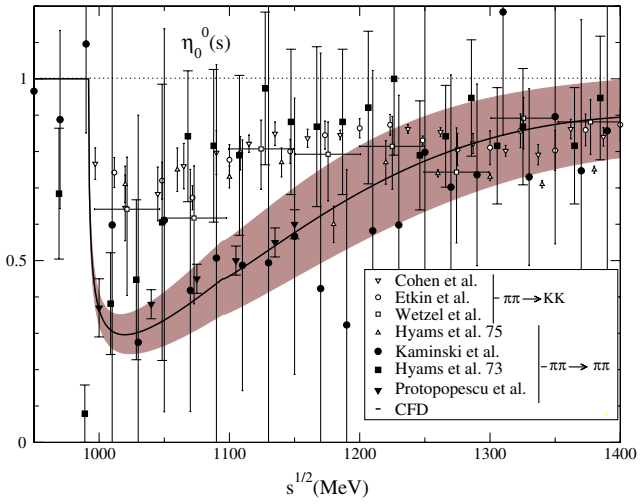

FIG. 18 (color online). CFD S0 wave inelasticity versus experimental data.

Concerning the S0 inelasticity, we show in Fig. 17 the difference between the UFD and CFD sets. It can be noticed that the difference lies essentially within the uncertainties (gray area), although the dip structure above 1000 MeV becomes even deeper in the CFD set. Finally, in Fig. 18 we show the CFD inelasticity versus all the existing experimental data.

Since the UFD set already provided a good description of the inelasticity data obtained from $\pi\pi \to \pi\pi$ experiments, as shown in Fig. 4, so does the CFD. For the same reason, it also fails to reproduce the inelasticity data from $\pi\pi \to K\bar{K}$, as we had already shown for the UFD case in Fig. 5. Note that this is due to the fact that both our UFD and CFD solutions show a dip structure between 1 and 1.1 GeV, which is seen in the data coming from $\pi\pi \to \pi\pi$, but not in those coming from $\pi\pi \to K\bar{K}$. This is a long-standing problem (see [21] and references therein) that we will address in the next subsection, showing that the "nondip" scenario is not able to satisfy the dispersive representation well even when allowing for a large deviation from the phase-shift data.

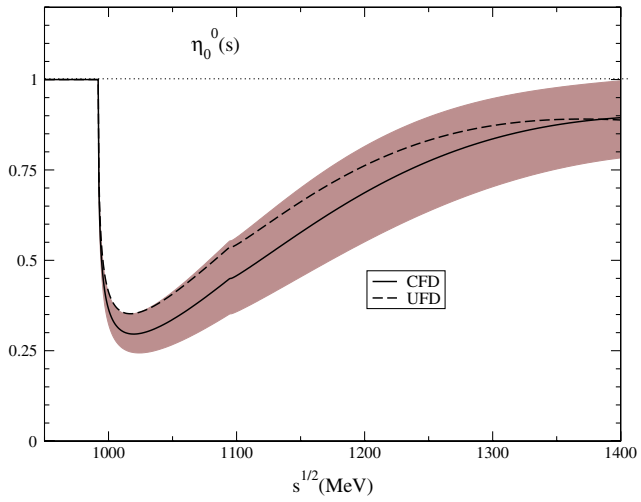

FIG. 17 (color online). Comparison between the UFD and CFD S0 wave inelasticity. The gray area corresponds to the CFD uncertainty. A similar size area should be associated with the UFD result, but for clarity we only show its central value. Note the dip structure between 1 and 1.1 GeV.

B. S0 inelasticity: The nondip scenario is disfavored

In order to show how much the nondip scenario is disfavored, we will first repeat the same procedure of this whole paper, but starting from the S0 inelasticity fitted to the nondip data, as shown in Fig. 19, while keeping the same UFD parametrization for all other waves and for the S0 phase. We will refer to this set as "ndUFD." The resulting averaged discrepancies $\bar{d}_i^2$ are relatively similar to those in Table I for our UFD, except for the S0 wave GKPY equations up to $\sqrt{s} \leq 1100$ MeV, whose averaged $\bar{d}_i^2$ rises from 2.42 to 4.77. This already disfavors the nondip scenario.

Of course, the dip-scenario UFD set was not doing very well either, but we were able to improve it by constraining the fit to data with dispersion relations, i.e., the CFD set. One could wonder if a similar quality fit can also be obtained by imposing the dispersive constraints, but starting from the ndUFD. Thus, we followed again the procedure described in previous sections, but now in order to arrive at a ndCFD set. Surprisingly, the S0 inelasticity barely changes, but the improvement comes from a bigger variation of the phase in the two-kaon subthreshold region. The resulting average discrepancies $\bar{d}_i^2$ are, in general, larger than for our CFD set, sometimes by a factor of 2, but still below 1. This may look like an agreement, but one

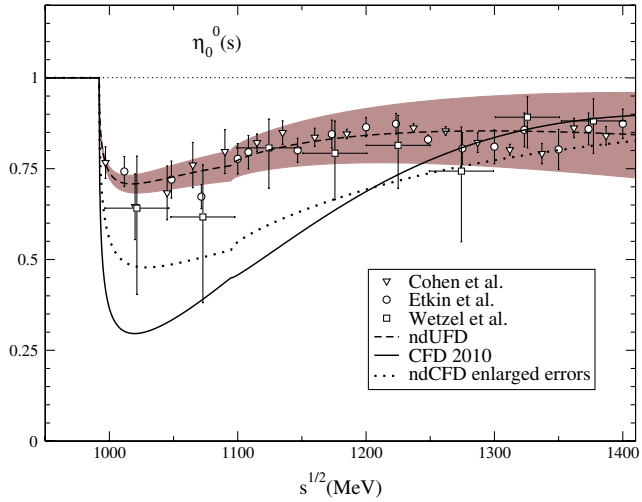

FIG. 19 (color online). S0 wave inelasticity versus the nondip $\pi\pi \to K\bar{K}$ data. We first show the ndUFD set obtained from a fit to these nondip data. Next, we show the ndCFD set obtained with enlarged errors to try to fulfill dispersion relations. This constrained fit satisfies the dispersive constraints better, but does not describe these nondip data, coming closer to the best CFD set, which actually describes the alternative dip data from $\pi\pi \to \pi\pi$.

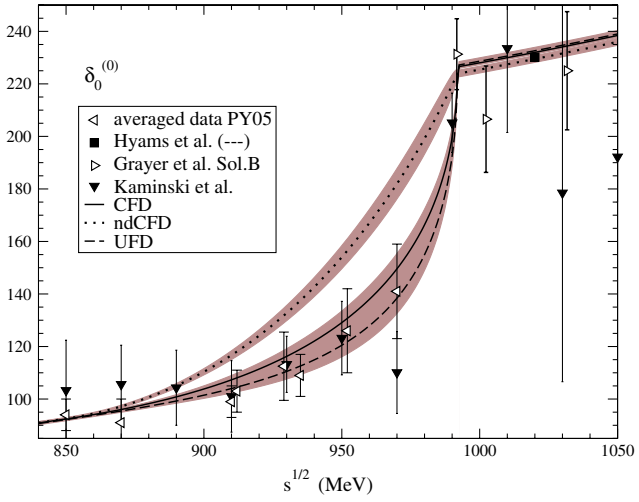

FIG. 20 (color online). Comparison of the UFD, CFD, and ndCFD solutions for the S0 phase in the 850 to 1050 MeV region. Note that the ndCFD parametrization is largely inconsistent with data, despite the fact that we are plotting the PY05 averaged data, which include our estimations of the large dominant systematic uncertainties.

should not be misguided now by these relatively low averaged $\bar{d}_i^2$ because, contrary to the CFD set where discrepancies are below 1 uniformly over the whole energy region, for the ndCFD set they are larger in the $f_0(980)$ resonance region.

In particular, in the interval between 950 and 1050 MeV, for the CFD set, the GKPY S0 equations have $\bar{d}^2 = 1.02$, whereas the ndCFD set has $\bar{d}^2 = 3.49$. This averaged discrepancy is unacceptable now, since this time we are using the dispersion relations as constraints to our fits. In addition, the crossing sum rule in Eq. (16) grows to $\bar{d}_I^2 = 2.0$.

Furthermore, as we show in Fig. 20, in the region from 900 MeV up to $K\bar{K}$ threshold, the resulting phase of this ndCFD scenario lies above all data points with a $\chi^2/\#\text{points} = 3.4$, which is a very bad fit, given the fact that these are data. In contrast, the CFD set has $\chi^2/\#\text{points} = 0.98$ in this region and is just a small modification from the UFD phase, which has $\chi^2/\#\text{points} = 0.63$. Moreover, the ndCFD parameters lie far from the original ndUFD ones, with the c parameter more than 6 standard deviations away from its ndUFD value. These numbers clearly show the incompatibility of the ndCFD set with the S0 wave $\pi\pi \to \pi\pi$ phase-shift scattering data. This disagreement cannot be mended by adding systematic uncertainties, since in this region we had already included large systematic uncertainties (see KPY08 and PY05 for details) and all points have total uncertainties of more than 10°.

One could wonder if our minimization procedure, that was good enough to reach $\bar{d}_i^2 < 1$ for the dip scenario, is badly tuned for the nondip one. This, of course is the role of the W_i weights in Eq. (21). For this reason, we have repeated the above procedure adding additional weight to the GKPY S0 wave equation above 900 MeV. The resulting ndCFD2 yields $\bar{d}^2 = 2.06$ for the GKPY S0 equation. Besides, the crossing sum rule in Eq. (16) is also $\bar{d}_i^2 = 1.43$. Although they still disfavor this solution, these numbers by themselves are not too bad. However, the phase-shift data between 950 and 1050 MeV has $\chi^2/\#\text{points} = 5.9$, so that it is described even worse than with the previous ndCFD.

Since we cannot fix the dispersive constraints without spoiling the data phase description, as a final check, we have allowed for larger errors in the inelasticity parameters of the nondip scenario, and applied the dispersive constraints. In so doing, we can obtain $\bar{d}_i^2 < 1$ uniformly over all energy regions for all GKPY equations except for the S0 wave between 950 and 1050 MeV, for which we obtain 1.42. However, the central value of the inelasticity for the resulting constrained nondip fit starts developing a dip as seen in Fig. 19. Therefore, we describe neither the nondip nor the dip scenario.

In conclusion, the nondip scenario, even when constrained with dispersion relations, is not able to describe the data and simultaneously satisfy forward dispersion relations, Roy and GKPY equations, plus certain crossing sum rules.

C. Comparison with other works

The results listed in Table IV for threshold parameters are remarkably compatible with the predictions of [11] using chiral perturbation theory and Roy equations:

$$a_0^{(0)} = 0.220 \pm 0.005, \qquad a_0^{(2)} = -0.0444 \pm 0.0010.$$

The agreement with that reference has also improved a great deal since the $\delta_0^{(0)}(M_K^2) - \delta_0^{(2)}(M_K^2) = (47.3 \pm 0.9)^\circ$ value, obtained directly from our CFD set, is now completely consistent with their value of $(47.7 \pm 1.5)^\circ$. Of course, for this agreement, it is essential that we do not consider the $K \to \pi\pi$ datum. Also, all the D wave threshold parameters are now in good agreement with those used in [11]. The remaining differences with respect to that work are rather small: The largest one is a 2.1 standard deviation disagreement, with respect to their predicted value $b_1 = (5.67 \pm 0.13) \times 10^{-3}$. In general, and up to 500 MeV, the results of [11] fall within roughly 1 standard deviation of our analysis. For instance, at the kaon mass, our CFD S0 wave phase shift is $\delta_0^{(0)}(M_K) = 39.1 \pm 0.6^\circ$, identical to theirs to the last digit, but our S2 wave is $\delta_0^{(2)}(M_K) = -8.2 \pm 0.6^\circ$, 0.3° more than theirs, which is half a standard deviation. This good agreement does not deteriorate much above that energy. For instance, at 800 MeV, which is their matching point between the calculated phase shifts and their input, they use an input value of $\delta_0^{(0)} = 82.3 \pm 3.4^\circ$. In contrast, we obtain $\delta_0^{(0)} = 85.2 \pm 0.5^\circ$ directly from the CFD set, whereas we find $\delta_0^{(0)} = 85.7 \pm 1.6^\circ$ when using the same CFD set inside GKPY equations, that is, one of their standard deviations. Above 800 MeV their amplitudes are part of the input and not solutions of Roy equations.

Finally, we would like to remark that our best values for the scalar scattering lengths in Eq. (28) are in very good agreement with the experimental results from pionic atoms [37,38], which yield

$$a_0^{(0)} - a_0^{(2)} = 0.280 \pm 0.013(\text{st}) \pm 0.008(\text{syst}) M_\pi^{-1},$$
$$a_0^{(0)} - a_0^{(2)} = 0.264^{+0.033}_{-0.020} M_\pi^{-1},$$

or $K_{3\pi}$ decays [39]:

$$a_0^{(0)} - a_0^{(2)} = 0.2571 \pm 0.0048(\text{st}) \pm 0.0025(\text{syst}) \pm 0.0014(\text{ext}) M_\pi^{-1}.$$

Had we used them as additional constraints with the statistical and systematic errors added linearly as we did with other decays, the difference with our best results would have been barely modified.

As we commented in Sec. III B, the phase difference $\delta_0^{(0)}(M_K^2) - \delta_0^{(2)}(M_K^2) = (52.5 \pm 0.8_{\text{exp}} \pm 2.8_{\text{exp}})^\circ$ has been recently reanalyzed [26]. This is a considerable shift from the previous value of $(57.27 \pm 0.82_{\text{exp}} \pm 3_{\text{rad}} \pm 1_{\text{ChPT appr}})^\circ$, in much better agreement with ours and other previous dispersive analyses. Note that the new number is also in good agreement with our results in Table IV.

VIII. SUMMARY

In this work, we have presented the derivation of a once-subtracted set of Roy-like dispersion relations—the GKPY equations. We have shown and explained that above 450 MeV, and up to 1115 MeV, they provide stronger constraints on $\pi\pi$ scattering amplitudes than other existing sets of dispersion relations.

We have then applied these new equations as constraints in our fits to data—together with the standard Roy equations and forward dispersion relations—in order to obtain a precise description of $\pi\pi$ scattering amplitudes. In contrast to previous works, we have extended the Roy and GKPY equations analysis from 932 MeV up to their applicability limit of 1100 MeV. Forward dispersion relations are considered up to 1420 MeV.

We have also made use of the final and very precise data on $K_{\ell 4}$ decays from NA48/2, including the isospin violation corrections proposed in [22], and we have removed a conflicting data point from $K \to 2\pi$ decay. With these changes in the data selection, most of the disagreement with previous Roy equation calculations [11] has disappeared below 800 MeV. The largest discrepancy that remains is on the P wave slope parameter, but just at the 2 standard deviation level.

In addition, we have improved our S0 wave parametrization to ensure a continuous matching between the low and intermediate energy parametrizations. Both parametrizations have been made more flexible, which allows the phase and inelasticity to include contributions from states different from $\pi\pi$ and $K\bar{K}$, above the $K\bar{K}$ threshold.

There are two sets of fits to data: UFD or CFD. In the UFD set each wave is independent of all others, but dispersion relations are satisfied only up to the two sigma level (in the sense explained in the text). In contrast, the CFD waves are all correlated, but they fulfill all dispersion relations under consideration within less than 1 standard deviation in the whole energy region. The CFD set can be considered as a very precise parametrization of experimental data consistent with the requirements of analyticity, unitarity, and crossing symmetry. Using this CFD set as an input in different sum rules and the dispersion relations themselves, we have also provided a precise determination of phases in the elastic regime, threshold parameters, and Adler zeros.

In addition, and concerning the conflicting data for the S0 wave inelasticity between the two-kaon threshold and 1100 MeV, the use of the new GKPY equations has allowed us to show that the sudden drop around 1050 MeV in the S0 wave inelasticity, or dip solution, is clearly favored with respect to the nondip solution. Actually, for the nondip inelasticity scenario to fulfill dispersion relations, it would require a very poor description of the phase-shift data, even when allowing for large systematic uncertainties.

In conclusion, we provide fits to data in terms of simple and ready-to-use parametrizations for the S0, S2, P, D0, D2, and F partial waves, between threshold and 1420 MeV.

Additional simple Regge parametrizations are given above that energy. In particular, the CFD set satisfies remarkably well all the analyticity and crossing symmetry constraints in the form of once- and twice-subtracted Roy equations and forward dispersion relations.

ACKNOWLEDGMENTS

At the early stages of this collaboration, we suffered the devastating loss of one of the authors, F. J. Ynduráin, whose contributions were essential for this work. He was an example of humanity and scientific dedication. We also thank I. Caprini, G. Colangelo, J. Gasser, and H. Leutwyler for many discussions and suggestions on possible improvements of our parametrizations, as well as D. V. Bugg for comments on the S0 wave inelasticity, and B. Kubis for his comments on $K_{3\pi}$ decays. This work is partly supported by DGICYT Contracts No. FIS2006-03438 and No. FPA2005-02327, Santander/Complutense Contract No. PR27/05-13955-BSCH and the EU Integrated Infrastructure Initiative Hadron Physics Project under Contract No. RII3-CT-2004-506078.

Note added in proof.—While this article was in proofs, one of us [42] has shown that our F and D waves satisfy the F and D wave GKPY equations fairly well up to 800 MeV, even though these equations have not been imposed in the constrained fits here. Above that energy the agreement deteriorates, and one could think about improving the D and F waves by including in our fit the D and F wave GKPY equations. However, we have seen that the F waves are negligible for our results here. In addition, since just a few percent change is all that seems to be needed for the D0 wave, which is more relevant than the D2 wave for the driving terms used here, we estimate that the net effect would be within the uncertainties of the results we provide here for the constrained S and P waves.

APPENDIX A: PARTIAL WAVE PARAMETRIZATIONS

In the following, we provide the parametrizations we use for each partial wave and, then, the parameters for the UFD and CFD sets. For brevity, we do not explain again why a specific parametrization for each wave has been chosen, since such details can be found in KPY08 [3]. In what follows we use $M_\pi = 139.57$ MeV, $M_K = 496$ MeV, and $M_\eta = 547.51$ MeV.

TABLE V. S0 wave parameters for the UFD and CFD sets. The first four lines correspond to the low energy parametrization, $\sqrt{s} \le 0.85$ GeV, and the last nine to the parametrization up to $\sqrt{s} = 1.42$ GeV.

S0 wave	UFD	CFD
B_0	7.26 ± 0.23	7.14 ± 0.23
B_1	-25.3 ± 0.5	-25.3 ± 0.5
B_2	-33.1 ± 1.2	-33.2 ± 1.2
B_3	-26.6 ± 2.3	-26.2 ± 2.3
z_0	M_π	M_π
d_0	$(227.1 \pm 1.3)°$	$(226.5 \pm 1.3)°$
c	$(-660 \pm 290)°$	$(-81 \pm 290)°$
B	$(94.0 \pm 2.3)°$	$(93.3 \pm 2.3)°$
C	$(40.4 \pm 2.9)°$	$(48.7 \pm 2.9)°$
D	$(-86.9 \pm 4.0)°$	$(-88.3 \pm 4.0)°$
$\tilde{\epsilon}_1$	4.7 ± 0.2	4.9 ± 0.2
$\tilde{\epsilon}_2$	-15.0 ± 0.8	-15.1 ± 0.8
$\tilde{\epsilon}_3$	4.7 ± 2.6	4.7 ± 2.6
$\tilde{\epsilon}_4$	0.38 ± 0.34	0.32 ± 0.34

1. S0 wave

This wave has been thoroughly discussed in the main text. However, for the sake of completeness, we repeat here the form of the parametrizations and provide the values of the parameters for the UFD and CFD sets in Table V.

For this wave we have set the matching point between the intermediate and low energy parametrizations at $s_M^{1/2} = 0.85$ GeV. Thus, at low energies $s \le s_M$, we use

$$\cot\delta_0^{(0)}(s) = \frac{s^{1/2}}{2k}\frac{M_\pi^2}{s - \frac{1}{2}z_0^2}\left\{\frac{z_0^2}{M_\pi\sqrt{s}} + B_0 + B_1 w(s) + B_2 w(s)^2 + B_3 w(s)^3\right\},$$
$$w(s) = \frac{\sqrt{s} - \sqrt{s_0 - s}}{\sqrt{s} + \sqrt{s_0 - s}}, \qquad s_0 = 4M_K^2. \tag{A1}$$

Above that energy, and up to 1.42 GeV, we use the KPY06 polynomial parametrization for the phase shift, but with one more term in the expansion. For definiteness, we provide here the polynomial parametrization once it has been matched to Eq. (A1) above, by imposing continuity and a continuous derivative at $s = s_M$, namely,

$$\delta_0^{(0)}(s) = \begin{cases} d_0\left(1 - \frac{|k_2|}{k_M}\right)^2 + \delta_M\frac{|k_2|}{k_M}\left(2 - \frac{|k_2|}{k_M}\right) + |k_2|(k_M - |k_2|)\left(8\delta'_M + c\frac{(k_M - |k_2|)}{M_K^3}\right) & (0.85\ \text{GeV})^2 < s < 4M_K^2 \\ d_0 + B\frac{k_2^2}{M_K^2} + C\frac{k_2^4}{M_K^4} + D\theta(s - 4M_\eta^2)\frac{k_3^2}{M_\eta^2} & 4M_K^2 < s < (1.42\ \text{GeV})^2, \end{cases} \tag{A3}$$

where $k_2 = \sqrt{s/4 - M_K^2}$. Note that we have defined $\delta_M = \delta(s_M)$ and $\delta'_M = d\delta(s_M)/ds$, which are obtained from Eq. (A1), and $k_M = |k_2(s_M)|$.

Finally, we assume an elastic S0 wave, $\eta_0^{(0)} = 1$, up to the two-kaon threshold, whereas above that energy, we use

$$\eta_0^{(0)}(s) = \exp\Big[\frac{-k_2(s)}{s^{1/2}}\Big(\tilde{\epsilon}_1 + \tilde{\epsilon}_2\frac{k_2}{s^{1/2}} + \tilde{\epsilon}_3\frac{k_2^2}{s}\Big)^2 - \tilde{\epsilon}_4\theta(s-4M_\eta^2)\frac{k_3(s)}{s^{1/2}}\Big]. \quad \text{(A4)}$$

We have collected the values of the parameters for the UFD and CFD sets in Table V.

2. S2 wave

As we have already done with the S0 wave, we have also set the matching point between intermediate and low energy parametrizations for this wave at $s_M^{1/2} = 850$ MeV. Thus, at energies $s^{1/2} \le s_M^{1/2}$ we use

$$\cot\delta_0^{(2)}(s) = \frac{s^{1/2}}{2k}\frac{M_\pi^2}{s-2z_2^2}\{B_0 + B_1 w_l(s)\},$$
$$w_l(s) = \frac{\sqrt{s}-\sqrt{s_l-s}}{\sqrt{s}+\sqrt{s_l-s}}, \qquad s_l^{1/2} = 1.05 \text{ GeV}, \quad \text{(A5)}$$

whereas at intermediate energies, 850 MeV $\le s^{1/2} \le$ 1420 MeV, we use

$$\cot\delta_0^{(2)}(s) = \frac{s^{1/2}}{2k}\frac{M_\pi^2}{s-2z_2^2}\{B_{h0} + B_{h1}[w_h(s) - w_h(s_M)] + B_{h2}[w_h(s) - w_h(s_M)]^2\},$$

where

$$w_h(s) = \frac{\sqrt{s}-\sqrt{s_h-s}}{\sqrt{s}+\sqrt{s_h-s}},$$
$$s_h^{1/2} = 1.42 \text{ GeV},$$
$$B_{h0} = B_0 + B_1 w_l(s_M),$$
$$B_{h1} = B_1\frac{\partial w_l(s)}{\partial w_h(s)}\Big|_{s=s_M} = B_1\frac{s_l}{s_h}\frac{\sqrt{s_h-s_M}}{\sqrt{s_l-s_M}}\Big(\frac{\sqrt{s_M}+\sqrt{s_h-s_M}}{\sqrt{s_M}+\sqrt{s_l-s_M}}\Big)^2. \quad \text{(A6)}$$

Note that, with these definitions, both the parametrization and its derivative are continuous at the matching point.

Note that we have explicitly factorized the Adler zero at $s_A = 2z_2^2$. For the unconstrained fit, z_2 is fixed to the pion mass. As explained in the main text in Sec. V B, we then calculate the Adler zero position using Roy and GKPY equations, and feed the weighted average into the constrained fit. This change is very small in terms of the total values and uncertainties of other quantities, but it is relevant in the differences when calculating the fulfillment of GKPY equations.

For the S2 inelasticity we use a purely phenomenological parametrization,

$$\eta_0^{(2)} = 1 - \epsilon(1 - s_l/s)^{3/2},$$

for $s^{1/2} > 1.05$ GeV and $\eta_0^{(2)} = 1$ otherwise.

The S2 wave parameters for UFD and CFD sets are given in Table VI.

TABLE VI. S2 wave parameters for the UFD and CFD sets.

S2 wave	UFD	CFD
B_0	-80.4 ± 2.8	-79.4 ± 2.8
B_1	-73.6 ± 10.5	-63.0 ± 10.5
z_2	M_π	143.5 ± 3.2 MeV
B_{h2}	112 ± 38	32 ± 38
ϵ	0.28 ± 0.12	0.28 ± 0.12

3. P wave

For this wave we have set the matching point between low and intermediate energy parametrizations at $s_M^{1/2} = 2M_K$. Thus, at low energies $s^{1/2} \le 2M_K$, we use

$$\cot\delta_1(s) = \frac{s^{1/2}}{2k^3}(M_\rho^2 - s)\Big\{\frac{2M_\pi^3}{M_\rho^2\sqrt{s}} + B_0 + B_1 w(s)\Big\},$$
$$w(s) = \frac{\sqrt{s}-\sqrt{s_0-s}}{\sqrt{s}+\sqrt{s_0-s}}, \qquad s_0^{1/2} = 1.05 \text{ GeV}, \quad \text{(A7)}$$

where the ρ mass is fixed to $M_\rho = 773.6 \pm 0.9$ MeV. At intermediate energies, $2M_K \le s^{1/2} \le 1420$ MeV, we use a purely phenomenological parametrization:

$$\delta_1(s) = \lambda_0 + \lambda_1(\sqrt{s}/2M_K - 1) + \lambda_2(\sqrt{s}/2M_K - 1)^2,$$
$$\eta_1(s) = 1 - \epsilon_1\sqrt{1-4M_K^2/s} - \epsilon_2(1-4M_K^2/s), \quad \text{(A8)}$$

where λ_0 is fixed from the value of $\delta_1(4M_K^2)$ obtained from the low energy parametrization, so that the phase shift is continuous. Note the possible presence of a discontinuity in the derivative, allowed by the presence of the $K\bar{K}$ threshold. The values of the UFD and CFD parameters are given in Table VII.

4. The D0 wave

As it was the case for the P wave, the matching energy between low and intermediate energies is now taken at $s_M^{1/2} = 2M_K$. At low energies, $s^{1/2} \le 2M_K$, we parametrize this wave by

$$\cot\delta_2^{(0)}(s) = \frac{s^{1/2}}{2k^5}(M_{f_2}^2 - s)M_\pi^2\{B_0 + B_1 w(s)\},$$
$$w(s) = \frac{\sqrt{s}-\sqrt{s_0-s}}{\sqrt{s}+\sqrt{s_0-s}}, \qquad s_0^{1/2} = 1.05 \text{ GeV}, \quad \text{(A9)}$$

TABLE VII. P wave parameters for the UFD and CFD sets.

P wave	UFD	CFD
B_0	1.055 ± 0.011	1.043 ± 0.011
B_1	0.15 ± 0.05	0.19 ± 0.05
λ_1	1.57 ± 0.18	1.39 ± 0.18
λ_2	-1.96 ± 0.49	-1.70 ± 0.49
ϵ_1	0.10 ± 0.06	0.00 ± 0.06
ϵ_2	0.11 ± 0.11	0.07 ± 0.11

TABLE VIII. D0 wave parameters for the UFD and CFD sets.

D0 wave	UFD	CFD
B_0	12.47 ± 0.12	12.40 ± 0.12
B_1	10.12 ± 0.16	10.06 ± 0.16
B_{h1}	43.7 ± 1.8	43.2 ± 1.8
ϵ	0.284 ± 0.030	0.254 ± 0.030
r	2.54 ± 0.31	2.29 ± 0.31

where the mass of the $f_2(1270)$ resonance is fixed at $M_{f_2} = 1275.4$ MeV. In the intermediate region, $2M_K \le s^{1/2} \le 1420$ MeV, we use a rather similar parametrization:

$$\cot\delta_2^{(0)}(s) = \frac{s^{1/2}}{2k^5}(M_{f_2}^2 - s)M_\pi^2\{B_{0h} + B_{1h}w_h(s)\},$$
$$w_h(s) = \frac{\sqrt{s} - \sqrt{s_h - s}}{\sqrt{s} + \sqrt{s_h - s}}, \qquad s_h^{1/2} = 1.45 \text{ GeV}. \tag{A10}$$

Imposing continuity at the matching point fixes B_{h0} from the value of $\delta_2^{(0)}(4M_K^2)$ obtained from the low energy parametrization. We take the inelasticity to be different from 1 only for $s > 4M_K^2$, in which case we write

$$\eta_2^{(0)} = 1 - \epsilon\left(\frac{1 - 4M_K^2/s}{1 - 4M_K^2/M_{f_2}^2}\right)^{5/2}\left[1 + r\left(1 - \frac{k_2(s)}{k_2(M_{f_2}^2)}\right)\right]. \tag{A11}$$

The parameters of the D0 wave are given in Table VIII.

5. The D2 wave

We use the following parametrization from threshold up to 1420 MeV:

$$\cot\delta_2^{(2)}(s) = \frac{s^{1/2}}{2k^5}\frac{M_\pi^4 s}{4(M_\pi^2 + \Delta^2) - s}\{B_0 + B_1 w(s) + B_2 w(s)^2\},$$
$$w(s) = \frac{\sqrt{s} - \sqrt{s_0 - s}}{\sqrt{s} + \sqrt{s_0 - s}}, \qquad s_0^{1/2} = 1.45 \text{ GeV}, \tag{A12}$$

and we consider that the inelasticity differs from 1 for $s^{1/2} > 1.05$ GeV, as follows:

$$\eta_2^{(2)}(s) = 1 - \epsilon(1 - \hat{s}/s)^3, \qquad \hat{s}^{1/2} = 1.05 \text{ GeV}, \tag{A13}$$

which is almost negligible up to 1.25 GeV. The values of the parameters for the UFD and CFD sets are given in Table IX.

6. The F wave

We neglect the inelasticity up to 1420 MeV and simply use the following parametrization from threshold:

$$\cot\delta_3(s) = \frac{s^{1/2}}{2k^7}M_\pi^6\left\{\frac{2\lambda M_\pi}{\sqrt{s}} + B_0 + B_1 w(s)\right\},$$
$$w(s) = \frac{\sqrt{s} - \sqrt{s_0 - s}}{\sqrt{s} + \sqrt{s_0 - s}}, \qquad s_0^{1/2} = 1.45 \text{ GeV}. \tag{A14}$$

TABLE IX. D2 wave parameters for the UFD and CFD sets.

D2 wave	UFD	CFD
B_0	$(2.4 \pm 0.5)10^3$	$(4.1 \pm 0.5)10^3$
B_1	$(7.8 \pm 1.0)10^3$	$(8.6 \pm 1.0)10^3$
B_2	$(23.7 \pm 4.2)10^3$	$(25.5 \pm 4.2)10^3$
Δ	196 ± 25 MeV	233 ± 25 MeV
ϵ	0.2 ± 0.2	0.0 ± 0.2

The parameters for the UFD and CFD sets are given in Table X. Note that they do not change at all from one set to another.

7. The G waves

The contribution of the G0 and G2 waves was shown to be completely negligible for the calculations. The details can be found in the Appendix of KPY08 [3].

8. Regge parametrizations

Next we show the Regge parametrizations that we use in the high energy region, i.e. above 1420 MeV. The forward ($t = 0$) Regge parametrizations were obtained from fits to high energy data [5]. For the $t \neq 0$ behavior we [3] simply covered the uncertainties between the different fits in [40]. These Regge fits are expected to represent *experimental* data when $1.42 \text{ GeV} \le s^{1/2} \le 20$ GeV and $4M_\pi^2 \ge t \ge -0.4$ GeV^2, somewhat less reliably for the most negative t values. This is enough to describe the region of interest that reaches $t = -0.42$ GeV^2. In particular, for the ρ Regge trajectory, we use the following expression for the imaginary part, which is all we need in the dispersive integrals:

$$\text{Im}F^{(I_t=1)}(s,t) = \beta_\rho \frac{1 + \alpha_\rho(t)}{1 + \alpha_\rho(0)}\varphi(t)e^{bt}\left(\frac{s}{\hat{s}}\right)^{\alpha_\rho(t)},$$
$$\alpha_\rho(t) = \alpha_\rho(0) + t\alpha'_\rho + \frac{1}{2}t^2\alpha''_\rho,$$
$$\varphi(t) = 1 + d_\rho t + e_\rho t^2, \tag{A15}$$

where we fix

$$\hat{s} = 1 \text{ GeV}^2, \qquad b = 2.4 \pm 0.2 \text{ GeV}^{-2},$$
$$\alpha'_\rho = 0.90 \text{ GeV}^{-2}, \qquad \alpha''_\rho = -0.3 \text{ GeV}^{-4}, \tag{A16}$$
$$d_\rho = 2.4 \pm 0.5 \text{ GeV}^{-2}, \qquad e_\rho = 0 \pm 2.5 \text{ GeV}^{-4},$$

whereas the rest of the parameters are allowed to vary in the fits.

TABLE X. F wave parameters for the UFD and CFD sets.

F wave	UFD	CFD
B_0	$(1.09 \pm 0.03)10^5$	$(1.09 \pm 0.03)10^5$
B_1	$(1.41 \pm 0.04)10^5$	$(1.41 \pm 0.04)10^5$
λ	0.051×10^5	0.051×10^5

TABLE XI. UFD and CFD parameters for the ρ, Pomeron, and $I = 2$ Regge contributions to $\pi\pi$ scattering amplitudes.

Regge parameters	UFD	CFD
β_ρ	1.22 ± 0.14	1.48 ± 0.14
$\alpha_\rho(0)$	0.46 ± 0.02	0.53 ± 0.02
β_P	2.54 ± 0.04	2.50 ± 0.04
c_P	0.0 ± 1.0 GeV^{-2}	0.6 ± 1.0 GeV^{-2}
$c_{P'}$	-0.4 ± 0.4 GeV^{-2}	-0.38 ± 0.4 GeV^{-2}
$\beta_{P'}$	0.83 ± 0.05	0.80 ± 0.05
$\alpha_{P'}(0)$	0.54 ± 0.02	0.53 ± 0.02
β_2	0.2 ± 0.2	0.08 ± 0.2

For both the Pomeron P and the P' pole, we have used, for $s^{1/2} = 1420$ MeV,

$$\begin{aligned}
&\mathrm{Im}\, F^{(I_t=0)}(s,t) = P(s,t) + P'(s,t),\\
&P(s,t) = \beta_P \Psi_P(t)\alpha_P(t)\frac{1+\alpha_P(t)}{2}\mathrm{e}^{bt}\left(\frac{s}{\hat{s}}\right)^{\alpha_P(t)},\\
&\alpha_P(t) = 1 + t\alpha'_P, \qquad \Psi_P(t) = 1 + c_P t,\\
&P'(s,t) = \beta_{P'}\Psi_{P'}(t)\frac{\alpha_{P'}(t)[1+\alpha_{P'}(t)]}{\alpha_{P'}(0)[1+\alpha_{P'}(0)]}\mathrm{e}^{bt}\left(\frac{s}{\hat{s}}\right)^{\alpha_{P'}(t)},\\
&\alpha_{P'}(t) = \alpha_{P'}(0) + t\alpha'_{P'}, \qquad \Psi_{P'}(t) = 1 + c_{P'}t,
\end{aligned} \tag{A17}$$

where, once again, we fix

$$\begin{aligned}
&\hat{s} = 1\,\mathrm{GeV}^2, \quad b = 2.4 \pm 0.2\,\mathrm{GeV}^{-2},\\
&\alpha'_P = 0.20 \pm 0.10\,\mathrm{GeV}^{-2}, \quad \alpha'_{P'} = 0.90\,\mathrm{GeV}^{-2},\\
&c_P = 0.0 \pm 1.0\,\mathrm{GeV}^{-2}, \quad c_{P'} = -0.4 \pm 0.4\,\mathrm{GeV}^{-2},
\end{aligned} \tag{A18}$$

and allow the rest of the parameters to vary in the fits.

Finally, the Regge exchange of isospin two is parametrized as

$$\mathrm{Im}\, F^{(I_t=2)} = \beta_2 \mathrm{e}^{bt}\left(\frac{s}{\hat{s}}\right)^{\alpha_\rho(t)+\alpha_\rho(0)-1}. \tag{A19}$$

In Table XI we show the values of the Regge parameters obtained from the direct fit to high energy data (UFD) and how they are modified when imposing the dispersive constraints in the fits (CFD).

APPENDIX B: DERIVATION OF THE ONCE-SUBTRACTED DISPERSION RELATIONS

A once-subtracted dispersion relation for a scattering amplitude of definite isospin I has the following expression:

$$\begin{aligned}
F^{(I)}(s,t) = F^{(I)}(s_0,t) &+ \frac{s-s_0}{\pi}\int_{4M_\pi^2}^{\infty} ds' \frac{\mathrm{Im}F^{(I)}(s',t)}{(s'-s_0)(s'-s)}\\
&+ \frac{s-s_0}{\pi}\int_{-t}^{-\infty} ds' \frac{\mathrm{Im}F^{(I)}(s',t)}{(s'-s_0)(s'-s)},
\end{aligned} \tag{B1}$$

with s_0 the subtraction point. This expression assumes that the point s is regular. However, we are especially interested in what happens for s in the physical region, that is, on the cuts of the function $F(s,t)$. The usual prescription is to define the amplitude for physical values of s as

$$F_{\mathrm{phys}}(s,t) = \lim_{\epsilon\to 0^+} F(s+i\epsilon,t).$$

With this prescription, we have

$$\begin{aligned}
F^{(I)}_{\mathrm{phys}}(s,t) &= \lim_{\epsilon\to 0^+} F^{(I)}(s+i\epsilon,t)\\
&= F^{(I)}(s_0,t)\\
&\quad + \frac{s-s_0+i\epsilon}{\pi}\int_{4M_\pi^2}^{\infty} ds' \frac{\mathrm{Im}F^{(I)}(s',t)}{(s'-s_0)(s'-s-i\epsilon)}\\
&\quad + \frac{s-s_0+i\epsilon}{\pi}\int_{-t}^{-\infty} ds' \frac{\mathrm{Im}F^{(I)}(s',t)}{(s'-s_0)(s'-s-i\epsilon)}.
\end{aligned}$$

To obtain the physical amplitude, we must take the limit $\epsilon \to 0^+$ in this expression. Suppose s is on the right-hand cut (RHC), $4M_\pi^2 < s < \infty$. Since

$$\frac{1}{x \pm i\epsilon} = \mathrm{P.P.}\left[\frac{1}{x}\right] \mp i\pi\delta(x), \qquad \epsilon \to 0^+,$$

we can write the RHC integral as

$$\frac{s-s_0}{\pi}\mathrm{P.P.}\int_{4M_\pi^2}^{\infty} ds' \frac{\mathrm{Im}F^{(I)}(s',t)}{(s'-s_0)(s'-s)} + i\,\mathrm{Im}F^{(I)}(s,t),$$

whereas the left-hand cut (LHC) integral presents no problems when ϵ vanishes. Then we have

$$\begin{aligned}
F^{(I)}_{\mathrm{phys}}(s,t) &= F^{(I)}(s_0,t) + i\,\mathrm{Im}F^{(I)}(s,t)\\
&\quad + \frac{s-s_0}{\pi}\mathrm{P.P.}\int_{4M_\pi^2}^{\infty} ds' \frac{\mathrm{Im}F^{(I)}(s',t)}{(s'-s_0)(s'-s)}\\
&\quad + \frac{s-s_0}{\pi}\int_{-t}^{-\infty} ds' \frac{\mathrm{Im}F^{(I)}(s',t)}{(s'-s_0)(s'-s)}.
\end{aligned}$$

Thus the dispersive integrals only reconstruct the *real part* of the amplitude, instead of the total amplitude. Had we chosen s to be on the LHC, the reasoning would be analogous, but the principal value should be taken on the LHC integral, instead of on the RHC one. We finally obtain

$$\mathrm{Re}\,F^{(I)}_{\mathrm{phys}}(s,t) = \mathrm{Re}F^{(I)}(s_0,t) + \frac{s-s_0}{\pi}\mathrm{P.P.}\int_{4M_\pi^2} ds' \frac{\mathrm{Im}F(I)(s',t)}{(s'-s_0)(s'-s)} + \frac{s-s_0}{\pi}\mathrm{P.P.}\int_{-t}^{-\infty} ds' \frac{\mathrm{Im}F^{(I)}(s',t)}{(s'-s_0)(s'-s)},$$

with the principal value taken on the cut on which s lies. This is valid for any s on the cuts of $F^{(I)}(s,t)$, i.e., for physical s. We can now recast the LHC integral on the s channel in Eq. (B1) in terms of the u-channel RHC by renaming the dummy variable s' as u' in the LHC integral and performing the substitution

$$u' \to 4M_\pi^2 - s' - t.$$

Taking both integrands under the same integral sign, and choosing $s_0 = 0$—in analogy with Roy's derivation—we obtain

$$\mathrm{Re}F^{(I)}(s,t) = \mathrm{Re}F^{(I)}(0,t) + \frac{s}{\pi}\int_{4M_\pi^2} ds' \times\left[\frac{\mathrm{Im}F^{(I)}(s',t)}{s'(s'-s)} - \frac{\mathrm{Im}F^{(I)}(u',t)}{u'(u'-s)}\right].$$

Each of these integrals is potentially divergent if taken by itself, due to the Pomeron contribution coming from the $I_t = 0$ channel, which grows like $\mathrm{Im}F^{(I_t=0)}(s,t) \sim s$ for large s. We now show that this is not the case when taken together.

Bose statistics require that the $I_t = 0$ amplitude be symmetric under $s - u$ exchange,

$$F^{(I_t=0)}(s,t) = F^{(I_t=0)}(u,t).$$

Since the amplitudes with well-defined isospin in the s and t channels are related via the usual crossing matrices,

$$C_{st} = \begin{pmatrix} 1/3 & 1 & 5/3 \\ 1/3 & 1/2 & -5/6 \\ 1/3 & -1/2 & 1/6 \end{pmatrix},$$

$$C_{su} = \begin{pmatrix} 1/3 & -1 & 5/3 \\ -1/3 & 1/2 & 5/6 \\ 1/3 & 1/2 & 1/6 \end{pmatrix},$$

we know that each amplitude with well-defined isospin in the s channel has a contribution from each of the amplitudes with well-defined isospin in the t channel. In particular, the contribution from the $I_t = 0$ channel to the integrand can be written as

$$\left[\frac{1}{s'(s'-s)} - \frac{1}{u'(u'-s)}\right]\mathrm{Im}F^{(I_t=0)}(s',t) = \frac{(s+t-4M_\pi^2)(2s'+t-4M_\pi^2)\,\mathrm{Im}F^{(I_t=0)}(s',t)}{s'(s'-s)(s'+t-4M_\pi^2)(s'+s+t-4M_\pi^2)}.$$

The s'^2 terms in the numerator cancel out, and the integrand decays as $1/s'^2$ when $s' \to \infty$, so that the integral converges. This is in contrast with the expected $1/s'$ asymptotic behavior, which would spoil convergence. The contributions from the other t-channel isospin contributions $I_t = 1, 2$ are not problematic, since they grow as $(s')^\alpha$ with $\alpha < 1$, and are convergent even if taking the integrals separately. Note that this cancellation does not depend on the explicit parametrizations we use for the Pomeron but, rather, on very general asymptotic properties of the amplitudes.

In order to rewrite the RHC contribution from the u channel in terms of amplitudes on the RHC s channel, we take into account the crossing symmetry relation:

$$F^{(I)}(4M_\pi^2 - s' - t, t) = \sum_{I'} C_{su}^{II'} F^{(I')}(s',t), \tag{B2}$$

with C_{su} the crossing matrix defined above. Also,

$$F^{(I)}(0,t) = \sum_{I''} C_{st}^{II''} F^{(I'')}(t,0), \tag{B3}$$

and we now write a dispersion relation for $F^{(I'')}(t,0)$:

$$F(I'')(t,0) = F(I'')(t_0,0) + \frac{t-t_0}{\pi}\int_{4M_\pi^2} ds'\left[\frac{\mathrm{Im}F^{(I'')}(s',0)}{(s'-t)(s'-t_0)} - \frac{\sum_{I'''} C_{su}^{I''I'''}\,\mathrm{Im}F^{(I''')}(s',0)}{(4M_\pi^2 - t - s')(4M_\pi^2 - s' - t_0)}\right]. \tag{B4}$$

Again, in analogy with Roy, we take $t_0 = 4M_\pi^2$. Thus

$$\mathrm{Re}\,F^{(I)}(s,t) = \sum_{I'} C_{st}^{II'} F^{(I')}(4M_\pi^2,0) + \frac{s}{\pi}\mathrm{P.P.}\int_{4M_\pi^2} ds'\left[\frac{\mathrm{Im}F^{(I)}(s',t)}{s'(s'-s)} - \frac{\sum_{I'} C_{su}^{II'}\,\mathrm{Im}F^{(I')}(s',t)}{(s'+t-4M_\pi^2)(s'+s+t-4M_\pi^2)}\right] + \frac{t-4M_\pi^2}{\pi}\mathrm{P.P.}\int_{4M_\pi^2}^{\infty} ds' \sum_{I''} C_{st}^{II''}\left[\frac{\mathrm{Im}F^{(I'')}(s',0)}{(s'-t)(s'-4M_\pi^2)} - \frac{\sum_{I'''} C^{I''I'''}\,\mathrm{Im}F^{(I''')}(s',0)}{s'(s'+t-4M_\pi^2)}\right].$$

Now, to project into partial waves, we define first the following kernels:

$$
\begin{aligned}
K_{\ell\ell'}(s,s') &= \frac{s}{\pi s'(s-s')}\int_0^1 dx P_\ell(x)P_{\ell'}(y),\\
L_{\ell\ell'}(s,s') &= \frac{s}{\pi}\int_0^1 dx P_\ell(x)\frac{P_{\ell'}(y)}{u'(u'-s)},\\
M_\ell(s,s') &= \frac{1}{\pi(s'-4M_\pi^2)}\int_0^1 dx P_\ell(x)\frac{t-4M_\pi^2}{s'-t},\\
N_\ell(s,s') &= \frac{1}{\pi s'}\int_0^1 dx P_\ell(x)\frac{4M_\pi^2-t}{u'},
\end{aligned}
\tag{B5}
$$

where $P_\ell(x)$ and $P_{\ell'}(y)$ are Legendre polynomials, and

$$
\begin{aligned}
t &= \frac{(s-4M_\pi^2)(x-1)}{2},\\
u' &= 4M_\pi^2 - s' - t,\\
y &= \frac{u'-t}{u'+t}.
\end{aligned}
$$

Note we have taken advantage of the symmetry of the integrands to change the integration limits from $(-1, 1)$ to $(0, 1)$.

With the normalization chosen in Sec. II B, and recalling that $a_0^{(1)} = 0$, we find

$$
\begin{aligned}
&\mathrm{Re}\,t_\ell^{(I)}(s)\\
&= \xi_\ell \sum_{I''} C_{st}^{II''} a_0^{(I'')} + \sum_{\ell'}(2\ell'+1)\int_{4M_\pi^2}^\infty ds'\Big\{K_{\ell\ell'}(s,s')\,\mathrm{Im}\,t_{\ell'}^{(I)}(s')\\
&\quad - L_{\ell\ell'}(s,s')\sum_{I'} C_{II'}^{su}\,\mathrm{Im}\,t_{\ell'}^{(I')}(s') + \sum_{I''} C_{II''}^{st}[M_\ell(s,s')\,\mathrm{Im}\,t_{\ell'}^{(I'')}(s')\\
&\quad - N_\ell(s,s')\sum_{I'''} C_{I''I'''}^{su}\,\mathrm{Im}\,t_{\ell'}^{(I''')}(s')]\Big\}.
\end{aligned}
$$

In order to simplify the previous expression, we define

$$
\begin{aligned}
\overline{K}_{\ell\ell'}^{II'}(s,s') = (2\ell'+1)[&K_{\ell\ell'}(s,s')\delta^{II'} - L_{\ell\ell'}(s,s')(C_{su})^{II'}\\
&+ M_\ell(s,s')(C_{st}^{II'}) - N_\ell(s,s')(C_{st}C_{su})^{II'}].
\end{aligned}
\tag{B6}
$$

We thus arrive at the final result used in Eq. (18):

$$
\begin{aligned}
\mathrm{Re}\,t_\ell^{(I)}(s) &= \overline{ST}_\ell^I + \overline{DT}_\ell^I(s)\\
&\quad + \sum_{I'=0}^{2}\sum_{\ell'=0}^{1}\mathrm{P.P.}\int_{4M_\pi^2}^{s_{\max}} ds'\overline{K}_{\ell\ell'}^{II'}(s,s')\,\mathrm{Im}\,t_{\ell'}^{I'}(s'),
\end{aligned}
$$

where, for simplicity, the high energy part of the integrals ($s' > s_{\max}$) and the higher partial waves ($\ell' > 1$) are grouped in the so-called driving terms $\overline{DT}_\ell^I(s)$. The subtraction terms $\overline{ST}_\ell^I$, which are now constant, are

$$
\overline{ST}_\ell^{\,I} = \xi_\ell \sum_{I''} C_{st}^{II''} a_0^{I''},
$$

with the ξ_ℓ coefficients defined in Eq. (B7). For our purposes we will only need $\xi_0 = 1$ and $\xi_1 = 1/2$. Note that the subtraction term $\overline{ST}_\ell^I$ is a *constant*, and does not depend on s. This is a relevant feature of GKPY equations versus Roy equations, as explained in Sec. IV E.

$$
\begin{aligned}
\xi_\ell &= \int_0^1 dx P_\ell(x)\\
&= \frac{\sqrt{\pi}}{2\Gamma(1-\frac{\ell}{2})\Gamma(\frac{3+\ell}{2})}\\
&= \begin{cases} 1 & \ell = 0\\ 0 & \ell = 2m,\ m > 0\\ \frac{(-1)^m}{2^{m+1}(m+1)!}\prod_{k=0}^{m-1}[2m-(2k+1)] & \ell = 2m+1. \end{cases}
\end{aligned}
\tag{B7}
$$

APPENDIX C: INTEGRAL KERNELS IN GKPY EQUATIONS

All kernels in Eqs. (B5) and (B6) can be calculated analytically. One has to note, however, that the $L_{\ell\ell'}(s,s')$ and $N_\ell(s,s')$ kernels are singular at $u' = 0$, namely, $x = -(2s' - s - 4M_\pi^2)/(s - 4M_\pi^2)$, where a principal value over the integral is understood.

In this work we need 18 $\overline{K}_{\ell\ell'}^{II'}(s,s')$ kernels, since we are considering the dispersion relation for the S0, P, and S2 waves, but using S0, P, S2, D0, D2, and F waves as input. However, following [41], we know that, since the K, L, M, and N kernels in Eqs. (B5) and (B6) do not depend on isospin, the $\overline{K}_{\ell\ell'}^{II'}(s,s')$ are not all independent and can be expressed in terms of four of the $K_{\ell\ell'}$ above, and eight combinations of the other kernels, which we call $I_{\ell\ell'}(s,s')$. Namely,

$$
\begin{aligned}
&\overline{K}_{00}^{00} = K_{00} - I_{00}/3, \quad \overline{K}_{00}^{02} = -\frac{5}{3}I_{00}, \quad \overline{K}_{01}^{01} = 3I_{01},\\
&\overline{K}_{02}^{00} = 5(K_{02} - \tfrac{1}{3}I_{02}), \quad \overline{K}_{02}^{02} = -\tfrac{25}{3}I_{02}, \quad \overline{K}_{03}^{01} = 7I_{03},\\
&\overline{K}_{10}^{10} = I_{10}/3, \quad \overline{K}_{10}^{12} = -\tfrac{5}{6}I_{10}, \quad \overline{K}_{11}^{11} = 3(K_{11} - \tfrac{1}{2}I_{11}),\\
&\overline{K}_{12}^{10} = \tfrac{5}{3}I_{12}, \quad \overline{K}_{12}^{12} = -\tfrac{25}{6}I_{12}, \quad \overline{K}_{13}^{11} = 7(K_{13} - \tfrac{1}{2}I_{13}),\\
&\overline{K}_{00}^{20} = -I_{00}/3, \quad \overline{K}_{00}^{22} = K_{00} - I_{00}/6, \quad \overline{K}_{01}^{21} = -\tfrac{3}{2}I_{01},\\
&\overline{K}_{02}^{20} = -\tfrac{5}{3}I_{02}, \quad \overline{K}_{02}^{22} = 5(K_{02} - \tfrac{1}{6}I_{02}), \quad \overline{K}_{03}^{21} = -\tfrac{7}{2}I_{03},
\end{aligned}
$$

where

$$
\begin{aligned}
I_{00} &= L_{00} - M_0 + N_0, & I_{01} &= L_{01} + M_0 - N_0,\\
I_{10} &= L_{10} + M_1 + N_1, & I_{11} &= L_{11} - M_1 - N_1,\\
I_{02} &= L_{02} - M_0 + N_0, & I_{03} &= L_{03} + M_0 - N_0,\\
I_{12} &= L_{12} + M_1 + N_1, & I_{13} &= L_{13} - M_1 - N_1.
\end{aligned}
\tag{C1}
$$

The analytic expressions for the $K_{\ell\ell'}$ kernels are

$$
\begin{aligned}
K_{00} &= -\frac{s}{\pi s'(s-s')},\\
K_{02} &= -\frac{s(4M_\pi^2 + s - 2s')}{2\pi s'(s'-4M_\pi^2)^2},\\
K_{11} &= \frac{s(8M_\pi^2 + s - 3s')}{6\pi s'(s-s')(s'-4M_\pi^2)},\\
K_{13} &= \frac{s(4M_\pi^2 + s - 2s')^2}{8\pi s'(s'-4M_\pi^2)^3}.
\end{aligned}
\tag{C2}
$$

The diagonal kernels $K_{00}(s, s')$ and $K_{11}(s, s')$ contain a singularity at $s = s'$, which is the only type of singularity in the GKPY equations.

By defining the following a_i functions,

$$
\begin{aligned}
a_1 &= \frac{s'}{s + s' - 4M_\pi^2}, \qquad a_2 = \frac{(s + 2s' - 4M_\pi^2)^2}{4(s + s' - 4M_\pi^2)^2},\\
a_3 &= -\frac{s^2 - 4(s' - 2M_\pi^2)^2}{4(s' - 4M_\pi^2)(s + s' - 4M_\pi^2)},\\
a_4 &= -\frac{(s - 2s' + 4M_\pi^2)(s + s' - 4M_\pi^2)}{(s' - 4M_\pi^2)(s + 2s' - 4M_\pi^2)},\\
a_5 &= \frac{s'(-s + 2s' - 4M_\pi^2)}{(s' - 4M_\pi^2)(s + 2s' - 4M_\pi^2)},\\
a_6 &= -\frac{(s - 2s' + 4M_\pi^2)(s + 2s' - 4M_\pi^2)}{4(s' - 4M_\pi^2)s'},
\end{aligned}
\tag{C3}
$$

the analytical expressions for the $I_{\ell\ell'}(s, s')$ can be recast as

$$
I_{00}(s, s') = 2\frac{(s - 4M_\pi^2)(s' - 2M_\pi^2)/(s' - 4M_\pi^2) + s'\log(a_1)}{\pi s'(s - 4M_\pi^2)},
\tag{C4}
$$

$$
I_{01}(s, s') = -\frac{2(s' - 2M_\pi^2)}{\pi(s' - 4M_\pi^2)s'} - 2\frac{(s' - 4M_\pi^2)s'\log(a_1) + ss'\log(a_2)}{\pi(s - 4M_\pi^2)(s' - 4M_\pi^2)s'},
\tag{C5}
$$

$$
I_{02}(s, s') = \frac{1}{\pi}\left\{\frac{6s}{(s' - 4M_\pi^2)^2} + \frac{1}{s' - 4M_\pi^2} + \frac{1}{s'}\right\} + \frac{1}{\pi(s - 4M_\pi^2)}\left\{2\log(a_1) + \frac{6s(s + s' - 4M_\pi^2)\log(a_2)}{(s' - 4M_\pi^2)^2}\right\},
\tag{C6}
$$

$$
\begin{aligned}
I_{03}(s, s') = -\frac{1}{\pi(s - 4M_\pi^2)}\Bigg\{&\frac{(s - 4M_\pi^2)(2s'^3 + 10(s - 2M_\pi^2)s'^2 + (25s^2 - 60M_\pi^2 s + 64M_\pi^4)s' - 64M_\pi^6)}{(s' - 4M_\pi^2)^3 s'}\\
&+ 2\log(a_1) + \frac{2s(10s^2 + 15(s' - 4M_\pi^2)s + 6(s' - 4M_\pi^2)^2)\log(a_2)}{(s' - 4M_\pi^2)^3}\Bigg\},
\end{aligned}
\tag{C7}
$$

$$
\begin{aligned}
I_{10}(s, s') = -\frac{2}{\pi(s - 4M_\pi^2)^2(s' - 4M_\pi^2)s'}&[s^2 M_\pi^2 + 2s'^2 s - 8s' s M_\pi^2 - 8sM_\pi^4 - 8s'^2 M_\pi^2 + 32s' M_\pi^4 + 16M_\pi^6\\
&+ (s' - 4M_\pi^2)s'\log(a_1)s + 2s'(s'^2 - 6s' M_\pi^2 + 8M_\pi^4)\log(a_1)],
\end{aligned}
\tag{C8}
$$

$$
\begin{aligned}
I_{11}(s, s') = \frac{2}{\pi(s - 4M_\pi^2)^2}\Bigg\{&\frac{(2s' + M_\pi^2)s^2 + 2(s'^2 - 8s' M_\pi^2 - 4M_\pi^4)s - 8(s'^2 - 4M_\pi^2 s' - 2M_\pi^4)M_\pi^2}{(s' - 4M_\pi^2)s'}\\
&+ \frac{1}{s' - 4M_\pi^2}[s(s + 3s' - 8M_\pi^2)\log(a_3) - (s^2 + 2(s' - 2M_\pi^2)s + 2(s'^2 - 6s' M_\pi^2 + 8M_\pi^4))\log(a_4)]\\
&+ 2(s' - 2M_\pi^2)\log(a_5) - s\log(a_6)\Bigg\},
\end{aligned}
\tag{C9}
$$

$$I_{12}(s,s') = \frac{1}{2\pi(s-4M_\pi^2)^2}\Bigg\{-\frac{2(s-4M_\pi^2)(9s's^2+2(6s'^2-17s'M_\pi^2-4M_\pi^4)s+4(s'^3-8s'^2M_\pi^2+14M_\pi^4s'+8M_\pi^6))}{(s'-4M_\pi^2)^2s'}$$
$$+\frac{4}{(s'-4M_\pi^2)^2}[s(3s^2+3(3s'-8M_\pi^2)s+7s'^2-44M_\pi^2s'+64M_\pi^4)\log(a_3^{-1})+(3s^3+3(3s'-8M_\pi^2)s^2$$
$$+6(s'^2-6s'M_\pi^2+8M_\pi^4)s+2(s'-4M_\pi^2)^2(s'-2M_\pi^2))\log(a_4)]-8(s'-2M_\pi^2)\log(a_5)+4s\log(a_6)\Bigg\}, \quad \text{(C10)}$$

$$I_{13}(s,s') = \frac{1}{2\pi(s-4M_\pi^2)^2}\Bigg\{\frac{2(s-4M_\pi^2)(85s's^3+5s'(33s'-100M_\pi^2)s^2+(72s'^3-510s'^2M_\pi^2+784M_\pi^4s'+96M_\pi^6)s)}{3(s'-4M_\pi^2)^3s'}$$
$$-\frac{4}{(s'-4M_\pi^2)^3}[s(10s^3+5(7s'-20M_\pi^2)s^2+12(3s'^2-19s'M_\pi^2+28M_\pi^4)s$$
$$+(s'-4M_\pi^2)^2(13s'-28M_\pi^2))\log(a_3^{-1})+(10s^4+5(7s'-20M_\pi^2)s^3+12(3s'^2-19s'M_\pi^2+28M_\pi^4)s^2$$
$$+12(s'-4M_\pi^2)^2(s'-2M_\pi^2)s+2(s'-4M_\pi^2)^3(s'-2M_\pi^2))\log(a_4)]+\frac{8(s-4M_\pi^2)(s'^2-4M_\pi^2s'-2M_\pi^4)}{(s'-4M_\pi^2)s'}$$
$$+8(s'-2M_\pi^2)\log(a_5)-4s\log(a_6)\Bigg\}. \quad \text{(C11)}$$

The behavior around threshold is also interesting when considering the expansions of the kernels around $s-4M_\pi^2$. In particular, the threshold expansions of $\overline{K}^{II'}_{\ell\ell'}(s,s')$ around $s=4M_\pi^2$ behave like $a+b(s-4M_\pi^2)+\ldots$.

TABLE XII. Phases from the dispersive data analysis. Central values are obtained as a weighted average between the output of Roy and GKPY equations, using the CFD fit as input. We do not weight the uncertainty but take the smallest of the two, since both results come from the same data.

$\sqrt{s}$ (MeV)	$\delta_0^0(^\circ)$	$\delta_1^1(^\circ)$	$\delta_0^2(^\circ)$
310	7.1 ± 0.3	0.2 ± 0.1	−1.5 ± 0.1
340	11.7 ± 0.5	0.6 ± 0.1	−2.5 ± 0.1
370	16.5 ± 0.7	1.2 ± 0.1	−3.5 ± 0.1
400	21.5 ± 1.0	1.9 ± 0.2	−4.6 ± 0.2
430	26.6 ± 1.3	2.8 ± 0.2	−5.7 ± 0.2
460	31.9 ± 1.8	3.9 ± 0.2	−6.7 ± 0.3
490	36.9 ± 3.0	5.3 ± 0.2	−7.8 ± 0.3
520	40.7 ± 7.5	7.0 ± 0.2	−8.9 ± 0.3
550	50.5 ± 5.4	9.1 ± 0.2	−9.9 ± 0.4
580	54.7 ± 3.2	12.0 ± 0.2	−11.0 ± 0.4
610	59.3 ± 2.5	15.9 ± 0.3	−12.0 ± 0.5
640	63.8 ± 2.1	20.7 ± 0.5	−13.1 ± 0.6
670	68.1 ± 1.8	28.7 ± 0.5	−14.1 ± 0.6
700	72.2 ± 1.7	40.6 ± 2.6	−15.1 ± 0.7
730	76.2 ± 1.6	56.1 ± 1.1	−16.2 ± 0.8
760	80.3 ± 1.6	79.0 ± 0.8	−17.2 ± 0.9
790	84.3 ± 1.6	101.8 ± 0.8	−18.2 ± 1.0
820	88.6 ± 1.7	118.0 ± 0.9	−19.2 ± 1.1
850	93.5 ± 1.8	128.3 ± 1.9	−20.2 ± 1.2
880	99.7 ± 2.2	142.0 ± 2.0	−21.2 ± 1.3
910	108.8 ± 3.4	147.0 ± 1.3	−22.1 ± 1.4
940	122.7 ± 7.0	150.5 ± 1.2	−22.9 ± 1.5
970	152.0 ± 6.3	153.3 ± 1.2	−23.9 ± 1.7

APPENDIX D: ROY-GKPY WEIGHTED PHASES

In Table XII we give the central values of the phase in the elastic regions, as the weighted average obtained from the output of Roy and GKPY equations, when using the CFD set as input. We do not weight the uncertainty but take the smallest of the two outputs, since both results come from the same data. These results could be understood as a traditional ''energy-dependent data analysis.''

[1] J. R. Pelaez and F. J. Yndurain, Phys. Rev. D **71**, 074016 (2005).
[2] R. Kaminski, J. R. Pelaez, and F. J. Yndurain, Phys. Rev. D **74**, 014001 (2006); **74**, 079903(E) (2006).
[3] R. Kaminski, J. R. Pelaez, and F. J. Yndurain, Phys. Rev. D **77**, 054015 (2008).
[4] J. Gasser and H. Leutwyler, Ann. Phys. (N.Y.) **158**, 142 (1984).
[5] J. R. Pelaez and F. J. Yndurain, Phys. Rev. D **69**, 114001 (2004).
[6] R. Garcia-Martin, J. R. Pelaez, and F. J. Yndurain, Phys. Rev. D **76**, 074034 (2007).
[7] L. Rosselet, P. Extermann, J. Fischer *et al.*, Phys. Rev. D **15**, 574 (1977); S. Pislak *et al.* (BNL-E865 Collaboration), Phys. Rev. Lett. **87**, 221801 (2001).
[8] J. R. Batley *et al.* (NA48/2 Collaboration), Eur. Phys. J. C **54**, 411 (2008).
[9] S. M. Roy, Phys. Lett. **36B**, 353 (1971).
[10] J. L. Basdevant, C. D. Froggatt, and J. L. Petersen, Phys. Lett. **41B**, 178 (1972); Nucl. Phys. **B72**, 413 (1974); M. R. Pennington, Ann. Phys. (N.Y.) **92**, 164 (1975).
[11] G. Colangelo, J. Gasser, and H. Leutwyler, Nucl. Phys. **B603**, 125 (2001); B. Ananthanarayan, G. Colangelo, J. Gasser, and H. Leutwyler, Phys. Rep. **353**, 207 (2001).
[12] R. Kaminski, L. Lesniak, and B. Loiseau, Phys. Lett. B **551**, 241 (2003).
[13] I. Caprini, G. Colangelo, and H. Leutwyler, Phys. Rev. Lett. **96**, 132001 (2006).
[14] K. Nakamura *et al.* (Particle Data Group), J. Phys. G **37**, 075021 (2010).
[15] A. Dobado and J. R. Pelaez, Phys. Rev. D **56**, 3057 (1997); J. A. Oller and E. Oset, Nucl. Phys. **A620**, 438 (1997); Z. Y. Zhou, G. Y. Qin, P. Zhang *et al.*, J. High Energy Phys. 02 (2005) 043; G. Mennessier, S. Narison, and W. Ochs, Nucl. Phys. B, Proc. Suppl. **181–182**, 238 (2008).
[16] R. L. Jaffe, Phys. Rev. D **15**, 267 (1977); AIP Conf. Proc. **964**, 1 (2007); Prog. Theor. Phys. Suppl. **168**, 127 (2007).
[17] M. R. Pennington, Phys. Rev. Lett. **97**, 011601 (2006); J. A. Oller and L. Roca, Eur. Phys. J. A **37**, 15 (2008); J. Bernabeu and J. Prades, Phys. Rev. Lett. **100**, 241804 (2008); R. Kaminski, G. Mennessier, and S. Narison, Phys. Lett. B **680**, 148 (2009).
[18] J. R. Pelaez, Phys. Rev. Lett. **92**, 102001 (2004); J. R. Pelaez and G. Rios, Phys. Rev. Lett. **97**, 242002 (2006).
[19] N. N. Achasov and G. N. Shestakov, Phys. Rev. Lett. **99**, 072001 (2007).
[20] J. R. Batley *et al.* (NA48/2 Collaboration), Eur. Phys. J. C **70**, 635 (2010).
[21] K. L. Au, D. Morgan, and M. R. Pennington, Phys. Rev. D **35**, 1633 (1987); D. Morgan and M. R. Pennington, Phys. Rev. D **48**, 1185 (1993); B. S. Zou and D. V. Bugg, Phys. Rev. D **48**, R3948 (1993); D. V. Bugg, Eur. Phys. J. C **47**, 45 (2006).
[22] G. Colangelo, J. Gasser, and A. Rusetsky, Eur. Phys. J. C **59**, 777 (2008).
[23] A. Aloisio *et al.* (KLOE Collaboration), Phys. Lett. B **537**, 21 (2002); V. Cirigliano, G. Ecker, H. Neufeld, and A. Pich, Eur. Phys. J. C **33**, 369 (2004); V. Cirigliano, C. Gatti, M. Moulson, and M. Palutan (FlaviaNet Kaon Working Group), arXiv:0807.5128.
[24] O. Nachtmann and E. de Rafael, CERN Report No. TH-1031, 1969 (unpublished); P. Pascual and F. J. Ynduráin, Nucl. Phys. **B83**, 362 (1974).
[25] G. Colangelo, Proc. Sci., KAON (2008) 038 [arXiv:0710.3050].
[26] V. Cirigliano, G. Ecker, and A. Pich, Phys. Lett. B **679**, 445 (2009).
[27] H. Leutwyler, AIP Conf. Proc. **892**, 58 (2007).
[28] We thank H. Leutwyer for this suggestion.
[29] B. Hyams *et al.*, Nucl. Phys. **B64**, 134 (1973); P. Estabrooks and A. D. Martin, Nucl. Phys. **B79**, 301 (1974); S. D. Protopopescu *et al.*, Phys. Rev. D **7**, 1279 (1973); R. Kamiński, L. Lesniak, and K. Rybicki, Z. Phys. C **74**, 79 (1997); Eur. Phys. J. direct C **4**, 1 (2002); B. Hyams *et al.*, Nucl. Phys. **B100**, 205 (1975); M. J. Losty *et al.*, Nucl. Phys. **B69**, 185 (1974); W. Hoogland *et al.*, Nucl. Phys. **B126**, 109 (1977); N. B. Durusoy *et al.*, Phys. Lett. **45B**, 517 (1973).
[30] G. Grayer *et al.*, Nucl. Phys. **B75**, 189 (1974).
[31] S. L. Adler, Phys. Rev. **137**, B1022 (1965).
[32] I. Caprini, Phys. Rev. D **77**, 114019 (2008).
[33] N. N. Achasov, S. A. Devyanin, and G. N. Shestakov, Z. Phys. C **22**, 53 (1984); N. N. Achasov and A. V. Kiselev, Phys. Rev. D **73**, 054029 (2006); **74**, 059902 (2006).
[34] R. Kaminski, R. Garcia-Martin, P. Grynkiewicz, J. R. Pelaez, and F. J. Yndurain, Int. J. Mod. Phys. A **24**, 402 (2009).
[35] R. Kaminski, R. Garcia-Martin, P. Grynkiewicz, and J. R. Pelaez, Nucl. Phys. B, Proc. Suppl. **186**, 318 (2009).
[36] We thank H. Leutwyler for his comments and suggestions on this issue.
[37] B. Adeva, A. Romero, and O. Vazquez Doce, Eur. Phys. J. A **31**, 522 (2007).
[38] B. Adeva *et al.* (DIRAC Collaboration), Phys. Lett. B **619**, 50 (2005).

[39] J. R. Batley *et al.*, Eur. Phys. J. C **64**, 589 (2009); N. Cabibbo and G. Isidori, J. High Energy Phys. 03 (2005) 021; G. Colangelo *et al.*, Phys. Lett. B **638**, 187 (2006); M. Bissegger *et al.*, Nucl. Phys. B **806**, 178 (2009).

[40] W. Rarita, R. J. Riddell, C. B. Chiu, and R. J. N. Phillips, Phys. Rev. **165**, 1615 (1968); C. D. Froggatt and J. L. Petersen, Nucl. Phys. **B129**, 89 (1977).

[41] G. Wanders, Eur. Phys. J. C **17**, 323 (2000).

[42] R. Kaminski, arXiv:1103.0882.

2.1.4 Publication: R. Garcia-Martin, R. Kaminski, J.R. Pelaez, J. Ruiz de Elvira, *Precise determination of the f0(600) and f0(980) pole parameters from a dispersive data analysis , Phys. Rev. Lett.* 107 (2011) 072001

Precise Determination of the $f_0(600)$ and $f_0(980)$ Pole Parameters from a Dispersive Data Analysis

R. García-Martín,[1] R. Kamiński,[2] J. R. Peláez,[1] and J. Ruiz de Elvira[1]

[1]*Departamento de Física Teórica II, Universidad Complutense de Madrid, 28040 Madrid, Spain*
[2]*Department of Theoretical Physics Henryk Niewodniczański Institute of Nuclear Physics, Polish Academy of Sciences, 31-342, Kraków, Poland*

(Received 14 April 2011; published 9 August 2011)

We use our latest dispersive analysis of $\pi\pi$ scattering data and the very recent $K_{\ell 4}$ experimental results to obtain the mass, width, and couplings of the two lightest scalar-isoscalar resonances. These parameters are defined from their associated poles in the complex plane. The analytic continuation to the complex plane is made in a model-independent way by means of once- and twice-subtracted dispersion relations for the partial waves, without any other theoretical assumption. We find the $f_0(600)$ pole at $(457^{+14}_{-13}) - i(279^{+11}_{-7})$ MeV and that of the $f_0(980)$ at $(996 \pm 7) - i(25^{+10}_{-6})$ MeV, whereas their respective couplings to two pions are $3.59^{+0.11}_{-0.13}$ and 2.3 ± 0.2 GeV.

DOI: 10.1103/PhysRevLett.107.072001 PACS numbers: 14.40.Be, 11.55.Fv, 13.75.Lb

The $f_0(600)$ or sigma and $f_0(980)$ resonances are of great interest in several fields of physics. First, the two-pion exchange in the scalar-isoscalar channel, $I = 0$, $J = 0$, where these resonances appear, plays a key role in nuclear physics, where the nucleon-nucleon attractive interaction has been long [1] modeled by the exchange of a ''sigma'' resonance. Second, this channel is also relevant for the QCD non-Abelian nature, since it is where the lightest glueball is expected to appear. However, the glueball identification is complicated by its possible mixing into different states, like the $f_0(600)$, $f_0(980)$, and heavier f_0 resonances, which may be $\bar{q}q$ mesons, tetraquarks, molecules, or most likely a mixture of them all. Actually, most of the controversy around these resonances comes from the identification of scalar multiplets—see the Review of Particle Physics (PDG) ''Note on Scalar Mesons'' [2]. Third, the $f_0(600)$, being the lightest hadronic resonance with vacuum quantum numbers, plays a relevant role in many models of QCD spontaneous chiral symmetry breaking. Furthermore, this state is of interest in order to understand why, despite being so light and strongly coupled to pions, it plays such a small role, if any, in the saturation [3] of the low energy constants of chiral perturbation theory (ChPT). Moreover, the position of this pole could be setting the limit of applicability of the chiral expansion. Finally, this state is of interest for electroweak physics due to its many similarities—but even more by its many differences—with the Higgs mechanism now under scrutiny at the LHC.

Still, the properties of these resonances are the subject of an intense debate. Let us recall that the σ was listed in the PDG as ''not well established'' until 1974, removed in 1976, and listed back in 1996. This was due to its width being comparable to its mass, so that it barely propagates and becomes a broad enhancement in the traditional, and often contradictory, $\pi\pi$ scattering analyses, extracted from $\pi N \to \pi\pi N$ experiments, using different models affected by large systematic uncertainties. After 2000, these resonances have been observed in decays of heavier mesons, with well defined initial states and very different systematics from $\pi\pi$ scattering, which led the PDG to consider, in 2002, the $f_0(600)$ as ''well established'' but keeping until today a too conservative estimate of ''mass: 400–1200 MeV'' and ''width: 600–1000 MeV.'' For the $f_0(980)$ the situation is not much better, with an estimated width ''from 40 to 100 MeV.'' However, not all the uncertainty comes from experiment. The shape of these resonances varies from process to process, and that is why their masses and widths are quoted from their process-independent pole positions, defined as $\sqrt{s_{\rm pole}} \sim M - i\Gamma/2$. But many models do not implement rigorous analytic continuations and lead to incorrect determinations when poles are deep in the complex plane or close to threshold cuts, as happens with the $f_0(600)$ and the $f_0(980)$, respectively. Actually, this is one of the main causes of the huge PDG uncertainties [2].

This model dependence can be avoided by using dispersive techniques, which follow from causality and crossing and provide integral relations and a rigorous analytic continuation of the amplitude in terms of its imaginary part in the physical region, which can be obtained from data. For example, dispersion relations combined with ChPT determine the σ pole at $440 - i245$ MeV [4] or $(470 \pm 50) - i(260 \pm 25)$ MeV [5]. We focus here on dispersive analyses, but other approaches yield similar values [6,7]—see Table I and Ref. [14] for a review and references.

Generically, the main difficulty lies in the calculation of the left cut integral, which in Refs. [4,5] was just approximated. This left cut is due to crossing symmetry and can be incorporated rigorously in a set of infinite coupled equations written long ago by Roy [15] (see also [16] for

TABLE I. Other recent determinations of the σ pole and coupling, using analyticity. Results come from Roy equations and ChPT [8], conformal fits to $K_{\ell 4}$ decays and averaged $\pi\pi$ data around 800–900 MeV with only statistical [9] or also systematic [10] uncertainties, the chiral unitary approach [11] (only statistical error), a K matrix with a form factor shape [12], and ChPT + elastic dispersion relations (two loops [13]).

Reference	$\sqrt{s_\sigma}$ (MeV)	$\lvert g_{\sigma\pi\pi}\rvert$ (GeV)
[8]	$(441^{+16}_{-8}) - i(272^{+9}_{-12.5})$	$3.31^{+0.35}_{-0.15}$
[9]	$(474 \pm 6) - i(254 \pm 4)$	3.58 ± 0.03
[10]	$(463 \pm 6^{+31}_{-17}) - i(254 \pm 6^{+33}_{-34})$	...
[11]	$(443 \pm 2) - i(216 \pm 4)$	2.97 ± 0.04
[12]	$(452 \pm 12) - i(260 \pm 15)$	2.65 ± 0.10
[13] (fit D)	$453 - i271$	3.5

applications and references). Recently, Roy equations have been used to study low energy $\pi\pi$ scattering [17], sometimes combined with ChPT [18], or also to test ChPT [19], as well as to solve old data ambiguities [20]. Most recently [8], the $f_0(600)$ and $f_0(980)$ poles were shown to lie within the applicability region of Roy equations. Since data were not reliable and to improve accuracy, Roy equations were supplemented by ChPT predictions in Ref. [8], to yield $\sqrt{s_\sigma} = (441^{+16}_{-8}) - i(272^{+9}_{-19.5})$ MeV, without using data below 800 MeV on S and P waves. In that work, an $f_0(980)$ pole is also found at $\sqrt{s} = 1001 - i14$ MeV. Note that, generically, $\pi\pi$ scattering data around 900 MeV tend to produce a narrower $f_0(980)$ [7,8,11] than that seen in production processes or the PDG estimate. In Table II, we list some other recent determinations of the $f_0(980)$ parameters.

Our aim in this work is to provide a precise and model-independent simultaneous determination of the $f_0(600)$ and $f_0(980)$ parameters from data alone, profiting from two relevant results developed over the past half year: on the one hand, the final analysis of $K_{\ell 4}$ decays by the NA48/2 Collaboration [26], which provides reliable and precise $\pi\pi$ scattering phases below the mass of the kaon and, on the other hand, a set of Roy-like equations—called García-Martín–Kamiński–Peláez–Yndurain (GKPY) equations and developed by our group [27]—which is much more stringent in the resonant region than standard Roy equations. The reason is that, in order to avoid divergences, dispersion relations are weighted at low energy with "subtractions," but then amplitudes are determined only up to a polynomial, whose coefficients depend on threshold parameters. Since Roy equations have two subtractions, they have an s polynomial term multiplied by the isospin-2 scalar scattering length, whose large uncertainty thus grows markedly in the $f_0(600)$ and $f_0(980)$ region. In contrast, the GKPY equations have just one subtraction, and their output, even without using ChPT predictions at all, provides [27] a very precise description of $\pi\pi$ scattering data, discarding a long-standing conflict concerning the inelasticity—and to a lesser extent the phase shift—right above the $f_0(980)$ region.

TABLE II. Recent determinations of $f_0(980)$ parameters. For Ref. [21] our estimate covers the six models considered there. The last three poles come from scattering matrices and the rest from production experiments.

Reference	$\sqrt{s_{f_0(980)}}$ (MeV)	$\lvert g_{f_0\pi\pi}\rvert$ (GeV)
[22]	$(978 \pm 12) - i(28 \pm 15)$	2.25 ± 0.20
[21]	$(988 \pm 10 \pm 6) - i(27 \pm 6 \pm 5)$	2.2 ± 0.2
[23]	$(977 \pm 5) - i(22 \pm 2)$	1.5 ± 0.2
[24]	$(965 \pm 10) - i(26 \pm 11)$	2.3 ± 0.2
[11]	$(986 \pm 3) - i(11 \pm 4)$	1.1 ± 0.2
[12]	$(981 \pm 34) - i(18 \pm 11)$	1.17 ± 0.26
[25]	$999 - i21$	1.88

If we now use these GKPY dispersion relations to continue analytically that amplitude, we find

$$\sqrt{s_\sigma} = (457^{+14}_{-13}) - i(279^{+11}_{-7}) \text{ MeV}, \quad (1)$$

$$\sqrt{s_{f_0(980)}} = (996 \pm 7) - i(25^{+10}_{-6}) \text{ MeV}. \quad (2)$$

Let us describe next the whole approach in detail and provide determinations for other quantities of interest, like their couplings and the $\rho(770)$ parameters, as well as other checks of our calculations from Roy equations.

Ours is what is traditionally called an "energy-dependent" analysis of $\pi\pi$ scattering and $K_{\ell 4}$ decay data [28,29]—in particular, the latest results from NA48/2 [26]. Our procedure, described in a series of works [27,30], was to obtain as a first step a simple set of *unconstrained* fits to these data (UFD) for each partial wave separately up to 1420 MeV and Regge fits above that energy. Next we obtained *constrained* fits to data (CFD) by varying the UFD parameters in order to satisfy within uncertainties two crossing sum rules, a complete set of forward dispersion relations as well as Roy and GKPY equations, while simultaneously describing the data. The details for all CFD waves can be found in Ref. [27], but since we are now interested in the scalar-isoscalar partial wave $t_0^{(0)}$, we show in Fig. 1 the resulting $\delta_0^{(0)}$ phase shift. It should be noticed that the CFD result is indistinguishable to the eye from the UFD, except in the 900–1000 MeV region, which we also show in detail and is essential for the determination of the $f_0(980)$ parameters. Note that both the UFD and CFD describe the data in that region, but the GKPY dispersion relations require the CFD phase to lie somewhat higher than the UFD one. This is relevant since it yields a wider $f_0(980)$, correcting the above-mentioned tendency to obtain a too narrow $f_0(980)$ from unconstrained fits to $\pi\pi$ scattering data alone. In the inner top panel, we show the good description of the latest NA48/2 data on $K_{\ell 4}$ decays, which are responsible for the small uncertainties in our input parametrization and constrain our subtraction constants. As seen in Fig. 1, the inelasticity $\eta_0^{(0)}$ shows a

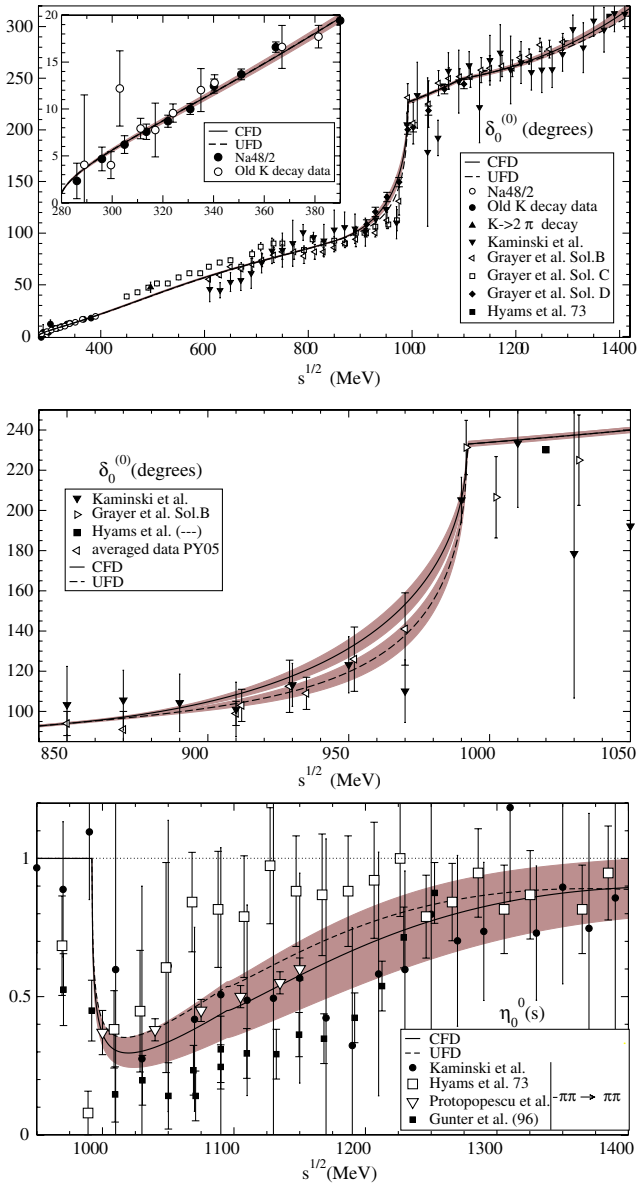

FIG. 1 (color online). S0 wave phase and inelasticity from UFD and CFD. Dark bands cover the uncertainties. The data come from Refs. [26,28].

"dip" structure above 1 GeV required by the GKPY equations [27], which disfavors the alternative "nondip" solution. Having this long-standing dip versus "no-dip" controversy [31] settled [27] is very relevant for a precise $f_0(980)$ determination.

The interest of this CFD parametrization is that, while describing the data, it satisfies within uncertainties Roy and GKPY relations up to their applicability range, namely, 1100 MeV, which includes the $f_0(980)$ region. In addition, the three forward dispersion relations are satisfied up to 1420 MeV. In Fig. 2, we show the fulfillment of the S0 wave Roy and GKPY equations and how, as explained above, the uncertainty in the Roy equation is much larger

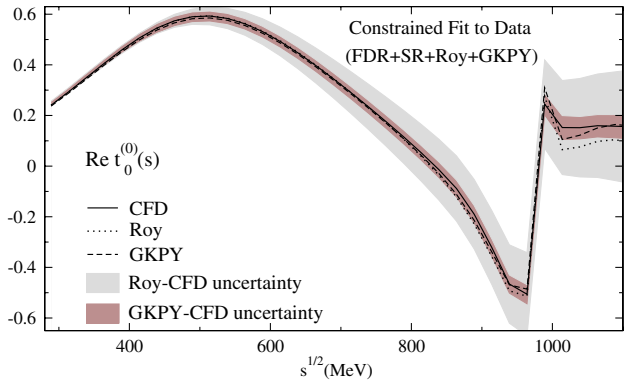

FIG. 2 (color online). Fulfillment of S0 wave Roy and GKPY equations. The CFD parametrization is the input to both the Roy and GKPY equations and is in remarkable agreement with their output. Note how the uncertainty in the Roy equation is much larger than that of the GKPY equation above roughly 500 MeV.

than for the GKPY equation in the resonance region. The latter will allow us now to obtain a precise determination of the $f_0(600)$ and $f_0(980)$ poles from data alone, i.e., without using ChPT predictions.

Hence, we now feed our CFD parameterizations as input for the GKPY and Roy equations, which provide a model-independent analytic continuation to the complex plane, and determine the position and residues of the second Riemann sheet poles. It has been shown [8] that the $f_0(600)$ and $f_0(980)$ poles lie well within the domain of validity of Roy equations, given by the constraint that the t values which are integrated to obtain the partial wave representation at a given s should be contained within a Lehmann-Martin ellipse. These are conditions on the analytic extension of the partial wave expansion, unrelated to the number of subtractions in the dispersion relation, and they equally apply to GKPY equations.

Thus, in Table III, we show the $f_0(600)$, $f_0(980)$, and $\rho(770)$ poles resulting from the use of the CFD parametrization inside Roy or GKPY equations. We consider that our best results are those coming from GKPY equations, since their uncertainties are smaller, although, of course, both results are compatible.

Several remarks are in order. First, statistical uncertainties are calculated by using a Monte Carlo Gaussian sampling of the CFD parameters with 7000 samples distributed

TABLE III. Poles and residues from Roy and GKPY equations.

	$\sqrt{s_{\text{pole}}}$ (MeV)	$\lvert g\rvert$
$f_0(600)^{\text{Roy}}$	$(445 \pm 25) - i(278^{+22}_{-18})$	3.4 ± 0.5 GeV
$f_0(980)^{\text{Roy}}$	$(1003^{+5}_{-27}) - i(21^{+10}_{-8})$	$2.5^{+0.2}_{-0.6}$ GeV
$\rho(770)^{\text{Roy}}$	$(761^{+4}_{-3}) - i(71.7^{+1.9}_{-2.3})$	$5.95^{+0.12}_{-0.08}$
$f_0(600)^{\text{GKPY}}$	$(457^{+14}_{-13}) - i(279^{+11}_{-7})$	$3.59^{+0.11}_{-0.13}$ GeV
$f_0(980)^{\text{GKPY}}$	$(996 \pm 7) - i(25^{+10}_{-6})$	2.3 ± 0.2 GeV
$\rho(770)^{\text{GKPY}}$	$(763.7^{+1.7}_{-1.5}) - i(73.2^{+1.0}_{-1.1})$	$6.01^{+0.04}_{-0.07}$

within 3 standard deviations. A systematic uncertainty due to the different charged and neutral kaon masses is relevant for the $f_0(980)$ due to the existence of two $\bar{K}K$ thresholds separated by roughly 8 MeV, which we have treated as a single $\bar{K}K$ threshold at $\hat{m}_K = (m_{K^0} - m_{K^+})/2 \simeq 992\,\mathrm{MeV}$. In order to estimate this systematic uncertainty, we have refitted the UFD and CFD sets to the extreme cases of using m_{K^0} or m_{K^+} instead of $\hat{m}_K$. As could be expected, the only significant variation is for the $f_0(980)$—actually, only for its half-width, which changes by ± 4.4 MeV for GKPY equations and ± 5.6 MeV for Roy equations. The $f_0(600)$ changes by roughly 1 MeV, and the $\rho(770)$ barely notices the change—less than 0.1 MeV. The effect on residues is smaller than that of rounding the numbers. We have added all these uncertainties in quadrature to the statistical ones. Second, both the mass and width of the $f_0(600)$ are compatible with those in Ref. [8] within 1 standard deviation. Since we are not using ChPT and Ref. [8] did not use data below 800 MeV, this is a remarkable check of the agreement between ChPT and low energy data. Third, the $f_0(980)$ width is no longer so narrow—as happens in typical $\pi\pi$ scattering analyses—and we find $\Gamma = 50^{+20}_{-12}$ MeV, very compatible with results from production processes. The mass overlaps within 1 standard deviation with the PDG estimate. These results show that the effect of the too narrow $f_0(980)$ pole and the use of further theoretical input like ChPT do not affect significantly the resulting $f_0(600)$ parameters.

In Table III, we also provide for each resonance its coupling to two pions, defined from its pole residue as

$$g^2 = -16\pi \lim_{s \to s_{\mathrm{pole}}} (s - s_{\mathrm{pole}}) t_\ell(s) (2\ell + 1)/(2p)^{2\ell}, \quad (3)$$

where $p^2 = s/4 - m_\pi^2$. This residue is relevant for models of the spectroscopic nature of these particles, particularly for the $f_0(600)$ [32], which are beyond the pure data analysis scope of this work. Differences between previous values of these couplings can be seen in Tables I and II.

In summary, using a recently developed dispersive formalism, which is especially accurate in the resonance region, we have been able to determine, in a model-independent way, the $f_0(600)$ and $f_0(980)$ poles and couplings from data with no further theoretical input. We hope this work helps to clarify the somewhat controversial situation regarding the parameters of these resonances.

[1] M. H. Johnson and E. Teller, Phys. Rev. **98**, 783 (1955).
[2] K. Nakamura *et al.* (Particle Data Group), J. Phys. G **37**, 075021 (2010).
[3] G. Ecker, J. Gasser, A. Pich, and E. de Rafael, Nucl. Phys. **B321**, 311 (1989); J. F. Donoghue, C. Ramirez, and G. Valencia, Phys. Rev. D **39**, 1947 (1989).
[4] A. Dobado and J. R. Pelaez, Phys. Rev. D **56**, 3057 (1997).
[5] Z. Y. Zhou *et al.*, J. High Energy Phys. 02 (2005) 043.
[6] E. van Beveren *et al.*, Z. Phys. C **30**, 615 (1986); R. Kaminski, L. Lesniak, and J. P. Maillet, Phys. Rev. D **50**, 3145 (1994); R. Delbourgo and M. D. Scadron, Mod. Phys. Lett. A **10**, 251 (1995); S. Ishida *et al.*, Prog. Theor. Phys. **95**, 745 (1996); M. Harada, F. Sannino, and J. Schechter, Phys. Rev. D **54**, 1991 (1996); N. A. Tornqvist and M. Roos, Phys. Rev. Lett. **76**, 1575 (1996); J. A. Oller and E. Oset, Nucl. Phys. **A620**, 438 (1997); **A652**, 407(E) (1999); D. Black *et al.*, Phys. Rev. D **59**, 074026 (1999); D. V. Bugg, Phys. Lett. B **572**, 1 (2003); **595**, 556(E) (2004); Phys. Rep. **397**, 257 (2004); M. Ablikim *et al.* (BES Collaboration), Phys. Lett. B **598**, 149 (2004); A. V. Anisovich *et al.*, arXiv:1105.5923.
[7] J. A. Oller, E. Oset, and J. R. Pelaez, Phys. Rev. D **59**, 074001 (1999); **60**, 099906(E) (1999); **75**, 099903(E) (2007); J. R. Pelaez, Mod. Phys. Lett. A **19**, 2879 (2004).
[8] I. Caprini, G. Colangelo, and H. Leutwyler, Phys. Rev. Lett. **96**, 132001 (2006); H. Leutwyler, AIP Conf. Proc. **1030**, 46 (2008).
[9] R. Garcia-Martin, J. R. Pelaez, and F. J. Yndurain, Phys. Rev. D **76**, 074034 (2007).
[10] I. Caprini, Phys. Rev. D **77**, 114019 (2008).
[11] J. A. Oller, Nucl. Phys. **A727**, 353 (2003).
[12] G. Mennessier, S. Narison, and X. -G. Wang, Nucl. Phys. B, Proc. Suppl. **207–208**, 177 (2010); Phys. Lett. B **696**, 40 (2011); **688**, 59 (2010); R. Kaminski, G. Mennessier, and S. Narison, Phys. Lett. B **680**, 148 (2009).
[13] J. R. Pelaez and G. Rios, Phys. Rev. D **82**, 114002 (2010).
[14] E. Klempt and A. Zaitsev, Phys. Rep. **454**, 1 (2007).
[15] S. M. Roy, Phys. Lett. **36B**, 353 (1971).
[16] M. R. Pennington and S. D. Protopopescu, Phys. Rev. D **7**, 1429 (1973); **7**, 2591 (1973); J. L. Basdevant, C. D. Froggatt, and J. L. Petersen, Phys. Lett. **41B**, 173 (1972); **41B**, 178 (1972); Nucl. Phys. **B72**, 413 (1974).
[17] B. Ananthanarayan *et al.*, Phys. Rep. **353**, 207 (2001).
[18] G. Colangelo, J. Gasser, and H. Leutwyler, Nucl. Phys. **B603**, 125 (2001).
[19] S. Descotes-Genon *et al.*, Eur. Phys. J. C **24**, 469 (2002).
[20] R. Kaminski, L. Lesniak, and B. Loiseau, Phys. Lett. B **551**, 241 (2003).
[21] D. Barberis *et al.* (WA102 Collaboration), Phys. Lett. B **462**, 462 (1999).
[22] R. R. Akhmetshin *et al.* (CMD-2 Collaboration), Phys. Lett. B **462**, 380 (1999).
[23] E. M. Aitala *et al.* (E791 Collaboration), Phys. Rev. Lett. **86**, 765 (2001).
[24] M. Ablikim *et al.* (BES Collaboration), Phys. Lett. B **607**, 243 (2005).
[25] Y. Mao *et al.*, Phys. Rev. D **79**, 116008 (2009).
[26] J. R. Batley *et al.* (NA48-2 Collaboration), Eur. Phys. J. C **70**, 635 (2010).
[27] R. Garcia-Martin *et al.*, Phys. Rev. D **83**, 074004 (2011).
[28] B. Hyams *et al.*, Nucl. Phys. **B64**, 134 (1973); G. Grayer *et al.*, Nucl. Phys. **B75**, 189 (1974).S. D. Protopopescu *et al.*, Phys. Rev. D **7**, 1279 (1973); R. Kaminski, L. Lesniak, and K. Rybicki, Z. Phys. C **74**, 79 (1997); Eur. Phys. J. C **4**, 4 (2002); J. Gunter *et al.* (E852 Collaboration), arXiv:hep-ex/9609010.
[29] L. Rosselet *et al.*, Phys. Rev. D **15**, 574 (1977); S. Pislak *et al.* (BNL-E865 Collaboration), Phys. Rev. Lett. **87**, 221801 (2001).

[30] R. Kaminski, J. R. Pelaez, and F. J. Yndurain, Phys. Rev. D **77**, 054015 (2008); **74**, 014001 (2006); J. R. Pelaez and F. J. Yndurain, Phys. Rev. D **71**, 074016 (2005); **69**, 114001 (2004).

[31] K. L. Au, D. Morgan, and M. R. Pennington, Phys. Rev. D **35**, 1633 (1987); D. Morgan and M. R. Pennington, Phys. Rev. D **48**, 1185 (1993).B. S. Zou and D. V. Bugg, Phys. Rev. D **48**, R3948 (1993).D. V. Bugg, Eur. Phys. J. C **47**, 45 (2006).

[32] M. R. Pennington, Phys. Rev. Lett. **97**, 011601 (2006); J. A. Oller and L. Roca, Eur. Phys. J. A **37**, 15 (2008).J. Bernabeu and J. Prades, Phys. Rev. Lett. **100**, 241804 (2008).

2.2 Nature of the lightest scalar resonances

2.2.1 Motivation

We have seen in Section 1.4, that the $1/N_c$ expansion is an analytic approximation to QCD in the whole energy region, that provides a clear definition of $\bar{q}q$ states. In addition, as reviewed in Section 1.4.4, the N_c scaling of the ChPT parameters is well known. Furthermore, we have seen in Section 1.6 how unitarization techniques allow us to reproduce or include explicitly different light resonances. Particularly, the IAM generates resonances not initially present in ChPT by ensuring unitarity in the elastic region and respecting the low energy ChPT expansion, without include any spurious parameters or unknown dependencies. Moreover, as we have commented briefly in Section 1.6, the coupled–channel IAM is a generalization of the elastic IAM described, which implements unitarity in coupled channels. However it cannot be derived in a model independent dispersive way, but it also generates the poles associated to the $f_0(980)$ and $a_0(980)$, $K^*(892)$ and κ.

In [211], it was shown, within a coupled–channel IAM formalism, that the vector resonances generated followed closely a N_c $\bar{q}q$ behaviour, whereas in the case of the lightest scalar poles this interpretation was very disfavored from the $1/N_c$ expansion. In Fig. 2.1, it is shown the evolution with N_c of the mass M and width Γ of the vectors $\rho(770)$ and $K^*(892)$ and the scalars $f_0(500)$ and κ, defined from the corresponding pole position, $\sqrt{s_{pole}} = M - i\Gamma/2$. The quantities are normalized to their value at $N_c = 3$, so they can be compared with the behaviour expected for a $\bar{q}q$ state, $M/M_{N_c=3} = 1$ and $\Gamma/\Gamma_{N_c=3} = 3/N_c$. The gray bands cover the uncertainty on the renormalization scale $\mu \sim 0.5 - 1$ GeV where to apply the $1/N_c$ scaling. It is clearly seen in Fig 2.1, that the vectors follow remarkably well the $1/N_c$ behaviour of $\bar{q}q$ states. However, the behaviour of the scalars σ and κ is quite different, and their width and mass grows with N_c. In addition, other results in the literature [213, 214, 215, 216, 217, 218] also found that near $N_c = 3$ the σ behaviour is not that expected one for a $\bar{q}q$ state.

It is important to remark that the main conclusion of this result is that the scalars do not behave predominantly as $\bar{q}q$ states. However, it was shown in [212] that only the pole dependence is robust not too far from $N_c = 3$, and that, beyond that regime, one could even find different qualitative behaviors. The main source of uncertainty in the one loop IAM, as we have seen in Section 1.3, is the choice of renormalization scale μ where the N_c scaling is applied. As seen in Fig. 2.2, that uncertainty is enough to change the large N_c behaviour, even when starting from exactly the same set of LECs at $N_c = 3$. Note that, only when μ is chosen between 0.5 and 1 GeV, the ρ pole behaves like a $\bar{q}q$ state. Nevertheless, still within that uncertainty band, the one loop IAM σ pole could move deep into the complex plane, or turn back into the real axis, at mass values smaller than the initial one or below two pion threshold. Moreover, the IAM cannot be applied for too large values of N_c because the underlying theory becomes weakly interacting, and, intuitively, unitarization makes much less sense. Further details can be found in [219].

In [220] the authors extended this analysis in SU(2) UChPT up to two-loops. The $O(p^6)$ best fit, although being compatible with the $O(p^4)$ ones at low N_c in that the σ is not predominantly a $\bar{q}q$ state, allows naturally for a subdominant $\bar{q}q$ component for the σ with a mass above 1

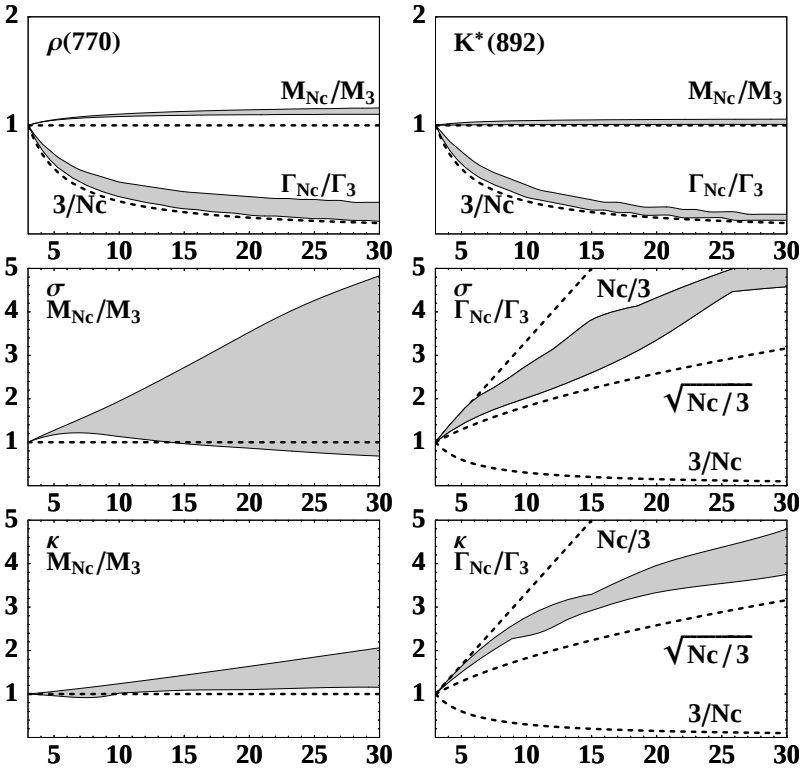

Figure 2.1: $1/N_c$ dependence found in [143], of the $\rho(770)$, $K^*(892)$, σ and κ poles positions defined as $\sqrt{s_{pole}} = M - i\Gamma/2$, normalized to their $N_c = 3$ values. The dashed lines show different N_c scaling laws, and the gray areas cover the uncertainty in $\mu = 0.5 - 1$ GeV.

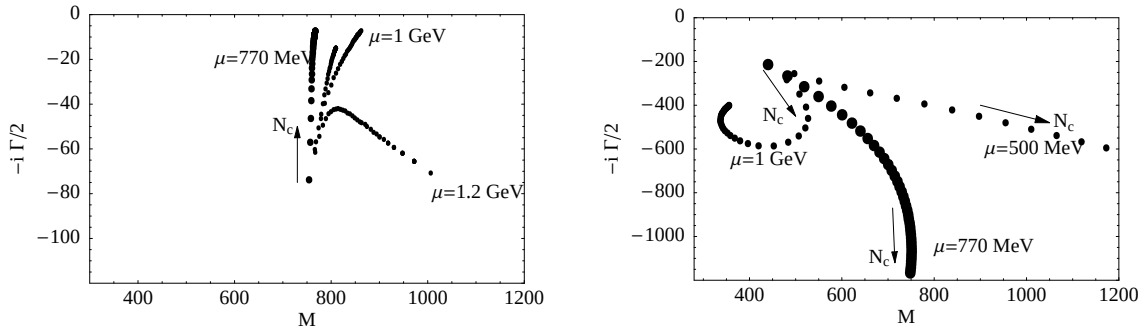

Figure 2.2: $1/N_c$ behaviour versus the renormalization scale choice from [212]. Left panel: The ρ pole tends to the real axis if 0.5 GeV < μ < 1 GeV, but not for μ = 1.2 GeV. Right panel: The sigma pole behaviour changes dramatically when μ changes from 0.5 to 1 GeV.

GeV arising as N_c grows. As we can see in Fig 2.3, the $f_0(500)$ pole still moves away from the 400–600 MeV region of the real axis, but then, the pole trajectory turns around moving back towards the real axis above 1 GeV as N_c becomes larger than 10 or so. This occurs rather

naturally in the two-loop results but was also hinted in some part of the one-loop parameter space. We have checked in this thesis that such a possibility actually occurs to one loop. Such a behaviour would indicate that, while the σ is predominantly non-$\bar{q}q$ at $Nc = 3$, it may have a subdominant $\bar{q}q$ component, but always originated above 1 GeV. However, as pointed out above, the fact that we have to choose the scale for which the $1/N_c$ scaling starts, implies that, even when this behaviour is favored at $O(p^6)$, we cannot exclude all those which lie within the uncertainty bands of Fig. 2.1.

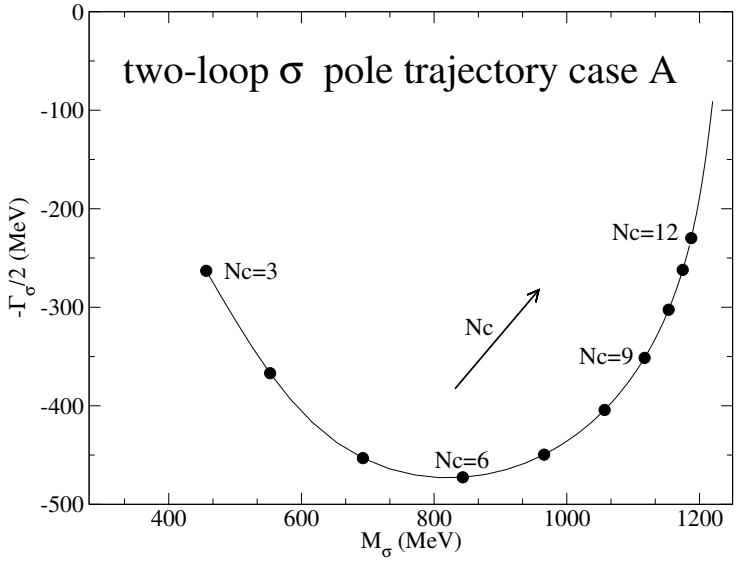

Figure 2.3: $1/N_c$ dependence found in [220] for the $f_0(500)$ pole. The mass and width start increasing as N_c increases. However, for $N_c = 6 \sim 8$, the pole trajectory turns around moving back towards the real axis above 1 GeV.

Given the situation we have just described, our motivation for our work has been the following: First, we wanted to find additional constraints on the N_c dependence of light scalars, in order to clarify their behavior and nature. Second we wanted to study whether the N_c behavior that had been found for the lightest scalar could be understood *naturally* from its composition in terms of states made explicitly of quarks and gluon components, starting from the QCD N_c expansion. Finally, we wanted to check if naturalness disfavors any other composition.

2.2.2 Outline of the results

Here we present the results of three published research articles in Sections 2.2.3, 2.2.4 and 2.2.5, as well as some preliminary results published in the proceedings of a conference, Section 2.2.7. In addition, we also include some still unpublished results in Sections 2.2.6 and 2.2.8.

In the publications of Sections 2.2.3, 2.2.4 and 2.2.5, we analyze the relation between the nature of the σ meson and semi-local duality. As we have seen in Section 1.8.3, semi-local duality constrains low energy scattering amplitudes, and the nature of the lightest resonances. In particular, the s-wave $I = 2$ $\pi\pi$-scattering channel is an exotic one, where there are no

resonances to contribute. Since Regge exchanges in the t-channel are related (dual) to the exchange of s-channel resonances, then the absence of scalar $I = 2$ resonances implies that the $I_t = 2$ t-channel amplitude has to be suppressed compared to those amplitudes with definite t-channel isospin where resonances can be exchanged. However, as we have seen in Section 1.7, this amplitude can be expressed as a combination of s-channel amplitudes:

$$T^{I_t=2}(s,t,u) = \frac{1}{3}T^{I_s=0}(s,t,u) - \frac{1}{2}T^{I_s=1}(s,t,u) + \frac{1}{6}T^{I_s=2}(s,t,u). \tag{2.1}$$

Since $T^{I_s=2}$ is repulsive and small, semi-local duality implies a strong cancellation between $T^{I_s=0}$ and $T^{I_s=1}$, which are saturated at low energies by the $f_0(500)$ and $\rho(770)$ resonances, respectively. Hence, semi-local duality requires the contribution of these two resonances to cancel "on average" in keeping with $I = 2$ exchange in the t-channel. This cancellation is expected to hold for all values of N_c. Therefore, any model where the N_c behaviour of the σ and $\rho(770)$ is different, does not ensure this cancellation and is in potential conflict with semi-local duality. In the publications of Sections 2.2.3, 2.2.4 and 2.2.5, we will show how unitarized ChPT, either using the IAM or the N/D method, is able to avoid this conflict.

The main results we obtain in the publication of Section 2.2.3 can be summarized as follows:

- In the first place, we check how well semi-local duality works from experimental data in the real world of $N_c = 3$ by comparing the Regge "prediction" with the partial wave parametrizations given in [149]. By including S, P and D waves, or just S and P waves, we analyze how well the integrals are dominated by just the lowest partial waves.

- We show then that the Regge parameters fixed from high energy NN and πN scattering yield the correct $\pi\pi$ P and D-wave scattering lengths, which have been obtained using the Froissart-Gribov representation for partial waves.

- Having confirmed that semi-local duality between resonances and Regge behaviour works for $N_c = 3$, we turn to the description of amplitudes using the IAM. We check that the IAM still fulfills semi-local duality for $N_c = 3$, which allows us to study this property as N_c increases.

- For $N_c > 3$, and as anticipated in [212], we find that even for $O(p^4)$, the estimated uncertainty from the choice of the renormalized scale μ, allows for different qualitative behaviors when N_c is not too close to 3. From those similar to the $O(p^6)$ result plotted in Fig. 2.3, to those where the sigma pole, after moving deep in the complex plane turns back to the real axis but with negative “mass squared” values.

- We check that for those cases in which the $f_0(500)$ pole moves to infinity, or to the left hand cut without a $\bar{q}q$ state appearing slightly above 1 GeV that survives as N_c increases, as it occurs in the cases depicted in Figs. 2.1 and 2.2, the cancellation between the σ and $\rho(770)$ fails, leading to a conflict with semi-local duality. We show that in order to satisfy semi-local duality, the σ pole cannot disappear completely in the complex plane, which actually occurs for the most part of one-loop unitarized chiral perturbation theory parameter space.

- However, we obtain that when the σ shows a $\bar{q}q$ subdominant component [220], showed in Fig. 2.1, semi-local duality for $I = 2$ exchanges is fulfilled as N_c increases.

- Finally, we checked that these results are still consistent when we include heavier resonances as the $f_0(980)$ or the $f_2(1270)$.

In the publications of Sections 2.2.4 and 2.2.5, we address again the problem of the nature of the σ meson by studying the role of the lightest resonances in semi-local duality and in spectral function sum rules, within a $U(3)$ ChPT framework (Section 1.3.4), which includes not only the pseudo-Goldstone octet π, K and η, as SU(3) ChPT, but also the singlet η'. Instead of considering the contributions from the higher order LECs, we introduce explicitly the resonance exchanges at tree level (Section 1.3.5), assuming that the LECs are saturated by the lightest resonances. Furthermore, we use the non-perturbative N/D approach (Section 1.6.2), to unitarize the meson-meson scattering amplitudes and the tree level resonance exchanges. One of the main motivations of this formalism is to discuss the N_c expansion since, as we have seen in Section 1.4.3, the η' becomes the ninth Goldstone boson at larger N_c. In order to perform this study, we assume, as it was pointed out in [5], that the N_c behaviour of the resonance coupling constants are $\mathcal{O}(\sqrt{N_c})$, that the resonance masses are $\mathcal{O}(1)$, and that the N_c subleading subtraction constants which appear in eq. (1.169) are $\mathcal{O}(1)$.

The main points of discussion of these publications are:

- We first fit the unknown parameters in the theory to a large amount of experimental data, consisting of phase shifts and inelasticities of $\pi\pi \to \pi\pi(K\bar{K})$ and $\pi K \to \pi K$ scattering, with different isospin and angular momentum numbers, and also the invariant mass distribution of the $\pi\eta$ system.

- From the previous fits, we obtain on the second Riemann sheet of the complex plane seven scalar and three vector resonances from our unitarized scattering amplitudes, namely: $f_0(500)$, $f_0(980)$, $f_0(1370)$, $K_0(800)$, $K_0(1430)$, $a_0(980)$, $a_0(1450)$, $\rho(770)$, $K(892)$ and $\phi(1020)$. Their masses and widths agree well with the PDG values. In addition, we also calculate the coupling strengths of the resonances to the pseudo-Goldstone boson pairs. It is remarkable that the $f_0(500)$ resonance is marginally coupled to η and η' mesons, which indicates that it is not affected by the η and η' dynamics.

- By studying the $I_t = 2$ $\pi\pi$-amplitude, we confirm the results obtained in the publication of Section 2.2.3, local-duality is also satisfied at $N_c = 3$ within this formalism.

- At larger N_c, we are able to satisfy local duality when ad hoc subleading N_c terms are included. As it was found in [221], within this approach, the $f_0(500)$ resonance fades away in the complex energy plane, so the strength needed to cancel the ρ resonance contribution, which as we have seen previously is required to satisfy local duality, comes from the singlet scalar, which is a subdominant part of the $f_0(980)$ for $N_c = 3$, but becomes dominant for higher values of N_c. This is a crucial source to oppose the $\rho(770)$ contribution and hence to guarantees the fulfillment of semi-local duality at large values of N_c.

- It is important to remark that in both works, in this U(3) N/D analysis and in the previous one within the IAM, it is a $\bar{q}q$ component with a mass around of 1 GeV, the one that compensates for the $\rho(770)$ contribution. This $\bar{q}q$ component is subdominant for both resonances at $N_c = 3$, but becomes dominant at larger N_c. Therefore, whereas the solution given in both analysis is similar, they show two different ways to reach it.

- Finally, we study another way to constrain the resonance properties, which is the use of spectral function sum rules that hold in the chiral limit [222, 223]. In particular, we calculate the scalar and pseudoscalar spectral functions which are obtained by using the appropriate form factors unitarized using the N/D method. From the parameters obtained in the previous fit, we conclude that they are satisfied in the chiral limit with a violation around 10% at most.

In Section 2.2.6, we study the N_c dependence of the couplings between several kinds of states, which correspond to different inner meson structures in terms of quarks and gluons. The N_c expansion of these couplings is of interest because current research efforts strive to understand the composition of hadrons in terms of the fundamental QCD degrees of freedom; i.e., quarks and gluons. In order to study a possible Fock expansion of the components of the controversial σ meson, we study the couplings, masses and widths of different QCD states compatible with the σ meson quantum numbers, namely, $\bar{q}q$, $(\bar{q}q)^2$, $\bar{q}\bar{q}qq$ and the glueball, where the second state refers to a tetraquark or molecular state, and the third one to an exotic tetraquark, called "polyquark". We find that none of them has the N_c behaviour found in [220], so we expect the $f_0(500)$ to be a mixture.

Thus, in publication 2.2.7, we present preliminary results about a possible Fock expansion for the σ meson in terms of just three QCD states, the ordinary $\bar{q}q$, the $\pi\pi$ molecule or tetraquark and the glueball:

$$|\sigma\rangle = \alpha|\bar{q}q\rangle + \beta|(\bar{q}q)^2\rangle + \gamma|gg\rangle, \tag{2.2}$$

where the coefficients, α, β and γ are in principle N_c dependent. The main discussion points addressed in this publication are:

- In order to obtain the value of these coefficients, we construct an effective 3×3 Hamiltonian, which is chosen to represent the scalar sector, and factorize the leading-N_c behaviour of its matrix elements, which we known from our previous N_c analysis, Section 2.2.6. Then, we diagonalize this Hamiltonian and identify the lowest one as the σ meson.

- The coefficients of the N_c powers of the different matrix elements are then fitted to the IAM results for the σ mass and width as a function of the number of colours obtained in [220], and depicted in Fig. 2.3.

- Given the large number of free parameters, we impose that they must be natural. From this fit we can extract the N_c dependence of the coefficients given in eq. (2.2), and therefore, obtain the σ meson composition for $N_c = 3$.

- In the preliminary results presented in Section 2.2.7, the σ meson at $N_c = 3$ is around 65% tetraquark or a $\pi\pi$ molecule, $\sim$ 25% $\bar{q}q$ and 10% or less glueball. However as N_c

increases this composition changes, and at $N_c = 8$ the $\bar{q}q$ component is more important that the molecular one. At $N_c = 20$ the σ is predominantly a $\bar{q}q$ state (90%), with only a 10% tetraquark and a negligible glueball contribution. Of course this result is slightly dependent on the way we impose naturality, but these numbers can be considered as a educated guess. This result is achieved with natural values of the Hamiltonian coefficients, masses and widths.

- Note that when we impose a dominant contributions for the glueball or the $q\bar{q}$ state, it leads to an important lack of naturalness in the free parameters, which as we have commented above, can be chosen of natural order of magnitude if the σ has a dominant meson-meson or tetraquark component.

Once we have shown that there is one natural solution, in terms of QCD degrees of freedom, to explain the N_c behaviour of the $f_0(500)$ found with the IAM, one might wonder if there are other natural explanations. Thus, in Section 2.2.8, we proceed to study briefly how the naturality assumption for the coefficients of the Hamiltonian described in the previous Section, can constraint the composition of the lightest scalar.

2.2.3 Publication: J.R. Pelaez , M.R. Pennington, J. Ruiz de Elvira, D.J. Wilson, *Chiral Perturbation Theory, the 1/Nc expansion and Regge behaviour determine the structure of the lightest scalar meson, Phys. Rev.* D84 096006 (2011)

PHYSICAL REVIEW D **84,** 096006 (2011)

Chiral perturbation theory, the $1/N_c$ expansion and Regge behavior determine the structure of the lightest scalar meson

J. R. Peláez,[1] M. R. Pennington,[2] J. Ruiz de Elvira,[1] and D. J. Wilson[3]

[1]*Departamento de Física Teórica II, Universidad Complutense de Madrid, 28040 Madrid, Spain*
[2]*Theory Center, Thomas Jefferson National Accelerator Facility, 12000 Jefferson Avenue, Newport News, Virginia 23606, USA*
[3]*Physics Division, Argonne National Laboratory, Argonne, Illinois 60439, USA*

(Received 7 October 2010; published 9 November 2011)

The leading $1/N_c$ behavior of unitarized chiral perturbation theory distinguishes the nature of the ρ and the σ: The ρ is a $\bar{q}q$ meson, while the σ is not. However, semilocal duality between resonances and Regge behavior cannot be satisfied for larger N_c, if such a distinction holds. While the σ at $N_c = 3$ is inevitably dominated by its di-pion component, unitarized chiral perturbation theory also suggests that as N_c increases above 6–8, the σ may have a subdominant $\bar{q}q$ fraction up at 1.2 GeV. Remarkably this ensures semilocal duality is fulfilled for the range of $N_c \lesssim$ 15–30, where the unitarization procedure adopted applies.

DOI: 10.1103/PhysRevD.84.096006 PACS numbers: 11.15.Pg, 12.39.Mk, 12.40.Nn, 13.75.Lb

I. INTRODUCTION

Long ago, Jaffe [1] identified the distinct nature of mesons: those built simply of a quark and an antiquark, and those with additional $\bar{q}q$ pairs. Of course, even well established $\bar{q}q$ resonances, like the ρ and ω, spend part of their time in four and six quark configurations as this is how they decay to $\pi\pi$ and 3π, respectively. However, the $1/N_c$ expansion [2] provides a method of clarifying such differences. If we could tune N_c up from 3, we would see that an intrinsically $\bar{q}q$ state would become narrower and narrower. As N_c increases, the underlying pole, which defines the resonant state, moves along the unphysical sheet(s) towards the real axis. In contrast, a tetraquark state would become wider and wider and its pole would effectively disappear from ''physical'' effect: if only we could tune N_c.

A long recognized feature of the world with $N_c = 3$ is that of ''local duality''[3–5]. In a scattering process, as the energy increases from threshold, distinct resonant structures give way to a smooth Regge behavior. At low energy the scattering amplitude is well represented by a sum of resonances (with a background), but as the energy increases the resonances (having more phase space for decay) become wider and increasingly overlap. This overlap generates a smooth behavior of the cross section most readily described not by a sum of a large number of resonances in the direct channel, but the contribution of a small number of crossed channel Regge exchanges. Indeed, detailed studies [4,6] of meson-baryon scattering processes show that the sum of resonance contributions at all energies ''averages'' (in a well-defined sense to be recalled below) the higher energy Regge behavior. Indeed, these early studies [3,4] revealed how this property starts right from the πN threshold, so that this ''local duality'' holds across the whole energy regime. Thus, resonances in the s channel know about Regge exchanges in the t channel. Indeed, these resonance and Regge components are not to be added like Feynman diagram contributions, but are ''dual'' to each other: one uses one *or* the other. Indeed, the wonderful formula discovered by Veneziano [7] is an explicit realization of this remarkable property. This has allowed the idea of ''duality'' first found in meson-nucleon reactions to be extended to baryon-antibaryon reactions, as well as to the simpler meson-meson scattering channel we consider here [8]. Unlike the idealized Veneziano model with its exact local duality, the real world, with finite width resonances, has a ''semilocal duality'' quantified by averaging over the typical spacing of resonance towers defined by the inverse of the slope of relevant Regge trajectory.

Regge exchanges too are built from $\bar{q}q$ and multiquark contributions. In a channel like that with isospin 2 in $\pi\pi$ scattering, or isospin $3/2$ in $K\pi$ scattering, there are no $\bar{q}q$ resonances, and so the Regge exchanges with these quantum numbers must involve multiquark components. Data teach us that even at $N_c = 3$ these components are suppressed compared to the dominant $\bar{q}q$ exchanges. Semilocal duality means that in $\pi^+\pi^- \to \pi^-\pi^+$ scattering, the low energy resonances must have contributions to the cross section that ''on the average'' cancel, since this process is purely isospin 2 in the t channel. The meaning of semilocal duality is that this cancellation happens right from the $\pi\pi$ threshold.

Now in $\pi\pi$ scattering below 900 MeV, there are just two low energy resonances: the ρ with $I = J = 1$ and the σ with $I = J = 0$. In the model of Veneziano, where resonances contribute as delta functions, exact local duality is achieved by the σ and ρ having exactly the same mass, and the coupling squared of the σ is $9/2$ times that of the ρ. Of course, the Veneziano amplitude is too simplistic and does not respect two body unitarity. Yet nevertheless, in the real world with $N_c = 3$ with finite width resonances ''semilocal'' duality is at play right from threshold. There

is a cancellation between the ρ with a width of 150 MeV, which is believed to be predominantly a $\bar{q}q$ state, and the σ, which is very broad, at least 500 MeV wide, with a shape that is not Breit-Wigner like, and might well be a tetraquark, molecular [9] or gluonic state [10,11], or possibly a mixture of all of these. Its short-lived nature certainly means it spends most of its existence in a di-pion configuration. The contribution of these two resonances to the $\pi^+\pi^-$ cross section do indeed ''on average'' cancel in keeping with $I = 2$ exchange in the t channel. However, such a distinct nature for the ρ and σ would prove a difficulty if we could increase N_c. A tetraquark σ would become still broader and its contribution to the cross section less and less, while its companion the ρ would become more delta-function-like and have nothing to cancel. Semilocal duality would fail. The correct Regge behavior would not be generated. It would just be a feature of the world with $N_c = 3$ and not for higher values. Yet our theoretical expectation is quite the contrary, the multiquark Regge exchange should be even better suppressed as N_c increases above 3. This paradox clearly poses a problem for the description of the σ as a non-$\bar{q}q$ state. The aim of this paper is to show how unitarized chiral perturbation theory provides a picture of how this paradox is resolved.

Chiral perturbation theory (χPT) [12] provides a systematic procedure for computing processes involving the Goldstone bosons of chiral symmetry breaking, particularly pions. The domain of applicability is naturally restricted to low energies where the pion momenta p and the pion mass m_π are much less than the natural scale of the theory specified by the pion decay constant f_π scaled by 4π, i.e. 1 GeV. The presence at low energies of elastic resonances, like the ρ and σ, means that the unitarity limit is reached at well below this scale of 1 GeV. Consequently, the fact that χPT satisfies unitarity order by order is not sufficiently fast for these key low energy resonances to be described beyond their near threshold tails. Much effort has been devoted to accelerating the process of unitarization [13–19]. Low orders in χPT must already contain information about key components at all orders for unitarization to be achieved. It surely pays to sum these known contributions up even when working ostensibly at low orders in perturbation theory. One method for achieving a unitarized chiral perturbation theory (UChPT) is the *inverse amplitude method* (IAM) [13–15,20]. This is based on the very simple idea that, in the region of elastic unitarity, the imaginary part of the inverse of each partial wave amplitude is determined by phase space—dynamics resides in the real part of the inverse amplitude. This procedure leads naturally to resonant effects in the strongly attractive $I = 0$ and $I = 1$ channels. At tree level χPT involves just one parameter, the pion decay constant. However, at higher orders new low energy constants (LECs) enter in the pion-pion scattering amplitudes: four at one loop order [12], six more at two loops [21], etc. These have to be fixed from experiment. Clearly, the predictive power of the theory, so apparent at tree level, where every pion process just depends on the scale set by f_π, becomes clouded as higher loops become significant with the LECs poorly known. While the elastic inverse amplitude method delays the onset of these new terms with their additional LECs, this is still restricted to the region below 1 GeV (or 1.2 GeV if the IAM is used within a coupled channel formalism, although this has other problems not present in the elastic treatment—see [18]).

A beauty of chiral Lagrangians is that the N_c dependence of the parameters is determined. Every LEC, starting with f_π has a well-defined leading N_c behavior [12,22], for instance, $f_\pi \sim \sqrt{N_c}$. At one-loop order with central values for the LECs, one of us (J. R. P.) has studied unitarized low energy $\pi\pi$ scattering as N_c increases [23], showing how the ρ does indeed become narrower (as expected of a $\bar{q}q$ resonance). In contrast, at least for not too large N_c, the σ pole became wider and moved away from the 400 to 600 MeV region of the real energy axis, as anticipated by a largely $\overline{qq}qq$ nature. As we shall discuss, and as already introduced, this means that for the central values and most parameter space, the semilocal duality implicit in finite energy sum rules (FESRs) is not satisfied as N_c increases.

Subsequently, one of us (J. R. P.) together with Rios showed [24] that the N_c behavior becomes more subtle when two-loop χPT effects are included. In particular, for the best fits of the unitarized two-loop χPT, there is a $\bar{q}q$ component of the σ, which while subdominant at $N_c = 3$, becomes increasingly important as N_c increases. The σ pole still moves away from the 400–600 MeV region of the real axis, but the pole trajectory turns around moving back towards the real axis above 1 GeV as N_c becomes larger than 10 or so. This occurs rather naturally in the two-loop results but was only hinted in some part of the one-loop parameter space. Such a behavior would indicate that, while the σ is predominantly non-$\bar{q}q$ at $N_c = 3$, it does have a $\bar{q}q$ component. As we show here, it is this component that ensures FESRs are satisfied. Regge expectations then hold at all N_c. Indeed, imposing this as a physical requirement places a constraint on the second order LECs: a constraint readily satisfied with LECs in fair agreement with current crude estimates.

Thus, chiral dynamics already contains the resolution of the paradox that was the motivation for this study: namely, how does the suppression of $I = 2$ Regge exchanges happen if resonances like the ρ and σ are intrinsically different. We will see that the σ may naturally contain a small but all important $\bar{q}q$ component. At large N_c this would be the seed of this state. As N_c is lowered this state will have an increased coupling to pions, and it is these that dominate its existence when $N_c = 3$. We will, of course, discuss the range of N_c for which the IAM applies and where replacing the LECs (at $N_c = 3$) with their leading N_c form is appropriate.

II. SEMILOCAL DUALITY AND FINITE ENERGY SUM RULES

A. Regge theory and semilocal duality

Regge considerations lead us to study s-channel $\pi\pi$ scattering amplitudes with definite isospin in the t channel, labeled $A^{tI}(s,t)$. These can, of course, be written in terms of amplitudes with definite isospin in the direct channel, $A^{sI}(s,t)$, using the well-known crossing relationships, so that

$$\begin{aligned} A^{t0}(s,t) &= \tfrac{1}{3}A^{s0}(s,t) + A^{s1}(s,t) + \tfrac{5}{3}A^{s2}(s,t) \\ A^{t1}(s,t) &= \tfrac{1}{3}A^{s0}(s,t) + \tfrac{1}{2}A^{s1}(s,t) - \tfrac{5}{6}A^{s2}(s,t) \\ A^{t2}(s,t) &= \tfrac{1}{3}A^{s0}(s,t) - \tfrac{1}{2}A^{s1}(s,t) + \tfrac{1}{6}A^{s2}(s,t). \end{aligned} \tag{1}$$

It is convenient to denote the common channel threshold by $s_{\rm th} \equiv t_{\rm th} \equiv 4m_\pi^2$. The amplitudes of Eq. (1) have definite symmetry under $s \rightarrow u$ and this will be reflected in writing them as functions of $\nu = (s-u)/2$, a variable for which $\nu = s = -u$ along the line $t = t_{\rm th}$. To check semilocal duality, we need to continue the well-known Regge asymptotics at fixed t down to threshold. To do this we follow [25] with

$$\mathrm{Im}\, A^{tI}_{\rm Regge}(\nu,t) = \sum_R \beta_R(t)\Theta(\nu)[\alpha'^2(\nu^2-\nu_{\rm th}^2)]^{\alpha_R(t)/2}, \tag{2}$$

where as usual the $\alpha_R(t)$ denote the Regge trajectories with the appropriate t-channel quantum numbers, $\beta_R(t)$ their Regge couplings, and α' is the universal slope of the $\bar{q}q$ meson trajectories (~ 0.9 GeV^{-2}). The crossing function $\Theta(\nu) = [1-\nu_{\rm th}^2/\nu^2]^{(1+\gamma)}$ having $\gamma = 0$ for $s-u$-even amplitudes, and $\gamma = 1/2$ if they are crossing odd, ensures the imaginary parts of the amplitudes vanish at threshold, while being unity when ν is large. $\nu_{\rm th}$ is the value of ν at threshold, viz. $\nu_{\rm th} = (s_{\rm th}+t)/2$. For the amplitude with $I = 1$ in the t channel, for which $\gamma = 1$, the sum in Eq. (2) will be dominated by ρ exchange with a trajectory $\alpha(t) = \alpha_0 + \alpha' t$ that has the value 1 at $t = m_\rho^2$ and 3 at $t = m_{\rho_3}^2$ [26], i.e. $\alpha_0 = 0.467$ and $\alpha' = 0.889$ GeV^{-2}. For isoscalar exchange the dominant trajectories are the Pomeron with $\alpha_P(t) = 1.083 + 0.25t$ (with t in GeV^2 units) [27][1] and the f_2 trajectory which is almost degenerate with that of the ρ. For the exotic $I = 2$ channel with its leading Regge exchange being a $\rho-\rho$ cut, we expect $\alpha(0) \ll \alpha_\rho(0)$, and its couplings to be correspondingly smaller.

Semilocal duality between Regge and resonance contributions teaches us that

$$\int_{\nu_1}^{\nu_2} d\nu \nu^{-n}\, \mathrm{Im}A^{tI}_{\rm resonance}(\nu,t) \simeq \int_{\nu_1}^{\nu_2} d\nu \nu^{-n}\, \mathrm{Im}A^{tI}_{\rm Regge}(\nu,t), \tag{3}$$

the "averaging" should take place over at least one resonance tower. Thus, the integration region $\nu_2 - \nu_1$ should be a multiple of $1/\alpha'$, typically 1 GeV^2. We will consider two ranges from threshold to 1 GeV^2 and up to 2 GeV^2.

This duality should hold for values of t close to the forward scattering direction, and so we consider both $t = 0$ and $t = t_{\rm th}$. The difference in results between these two gives us a measure of the accuracy of semilocal duality, as expressed in Eq. (3). Since we are interested in the resonance integrals being saturated by the lightest states, we consider values of $n = 0$ to $n = 3$. We will find that with $n = 1, 2, 3$ the low mass resonances do indeed control these finite energy sum rules.

B. Finite energy sum rules from data (i.e. $N_c = 3$)

Let us first look at $\pi\pi$ scattering data and see how well it approximates this relationship, before we consider the various resonances contributions that make up the "data" and in turn how these might change with N_c. To do this it is useful to define the following ratio:

$$R^I_n = \frac{\int_{\nu_1}^{\nu_2} d\nu \nu^{-n}\, \mathrm{Im}A^{tI}(\nu,t)}{\int_{\nu_1}^{\nu_3} d\nu \nu^{-n}\, \mathrm{Im}A^{tI}(\nu,t)}. \tag{4}$$

The behavior of such a ratio tests the way the low energy amplitudes average the expected leading Regge energy dependence of Eq. (2)—the leading Regge behavior because only then does the Regge coupling $\beta_R(t)$ cancel out in the ratio. We will consider these ratios with ν_1 at its threshold value, $\nu_2 = 1$ GeV^2 and $\nu_3 = 2$ GeV^2. In evaluating the amplitudes in Eq. (1), we represent them by a sum of s-channel partial waves, so that

$$\mathrm{Im}\, A^{sI}(s,t) = \sum_\ell (2\ell+1)\, \mathrm{Im}\mathcal{A}^I_\ell(s) P_\ell(z_s), \tag{5}$$

where the sum involves only even ℓ for $I = 0, 2$ and odd ℓ for $I = 1$. $P_\ell(z_s)$ are the usual Legendre polynomials, with z_s the cosine of the s channel c.m. scattering angle related to the Mandelstam variables by $z_s = 1 + 2t/(s-s_{\rm th})$. It is useful to note that the partial wave amplitudes behave towards threshold like $\mathcal{A}_\ell \sim (s-s_{\rm th})^\ell$, so that the imaginary parts that appear in Eqs. (3)–(5) behave like $(s-s_{\rm th})^{2\ell+1}$ from unitarity.

We use the partial wave parametrization from Kamiński, Peláez, and Yndurain (KPY) [29] to represent the data. The partial wave sum is performed in two ways: first including partial waves up to and including $\ell = 2$, and second with just the S and P waves. We compare each of these in Table I with the evaluation of the ratios in Eq. (4) using the leading Regge pole contribution. This serves as a guide as to

[1] Because of the rapid convergence of the sum rules we consider, the fact the Pomeron form used violates the Froissart bound is of no consequence. This has been explicitly checked by also using the parametrization of Cudell *et al.* [28].

TABLE I. R_n^I ratios defined in Eq. (4) evaluated using the Regge model of Eq. (2) and the KPY $\pi\pi$ parametrization [29] with and without D waves.

		$I_t = 0$		$I_t = 1$	
	n	$t = t_{\rm th}$	$t = 0$	$t = t_{\rm th}$	$t = 0$
REGGE	0	0.225	0.233	0.325	0.353
	1	0.425	0.452	0.578	0.642
	2	0.705	0.765	0.839	0.908
	3	0.916	0.958	0.966	0.990
KPY S, P, D	0	0.337 ± 0.093	0.342 ± 0.083	0.479 ± 0.213	0.492 ± 0.191
	1	0.567 ± 0.095	0.582 ± 0.082	0.725 ± 0.157	0.741 ± 0.131
	2	0.788 ± 0.061	0.815 ± 0.047	0.894 ± 0.072	0.911 ± 0.052
	3	0.927 ± 0.023	0.953 ± 0.013	0.971 ± 0.022	0.982 ± 0.011
KPY S, P	0	0.615 ± 0.169	0.572 ± 0.133	0.743 ± 0.187	0.709 ± 0.103
	1	0.796 ± 0.145	0.771 ± 0.120	0.874 ± 0.123	0.861 ± 0.064
	2	0.912 ± 0.088	0.909 ± 0.068	0.950 ± 0.062	0.950 ± 0.026
	3	0.971 ± 0.038	0.977 ± 0.021	0.984 ± 0.023	0.989 ± 0.006

(i) how well semilocal duality of Eq. (3) works from experimental data in the world of $N_c = 3$ by comparing the Regge "prediction" with the KPY representation of experiment, and

(ii) by comparing how well the integrals are dominated by just the lowest partial waves $\ell \leq 1$ with $\ell \leq 2$.

This will be needed to address how the duality relation of Eq. (3) puts constraints on the nature of the ρ and σ resonances. We present these results in Table I. The $n = 1$ integral would with $t = 0$ be closest to averaging the total cross section. The table shows that the data follow the expectations of semilocal duality from the dominant Pomeron and ρ Regge exchange immediately above threshold to 1 and 2 GeV^2. As expected this works best for $n \geq 1$ when the low energy regime dominates. We see that including just S and P waves is not sufficient for this agreement. For the $n = 0$ sum rule even higher waves than D are crucial in integrating up to 2 GeV^2. In contrast for $n = 3$ of course just S and P are naturally sufficient. Higher values of n would weight the near threshold behavior of all waves even more and this region is less directly controlled by resonance contributions alone but their tails down to threshold, where Regge averaging is less likely to be valid. Thus, we restrict attention to our finite energy sum rules with $n = 1$–3. It is important to note that all we require is the fact that the $I_t = 2$ exchange is lower lying than those with $I_t = 0, 1$. That the continuation of Regge behavior for the absorptive parts of the amplitude actually does average resonance-dominated low energy data even with sum rules with $n = 2, 3$ is proved by considering the P and D-wave scattering lengths. With scattering lengths defined by being the limit of the real part of the appropriate partial waves, Eq. (5), as the momentum tends to zero:

$$a_\ell^I = \lim_{p\to 0} \mathcal{A}_\ell^I(s)/(p/m_\pi)^{2\ell}, \tag{6}$$

where $p = \frac{1}{2}\sqrt{s - s_{\rm th}}$. Then by using the Froissart-Gribov representation for the partial wave amplitudes, we have

$$a_1^1 = \frac{4}{3\pi}\int_{s_{\rm th}}^{\infty} \frac{ds}{s^2}\, {\rm Im}A^{t1}(s, t_{\rm th}) \tag{7}$$

$$a_2^0 = \frac{16}{15\pi}\int_{s_{\rm th}}^{\infty} \frac{ds}{s^3}\, {\rm Im}A^{t0}(s, t_{\rm th}). \tag{8}$$

If we evaluate these integrals using just the Regge representation from threshold up, we find the following result:

$$m_\pi^2 a_1^1 = \frac{1}{12\pi}\beta_\rho(t_{\rm th})(\alpha' s_{\rm th})^{\alpha_\rho}\Gamma\left(\frac{5}{2} + \frac{\alpha_\rho}{2}\right)\Gamma\left(\frac{1}{2} - \frac{\alpha_\rho}{2}\right), \tag{9}$$

$$m_\pi^4 a_2^0 = \frac{1}{120\pi}\sum_{R=P,f_2}\beta_R(t_{\rm th})(\alpha' s_{\rm th})^{\alpha_R}\Gamma\left(2 + \frac{\alpha_R}{2}\right) \times \Gamma\left(1 - \frac{\alpha_R}{2}\right), \tag{10}$$

where each α_R is to be evaluated at $t = t_{\rm th}$. Analysis of high energy NN and πN scattering [30,31] determines the couplings β_R of the contributing Regge poles to $\pi\pi$ scattering through factorization [25]. In the case of the ρ, the value of the residue is known to be almost proportional to $\alpha_\rho(t)$ putting a zero close to $t \simeq -0.5$ (GeV^2) and reproducing the correct $\rho\pi\pi$ coupling at $t = m_\rho^2$. This is more like the shape shown in Ref. [32] than that proposed earlier by Rarita *et al.* [30,31]. This fixes $\beta_\rho(t = t_{\rm th}) = 0.84 \pm 0.13$ from the "best value" of the analysis of Ref. [31].[2] The suppression of $I = 2$ s-channel amplitudes that is basic to our assumptions here requires an exchange degeneracy between the ρ and f_2 trajectories, so that

[2]Note that the amplitudes defined in [31] are $\pi/4$ times those used here.

$\beta_{f_2} = 3\beta_\rho/2$, as in the "best value" fit of Ref. [31]. With the Pomeron contribution proportional to a $\pi\pi$ cross section of 16 ± 2 mb for $s \simeq 5$–8 GeV^2. This gives

$$m_\pi^2 a_1^1 = (3.4 \pm 0.5) \times 10^{-2}, \quad m_\pi^4 a_2^0 = (1.67 \pm 0.19) \times 10^{-3} \tag{11}$$

to be compared with the precise values found by Colangelo, Gasser, and Leutwyler [33] from a dispersive analysis of $\pi\pi$ amplitudes combining Roy equations and χPT predictions

$$m_\pi^2 a_1^1 = (3.79 \pm 0.06) \times 10^{-2}, \quad m_\pi^4 a_2^0 = (1.75 \pm 0.03) \times 10^{-3}, \tag{12}$$

or the recent dispersive analysis by two of us and other collaborators in [34], which includes the latest NA48/2 K_{e4} decay results [35] and no χPT,

$$m_\pi^2 a_1^1 = (3.81 \pm 0.09) \times 10^{-2}, \quad m_\pi^4 a_2^0 = (1.78 \pm 0.03) \times 10^{-3}. \tag{13}$$

We see that the presumption that Regge parametrization averages the low energy scattering in terms of sum rules with $n = 2, 3$ is borne out with remarkable accuracy: far greater accuracy than underlies our fundamental assumption that $I = 2$ s-channel resonances and t-channel exchanges are suppressed relative to those with $I = 0$ and 1. This is further supported by the fact that the $I = 2$ D-wave scattering length as determined in [33,34] is indeed a factor of 10 smaller than that for $I = 0$. The required cancellation between the ρ and the σ contributions that is the subject of this paper requires a less stringent relation than nature imposes at $N_c = 3$.

III. N_c DEPENDENCE OF $\pi\pi$ SCATTERING TO ONE-LOOP UCHPT: DOMINANT NON-$\bar{q}q$ BEHAVIOR OF THE σ

Having confirmed that semilocal duality between resonances and Regge behavior works for $N_c = 3$, we turn to the description of amplitudes within chiral perturbation theory and the inverse amplitude method (IAM). For orientation we recapitulate first the central results of Ref. [23] and we will discuss the uncertainties at the end. We plot in Fig. 1 the imaginary part of the $\pi\pi$ scattering partial waves, T_J^I, with $I = J = 0$ and $I = J = 1$ from unitarized one-loop $SU(3)$ χPT, which fits the experimental data very well for $N_c = 3$. The virtue of χPT is the fact that the constants all have a dependence on N_c that is well defined at leading order.

As anticipated by the work of one of us (J. R. P.) [23], Fig. 1 shows how the ρ peak narrows as N_c increases and how its mass barely moves (for the LECs used here the mass decreases slightly, whereas for those in [23], with a coupled channel IAM, it increases, but again by very little). In contrast, any scalar resonance contribution to the isoscalar amplitude becomes smaller and flatter below 1 GeV. Indeed, the positions of the ρ and σ poles move along the unphysical sheet as N_c increases from 3. It is useful to replicate these results here, as shown in Fig. 2. We see the ρ pole move towards the real axis, while that for the σ moves away from the real axis region below 1 GeV. This is, of course, reflected in the behavior of the amplitudes with definite t-channel isospin, Eq. (1).

The one-loop LECs we have used are those from Ref. [36]. These are listed in Table II. Constructing the IAM analysis of [24] using these LECs, we show in Fig. 3 the imaginary parts of the resulting amplitudes as functions of s. We see for instance in looking at $\mathrm{Im}A^{t2}(\nu, t_{\mathrm{th}})/\nu^2$ that

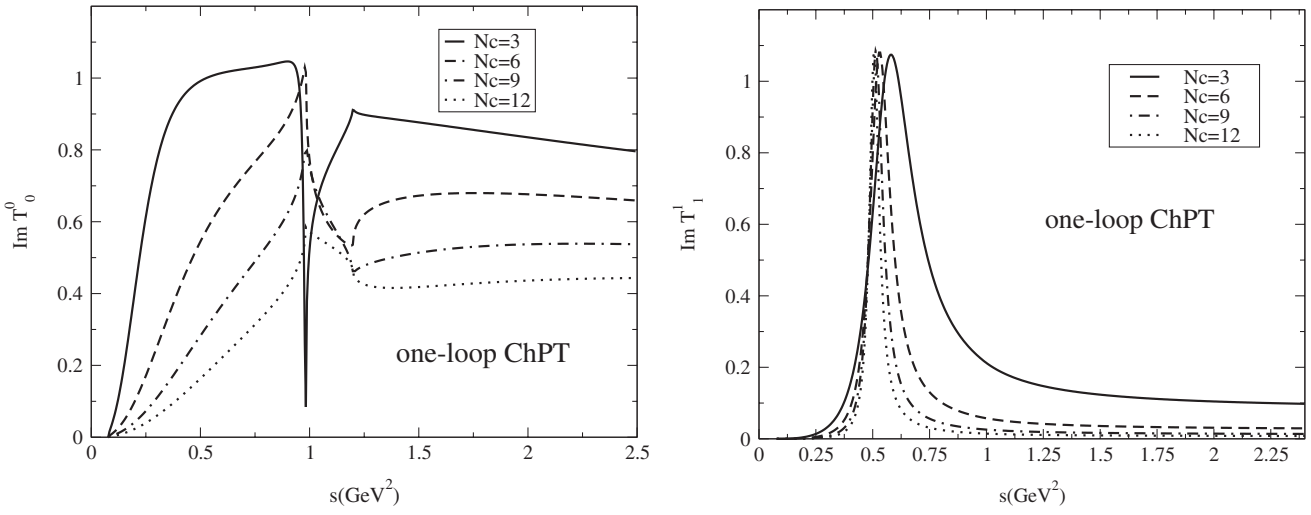

FIG. 1. Absorptive parts of key partial wave amplitudes, $\mathrm{Im}T_J^I(s)$ with $I = J = 0$ and $I = J = 1$. Parameters are fixed from a coupled channel $SU(3)$ chiral fit at $N_c = 3$ to data.

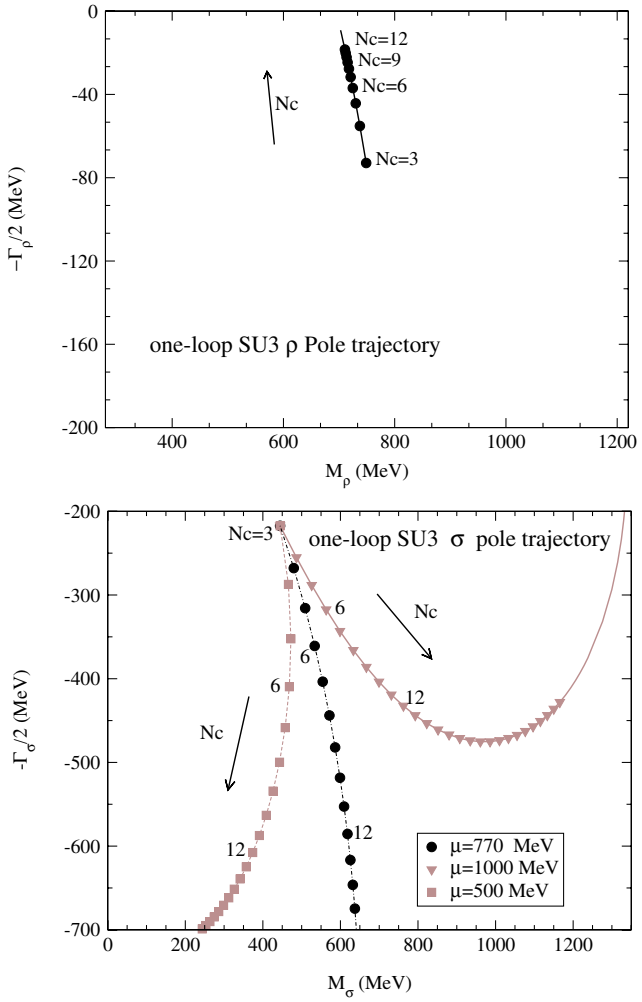

FIG. 2 (color online). Position of the ρ and σ poles in the complex energy plane as a function of N_c in one-loop χPT. Black lines correspond to the fit described in the text [36] imposing the leading $1/N_c$ behavior of the LECs at the usual renormalization scale $\mu = 770$ MeV. Note the different vertical scales for the ρ and σ poles. The lighter points delineate the estimated uncertainty from the choice of μ. This range is not plotted for the ρ, since it is so very close to the central line.

at $N_c = 3$ the positive σ and negative ρ components cancel. This is not the case as N_c increases to 12.

To quantify the N_c dependence at different orders in χPT and with different choices of LECs, we calculate the value of finite energy sum rules (FESR) ratios:

$$F_n^{II'}(t) = \frac{\int_{\nu_{\rm th}}^{\nu_{\rm max}} d\nu\, {\rm Im}A^{tI}(\nu, t, N_c)/\nu^n}{\int_{\nu_{\rm th}}^{\nu_{\rm max}} d\nu\, {\rm Im}A^{tI'}(\nu, t, N_c)/\nu^n}, \qquad (14)$$

for different values of $n = 0$–3, and N_c, t, $\nu_{\rm max}$, and isospin t channels I, I'. The ratio F^{10} compares the amplitude given by ρ Regge exchange with that controlled by the Pomeron, while the ratio F^{21} compares the "exotic" four quark exchange with $\bar{q}q$ ρ exchange.

TABLE II. One-loop IAM LECs we have used [36].

LECs($\times 10^3$)	One-loop IAM
L_1^r	0.60 ± 0.09
L_2^r	1.22 ± 0.08
L_3^r	-3.02 ± 0.06
L_4^r	0(fixed)
L_5^r	1.90 ± 0.03
L_6^r	-0.07 ± 0.20
L_7^r	-0.25 ± 0.18
L_8^r	0.84 ± 0.23

We show the results in Table III and plot the data in Fig. 4. If Regge expectations were working at one-loop order, we would expect F^{10} to tend to 0.66 and for F^{21} to be very small in magnitude, just as they are at $N_c = 3$, particularly for a cutoff of 2 GeV^2, the results for which are shown as the bolder lines. However, as N_c increases we find that the ratio F^{10} tends to 0.5, while that for F^{21} tends to -1. This is in accord with the $n = 1, 2$ sum rules becoming increasingly dominated by the ρ with very little scalar contribution. This difference is a consequence of the seeming largely non-$\bar{q}q$ nature of the σ being incompatible with Regge expectations. All these results use values for the one-loop LECs that accurately fit the low energy $\pi\pi$ phase shifts up to 1 GeV.

Finally, let us recall that the LECs carry a dependence on the regularization scale μ that cancels with those of the loop functions to give a finite result order by order. As a consequence, when rescaling the LECs with N_c, a specific choice of μ has to be made. In other words, despite the χPT and IAM amplitudes being scale independent, the N_c evolution is not. Intuitively, μ is related to a heavier scale, which has been integrated out in χPT and it is customary to take μ between 0.5 and 1 GeV [23,37]. This range is confirmed by the fact that at these scales the measured LECs satisfy their leading $1/N_c$ relations fairly well [37]. All the previous considerations about the one-loop IAM have been made with an N_c scaling at the usual choice of renormalization scale $\mu = 770$ MeV $\simeq M_\rho$, which is the most natural choice given the fact that the values of the LECs are mainly saturated by the first octet of vector resonances, with additional contributions from scalars above 1 GeV [37].

Thus, in Fig. 2 we have also illustrated the uncertainties in the pole movements for the $\rho(770)$ and $f_0(600)$ due to the choice of μ. Note that the $\rho(770)\bar{q}q$ behavior is rather stable, since for the LECs in Table II the variation is negligible. Other sets of LECs [23,38], which also provide a relatively good description of the $\rho(770)$, show a bigger variation with μ, but they always lead to the expected $\bar{q}q$ behavior. In contrast, we observe that the only robust

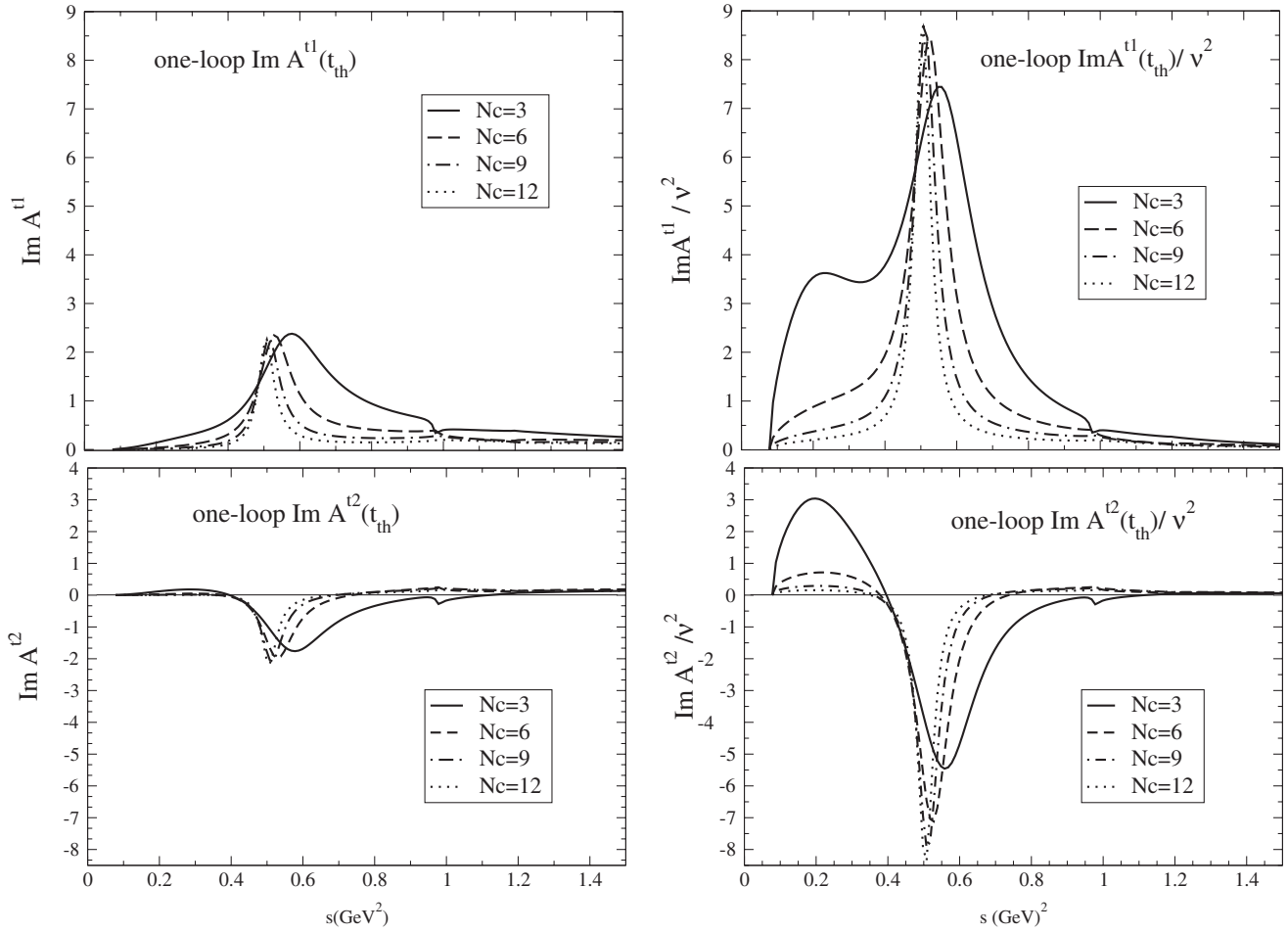

FIG. 3. Absorptive part of amplitudes with definite t-channel isospin, $\mathrm{Im}A^{IJ}(s, t_{\mathrm{th}})/\nu^n$. The top pair of graphs has $I = 1$ and the lower with $I = 2$, and on the left hand $n = 0$ and right hand $n = 2$. Parameters have been fixed from a coupled channel $SU(3)$ chiral fit at $N_c = 3$ to data.

feature of the $f_0(600)$ is that it does not behave predominantly as a $\bar{q}q$. Unfortunately, its detailed pole behavior is not well determined except for the fact that it moves away from the 400 to 600 MeV region of the real axis and that at N_c below 15 its width always increases. However, for N_c around 20 or more and for the higher values of the μ range, the width may start decreasing again and the pole would start behaving as a $\bar{q}q$.

In Fig. 5 we show how the IAM uncertainty translates into our calculations of the F_n^{21} ratio for the most interesting cases $n = 2, 3$. The thick continuous line stands for the central values we have been discussing so far, which at larger N_c tend to grow in absolute value and, as already commented, spoil semilocal duality. The situation is even worse when the N_c scaling of our LECs is performed at $\mu = 500$ MeV. This is due to the fact, seen in Fig. 2, that, with this choice of μ, the σ pole moves deeper and deeper into the complex plane and its mass even decreases. Let us note that this behavior—compatible with our IAM results when the uncertainty in μ is taken into account—is also found when studying the leading N_c behavior within other unitarization schemes, or for certain values of the LECs within the one-loop IAM [39,40]. We would therefore also expect that in these treatments semilocal duality would deteriorate very rapidly. In [39], there is the $f_0(980)$, as well as other scalar states above 1300 MeV, but all of them seem insufficient to compensate for the disappearance of the σ pole. As we will discuss in Sec. V, this is because the contributions of the $f_0(980)$ resonance and the region above 1300 MeV to our F_n^{IJ} ratios are rather small, and in [39] they seem to become even smaller, since all those resonances become narrower as N_c increases. Of course, as pointed out in [39] this deserves a detailed calculation within their approach.

TABLE III. Ratios for one loop UChPT using LECs from a single channel fit.

			One loop $SU(3)$ IAM			
			$t = t_{\rm th}$		$t = 0$	
	n	N_c	$\nu_{\rm max} = 1$ GeV^2	$\nu_{\rm max} = 2$ GeV^2	$\nu_{\rm max} = 1$ GeV^2	$\nu_{\rm max} = 2$ GeV^2
F_n^{10}	0	3	0.503 ± 0.008	0.385 ± 0.023	0.500 ± 0.010	0.364 ± 0.027
		6	0.527 ± 0.013	0.475 ± 0.033	0.534 ± 0.017	0.468 ± 0.038
		9	0.528 ± 0.015	0.522 ± 0.039	0.537 ± 0.020	0.524 ± 0.046
		12	0.524 ± 0.015	0.545 ± 0.042	0.533 ± 0.021	0.552 ± 0.050
	1	3	0.521 ± 0.008	0.457 ± 0.016	0.526 ± 0.011	0.452 ± 0.019
		6	0.529 ± 0.011	0.506 ± 0.022	0.538 ± 0.015	0.507 ± 0.026
		9	0.525 ± 0.013	0.525 ± 0.024	0.532 ± 0.016	0.530 ± 0.029
		2	0.520 ± 0.012	0.531 ± 0.027	0.526 ± 0.016	0.538 ± 0.030
	2	3	0.551 ± 0.011	0.522 ± 0.013	0.575 ± 0.013	0.544 ± 0.016
		6	0.536 ± 0.012	0.526 ± 0.016	0.550 ± 0.015	0.538 ± 0.019
		9	0.525 ± 0.011	0.525 ± 0.016	0.534 ± 0.015	0.533 ± 0.020
		12	0.517 ± 0.010	0.523 ± 0.016	0.524 ± 0.013	0.529 ± 0.019
	3	3	0.599 ± 0.015	0.588 ± 0.015	0.654 ± 0.017	0.645 ± 0.017
		6	0.551 ± 0.014	0.547 ± 0.015	0.579 ± 0.017	0.575 ± 0.018
		9	0.530 ± 0.012	0.530 ± 0.014	0.547 ± 0.016	0.547 ± 0.017
		12	0.519 ± 0.010	0.521 ± 0.012	0.530 ± 0.013	0.532 ± 0.015
F_n^{21}	0	3	-0.441 ± 0.021	-0.220 ± 0.045	-0.312 ± 0.029	-0.073 ± 0.058
		6	-0.415 ± 0.050	0.012 ± 0.057	-0.259 ± 0.057	0.180 ± 0.059
		9	-0.479 ± 0.068	0.059 ± 0.083	-0.319 ± 0.080	0.230 ± 0.079
		12	-0.552 ± 0.074	0.047 ± 0.105	-0.399 ± 0.073	0.221 ± 0.097
	1	3	-0.355 ± 0.021	-0.269 ± 0.021	-0.193 ± 0.022	-0.104 ± 0.023
		6	-0.438 ± 0.047	-0.228 ± 0.052	-0.284 ± 0.051	-0.074 ± 0.052
		9	-0.538 ± 0.054	-0.262 ± 0.077	-0.396 ± 0.068	-0.113 ± 0.078
		12	-0.621 ± 0.060	-0.317 ± 0.093	-0.493 ± 0.073	-0.170 ± 0.097
	2	3	-0.157 ± 0.043	-0.133 ± 0.036	0.107 ± 0.039	0.123 ± 0.032
		6	-0.382 ± 0.053	-0.299 ± 0.054	-0.171 ± 0.054	-0.100 ± 0.053
		9	-0.530 ± 0.056	-0.415 ± 0.066	-0.354 ± 0.063	-0.247 ± 0.069
		12	-0.630 ± 0.053	-0.505 ± 0.072	-0.481 ± 0.062	-0.355 ± 0.078
	3	3	0.175 ± 0.062	0.176 ± 0.058	0.578 ± 0.042	0.577 ± 0.040
		6	-0.193 ± 0.066	-0.169 ± 0.065	0.204 ± 0.057	0.217 ± 0.056
		9	-0.407 ± 0.062	-0.369 ± 0.066	-0.054 ± 0.061	-0.030 ± 0.063
		12	-0.541 ± 0.055	-0.497 ± 0.063	-0.233 ± 0.060	-0.200 ± 0.064

In Fig. 5 we also find that the F_n^{21} are much smaller and may even seem to stabilize if we apply the N_c scaling of the LECs at $\mu = 1000$ MeV. In such a case, the σ pole, after moving away from the real axis, returns back at higher masses, above roughly 1 GeV. For simplicity we only show F_n^{21} for the $t = 0$ case, but a similar pattern is found at $t = 4M_\pi^2$: the turning back of the σ pole at higher masses helps to keep the F_n^{21} ratios smaller. This behavior follows from the existence of a subdominant $\bar{q}q$ component within the $f_0(600)$ with a mass which is at least twice that of the original $f_0(600)$ pole. However, at one-loop order such behavior only occurs at one extreme of the μ range. In contrast, as we will see next, it appears in a rather natural way in the two-loop analysis.

IV. N_c DEPENDENCE OF $\pi\pi$ SCATTERING TO TWO-LOOP UCHPT: SUBDOMINANT $\bar{q}q$ COMPONENT OF THE σ

Now let us move to two-loop order in χPT [21] and see if this situation changes. The IAM to two loops for pion-pion scattering was first formulated in [15], and first analyzed in [19]. With a larger number of LECs appearing, we clearly have more freedom. In studying the $1/N_c$

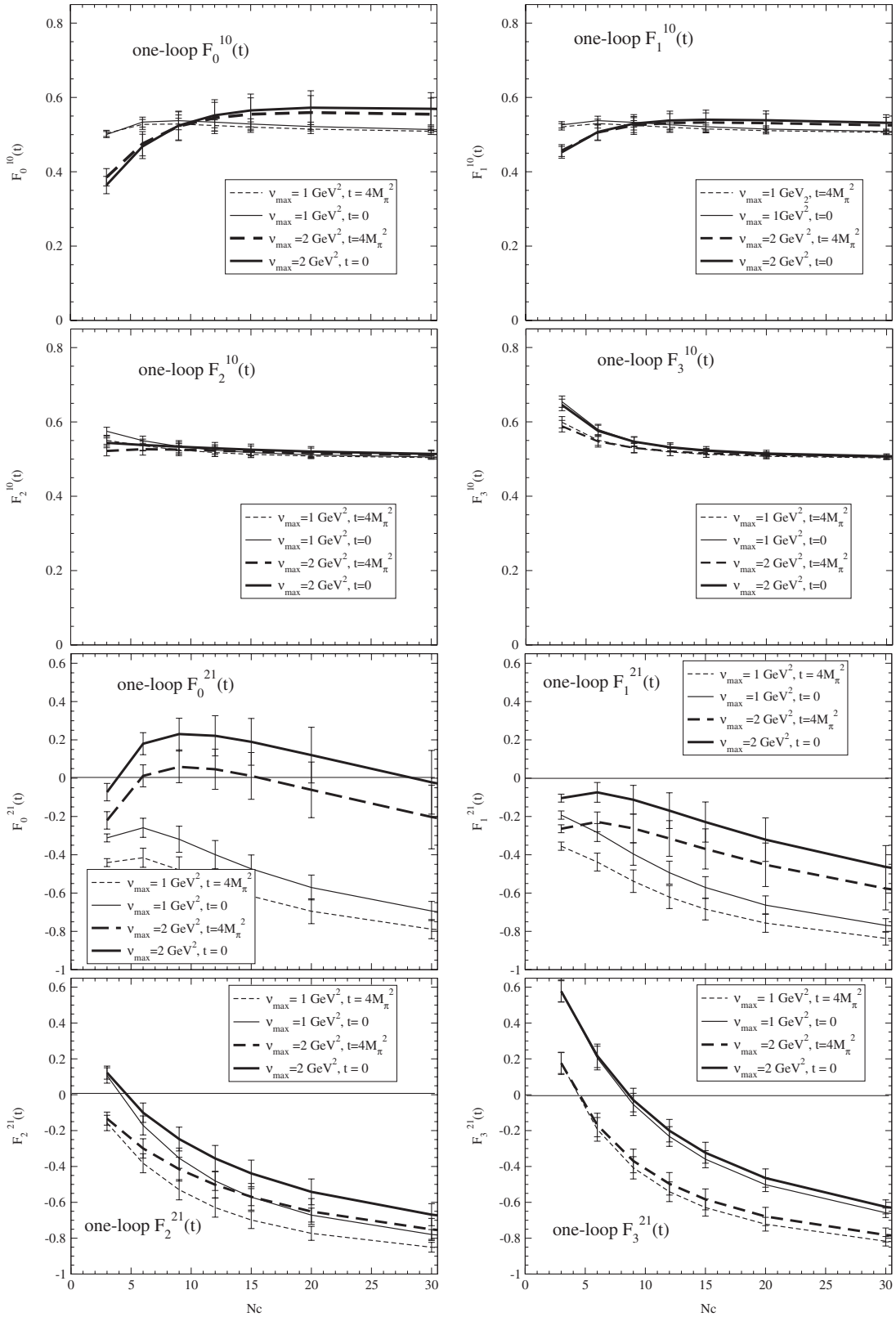

FIG. 4. Ratios $F_n^{II'}$ of Eq. (13) with $n = 0$–3. The top four graphs are for F^{10}, and the lower four for F^{21}. One-loop χPT IAM parameters are from a coupled channel $SU(3)$ fit with $N_c = 3$ to data.

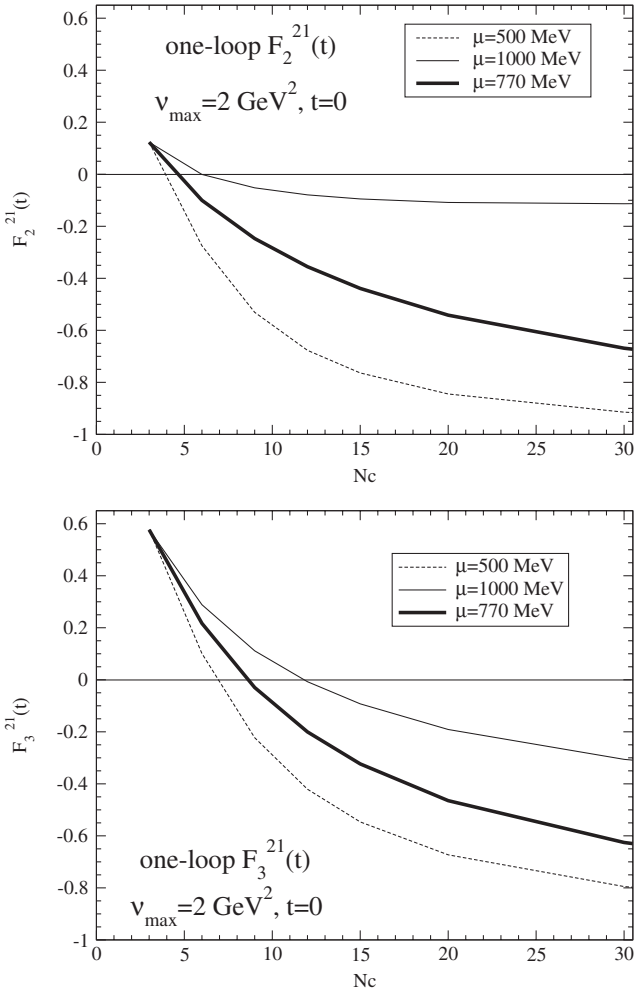

FIG. 5. Evolution of the F_n^{21} ratio calculated with the one-loop IAM when the leading $1/N_c$ behavior of the LECs is imposed at different choices of the renormalization scale μ.

behavior, Peláez and Rios [24] consider three alternatives within single channel $SU(2)$ chiral theory for fixing these, which we follow here too. These three cases involve combining agreement with experiment with different underlying structures for the ρ and σ. Agreement with experiment for the $I = 0$ and 2 S waves and the $I = 1$ P wave is imposed by minimizing a suitable $\chi^2_{\rm data}$. Our whole approach is one of considering the $1/N_c$ corrections to the physical $N_c = 3$ results. Consequently, to impose an underlying structure for the resonances, we note that if a resonance is predominantly a $\bar{q}q$ meson, then as a function of N_c, its mass $M \sim O(1)$ and width $\Gamma \sim O(1/N_c)$. Taking into account the subleading orders in $1/N_c$, it is sufficient to consider a resonance a $\bar{q}q$ state, if

$$M_{N_c}^{\bar{q}q} = M_0\left(1 + \frac{\epsilon_M}{N_c}\right), \qquad \Gamma_{N_c}^{\bar{q}q} = \frac{\Gamma_0}{N_c}\left(1 + \frac{\epsilon_\Gamma}{N_c}\right), \tag{15}$$

where M_0 and Γ_0 are unknown but N_c independent, with ϵ_M and ϵ_Γ naturally taken to be one. Thus, for a $\bar{q}q$ state the expected M_{N_c} and Γ_{N_c} can be obtained from those generated by the IAM,

$$\begin{aligned} M_{N_c}^{\bar{q}q} &\simeq M_{N_c-1}\left[1 + \epsilon_M\left(\frac{1}{N_c} - \frac{1}{N_c - 1}\right)\right] \\ &= M_{N_c-1} + \Delta M_{N_c}^{\bar{q}q}, \end{aligned} \tag{16}$$

$$\begin{aligned} \Gamma_{N_c}^{\bar{q}q} &\simeq \frac{N_c - 1}{N_c}\Gamma_{N_c-1}\left[1 + \epsilon_\Gamma\left(\frac{1}{N_c} - \frac{1}{N_c - 1}\right)\right] \\ &= \frac{N_c - 1}{N_c}\Gamma_{N_c-1} + \Delta\Gamma_{N_c}^{\bar{q}q}. \end{aligned} \tag{17}$$

We therefore define an averaged $\chi^2_{\bar{q}q}$ to measure how close a resonance is to a $\bar{q}q$ behavior, using as uncertainty the $\Delta M_{N_c}^{\bar{q}q}$ and $\Delta\Gamma_{N_c}^{\bar{q}q}$:

$$\chi^2_{\bar{q}q} = \frac{1}{2n}\sum_{N_c=4}^{n}\left[\left(\frac{M_{N_c}^{\bar{q}q} - M_{N_c}}{\Delta M_{N_c}^{\bar{q}q}}\right)^2 + \left(\frac{\Gamma_{N_c}^{\bar{q}q} - \Gamma_{N_c}}{\Delta\Gamma_{N_c}^{\bar{q}q}}\right)^2\right]. \tag{18}$$

This χ^2 is added to $\chi^2_{\rm data}$ and the sum is minimized. Case A is where the data are fitted assuming that the ρ is a $\bar{q}q$ meson, while case B assumes that both the σ and the ρ are $\bar{q}q$ states. Last, case C is where we minimize $\chi^2_{\rm data}$ and just $\chi^2_{\bar{q}q}$ for the σ.

We show in Table IV the values of the χ^2 contributions for each case, where we sum over N_c from 3 to 12. The two-loop LECs [24] for each case are shown in Table V. We see from Table IV that constraining the ρ to be a $\bar{q}q$ state by imposing Eq. (17) is completely compatible with data at $N_c = 3$. In contrast, imposing a $\bar{q}q$ configuration for the σ gives much poorer agreement with data and can distort the

TABLE IV. Values of the χ^2 for the different $SU(2)$ fits.

IAM Fit	$\chi^2_{\rm data}$	$\chi^2_{\rho,\bar{q}q}$	$\chi^2_{\sigma,\bar{q}q}$	$\chi^2_{\sigma,\bar{q}q,N_c=9}$	$\chi^2_{\sigma,\bar{q}q,N_c=12}$
Case A: ρ as $\bar{q}q$	1.1	0.9	15.0	4.8	3.4
Case B: ρ and σ as $\bar{q}q$	1.5	1.3	4.0	0.8	0.5
Case C: σ as $\bar{q}q$	1.4	2.0	3.5	0.6	0.5

TABLE V. Two-loop IAM LECs for the different cases we have used [24].

LECs	Case A	Case B	Case C
$l_1^r(\times 10^3)$	−5.4	−5.7	−5.7
$l_2^r(\times 10^3)$	1.8	2.5	2.6
$l_3^r(\times 10^3)$	1.5	0.39	−1.7
$l_4^r(\times 10^3)$	9.0	3.5	1.7
$r_1(\times 10^4)$	−0.6	−0.58	−0.6
$r_2(\times 10^4)$	1.5	1.5	1.3
$r_3(\times 10^4)$	−1.4	−3.2	−4.4
$r_4(\times 10^4)$	1.4	−0.49	−0.03
$r_5(\times 10^4)$	2.4	2.7	2.7
$r_6(\times 10^4)$	−0.6	−0.62	−0.7

simple structure for the ρ. It is interesting to point out that, the lower energy at which such a sigma's $\bar{q}q$ behavior emerges, the higher energy at which the ρ pole moves with N_c. Therefore, as much as we try to force the σ to behave as a $\bar{q}q$ meson, less the ρ meson does. However, requiring a $\bar{q}q$ composition for the σ for larger N_c causes no such distortion.

In all parameter sets at two loops, including case A, which fits the data best and in which the ρ has a clear $\bar{q}q$ structure, we do see a subleading $\bar{q}q$ behavior for the σ meson emerge between 1 and 1.5 GeV^2. This is evident from Fig. 6 where the imaginary part of the $I = J = 0$ amplitude is plotted. We see a clear enhancement above 1 GeV emerge as N_c increases. That this enhancement is related to the σ at larger N_c can be seen by tracking the movement of the ρ and σ poles at two loops, and comparing this with the one-loop trajectories in Fig. 2.

We see clearly how the σ pole moves away as N_c increases above 3, just as in the one-loop case, but then subleading terms take over as N_c increases above 6 and the σ pole moves back to the real axis close to 1.2 GeV. This clearly indicates dominance of a $\bar{q}q$ component in its Fock space, which may well be related to the existence of a scalar $\bar{q}q$ nonet above 1 GeV, as suggested in [17,41–44]. This is directly correlated with the enhancement seen in Fig. 6 (the pole movement shown in Fig. 7) and of course

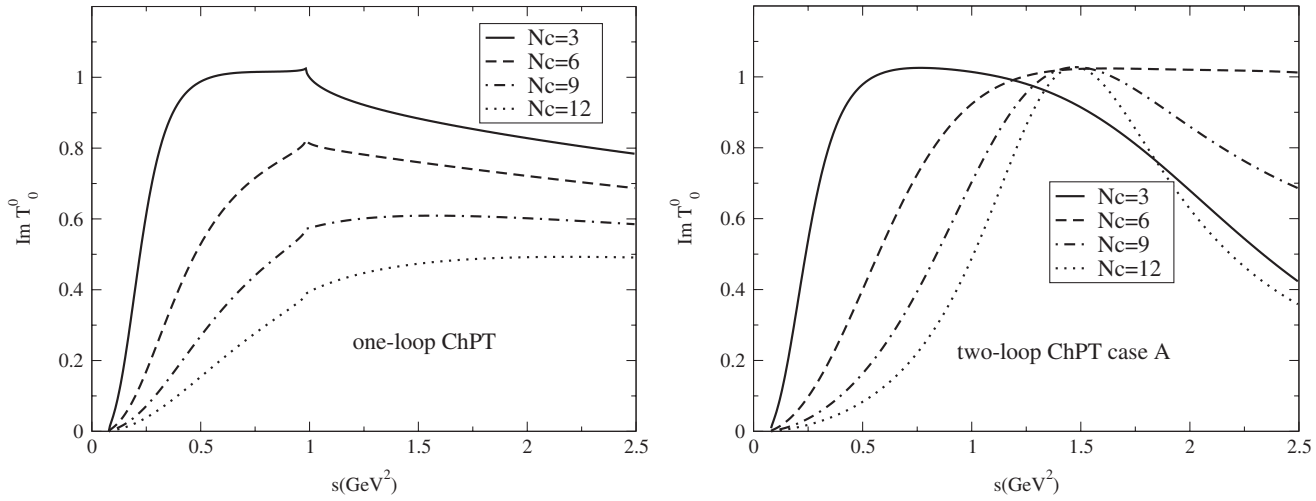

FIG. 6. Absorptive parts of the $I = J = 0$ partial wave amplitude, $\mathrm{Im}T^0_0(s)$, at one loop with the parameters of an $SU(3)$ fit (cf. the corresponding coupled channel fit in Fig. 1) and at two loops an $SU(2)$ fit with $N_c = 3$ to data below 0.9 GeV. These both involve only the $\pi\pi$ channel and so the strong inelastic effects from $\bar{K}K$ threshold are not included, in contrast to Fig. 1.

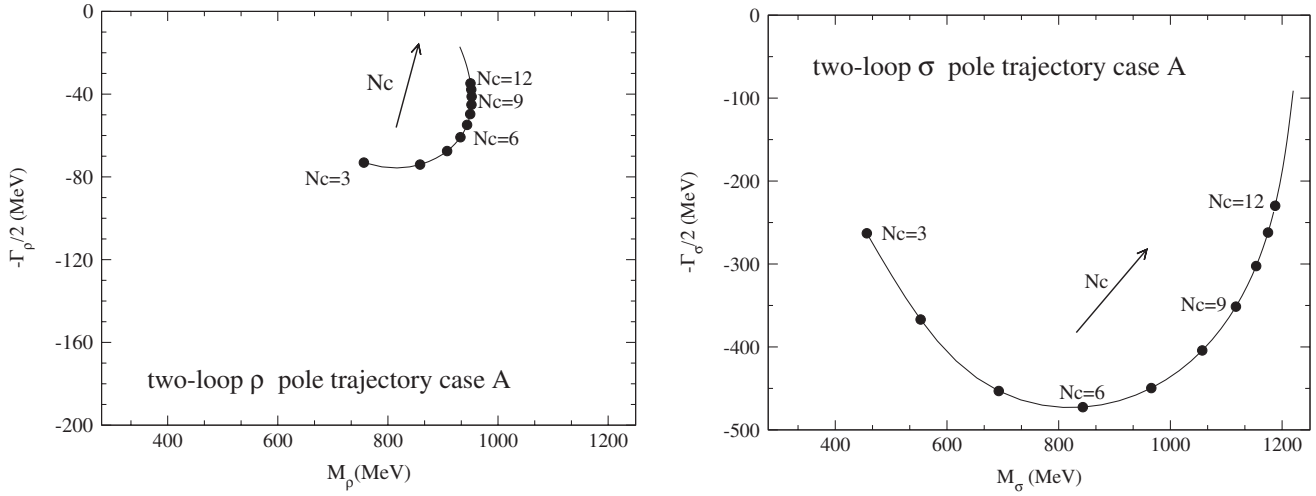

FIG. 7. Position of the ρ and σ poles in the complex energy plane as a function of N_c in two-loop χPT with parameters from the $SU(2)$ fit A of Table IV. This is to be compared with the one-loop trajectories of Fig. 2. Note the different vertical scales for the ρ and σ plots.

this enhancement makes its presence felt in the amplitudes with definite t-channel isospin. Indeed, with $I_t = 2$ we see the growth of a positive contribution to the imaginary part that might cancel the negative ρ component as N_c increases: see Fig. 8 and compare with the one-loop forms in Fig. 3.

In addition, and though these ratios have only been evaluated at one-loop order, as shown in Fig. 1, to go further one would need to extend this analysis to two or more loops. Notwithstanding this caveat, we now compute the finite energy sum rule ratios, $F(t)_n^{II'}$ of Eq. (6) with these same two-loop parameters. These ratios are set out in Table VI.

We should be just a little cautious in recognizing the limitations of the single channel approach we use here at two loop in χPT. Despite the unitarization, we are restricted to a region below 1 GeV, where strong coupling inelastic channels are not important. We see in Fig. 7 (and Fig. 6) that the subdominant $\bar{q}q$ components move above 1 GeV as N_c increases beyond 10 or 12. Consequently, if we take N_c much beyond 15 without including coupled channels, we do not expect to have a detailed description of the resonances up to 2 GeV^2. However, in the scenario where the sigma has a subdominant $\bar{q}q$, it should be interpreted as a Fock space state that is mixed in all the f_0 resonant structures in that region [45], which survives as N_c increases. Then it is easy to see that its contribution would be dominant in our ratios, and still provide a large cancellation with the ρ contribution. The reason is that, when this subdominant $\bar{q}q$ component approaches the real axis above 1 GeV, it has a much larger width than any other f_0 resonant state in that region. For instance, we see in Fig. 7 that for $N_c = 12$, the width of the $\bar{q}q$ subcomponent in the sigma is roughly 450 MeV, whereas the width of any other $\bar{q}q$ component that may exist in that region would have already decreased by $3/12 = 1/4$. Since the other

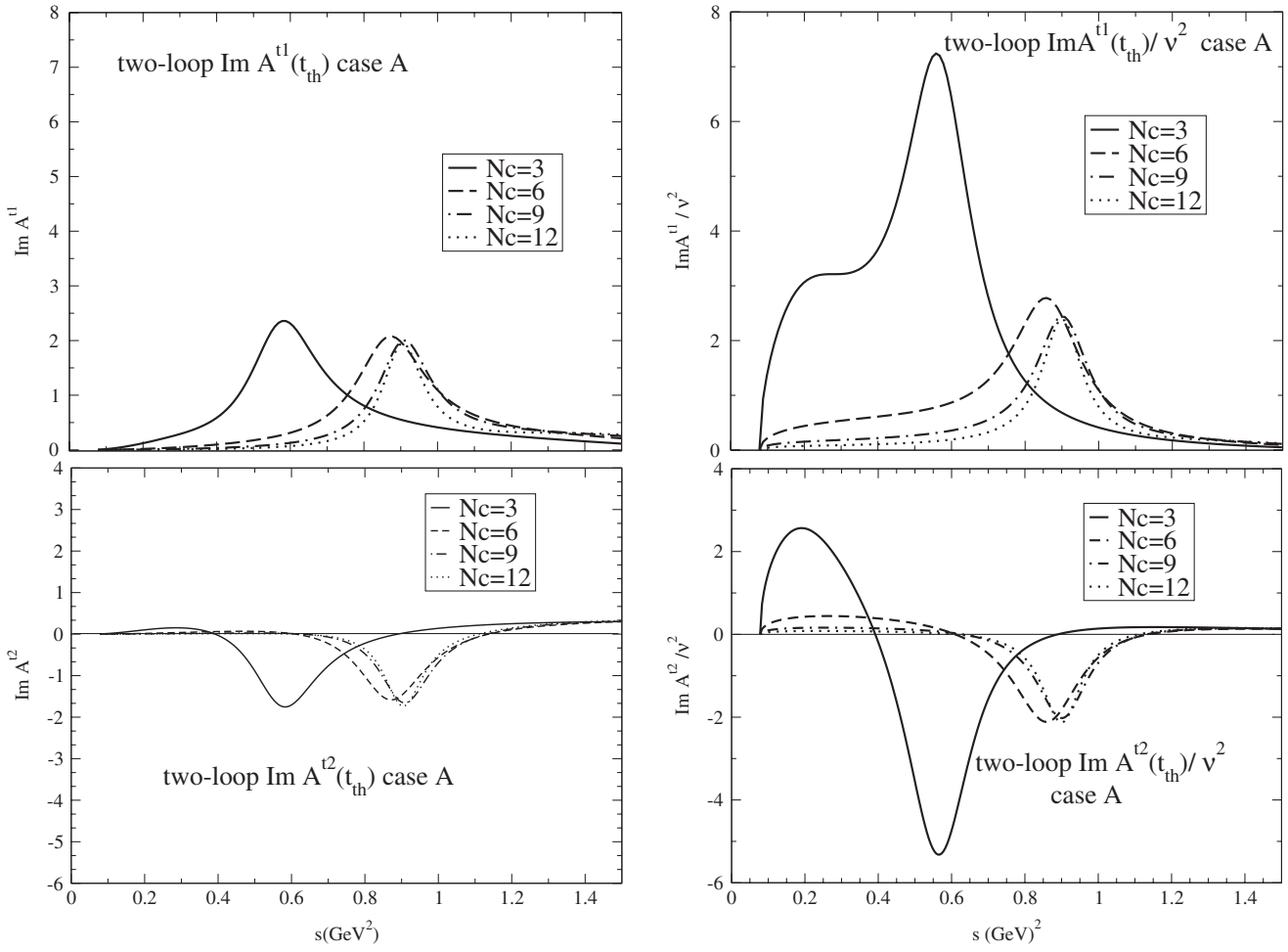

FIG. 8. Absorptive parts of amplitudes with definite t-channel isospin, $\mathrm{Im}A^{tI}(s, t_{\mathrm{th}})/\nu^n$, using the parameters of the two-loop $SU(2)$ fit case A. The top pair of graphs has $I = 1$ and the lower with $I = 2$, on the left hand $n = 0$ and right hand $n = 2$. One sees from the lower pair how integrating the curves the positive and negative contributions cancel for all N_c.

TABLE VI. Ratios for two-loop UChPT using the LECs of case A.

			Two loops $SU2$ ρ as $\bar{q}q$			
			$t = 4M_\pi^2$		$t = 0$	
	n	N_c	$\nu_{\max} = 1$ GeV^2	$\nu_{\max} = 2$ GeV^2	$\nu_{\max} = 1$ GeV^2	$\nu_{\max} = 2$ GeV^2
F_n^{10}	0	3	0.493	0.359	0.488	0.334
		6	0.494	0.370	0.492	0.349
		9	0.491	0.395	0.490	0.376
		12	0.489	0.422	0.488	0.404
	1	3	0.509	0.442	0.511	0.434
		6	0.496	0.419	0.494	0.407
		9	0.488	0.430	0.487	0.418
		12	0.485	0.447	0.483	0.436
	2	3	0.533	0.505	0.551	0.522
		6	0.498	0.457	0.498	0.454
		9	0.482	0.452	0.479	0.445
		12	0.477	0.460	0.472	0.452
	3	3	0.572	0.563	0.618	0.611
		6	0.503	0.485	0.511	0.495
		9	0.472	0.460	0.468	0.456
		12	0.461	0.457	0.451	0.447
F_n^{21}	0	3	−0.421	−0.060	−0.280	0.135
		6	−0.536	−0.086	−0.454	0.058
		9	−0.648	−0.061	−0.579	0.073
		12	−0.748	−0.038	−0.686	0.090
	1	3	−0.351	−0.202	−0.183	−0.028
		6	−0.438	−0.196	−0.335	−0.069
		9	−0.578	−0.215	−0.497	−0.102
		12	−0.699	−0.227	−0.629	−0.121
	2	3	−0.173	−0.123	0.097	0.139
		6	−0.249	−0.152	−0.069	0.027
		9	−0.435	−0.248	−0.294	−0.105
		12	−0.594	−0.314	−0.477	−0.192
	3	3	0.146	0.156	0.570	0.575
		6	0.102	0.112	0.485	0.488
		9	−0.121	−0.073	0.249	0.275
		12	−0.332	−0.216	0.012	0.092

components would be heavier and much narrower, their contributions would be much smaller than that of the $\bar{q}q$ state subdominant in the σ. Note that it is also likely that some of the f_0's may have large glueball components (see, for instance, [44]), which also survive as N_c increase, but then their widths would decrease even faster—like $1/N_c^2$, and our argument would apply even better. For the scenario when we do not see the sigma subdominant component (as in Fig. 4), we still expect that the other resonances by themselves will not be able to cancel the ρ contribution, so that the IAM would still provide a qualitatively good picture of this "noncancellation." For this reason, although the IAM much beyond $N_c = 15$ may not necessarily yield a detailed description of the resonance structure, we expect the N_c behavior of the ratios to be qualitatively correct for both scenarios even at larger N_c.

Additional arguments to consider the IAM only as a qualitative description beyond $N_c = 15$ or 30 have been given in [38] since the error made in approximating the left cut, as well as the effect of the η' may start to become numerically relevant around those N_c values.

Remarkably we see with two-loop χPT, that the unitarized amplitudes do reflect semilocal duality with $I = 2$ in the t channel suppressed. This is most readily seen from the plots of the ratios $F_n^{II'}$ for the two-loop amplitudes shown in Fig. 9 (to be compared with the one-loop ratios of Fig. 4). For F_n^{21}, it is clear that, if only considering the integrals up to 1 GeV^2, the ratios are still not small in

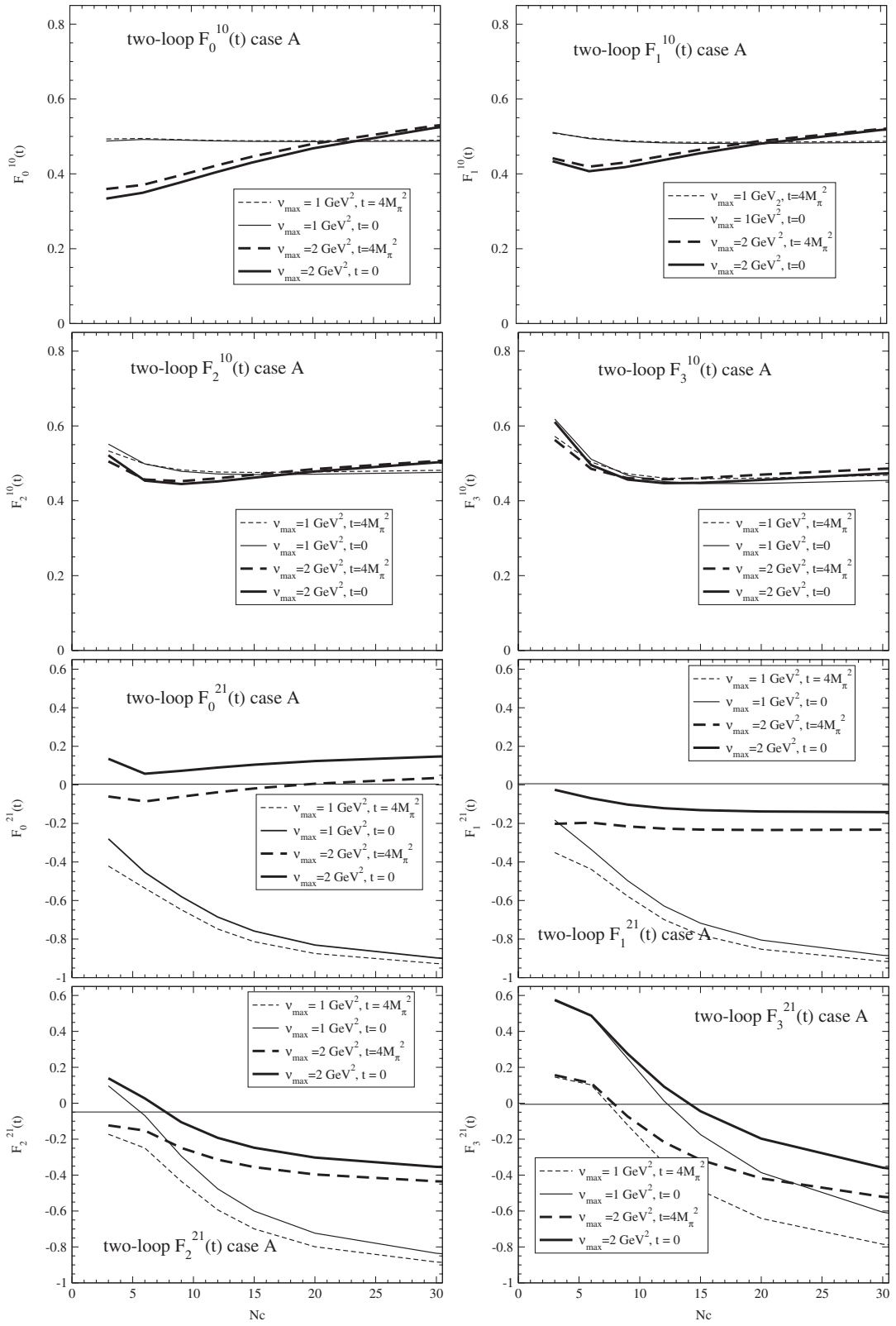

FIG. 9. Ratios $F_n^{II'}$ of Eq. (6) with $n = 0$–3. The top four graphs are for F^{10}, and the lower four for F^{21}. Two-loop χPT IAM parameters are from the $SU(2)$ fit with $N_c = 3$ to data: case A.

magnitude. Indeed, their absolute value increases with N_c. However, integrating up to 2 GeV^2 takes into account the subdominant component, and then the ratios stabilize at much smaller values for all N_c, consistent with expectations from semilocal duality.

V. THE EFFECT OF HEAVIER RESONANCES

So far we have restricted the analysis of the N_c behavior to the ρ and σ resonances. Of course, one may wonder what is the effect of heavier resonances on our analysis and conclusions. In particular, since the subdominant $\bar{q}q$ component of the σ emerges between 1 and 1.5 GeV^2, one might worry about the $f_0(980)$ and even the $f_0(1370)$ resonance, since the latter has a width of several hundred MeV and may overlap with the region of interest. [The $f_0(1500)$ and $f_0(1710)$ lie beyond that energy range and are therefore suppressed by the $1/s^n$ in the denominator.] In addition, we might worry about resonances in higher waves; in this case the $f_2(1270)$ in the D wave would yield the largest contribution.

Actually, Fig. 1 has been calculated in an $SU(3)$ coupled channel formalism and includes the $f_0(980)$ as a very sharp drop in $\mathrm{Im}T_0^0$, which disappears as N_c increases. By comparing with Fig. 6, with no $f_0(980)$ present, it is clear that, by removing the $f_0(980)$ the variation in the $\mathrm{Im}T_0^0$ integrals, and therefore in the $F_n^{II'}$ of Eq. (6), is small compared to the systematic uncertainty that we have estimated as the difference between the $t = 0$ and $t = t_{\mathrm{th}}$ calculations. Actually, if the $f_0(980)$ is included in a coupled channel IAM calculation, as in Fig. 1, the new F_n^{21} values would all lie between our $t = 0$ and $t = t_{\mathrm{th}}$ results listed in Table III without the $f_0(980)$. The error we make by ignoring the $f_0(980)$ is, at most, 30% of the estimated systematic uncertainty. For sure the $f_0(980)$ will not be able to compensate the ρ contribution. Still, one might wonder whether this is also the case at two loops if the $f_0(980)$ or $f_0(1370)$ have a $\bar{q}q$ component around 1 to 1.5 GeV^2 that survives when N_c increases. However, at least the lightest such component would be precisely the same $\bar{q}q$ state that we already see in the $f_0(600)$. Actually the interpretation of the IAM results is that all these scalars are a combination of all possible states from Fock space [45], namely, $\bar{q}q$, tetraquarks, molecules, glueballs, etc..., but as N_c grows only the $\bar{q}q$ survives between 1 and 1.5 GeV^2, whereas the other components are either more massive or disappear in the deep complex plane. It is precisely that component, which we already have in our calculation, the one compensating the ρ contributions, as we have just seen above.

In the very preliminary interpretation of [45], the $\bar{q}q$ subdominant component of the $f_0(600)$ within the IAM naturally accounts for 20%–30% of its total composition. This is in fairly good agreement with the 40% estimated in [46]. Indeed, given the two caveats raised by the authors of [46], their 40% may be considered an upper bound. First, this 40% refers to the "tree level masses" of the scalar states. These mesons, of course, only acquire their physical mass and width after unitarization, which is essentially generated by $\pi\pi$ final state interactions. Intuitively we would expect these to enhance the non-$\bar{q}q$ component, and so bring the $\bar{q}q$ fraction below the "bare" 40%. Second, in [46] the authors also suggest that "a possible glueball state is another relevant effect" not included in their analysis. In [45], the glueball component is of the order of 10%. Consequently, the results of [46], those presented here and in [45], are all quite consistent.

Finally, we will show that the contribution of the $f_2(1270)$ to the FESR cancellation, even assuming it follows exactly a $\bar{q}q$ leading N_c behavior, is rather small and does not alter our conclusions. All other resonances coupling to $\pi\pi$ are more massive and therefore less relevant.

In order to describe the $I = 0$ $J = 2$ channel we will again use the parametrization of KPY in terms of the corresponding phase shift δ_2^0, namely,

$$\mathcal{A}_{\ 2}^{\ 0} = \frac{1}{\sigma(s)} \frac{1}{\cot\delta_{(2)}^0 - \imath}, \tag{19}$$

where $\cot\delta_2^0$, which is proportional to $s - M_{f_2}^2$, is given in detail in the Appendix of KPY [29]. Now, by replacing

$$\cot\delta_2^0 \to \frac{N_c}{3} \cot\delta_2^0, \tag{20}$$

we ensure that the amplitude itself scales as $1/N_c$. This also ensures that the resonance mass M_{f_2} is constant, and its width scales as $1/N_c$. We require the $f_2(1270)$ to behave as a perfect $\bar{q}q$ at leading order in $1/N_c$, while reproducing the KPY fit to the D wave at $N_c = 3$. As can be noticed in Fig. 10, for F_2^{21} and F_3^{21}, which are the most relevant ratios for our arguments, the difference between adding this D-wave contribution to our previous results is smaller than the effect of the sigma $\bar{q}q$ component around 1 to 1.5 GeV^2. For the ratio F_3^{21}, the effect of the D-wave contribution is larger, but it is the effect of the sigma $\bar{q}q$ subcomponent the one that makes the curves flatter and bounded between -0.2 and 0.2, whereas the slope is clearly negative without such a contribution and the absolute value of the ratio can be as large as 0.5 and still growing. Note that in Fig. 10 we compare our previous one- and two-loop F_n^{21} calculations (bolder line) to those which include the $f_2(1270)$ resonance as a pure $\bar{q}q$ (thin lines). Therefore the effect of including the $f_2(1270)$ does not modify our conclusions. The main FESR cancellation at N_c larger than 3 is between the $\rho(770)$ and the subdominant $\bar{q}q$ component of the $f_0(600)$ resonance, which appears around 1 to 1.5 GeV^2.

This is even more evident if we extrapolate our results to even higher N_c, as in Fig. 11, where all curves include the effect of the $f_2(1275)$. As already explained above, for such high N_c the IAM cannot be trusted as a precise description, but just as a qualitative model of the effect of a $\bar{q}q$ state around 1 to 1.5 GeV^2, which has a width

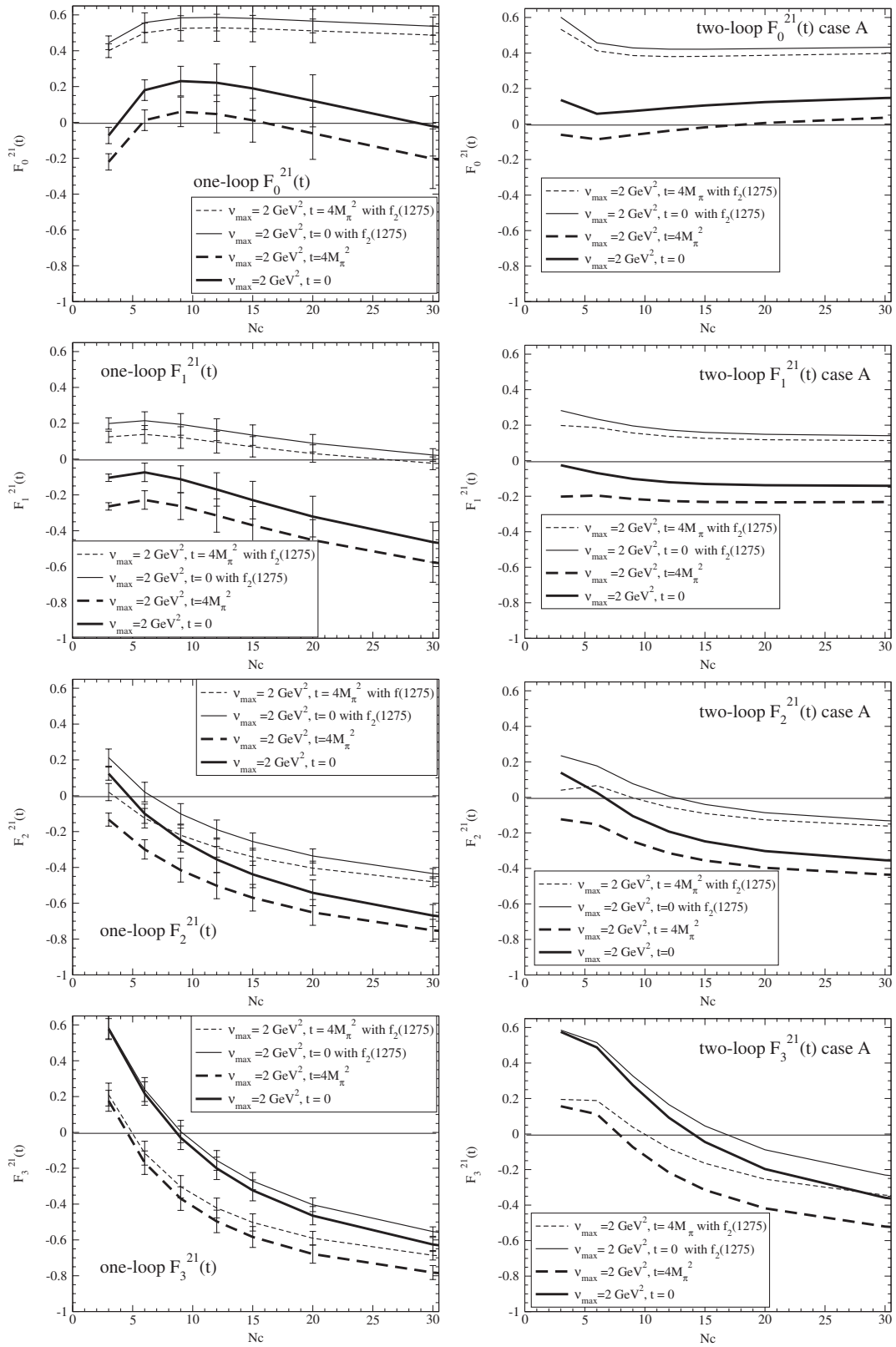

FIG. 10. Results for F_n^{21} with and without the $f_2(1270)$ resonance scaled as a pure $\bar{q}q$ (thin and bolder lines, respectively). The left panels are for one-loop IAM results, and the right ones for the two-loop results. The latter contain a subdominant $\bar{q}q$ component of the $f_0(600)$ around 1 to 1.5 GeV^2 whose effect is relevant for the cancellation of F_n^{21}.

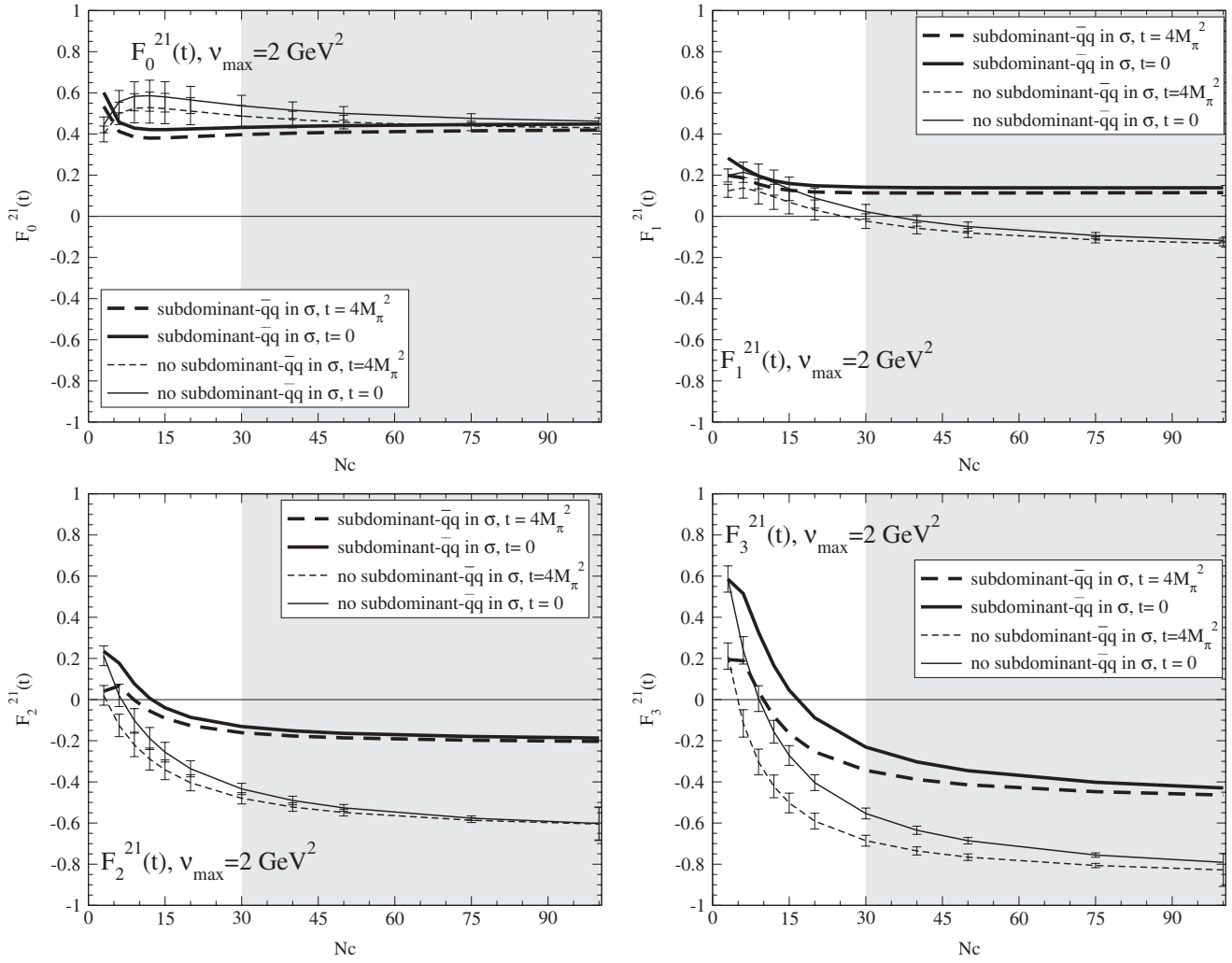

FIG. 11. Results for the F_n^{21} ratios including the $f_2(1275)$ model to the χPT unitarized S and P waves. The bolder lines correspond to our two-loop calculation that yields a subdominant $\bar{q}q$ component around 1 to 2 GeV^2, whereas the thin lines are the one-loop unitarized calculation that does not contain such a component. As explained in the text, beyond $N_c = 15$ or 30 (gray area) we consider the unitarized amplitudes to provide just a qualitative description of the dominant $\bar{q}q$ state in the 1 to 1.5 GeV^2 region. It is nevertheless clear that the effect of such a $\bar{q}q$ component brings a large cancellation in the ratios, improving the fulfillment of semilocal duality.

much larger than the states seen there at $N_c = 3$ and will dominate the integrals in F_n^{21}. It is clearly seen that the effect of such a state will compensate the $\rho(770)$ contribution and preserve semilocal duality. Other states that survive the N_c limit in that region—which would be heavier and much narrower—would only provide smaller corrections to this qualitative picture. Nevertheless, it would be desirable to extend this study to a more ambitious treatment of the higher mass states in future work.

VI. DISCUSSION

It is a remarkable fact that hadronic scattering amplitudes from threshold upwards build their high energy Regge behavior. This was learnt from detailed studies of meson-nucleon interactions more than 40 years ago. This property is embodied in semilocal duality, expressed through finite energy sum rules. Perhaps just as remarkably we have shown here that the Regge parameters fixed from high energy NN and πN scattering yield the correct $\pi\pi$ P and D-wave scattering lengths, cf. Eqs. (11) and (12). Indeed, there is probably no closer link between amplitudes with definite t-channel quantum numbers and their low energy behavior in the s-channel physics region than that shown here. What is more, such a relationship should hold at all values of N_c. At low energy the scattering amplitudes of pseudo-Goldstone bosons are known to be well described by their chiral dynamics, and their contribution to finite energy sum rules is dominated by the $\rho(770)$ and $f_0(600)$ contributions. However, there are many proposals in the

literature, including the N_c dependence of the unitarized chiral amplitudes, suggesting that the $f_0(600)$, contrary to the $\rho(770)$, may not be an ordinary $\bar{q}q$ meson. This is a potential problem for the concept of semilocal duality between resonances and Regge exchanges. The reason is that for $I = 2$ t-channel exchange it requires a cancellation between the $\rho(770)$ and $f_0(600)$ resonances, which may no longer occur if the $f_0(600)$ contribution becomes comparatively smaller and smaller as N_c increases.

This conflict actually occurs for the most part of one-loop unitarized chiral perturbation theory parameter space. In contrast, for a small part of the one-loop parameter space and in a very natural way at higher order in the chiral expansion, the σ may have a $\bar{q}q$ component in its Fock space, which though subdominant at $N_c = 3$, becomes increasingly important as N_c increases. This is critical, as we have shown here, in ensuring semilocal duality for $I = 2$ exchanges is fulfilled as N_c increases. As we show in Fig. 11 this better fulfillment of semilocal duality keeps improving even at much larger N_c, where the IAM can only be interpreted as a very qualitative average description.

Thus, the chiral expansion contains the solution to the seeming paradox of how a distinctive nature for the ρ, σ at $N_c = 3$ is reconciled with semilocal duality at larger values of N_c. Indeed, despite the additional freedom brought about by the extra low energy constants at two-loop order, fixing these from experiment at $N_c = 3$ automatically brings this compatibility with semilocal duality as N_c increases. This is a most satisfying result.

The P and D-wave scattering lengths evaluated using Eqs. (7) and (8) that agree so well with local duality at $N_c = 3$ can, of course, be computed at larger N_c by inputting chiral amplitudes on each side of the defining equations. The scattering lengths themselves involve only the real parts, while the Froissart-Gribov integrals require the imaginary parts that are determined by the unitarization procedure. Explicit calculation shows that these agree as N_c increases. While the agreement at one-loop order is straightforward, at two loops there is a subtle interplay of dominant and subdominant terms placing constraints on the precise values of the LECs. As this takes us beyond the scope of the present work, we leave this for a separate study.

Though beyond the scope of this work, we can then ask what does this tell us about the nature of the enigmatic scalars [9]? At $N_c = 3$, the behavior of the σ is controlled by its coupling to $\pi\pi$. Its Fock space is dominated by this non-$\bar{q}q$ component [42,43,45]. In dynamical calculations of resonances and their propagators, like that of van Beveren, Rupp, and their collaborators [41] and of Tornqvist [47], the seeds for the lightest scalars are an ideally mixed $\bar{q}q$ multiplet of higher mass. These seeds may leave a conventional $\bar{q}q$ nonet near 1.4 GeV [17,41,43,44], while the dressing by hadron loops dynamically generates a second set of states, whose decay channels dominate their behavior at $N_c = 3$ and pull their masses close to the threshold of their major decay: the σ down towards $\pi\pi$ threshold, and the $f_0(980)$ and $a_0(980)$ to $\bar{K}K$ threshold. The leading order in the $1/N_c$ expansion discussed here may be regarded *a posteriori* as providing a quantitative basis for this. The scalars are at N_c larger than 3 controlled by $\bar{q}q$ seeds of mass well above 1 GeV (1.2 GeV for the intrinsically nonstrange scalar). Switching on decay channels, as one does as N_c decreases, changes their nature dramatically, inevitably producing non-$\bar{q}q$ or di-meson components in their Fock space at $N_c = 3$ [9]. We see here that the σ having a subdominant $\bar{q}q$ component with a mass above 1 GeV is essential for semilocal duality, that suppresses $I = 2$ amplitudes, to hold.

ACKNOWLEDGMENTS

M. R. P is grateful to Bob Jaffe for discussions about the issues raised at the start of this study. The authors (J. R. de E, M. R. P and D. J. W) acknowledge partial support of the EU-RTN Programme, Contract No. MRTN–CT-2006-035482, "Flavianet" for this work, while at the IPPP in Durham. D. J. W is grateful to the UK STFC for the award of a postgraduate studentship and to Jefferson Laboratory for hospitality while this work was completed. This work was supported in part by DOE Contract No. DE-AC05-06OR23177, under which Jefferson Science Associates, LLC, operates Jefferson Laboratory.

[1] R. L. Jaffe, Phys. Rev. D **15**, 267 (1977).
[2] G. 't Hooft, Nucl. Phys. **B72**, 461 (1974); E. Witten, Ann. Phys. (N.Y.) **128**, 363 (1980).
[3] R. Dolen, D. Horn, and C. Schmid, Phys. Rev. Lett. **19**, 402 (1967); Phys. Rev. **166**, 1768 (1968).
[4] C. Schmid, Phys. Rev. Lett. **20**, 628 (1968); **20**, 689 (1968).
[5] S. Donnachie, H. G. Dosch, O. Nachtmann, and P. Landshoff, Cambridge Monogr. Part. Phys., Nucl. Phys., Cosmol. **19**, 1 (2002).
[6] K. Shiga, K. Kinoshita, and F. Togoda, Nucl. Phys. **B24**, 490 (1970).
[7] G. Veneziano, Nuovo Cimento A **57**, 190 (1968).
[8] C. Schmid and J. Yellin, Phys. Rev. **182**, 1449 (1969); T. Eguchi and K. Igi, Phys. Lett. **40B**, 245 (1972).
[9] M. R. Pennington, AIP Conf. Proc. **1257**, 27 (2010).
[10] P. Minkowski and W. Ochs, Eur. Phys. J. C **9**, 283 (1999).
[11] G. Mennessier, S. Narison, and W. Ochs, Phys. Lett. B **665**, 205 (2008); Nucl. Phys. Proc. Suppl. **181–182**, 238 (2008).

[12] S. Weinberg, Physica A (Amsterdam) **96**, 327 (1979); J. Gasser and H. Leutwyler, Ann. Phys. (N.Y.) **158**, 142 (1984); Nucl. Phys. **B250**, 465 (1985).

[13] T. N. Truong, Phys. Rev. Lett. **61**, 2526 (1988); **67**, 2260 (1991); A. Dobado *et al.*, Phys. Lett. B **235**, 134 (1990).

[14] A. Dobado and J. R. Peláez, Phys. Rev. D **47**, 4883 (1993).

[15] A. Dobado and J. R. Peláez, Phys. Rev. D **56**, 3057 (1997).

[16] J. A. Oller and E. Oset, Nucl. Phys. **A620**, 438 (1997); **A652**, 407 (1999); J. A. Oller, E. Oset, and J. R. Peláez, Phys. Rev. Lett. **80**, 3452 (1998); Phys. Rev. D **59**, 074001 (1999); **60**, 099906(E) (1999); **75**, 099903(E) (2007); **62**, 114017 (2000); J. Nieves and E. Ruiz Arriola, Phys. Lett. B **455**, 30 (1999); F. Guerrero and J. A. Oller, Nucl. Phys. B **B537**, 459 (1999); **B602**, 641 (2001).

[17] J. A. Oller and E. Oset, Phys. Rev. D **60**, 074023 (1999).

[18] A. Gomez Nicola and J. R. Peláez, Phys. Rev. D **65**, 054009 (2002); J. R. Peláez and G. Rios, arXiv:0905.4689.

[19] J. Nieves, M. Pavon Valderrama, and E. Ruiz Arriola, Phys. Rev. D **65**, 036002 (2002).

[20] A. Gomez Nicola, J. R. Peláez, and G. Rios, Phys. Rev. D **77**, 056006 (2008).

[21] J. Bijnens, G. Colangelo, G. Ecker, J. Gasser, and M. E. Sainio, Nucl. Phys. **B508**, 263 (1997); **B517**, 639(E) (1998).

[22] S. Peris and E. de Rafael, Phys. Lett. B **348**, 539 (1995).

[23] J. R. Peláez, Phys. Rev. Lett. **92**, 102001 (2004).

[24] J. R. Peláez and G. Rios, Phys. Rev. Lett. **97**, 242002 (2006).

[25] V. D. Barger and D. B. Cline, *Phenomenological Theories of High Energy Scattering* (W.A. Benjamin, New York, 1969).

[26] C. Amsler *et al.* (Particle Data Group), Phys. Lett. B **667**, 1 (2008).

[27] A. Donnachie and P. V. Landshoff, Nucl. Phys. **B267**, 690 (1986).

[28] J. R. Cudell *et al.* (COMPETE Collaboration), Phys. Rev. D **65**, 074024 (2002).

[29] R. Kaminski, J. R. Peláez, and F. J. Yndurain, Phys. Rev. D **77**, 054015 (2008).

[30] W. Rarita, R. J. Riddell, C. Chiu, and R. J. N. Phillips, Phys. Rev. **165**, 1615 (1968).

[31] J. R. Peláez and F. J. Yndurain, Phys. Rev. D **69**, 11401 (2004).

[32] M. R. Pennington, Ann. Phys. (N.Y.) **92**, 164 (1975).

[33] G. Colangelo, J. Gasser, and H. Leutwyler, Nucl. Phys. **B603**, 125 (2001).

[34] R. Garcia-Martin, R. Kaminski, J. R. Pelaez, J. Ruiz de Elvira, and F. J. Yndurain, Phys. Rev. D **83**, 074004 (2011).

[35] J. R. Batley *et al.* (NA48-2 Collaboration), Eur. Phys. J. C **70**, 635 (2010).

[36] J. R. Peláez, Mod. Phys. Lett. A **19**, 2879 (2004).

[37] J. F. Donoghue, C. Ramirez, and G. Valencia, Phys. Rev. D **39**, 1947 (1989); G. Ecker, J. Gasser, A. Pich, and E. de Rafael, Nucl. Phys. **B321**, 311 (1989).

[38] J. R. Pelaez, J. Nebreda, and G. Rios, Prog. Theor. Phys. Suppl. **186**, 113 (2010); J. R. Pelaez and G. Rios, Acta Phys. Polon. Suppl. **2**, 215 (2009); J. R. Pelaez, arXiv:hep-ph/0509284; in *Proceedings of the 11th International Conference on Elastic and Diffractive Scattering, Blois, France, 2005* (The Gioi Publishers, Hanoi, Vietnam, 2005).

[39] Z.-H. Guo and J. A. Oller, Phys. Rev. D **84**, 034005 (2011).

[40] Z. X. Sun, L. Y. Xiao, Z. Xiao, and H. Q. Zheng, Mod. Phys. Lett. A **22**, 711 (2007); E. van Beveren and G. Rupp, Eur. Phys. J. C **22**, 493 (2001).

[41] E. van Beveren, T. A. Rijken, K. Metzger, C. Dullemond, G. Rupp, and J. E. Ribeiro, Z. Phys. C **30**, 615 (1986); E. van Beveren, D. V. Bugg, F. Kleefeld, and G. Rupp, Phys. Lett. B **641**, 265 (2006).

[42] R. L. Jaffe, in *Proceedings of the International Symposium on Lepton and Photon Interactions at High Energies* (University of Bonn, Germany, 1981); M. Harada, F. Sannino, and J. Schechter, Phys. Rev. D **69**, 034005 (2004).

[43] D. Black, A. H. Fariborz, F. Sannino, and J. Schechter, Phys. Rev. D **59**, 074026 (1999); L. Maiani, F. Piccinini, A. D. Polosa, and V. Riquer, Phys. Rev. Lett. **93**, 212002 (2004); F. Giacosa, Phys. Rev. D **75**, 054007 (2007).

[44] F. E. Close and N. A. Tornqvist, J. Phys. G **28**, R249 (2002).

[45] F. J. Llanes-Estrada, J. R. Pelaez, and J. Ruiz de Elvira, Nucl. Phys. Proc. Suppl. **207–208**, 169 (2010).

[46] A. H. Fariborz, R. Jora, and J. Schechter, Phys. Rev. D **79**, 074014 (2009); arXiv:0902.2825; A. H. Fariborz, R. Jora, J. Schechter, and M. N. Shahid, arXiv:1106.4538.

[47] N. A. Tornqvist, Z. Phys. C **68**, 647 (1995).

2.2.4 Publication: Zhi-Hui Guo, J.A. Oller, J. Ruiz de Elvira, *Chiral dynamics in U(3) unitary chiral perturbation theory, Phys. Lett.* B712 407-412 (2012)

Physics Letters B 712 (2012) 407–412

Contents lists available at SciVerse ScienceDirect

Physics Letters B

www.elsevier.com/locate/physletb

Chiral dynamics in $U(3)$ unitary chiral perturbation theory

Zhi-Hui Guo [a,b,*], J.A. Oller [b], J. Ruiz de Elvira [c]

[a] Department of Physics, Hebei Normal University, 050024 Shijiazhuang, PR China
[b] Departamento de Física, Universidad de Murcia, E-30071 Murcia, Spain
[c] Departamento de Física Teórica II, Universidad Complutense de Madrid, E-28040 Madrid, Spain

ARTICLE INFO

Article history:
Received 21 March 2012
Received in revised form 26 April 2012
Accepted 10 May 2012
Available online 14 May 2012
Editor: B. Grinstein

Keywords:
Chiral perturbation theory
Weinberg sum rules
Semi-local duality
$1/N_C$ expansion

ABSTRACT

We perform a complete one-loop calculation of meson–meson scattering, and of the scalar and pseudoscalar form factors in $U(3)$ chiral perturbation theory with the inclusion of explicit resonance fields. This effective field theory takes into account the low-energy effects of the QCD $U_A(1)$ anomaly explicitly in the dynamics. The calculations are supplied by non-perturbative unitarization techniques that provide the final results for the meson–meson scattering partial waves and the scalar form factors considered. We present thorough analyses on the scattering data, resonance spectroscopy, spectral functions, Weinberg-like sum rules and semi-local duality. The last two requirements establish relations between the scalar spectrum with the pseudoscalar and vector ones, respectively. The N_C extrapolation of the various quantities is studied as well. The fulfillment of all these non-trivial aspects of the QCD dynamics by our results gives a strong support to the emerging picture for the scalar dynamics and its related spectrum.

Chiral symmetry and $U_A(1)$ anomaly are two prominent features of QCD in the low energy sector. Chiral perturbation theory (χPT) [1–3] that exhaustively exploits chiral symmetry as well as its spontaneous and explicit breaking to constrain the dynamics allowed, has proven as a reliable tool to analyze the QCD low energy processes involving the octet of pseudo-Goldstone bosons π, K and η. On the other hand, the $U_A(1)$ anomaly of QCD provides a natural explanation of the massive state η' [4]. The consideration of a variable number of colors (N_C) in QCD is enlightening. An important finding from large N_C QCD [5] is that the $U_A(1)$ anomaly is $1/N_C$ suppressed and thus the η' meson becomes the ninth Goldstone boson at large N_C in the chiral limit [6]. This poses strong constraints on the allowed forms of the chiral operators involving the η' field, which generalizes the conventional $SU(3)$ χPT [3] to the $U(3)$ version [4,7,8]. Thus $U(3)$ χPT is a serious theory to incorporate the η' as a dynamical degree of freedom in the chiral effective Lagrangian approach and hence deserves of detailed calculations. Though the one-loop renormalization and construction of the corresponding $\mathcal{O}(p^4)$ Lagrangian are performed in Refs. [7,8], further calculations still need to be carried out. Recently the calculation of the one-loop meson–meson scattering amplitudes was completed in Ref. [9], and the non-strangeness changing scalar and pseudoscalar form factors are calculated in the present work.

Based on the calculated scattering amplitudes and form factors from $U(3)$ χPT, we then study semi-local duality [10,11] between Regge theory and the hadronic degrees of freedom (h.d.f.) and construct the spectral functions to investigate the Weinberg-like spectral function sum rules [12] among the scalar and pseudoscalar correlators. The N_C evolution of the resonance poles, semi-local duality and two-point correlators are also studied. In the physical case, i.e. $N_C = 3$, the $f_0(600)$ resonance (also called σ) plays important roles for the fulfillment of both semi-local duality and the Weinberg-like spectral function sum rules. However, according to the study of Ref. [9] that employs a similar approach as the one used here, when N_C increases the $f_0(600)$ resonance evolves deeper in the complex energy plane and barely contributes at large N_C. Interestingly, we find that at large N_C the contribution from the singlet scalar resonance S_1 with a mass around 1 GeV, that is part of the $f_0(980)$ resonance at $N_C = 3$, becomes more and more important for larger values of N_C. Then, two markedly different pictures for the scalar dynamics emerge as a function of N_C. For the physical case the $f_0(600)$ is the scalar resonance mainly responsible to counterbalance the vector resonance $\rho(770)$ in semi-local duality. It also counterbalances the contributions from the octet of scalar resonances, the nonet of the pseudo-Goldstone bosons and also from the lightest multiplet of pseudoscalar resonances in the Weinberg-like spectral sum rules.

* Corresponding author at: Department of Physics, Hebei Normal University, 050024 Shijiazhuang, PR China and Departamento de Física, Universidad de Murcia, E-30071 Murcia, Spain.
E-mail address: guo@um.es (Z.-H. Guo).

0370-2693/$ – see front matter
http://dx.doi.org/10.1016/j.physletb.2012.05.021

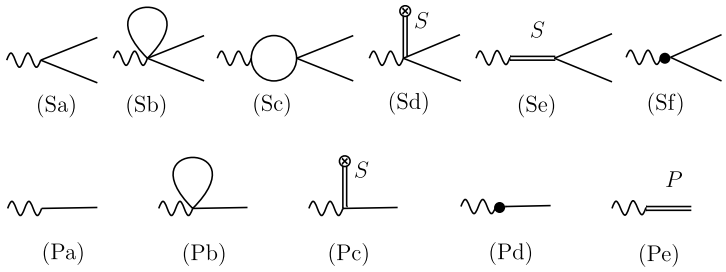

Fig. 1. Feynman diagrams for the calculations of the scalar (first row) and pseudoscalar (second row) form factors. The wavy lines denote either the scalar or the pseudoscalar external source. See the text for more details.

However, at large N_C the remnant component (a $\bar{q}q$-like one) of the $f_0(980)$ is responsible for the strength in the scalar dynamics. Though these two pictures differ dramatically they evolve continuously from one to the other as N_C varies. We present the discussions in more detail next.

In the perturbative calculations, we include the tree level exchanges of resonances explicitly [13], instead of considering the local chiral operators from the higher order Lagrangian [7,8]. We then assume tacitly the saturation by resonance exchange of the (next-to-leading) chiral counterterms [13]. The relevant Lagrangian has been presented in detail in Ref. [9]. In addition we also include the exchange of pseudoscalar resonances here, which are absent in [9]. Their effects in meson–meson scattering turn out to be small, but they play a crucial role to establish the Weinberg-like spectral sum rules for the difference between the scalar–scalar (SS) and pseudoscalar–pseudoscalar (PP) correlators (SS–PP).

The pseudoscalar resonance Lagrangian introduced in [13] produces the mixing between the pseudoscalar resonances and the pseudo-Goldstone bosons. Nevertheless this mixing can be eliminated at the Lagrangian level through a chiral covariant redefinition of the resonance fields, which results in two local chiral operators at the $\mathcal{O}(p^4)$ level [14]. We remind that the nature of the pseudoscalar resonances is still a controversial issue and their parameters are not accurately measured yet [15]. So in order to compensate the uncertainties on the pseudoscalar resonance properties, as well as our simple parameterization here in terms of simple bare propagators in the spirit of the narrow resonance approach,[1] we include an L_8-like operator [3].

We show the pertinent Feynman graphs for the scalar form factors of the pseudo-Goldstone pairs and the pseudoscalar form factors in the first and second rows of Fig. 1, in order. The scalar form factor of a pseudo-Goldstone boson pair PQ, $F^a_{PQ}(s)$, is defined as

$$F^a_{PQ}(s) = \frac{1}{B}\langle 0|S^a|PQ\rangle, \tag{1}$$

while the pseudoscalar form factor of the pseudoscalar P, $H^a_P(s)$, corresponds to

$$H^a_P(s) = \frac{1}{B}\langle 0|P^a|P\rangle. \tag{2}$$

In the equations above the scalar and pseudoscalar currents are $S^a = \bar{q}\lambda_a q$ and $P^a = i\bar{q}\gamma_5\lambda_a q$, in order, with λ_a the Gell-Mann matrices for $a = 1,\ldots,8$ and $\lambda_0 = I_{3\times 3}\sqrt{2/3}$ for $a = 0$. On the other hand, B is proportional to the quark condensate in the chiral limit [9]. In Fig. 1 the wavy lines correspond to either the scalar or pseudoscalar external sources, the single straight lines to the pseudo-Goldstone bosons and the double lines to the scalar (S) and pseudoscalar (P) resonances. The cross in diagram (Sd) and (Pc) indicates the coupling between the scalar resonance and the vacuum. The dot in the diagrams (Sf) and (Pd) corresponds to the vertices involving only pseudo-Goldstone bosons beyond the leading order. They can stem from many sources, such as from the local terms that originate after removing the mixing between the pseudo-Goldstone bosons and the pseudoscalar resonances. A detailed account, including explicitly all the relevant expressions, will be presented in Ref. [14].

In $U(3)$ χPT it is necessary to resum the unitarity loops due to the large s-quark mass and the large anomaly mass. Consequently, the pseudo-Goldstone boson thresholds are much larger than the typical three-momenta in many kinematical regions, which increases the contributions from the reducible two pseudo-Goldstone boson loops [17]. Moreover, we are also interested in the resonance energy region where the unitarity upper bound in partial wave amplitudes can be easily reached, so that it does not make sense to treat unitarity perturbatively as in χPT for these energy regions. Hence one must resum the unitary cut and we use Unitary χPT (UχPT) to accomplish this resummation. This approach is based on the N/D method [18] to resum the unitarity chiral loops both for the partial wave scattering amplitudes and the form factors. The application of these unitarization techniques to the form factors is discussed in Refs. [19–21]. The partial waves from $U(3)$ unitary χPT plus the resonance exchanges at tree level were already discussed in Ref. [9], we now build the unitarized scalar form factors in a similar fashion [20]. Our master equation in matrix notation is

$$F^I(s) = \left[1 + N^{IJ}(s)g^{IJ}(s)\right]^{-1} R^I(s), \tag{3}$$

where

$$R^I(s) = F^I(s)^{(2)+\mathrm{Res}+\mathrm{Loop}} + T^{IJ}(s)^{(2)} g^{IJ}(s) F^I(s)^{(2)}. \tag{4}$$

In the previous equation $T^{IJ}(s)$ is a matrix whose elements are the partial wave scattering amplitudes with definite isospin I and angular momentum J. We refer to Ref. [9] for details about $T^{IJ}(s)$, $N^{IJ}(s)$ and $g^{IJ}(s)$. The quantity $F^I(s)^{(2)+\mathrm{Res}+\mathrm{Loop}}$ denotes the scalar form factors of the Goldstone pairs depicted in the first row of Fig. 1. The superscripts (2), Res and Loop stand for the perturbative results from the leading order, resonance contributions and chiral loops, respectively. The vector function $R^I(s)$ in Eq. (4) stems from the perturbative calculations of the form factors and it does not contain any cut singularity [19,20].

The two-point scalar and pseudoscalar correlators, Π_{S^a} and Π_{P^a}, respectively, are defined as

$$\delta^{ab}\Pi_R(p^2) = i\int d^4x\, e^{ip\cdot x}\langle 0|T\left[R^a(x)R^b(0)\right]|0\rangle, \tag{5}$$

with $R^a = S^a$ or P^a. After the establishment of the unitarized scalar form factors in Eq. (3), we are ready to calculate the scalar

[1] E.g. see Ref. [16] for a refined treatment of the pseudoscalar resonances as dynamically generated resonances from the interactions between the scalar resonances and the pseudo-Goldstone bosons.

spectral function or the imaginary part of the two-point scalar correlator

$$\operatorname{Im}\Pi_{S^a}(s)=\sum_i \rho_i(s)\left|F_i^a(s)\right|^2\theta\left(s-s_i^{\rm th}\right), \tag{6}$$

with $\theta(x)$ the Heaviside step function. The kinetic space factor $\rho_i(s)$ is defined as

$$\rho_i(s)=\frac{\sqrt{[s-(m_A+m_B)^2][s-(m_A-m_B)^2]}}{16\pi s}, \tag{7}$$

where m_A, m_B are the masses of the two particles in the ith channel, s is the energy squared in the center of mass frame and $s_i^{\rm th}=(m_A+m_B)^2$ denotes the threshold. We focus on the cases with $a=0$, 3 and 8, which conserve strangeness. The values $a=0$ and 8 correspond to the isoscalar case $I=0$, and there are five relevant channels: $\pi\pi$, $K\bar{K}$, $\eta\eta$, $\eta\eta'$ and $\eta'\eta'$. For $a=3$ one has the isovector case $I=1$ and three channels are involved: $\pi\eta$, $K\bar{K}$ and $\pi\eta'$. We adopt the isospin bases and employ the unitarity normalization as used in Ref. [9]. Another important observable that can be extracted from the scalar form factor is the quadratic pion scalar radius $\langle r^2\rangle_S^\pi$ defined from the Taylor expansion around the origin of the pion scalar form factor as

$$F_{\pi\pi}^{\bar{u}u+\bar{d}d}(s)=F_{\pi\pi}^{\bar{u}u+\bar{d}d}(0)\left[1+\frac{1}{6}\langle r^2\rangle_S^\pi s+\cdots\right], \tag{8}$$

with

$$\begin{aligned} m_\pi^2 F_{\pi\pi}^{\bar{u}u+\bar{d}d}(s)&\equiv 2Bm\langle 0|\bar{u}u+\bar{d}d|\pi\pi\rangle \\ &=2Bm\left[\frac{F_{\pi\pi}^{a=8}(s)}{\sqrt{3}}+\frac{\sqrt{2}F_{\pi\pi}^{a=0}(s)}{\sqrt{3}}\right], \end{aligned} \tag{9}$$

where m is the up or down current quark mass (isospin breaking is not considered in this work).

The pseudoscalar spectral function is related to the pseudoscalar form factors, $H_P^a(s)$, depicted in the second row of Fig. 1, by

$$\operatorname{Im}\Pi_{P^a}(s)=\sum_i \pi\delta\left(s-m_{P_i}^2\right)\left|H_i^a(s)\right|^2, \tag{10}$$

where we do not consider multiple-particle intermediate states. In the above equation $\delta(x)$ stands for the Dirac δ function, m_{P_i} corresponds to the masses of the pseudo-Goldstone bosons or the pseudoscalar resonances with the same quantum numbers as the considered spectral function.

Another interesting object that we study is the so-called semi-local (or average) duality in scattering [10,11]. We quantify semi-local duality in $\pi\pi$ scattering between the Regge theory and h.d.f., by employing the useful ratio between the amplitudes with well-defined I in the t-channel, as proposed in [11],

$$F_n^{II'}=\frac{\int_{\nu_1}^{\nu_{\rm max}}\nu^{-n}\operatorname{Im}T_{\rm t}^{(I)}(\nu,t)\,d\nu}{\int_{\nu_1}^{\nu_{\rm max}}\nu^{-n}\operatorname{Im}T_{\rm t}^{(I')}(\nu,t)\,d\nu}. \tag{11}$$

In this equation the isospin is indicated by the superscript and $\nu=\frac{s-u}{2}=\frac{2s+t-4m_\pi^2}{2}$, with s, t and u the standard Mandelstam variables. The relations between the t-channel well-defined isospin amplitudes, $T_{\rm t}^{(I)}(s,t)$, and those with well-defined isospin in the s-channel, $T_{\rm s}^{(I)}(s,t)$, are [10]

$$\begin{aligned} T_{\rm t}^{(0)}(s,t)&=\frac{1}{3}T_{\rm s}^{(0)}(s,t)+T_{\rm s}^{(1)}(s,t)+\frac{5}{3}T_{\rm s}^{(2)}(s,t),\\ T_{\rm t}^{(1)}(s,t)&=\frac{1}{3}T_{\rm s}^{(0)}(s,t)+\frac{1}{2}T_{\rm s}^{(1)}(s,t)-\frac{5}{6}T_{\rm s}^{(2)}(s,t),\\ T_{\rm t}^{(2)}(s,t)&=\frac{1}{3}T_{\rm s}^{(0)}(s,t)-\frac{1}{2}T_{\rm s}^{(1)}(s,t)+\frac{1}{6}T_{\rm s}^{(2)}(s,t). \end{aligned} \tag{12}$$

Since Regge exchange is highly suppressed for the exotic $I=2$ case in the t-channel, Regge theory predicts a vanishing value for the ratios F_n^{21} and F_n^{20}. In the following we shall focus on the ratio F_n^{21} to test semi-local duality in order to make a close comparison with Ref. [11]. We study the scattering for two values of t, $t=0$ (forward scattering) and $t=4m_\pi^2$, in order to test the stability of the results for different small values of t compared with GeV^2. The lower integration limit ν_1 is always set to the threshold point and we concentrate on the energy region with $\nu_{\rm max}=2$ GeV^2 for the ratio in Eq. (11). To calculate in Eq. (12) the imaginary parts of the t-channel well-defined isospin amplitudes, $\operatorname{Im}T_{\rm t}^{(I)}(s,t)$, we need to know $\operatorname{Im}T_{\rm s}^{(I)}(s,t)$, which can be decomposed in the center of mass frame in a partial wave expansion as

$$\operatorname{Im}T_{\rm s}^{(I)}(\nu,t)=\sum_J(2J+1)\operatorname{Im}T^{IJ}(s)P_J(z_s), \tag{13}$$

with $z_s=1+2t/(s-4m_\pi^2)$, the cosine of the scattering angle, and $P_J(z_s)$ the Legendre polynomials. The partial waves $T^{IJ}(s)$ were already carefully studied in Ref. [9] within $U(3)$ unitary χPT, and we extend the results there by including the contributions from the exchange of the pseudoscalar resonances.

We point out that all the parameters entering the form factors also appear in the unitarized scattering amplitudes and in the expressions for the masses of the pseudo-Goldstone bosons. Hence, once the unknown parameters are determined by the fit to scattering data and the pseudo-Goldstone masses, we can completely predict the form factors and spectral functions. By using the best fit in Eq. (55) of Ref. [9] for the calculation of the pion scalar form factor, a small quadratic pion scalar radius is obtained $\langle r^2\rangle_S^\pi=0.43$ fm^2, which is around 30% less than the dispersive result 0.61 fm^2 in [22]. One way to improve the pion scalar radius is to increase the value of L_5 [3]. It is found in Ref. [23] that a second multiplet of scalar resonances around 2 GeV contributes around 50% of L_5. Thus, we shall include this second scalar multiplet in our analysis and we take the values for its resonance parameters from the preferred fit Eq. (6.10) of Ref. [23]. The inclusion of this second scalar nonet and of the pseudoscalar resonance exchanges requires to perform a new fit. The resulting quality of the new fit and also the resonance spectroscopy, which will be given in detail in Ref. [14], are quite similar to the ones of Ref. [9], so we refrain from discussing them further here. But the new fit improves the pion scalar radius to $0.49^{+0.01}_{-0.03}$ fm^2, being around a 14% larger than the result from the best fit of Ref. [9].

Let us consider other interesting consequences of the new fit. As we commented previously, an important advantage of $U(3)$ χPT, compared with the $SU(2)$ or $SU(3)$ versions, is that it incorporates the singlet η_1 that becomes the ninth Goldstone boson at large N_C in the chiral limit and thus $U(3)$ χPT is more adequate to discuss the large N_C dynamics. The leading order N_C scaling for the various parameters in our theory was already given in [9]. For the pion decay constant F_π, we always take both the leading and sub-leading N_C terms which were calculated in Ref. [9] at the one-loop level in $U(3)$ χPT. In addition to only including the leading N_C behavior for the remaining parameters, referred as Scenario 1, we also consider other three scenarios that include sub-leading N_C scaling for the resonance parameters. Through the fit to experimental data, we determine the values of the parameters at $N_C=3$. By imposing short distance constraints, the resonance parameters that then result at large N_C are already discussed in many contexts [24–27]. Among these constraints, we take the one from the vector resonance sector, which should be quite reliable due to the well established $\rho(770)$ $\bar{q}q$-like resonance at large N_C. An updated version of the constraint on G_V, a coupling describing

Table 1
Description of Scenarios 1–4. In the second and third columns the symbol √ (–) denotes that the sub-leading N_C scaling for the corresponding parameters is (not) considered. In the last column, the symbol √ (–) means that we do (not) consider the contribution from the D-waves.

	G_V	M_ρ, M_{S_1}	D-wave
Scenario 1	–	–	–
Scenario 2	√	–	–
Scenario 3	√	√	–
Scenario 4	√	√	√

the vertices of the $\rho(770)$ with pions, is revealed in many recent works [25–27,9] as

$$G_V = \frac{F}{\sqrt{3}}, \tag{14}$$

with F the pion decay constant at large N_C. The extrapolation function for G_V is uniquely fixed if one considers contributions up to and including next-to-leading order in the large N_C expansion and requires G_V to take the value given by the fit at $N_C = 3$ and the result in Eq. (14) at large N_C. We present the detailed expressions in Ref. [14]. We refer the situation including the sub-leading piece for G_V as Scenario 2. In Scenario 3, on top of the setups in Scenario 2, we impose that M_ρ and M_{S_1} approach to the same value at large N_C, which can be realized naturally by tuning the corresponding parameters at the level of 16% from the values at $N_C = 3$. While in Scenario 4, we keep all the constraints from Scenario 3 and include the tensor resonances, which are the dominant contributions to the D-wave amplitudes. We follow Ref. [28] to include the tensor resonances in meson–meson scattering and also take the numerical value for the tensor coupling as determined there. The explicit calculation will be also given in detail in Ref. [14]. The characteristics of the different scenarios considered are summarized in Table 1. As proposed in Ref. [11], F_n^{21} with $n = 0, 1, 2$ and 3 are the relevant ratios in our considered energy region. We show the N_C evolution of the ratio F_n^{21} from Eq. (11) in Fig. 2 for $n = 0$ and 3. And more details for $n = 1$ and 2 will be given in Ref. [14].

Notice that if the required cancellations between the $I = 0$ and $I = 1$ partial wave amplitudes in Eq. (12) did not take place for $T_t^{(2)}(s,t)$, as they are required by Regge exchange theory, the natural value for $|F_n^{21}|$ would be around 1. While if the semi-local duality is satisfied, $|F_n^{21}|$ should approach to zero. So we conclude that Scenario 3 is the best one of the four situations. The main problem in Scenario 4 is that the tensor resonances give too large contributions and overbalance the $\rho(770)$ resonance for $n = 0$. This seems to indicate that once the tensor resonances are included, heavier vector resonances are needed so as to fulfill better semi-local duality for $n = 0$. A remarkably valuable information that we can get from the study of semi-local duality is its capacity to distinguish clearly between the different scenarios proposed and hence it provides a tight constraint on the N_C evolution of the resonance parameters. In the following we shall only focus on the N_C running within Scenario 3, since it is the one that satisfies best semi-local duality.

Now, we study the Weinberg-like spectral sum rules in the scalar and pseudoscalar sectors, which are given by

$$\int_0^{s_0} \left[\mathrm{Im}\,\Pi_R(s) - \mathrm{Im}\,\Pi_{R'}(s)\right] ds + \int_{s_0}^{\infty} \left[\mathrm{Im}\,\Pi_R(s) - \mathrm{Im}\,\Pi_{R'}(s)\right] ds = 0, \tag{15}$$

where $R, R' = S^a$ or P^a, with $a = 0, 8, 3$. With a proper choice of s_0, we can calculate the first integral employing the results from the present study in the non-perturbative region and use the results from the operator product expansion (OPE) to calculate the second one. According to the OPE study of Ref. [29] the different spectral functions considered here are equal in the asymptotic region in the chiral limit.[2] As a result the second integral in Eq. (15) is zero and to test how well the Weinberg-like spectral function sum rules hold reduces to the evaluation of the first integral in Eq. (15) in the energy region below $\sqrt{s_0}$. The relevant spectral functions $\mathrm{Im}\,\Pi_R$ are calculated through Eq. (6) for the scalar case and from Eq. (10) for the pseudoscalar one. To study the dependences of the first integral in Eq. (15) with s_0, we try three values of s_0, namely, $s_0 = 2.5$, 3.0 and 3.5 GeV^2 and we confirm that the results are quite stable for the different values taken. In order to display the results in a more compact way, we show the value of the integral separately for each spectral function

$$W_i = 16\pi \int_0^{s_0} \mathrm{Im}\,\Pi_i(s)\, ds, \quad i = S^8, S^0, S^3, P^0, P^8, P^3, \tag{16}$$

instead of the differences between the various correlators. We show the results for $W_i \times 3/N_C$ in Fig. 3 at the physical point and also their N_C evolution in the chiral limit. In order to study W_i in the chiral limit, we need to perform the chiral extrapolation. Though the resonance parameters are independent on the quark masses, the subtraction constants introduced through the unitarization procedure depend on them. Indeed it is shown in Ref. [30]

[2] The calculation in Ref. [29] is done up to $\mathcal{O}(\alpha_s)$ and including up to dimension 5 operators.

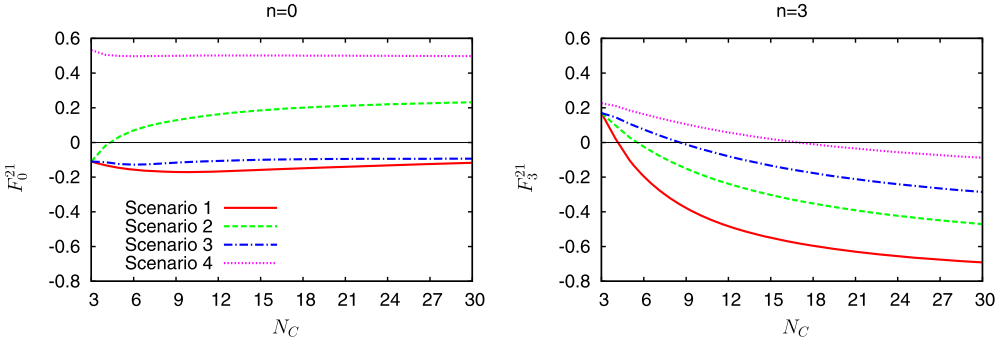

Fig. 2. Evolution of $F_n^{21}(t = 4m_\pi^2)$ from $N_C = 3$ to 30 for the four scenarios considered. See the text and Table 1 for the meaning of each scenario. We verify that the ratios evaluated at $t = 0$ are similar.

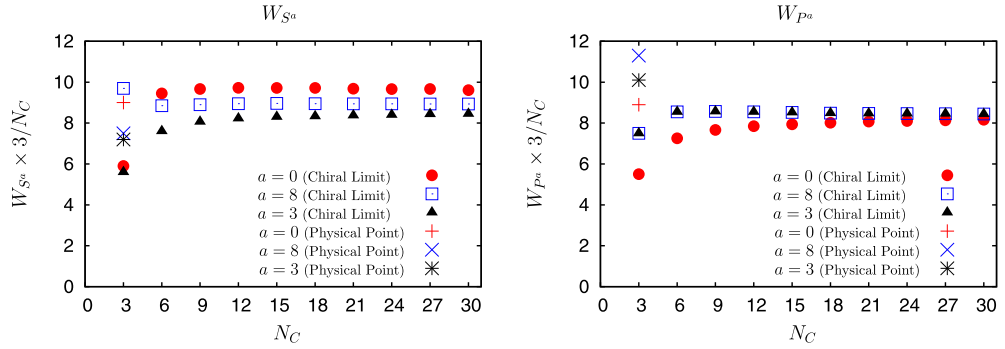

Fig. 3. $W_i \times 3/N_C$ as a function of N_C within Scenario 3. All of the results are calculated by setting the upper limit of the integral in Eq. (16) to $s_0 = 3$ GeV^2. We check that the results with $s_0 = 2.5$ GeV^2 and $s_0 = 3.5$ GeV^2 are quite similar.

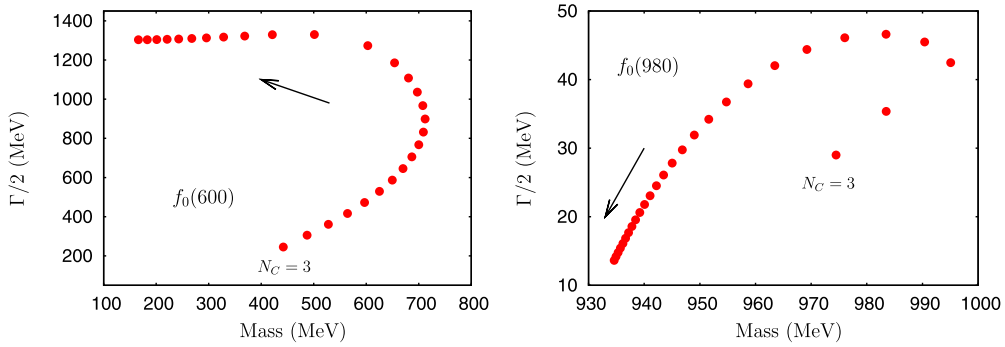

Fig. 4. Pole trajectories as a function of N_C for the resonances $f_0(600)$ and $f_0(980)$. We show the results from $N_C = 3$ to 30 in one unit step.

that in the $SU(3)$ limit case (as in the chiral limit) all of them should be the same for any PQ pair involving the π, K and η_8 pseudoscalars. Indeed, we find that in the chiral limit there exists a reasonable region for a common value of all the subtraction constants where the values of the two-point correlators are stable and Weinberg sum rules are improved comparing with the physical situation. This region includes values similar to the ones fitted. In Fig. 3, we show the typical result in this region and normalize by the factor $3/N_C$ because W_i scales as N_C, as it is also clear from the results plotted in the figure. Focusing on the points at the chiral limit case in Fig. 3, the relative variance among the six numbers, i.e. the square root of the variance divided by their mean value [14], is found to be 10%, implying that the Weinberg-like spectral function sum rules in the SS–SS, PP–PP and SS–PP sectors hold quite accurately. The fulfillment of these sum rules even improves at large N_C and the relative variance reduces to 5% for $N_C = 30$.

Up to now, we have shown that our formalism can simultaneously fulfill semi-local duality between the Regge theory and h.d.f. and the Weinberg-like spectral function sum rules both for the physical case and large values of N_C. Of course this success is based on the fact that we properly take the N_C scaling for the resonance parameters dictated by the short distance constraint. It is interesting to de-construct the ratio F_n^{21} and the Weinberg-like spectral sum rules to see how different resonances contribute to them. At the physical case, we obtain the spectroscopy for various resonances, such as $f_0(600)$, $f_0(980)$, $f_0(1370)$, $a_0(980)$, $a_0(1450)$, $K_0^*(800)$ (also called κ), $K_0^*(1430)$, $\rho(770)$, $K^*(892)$ and $\phi(1020)$, and they agree quite well with their properties reported in the PDG [15]. Taking F_3^{21} as an example, we observe an interesting interplay between the $f_0(600)$ and $f_0(980)$ resonances in the N_C evolution. In Fig. 4, we show the N_C trajectories for the $f_0(600)$ and $f_0(980)$, from left to right, respectively. More details about the other resonances will be displayed elsewhere [14]. For the physical situation, both $f_0(600)$ and $\rho(770)$ give important contributions to F_3^{21}, which leads to a significant cancellation between each other, that is necessary in order to guarantee semi-local duality. While the $f_0(980)$ only plays a marginal role. But when N_C increases, the $f_0(600)$ pole as shown in Fig. 4 and in Ref. [9], blows up in the complex energy plane and does not play any significant role at large N_C. In contrast, the $\rho(770)$ resonance falls down to the real axis [31,9], behaving as a standard $\bar{q}q$-like resonance at large N_C, and definitely contributes to the ratio F_3^{21}. The scalar strength to cancel the contribution from the $\rho(770)$ comes now from the $f_0(980)$ resonance, which gradually evolves to the singlet scalar $\bar{q}q$-like S_1 when increasing N_C.

It is also worth comparing our results with those from the previous works [11,31,32] based on the use of the Inverse Amplitude Method [33]. The N_C trajectories shown in Fig. 4, confirm again the results obtained in [31,32] which predict a non-dominant $\bar{q}q$ behavior for the $f_0(600)$. The latter was explained in terms of different kind of resonances in Ref. [34]. Note that the $f_0(600)$ behavior in Fig. 4, moving towards lower masses and larger widths, was found in Refs. [11,35] by varying the renormalization scale where the N_C scaling of the χPT low energy constants applies. Let us remark that, as it happens in Ref. [11], in order to satisfy semi-local duality, we also need a $\bar{q}q$ component around 1 GeV. However, this work presents an alternative to Refs. [32,11] because at $N_C = 3$ such a $\bar{q}q$ component would belong to the $f_0(980)$ instead to the $f_0(600)$.

Large cancellations are also required to satisfy the Weinberg-like spectral function sum rules. For the physical case, the singlet correlator W_{S^0} receives important contributions both from the $f_0(600)$ and $f_0(980)$. The octet W_{S^8} mainly gets contribution from the $f_0(1370)$ resonance and is also slightly contributed by the $f_0(600)$ and $f_0(980)$. For W_{S^3}, the $a_0(980)$ peak dominates its

spectral function, though it receives non-negligible contributions from the $a_0(1450)$. However at large N_C, the $a_0(980)$ resonance goes deep in the complex energy plane, like the $f_0(600)$ for the isoscalar case, and hence it does not contribute to W_{S^3} any more. Instead, the $a_0(1450)$ becomes more important when increasing N_C and finally matches the contributions from the $f_0(980)$ in the singlet correlator W_{S^0} and $f_0(1370)$ in W_{S^8}, so that the Weinberg-like spectral function sum rules at large N_C are well satisfied.

Finally, we summarize briefly our work. We perform a complete one-loop calculation of the scalar and pseudoscalar form factors within $U(3)$ unitary χPT, including the tree-level exchange of resonances. The spectral functions of the two-point correlators are constructed by using the resulting form factors (which are unitarized for the case of the scalar ones). After updating the fit in Ref. [9], which is also extended by including the explicit exchange of pseudoscalar resonances, we study the resonance spectroscopy, quadratic pion scalar radius, and the fulfillment of semi-local duality and the Weinberg-like spectral function sum rules in the *SS–SS*, *PP–PP* and *SS–PP* cases, which are well satisfied. We show that it is important to take under consideration the high energy constraint for G_V, Eq. (14), in order to keep semi-local duality when varying N_C. An interesting interplay between different resonances when studying the N_C evolution of semi-local duality and the Weinberg-like spectral sum rules is revealed. In the former case the scalar and vector spectra appear tightly related and in the latter one the same can be stated for the scalar and pseudoscalar ones.

The idea to study the Weinberg sum rules in $U(3)$ χPT was brought up by our colleague J. Prades, who unfortunately passed away. We would like to express our gratitude to his help in this subject. We also acknowledge the valuable discussions with J.R. Peláez. This work is partially funded by the grants MEC FPA2010-17806, the Fundación Séneca 11871/PI/09, the BMBF grant 06BN411, the EU-Research Infrastructure Integrating Activity "Study of Strongly Interacting Matter" (HadronPhysics2, grant No. 227431) under the Seventh Framework Program of EU and the Consolider-Ingenio 2010 Programme CPAN (CSD2007-00042). Z.H.G. also acknowledges the grants National Natural Science Foundation of China (NSFC) under contract No. 11105038, Natural Science Foundation of Hebei Province with contract No. A2011205093 and Doctor Foundation of Hebei Normal University with contract No. L2010B04.

References

[1] S. Weinberg, Phys. A 96 (1979) 327.
[2] J. Gasser, H. Leutwyler, Ann. Phys. 158 (1984) 142.
[3] J. Gasser, H. Leutwyler, Nucl. Phys. B 250 (1985) 465.
[4] P. Di Vecchia, G. Veneziano, Nucl. Phys. B 171 (1980) 253;
C. Rosenzweig, J. Schechter, T. Trahem, Phys. Rev. D 21 (1980) 3388;
E. Witten, Ann. Phys. 128 (1980) 363.
[5] G. 't Hooft, Nucl. Phys. B 72 (1974) 461;
E. Witten, Nucl. Phys. B 160 (1979) 57.
[6] E. Witten, Nucl. Phys. B 156 (1979) 269.
[7] P. Herrera-Siklody, J.I. Latorre, P. Pascual, J. Taron, Nucl. Phys. B 497 (1997) 345.
[8] R. Kaiser, H. Leutwyler, Eur. Phys. J. C 17 (2000) 623.
[9] Z.-H. Guo, J.A. Oller, Phys. Rev. D 84 (2011) 034005.
[10] P.D.B. Collins, An Introduction to Regge Theory and High Energy Physics, Cambridge University Press, Cambridge, 1977.
[11] J.R. Peláez, M.R. Pennington, J. Ruiz de Elvira, D.J. Wilson, Phys. Rev. D 84 (2011) 096006.
[12] S. Weinberg, Phys. Rev. Lett. 18 (1967) 507;
C.W. Bernard, A. Duncan, J. LoSecco, S. Weinberg, Phys. Rev. D 12 (1975) 792.
[13] G. Ecker, J. Gasser, A. Pich, E. de Rafael, Nucl. Phys. B 321 (1989) 311.
[14] Z.-H. Guo, J.A. Oller, J. Ruiz de Elvira, forthcoming.
[15] K. Nakamura, et al., J. Phys. G 37 (2010) 075021.
[16] M. Albaladejo, J.A. Oller, L. Roca, Phys. Rev. D 82 (2010) 094019.
[17] S. Weinberg, Nucl. Phys. B 363 (1991) 3.
[18] J.A. Oller, E. Oset, Phys. Rev. D 60 (1999) 074023.
[19] J.A. Oller, E. Oset, J.E. Palomar, Phys. Rev. D 63 (2001) 114009.
[20] U.-G. Meißner, J.A. Oller, Nucl. Phys. A 679 (2001) 671.
[21] J.A. Oller, Phys. Rev. D 71 (2005) 054030.
[22] G. Colangelo, J. Gasser, H. Leutwyler, Nucl. Phys. B 603 (2001) 125.
[23] M. Jamin, J.A. Oller, A. Pich, Nucl. Phys. B 622 (2002) 279.
[24] G. Ecker, J. Gasser, H. Leutwyler, A. Pich, E. de Rafael, Phys. Lett. B 223 (1989) 425.
[25] A. Pich, I. Rosell, J.J. Sanz-Cillero, JHEP 1102 (2011) 109.
[26] Z.-H. Guo, P. Roig, Phys. Rev. D 82 (2010) 113016.
[27] Z.-H. Guo, J.J. Sanz-Cillero, H.-Q. Zheng, JHEP 0706 (2007) 030.
[28] G. Ecker, C. Zauner, Eur. Phys. J. C 52 (2007) 315.
[29] M. Jamin, M. Munz, Z. Phys. C 60 (1993) 569.
[30] D. Jido, J.A. Oller, E. Oset, A. Ramos, U.G. Meissner, Nucl. Phys. A 725 (2003) 181.
[31] J.R. Peláez, Phys. Rev. Lett. 92 (2004) 102001.
[32] J.R. Peláez, G. Rios, Phys. Rev. Lett. 97 (2006) 242002.
[33] A. Dobado, M.J. Herrero, T.N. Truong, Phys. Lett. B 235 (1990) 134;
A. Dobado, J.R. Peláez, Phys. Rev. D 56 (1997) 3057;
J.A. Oller, E. Oset, J.R. Peláez, Phys. Rev. Lett. 80 (1998) 3452;
J.A. Oller, E. Oset, J.R. Peláez, Phys. Rev. D 59 (1999) 074001;
J.A. Oller, E. Oset, J.R. Peláez, Phys. Rev. D 60 (1999) 099906 (Erratum);
J.A. Oller, E. Oset, J.R. Peláez, Phys. Rev. D 75 (2007) 099903 (Erratum).
[34] F.J. Llanes-Estrada, J.R. Pelaez, J. Ruiz de Elvira, Nucl. Phys. B (Proc. Suppl.) 207–208 (2010) 169.
[35] J.R. Pelaez, hep-ph/0509284.

2.2.5 Publication:Zhi-Hui Guo, J.A. Oller, J. Ruiz de Elvira, *Chiral dynamics in form factors, spectral-function sum rules, meson-meson scattering and semi-local duality, Phys. Rev.* D86 054006 (2012)

PHYSICAL REVIEW D **86,** 054006 (2012)

Chiral dynamics in form factors, spectral-function sum rules, meson-meson scattering and semilocal duality

Zhi-Hui Guo,[1,2,*] J. A. Oller,[2,†] and J. Ruiz de Elvira[3,‡]

[1]*Department of Physics, Hebei Normal University, 050024 Shijiazhuang, People's Republic of China*
[2]*Departamento de Física, Universidad de Murcia, E-30071 Murcia, Spain*
[3]*Departamento de Física Teórica II, Universidad Complutense de Madrid, E-28040 Madrid, Spain*

(Received 22 June 2012; published 7 September 2012)

In this work, we perform the one-loop calculation of the scalar and pseudoscalar form factors in the framework of $U(3)$ chiral perturbation theory with explicit tree level exchanges of resonances. The meson-meson scattering calculation from Guo and Oller [Phys. Rev. D **84**, 034005 (2011)] is extended as well. The spectral functions of the nonet scalar-scalar (SS) and pseudoscalar-pseudoscalar (PP) correlators are constructed by using the corresponding form factors. After fitting the unknown parameters to the scattering data, we discuss the resonance content of the resulting scattering amplitudes. We also study spectral-function sum rules in the $SS-SS$, $PP-PP$, and $SS-PP$ sectors as well as semilocal duality from scattering. The former relate the scalar and pseudoscalar spectra between themselves while the latter mainly connects the scalar spectrum with the vector one. Finally we investigate these items as a function of N_C for $N_C > 3$. All these results pose strong constraints on the scalar dynamics and spectroscopy that are discussed. They are successfully fulfilled by our meson-meson scattering amplitudes and spectral functions.

DOI: 10.1103/PhysRevD.86.054006 PACS numbers: 12.39.Fe, 11.15.Pg, 11.55.Hx, 12.40.Nn

I. INTRODUCTION

Spectral functions of current-current correlators are interesting objects in hadron physics. They are sensitive to both low- and high-energy dynamics of QCD, which can be evaluated in two reliable approaches: chiral perturbation theory (χPT) [1–3] in the low-energy region and the operator product expansion (OPE) [4,5] for the higher one. The celebrated Weinberg sum rules are in fact derived by studying the differences of the vector-vector and axial-vector–axial-vector spectral functions [6], where not only the low and asymptotic energy regions but also the resonance region are considered. After that, great progress, on both the experimental and theoretical sides [7], has been made along this research line. The vector and axial-vector spectral functions are experimentally measurable quantities, mainly through the τ decays, due to the noticeable $V-A$ nature of the Standard Model in the energy region well below the W boson mass.

Concerning the scalar and pseudoscalar spectral functions, there are no direct experimental data. However, great efforts have been made on the theoretical sides both in perturbative QCD calculations [8–10], which are important to reduce the QCD background in the search of the Higgs particle, and in the nonperturbative QCD region [2,11–19]. Through the matching between the low- and high-energy behaviors of the spectral functions, valuable information can be obtained: light quark masses and Cabibbo angle $|V_{us}|$ [8,17,18], determination of the low-energy constants (LECs) in χPT [11,12,15,16,20], and constraints on resonance parameters [13,15,16,19,21,22].

On the other hand, in the past decade scalar dynamics in the nonperturbative QCD region has been greatly put forward thanks to the combination of χPT and nonperturbative approaches from the S-matrix theory [23–34]. One of the main results is the reappearance of the broad $f_0(500)$ (traditionally called σ), the lightest resonance in the QCD spectrum, after its long absence in the Particle Data Group (PDG) list [35]. Later on the $K_0^*(800)$ or κ resonance in $K\pi$ scattering was also confirmed [35]. Though the mass and width of these broad scalar resonances predicted by different groups are rather consistent among each other, other properties about the resonances in the scalar family are still under a vivid debate (e.g. their nature).

The scalar-scalar (SS) and pseudoscalar-pseudoscalar (PP) correlation functions provide us another theoretical tool to further study the scalar resonances [36], once the phase shifts and inelasticities in meson-meson scattering are well reproduced [24–26,28–34,37]. As derived in Refs. [11,12,19,38,39] these correlator functions should fulfill a set of spectral-function sum rules that imply tight constraints to the scalar and pseudoscalar spectra, involving nontrivial relations between them.

We take, and further study, the meson-meson scattering amplitudes of Ref. [40] that are calculated in one-loop $U(3)$ χPT plus the explicit scalar and vector resonance exchanges at tree level within the framework of resonance chiral theory (RχT) [41]. As a novelty, we include the contributions from the tree level exchange of pseudoscalar resonances in this work so that a new fit to data is also

*guo@um.es
†oller@um.es
‡jacobore@rect.ucm.es

discussed. The unitarized $U(3)$ χPT amplitudes are more appropriate to incorporate the heavier f_0 scalar resonances since the channels involving the η and η' mesons can be taken into account [while $SU(3)$ χPT [3] only contains the pure octet η_8 field]. As noticed in Ref. [25], further developed later in Refs. [33,40,42–48], the study of the resonance pole trajectories with increasing number of colors of QCD, N_C, is of interest to discern possible natures of the scalar resonances. For example, a $\bar{q}q$ resonance evolves with a mass $M \sim \mathcal{O}(N_C^0)$, while its width decreases as $\Gamma \sim \mathcal{O}(N_C^{-1})$. For the case of a glueball its mass behaves also as $M \sim \mathcal{O}(N_C^0)$ with a width that decreases faster with N_C as $\Gamma \sim \mathcal{O}(N_C^{-2})$ [49,50]. In this respect $U(3)$ χPT is also more adequate than the $SU(3)$ version to discuss the large N_C limit because $U(3)$ χPT includes not only the pseudo-Goldstone octet, as $SU(3)$ does, but also the singlet η_1 that in the chiral limit is the ninth Goldstone boson at large N_C [51]. In this way, $U(3)$ χPT has the appropriate low-energy degrees of freedom in the chiral limit at large N_C. Additionally, as stressed in Ref. [40], the η meson quickly becomes much lighter with increasing N_C [52]. This fact has a strong impact on the dependence with N_C of the pole trajectories of the scalar resonances, except for the $f_0(500)$, because of its weak couplings to the channels with η and η' [40]. We show below the N_C pole trajectories for the different resonances involved in our study from the new fit to data.

Another interesting property of strong interactions that can be used to restrict meson-meson scattering is average or semilocal duality [53]. It allows one to relate the crossed channel dynamics with the s-channel one, which supplies another stringent constraint on the resonance properties involved in scattering. In a recent work [54], Peláez *et al.* have investigated how semilocal duality between the light resonances of QCD and Regge theory can be satisfied in $\pi\pi$ scattering. These authors employ the inverse amplitude method (IAM) [55–58] to unitarize the $SU(3)$ one-loop and $SU(2)$ two-loop χPT amplitudes. The main conclusion of Ref. [54] is that in the physical case, i.e. when $N_C = 3$, the $f_0(500)$ resonance, with its pole position around $440 - i250$ MeV, plays a crucial role to oppose the vector strength from the $\rho(770)$ resonance, which guarantees the fulfillment of semilocal duality.

Having introduced the main research topics considered here for the sake of clarity, we summarize our work and briefly comment on the main points and results obtained by considering these topics. A complete one-loop calculation of the scalar and pseudoscalar form factors within $U(3)$ unitary χPT, including the tree level exchange of scalar, pseudoscalar, and vector resonances, is undertaken. The spectral functions of the SS and PP two-point correlators are constructed by using the resulting scalar and pseudoscalar form factors, respectively, which are unitarized for the case of the scalar ones. After updating the fit in Ref. [40], which is also extended by including the explicit exchange of pseudoscalar resonances, we study the resonance spectroscopy, quadratic pion scalar radius, the fulfillment of semilocal duality, and the spectral-function sum rules in the $SS - SS$, $PP - PP$, and $SS - PP$ cases, which are remarkably well satisfied simultaneously. We show that it is important to take under consideration the high-energy constraint for the coupling of the vector resonances to pseudo-Goldstone bosons, in order to keep semilocal duality when varying N_C. An interesting interplay between different resonances when studying the N_C evolution of semilocal duality and the spectral-function sum rules is revealed. In the former case the scalar and vector spectra appear tightly related, and in the latter one the same can be stated for the scalar and pseudoscalar ones. This issue is closely connected with the evolution of the resonance pole position with varying N_C of the pseudoscalar, vector, and scalar resonances.

In this respect, for larger N_C, the authors of Ref. [54] revealed that a $\bar{q}q$ subdominant component for the $f_0(500)$, with a mass around 1 GeV and obtained for some sets of LECs in both one-loop and two-loop calculations, is needed in order to fulfill semilocal duality. For those solutions, the $f_0(500)$ pole moves away from the 400–700 MeV region of the real axis, but it turns around moving back toward the real axis above 1 GeV as N_C becomes larger than 8 or so. The interpretation of these results was studied preliminarily in Ref. [59], where the $f_0(500)$ is considered as a combination of several states and it was found that the weight of the subdominant $\bar{q}q$ component in the $f_0(500)$ grows with increasing N_C. Immediately, one can ask a question: apart from the $f_0(500)$ resonance, which is only marginally contributed by this $\bar{q}q$ component, are there any other more obvious effects from the $\bar{q}q$ seed at $N_C = 3$? If there are, what kind of role do these effects play in the fulfillment of semilocal duality?

Concerning the first question, we provide here, confirming Refs. [25,40], a scenario for an affirmative answer. A bare singlet scalar resonance S_1, with its bare mass around 1 GeV, is found significant [40] to reproduce the $\pi\pi$ and $K\bar{K}$ scattering data around the $f_0(980)$ energy region and, thus, becomes an important part of the $f_0(980)$ resonance in the physical case, i.e. at $N_C = 3$. When increasing N_C, the physical $f_0(980)$ resonance gradually evolves to the singlet S_1, which acts as the role of the $\bar{q}q$ seed described in Refs. [54,59]. Apparently, the scenario that we provide now is different from that in Ref. [54], since in the latter reference the signal of the $f_0(980)$ resonance gradually disappears when increasing N_C.[1] Regarding the second question raised in the previous paragraph we find here that its role for fulfilling the requirements of semilocal duality becomes more important with increasing N_C, being only of little importance at $N_C = 3$. This behavior is in qualitative agreement with the results of [54].

[1]See the left panel of Fig. 1 in Ref. [54]. It is verified that the peak around 1 GeV^2 finally disappears with larger values of N_C.

In addition to the results presented in our short letter [36], we show our theoretical calculations in detail and discuss more phenomenological materials in this work, such as the fit results, resonance pole positions and their coupling strengths, and N_C trajectories for all the relevant resonances. The contents of this article are organized as follows. Section II is devoted to the introduction of the relevant chiral Lagrangian. In Secs. III and IV, we present the details of the calculations of the spectral functions and the quantities to measure the degree of fulfillment of semilocal duality, respectively. The phenomenological discussions are given in Sec. V, which include the fit of unknown parameters to the experimental data and its consequences on the form factors, spectral functions, spectral-function sum rules, and semilocal duality. Section VI is then devoted to the study of the N_C evolution of these quantities. Finally, we conclude in Sec. VII.

II. CHIRAL LAGRANGIAN

The theoretical framework that we use in the present work is $U(3)$ χPT [60,61], the tree level resonance exchanges from chiral invariant Lagrangians [41] and unitary χPT [25,62]. The $U(3) \otimes U(3)$ chiral symmetry in u, d, s massless QCD is broken because of quantum effects that violate the conservation of the singlet axial-vector current by the $U_A(1)$ anomaly [63–65]. As a result the pseudoscalar η' is not a pseudo-Goldstone boson [66]. Nevertheless, from the large N_C QCD point of view the quark loop responsible for the $U_A(1)$ anomaly [63] is $1/N_C$ suppressed. In this way, the η' becomes the ninth pseudo-Goldstone boson in the large N_C limit [51]. In large N_C QCD the singlet field η_1 can be conveniently incorporated into the effective field theory by enlarging the number of degrees of freedom of the theory from an octet to a nonet of pseudo-Goldstone bosons, which is usually called $U(3)$ χPT [60]. In this theory there are three expansion parameters: momentum, quark masses, and $1/N_C$, giving rise to a joint triple expansion $\delta \sim p^2 \sim m_q \sim 1/N_C$. We briefly recapitulate the relevant chiral Lagrangians for our work.

The leading order Lagrangian in $U(3)$ χPT reads [60]

$$\mathcal{L}_\chi = \frac{F^2}{4}\langle u_\mu u^\mu\rangle + \frac{F^2}{4}\langle \chi_+\rangle + \frac{F^2}{3}M_0^2 \ln^2 \det u, \quad (1)$$

where $\langle\cdots\rangle$ stands for the trace in flavor space and the last operator is the $U_A(1)$ anomaly term that gives rise to the singlet η_1 mass. The definitions for the chiral building blocks are

$$\begin{aligned} u_\mu &= iu^+ D_\mu U u^+, \qquad \chi_\pm = u^+\chi u^+ \pm u\chi^+ u, \\ U &= u^2 = e^{i\frac{\sqrt{2}\Phi}{F}}, \qquad D_\mu U = \partial_\mu U - ir_\mu U + iUl_\mu, \\ &\chi = 2B(s+ip), \end{aligned} \quad (2)$$

where r_μ, l_μ, s, p are external sources [2] and the pseudo-Goldstone bosons are collected in the matrix

$$\Phi = \begin{pmatrix} \frac{1}{\sqrt{2}}\pi^0 + \frac{1}{\sqrt{6}}\eta_8 + \frac{1}{\sqrt{3}}\eta_1 & \pi^+ & K^+ \\ \pi^- & \frac{-1}{\sqrt{2}}\pi^0 + \frac{1}{\sqrt{6}}\eta_8 + \frac{1}{\sqrt{3}}\eta_1 & K^0 \\ K^- & \bar{K}^0 & \frac{-2}{\sqrt{6}}\eta_8 + \frac{1}{\sqrt{3}}\eta_1 \end{pmatrix}. \quad (3)$$

The axial decay constant of the pseudo-Goldstone bosons in the simultaneous chiral and large N_C limit is denoted by F. In the same limit the parameter B is related to the quark condensate through $\langle 0|\bar{q}^i q^j|0\rangle = -F^2 B\delta^{ij}$. We do not consider isospin (I) breaking effects throughout.

In the present work, we exploit the assumption on the resonance saturation of the LECs [41,67], so that, instead of local chiral terms contributing to meson-meson scattering, we take the tree level exchanges of the scalar, pseudoscalar, and vector resonances. In this way we keep all local contributions to meson-meson scattering up to and including $\mathcal{O}(\delta^3)$, while also generating higher order ones. We also include the one-loop contributions that count one order higher in δ, as calculated in Ref. [40].

The terms that describe the interactions between scalar resonances and pseudo-Goldstone bosons in RχT are[2] [41]

$$\mathcal{L}_S = c_d\langle S_8 u_\mu u^\mu\rangle + c_m\langle S_8\chi_+\rangle + \tilde{c}_d S_1\langle u_\mu u^\mu\rangle + \tilde{c}_m S_1\langle\chi_+\rangle, \quad (4)$$

and for the vector resonances it reads

$$\mathcal{L}_V = \frac{iG_V}{2\sqrt{2}}\langle V_{\mu\nu}[u^\mu, u^\nu]\rangle, \quad (5)$$

where the antisymmetric tensor formalism is used to describe the vector resonances [41]. In addition, we also include the pseudoscalar resonances in this work, which are not considered in Ref. [40]. The relevant Lagrangian reads [41]

$$\mathcal{L}_P = id_m\langle P_8\chi_-\rangle + i\tilde{d}_m P_1\langle\chi_-\rangle. \quad (6)$$

The corresponding kinetic terms for the resonance fields are [41]

$$\mathcal{L}_{\rm kin}^V = -\frac{1}{2}\left\langle \nabla^\lambda V_{\lambda\mu}\nabla_\nu V^{\nu\mu} - \frac{1}{2}M_V^2 V_{\mu\nu}V^{\mu\nu}\right\rangle, \quad (7)$$

[2]The terms $\hat{c}_d\langle S_9 u_\mu\rangle\langle u_\mu\rangle + \hat{c}_m S_1 \ln^2\det u$ were also introduced in Ref. [40] but found phenomenologically irrelevant. This is in agreement with the fact that from the exchange of scalar resonances they start to generate tree level meson-meson contributions that are of higher order, $\mathcal{O}(\delta^4)$.

$$\mathcal{L}_{\rm kin}^{R} = \frac{1}{2}\langle \nabla^{\mu} R_8 \nabla_{\mu} R_8 - M_{R_8}^2 R_8^2 \rangle + \frac{1}{2}(\partial^{\mu} R_1 \partial_{\mu} R_1 - M_{R_1}^2 R_1^2), \tag{8}$$

where the symbol R refers to either scalar or pseudoscalar resonances.

One should notice that the operators appearing in Eq. (6) cause mixing terms proportional to the quark masses between the pseudoscalar resonances and the pseudo-Goldstone bosons. Though it is not a problem to consider this effect in the calculation of Feynman diagrams, it would be convenient to eliminate the mixing terms at the Lagrangian level. Indeed this can be accomplished by performing the following field redefinition in a chiral covariant way:

$$\begin{aligned} P_8 &\to \bar{P}_8 + i\frac{d_m}{M_{P_8}^2}\left(\chi_- - \frac{1}{3}\langle \chi_- \rangle I_{3\times 3}\right), \\ P_1 &\to \bar{P}_1 + i\frac{\tilde{d}_m}{M_{P_1}^2}\langle \chi_- \rangle, \end{aligned} \tag{9}$$

with $I_{3\times 3}$ the unit 3×3 matrix. Substituting Eq. (9) into Eqs. (6) and (8), we have the new Lagrangian

$$\begin{aligned} \mathcal{L}_{\bar{P}} =& \frac{1}{2}\langle \nabla^{\mu}\bar{P}_8 \nabla_{\mu}\bar{P}_8 - M_{P_8}^2 \bar{P}_8^2 \rangle + \frac{1}{2}(\partial^{\mu}\bar{P}_1 \partial_{\mu}\bar{P}_1 - M_{P_1}^2 \bar{P}_1^2) \\ &+ i\frac{d_m}{M_{P_8}^2}\langle \nabla_{\mu}\bar{P}_8 \nabla^{\mu}\chi_- \rangle + i\frac{\tilde{d}_m}{M_{P_1}^2}\nabla_{\mu}\bar{P}_1 \nabla^{\mu}\langle \chi_- \rangle \\ &- \frac{d_m^2}{2M_{P_8}^2}\langle \chi_- \chi_- \rangle + \left(\frac{d_m^2}{6M_{P_8}^2} - \frac{\tilde{d}_m^2}{2M_{P_1}^2}\right)\langle \chi_- \rangle\langle \chi_- \rangle + \cdots, \end{aligned} \tag{10}$$

where the omitted terms, represented by the dots in the last line, denote the local chiral operators that describe the interactions between the pseudo-Goldstone bosons at $\mathcal{O}(p^6)$ that we disregard throughout. We point out that the above procedure only eliminates the mixing terms between the pseudoscalar resonances and pseudo-Goldstone bosons that are linearly proportional to quark masses. The new mixing terms with higher power of quark masses that arise through the operators in the second line of Eq. (10) are $\mathcal{O}(p^6)$ contributions, which are then not considered in this work. It is interesting to point out that after the field redefinition of Eq. (9), two new operators describing interactions between pseudo-Goldstone bosons appear, i.e. the ones in the third line of Eq. (10). They coincide with the $\mathcal{O}(p^4)$ terms that result from the integration of the pseudoscalar resonances [41].

We remind the reader that the nature of the pseudoscalar resonances is still a somewhat debated issue and also that typically the parameters of those resonances are not determined accurately [35]. In Ref. [68] the pseudoscalar resonances are generated dynamically due to the interactions between the scalar resonances and the pseudo-Goldstone bosons, instead of introducing them as basic degrees of freedom at the Lagrangian level. In order to compensate for the uncertainties arising from the not well settled properties of the pseudoscalar resonances, as well as from the simple tree level exchanges with bare propagators that we take here to describe them (neglecting more involved contributions as those pointed out in Ref. [68]), we introduce an L_8-like operator [3] in our study

$$\frac{\delta L_8}{2}\langle \chi_+\chi_+ + \chi_-\chi_- \rangle. \tag{11}$$

The reason behind is that only L_8 and L_7 could receive contributions at the $\mathcal{O}(p^4)$ level after the integration of the pseudoscalar resonances from Eqs. (6) and (8). Nevertheless the L_7 term vanishes if one further imposes the large N_C relations for the pseudoscalar resonances (as we take here)

$$\tilde{d}_m = \frac{d_m}{\sqrt{3}}, \tag{12}$$

$$M_{P_1} = M_{P_8}. \tag{13}$$

We stress that δL_8 is different from L_8 in the χPT Lagrangian [3] and their relation can be written as

$$L_8^{\chi\rm PT} = L_8^{\rm Resonances} + \delta L_8. \tag{14}$$

So that we interpret δL_8 as the contributions from some remnant pieces that are subleading in $1/N_C$, minding that the leading N_C contributions are already included in the resonance part.

Finally, there are two relevant terms at $\mathcal{O}(\delta)$ that only incorporate pseudo-Goldstone bosons [69] and cannot be generated from the exchange of the explicit resonance fields discussed above. These contributions are

$$\begin{aligned} &\mathcal{L}_{\Lambda} = \Lambda_1 \frac{F^2}{12} D_{\mu}\psi D^{\mu}\psi - i\Lambda_2 \frac{F^2}{12}\langle U^+\chi - \chi^+ U\rangle\psi, \\ &\psi = -i\,\mathrm{ln}\,\mathrm{det}U, \qquad D_{\mu}\psi = \partial_{\mu}\psi - 2\langle a_{\mu}\rangle, \end{aligned} \tag{15}$$

with $a_{\mu} = (r_{\mu} - l_{\mu})/2$. As we commented in Ref. [40] the Λ_1 parameter only affects the calculation of the masses, scattering amplitudes, and also the scalar and pseudoscalar form factors in an indirect way, i.e. through the renormalization of the η_1 field, and its effect in the global fit is tiny. We explicitly check that if we include Λ_1 in our discussion, the fitted value for this parameter approaches zero. This operator is not considered in the following.

For the remaining definitions of the basic chiral building blocks, the reader is referred to Ref. [40] and references therein for further details.

III. SPECTRAL FUNCTIONS AND FORM FACTORS

The two-point correlation function is defined as

$$\delta^{ab}\Pi_R(p^2) = i\int d^4x e^{ip\cdot x}\langle 0|T[R^a(x)R^b(0)]|0\rangle, \quad (16)$$

where the scalar and pseudoscalar densities correspond to $R^a \equiv S^a = \bar{q}\lambda_a q$ and $R^a \equiv P^a = i\bar{q}\gamma_5\lambda_a q$, in order, with λ_a the Gell-Mann matrices for $a = 1,\ldots,8$ and $\lambda_0 = I_{3\times3}\sqrt{2/3}$ for $a = 0$. The spectral-function sum rule in the chiral limit can then be represented as

$$\int_0^\infty [\mathrm{Im}\Pi_R(s) - \mathrm{Im}\Pi_{R'}(s)]ds = 0, \quad (17)$$

where R and R' are different scalar or pseudoscalar densities mentioned above. The imaginary part of the two-point correlation function $\mathrm{Im}\Pi_R$, also called the spectral function, is one of the key quantities that we calculate in this work.

A. Scalar sector

The scalar form factor of a pseudo-Goldstone boson pair PQ is defined as

$$F^a_{PQ}(s) = \frac{1}{B}\langle 0|\bar{q}\lambda_a q|PQ\rangle. \quad (18)$$

In the present work, we focus on the chiral dynamics for the components with $a = 0, 1, 2, 3, 8$, which preserve the strangeness. By imposing the isospin symmetry, only three of the five components are independent. We take the neutral ones, i.e. $a = 0, 8, 3$, which correspond to the singlet and $I = 0, 1$ octet $SU(3)$ densities, respectively. The scalar form factors with components $a = 4, 5, 6, 7$ correspond to the strangeness changing ones with $I = \frac{1}{2}$ and $\frac{3}{2}$, which were studied in [22].

The scalar spectral function is related to the scalar form factors through

$$\mathrm{Im}\,\Pi_{S^a}(s) = \sum_i \rho_i(s)|F^a_i(s)|^2\theta(s - s_i^{\mathrm{th}}), \quad (19)$$

where $\theta(x)$ is the Heaviside step function and the sum on i extends over the different pseudo-Goldstone boson pairs. In addition, s is the energy squared in the center of mass frame, $s_i^{\mathrm{th}} = (m_A + m_B)^2$ is the threshold of the ith channel, and m_A, m_B are the masses of the corresponding two particles. In the previous equation only two-body intermediate states are considered, the same ones as taken in Ref. [40] to study meson-meson scattering. We point out that the unitarized scalar form factors, among others, include the contributions of the single resonance exchanges to the spectral functions. We proof below, when discussing the evolution with N_C, that the two-point correlator in our analysis reduces to the single resonance exchange diagram at large N_C [70].

The phase space factor for the ith channel in Eq. (19) is

$$\rho_i(s) = \frac{\sqrt{[s-(m_A+m_B)^2][s-(m_A-m_B)^2]}}{16\pi s} = \frac{q_i}{8\pi\sqrt{s}}, \quad (20)$$

with q_i the three momentum in the center of mass frame.

For the isoscalar case, there are five two-particle intermediate states made by a pseudo-Goldstone pair in $U(3)$ χPT, namely, $\pi\pi$, $K\bar{K}$, $\eta\eta$, $\eta\eta'$, and $\eta'\eta'$. For the isovector case, there are three channels: $\pi\eta$, $K\bar{K}$, and $\pi\eta'$. The two-particle states with well-defined isospin for the isoscalar case read

$$|\pi\pi\rangle_{I=0} = -\frac{1}{\sqrt{2}}\frac{|\pi^+\pi^-\rangle + |\pi^-\pi^+\rangle + |\pi^0\pi^0\rangle}{\sqrt{3}},$$
$$|K\bar{K}\rangle_{I=0} = -\frac{|K^+K^-\rangle + |K^0\bar{K}^0\rangle}{\sqrt{2}}, \quad |\eta\eta\rangle_{I=0} = \frac{|\eta\eta\rangle}{\sqrt{2}}, \quad (21)$$
$$|\eta\eta'\rangle_{I=0} = |\eta\eta'\rangle, \quad |\eta'\eta'\rangle_{I=0} = \frac{|\eta'\eta'\rangle}{\sqrt{2}}.$$

For the isovector case they are

$$|\pi\eta\rangle_{I=1} = |\pi\eta\rangle, \qquad |K\bar{K}\rangle_{I=1} = -\frac{|K^+K^-\rangle - |K^0\bar{K}^0\rangle}{\sqrt{2}},$$
$$|\pi\eta'\rangle_{I=1} = |\pi\eta'\rangle. \quad (22)$$

We point out that the so-called unitary normalization for the identical particles, as proposed in Ref. [24], has been used in Eq. (21) for the $\pi\pi$, $\eta\eta$, and $\eta'\eta'$ states. In this way, the normalization that we employ in this work coincides with the one used in [40]. We can then construct the unitarized form factors by using the partial wave scattering amplitudes calculated in [40] without any adjustment in the normalization.

The perturbative calculation of the scalar form factors of the pseudo-Goldstone pairs at the one-loop level consists of evaluating the Feynman graphs shown in Fig. 1. As we have done for the scattering in Ref. [40], the contributions beyond the leading order to the form factors are calculated in terms of $\bar{\eta}$ and $\bar{\eta}'$ fields that result by diagonalizing the fields η_8 and η_1 at leading order from Eq. (1)

$$\eta_8 = c_\theta\bar{\eta} + s_\theta\bar{\eta}', \qquad \eta_1 = -s_\theta\bar{\eta} + c_\theta\bar{\eta}', \quad (23)$$

with $c_\theta = \cos\theta$ and $s_\theta = \sin\theta$. Compared to the basis with the fields η_8 and η_1, the use of the fields $\bar{\eta}$ and $\bar{\eta}'$ allows us to include the relevant Feynman diagrams conveniently in the calculation. As discussed in Ref. [40] we avoid in this way having to include an arbitrary number of insertions of the leading order η_8-η_1 mixing. As a result, one can consider the η and η' mixing effects in the form factors order by order in the δ counting scheme.

There are several sources that contribute to diagram (f) in Fig. 1: $\bar{\eta}$-$\bar{\eta}'$ mixing (notice that it is different from η_1–η_8 mixing [40], as just discussed), and the local contributions from the last two terms in Eq. (10) and the

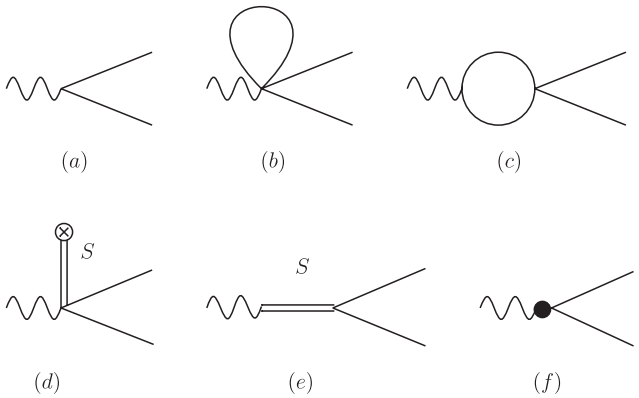

FIG. 1. Feynman diagrams for the calculation of the scalar form factor in one-loop $U(3)$ χPT. The wavy line denotes the scalar external source. The cross in diagram (d) indicates the coupling between the scalar resonance and the vacuum. The filled circle in diagram (f) corresponds to the vertices that only involve the pseudo-Goldstone bosons and are beyond leading order from Eq. (1). The different terms that contribute to diagram (f) are explained in detail in the text.

operators in Eqs. (11) and (15). The contributions from the $\bar{\eta}$-$\bar{\eta}'$ mixing to the form factors are calculated in the same way as for the calculation of scattering amplitudes in Ref. [40]. First, we substitute Eq. (16) of Ref. [40], which parametrizes the relations between $\bar{\eta}$, $\bar{\eta}'$ and the physical states η, η', into the leading order Lagrangian Eq. (1). Afterwards, we calculate the form factors in terms of the physical states η and η'. Because of the inclusion of the pseudoscalar resonances and the operator in Eq. (11), which contribute to the $\bar{\eta}$-$\bar{\eta}'$ mixing parameters δ_i in Eq. (14) of Ref. [40], we present the updated results in Appendix A. In addition, the wave function renormalization of the pseudo-Goldstone bosons, which has been calculated in Ref. [40], also contributes to the scalar form factors. The explicit expressions for the scalar form factors are given in Appendix B.

In $U(3)$ χPT the resummation of the unitarity chiral loops is essential because of the large mass of the s quark and the large anomaly mass in Eq. (1). Then, in many kinematical regions the resulting pseudo-Goldstone thresholds are much larger than the three-momenta involved, and this enhances the two-pseudo-Goldstone reducible loop contributions [71]. In addition, we are also interested in the chiral dynamics involving the resonance region where the unitarity upper bound in partial waves could easily be found to be saturated. So it is not meaningful to treat unitarity in a perturbative way as in χPT. As a result, one must resum the right-hand cut that stems from unitarity, and for that we employ Unitary χPT (UχPT), for calculating both the meson-meson partial wave amplitudes [21,25,40] and the scalar form factors [72–74].

The unitarization method that we use to resum the unitarity cut for the scalar form factors was developed in Refs. [72,73]. It is based on the N/D method and was first applied to meson-meson scattering in Ref. [25]. For completeness, we recapitulate the essentials of this method here.

In the case of two-particle intermediate states, the absorptive part of the form factor obeys the relation

$$\mathrm{Im}\, F_j^I(s) = \sum_{k=1}^{Z} T_{jk}^{IJ}(s)^* \rho_k(s) F_k^I(s), \tag{24}$$

where $T^{IJ}(s)$ denotes the partial wave scattering amplitudes with definite isospin number I and angular momentum J and Z is the number of channels with the same quantum numbers IJ. The T-matrix $T^{00}(s)$, relevant to the scalar form factors with $a = 0, 8$, is a 5×5 matrix, and $T^{10}(s)$, relevant to $a = 3$, is a 3×3 matrix. Both of them are studied in detail in Ref. [40]. Nevertheless because of the fact that now we also include the pseudoscalar resonances and the δL_8 operator, we need to consider their contributions in the scattering amplitudes as well. The effect from the pseudoscalar resonances can easily be included, since after the field redefinition the only relevant terms are the last two operators in Eq. (10). The pertinent expressions for the perturbative scattering amplitudes from $U(3)$ χPT including explicit exchanges of scalar and vector resonances [40] is given in Ref. [75]. The new contributions from the δL_8 operator and pseudoscalar resonances (as well as from tensor resonances, introduced below) are given in [76], together with the expressions for the form factors.

Following the method elaborated in Refs. [72,73] (see Ref. [74] for a simplified discussion), the unitarized scalar form factor can be cast as

$$F^I(s) = [1 + N^{IJ}(s) g^{IJ}(s)]^{-1} R^I(s), \tag{25}$$

where

$$\begin{aligned} N^{IJ}(s) &= T^{IJ}(s)^{(2)+\mathrm{Res}+\mathrm{Loop}} + T^{IJ}(s)^{(2)} g^{IJ}(s) T^{IJ}(s)^{(2)}, \\ R^I(s) &= F^I(s)^{(2)+\mathrm{Res}+\mathrm{Loop}} + N^{IJ}(s)^{(2)} g^{IJ}(s) F^I(s)^{(2)}. \end{aligned} \tag{26}$$

The matrix $N^{IJ}(s)$ contains the crossed-channel cuts from the meson-meson scattering and the bare resonance poles. It was calculated in Ref. [40] and extended here by including the pseudoscalar resonance exchanges and the δL_8 operator. The superscripts (2), Res, and Loop in Eq. (26) denote the perturbative calculations from the tree level result using the leading order Lagrangian Eq. (1), resonance contributions [also including the operators in Eqs. (11) and (15)], and pseudo-Goldstone loops, respectively. On the other hand, $R^I(s)$ is a vector with Z rows constructed from the $U(3)$ χPT form factors similarly as $N^{IJ}(s)$ is calculated for scattering. The vector $R^I(s)$ does not contain any cut singularity and is real [72,73].

The matrix $g^{IJ}(s)$ in Eq. (26) is a diagonal $Z \times Z$ matrix, with its ith nonvanishing matrix element given by

$$16\pi^2 g^{IJ}(s)_i = a_{SL}(\mu) + \log\frac{m_B^2}{\mu^2} - x_+ \log\frac{x_+ - 1}{x_+} - x_- \log\frac{x_- - 1}{x_-},$$
$$x_\pm = \frac{s + m_A^2 - m_B^2}{2s} \pm \frac{1}{2s}\sqrt{-4s(m_A^2 - i0^+) + (s + m_A^2 - m_B^2)^2}, \quad (27)$$

where $a_{SL}(\mu)$ is a subtraction constant. The matrix $g^{IJ}(s)$ collects the discontinuity caused by the two-particle intermediate states along the right-hand cut and plays a key role in the N/D unitarization approach. We refer to Sec. IV of Ref. [40], and references therein, for detailed discussions on the calculation of the scattering T matrix. The latter is given by a similar expression to Eq. (25) in terms of $N^{IJ}(s)$ and $g^{IJ}(s)$,

$$T^{IJ}(s) = [1 + N^{IJ}(s)g^{IJ}(s)]^{-1}N^{IJ}(s). \quad (28)$$

Before ending this section, we introduce the scalar form factors in the quark flavor basis instead of in the singlet-octet flavor basis. There are two kinds of isoscalar scalar densities in the quark flavor basis: $\bar{u}u + \bar{d}d$ and $\bar{s}s$. The relations between the form factors in the two different bases read

$$F^{\bar{u}u+\bar{d}d} = \frac{1}{\sqrt{3}}F^{a=8} + \sqrt{\frac{2}{3}}F^{a=0}, \quad (29)$$

$$F^{\bar{s}s} = -\frac{1}{\sqrt{3}}F^{a=8} + \frac{1}{\sqrt{6}}F^{a=0}. \quad (30)$$

The pion scalar radius $\langle r^2\rangle_S^\pi$, an important low-energy observable, is defined through the low-energy Taylor expansion of the pion scalar form factor in the quark flavor basis [77,78]

$$F_{\pi\pi}^{\bar{u}u+\bar{d}d}(s) = F_{\pi\pi}^{\bar{u}u+\bar{d}d}(0)\left[1 + \frac{1}{6}\langle r^2\rangle_S^\pi s + \ldots\right], \quad (31)$$

with

$$m_\pi^2 F_{\pi\pi}^{\bar{u}u+\bar{d}d}(s) \equiv 2Bm\langle 0|\bar{u}u + \bar{d}d|\pi\pi\rangle_{I=0}. \quad (32)$$

In the above equation, m stands for the up or down quark mass (we ignore isospin breaking) so that $2Bm = \bar{m}_\pi^2$, with $\bar{m}_\pi$ the leading order pion mass from Eq. (1). The relation between the physical mass square of the pion, m_π^2, and the leading order one, $\bar{m}_\pi^2$, was given in the Appendix of Ref. [40]. The updated version that includes the pseudoscalar resonances and the δL_8 effect is collected in Appendix A.

B. Pseudoscalar sector

For the pseudoscalar spectral function, the leading order contribution is due to the single pseudo-Goldstone boson exchange. The next nonvanishing contribution from the pure pseudo-Goldstone system requires at least three intermediate mesons, which belongs to a two-loop calculation that is beyond the scope of our current discussion. In order to take into account the chiral dynamics above 1 GeV in the pseudoscalar spectral function, we include the pseudoscalar resonance exchanges explicitly making use of the chiral invariant Lagrangian, Eq. (10). In light of the results of the work [68], where the pseudoscalar resonances were dynamically generated through the scattering of the scalar resonances and the pseudo-Goldstone bosons, we could instead consider the scalar resonances and the pseudo-Goldstone bosons in the intermediate states. This is left for future work.

The pseudoscalar spectral function is related to the pseudoscalar form factors calculated here in a simple way

$$\mathrm{Im}\,\Pi_{P^a}(s) = \sum_i \pi\delta(s - m_{P_i}^2)|H_i^a(s)|^2, \quad (33)$$

where $\delta(x)$ is the standard Dirac δ function, and m_{P_i} denotes the masses of the pseudo-Goldstone bosons and the pseudoscalar resonances with the same isospin as the considered spectral function. Finally, $H_i^a(s)$ is the corresponding pseudoscalar form factor

$$H_i^a(s) = \frac{1}{B}\langle 0|i\bar{q}\gamma_5\lambda_a q|P_i\rangle. \quad (34)$$

The calculation of the pseudoscalar form factor for the pseudo-Goldstone boson consists of evaluating the Feynman diagrams (a)–(d) in Fig. 2. Only the Feynman diagram (e) in Fig. 2 is relevant for the calculation of the pseudoscalar form factor for the pseudoscalar resonances. This diagram stems from the operators in the second line of Eq. (10). Moreover, we also consider the effects from the wave function renormalization of the pseudo-Goldstone

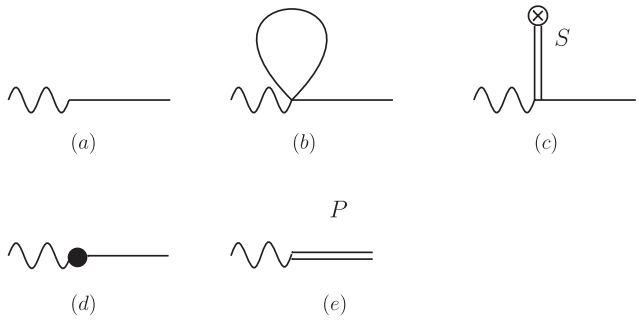

FIG. 2. Pseudoscalar form factors of the pseudo-Goldstone bosons and pseudoscalar resonances. The symbols have the same meanings as those in Fig. 1, except that the wavy line now stands for the pseudoscalar external source. See the text for further details.

bosons and express in the final results the pion decay constant F in the chiral and large N_C limits by the physical one F_π. The latter was calculated in Ref. [40]. This reshuffling in the expressions was also done for the scattering amplitudes in Ref. [40].

IV. REMARKS ON SEMILOCAL DUALITY

In this section, we introduce the basic idea of Regge theory in order to formulate the notation used in this work. For a detailed account on Regge theory see e.g. Ref. [53]. Regge theory relates the dynamics in the t channel with the s channel for the scattering processes. In $\pi\pi$ scattering, the isospin well-defined amplitudes from both channels are related through [53]

$$\begin{aligned} T_t^{(0)}(s,t) &= \frac{1}{3}T_s^{(0)}(s,t) + T_s^{(1)}(s,t) + \frac{5}{3}T_s^{(2)}(s,t), \\ T_t^{(1)}(s,t) &= \frac{1}{3}T_s^{(0)}(s,t) + \frac{1}{2}T_s^{(1)}(s,t) - \frac{5}{6}T_s^{(2)}(s,t), \\ T_t^{(2)}(s,t) &= \frac{1}{3}T_s^{(0)}(s,t) - \frac{1}{2}T_s^{(1)}(s,t) + \frac{1}{6}T_s^{(2)}(s,t), \end{aligned} \tag{35}$$

where the subscript of T denotes the t or s channel and the superscript refers to the proper isospin quantum number I in the t or s channel, respectively.

The object of the Regge theory is the fixed-t scattering amplitude and the proposed quantity to quantify the fulfillment of semilocal (or average) duality between Regge theory and hadronic degrees of freedom (h.d.f.) in Ref. [54] is

$$\int_{\nu_1}^{\nu_2} \nu^{-n}\,\mathrm{Im}T^{(I)}_{t,\mathrm{Regge}}(\nu,t)d\nu = \int_{\nu_1}^{\nu_2} \nu^{-n}\,\mathrm{Im}T^{(I)}_{t,\mathrm{Hadrons}}(\nu,t)d\nu, \tag{36}$$

where $\nu = \frac{s-u}{2} = \frac{2s+t-4m_\pi^2}{2}$ and s, t, u are the standard Mandelstam variables. The "averaging" should take place over at least one resonance tower. Therefore, the integration region $\nu_2 - \nu_1$ is typically taken as a multiple of 1 GeV^2. In this work, we shall focus on the energy region below 2 GeV^2. Semilocal duality should be well satisfied for forward scattering, i.e. with $t = 0$, where the leading Regge trajectory (the one taken here into account) dominates. As in Ref. [54], we also evaluate Eq. (36) at the threshold point $t = t_{\mathrm{th}} = 4m_\pi^2$ to show the robustness of the approach under changes of t (still small compared with GeV^2). Different choices for n enable us to test the different energy regions that dominate the integrals in Eq. (36). For negative values of n, the dynamics in the high-energy region definitely plays a more important role, and it is beyond the scope of the current work. For large positive values of n, the integrations in Eq. (36) are then dominated by the very low-energy physics, where resonances marginally contribute. In this work we test semilocal duality by taking n from 0 to 3, as suggested in Ref. [54], which is an adequate choice for the intermediate energy region from threshold up to 2 GeV^2, where several resonances contribute.

To evaluate the left-hand side of Eq. (36), the Regge asymptotic results continued down to threshold for $\mathrm{Im}T^{(I)}_{t,\mathrm{Regge}}(\nu,t)$ at fixed t are needed. The explicit formulas and detailed discussions can be found in Ref. [54] and references therein. We do not repeat here the formulation. For the right-hand side of Eq. (36), one can decompose the isospin amplitudes into a sum of partial waves

$$\mathrm{Im}\,T_s^{(I)}(\nu,t) = \sum_J (2J+1)\mathrm{Im}T^{IJ}(s)P_J(z_s), \tag{37}$$

where $z_s = 1 + 2t/(s-4m_\pi^2)$ is the cosine of the scattering angle in the s-channel center of mass frame and $P_J(z_s)$ denotes the Legendre polynomials. By substituting Eq. (37) into Eq. (35) $\mathrm{Im}T^{(I)}_{t,\mathrm{Hadrons}}(\nu,t)$ is obtained, and then the right-hand side of Eq. (36) can be compared with the results from Regge theory.

In order to quantify the fulfillment of semilocal duality we define, as in Ref. [54], two types of ratios of integrals such as these in Eq. (36), instead of comparing directly the value of the integration from the Regge theory and the h.d.f. The first one, R_n^I, is defined as

$$R_n^I = \frac{\int_{\nu_1}^{\nu_2} \nu^{-n}\,\mathrm{Im}T_{\mathrm{t}}^{(I)}(\nu,t)d\nu}{\int_{\nu_1}^{\nu_3} \nu^{-n}\,\mathrm{Im}T_{\mathrm{t}}^{(I)}(\nu,t)d\nu}. \tag{38}$$

To make closer the comparison with Ref. [54], we set in the following ν_1 at threshold, $\nu_2 = 1$ GeV^2, and $\nu_3 = 2$ GeV^2.

Other interesting objects to consider are the finite energy sum rule (FESR) between different isospin amplitudes with the same upper integration limit

$$F_n^{II'} = \frac{\int_{\nu_1}^{\nu_{\max}} \nu^{-n}\,\mathrm{Im}T_{\mathrm{t}}^{(I)}(\nu,t)d\nu}{\int_{\nu_1}^{\nu_{\max}} \nu^{-n}\,\mathrm{Im}T_{\mathrm{t}}^{(I')}(\nu,t)d\nu}, \tag{39}$$

where $\nu_{\max} = 1$ GeV^2 or 2 GeV^2 in the later discussions.

Among the various cases to investigate semilocal duality between h.d.f. and Regge theory in $\pi\pi$ scattering, the golden mode is the isotensor one in the t channel, since then the Regge exchange is highly suppressed (as there are no $\bar{q}q$ states with $I = 2$). As a result, the ratios F_n^{21} and F_n^{20} should tend to vanish in order to satisfy semilocal duality. In contrast, the dual direct s-channel allows the exchanges of several resonances with isospin $I = 0$, 1; see Eq. (35). Thus, if semilocal duality is fulfilled, one should expect the cancellation between the different resonances exchanged in the s channel, which sheds light on the resonance properties. Indeed, it establishes serious relations between the scalar and vector spectra, as we discuss later.

Finally, for the evaluation of the quantities in Eqs. (38) and (39) that quantify semilocal duality, the key ingredients are the partial waves $\mathrm{Im}\,T^{IJ}(s)$ in Eq. (37), which

were studied by us in Refs. [36,40]. This method is different from the one used in Ref. [54], where the resonances are regenerated by unitarizing the perturbative χPT amplitudes within the IAM [42,43]. An important difference is that instead of the explicit resonance states, as we employ here, the IAM depends on the LECs from $SU(2)$ or $SU(3)$ χPT [1–3]. Nevertheless, including the explicit resonance states in the Lagrangian is not enough to guarantee that one can apply the theory to higher energies because of the important contribution from the pseudo-Goldstone boson loops. In this case, one needs to resum the unitarity chiral loops, and a sophisticated approach based on the N/D method is formulated in Ref. [25] and already used to construct the unitarized scalar form factors in the previous section where we also discussed why $U(3)$ χPT should be unitarized. Through the procedure to resum the chiral loops, in addition to extending the application energy region of RχT, one also generates physical resonances with finite widths [21,24,25,40,79–81] in contrast to the zero-width resonances in the bare chiral Lagrangian. In the following, we employ the partial wave amplitudes from this procedure to analyze the semilocal duality.

V. PHENOMENOLOGICAL DISCUSSIONS

In this section, we study the phenomenological results of the several different types of spectral-function sum rules presented in Eq. (17) and the ratios in Eqs. (38) and (39) that quantify the fulfillment of semilocal duality. In order to perform the analyses, we need to provide the values for the resonance parameters, the low-energy constants in Eqs. (11) and (15), and the subtraction constants in Eq. (27) introduced by the unitarization procedure.

We want to stress that all the parameters in the form factors already appear in the meson-meson scattering amplitudes and the pseudo-Goldstone masses. Thus, once we determine them by fitting the scattering data and the η and η' masses, the form factors and the spectral functions are all predictions.

A. Former fit

We employ here the best fit in Eq. (55) of Ref. [40], which is referred to as "former fit" from now on, to calculate the form factors and spectral functions. In Figs. 3 and 4, we show in order the results for the pion

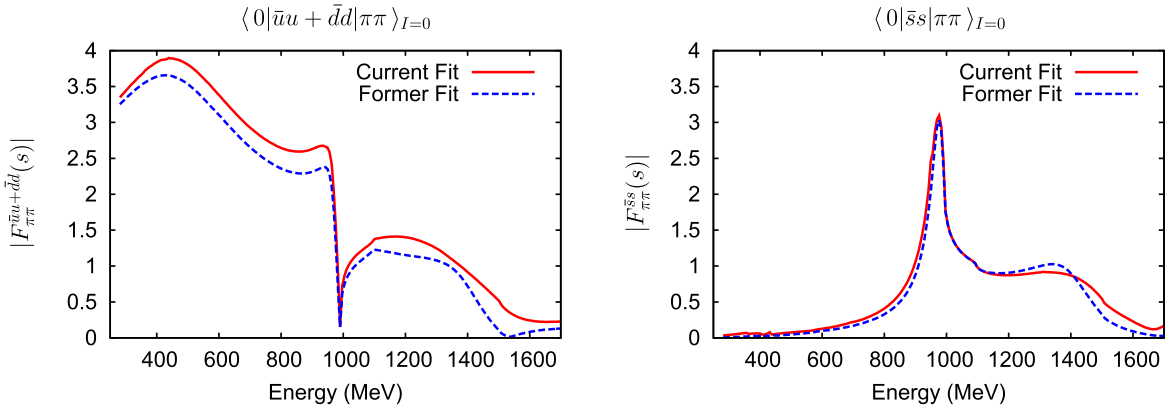

FIG. 3 (color online). The $\bar{u}u + \bar{d}d$ (left panel) and $\bar{s}s$ (right panel) scalar form factors of the pion in the quark flavor basis. The (red) solid lines are for the current fit and the (blue) dashed ones for the former fit.

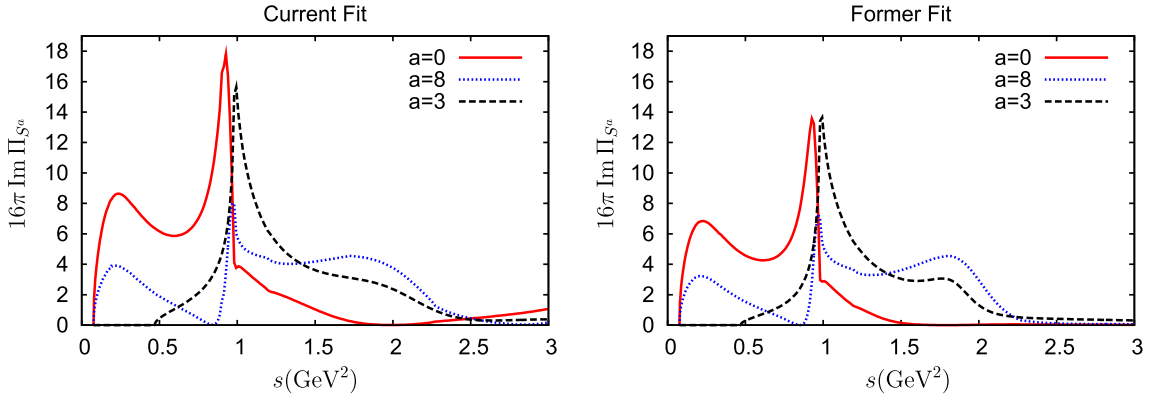

FIG. 4 (color online). The scalar spectral functions for the $a = 0$ (solid line), 8 (dotted line), and 3 (dashed line) correlators. The left panel is for the current fit and the right one for the former fit.

scalar form factors in the quark flavor basis and the spectral functions with $a = 0$, 3, and 8.

The quadratic pion scalar radius defined in Eq. (31) is found to be

$$\langle r^2\rangle_S^\pi = 0.43 \pm 0.01 \text{ fm}^2. \tag{40}$$

Compared to the dispersive result from Ref. [82]

$$\langle r^2\rangle_S^\pi = 0.61 \pm 0.04 \text{ fm}^2, \tag{41}$$

our result is about 30% smaller than this well-accepted value [82,83]. The main reason for getting a smaller value for the pion scalar radius is that our predictions for the low-energy constants L_4 and L_5 are quite small by using the resonance parameters from the best fit in Ref. [40]

$$\begin{aligned} L_4(\mu = 770 \text{ MeV}) &= (0.03^{+0.08}_{-0.05}) \times 10^{-3}, \\ L_5(\mu = 770 \text{ MeV}) &= (0.26^{+0.11}_{-0.18}) \times 10^{-3}. \end{aligned} \tag{42}$$

These two low-energy constants are important in the determination of the pion scalar radius [77]. So in order to improve its determination, we need to increase the values of L_4 and L_5 from the resonance contribution. In Ref. [22], it is realized that about 50% of L_5 is in fact contributed by a second nonet of scalar resonances. Thus we decide to include a second multiplet of scalar resonances in our discussion so as to achieve a bigger pion scalar radius. This requires us to update the fit we did in Ref. [40], which we discuss in detail in the next section. Another motivation to start a new fit is that we also include the pseudoscalar resonances in the present work, which turn out to be important in the spectral-function sum rules that we discuss below.

B. Current fit

Since we do not include the 4π channel, which turns out to be important in the energy region above 1.3 GeV in the isoscalar scalar case [34], we fit the scattering data in the $IJ = 00$ channel up to 1.3 GeV as was done in Ref. [40]. In this way, the second multiplet of scalar resonances around 2 GeV [21,22] behaves more like a background in our study, and we cannot fit its parameters in a precise manner. Instead, we take the values for the resonance parameters of the second multiplet of scalar resonances from the preferred fit of Ref. [21], given in its Eq. (6.10)[3]:

$$\begin{aligned} c_d' = \sqrt{3}\tilde{c}_d' = c_m' = \sqrt{3}\tilde{c}_m' \simeq 40 \text{ MeV}, \\ M_{S_1'} = M_{S_8'} = 2570 \text{ MeV}. \end{aligned} \tag{43}$$

In this reference the scattering data in the $IJ = \frac{1}{2}0$ and $IJ = \frac{3}{2}0$ channels were investigated in a similar approach as we use here up to around 2 GeV. About the pseudoscalar resonances, we take $d_m = \sqrt{3}\tilde{d}_m = 30$ MeV and $M_{P_8} = M_{P_1} = 1350$ MeV, which lie in the commonly determined regions of these parameters [16,19,41].

In Ref. [40] we found that the scalar resonance couplings from the fit perfectly obey the large N_C relations

$$\tilde{c}_{\,d} = \frac{c_d}{\sqrt{3}}, \qquad \tilde{c}_m = \frac{c_m}{\sqrt{3}}, \tag{44}$$

so that in the current fit we also impose them. For the subtraction constants we always keep the isospin constraints on them [40]. Finally, in the updated fit we have 18 free parameters and the fit results are

$$\begin{aligned} c_d &= (19.8^{+2.0}_{-5.2}) \text{ MeV}, & c_m &= (41.9^{+3.9}_{-9.2}) \text{ MeV}, \\ M_{S_8} &= (1397^{+73}_{-61}) \text{ MeV}, & M_{S_1} &= (1100^{+30}_{-63}) \text{ MeV}, \\ M_\rho &= (801.2^{+8.2}_{-6.9}) \text{ MeV}, & M_{K^*} &= (910.0^{+7.0}_{-9.1}) \text{ MeV}, \\ G_V &= (62.1^{+1.9}_{-2.1}) \text{ MeV}, & a_{SL}^{10,\pi\eta} &= 2.0^{+3.3}_{-4.5}, \\ a_{SL}^{00,\pi\pi} &= -1.27^{+0.12}_{-0.12}, & a_{SL}^{00,K\bar{K}} &= -0.95^{+0.33}_{-0.16}, \\ a_{SL}^{\frac{1}{2}0,K\pi} &= -1.12^{+0.12}_{-0.17}, & a_{SL}^{\frac{1}{2}0,K\eta} &= -0.08^{+0.38}_{-1.04}, \\ a_{SL}^{10,K\eta'} &= -1.25^{+1.11}_{-1.23}, & \delta L_8 &= 0.23^{+0.29}_{-0.19} \times 10^{-3}, \\ M_0 &= (951^{+50}_{-50}) \text{ MeV}, & \Lambda_2 &= -0.37^{+0.19}_{-0.19}, \\ \mathcal{N} &= (0.76^{+0.36}_{-0.35}) \text{ MeV}^{-2}, & c &= 1.05^{+0.43}_{-0.33}, \end{aligned} \tag{45}$$

with $\chi^2/(\text{degrees of freedom}) = 784/(348 - 18) \simeq 2.38$. For the remaining subtraction constants, we impose the following relations in the fit:

$$\begin{aligned} a_{SL}^{00,\eta\eta} &= a_{SL}^{00,\eta\eta'} = a_{SL}^{00,\eta'\eta'} = a_{SL}^{00,K\bar{K}}, \\ a_{SL}^{20,\pi\pi} &= a_{SL}^{00,\pi\pi}, \qquad a_{SL}^{\frac{3}{2}0,K\pi} = a_{SL}^{\frac{1}{2}0,K\pi}, \\ a_{SL}^{10,\pi\eta'} &= a_{SL}^{10,K\bar{K}} = a_{SL}^{00,K\bar{K}}, \end{aligned} \tag{46}$$

and all of the subtraction constants in the vector channels (which are barely sensitive to them while they are of natural size [62]) are set equal to $a_{SL}^{00,\pi\pi}$. The parameters $\mathcal{N}$ and c in Eq. (45) are introduced to describe the $\pi\eta$ distribution

$$\frac{dN_{\pi\eta}}{dE_{\pi\eta}} = q_{\pi\eta}\mathcal{N}|T^{10}_{K\bar{K}\to\pi\eta}(s) + cT^{10}_{\pi\eta\to\pi\eta}(s)|^2, \tag{47}$$

with $q_{\pi\eta}$ the three momentum of the $\pi\eta$ system in the center of mass frame.

The resulting plots from the fit in Eq. (45) are shown in Figs. 5–7, by the solid curves, where we have also shown the best fit results from Ref. [40] by the dashed lines. The masses of η and η' from the new fit read

$$m_\eta = 536.7^{+43.3}_{-39.6} \text{ MeV}, \qquad m_{\eta'} = 956^{+45.9}_{-30.4} \text{ MeV}, \tag{48}$$

which are clearly improved compared with the ones from Ref. [40]. And the leading order mixing angle of η_1 and η_8 introduced in Eq. (23) is

[3]The bare mass of the second nonet of scalar resonances is not either well fixed from Ref. [21]. For example, in its fit (6.11) its bare mass is ~2 GeV. The range 2–2.5 GeV is then a realistic one for the bare mass of the second nonet of scalar resonances as follows from Ref. [21].

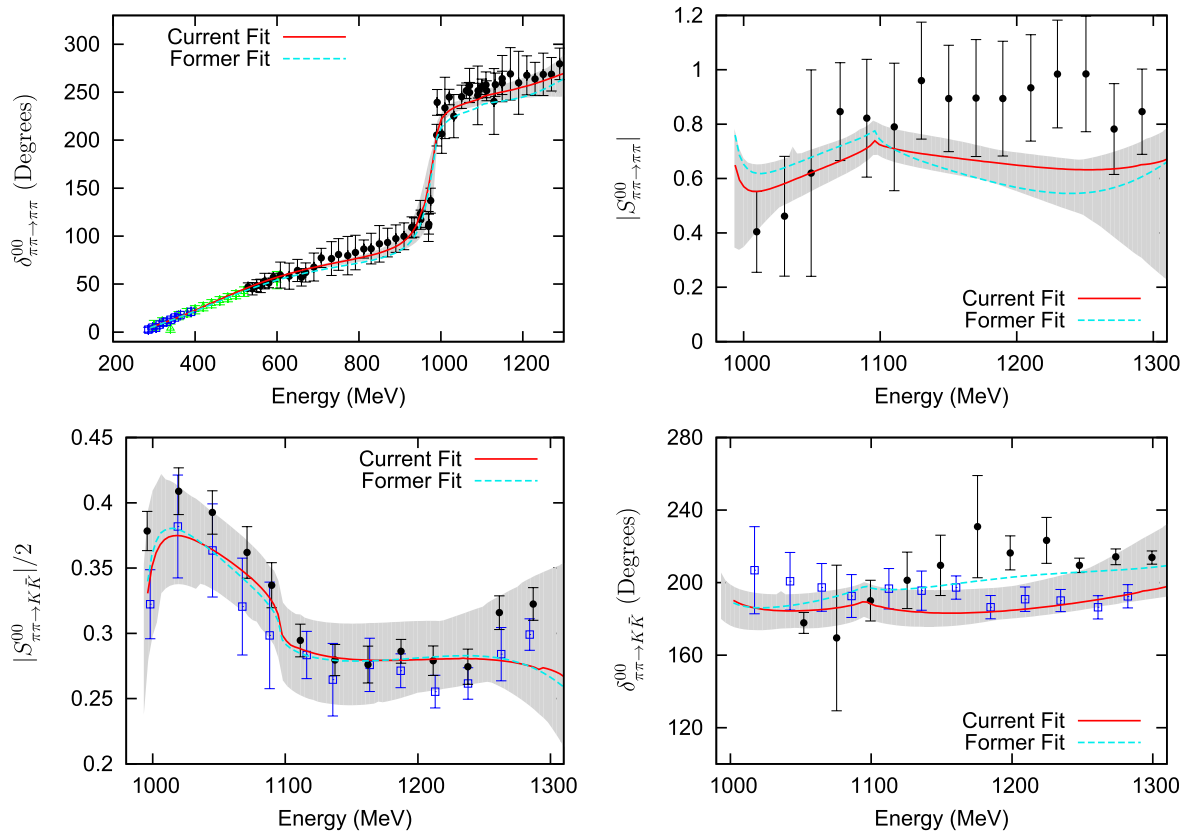

FIG. 5 (color online). The $IJ = 00$ case from the current and former fits. From top to bottom and left to right: the $\pi\pi \to \pi\pi$ phase shifts ($\delta^{00}_{\pi\pi\to\pi\pi}$), the modulus of the $\pi\pi \to \pi\pi$ S-matrix element ($|S^{00}_{\pi\pi\to\pi\pi}|$), one-half of the modulus of the $\pi\pi \to K\bar{K}$ S-matrix element ($|S^{00}_{\pi\pi\to K\bar{K}}|/2$), and the $\pi\pi \to K\bar{K}$ phase shifts ($\delta^{00}_{\pi\pi\to K\bar{K}}$). The solid (red) line corresponds to the current fit, Eq. (45), and the dashed (blue) line represents the former fit of Ref. [40]. The error bands are represented by the shadowed areas, which are calculated using Eq. (45). The data for $\delta^{00}_{\pi\pi\to\pi\pi}$ are from Refs. [102] (green triangles), [103] (blue squares), and the average data from Refs. [104–106] (black circles), as used in Ref. [25]. The data for $|S^{00}_{\pi\pi\to\pi\pi}|$ are from Ref. [104] while those for $|S^{00}_{\pi\pi\to K\bar{K}}|/2$ are from Refs. [107] (blue squares) and [108] (black circles). The phase shifts $\delta^{00}_{\pi\pi\to K\bar{K}}$ correspond to the data from Refs. [107] (blue squares) and [109] (black circles).

$$\theta = -(15.1^{+2.4}_{-2.4})^{\circ}. \tag{49}$$

Compared to the former fit from Ref. [40], three more subtraction constants, $a^{00,K\bar{K}}_{SL}$, $a^{\frac{1}{2}0,K\eta}_{SL}$, and $a^{\frac{1}{2}0,K\eta'}_{SL}$ are set free in the current fit Eq. (45), while we reduce now the scalar resonance parameters by explicitly imposing the large N_C relations of Eq. (44). For the subtraction constants in the isoscalar scalar channel, $a^{00,\pi\bar{\pi}}_{SL}$ and $a^{00,K\bar{K}}_{SL}$ are compatible with the former fit within error bands. For the $IJ = \frac{1}{2}0$ channel, $a^{\frac{1}{2}0,K\pi}_{SL}$ and $a^{\frac{1}{2}0,K\eta'}_{SL}$ are quite similar and obey nonet symmetry approximately, while $a^{\frac{1}{2}0,K\eta}_{SL}$ is much more different. Nevertheless, one should notice that both $a^{\frac{1}{2}0,K\eta}_{SL}$ and $a^{\frac{1}{2}0,K\eta'}_{SL}$ carry especially large error bars. About the resonance parameter c_d, its value from the new fit is larger by about 30% than the one from the former fit in Ref. [40]. This new value is closer to those determined in other works [21,25,84]. The figure $c_d = 19.1^{+2.4}_{-2.1}$ MeV was reported in Ref. [25], and $c_d = 23.8$ MeV and $c_d = 26 \pm 7$ MeV were given in Refs. [21,84], respectively. For the parameter c_m, its value from the new fit also increases about 30% compared to that from the former fit in Ref. [40]. However, the error bars accompanying c_m are now considerably smaller. This is because in the new fit we impose the large N_C relation for the singlet couplings, Eq. (44). Concerning the bare masses, both for the resonances (scalar and vector) and for the singlet η_1, no appreciable changes in the new fit are seen, compared with the ones from the previous one [40]. The central value of Λ_2 is now about 60% of that from the best fit in Eq. (55) of Ref. [40], though both determinations are affected by large uncertainties. For the vector resonance coupling G_V, the results from the current fit and the previous one in Ref. [40] perfectly agree with each other. Concerning δL_8, which is introduced to compensate the uncertainties in the pseudoscalar resonance sector, it also carries large error bars.

The quality of the current fit in Eq. (45) and the best fit in Ref. [40] is quite similar, as one can see from Figs. 5–7. Nevertheless, the prediction for L_5 from

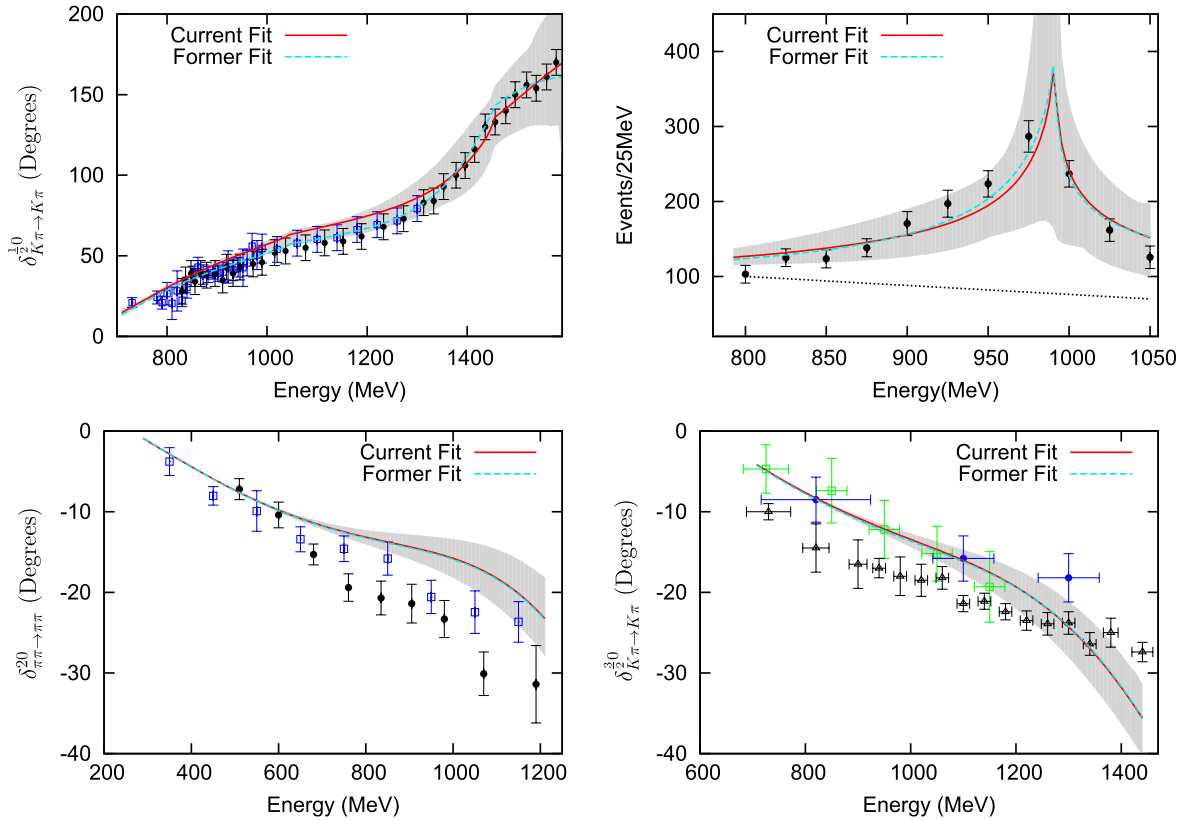

FIG. 6 (color online). From top to bottom and left to right: the $K\pi \to K\pi$ phase shifts with quantum numbers $IJ = \frac{1}{2}0$ ($\delta^{\frac{1}{2}0}_{K\pi\to K\pi}$), the $\pi\eta$ event distribution with $IJ = 10$, the $\pi\pi \to \pi\pi$ phase shifts with $IJ = 20$ ($\delta^{20}_{\pi\pi\to\pi\pi}$), and the $K\pi \to K\pi$ phase shifts with $IJ = \frac{3}{2}0$ ($\delta^{\frac{3}{2}0}_{K\pi\to K\pi}$). The experimental points for $\delta^{\frac{1}{2}0}_{K\pi\to K\pi}$ correspond to the average data from Refs. [110–112] (blue squares), as employed in Ref. [25], and Ref. [113] (black circles). Data points for the $\pi\eta$ event distribution are taken from Ref. [114], and the dotted line stands for the background [25]. The data for $\delta^{20}_{\pi\pi\to\pi\pi}$ correspond to Refs. [115] (blue squares) and [116] (black circles). The experimental data of $\delta^{\frac{3}{2}0}_{K\pi\to K\pi}$ are from Refs. [117] (green squares), [118] (blue circles), and [111] (black triangles). For the notation on the lines see Fig. 5.

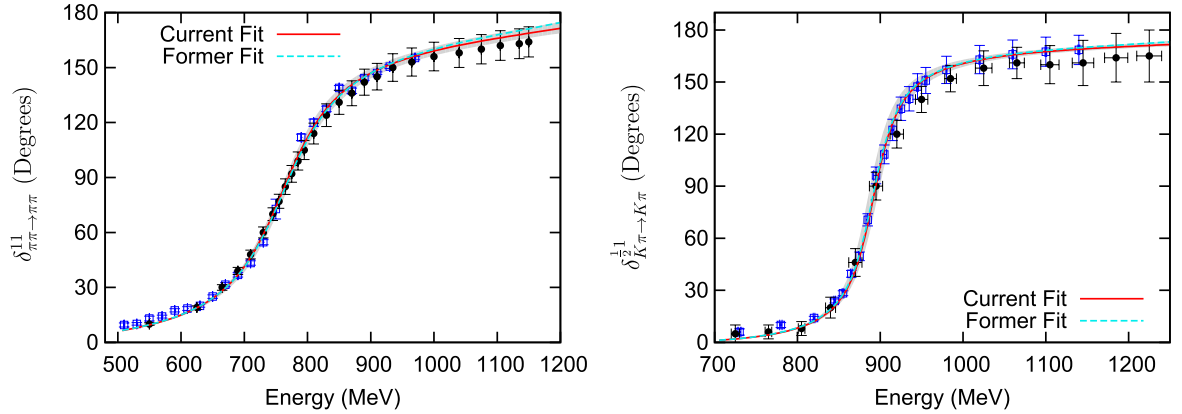

FIG. 7 (color online). The left panel displays the results for the $IJ = 11$ channel and the right one is for the $IJ = \frac{1}{2}1$ case. The $\pi\pi \to \pi\pi$ phase shifts in the $IJ = 11$ case, $\delta^{11}_{\pi\pi\to\pi\pi}$, correspond to Refs. [119] (blue squares) and [120] (black circles). The $K\pi \to K\pi$ phase shifts with $IJ = \frac{1}{2}1$, $\delta^{\frac{1}{2}1}_{K\pi\to K\pi}$, are taken from Refs. [110] (black circles) and [111] (blue squares). For the notation on the lines see Fig. 5.

resonance contributions using the new fit Eq. (45) is considerably increased, compared to the results in Eq. (42), because of the inclusion of the second scalar multiplet. The resulting values for L_4 and L_5 are now

$$L_4(\mu = 770\ \text{MeV}) = (0.09^{+0.02}_{-0.04}) \times 10^{-3},$$
$$L_5(\mu = 770\ \text{MeV}) = (0.67^{+0.04}_{-0.17}) \times 10^{-3}. \quad (50)$$

The new value for L_5 agrees well with the recent determination $L_5 = (0.58 \pm 0.13) \times 10^{-3}$ from the latest $\mathcal{O}(p^6)$ $SU(3)$ χPT fits of Ref. [85]. Concerning L_4 the latest reference cannot pin down a precise value, giving the result $L_4 = (0.75 \pm 0.75) \times 10^{-3}$. Our determination in Eq. (50) is compatible with the latter number given its large uncertainty. Related to the larger value for L_5 in Eq. (50), the quadratic pion scalar radius from the new fit is also improved with the resulting value

$$\langle r^2 \rangle^{\pi}_S = 0.49^{+0.01}_{-0.03}\ \text{fm}^2, \quad (51)$$

increasing about 14% compared to the value in Eq. (40) from the former fit, Eq. (55) of Ref. [40]. The resulting scalar pion form factors and spectral functions are displayed in Figs. 3 and 4, respectively, together with the results from the former fit [40].

The resulting resonance pole positions on the complex plane from the new fit Eq. (45) are collected in Table I. We refer to Ref. [40] for the discussions on how to perform the extrapolation from the physical sheet to the unphysical Riemann sheets. Around a resonance pole s_R, corresponding to a resonance R, the partial wave amplitude $T^I_J(s)_{i\to j}$ tends to

$$T^I_J(s)_{i\to j} \to -\frac{g_{R\to i} g_{R\to j}}{s - s_R}. \quad (52)$$

By calculating the residue of the resonance pole, we then obtain the product of the couplings to the corresponding decay modes, $g_{R\to i} g_{R\to j}$. The pole positions for the vector resonances $\rho(770)$, $K^*(892)$, and $\phi(1020)$ agree perfectly with those in Ref. [40]. Only slight changes are observed for the $f_0(500)$, $f_0(980)$, $K^*_0(800)$, and $a_0(980)$ resonances, while all of the excited scalar resonances, such as the $f_0(1370)$, $K^*_0(1430)$, and $a_0(1450)$, have larger widths in the new fit Eq. (45) than in the previous one [40].

C. Phenomenological results of semilocal duality

We show in Table II the values of the ratios defined in Eqs. (38) and (39) from the current fit, Eq. (45). The dependence of these ratios with $N_C > 3$ is discussed later. We also consider the contributions of the D waves to the integrals in Eqs. (38) and (39), in addition to the S and P waves. For including the tensor resonances, which originate the D waves, we follow the formalism of Ref. [86] and take for the couplings the values determined there. The bare mass is adjusted such that the physical mass of the $f_2(1270)$ from the pole position agrees with the value in the PDG [35]. To avoid interrupting the current discussion, we give the expressions for the tensor contributions to meson-meson scattering in Appendix C.

In the leftmost column in Table II we indicate the partial waves involved in the evaluation of the integrals in Eqs. (38) and (39). The values of n considered are given in the second column. In the rest of the columns we give the quantities R^I_n and F^{21}_n, as indicated in the top row. The

TABLE I. Pole positions for the different resonances in $\sqrt{s} \equiv (\text{M}, -i\frac{\Gamma}{2})$. The mass (M) and the half-width ($\Gamma/2$) are given in units of MeV. The modulus of the square root of a residue is given in units of GeV, which corresponds to the coupling of the resonance with the first channel (specified inside the parentheses). The last two columns are the ratios of the coupling strengths of the same resonance to the remaining channels with respect to the first one. Note that the residues for $\pi\pi$, $\eta\eta$, and $\eta'\eta'$ are given in the unitary normalization; see Ref. [40].

R	M (MeV)	$\Gamma/2$ (MeV)	$\lvert\text{Residues}\rvert^{1/2}$ (GeV)	Ratios	
$f_0(500)$	442^{+4}_{-4}	246^{+7}_{-5}	$3.02^{+0.03}_{-0.04}(\pi\pi)$	$0.50^{+0.04}_{-0.08}(K\bar{K}/\pi\pi)$	$0.17^{+0.09}_{-0.09}(\eta\eta/\pi\pi)$
				$0.33^{+0.06}_{-0.10}(\eta\eta'/\pi\pi)$	$0.11^{+0.05}_{-0.06}(\eta'\eta'/\pi\pi)$
$f_0(980)$	978^{+17}_{-11}	29^{+9}_{-11}	$1.8^{+0.2}_{-0.3}(\pi\pi)$	$2.6^{+0.2}_{-0.3}(K\bar{K}/\pi\pi)$	$1.6^{+0.4}_{-0.2}(\eta\eta/\pi\pi)$
				$1.0^{+0.3}_{-0.2}(\eta\eta'/\pi\pi)$	$0.7^{+0.2}_{-0.3}(\eta'\eta'/\pi\pi)$
$f_0(1370)$	1360^{+80}_{-60}	170^{+55}_{-55}	$3.2^{+0.6}_{-0.5}(\pi\pi)$	$1.0^{+0.7}_{-0.3}(K\bar{K}/\pi\pi)$	$1.2^{+0.7}_{-0.3}(\eta\eta/\pi\pi)$
				$1.5^{+0.4}_{-0.5}(\eta\eta'/\pi\pi)$	$0.7^{+0.2}_{-0.3}(\eta'\eta'/\pi\pi)$
$K^*_0(800)$	643^{+75}_{-30}	303^{+25}_{-75}	$4.8^{+0.5}_{-1.0}(K\pi)$	$0.9^{+0.2}_{-0.3}(K\eta/K\pi)$	$0.7^{+0.2}_{-0.3}(K\eta'/K\pi)$
$K^*_0(1430)$	1482^{+55}_{-110}	132^{+40}_{-90}	$4.4^{+0.2}_{-1.1}(K\pi)$	$0.3^{+0.3}_{-0.3}(K\eta/K\pi)$	$1.2^{+0.2}_{-0.2}(K\eta'/K\pi)$
$a_0(980)$	1007^{+75}_{-10}	22^{+90}_{-10}	$2.4^{+3.2}_{-0.4}(\pi\eta)$	$1.9^{+0.2}_{-0.5}(K\bar{K}/\pi\eta)$	$0.03^{+0.10}_{-0.03}(\pi\eta'/\pi\eta)$
$a_0(1450)$	1459^{+70}_{-95}	174^{+110}_{-100}	$4.5^{+0.6}_{-1.7}(\pi\eta)$	$0.4^{+1.2}_{-0.2}(K\bar{K}/\pi\eta)$	$1.0^{+0.8}_{-0.3}(\pi\eta'/\pi\eta)$
$\rho(770)$	760^{+7}_{-5}	71^{+4}_{-5}	$2.4^{+0.1}_{-0.1}(\pi\pi)$	$0.64^{+0.01}_{-0.02}(K\bar{K}/\pi\pi)$	
$K^*(892)$	892^{+5}_{-7}	25^{+2}_{-2}	$1.85^{+0.07}_{-0.07}(K\pi)$	$0.91^{+0.03}_{-0.02}(K\eta/K\pi)$	$0.41^{+0.07}_{-0.06}(K\eta'/K\pi)$
$\phi(1020)$	$1019.1^{+0.5}_{-0.6}$	$1.9^{+0.1}_{-0.1}$	$0.85^{+0.01}_{-0.02}(K\bar{K})$		

TABLE II. Current fit: R_n^I and $F_n^{II'}$ are defined in Eqs. (38) and (39), respectively. In the first column from the left the amplitudes involved in their evaluation are shown. The different values of n are given in the second column. The rest of the columns correspond to R_n^I and F_n^{21} as indicated. Two values of t, 0, and $t_{\rm th} \equiv 4m_\pi^2$, are considered, as shown in the second row.

	n	R_n^0 $t = t_{\rm th}$	R_n^0 $t = 0$	R_n^1 $t = t_{\rm th}$	R_n^1 $t = 0$	F_n^{21} $t = t_{\rm th}$ $\nu_{\rm max} = 2$ GeV^2	F_n^{21} $t = 0$ $\nu_{\rm max} = 2$ GeV^2
Regge	0	0.225	0.233	0.325	0.353	~ 0	~ 0
	1	0.425	0.452	0.578	0.642	~ 0	~ 0
	2	0.705	0.765	0.839	0.908	~ 0	~ 0
	3	0.916	0.958	0.966	0.990	~ 0	~ 0
Ours	0	0.669	0.628	0.836	0.817	-0.113	0.040
$S + P$	1	0.837	0.812	0.919	0.908	-0.230	-0.087
waves	2	0.934	0.924	0.966	0.962	-0.129	0.028
	3	0.979	0.976	0.989	0.988	0.169	0.345
Ours	0	0.410	0.400	0.453	0.468	0.531	0.587
$S + P + D$	1	0.653	0.643	0.694	0.706	0.154	0.236
waves	2	0.850	0.844	0.875	0.882	0.027	0.155
	3	0.954	0.953	0.965	0.968	0.225	0.388

values $t = 0$ and $t = 4m_\pi^2$ are used in order to show the stability of the results under changes in t that are small compared with GeV^2. For the different quantities one should compare the numbers from Regge exchange and those obtained by including only the $(S + P)$ waves or in addition including as well the D waves. Our results in Table II quantitatively confirm the conclusions of Ref. [54], that semilocal duality for $n = 3$ with $I_t = 0$ and 1 can be perfectly satisfied by including only the S and P waves, while the fulfillment for $n = 2$ is already marginal. For smaller values of n, the higher partial waves and higher cutoffs are crucial in order to satisfy semilocal duality. In this respect, we observe that once the D waves are included semilocal duality is satisfied better for all the n values discussed, but particularly for $n = 0$ and 1. We have also considered the role of the $\rho(1450)$, but it is negligible if one takes the $\pi\pi$ branching decay ratio from the PDG [35], which is only 6%.

For $I_t = 2$ the situation is somewhat different. Before discussing the different numbers for F_n^{21} in Table II, let us first comment on some specific values for the ratio F_n^{21} in order to set up a criterion that allows one to consider a value small and then acceptable for satisfying semilocal duality. From Eq. (35), one has that $F_n^{21} \to -1$, if the scalar contribution is dropped (the absorptive part of the $I = 2$ channel should be negligible compared with that of the scalar and vector channels). In contrast, $F_n^{21} \to 1$ results by neglecting the vector contribution. As we commented before, the ratio of F_n^{21} should vanish if semilocal duality works well. Taking this in mind we then see that with the S and P waves, we do not find any significant signal that semilocal duality is better satisfied for a specific value of n, even in some cases duality is satisfied worse for a larger value of n, in contrast to the situations with $I_t = 0$ and $I_t = 1$. However, in all cases the numbers are much smaller than 1 in absolute value, so that semilocal duality seems to be fulfilled quite accurately. In our scattering amplitudes higher scalar resonances are generated, instead of only the $f_0(500)$ as in Ref. [54], which leads to an improvement for the $I_t = 2$ channel by comparing the numbers for F_n^{21} in Table II with the ones in Table VI of Ref. [54]. The masses of the heavier scalar resonances in our scattering amplitudes are close to or larger than 1 GeV^2, as shown in Table I. Hence, only their effects can be taken into account in the discussion of semilocal duality when the integration upper limit $\nu_{\rm max}$ in Eq. (39) is larger than 1 GeV^2. Indeed, had we set instead $\nu_{\rm max} =$ 1 GeV^2 the fulfillment of semilocal duality would be much worse than for the $\nu_{\rm max} = 2$ GeV^2 case, especially for $n = 0$ and 1. Then, in the later discussions, we only consider the ratio F_n^{21} in Eq. (39) calculated at $\nu_{\rm max} = 2$ GeV^2. On the other hand, we find that the introduction of the D waves, instead of narrowing the gap between the Regge prediction and the h.d.f., worsens the situation for $I_t = 2$ in the $n = 0$ case. It is then advisable to focus in this work on $n > 0$ for F_n^{21} [87].

The ratios F_n^{20} are smaller in absolute value than F_n^{21} because the coefficient multiplying $T_s^{(1)}$ in Eq. (35) is larger by a factor of 2 for $T_t^{(0)}$ than for $T_t^{(1)}$. In Table II we do not display their values since they cannot reveal any new information compared with F_n^{21}.

D. Study of spectral-function sum rules

After fixing the unknown parameters through the fit to data, we are ready to investigate the spectral-function sum rules presented in Eq. (17). To study them one has to include not only nonperturbative QCD dynamics but also perturbative QCD and OPE [4,5]. In this way we split the integral into two parts

TABLE III. Results from the integration of the spectral functions from 0 up to s_0 [Eq. (54)]. We show three results in the columns W_{S^0}, W_{S^8}, and W_{S^3} by taking three different values for s_0: 2.5, 3, 3.5 GeV^2. The results for the pseudoscalar cases are not changed for different s_0, since the pseudoscalar spectral functions are just some Dirac δ functions [Eq. (33)]. W_i with $i = S^0, S^8, S^3, P^0, P^8, P^3$, the mean value $\bar{W}$, and σ_W are defined in Eqs. (54)–(56), which are given in units of GeV^2. In the last column we show the relative variance $\sigma_W/\bar{W}$.

	W_{S^0}	W_{S^8}	W_{S^3}	W_{P^0}	W_{P^8}	W_{P^3}	$\bar{W}$	σ_W	$\sigma_W/\bar{W}$
Physical masses									
Current fit	8.6 9.0 9.6	7.4 7.5 7.7	7.0 7.2 7.4	8.9	11.3	10.1	9.0	1.5	0.16
Former fit	6.1 6.1 6.1	6.1 6.1 6.1	5.8 5.9 6.1	1.8	5.0	5.1	5.0	1.5	0.31
$m_q = 0$									
Current fit	6.9 7.0 7.1	6.8 7.0 7.3	6.6 6.8 7.0	5.5	7.4	7.4	6.9	0.7	0.10
Former fit	5.2 5.3 5.5	5.5 5.7 6.0	5.2 5.3 5.5	0.3	3.0	3.0	3.8	2.0	0.53

$$\int_0^{s_0}[\mathrm{Im}\Pi_R(s) - \mathrm{Im}\Pi_{R'}(s)]ds + \int_{s_0}^{\infty}[\mathrm{Im}\Pi_R(s) - \mathrm{Im}\Pi_{R'}(s)]ds = 0. \quad (53)$$

The first integral, which extends along the lower-energy regime, comprises the nonperturbative region, and we use our results in terms of h.d.f. to evaluate it. For the second one, higher in energy, the results from OPE are employed to evaluate the theoretical spectral functions. According to the OPE study of Ref. [9], the different spectral functions with $R = S, P$ and $R' = S, P$ are equal in the asymptotic region in the chiral limit.[4] As a result, the second integral in Eq. (53) is zero. Then, testing how well a spectral-function sum rule is satisfied reduces to evaluating the first integral, which extends along the energy region below $\sqrt{s_0}$. This is exactly the key object of our current study in this section.

As discussed above, we consider the strangeness conserving scalar and pseudoscalar spectral functions for $a = 0, 8, 3$. Hence there are 15 types of nontrivial spectral-function sum rules as those in Eq. (53). In order to show the results in a compact way, we display the individual values for the integration up to s_0 for each of the phenomenological spectral functions in Table III, instead of the differences between the different spectral functions. Note that the second integral for $s > s_0$ is divergent, unless the difference between the spectral functions is taken as in Eq. (53). This divergent behavior is not an issue for the first integral because, as shown in Fig. 4, the phenomenological spectral functions are already very small for $s \gtrsim 2.5$ GeV^2. In this way, the results from the integration do not depend so much on s_0 as soon as they are larger than $\sim$2.5 GeV^2. This vanishing behavior should be expected from Eq. (19). In the latter only a finite number of two-body channels are considered so that if the form factors vanish for $s \to \infty$ (as expected from QCD counting rules [88]), then their contribution to the spectral function does as well. Note also that $\rho_i(s)$, given in Eq. (20), tends to constant for $s \to \infty$. The definitions of the different quantities in Table III are

$$W_i = 16\pi \int_0^{s_0} \mathrm{Im}\Pi_i(s)ds, \quad (54)$$

$$\bar{W} = \frac{1}{3\times 6}\sum_i W_i, \quad (55)$$

$$\sigma_W^2 = \sum_i \frac{(W_i - \bar{W})^2}{17}, \quad i = S^8, S^0, S^3, P^0, P^8, P^3, \quad (56)$$

where we take three different values of s_0 to evaluate the integrations in order to show the dependences of the integrated results on s_0. The relative variance $\sigma_W/\bar{W}$ serves as a parameter to quantify how well the spectral-function sum rules in the scalar and pseudoscalar cases hold.

Two situations by taking different masses for the pseudo-Goldstone bosons are investigated: the physical case and the chiral limit. In order to study the results at the chiral limit, it is necessary to perform the chiral extrapolation of our spectral functions. Though the resonance parameters in Eqs. (4)–(8) do not depend on the quark masses, the subtraction constants a_{SL} in Eq. (27) introduced through the unitarization procedure vary with them. In Ref. [89], it is demonstrated that in the $SU(3)$ limit (as also in the chiral limit) all the subtraction constants should be equal for any pseudo-Goldstone pair made of the π, K, and η_8 mesons. Thus we need to extrapolate the subtraction constants from the fit, which are not necessarily equal to each other, to a common value. We find that at the chiral limit such a value indeed exists in a reasonable region (roughly from -1 to 0), where the results of the two-point correlators are stable and the spectral-function sum rules are better satisfied compared to the physical situation. In the following, we show the typical results in this region (with a common value taken for the subtraction constant at the chiral limit of -0.5).

The corresponding scalar spectral functions at the chiral limit are shown in Fig. 8.[5] It is easy to conclude from

[4]The calculation in Ref. [9] is done up to $\mathcal{O}(\alpha_s)$ and includes up to dimension 5 operators.

[5]We show for later convenience the same spectral functions with $N_C = 30$ in the right panel of Fig. 8.

Table III that the spectral-function sum rules are much better fulfilled by the new fit in Eq. (45) than by the former one of [40]. The most significant changes in W_i from both fits happen for the pseudoscalar cases, with $i = P^0, P^8$, and P^3, which are caused by the pseudoscalar resonances that are now included in the new fit. We obtain that the smallest value for the violation of the spectral-function sum rules, around 10%, takes place at the chiral limit by using the new fit result. Nevertheless, the result for the physical case from the new fit is also quite similar, with a violation of around 16%.

In the left panel of Fig. 8 the singlet spectral function (solid line) is clearly dominated in the low-energy region by a peak corresponding to a pole that evolves continuously with the pseudo-Goldstone boson masses from the $f_0(500)$ resonance pole at the physical case. This affinity of the $f_0(500)$ resonance to the singlet scalar source is in agreement with the study of Ref. [90], which determined that the $f_0(500)$ meson was mostly a $SU(3)$ singlet. For the octet spectral function with $a = 3$ one observes neatly another low-energy peak (this is better seen in the inset of the left panel where the scale is changed to cover more adequately the values for $a = 3$ and 8). This peak is because of the $a_0(980)$ resonance in the chiral limit, as we have checked. The higher energy peak at around 2.3 GeV^2 for $a = 3, 8$ is caused by the bare octet of scalar resonances with a common mass $M_{S_8} \simeq$ 1.4 GeV, Eq. (45), shifted to somewhat higher energies by interference with nonresonant dynamical contributions. Finally, the strong peak in the singlet spectral function at around 1.4 GeV^2 comes from several sources involving the bare singlet resonance S_1 with a mass $M_{S_1} \simeq 1.1$ GeV, Eq. (45), and coupled channel dynamics with the $\eta\eta'$ state. The lightest scalar resonances in the chiral limit were studied earlier in Ref. [25], and the pole positions for the $f_0(500)$ and $a_0(980)$ obtained there are in agreement with ours.

VI. RESULTS FROM THE EXTRAPOLATION OF N_C

Through the fit to experimental data in Sec. V B, we get the unknown couplings that appear in the chiral Lagrangians as well as the subtraction constants. One advantage of employing the chiral Lagrangian approach in the phenomenological study is that once the chiral couplings are determined from one or several sets of data, we completely predict the other quantities that can be calculated from the same theory. For example, the resonance pole positions, pion scalar radius, spectral functions, spectral-function sum rules, and semilocal duality that were discussed previously are all predictions from the fit to the scattering data.

Another advantage of using the chiral Lagrangian approach is studying the behavior of the various quantities by extrapolating the number of colors of QCD, N_C, and then comparing with the results from large N_C QCD [49]. This is straightforward in the chiral Lagrangian approach once the N_C behavior of the parameters from the chiral Lagrangians are known [3,41]. Moreover, $U(3)$ χPT is more appropriate for discussing the large N_C running compared to $SU(3)$ or $SU(2)$ χPT [2,3], since the singlet η_1, explicitly included in the $U(3)$ chiral theory, becomes the ninth pseudo-Goldstone boson in the large N_C and chiral limits. Notice that this relevant degree of freedom is not treated as a dynamical active one in $SU(2)$ or $SU(3)$ χPT [2,3]. It is also worth stressing that the η becomes much lighter with increasing N_C [52], as explicitly shown in Ref. [40], an effect disregarded in previous studies [33,42–48].

Only the leading order scaling with N_C of the resonance parameters, such as couplings and masses, is known without ambiguities [41]. To show how robust is our knowledge of the N_C behavior for the various quantities studied, the subleading orders for the parameters in the N_C counting are necessary and could also be important [33,40,44,47,54]. In Ref. [54], this uncertainty induced by the subleading terms

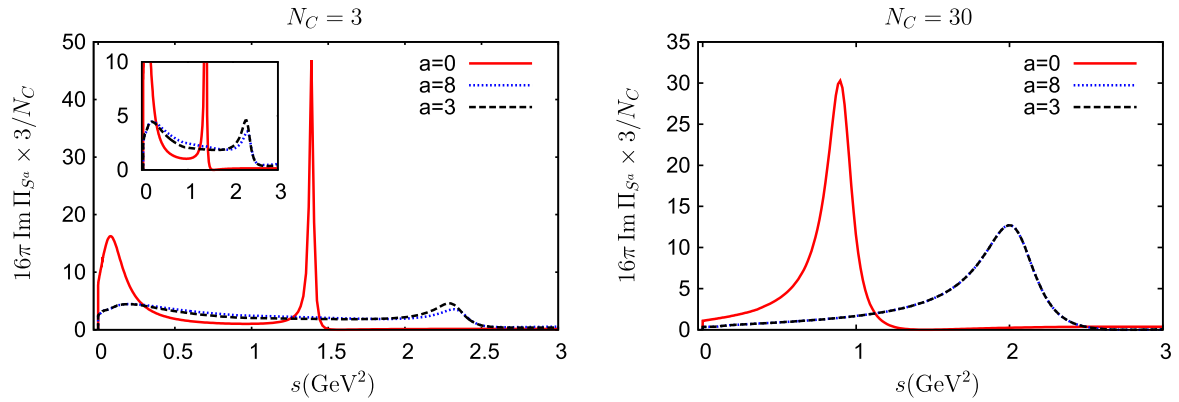

FIG. 8 (color online). The scalar spectral functions at the chiral limit for $N_C = 3$ (left panel) and $N_C = 30$ (right panel) with the new fit of Eq. (45). The values $a = 0$ (red solid line), 3 (black dashed line), and 8 (blue dotted line) are considered. The inset in the left panel shows the same figure with reducing scale, so that the spectral functions with $a = 3$ and 8 are better seen.

in the $1/N_C$ expansion of the LECs is estimated approximately by taking different values of the renormalization scale μ. We adopt a direct way to estimate the subleading order of $1/N_C$ effects, which has been used in Ref. [33]. The idea is that through the fit to data, one can determine the bare resonance couplings and masses from the Lagrangian, which represent their values at $N_C = 3$. Once their values at large N_C are known, we perform the most general smooth extrapolation from $N_C = 3$ to the large N_C values up to and including $1/N_C$ suppressed corrections. Of course, the values at large N_C are not accessible directly by experiment and can be ascertained only through theoretical considerations. In the past decades, great progress along this line has been achieved in the analyses of short distance constraints of two- and three-point Green functions, form factors, τ decays, and $\pi\pi$ scattering within RχT [22,33,46,67,91–94].

The pion decay constant F_π is calculated from the one-loop $U(3)$ χPT in Ref. [40], which also includes subleading terms in the $1/N_C$ expansion. Throughout we always consider both the leading and subleading N_C scaling for F_π when varying N_C as given in Ref. [40]. The values for the fit parameters in Eq. (45) are the ones taken for $N_C = 3$. On the other hand, because of the uncertainties of the values for the resonance parameters at large N_C, we consider several scenarios:

(1) *Scenario 1*: We take only the leading order running with large N_C for all the resonance parameters, starting with their values at $N_C = 3$. As discussed in more detail in Refs. [40,41] the leading running with N_C for the resonance parameters and meson-meson subtraction constants, a_{SL}, is given by

$$\{c_d(N_C), c_m(N_C), G_V(N_C), d_m(N_C)\} = \{c_d(3), c_m(3), G_V(3), d_m(3)\} \times \sqrt{\frac{N_C}{3}},$$
$$\{M_{S_1}(N_C), M_{S_8}(N_C), M_\rho(N_C), M_{K^*}(N_C), M_\omega(N_C), M_\phi(N_C), M_{P_1}(N_C), M_{P_8}(N_C), a_{SL}(N_C)\}$$
$$= \{M_{S_1}(3), M_{S_8}(3), M_\rho(3), M_{K^*}(3), M_\omega(3), M_\phi(3), M_{P_1}(3), M_{P_8}(3), a_{SL}(3)\}. \quad (57)$$

For the singlet couplings $\tilde{c}_d$, $\tilde{c}_m$, and $\tilde{d}_m$, we take the large N_C constraints in Eqs. (44) and (12).

About the N_C running of the subtraction constant a_{SL}, we argue that it is natural to assume its constant behavior at large N_C, though some subleading N_C corrections may exist. This is based on the fact that the unitarized scattering amplitude, defined in Eq. (28), is, in fact, the sum of a series of bubble diagrams with the kernel $N^{IJ}(s)$, since Eq. (28) can be expanded as

$$T^{IJ}(s) = N^{IJ}(s) - N^{IJ}(s)g^{IJ}(s)N^{IJ}(s) + N^{IJ}(s)[g^{IJ}(s)N^{IJ}(s)]^2 + \ldots. \quad (58)$$

Within large N_C QCD it is well known that the leading N_C behavior of a meson-meson scattering amplitude, ${N_C}^\alpha$, corresponds to $\alpha = -1$, and it can also contain other subleading pieces with $\alpha = -2, -3, \ldots$ [49]. This feature for meson-meson scattering is inherited by the construction of χPT [3]. Each single diagram in the geometric series expansion in powers of $g^{IJ}(s)$ of the unitarized amplitude in Eq. (58) should decrease with N_C at least as $1/N_C$. Focusing on the first term in Eq. (58), i.e. the kernel $N^{IJ}(s)$, it represents the perturbative results calculated from χPT, and hence regardless of the resummation it should inherit the N_C behavior of meson-meson scattering amplitudes dictated by large N_C QCD. Its calculation within χPT tells us that it scales as N_C^α with $\alpha = -1$, including typically other subleading components. An immediate conclusion that follows is that the N_C scaling index α for $g^{IJ}(s)$ can be only an integer, following the above arguments. Moreover, $\alpha \geq 2$ can also be simply excluded, otherwise the terms with $g^{IJ}(s)$ in Eq. (58) could violate the large N_C QCD prediction to the scattering amplitudes. The case $\alpha = 0$, i.e. $g^{IJ}(s)$ behaves as a constant at large N_C, is indeed the natural choice for the following reasons:

(a) The relative size between a term and the next one in the expansion of Eq. (58) is $g^{IJ}(s)N^{IJ}(s)$. At leading order $N^{IJ}(s)$ behaves as p^2/F^2, with p^2 a typical soft external four-momentum squared attached to the pseudo-Goldstone bosons. From the subtraction constant a_{SL} in Eq. (27) we then have the suppression factor

$$\frac{a_{SL}p^2}{(4\pi F)^2}. \quad (59)$$

For subtraction constants a_{SL} of $\mathcal{O}(1)$ size, as the fitted values shown in Eq. (45), one then has the typical suppression for unitarity loops in χPT, given in terms of the chiral symmetry breaking scale $\Lambda_{\chi\text{PT}} = 4\pi F$ [95]. In order to keep this interpretation with running N_C it is necessary that every unitarity loop is suppressed by an extra power of $1/N_C$ and, for that, the subtraction constants a_{SL} should be $\mathcal{O}(N_C^0)$.

(b) The combination

$$a_{SL}(\mu) - \log\mu^2 \quad (60)$$

in Eq. (27) is independent of the renormalization scale μ. Let us consider another value μ'

for which $a_{SL}(\mu') = 0$. From the previous equation it follows that

$$\mu' = \mu e^{-a_{SL}(\mu)/2}. \tag{61}$$

From here it is obvious that if $|a_{SL}(\mu)|$ is too different from 1, then μ' exponentially diverges for $a_{SL}(\mu) \ll -1$ or tends to 0 for $a_{SL} \gg 1$. In both cases one has too different values from the typical one for a renormalization scale in χPT, $\mu \sim 0.5$–1 GeV, of the similar size to the previously introduced chiral symmetry breaking scale $\sim$1 GeV or the mass of the ρ resonance. The fitted values for the subtraction constants in Eq. (45) have the right size so as to keep an adequate value for μ', which does not scale with N_C [nor should the $a_{SL}(\mu)$ so that Eq. (61) is meaningful].

As commented in Eq. (14), since we explicitly include the resonance contributions to L_8, which grows like N_C in the $1/N_C$ expansion [41], we consider that δL_8 is just some remnant piece subleading in N_C. So we take

$$\delta L_8(N_C) = \delta L_8(3), \tag{62}$$

throughout the following discussion. Concerning the parameters Λ_2 and M_0, their leading N_C scaling reads [69]

$$\{\Lambda_2(N_C), M_0^2(N_C)\} = \{\Lambda_2(3), M_0^2(3)\} \times \frac{3}{N_C}. \tag{63}$$

(2) *Scenario 2*: Comparing with Scenario 1, we include the subleading N_C scaling for the vector resonance parameter G_V in Eq. (5), which describes the interaction between the vector resonances and the pseudo-Goldstone boson pairs, e.g. the $\rho(770)\pi\pi$ coupling. The original type of Kawarabayashi-Suzuki-Riazuddin-Fayyazuddin (KSRF) relation [96] predicts $G_V = F/\sqrt{2}$. This relation was also derived from the high-energy constraint of the pion vector form factor at tree level [67]. An updated study of the vector form factor at the one-loop level [93] revealed a new version for the constraint:

$$G_V = \frac{F}{\sqrt{3}}. \tag{64}$$

This modified KSRF-like relation has also been confirmed in various contexts: partial wave $\pi\pi$ scattering [40,46], radiative tau decay [94], and extradimension model for $\pi\pi$ scattering [97]. The large N_C value for the pion decay constant in the chiral limit can be deduced from the $U(3)$ χPT study of Ref. [40] with the current fit results in Eq. (45), leading to $F \simeq 80\sqrt{\frac{N_C}{3}}$ MeV.

We impose the constraint for G_V given in Eq. (64) at large N_C, and the extrapolation function between $N_C = 3$ and $N_C \to \infty$ with $1/N_C$ suppressed corrections included is

$$G_V(N_C) = G_V(N_C = 3)\sqrt{\frac{N_C}{3}} \times \left[1 + \frac{G_V(N_C = 3) - G_V^{\rm Nor}(N_C \to \infty)}{G_V(N_C = 3)} \times \left(\frac{3}{N_C} - 1\right)\right], \tag{65}$$

where $G_V^{\rm Nor}(N_C \to \infty) = G_V(N_C \to \infty)\sqrt{\frac{3}{N_C}}$ and $G_V(N_C \to \infty)$ is given by Eq. (64). Notice that $G_V^{\rm Nor}(N_C \to \infty)$ is finite in the large N_C limit. With the running of F_π as a function of N_C from Ref. [40] we have the numerical value

$$G_V^{\rm Nor}(N_C \to \infty) \simeq 46 \text{ MeV}. \tag{66}$$

Were the subleading N_C scaling for G_V not considered, i.e. if

$$G_V^{\rm Nor}(N_C \to \infty) = G_V(N_C = 3), \tag{67}$$

then Eq. (65) reduces to the leading behavior $G_V(N_C) = G_V(N_C = 3)\sqrt{\frac{N_C}{3}}$, as in Eq. (57). We stress that the extrapolation function in Eq. (65) is unique if one considers only the next-to-leading order in the $1/N_C$ scaling for the considered parameter. Similar extrapolation functions are also used for the other resonance parameters when needed, as specified below. For the other parameters, we keep the same setups from Scenario 1.

(3) *Scenario 3*: Here, in addition to Eq. (65) of Scenario 2, we also assume that the bare masses of the $\rho(770)$ resonance and the singlet scalar resonance S_1 [an important component of the $f_0(980)$ at $N_C = 3$] approach the same value at large N_C. We can realize this scenario by increasing the bare $\rho(770)$ mass by 16% and decreasing the bare S_1 mass by another 16%, so that their large N_C masses meet around 930 MeV. This value is indeed quite close to the preferred one for the $\rho(770)$ in Ref. [54] in the large N_C limit. We take as the extrapolation function the analogous one to Eq. (65):

$$M^2(N_C) = M^2(N_C = 3) \times \left[1 + \frac{M^2(N_C = 3) - M^2(N_C \to \infty)}{M^2(N_C = 3)} \times \left(\frac{3}{N_C} - 1\right)\right], \tag{68}$$

with M either the $\rho(770)$ or S_1 bare mass.

TABLE IV. Description of Scenarios 1–4. In the second and third columns the symbol − denotes that the subleading N_C scaling for the corresponding parameters (indicated in the first row) is not considered. In turn, $\surd$ denotes that the subleading N_C scaling is taken into account. In the last column, the symbol − means that we do not consider the contribution from the D waves and $\surd$ indicates that the latter are taken into account.

	G_V	M_ρ, M_{S_1}	D wave
Scenario 1	−	−	−
Scenario 2	$\surd$	−	−
Scenario 3	$\surd$	$\surd$	−
Scenario 4	$\surd$	$\surd$	$\surd$

(4) *Scenario 4*: On top of the considerations in Scenario 3 we now consider the effects of the D waves, which include additionally the contributions from the tensor resonances. For their resonance parameters in Eq. (C1), we take the leading order scaling with N_C,

$$g_T(N_C) = g_T(3) \times \sqrt{\frac{N_C}{3}}, \quad M_T(N_C) = M_T(3). \quad (69)$$

We summarize the different Scenarios 1–4 in Table IV. We also considered another situation in which together with the characteristics of Scenario 3 we take at large N_C the mass of the octet of scalar resonances to be the same as that of the S_1 and $\rho(770)$. However, we checked that this new addition produces negligible contributions to the ratios $F_n^{II'}$ and R_n^I. The reason is because the coupling of the octet of scalar resonances to $\pi\pi$ is suppressed numerically compared with that of the singlet scalar resonance. Because of the fact that at large N_C the $\bar{q}q$ resonances fall down to the bare mass position in the real axis, it will cause noticeable changes for the octet resonance pole trajectories. Nevertheless since the reason is obvious, we do not discuss any further this scenario.

A. Semilocal duality for $N_C > 3$

For all the scenarios we plot in Fig. 9 the N_C trajectories of the ratio F_n^{21} with $t = 4m_\pi^2$, defined in Eq. (39). We verify that the results for $t = 0$ are quite similar. The (red) solid line is for Scenario 1, the (green) dashed line is for Scenario 2, the (blue) dot-dashed line corresponds to

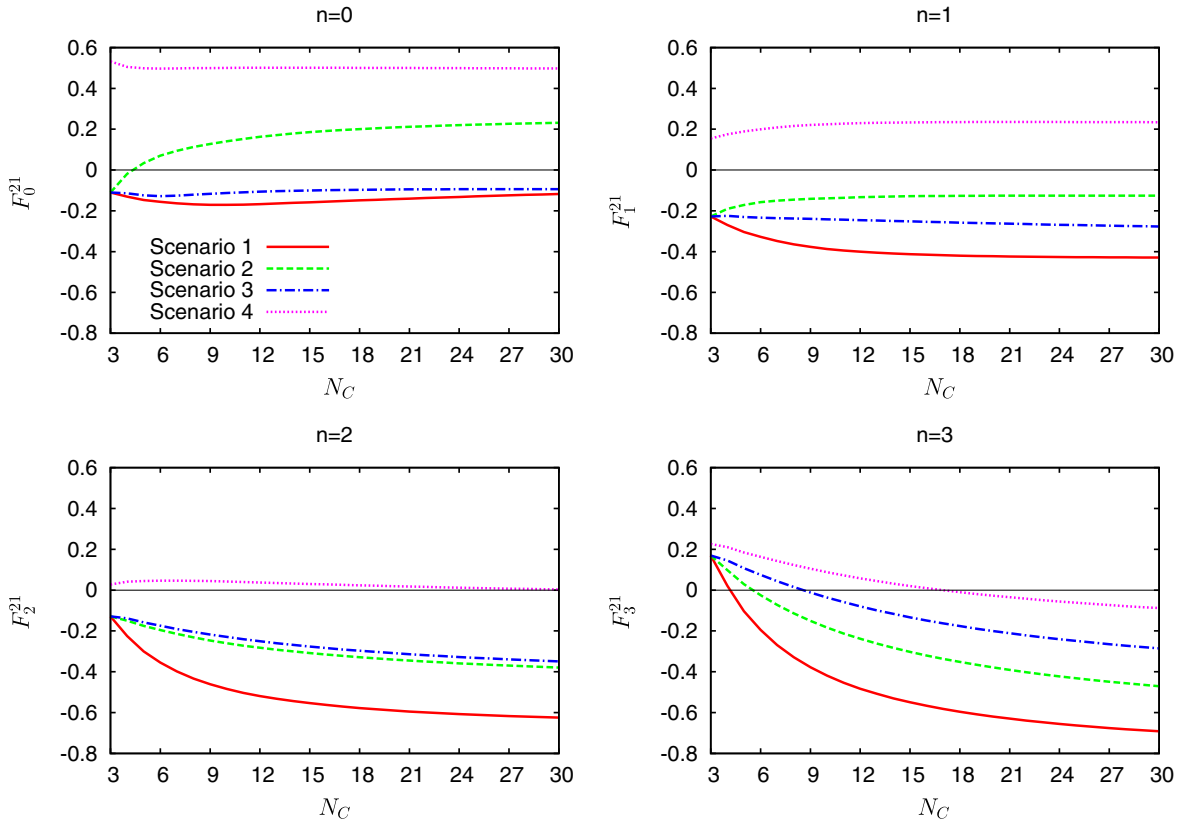

FIG. 9 (color online). $F_n^{21}(t = 4m_\pi^2)$. The solid (red) lines correspond to the current fit, and only the leading order of the N_C scaling for the resonance parameters is considered, i.e. Scenario 1. The dashed (green) lines additionally include the subleading N_C scaling for G_V, i.e. Scenario 2. The dot-dashed (blue) lines correspond to take into account the subleading N_C scaling for G_V, M_ρ, and M_{S_1}, i.e. Scenario 3. The dotted (magenta) lines show Scenario 4 so that the D-wave contribution is included as well.

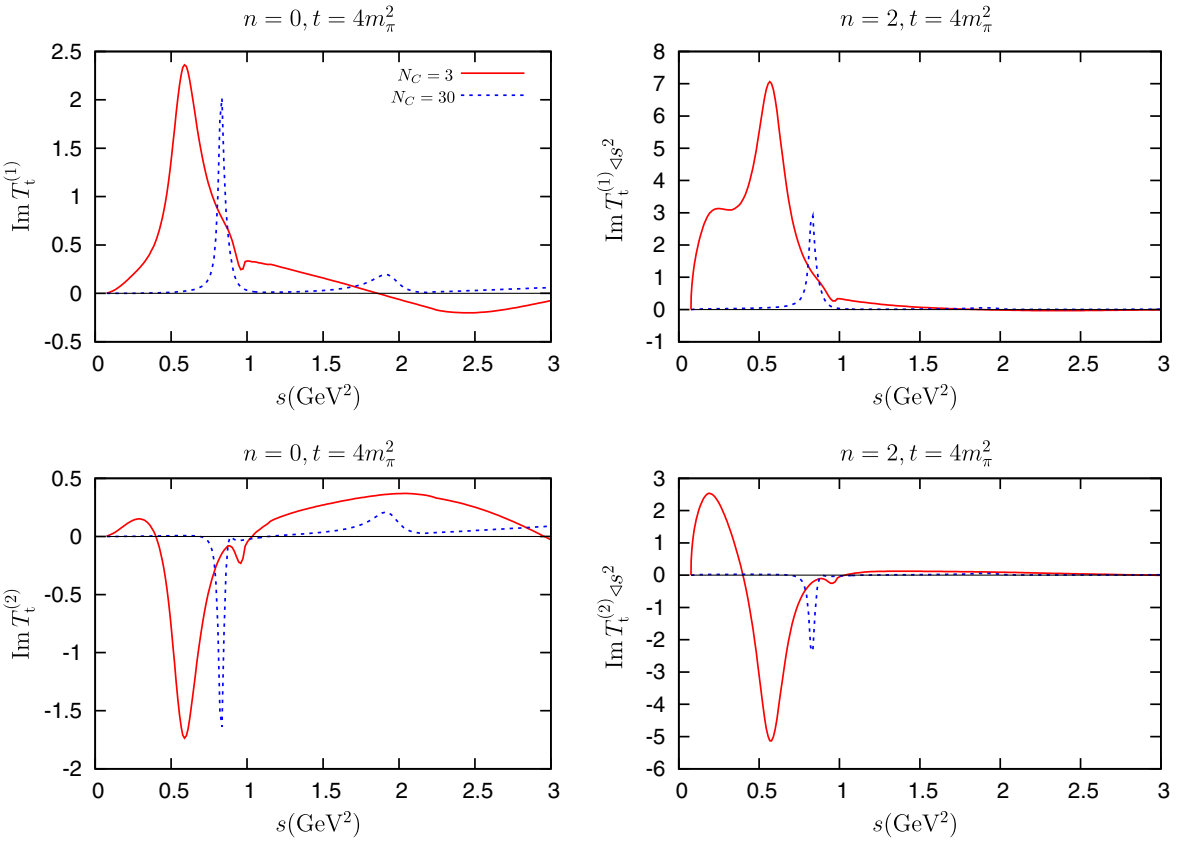

FIG. 10 (color online). For Scenario 3, we show $\mathrm{Im}T_t^{(1)}(t = 4m_\pi^2)$ in the two panels of the top row and $\mathrm{Im}T_t^{(2)}(t = 4m_\pi^2)$ in the ones at the bottom. The results from $N_C = 3$ (red solid lines) and 30 (dashed blue lines) are displayed for all four figures.

Scenario 3, and the (magenta) dotted line corresponds to Scenario 4. Among the first three scenarios the best is the third one since then the curves have the smallest absolute values for most of the N_C axis, as required by the Regge theory and semilocal duality. The only exception is F_1^{21} where Scenario 2 gives smaller values. Concerning Scenario 4, though it gives better results for $n = 2$, 3 than the others, it leads to too large values for the $n = 0$ case. In Fig. 10, we show the imaginary part of the amplitudes with well-defined isospin in the t channel for Scenario 3 at $N_C = 3$ and $N_C = 30$. Their integration, according to Eq. (39), gives F_n^{21}. For $N_C = 3$ one can clearly see in the bottom-left plot of Fig. 10 a resonant bump in the 1–3 GeV^2 region, which is absent in Ref. [54]. This is mainly contributed by the higher scalar resonance $f_0(1370)$, and it plays an important role to balance the contribution of the $\rho(770)$ resonance. Nonetheless, its contribution becomes less important with increasing N_C, and for $n \geq 2$ it has only a marginal contribution for all the N_C values. When N_C grows, the $f_0(500)$ resonance pole obtained in unitarized $U(3)$ RχT moves deeper and deeper in the complex energy plane and thus barely contributes. The role played in Ref. [54] by the subdominant $\bar{q}q$ component for the $f_0(500)$ with a mass around 1 GeV to cancel the $\rho(770)$ contribution for $n = 2, 3$, is played in this work by the $f_0(980)$ resonance, which gradually evolves to the scalar singlet S_1 resonance and starts behaving as a $\bar{q}q$ state for $N_C > 6$. In both works, a $\bar{q}q$ scalar state with a mass around 1 GeV is needed in order to satisfy local duality. The evolution of the resonance poles with increasing N_C will be discussed in detail in the next section.

Focusing on the solid (red) lines in the four panels of Fig. 9, resulting from Scenario 1, one can immediately conclude that semilocal duality, though satisfied at $N_C = 3$ for all the values of n, is not well satisfied at large N_C for $n \geq 1$. Indeed, the situation taking place for Scenario 1 is quite similar to the one-loop IAM case of Ref. [54] where the $f_0(500)$ does not show a subleading $\bar{q}q$ component. For $n = 0$, both the one- and two-loop IAM results satisfy approximately semilocal duality at large N_C, while only the results that include the $\bar{q}q$ subleading component for the $f_0(500)$ [54] show a clear sign of duality for $n = 1$, 2, and 3. The appearance of this $\bar{q}q$ subdominant component, which approaches the real axis in the complex energy plane at large N_C, plays the fundamental role in the fulfillment of duality in Ref. [54]. However, one should also keep in mind that the N_C behavior for the $\rho(770)$ resonance in the two-loop result, with its pole position at $\sqrt{s_\rho} = M_\rho - i\Gamma_\rho/2 = (950.0 - i34.8)$ MeV for $N_C = 12$, is quantitatively different compared with the one-loop result for the same value of

N_C, $\sqrt{s_\rho} = (710.5 - i18.4)$ MeV [54]. Because of the small ratios of Γ_ρ/M_ρ for $N_C = 12$ (in both cases it is less than 0.1), a reasonable approximation consists of using the narrow resonance approximate formula to estimate the $\rho(770)$ contribution in both cases to $\mathrm{Im}T^{IJ=11}(s)$. It reads [53]

$$\mathrm{Im}\, T^{11}(s) = 16\pi^2 \frac{M_\rho \Gamma_\rho}{\bar{\sigma}(M_\rho^2)} \delta(s - M_\rho^2), \tag{70}$$

where $\bar{\sigma}(s) = \sqrt{1 - 4m_\pi^2/s}$. We have adjusted the normalization of the partial wave amplitude in Eq. (70) to the one defined in Ref. [40] and used in this work. Now, one can analytically calculate the $\rho(770)$ contribution to the right-hand side of Eq. (36), which finally enters in the ratios of Eqs. (38) and (39). By applying Eq. (70), the $\rho(770)$ contribution to the FESR for $I_t = 2$ in terms of its width and mass is

$$\int_{\nu_1}^{\nu_{\max}} \nu^{-n}\, \mathrm{Im}T_{t,\rho}^{I=2}(\nu, t) d\nu = -24\pi^2 \frac{\Gamma_\rho M_\rho^{1-2n}}{\bar{\sigma}(M_\rho^2)}, \tag{71}$$

where the integration region between ν_1 and $\nu_{\max}$ always covers the $\rho(770)$ mass. For simplicity we show in the previous equation the result at $t = 0$, and similar results can be straightforwardly deduced for other values of t. The ratio of the $\rho(770)$ contribution between the two- and one-loop cases from [54] as follows from Eq. (71) is

$$\frac{\Gamma_{\rho,\mathrm{two-loop}}}{\Gamma_{\rho,\mathrm{one-loop}}} \left(\frac{M_{\rho,\mathrm{two-loop}}}{M_{\rho,\mathrm{one-loop}}}\right)^{1-2n} \frac{\bar{\sigma}(M^2_{\rho,\mathrm{one-loop}})}{\bar{\sigma}(M^2_{\rho,\mathrm{two-loop}})}. \tag{72}$$

Taking into account the $\rho(770)$ pole positions for $N_C = 12$ from Ref. [54], which were explicitly shown above, the ratio in the previous equation is 0.43 for $n = 3$. This implies that the $\rho(770)$ contribution is reduced by more than 50% in the two-loop result compared with the one-loop case in the IAM study of Ref. [54]. When increasing N_C this ratio will stay put since the $\rho(770)$ resonance already starts to behave as a standard $\bar{q}q$ resonance at $N_C = 12$, with its mass approaching a constant and its width decreasing as $1/N_C$ [42,43,54]. Though this N_C behavior of the $\rho(770)$ pole is not essential in Ref. [54] to satisfy local duality, it definitely helps to improve it.

This reduction of the ρ signal with increasing N_C is explained by our present approach in a quite transparent way. For that one needs to take into account the subleading N_C scaling of the resonance parameters. It is also the case that when the latter are taken into account semilocal duality is also better fulfilled. Among the estimates of the subleading scaling for various resonance parameters, G_V is the most reliable one, since it can be directly derived by requiring a proper high-energy behavior of the partial wave amplitudes, which are the key input in the study of semilocal duality. In addition, this constraint has also been confirmed in different processes, as already discussed above [40,46,93,94,97]. It turns out that the large N_C condition Eq. (64) considerably improves the fulfillment of semilocal duality. Thus, we provide another hint to confirm this constraint. This improvement is displayed in Fig. 9 by the difference between the solid (red) lines and the dashed (green) lines. The slight readjustment of the bare masses for the $\rho(770)$ and S_1 at large N_C seems to improve the situations for $n = 0$ and $n = 3$, which can be seen from the differences between the dashed (green) lines and the dot-dashed (blue) ones. It causes significant effects for $n = 0$ by alternating the sign of the ratio; nevertheless the magnitudes are always less than 0.2.

Finally, we comment on the D-wave effects. Though the D-wave amplitudes can gain contributions from many sources, such as chiral loops, scalar, pseudoscalar, and vector resonances exchanged in crossed channels, one expects from phenomenological reasons that the most important ones correspond to the tensor resonances [98,99]. From the change between the dot-dashed (blue) lines and the dotted (magenta) ones in Fig. 9, one can discern the role that the D waves play in the FESR. As one can see, it is significant for $n = 0$, 1, 2 and slight for $n = 3$ (and it should be even smaller for larger values of n since then low-energy physics is enhanced, as already commented). For $n = 1$, though the tensor resonances alternate the sign of the ratios, the magnitudes are still quite small when varying N_C. It also clearly improves the condition for $n = 2$ and $n = 3$, though for $n = 0$ it clearly deteriorates the fulfillment of semilocal duality. We observe that the D waves give rise to a large contribution that overbalances the one of the $\rho(770)$. This hints that higher vector resonances are necessary to cancel the D-wave contributions. In order to give a rough idea on whether the $\rho(1450)$ resonance in PDG [35] can counteract the D-wave contribution, we include another heavier vector resonance in $\pi\pi$ scattering following the formula in Eq. (70). We refer this resonance as ρ' in the following. The only difference now is that $\Gamma_{\rho'}$ in Eq. (70) should be understood as the partial decay width $\Gamma_{\rho' \to \pi\pi}$. Moreover, since we focus on semilocal duality below 2 GeV^2, we simply set the ρ' mass as 1350 MeV in order to cover its peak for the integral in Eq. (36). We find the $\rho(1450)$-type resonance gives a negligible contribution for all the values of n, because of its too small decay branching ratio to $\pi\pi$ (about 6%), as follows from the present information in PDG [35]. We verify that the decay branching ratio to $\pi\pi$ of the hypothetical resonance ρ' needs to be about 40% in order to decrease the large contribution by the D wave for the $n = 0$ case down to 0.2. This is a hint in favor of the existence of a heavy ρ' with a significant branching decay ratio to $\pi\pi$. For $n = 1$, 2, 3 no cancellations or just small ones are, in fact, needed in order to have a rather suppressed FESR with $I = 2$ in the t channel. Nevertheless, if included for these values of n, the resulting curves are equally satisfactory (even better for $n = 1$).

B. Resonance pole trajectories with varying N_C

Unless the opposite is stated, all the N_C pole-trajectory evolutions studied from now on correspond to Scenario 3 in Table IV. This is also the scenario that satisfies best semilocal duality, as seen in Sec. VI A.

Because of the N_C behavior of the singlet η_1 mass M_0 in Eq. (63), a novel feature of $U(3)$ χPT, as compared with the $SU(3)$ version, is that the masses of the pseudo-Goldstone bosons at large N_C, especially for η and η', can be significantly different from their physical values at $N_C = 3$, as shown in Ref. [40]. On the other hand, the masses of the pion and kaon barely change when varying N_C. Similar results are obtained from the new fit in Eq. (45), which are depicted in Fig. 11. One can see there that for $N_C = 30$, the η and η' masses decrease from their physical values down to around 300 MeV and 700 MeV, respectively. We point out the η' retains a somewhat heavy mass at large values of N_C mainly caused by the kaon mass [40]. This is easily seen by the leading order expression of the η and η' masses from $U(3)$ χPT [40]. They result from the tree level calculation using the leading order Lagrangian Eq. (1) at the large N_C limit, i.e. $M_0 \to 0$,

$$\bar{m}_\eta^2 = \bar{m}_\pi^2, \qquad \bar{m}_{\eta'}^2 = 2\bar{m}_K^2 - \bar{m}_\pi^2, \tag{73}$$

where $\bar{m}_\eta$ and $\bar{m}_{\eta'}$ stand for the η and η' masses, respectively.

The expressions that relate $\bar{m}_\pi^2$ and $\bar{m}_K^2$ with m_π^2 and m_K^2 at the one-loop level are given by Eqs. (A1), (B2), (B4), and (B7) of Ref. [40] to which one must add the new contribution Eq. (A1), because of δL_8 and the exchange of the pseudoscalar resonances. The numerical values from the new fit in Eq. (45) for the pion and kaon leading-order masses extracted at the one-loop level are

$$\bar{m}_\pi = 136.4^{+2.3}_{-1.7}\,\text{MeV}, \quad \bar{m}_K = 499.6^{+30.6}_{-30.4}\,\text{MeV}, \tag{74}$$

which leads to

$$\bar{m}_\eta = 136.4^{+2.3}_{-1.7}\,\text{MeV}, \quad \bar{m}_{\eta'} = 693.3^{+43.7}_{-43.8}\,\text{MeV}, \tag{75}$$

according to Eq. (73). We point out that at the chiral and large N_C limits, all the masses of the nonet of Goldstone bosons vanish. The N_C evolution of the leading order mixing angle in Eq. (23), given explicitly in Eq. (B7) of Ref. [40], is displayed in Fig. 12. At large N_C it corresponds to ideal mixing, as it should.

In the study of the evolutions of the resonance pole positions we always take the N_C running masses for the pseudo-Goldstone bosons as shown in Fig. 11. The resulting N_C trajectories of the various resonance poles and their residues were studied in detail in Ref. [40]. Qualitatively speaking we do not find any significant changes in the trajectories by using the new fit in Eq. (45), and thus we confirm the conclusions obtained in this reference: the $f_0(500)$, $K_0^*(800)$, and $a_0(980)$ resonances go deeper in the complex energy plane when increasing the values of N_C. For the other resonances, $f_0(980)$, $f_0(1370)$, $K_0^*(1430)$, $a_0(1450)$, $\rho(980)$, $K^*(892)$, and $\phi(1020)$ approach the real axis and behave like the standard $\bar{q}q$ resonances at large N_C. Notice that the $f_0(980)$ for not so large values of N_C does not follow the standard $\bar{q}q$ pattern (compare with the pole trajectories for the vector resonances in Fig. 15 below). For example, its width indeed clearly increases up to $N_C \simeq 7$. This is a signal of the fact that the $f_0(980)$ has also a strong contribution to its nature as a $K\bar{K}$ bound state [24].

Two variant approximations, named *vector reduced* and *mimic* $SU(3)$, were studied to explore the N_C trajectories of the resonance pole positions in Ref. [40]. In the vector reduced case, we freeze out the full propagators of the vector resonances in the scattering amplitudes and keep only the leading local terms generated from them, which are $\mathcal{O}(p^4)$ in the chiral counting [or $\mathcal{O}(\delta^3)$]. The purpose

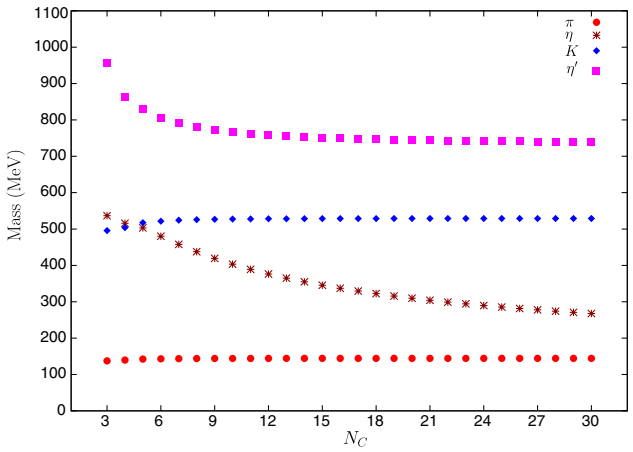

FIG. 11 (color online). N_C running for the masses of pseudo-Goldstone bosons.

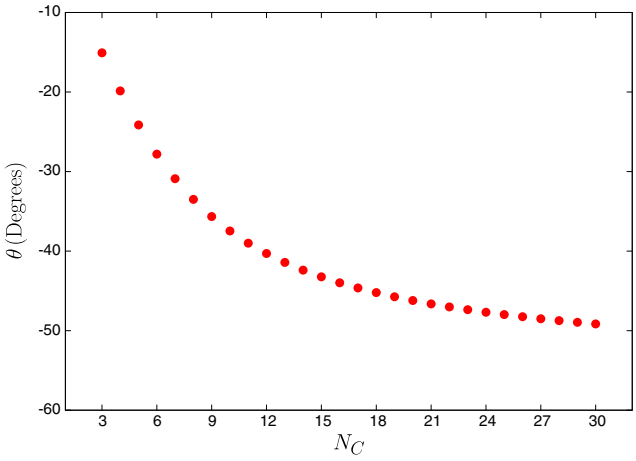

FIG. 12 (color online). N_C running for the leading order $\eta - \eta'$ mixing angle θ introduced in Eq. (23).

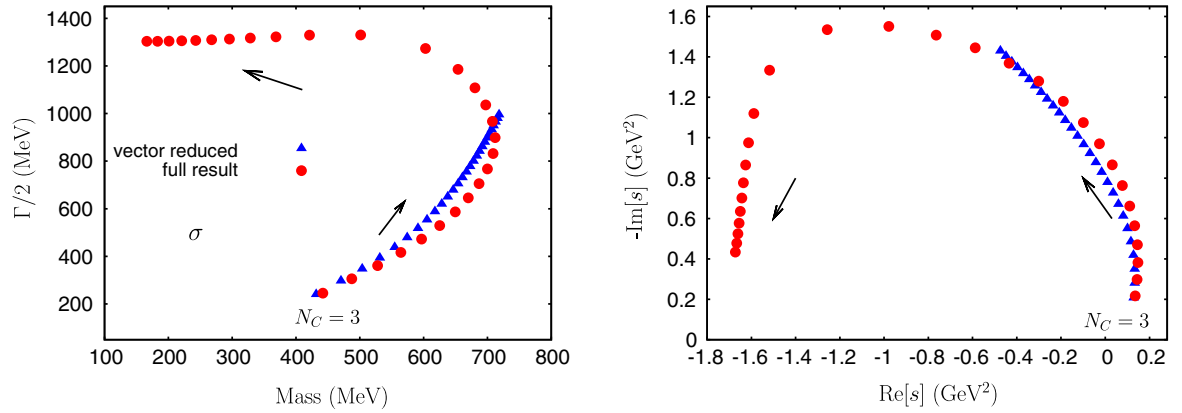

FIG. 13 (color online). N_C running of the pole positions for the $f_0(500)$ (or σ) resonance. We give the results for N_C from 3 to 30 with one unit step. Both the full results and the ones from the vector reduced approximation are displayed. The left panel shows $\sqrt{s_\sigma}$ and the right one s_σ.

for introducing this approximation is to highlight the difference between using the tree level resonance exchanges and the local LECs in the meson-meson scattering amplitudes. As discussed in Ref. [40], we find that freezing the bare scalar resonances in the amplitudes does not lead to significant effects for the $f_0(500)$ resonance. This is why we only discuss the vector reduced case. In the approximation of mimic $SU(3)$, instead of taking the N_C running masses for the pseudo-Goldstone bosons, we freeze them throughout and, in addition, we do not consider any $\eta - \eta'$ mixing terms. Thus, in this case, the η and η' correspond to the octet η_8 and singlet η_1, respectively. The masses of π, K, and η are fixed at the physical values, and the η' mass is taken from the leading order prediction of Eq. (1), which is around 1040 MeV. This mimics the conditions of $SU(3)$ χPT that we consider for comparison with our $U(3)$ χPT results.

In Fig 13, we explicitly show the full (circles) and vector reduced (triangles) results for the $f_0(500)$ resonance pole (s_σ) from $N_C = 3$ up to $N_C = 30$ in one unit step (as will also be the case for the rest of the pole trajectories). Though different strategies to estimate the subleading N_C scaling for the resonance parameters have been used in the current work, the N_C trajectories for the $f_0(500)$ are qualitatively consistent with those found in Ref. [40]. That is, the $f_0(500)$ resonance from the full calculation tends to fall down to the negative real axis in the s_σ-complex plane and moves farther and farther away along the nearby s_σ negative axis as N_C increases. For the vector reduced case this is not the case. The outcome from the latter resembles the $f_0(500)$ pole trajectory from the one-loop IAM [42,44], and the full result trajectory is also one of the different $f_0(500)$ pole trajectories [54,100]. It is important to remark that both results, as well as the ones of Ref. [54], are compatible for values of $N_C < 10$ and confirm again the results obtained in [42,43], which predict a nondominant $\bar{q}q$ behavior for the $f_0(500)$. The outcome from the mimic $SU(3)$ approximation, which is not explicitly shown in the figure, is quite close to the full results, indicating the insensitivity of the σ resonance to the η and η' mesons, even when quite different masses result for these two particles as a function of N_C. As explained in Ref. [40] this relative insensitivity is because of the small couplings of the $f_0(500)$ to the $\eta\eta$, $\eta\eta'$, and $\eta'\eta'$, even though these couplings are somewhat larger in the new fit than in the previous one. However, the largest couplings to $\pi\pi$ and $K\bar{K}$ are almost the same as in Ref. [40]. This pole trajectory clearly indicates that the $f_0(500)$ resonance has no significant $q\bar{q}$ or glueball components, and it is in agreement with its dynamical generation from the isoscalar scalar $\pi\pi$ interactions. Reference [37] calculates the quadratic scalar radius of the σ, $\langle r^2\rangle^s_\sigma = (0.19 \pm 0.02) - i(0.06 \pm 0.02)\,\mathrm{fm}^2$, so that it is concluded that this resonance is a compact one and the two pions merge inside it. As a result, a four-quark picture is more favorable than the molecular description.

On the other hand, the resulting pole trajectories of the heavier scalar resonances for the full result and the mimic $SU(3)$ approximation are quite different from each other, as one can see in Fig. 14. This tells us that the scalar resonances $f_0(980)$, $f_0(1370)$, $K_0^*(1430)$, and $a_0(1450)$ are sensitive to the η and η' states, to which they couple strongly as shown in Table I. For the vector resonances, we show the N_C trajectories in Fig. 15, where the different treatments of the η and η' mesons barely change the $\rho(770)$ resonance and only a little the $K^*(892)$. A kink structure has been found for the coupling strength between the $K^*(892)$ resonance and the $K\eta$ channel in the full result around $N_C = 14$ [40], which is caused by the crossover of the $K^*(892)$ mass by the $K\eta$ threshold. This is mainly due to the variation of the η mass. We find the structure from the new fit is quite similar to the one in Ref. [40]. For the $\phi(1020)$ and $\omega(780)$ resonances, we verify that it is also well behaved as a $\bar{q}q$ resonance at large N_C. The situation

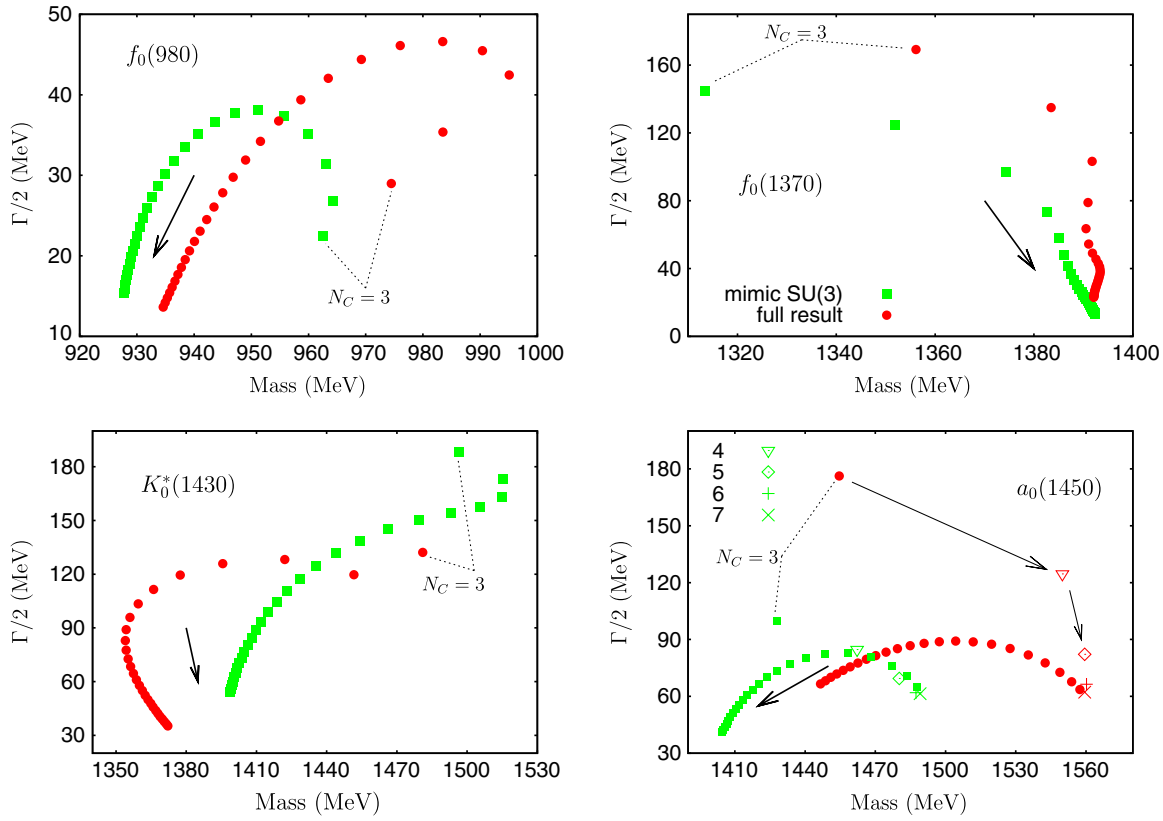

FIG. 14 (color online). N_C trajectories of the scalar resonances $f_0(980)$, $f_0(1370)$, $K_0^*(1430)$, and $a_0(1450)$. We show the results for N_C from 3 to 30 with one unit step. The results for both the full (circles) and the mimic $SU(3)$ (squares) calculations are shown. The differences between the two sets of trajectories show the sensitivity of the corresponding resonances to the η and η' mesons. Specific symbols are assigned to the $a_0(1450)$ resonance for $N_C = 4, 5, 6, 7$ in order to show more clearly its pole trajectory.

is even simpler in this case, since it only involves the $K\bar{K}$ channel in our approach.[6] For the $K_0^*(800)$ and $a_0(980)$ resonances, we reconfirm as in Ref. [40] that their pole positions go deeper in the complex energy plane when increasing N_C, which are displayed in Fig 16.

C. Spectral-function sum rules for $N_C > 3$

As a further application, we study the N_C evolution of the spectral functions and the spectral-function sum rules in this section. The scaling with N_C for the two-point correlators, i.e. W_i in Eq. (54), is proportional to N_C in the large N_C QCD [49]. The situation for the pseudoscalar correlators is obvious, since after substituting Eqs. (33), (B6), and (B7) into Eq. (54) one has

$$W_i \propto F_\pi^2 + 8d_m^2 + \cdots, \qquad i = P^0, P^8, P^3, \tag{76}$$

where the ellipsis stand for both subleading N_C or suppressed pieces in the chiral counting. From Eq. (57) and the fact that F_π scales as $\sqrt{N_C}$, it results that the leading N_C scaling of the pseudoscalar correlators is proportional to N_C.

However, the situation for the scalar correlators is not so obvious. In fact, if we simply use the tree level results in Eqs. (B1)–(B3), from the Lagrangian in Eq. (1) and substitute them into Eq. (19) to calculate the correlators in Eq. (54), we would conclude that the latter behaves as a constant at large N_C, instead of running like N_C. The subtlety, as shown in detail below, comes from the fact that at large N_C the width of a $\bar{q}q$-like resonance tends to zero and the imaginary part of its propagator behaves then as a Dirac δ function, which is the dominant contribution to the correlators in Eq. (54).

In the following discussion, we demonstrate that by properly taking into account the resonance contributions in the unitarized scalar form factors [Eq. (25)] for the pseudo-Goldstone boson pairs, the scalar correlators in our formalism also scale like N_C, as required by large N_C QCD. In order to make the analytical discussion neatly, we illustrate the proof in the chiral limit and consider the single channel case; i.e. we only include the $\pi\pi$ channel for both the scalar form factor and the scattering. The relevant parts $R^I(s)$, $N^{IJ}(s)$, and $g^{IJ}(s)$ in Eq. (25) are

[6] In the present study we are missing the important 3π channel for a realistic treatment of the $\omega(780)$ resonance. We can only then study its mass, which can be fixed to its experimental value by tuning its bare mass, as similarly done for the other vector resonances.

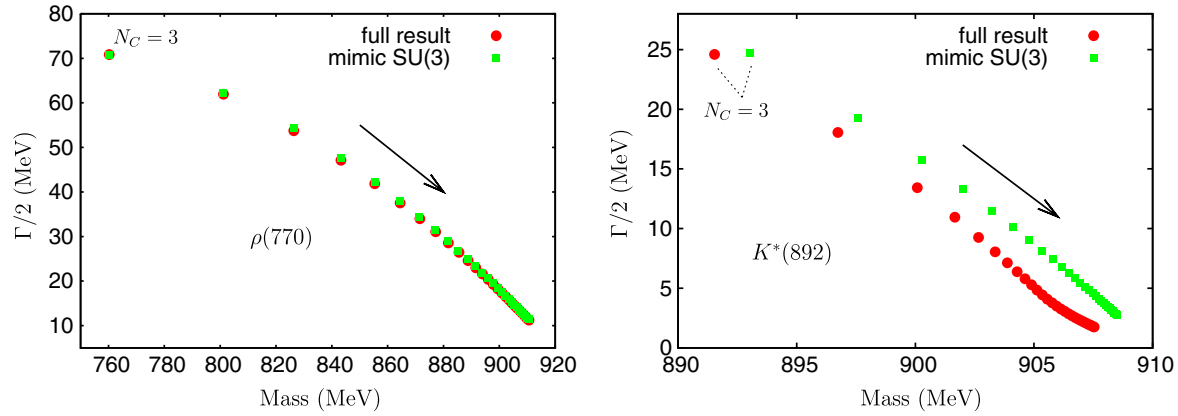

FIG. 15 (color online). N_C running of the pole positions for the $\rho(770)$ and $K^*(892)$ resonances. For notation see Fig. 14.

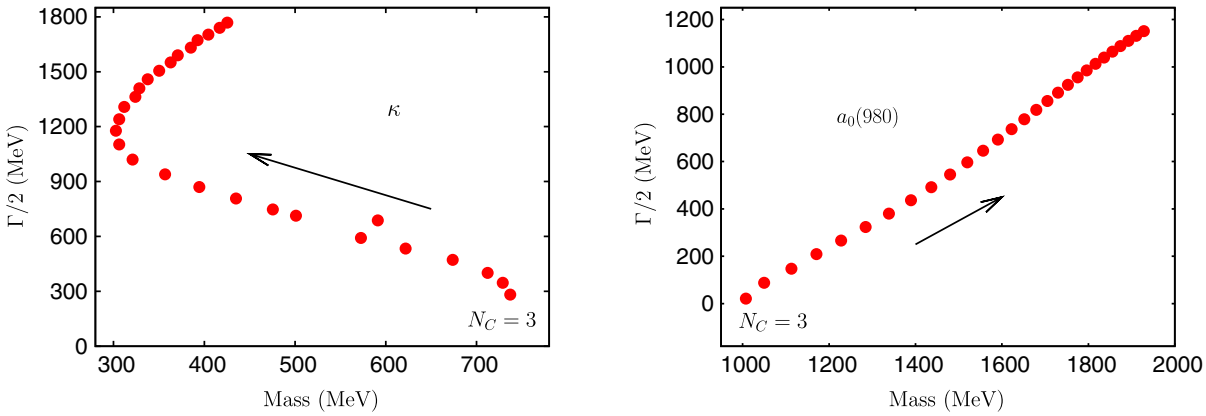

FIG. 16 (color online). N_C dependences of the $K_0^*(800)$ and $a_0(980)$ resonances both in the fourth Riemann sheets from $N_C = 3$ to 30 with one unit step. See Ref. [40] for details on the definitions of the different Riemann sheets.

just functions not matrices for the single channel. Notice also that in the large N_C limit, only the tree level contributions, i.e. the (2) + Res parts in Eq. (26), can survive. We focus on the case $a = 0$, while the others can be obtained analogously. The corresponding expressions in the chiral and large N_C limits are

$$R^{a=0}(s) = -2 - \frac{8c_d c_m}{F^2}\frac{s}{M_S^2 - s}, \tag{77}$$

$$N^{00}(s) = \frac{s}{F^2} - \frac{G_V^2(2M_\rho^2 + 3s)}{F^4} + \frac{2G_V^2 M_\rho^2(M_\rho^2 + 2s)}{F^4 s} \times \log\left[1 + \frac{s}{M_\rho^2}\right] + \frac{2c_d^2 M_S^4}{F^4 s}\log\left[1 + \frac{s}{M_S^2}\right] + \frac{c_d^2}{F^4}\frac{(2s - M_S^2)(s + 2M_S^2)}{M_S^2 - s}, \tag{78}$$

where we assume exact large N_C nonet symmetry for the scalar resonances in Eqs. (4) and (8), i.e. imposing that the masses for singlet and octet scalar resonances are equal and taking the large N_C relations in Eq. (44). In the previous equation M_S denotes the bare mass of the scalar nonet. In fact, for the scalar resonances, only the combination $\sqrt{\frac{1}{3}}S_8 + \sqrt{\frac{2}{3}}S_0$ is the one relevant in the large N_C limit for the $\pi\pi$ form factor and scattering. The interaction between the other orthogonal combination $\sqrt{\frac{1}{3}}S_0 - \sqrt{\frac{2}{3}}S_8$ and $\pi\pi$ is $1/N_C$ suppressed.

Let us concentrate on the s region around the bare resonance pole at $s = M_S^2$ in Eqs. (77) and (78). Substituting Eqs. (77) and (78) into Eq. (25), we have the simple expression around the resonance pole $s \to M_S^2$ for the unitarized form factor

$$F_{\pi\pi}^{a=0}(s) = -\frac{8c_d c_m M_S^2}{F^2}\frac{1}{M_S^2 - s - i\frac{3c_d^2 M_S^4}{16\pi F^4}}, \tag{79}$$

where we have dropped the tiny contribution that stems from the real part of the function $g^{00}(s)$ (that would give rise to a self-energy contribution to the resonance bare mass) and explicitly show the contribution from the imaginary part in the chiral limit

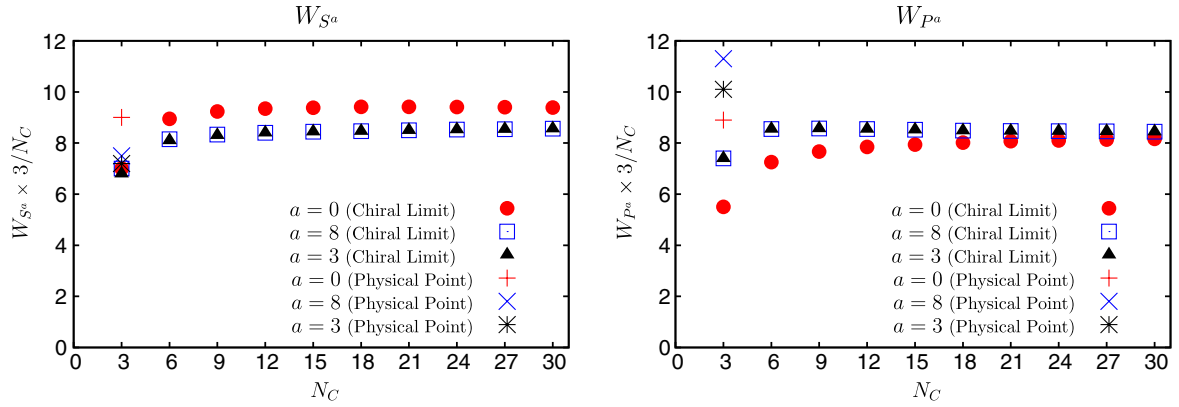

FIG. 17 (color online). $W_i \times 3/N_C$ as a function of N_C within Scenario 3. We distinguish between the chiral limit and the physical case as indicated in the panels. We also show the corresponding value of a for each point.

$$\mathrm{Im}\, g^{00} = -\frac{1}{16\pi}. \tag{80}$$

By substituting the tree level decay width of $S \equiv \sqrt{\frac{1}{3}}S_8 + \sqrt{\frac{2}{3}}S_0$ to $\pi\pi$ calculated from the Lagrangian in Eq. (4) at the chiral limit [46]

$$\Gamma_S = \frac{3c_d^2 M_S^3}{16\pi F^4}, \tag{81}$$

into Eq. (79), we get the standard Breit-Wigner propagator for the scalar resonance

$$F_{\pi\pi}^{a=0}(s) = -\frac{8c_d c_m M_S^2}{F^2}\frac{1}{M_S^2 - s - iM_S\Gamma_S}. \tag{82}$$

Because of the fact that Γ_S behaves as $1/N_C$ in the large N_C limit, we can use the standard narrow width approximation to write the form factor squared in terms of the Dirac δ function

$$|F_{\pi\pi}^{a=0}(s)|^2 = \frac{64c_d^2 c_m^2 M_S^4}{F^4}\frac{1}{(M_S^2 - s)^2 + (M_S\Gamma_S)^2} \Rightarrow \frac{1024\pi^2}{3}c_m^2\delta(s - M_S^2), \tag{83}$$

where we have used Eq. (81) and the following way to approach the Dirac δ function:

$$\frac{1}{\pi}\frac{M_S\Gamma_S}{(M_S^2 - s)^2 + (M_S\Gamma_S)^2} \Rightarrow \delta(s - M_S^2), \quad \text{when } M_S\Gamma_S \to 0. \tag{84}$$

By combining Eqs. (19), (83), (54), and (57) we obtain the leading N_C behavior for the singlet two-point scalar correlator

$$W_{S^0} \propto c_m^2 \propto N_C, \tag{85}$$

which has the same scaling as the pseudoscalar case Eq. (76). This is important because otherwise we would run into the contradiction that it would not make sense to consider the spectral-function sum rules as a function of N_C. The generalization to the cases with $a = 3$ and 8 is straightforward.

We stress that we can make a close analytical discussion only at the leading order in N_C and in the single channel case. Beyond these two conditions, it is rather difficult to perform the discussions analytically even in the chiral limit. Instead, our full calculations for the two-point correlators, which include both the subleading N_C parts, such as the chiral loops, and the multiple-channel dynamics, are carried out numerically. We show $W_i \times 3/N_C$ in Fig. 17 for $i = S^0, S^8, S^3$ (left panel) and P^0, P^8, P^3 (right panel). The flat behavior at large N_C clearly shows that all the two-point correlators W_i are proportional to N_C for large values of N_C. In addition, the asymptotic value is reached rather quickly with N_C, establishing already for $N_C \gtrsim 10$. The W_i results are nearly the same at large values of N_C either for the SS correlators or the PP ones as it is required by the spectral-function sum rules, Eqs. (17) [the discussion after Eq. (53) should be taken into account]. To be more precise, we find that the relative variance $\sigma_W/\overline{W}$ for the six points at $N_C = 30$ in Fig. 17 is only 5%. This indicates that the spectral-function sum rules are better satisfied in large N_C than for the $N_C = 3$ case, reported in Table III with a relative variance of 10%.

The reason behind this improvement can be attributed to the fact that at large N_C the correlators reduce to the single resonance or pseudo-Goldstone exchanges and the large N_C constraints from the $SS - PP$ sector requires that (as previously worked out in Ref. [19])

$$c_m^2 = d_m^2 + \frac{F^2}{8}. \tag{86}$$

This is perfectly satisfied by the results from our research, with c_m determined from the fit in Eq. (45), $d_m = 30$ MeV adopted in this work [16,19,41], and $F \simeq 80$ MeV predicted from the scalar resonance parameters in the fit

Eq. (45) using the $U(3)$ χPT one-loop calculation of Ref. [40].

It is also worth considering the evolution with N_C of the scalar spectral functions. In the right panel of Fig. 8 the latter is shown for $N_C = 30$. It is clear that the spectral functions are then completely dominated by the bare scalar pole S_1 and the octet of scalar resonances at around $\sqrt{s} = 1.4$ GeV. The low-energy peaks in the left panel of Fig. 8 disappear for large N_C because of its meson-meson dynamically generated nature, in agreement with what was already shown for the pole trajectories with N_C in Sec. VI B.

All the points in Fig. 17 are calculated by setting the upper limit of the integral in Eq. (54) to $s_0 = 3$ GeV^2. We verify that the results are quite stable for $s_0 = 2.5$ GeV^2 and 3.5 GeV^2, as it was already discussed for $N_C = 3$ in Table III.

VII. CONCLUSIONS

In this work, we perform a complete one-loop calculation of the strangeness conserving scalar and pseudoscalar form factors within $U(3)$ χPT. We employ the resonance chiral Lagrangian to include the tree level resonance exchanges, instead of using the LECs from the local operators at higher chiral orders (which are supposed to be saturated by the resonance exchanges within the assumption of resonance saturation [41]). We extend the previous one-loop calculation on meson-meson scattering [40] by including the pseudoscalar resonance exchanges. The full results for the scalar form factors are calculated by using the unitarization method in Refs. [72,73], based on the N/D method, taking as input the perturbative calculations of the scalar form factors and the partial wave scattering amplitudes. Then, we employ different form factors to calculate the various spectral functions, which allows us to study the spectral-function sum rules in the scalar and pseudoscalar sectors.

The unknown parameters in our theory are fitted to the experimental data. Comparing with the discussion in Ref. [40], a new fit is carried out in the present work, because of the inclusion of new ingredients, such as the pseudoscalar resonances and the second multiplet of scalar resonances. Various poles in the complex energy plane for the $f_0(500)$, $f_0(980)$, $f_0(1370)$, $a_0(980)$, $a_0(1450)$, $K_0^*(800)$, $K_0^*(1430)$, $\rho(770)$, $K^*(892)$, and $\phi(1020)$ resonances are found, and they agree well with the values from PDG [35]. The coupling strengths of the various resonances to the pseudo-Goldstone boson pairs are also calculated. The resonance content of the new fit presented here and that of Ref. [40] is quite similar, at both the qualitative and quantitative levels. However, the new fit gives a better numerical value for the pion scalar radius than the one in Ref. [40]. The former also contains the pseudoscalar resonance exchanges, which implies that the spectral-function sum rules in the scalar and pseudoscalar cases are satisfactorily fulfilled at the level of about 10%. In addition, the new fit results are employed to investigate semilocal duality in $\pi\pi$ scattering between Regge theory and the dynamics in terms of hadronic degree of freedom. We conclude that semilocal duality is well satisfied in general terms for $n \geq 1$.

An important advantage of working within the chiral Lagrangian approach is that it allows us to study the N_C evolution of the various quantities calculated, once the N_C scaling behavior of the parameters in the theory is settled. The leading evolution with N_C is known unambiguously, while this is not the case for the subleading one. We propose three scenarios to take into account the uncertainties of the subleading N_C scaling for the resonance parameters and another one to include the tensor resonances in the study of semilocal duality. Interestingly, we find that semilocal duality at large N_C imposes strong constraints on the resonance parameters and Scenario 3 turns out to be the best one. Under this scenario we then study the extrapolation of $N_C > 3$ for many other quantities: the masses of the pseudo-Goldstone bosons, the leading order $\eta - \eta'$ mixing angle, the various resonance poles, and the two-point correlators. We find that semilocal duality and the spectral-function sum rules in the scalar and pseudoscalar cases are well satisfied by using the parameters from the fit to experimental data, both for the physical case at $N_C = 3$ and for varying $N_C > 3$. It is important to stress that the fulfillment of semilocal duality and the spectral-function sum rules in the scalar and pseudoscalar sectors for both the physical and the large N_C cases is not trivial and gives a deep insight into the isoscalar scalar spectrum for $\sqrt{s} \lesssim 1$ GeV. In the physical case, the $f_0(500)$ resonance plays an important role for both semilocal duality and spectral-function sum rules, dominating the strength in the low-energy scalar isoscalar channel. However, when N_C increases, this resonance moves deeper in the complex energy plane and its contribution tends to vanish. Instead, the $f_0(980)$ resonance, which gradually evolves to the singlet scalar bare resonance S_1 when increasing N_C, plays the key role for the fulfillments of semilocal duality and spectral-function sum rules. It is then clear that the physical picture for the scalar isoscalar sector in the real and large N_C worlds are very different. The former case is dominated by the $f_0(500)$ resonance, which should not have a significant $\bar{q}q$ or glueball components as it is clear from its N_C pole trajectory. Within our approach it is dynamically generated by the $\pi\pi$ self-interactions. On the other hand, in the large N_C limit the lightest resonance is the singlet S_1 bare or preexisting resonance with a mass around 0.9–1.0 GeV, which for $N_C = 3$ is a component of the $f_0(980)$.

ACKNOWLEDGMENTS

We would like to thank J. R. Peláez for interesting discussions. This work is partially funded by MEC Grant No. FPA2010-17806 and the Fundación Séneca Grant

No. 11871/PI/09. We also appreciate the financial support from the BMBF Grant No. 06BN411, the EU-Research Infrastructure Integrating Activity "Study of Strongly Interacting Matter" (HadronPhysics2, Grant No. 227431) under the Seventh Framework Program of EU, and the Consolider-Ingenio 2010 Programme CPAN (CSD2007-00042). Z. H. G. acknowledges a CPAN postdoc contract in the Universidad de Murcia and financial support from the National Natural Science Foundation of China (NSFC) under Contract No. 11105038, Natural Science Foundation of Hebei Province with Contract No. A2011205093, and Doctor Foundation of Hebei Normal University with Contract No. L2010B04.

APPENDIX A: MASSES AND MIXING PARAMETERS

In this section, we provide the contributions to the self-energies of the pseudo-Goldstone bosons that stem from the exchange of the pseudoscalar resonances, i.e. the operators in the last line of Eq. (10), and the δL_8 operator in Eq. (11). About the second multiplet of scalar resonances, its contributions share the same form as the lowest multiplet given in [40] with the obvious changes in couplings and masses. Hence, we do not reproduce them here. Notice that one needs to combine the results in the present section and those in the Appendices of Ref. [40] to get the full expressions.

We point out that the exchange of pseudoscalar resonances and the δL_8 operator do not contribute to the wave function renormalization of the pseudo-Goldstone bosons and the kinetic terms of $\bar\eta$-$\bar\eta'$ mixing parametrized by δ_η, $\delta_{\eta'}$, and δ_k in Eq. (14) of Ref. [40]. For the pion and kaon masses these new contributions read

$$m_\pi^2 = \bar m_\pi^2 + \frac{16m_\pi^4}{F_\pi^2}\left(\delta L_8 - \frac{d_m^2}{2M_{P_8}^2}\right), \tag{A1}$$

$$m_K^2 = \bar m_K^2 + \frac{16m_K^4}{F_\pi^2}\left(\delta L_8 - \frac{d_m^2}{2M_{P_8}^2}\right). \tag{A2}$$

The mass terms in the $\bar\eta$-$\bar\eta'$ mixing are

$$\begin{aligned}\delta_{m^2_{\bar\eta}} =& -\frac{8d_m^2[c_\theta^2(m_\pi^2-4m_K^2)^2+4\sqrt{2}c_\theta s_\theta(4m_K^4-5m_K^2m_\pi^2+m_\pi^4)+8s_\theta^2(m_\pi^2-m_K^2)^2]}{9F_\pi^2M_{P_8}^2}\\ &-\frac{8\tilde d_m^2[8c_\theta^2(m_\pi^2-m_K^2)^2+4\sqrt{2}c_\theta s_\theta(2m_K^4-m_K^2m_\pi^2-m_\pi^4)+s_\theta^2(m_\pi^2+2m_K^2)^2]}{3F_\pi^2M_{P_1}^2}\\ &+\frac{16\delta L_8}{3F_\pi^2}[c_\theta^2(8m_K^4-8m_K^2m_\pi^2+3m_\pi^4)+8\sqrt{2}c_\theta s_\theta m_K^2(m_K^2-m_\pi^2)+s_\theta^2(4m_K^4-4m_K^2m_\pi^2+3m_\pi^4)],\end{aligned} \tag{A3}$$

$$\begin{aligned}\delta_{m^2_{\bar\eta'}} =& -\frac{8d_m^2[8c_\theta^2(m_\pi^2-m_K^2)^2-4\sqrt{2}c_\theta s_\theta(4m_K^4-5m_K^2m_\pi^2+m_\pi^4)+s_\theta^2(m_\pi^2-4m_K^2)^2]}{9F_\pi^2M_{P_8}^2}\\ &-\frac{8\tilde d_m^2[c_\theta^2(m_\pi^2+2m_K^2)^2-4\sqrt{2}c_\theta s_\theta(2m_K^4-m_K^2m_\pi^2-m_\pi^4)+8s_\theta^2(m_\pi^2-m_K^2)^2]}{3F_\pi^2M_{P_1}^2}\\ &+\frac{16\delta L_8}{3F_\pi^2}[c_\theta^2(4m_K^4-4m_K^2m_\pi^2+3m_\pi^4)-8\sqrt{2}c_\theta s_\theta m_K^2(m_K^2-m_\pi^2)+s_\theta^2(8m_K^4-8m_K^2m_\pi^2+3m_\pi^4)],\end{aligned} \tag{A4}$$

$$\begin{aligned}\delta_{m^2} =& \frac{8d_m^2}{9F_\pi^2M_{P_8}^2}[2\sqrt{2}c_\theta^2(4m_K^4-5m_K^2m_\pi^2+m_\pi^4)+c_\theta s_\theta(-8m_K^4-8m_K^2m_\pi^2+7m_\pi^4)-2\sqrt{2}s_\theta^2(4m_K^4-5m_K^2m_\pi^2+m_\pi^4)]\\ &+\frac{8\tilde d_m^2}{3F_\pi^2M_{P_1}^2}[2\sqrt{2}c_\theta^2(2m_K^4-m_K^2m_\pi^2-m_\pi^4)+c_\theta s_\theta(-4m_K^4+20m_K^2m_\pi^2-7m_\pi^4)+2\sqrt{2}s_\theta^2(-2m_K^4+m_K^2m_\pi^2+m_\pi^4)]\\ &+\frac{64\delta L_8m_K^2(m_\pi^2-m_K^2)(\sqrt{2}c_\theta^2-c_\theta s_\theta-\sqrt{2}s_\theta^2)}{3F_\pi^2},\end{aligned} \tag{A5}$$

where $\delta_{m^2_{\bar\eta}}$, $\delta_{m^2_{\bar\eta'}}$, and δ_{m^2} are defined in Eq. (14) of Ref. [40]. Notice that the two operators in the last line of the pseudoscalar resonance Lagrangian in Eq. (10) and the δL_8 operator of Eq. (11) do not contribute to the pion decay constant F_π.

APPENDIX B: ANALYTIC EXPRESSIONS FOR SCALAR AND PSEUDOSCALAR FORM FACTORS

In order to calculate the scalar form factors in the isospin basis of Eqs. (21) and (22), we need to evaluate for the isoscalar case eight form factors in the charged bases, namely, $F^{0,8}_{\pi^0\pi^0}$, $F^{0,8}_{\pi^+\pi^-}$, $F^{0,8}_{\pi^-\pi^+}$, $F^{0,8}_{K^+K^-}$, $F^{0,8}_{K^0\bar{K}^0}$, $F^{0,8}_{\eta\eta}$, $F^{0,8}_{\eta\eta'}$, and $F^{0,8}_{\eta'\eta'}$. For the isovector case, one needs $F^{3}_{\pi^0\eta}$, $F^{3}_{K^+K^-}$, $F^{3}_{K^0\bar{K}^0}$, and $F^{3}_{\pi^0\eta'}$.

The leading order contributions to the scalar form factors defined in Eq. (18) stem from the Lagrangian in Eq. (1). The expressions for $a = 0$ read

$$F^0_{\pi^0\pi^0} = F^0_{\pi^+\pi^-} = F^0_{\pi^-\pi^+} = 2\sqrt{\frac{2}{3}}, \quad F^0_{K^+K^-} = F^0_{K^0\bar{K}^0} = 2\sqrt{\frac{2}{3}}, \quad F^0_{\eta\eta} = 2\sqrt{\frac{2}{3}}, \quad F^0_{\eta\eta'} = 0, \quad F^0_{\eta'\eta'} = 2\sqrt{\frac{2}{3}}. \tag{B1}$$

For $a = 8$ one has

$$\begin{aligned} F^8_{\pi^0\pi^0} &= F^8_{\pi^+\pi^-} = F^8_{\pi^-\pi^+} = \frac{2}{\sqrt{3}}, \qquad F^8_{K^+K^-} = F^8_{K^0\bar{K}^0} = -\frac{1}{\sqrt{3}}, \qquad F^8_{\eta\eta} = -\frac{2c_\theta(c_\theta + 2\sqrt{2}s_\theta)}{\sqrt{3}}, \\ F^8_{\eta\eta'} &= \frac{2(\sqrt{2}c_\theta^2 - c_\theta s_\theta - \sqrt{2}s_\theta^2)}{\sqrt{3}}, \qquad F^8_{\eta'\eta'} = \frac{2s_\theta(2\sqrt{2}c_\theta - s_\theta)}{\sqrt{3}}. \end{aligned} \tag{B2}$$

And the results for $a = 3$ are

$$F^3_{\pi^0\eta} = \frac{2(c_\theta - \sqrt{2}s_\theta)}{\sqrt{3}}, \qquad F^3_{K^+K^-} = -F^3_{K^0\bar{K}^0} = 1, \qquad F^3_{\pi^0\eta'} = \frac{2(\sqrt{2}c_\theta + s_\theta)}{\sqrt{3}}. \tag{B3}$$

The scalar form factors in the quark flavor basis defined in Eqs. (29) at leading order are

$$\begin{aligned} F^{\bar{u}u+\bar{d}d}_{\pi^0\pi^0} &= F^{\bar{u}u+\bar{d}d}_{\pi^+\pi^-} = F^{\bar{u}u+\bar{d}d}_{\pi^-\pi^+} = 2, \qquad F^{\bar{u}u+\bar{d}d}_{K^+K^-} = F^{\bar{u}u+\bar{d}d}_{K^0\bar{K}^0} = 1, \qquad F^{\bar{u}u+\bar{d}d}_{\eta\eta} = -\frac{2}{3}(c_\theta^2 + 2\sqrt{2}c_\theta s_\theta - 2), \\ F^{\bar{u}u+\bar{d}d}_{\eta\eta'} &= \frac{2}{3}(\sqrt{2}c_\theta^2 - c_\theta s_\theta - \sqrt{2}s_\theta^2), \qquad F^{\bar{u}u+\bar{d}d}_{\eta'\eta'} = \frac{2}{3}(-s_\theta^2 + 2\sqrt{2}c_\theta s_\theta + 2), \end{aligned} \tag{B4}$$

and

$$\begin{aligned} F^{\bar{s}s}_{\pi^0\pi^0} &= F^{\bar{s}s}_{\pi^+\pi^-} = F^{\bar{s}s}_{\pi^-\pi^+} = 0, \qquad F^{\bar{s}s}_{K^+K^-} = F^{\bar{s}s}_{K^0\bar{K}^0} = 1, \qquad F^{\bar{s}s}_{\eta\eta} = \frac{2}{3}(c_\theta^2 + 2\sqrt{2}c_\theta s_\theta + 1), \\ F^{\bar{s}s}_{\eta\eta'} &= -\frac{2}{3}(\sqrt{2}c_\theta^2 - c_\theta s_\theta - \sqrt{2}s_\theta^2), \qquad F^{\bar{s}s}_{\eta'\eta'} = \frac{2}{3}(s_\theta^2 - 2\sqrt{2}c_\theta s_\theta + 1). \end{aligned} \tag{B5}$$

At the same order, the pseudoscalar form factors for the pseudo-Goldstone bosons defined in Eq. (34) are

$$\begin{aligned} &H^0_{\pi^0} = 0, \qquad H^0_{\eta} = -2F_\pi s_\theta, \qquad H^0_{\eta'} = 2F_\pi c_\theta, \qquad H^8_{\pi^0} = 0, \qquad H^8_{\eta} = 2F_\pi c_\theta, \\ &H^8_{\eta'} = 2F_\pi s_\theta, \qquad H^3_{\pi^0} = 2F_\pi, \qquad H^3_{\eta} = 0, \qquad H^3_{\eta'} = 0, \end{aligned} \tag{B6}$$

and for the pseudoscalar resonances they read

$$H^0_{\text{Pseudoscalar Resonances}} = -4\sqrt{6}\tilde{d}_m, \qquad H^8_{\text{Pseudoscalar Resonances}} = -4\sqrt{2}d_m, \qquad H^3_{\text{Pseudoscalar Resonances}} = -4\sqrt{2}d_m. \tag{B7}$$

We provide the remaining expressions, such as those from the chiral loops, scalar resonances, pseudoscalar resonances, Λ_2 and δL_8, in the MATHEMATICA code [76].

APPENDIX C: TENSOR RESONANCES IN MESON-MESON SCATTERING

We follow the framework proposed in Ref. [86] to include the tensor resonances in meson-meson scattering. The relevant Lagrangian reads

$$\mathcal{L}_T = -\frac{1}{2}\langle T_{\mu\nu} D^{\mu\nu,\rho\sigma}_{\mathrm{T}} T_{\rho\sigma}\rangle + g_T\langle T_{\mu\nu}\{u^\mu, u^\nu\}\rangle + \beta\langle T^\mu_\mu u_\nu u^\nu\rangle + \gamma\langle T^\mu_\mu \chi_+\rangle, \tag{C1}$$

where the nonet of the tensor resonances are collected in the matrix

$$T_{\mu\nu} = \begin{pmatrix} \frac{a_2^0}{\sqrt{2}} + \frac{f_2^8}{\sqrt{6}} + \frac{f_2^1}{\sqrt{3}} & a_2^+ & K_2^{*+} \\ a_2^- & -\frac{a_2^0}{\sqrt{2}} + \frac{f_2^8}{\sqrt{6}} + \frac{f_2^1}{\sqrt{3}} & K_2^{*0} \\ K_2^{*-} & \bar{K}_2^{*0} & -\frac{2f_2^8}{\sqrt{6}} + \frac{f_2^1}{\sqrt{3}} \end{pmatrix}_{\mu\nu}. \tag{C2}$$

See Ref. [41] for the definition of the remaining chiral building blocks. As in the vector resonance case [40], ideal mixing is also assumed for the tensor resonances:

$$f_2(1270) = \sqrt{\frac{2}{3}} f_2^1 + \sqrt{\frac{1}{3}} f_2^8, \quad f_2' = \sqrt{\frac{1}{3}} f_2^1 - \sqrt{\frac{2}{3}} f_2^8. \tag{C3}$$

In the present work, the purpose for introducing the tensor resonances is to discuss semilocal duality in $\pi\pi$ scattering. So we will set equal all the tensor masses, which is determined by the most relevant resonance $f_2(1270)$. The first operator in Eq. (C1) corresponds to the kinetic term while the remaining terms describe the interactions between the tensor resonances and the pseudo-Goldstone boson pairs. The terms proportional to β and γ do not contribute to the on-shell decay of the tensor resonances because the tensor field is traceless in the space-time indices [86]. Nevertheless, they do contribute to meson-meson scattering. It is argued in Ref. [86] that though the final result is independent of the choice of β, it is convenient to set $\beta = -g_T$ to avoid the inclusion of the $\mathcal{O}(p^6)$ LECs in order to fulfill the high-energy constraints for the forward $\pi\pi$ scattering. The γ operator is always accompanied by quark masses, and its effects should be much less important than the β term. So we will omit the former term throughout as done in Ref. [86].

Last but not least, one should guarantee the right high-energy behavior of meson-meson scattering in the presence of tensor resonances resulting from the Lagrangian in Eq. (C1). The high-energy constraint imposed in Ref. [86] concerns the fulfillment of a once subtracted forward dispersion relation for $\pi^+\pi^0$ elastic scattering, which turns out to play a crucial role to get the correct prediction for the LECs. We follow the same approach here to satisfy this high-energy constraint. Moreover we calculate all the relevant meson-meson coupled channels for scattering in $U(3)$ χPT, not just $\pi\pi$, since the other processes can enter through the unitarization procedure [40] that couples the different states with the same quantum numbers.

The final results for meson-meson scattering contributed by the tensor resonances and the high-energy constraints are given in the MATHEMATICA code [76]. Because of the consideration of the scattering processes involving η and η', additional LECs are needed to guarantee the proper short distance constraint imposed by the forward scattering. The short distance constraints that we find here are

$$\begin{aligned} \beta_{13}^{SD} &= \frac{4g_T^2}{M_T^2}, & \beta_{14}^{SD} &= -\frac{g_T^2}{M_T^2}, \\ \beta_{15}^{SD} &= -\frac{2g_T^2}{M_T^2}, & \beta_{16}^{SD} &= -\frac{g_T^2}{2M_T^2}, \end{aligned} \tag{C4}$$

in addition to the ones determined in Ref. [86]

$$\beta_1^{SD} = -\frac{g_T^2}{2M_T^2}, \quad \beta_2^{SD} = -\frac{g_T^2}{M_T^2}, \quad \beta_3^{SD} = \frac{2g_T^2}{M_T^2}. \tag{C5}$$

The convention to label the LECs in Eq. (C4) is the same as in Ref. [101], where one can also find the corresponding monomials multiplied by the coefficients with $i = 1, 2, 3, 13, 14, 15$, and 16. We checked that only after the short distance constraints are fulfilled, the introduction of the tensor resonances does not spoil the fit that we obtained in Ref. [40] and the new one in Eq. (45).

For the value of g_T, we take the result $g_T = 28$ MeV from Ref. [86]. As in the vector channels [40], because of the dominant role played by the tree level tensor resonances, one does not expect the subtraction constants arising from the unitarization procedure to play an important role in $IJ = 02$. We simply fix their values to the $IJ = 00$ channel and checked that the results are stable under $\mathcal{O}(1)$ changes in these numbers, so that the subtraction constants keep natural values in Eq. (45). The bare mass of the tensor resonances is adjusted to $M_T = 1300$ MeV, leading to the pole position $\sqrt{s} = (1275.2 - i75.8)$ MeV, which is close to the values of the $f_2(1270)$ resonance given in the PDG [35].

[1] S. Weinberg, Physica A (Amsterdam) **96**, 327 (1979).
[2] J. Gasser and H. Leutwyler, Ann. Phys. (N.Y.) **158**, 142 (1984).
[3] J. Gasser and H. Leutwyler, Nucl. Phys. **B250**, 465 (1985).
[4] K. G. Wilson, Phys. Rev. **179**, 1499 (1969).
[5] P. Pascual and R. Tarrach, *QCD: Renormalization for the Practitioner* (Springer-Verlag, Berlin, 1984).
[6] S. Weinberg, Phys. Rev. Lett. **18**, 507 (1967).
[7] For a recent review, M. Davier, A. Hocker, and Z. Zhang, Rev. Mod. Phys. **78**, 1043 (2006).
[8] S. Narison, N. Paver, E. de Rafael, and D. Treleani, Nucl. Phys. **B212**, 365 (1983).

[9] M. Jamin and M. Munz, Z. Phys. C **60**, 569 (1993).
[10] P. A. Baikov and K. G. Chetyrkin, Phys. Rev. Lett. **97**, 061803 (2006).
[11] B. Moussallam, Eur. Phys. J. C **14**, 111 (2000).
[12] B. Moussallam, J. High Energy Phys. 08 (2000) 005.
[13] S. Peris, M. Perrottet, and E. de Rafael, J. High Energy Phys. 05 (1998) 011.
[14] J. Bijnens, E. Gamiz, and J. Prades, J. High Energy Phys. 10 (2001) 009.
[15] J. Bijnens, E. Gamiz, and J. Prades, J. High Energy Phys. 04 (2003) 055.
[16] J. J. Sanz-Cillero and J. Trnka, Phys. Rev. D **81**, 056005 (2010).
[17] M. Jamin, J. A. Oller, and A. Pich, Eur. Phys. J. C **24**, 237 (2002); Phys. Rev. D **74**, 074009 (2006).
[18] A. Dominguez-Clarimon, E. de Rafael, and J. Taron, Phys. Lett. B **660**, 49 (2008).
[19] M. F. L. Golterman and S. Peris, Phys. Rev. D **61**, 034018 (2000).
[20] M. Jamin, J. A. Oller, and A. Pich, J. High Energy Phys. 02 (2004) 047.
[21] M. Jamin, J. A. Oller, and A. Pich, Nucl. Phys. **B587**, 331 (2000).
[22] M. Jamin, J. A. Oller, and A. Pich, Nucl. Phys. **B622**, 279 (2002).
[23] N. Kaiser, P. B. Siegel, and W. Weise, Nucl. Phys. **A594**, 325 (1995).
[24] J. Oller and E. Oset, Nucl. Phys. **A620**, 438 (1997); **A652**, 407(E) (1999).
[25] J. A. Oller and E. Oset, Phys. Rev. D **60**, 074023 (1999).
[26] R. Kaminski, J. R. Peláez, and F. J. Ynduráin, Phys. Rev. D **77**, 054015 (2008); R. Garcia-Martin, R. Kaminski, J. R. Peláez, J. Ruiz de Elvira, and F. J. Yndurain, Phys. Rev. D **83**, 074004 (2011).
[27] J. Nieves, M. Pavón Valderrama, and E. Ruiaz Arriola, Phys. Rev. D **65**, 036002 (2002).
[28] I. Caprini, G. Colangelo, and H. Leutwyler, Phys. Rev. Lett. **96**, 132001 (2006).
[29] S. Descotes-Genon and B. Moussallam, Eur. Phys. J. C **48**, 553 (2006).
[30] Z. Xiao and H. Q. Zheng, Nucl. Phys. **A695**, 273 (2001).
[31] H. Q. Zheng, Z. Y. Zhou, G. Y. Qin, Z. Xiao, J. J. Wang, and N. Wu, Nucl. Phys. **A733**, 235 (2004).
[32] Z.-Y. Zhou and Z. Xiao, Phys. Rev. D **83**, 014010 (2011).
[33] J. Nieves, A. Pich, and E. Ruiz Arriola, Phys. Rev. D **84**, 096002 (2011).
[34] M. Albaladejo and J. A. Oller, Phys. Rev. Lett. **101**, 252002 (2008).
[35] J. Beringer *et al.* (Particle Data Group), Phys. Rev. D **86**, 010001 (2012).
[36] Z.-H. Guo, J. A. Oller, and J. Ruiz de Elvira, Phys. Lett. B **712**, 407 (2012).
[37] M. Albaladejo and J. A. Oller, Phys. Rev. D **86**, 034003 (2012).
[38] C. W. Bernard, A. Duncan, J. LoSecco, and S. Weinberg, Phys. Rev. D **12**, 792 (1975).
[39] H. Leutwyler, Nucl. Phys. **B337**, 108 (1990).
[40] Zhi-Hui Guo and J. A. Oller, Phys. Rev. D **84**, 034005 (2011).
[41] G. Ecker, J. Gasser, A. Pich, and E. de Rafael, Nucl. Phys. **B321**, 311 (1989).
[42] J. R. Peláez, Phys. Rev. Lett. **92**, 102001 (2004).
[43] J. R. Peláez and G. Rios, Phys. Rev. Lett. **97**, 242002 (2006).
[44] Z. X. Sun, L. Y. Xiao, Z. Xiao, and H. Q. Zheng, Mod. Phys. Lett. A **22**, 711 (2007).
[45] L. Y. Xiao, Z.-H. Guo, and H. Q. Zheng, Int. J. Mod. Phys. A **22**, 4603 (2007).
[46] Z.-H. Guo, J. J. Sanz-Cillero, and H.-Q. Zheng, J. High Energy Phys. 06 (2007) 030.
[47] J. Nieves and E. Ruiz Arriola, Phys. Rev. D **80**, 045023 (2009).
[48] L. Y. Dai, X. G. Wang, and H. Q. Zheng, Commun. Theor. Phys. **57**, 841 (2012).
[49] G. 't Hooft, Nucl. Phys. **B72**, 461 (1974); E. Witten, Nucl. Phys. **B160**, 57 (1979).
[50] A. V. Manohar, arXiv:hep-ph/9802419.
[51] E. Witten, Nucl. Phys. **B156**, 269 (1979); S. Coleman and E. Witten, Phys. Rev. Lett. **45**, 100 (1980); G. Veneziano, Phys. Lett. **95B**, 90 (1980).
[52] S. Weinberg, Phys. Rev. D **11**, 3583 (1975).
[53] P. D. B. Collins, *An Introduction to Regge Theory and High Energy Physics* (Cambridge University Press, Cambridge, 1977).
[54] J. R. Peláez, M. R. Pennington, J. Ruiz de Elvira, and D. J. Wilson, Phys. Rev. D **84**, 096006 (2011).
[55] T. N. Truong, Phys. Rev. Lett. **61**, 2526 (1988).
[56] A. Dobado, M. J. Herrero, and T. N. Truong, Phys. Lett. B **235**, 134 (1990).
[57] A. Dobado and J. R. Peláez, Phys. Rev. D **56**, 3057 (1997).
[58] J. A. Oller, E. Oset, and J. R. Peláez, Phys. Rev. Lett. **80**, 3452 (1998); Phys. Rev. D **59**, 074001 (1999); **60**, 099906 (E) (1999); **75**, 099903(E) (2007).
[59] F. J. Llanes-Estrada, J. R. Pelaez, and J. Ruiz de Elvira, Nucl. Phys. B, Proc. Suppl. **207–208**, 169 (2010).
[60] P. Di Vecchia and G. Veneziano, Nucl. Phys. **B171**, 253 (1980); C. Rosenzweig, J. Schechter, and T. Trahem, Phys. Rev. D **21**, 3388 (1980); E. Witten, Ann. Phys. (N.Y.) **128**, 363 (1980).
[61] K. Karawabayashi and N. Ohta, Nucl. Phys. **B175**, 477 (1980); Prog. Theor. Phys. **66**, 1789 (1981).
[62] J. A. Oller and U.-G. Meißner, Phys. Lett. B **500**, 263 (2001).
[63] W. A. Bardeen, Phys. Rev. **184**, 1848 (1969).
[64] K. Fujikawa, Phys. Rev. D **21**, 2848 (1980).
[65] S. L. Adler and W. A. Bardeen, Phys. Rev. **182**, 1517 (1969).
[66] G.'t Hooft, Phys. Rev. D **14**, 3432 (1976); Phys. Rep. **142**, 357 (1986).
[67] G. Ecker, J. Gasser, H. Leutwyler, A. Pich, and E. de Rafael, Phys. Lett. B **223**, 425 (1989).
[68] M. Albaladejo, J. A. Oller, and L. Roca, Phys. Rev. D **82**, 094019 (2010).
[69] R. Kaiser and H. Leutwyler, Eur. Phys. J. C **17**, 623 (2000).
[70] A. Pich, I. Rosell, and J. J. Sanz-Cillero, J. High Energy Phys. 07 (2008) 014.
[71] S. Weinberg, Nucl. Phys. **B363**, 3 (1991).
[72] U.-G. Meißner and J. A. Oller, Nucl. Phys. **A679**, 671 (2001).
[73] J. A. Oller, E. Oset, and J. E. Palomar, Phys. Rev. D **63**, 114009 (2001).

[74] J. A. Oller, Phys. Rev. D **71**, 054030 (2005).
[75] http://www.um.es/oller/u3FullAmp16.nb.
[76] http://www.um.es/oller/AmpFF.nb.
[77] J. Gasser and H. Leutwyler, Nucl. Phys. **B250**, 517 (1985).
[78] J. F. Donoghue, J. Gasser, and H. Leutwyler, Nucl. Phys. **B343**, 341 (1990).
[79] J. A. Oller, Phys. Lett. B **477**, 187 (2000).
[80] U.-G. Meißner and J. A. Oller, Nucl. Phys. **A673**, 311 (2000).
[81] J. A. Oller, E. Oset, and A. Ramos, Prog. Part. Nucl. Phys. **45**, 157 (2000).
[82] G. Colangelo, J. Gasser, and H. Leutwyler, Nucl. Phys. **B603**, 125 (2001).
[83] J. A. Oller and L. Roca, Phys. Lett. B **651**, 139 (2007).
[84] Z. H. Guo and J. J. Sanz-Cillero, Phys. Rev. D **79**, 096006 (2009).
[85] J. Bijnens and I. Jemos, Nucl. Phys. **B854**, 631 (2012).
[86] G. Ecker and C. Zauner, Eur. Phys. J. C **52**, 315 (2007).
[87] J. Ruiz de Elvira, J. R. Pelaez, M. R. Pennington, and D. J. Wilson, AIP Conf. Proc. **1257**, 467 (2010).
[88] G. P. Lepage and S. J. Brodsky, Phys. Rev. D **22**, 2157 (1980).
[89] D. Jido, J. A. Oller, E. Oset, A. Ramos, and U. G. Meissner, Nucl. Phys. **A725**, 181 (2003).
[90] J. A. Oller, Nucl. Phys. **A727**, 353 (2003).
[91] A. Pich, arXiv:hep-ph/0205030.
[92] V. Cirigliano, G. Ecker, M. Eidemuller, R. Kaiser, A. Pich, and J. Portoles, J. High Energy Phys. 04 (2005) 006.
[93] A. Pich, I. Rosell, and J. J. Sanz-Cillero, J. High Energy Phys. 02 (2011) 109.
[94] Z.-H. Guo and P. Roig, Phys. Rev. D **82**, 113016 (2010).
[95] H. Georgi, *Weak Interactions and Modern Particle Theory* (Dover Publications, Mineola, NY, 2009).
[96] K. Kawarabayashi and M. Suzuki, Phys. Rev. Lett. **16**, 255 (1966); Riazuddin and Fayyazuddin, Phys. Rev. **147**, 1071 (1966).
[97] R. S. Chivukula, E. H. Simmons, H.-J. He, M. Kurachi, and M. Tanabashi, Phys. Rev. D **75**, 035005 (2007).
[98] J. A. Oller and E. Oset, Nucl. Phys. **A629**, 739 (1998).
[99] A. Dobado and J. R. Pelaez, Phys. Rev. D **65**, 077502 (2002).
[100] J. R. Pelaez, arXiv:hep-ph/0509284.
[101] P. Herrera-Siklody, J. I. Latorre, P. Pascual, and J. Taron, Nucl. Phys. **B497**, 345 (1997).
[102] C. D. Frogratt and J. L. Petersen, Nucl. Phys. **B129**, 89 (1977).
[103] J. R. Batley *et al.* (NA48/2 Collaboration), Eur. Phys. J. C **54**, 411 (2008).
[104] W. Ochs, Ph.D. thesis, University of Munich, 1974.
[105] B. Hyams *et al.*, Nucl. Phys. **B64**, 134 (1973); P. Estabrooks *et al.*, AIP Conf. Proc. **13**, 37 (1973); G. Grayer *et al.*, *Proceedings of the 3rd Philadelphia Conference on Experimental Meson Spectroscopy* (American Institute of Physics, New York, 1972), p. 5; S. D. Protopopescu and M. Alson-Garnjost, Phys. Rev. D **7**, 1279 (1973).
[106] R. Kaminski, L. Lesniak, and K. Rybicki, Z. Phys. C **74**, 79 (1997).
[107] D. Cohen, D. S. Ayres, R. Diebold, S. L. Kramer, A. J. Pawlicki, and A. B. Wicklund, Phys. Rev. D **22**, 2595 (1980).
[108] A. D. Martin and E. N. Ozmutlu, Nucl. Phys. **B158**, 520 (1979).
[109] A. Etkin *et al.*, Phys. Rev. D **25**, 1786 (1982).
[110] A. Mercer *et al.*, Nucl. Phys. **B32**, 381 (1971).
[111] P. Estabrooks, R. K. Carnegie, A. D. Martin, W. M. Dunwoodie, T. A. Lasinski, and D. W. G. S. Leith, Nucl. Phys. **B133**, 490 (1978).
[112] H. H. Bingham *et al.*, Nucl. Phys. **B41**, 1 (1972).
[113] D. Aston *et al.*, Nucl. Phys. **B296**, 493 (1988).
[114] T. A. Armstrong *et al.*, Z. Phys. C **52**, 389 (1991).
[115] W. Hoogland *et al.*, Nucl. Phys. **B126**, 109 (1977).
[116] M. J. Losty, M. J. Losty, V. Chaloupka, A. Ferrando, L. Montanet, E. Paul, D. Yaffe, A. Zieminski, J. Alitti, B. Gandois, and J. Louie, Nucl. Phys. **B69**, 185 (1974).
[117] A. M. Bakker *et al.*, Nucl. Phys. **B24**, 211 (1970).
[118] Y. Cho *et al.*, Phys. Lett. **32B**, 409 (1970).
[119] S. J. Lindenbaum and R. S. Longacre, Phys. Lett. B **274**, 492 (1992).
[120] P. Estabrooks and A. D. Martin, Nucl. Phys. **B79**, 301 (1974).

2.2.6 Meson coupling and the $1/N_c$ expansion

Introduction

As we have commented in Section 1.1.2, the properties and nature of light scalar mesons, and even the existence in the case of the κ resonance, are the subject of an intense debate. In particular, in the case of the $f_0(500)$, the analysis of its nature has led to different interpretations: whereas there are many groups which assume that it is a tetraquark [12, 13, 16, 211] or a $\pi\pi$-molecular state [23], there are other groups which claim it is a glueball [20, 24] or even a $\bar{q}q$ state [33, 224].

Current research efforts strive to understand the composition of hadrons in terms of the fundamental QCD degrees of freedom, quarks and gluons, as a a Fock space expansion. In the case of scalar mesons, it reads:

$$|M\rangle = \sum \int \left(\alpha_{q\bar{q}}|q\bar{q}\rangle + \alpha_{gg}|g\bar{g}\rangle + \alpha_{qq\bar{q}\bar{q}}|qq\bar{q}\bar{q}\rangle \dots\right) \tag{2.3}$$

(where the sum/integral signs remind us of spin, momentum and other degrees of freedom that we will omit). The full detail of this expansion in terms of quarks and transverse gluons is well defined in Coulomb gauge QCD [225], that can be formulated without ghosts nor longitudinal gluons. At least for heavy mesons decaying to open-flavor channels, the intrinsic $q\bar{q}$ component can be identified in a model-independent way [226]. The setback of this full quantum-mechanical answer is that it is frame and gauge dependent, presumably defined in the rest frame of the hadron [227]. This makes it less attractive for light hadrons where speeds can be large.

Furthermore, the $1/N_c$ expansion of QCD amplitudes and matrix elements around $N_c = 3$ does provide frame and gauge-independent information. In particular it characterizes the scaling with N_c of masses, decay widths and couplings of the QCD configurations, so it is a useful way to analyze the nature of scalar mesons and, in this section, we are going to analyze the N_c expansion of the most relevant meson couplings. However, it is important to remark that large N_c can only separate classes of equivalence of states whose mass and decays behave in the same way under N_c. Thus when we refer to a component of Eq.(2.3) as $q\bar{q}$ or $g\bar{g}$, it should be understood as $q\bar{q}$-like or $g\bar{g}$-like under the large N_c expansion. Namely, for a $q\bar{q}$-like state, its mass behaves as $O(1)$, its width as $O(1/N_c)$, etc... A large part of this contribution is dedicated to the scaling with N_c of the tetraquark Fock-space component. This is because the concept of "four-quark" or molecule state is ambiguous when considering large N_c.

Indeed Jaffe [228, 229] noticed that the diquark-antidiquark meson could be extended to larger N_c in two different ways. The first leaves the quark number fixed, that is, $qq\overline{qq}$ for all N_c, that corresponds to a tetraquark or molecule. The second scales both the number of quarks and antiquarks as $N_c - 1$, a configuration that we will call "polyquark" to avoid committing to a particular dynamic model (such as baryonium, that one should like to think of as a baryon-antibaryon state overlapping with the same color configuration).

In particular, for the "tetraquark/molecule"-like configuration we write its wave function as $\delta_{ij}\delta_{kl}|q_i q_k \bar{q}_j \bar{q}_l\rangle$, independently of N_c. Note that we write "tetraquark/molecule", because

	$q\bar{q}$	gg	$q\bar{q}g$	$q\bar{q}q\bar{q}$	$(N_c-1)q\bar{q}$
M	$O(1)$	$O(1)$	$O(1)$	$O(1)$	$O(N_c)$
Γ_{Tot}	$O(1/N_c)$	$O(1/N_c^2)$	$O(1/N_c)$	$O(1)$	$O\left(\frac{N_c!^2 c^{N_c}}{N_c^{N_c+1}}\right)$

Table 2.1: Leading behavior in the $1/N_c$ expansion of the mass and width for various configurations in QCD.

the "tetraquark" and the "molecule" are undistinguishable to the N_c counting. To introduce the polyquark, note that we could have also written a color singlet wave function as $\epsilon^{ijm}\epsilon^{klm}|q_i q_j \bar{q}_k \bar{q}_l\rangle$, created from the vacuum by the action of the field (also explicitly showing spin and color indices):

$$\bar{\mathbb{Q}}_{ia} = \epsilon_{ijk}\epsilon_{abc}(\mathrm{i}\sigma_2)_{\alpha\beta} q_\alpha^{jb} q_\beta^{kc}, \tag{2.4}$$

$$\mathbb{Q}_{ia} = \epsilon_{ijk}\epsilon_{abc}(\mathrm{i}\sigma_2)_{\alpha\beta} \bar{q}_\alpha^{jb} \bar{q}_\beta^{kc}, \tag{2.5}$$

For the latter we can extend the wave function to arbitrary N_c as:

$$\bar{\mathbb{Q}}^a \mathbb{Q}_a = \epsilon^{a\, j_i \cdots j_{N_c-1}} \epsilon_{a\, i_1 \cdots i_{N_c-1}} q^{i_1} \cdots q^{i_{N_c-1}} \bar{q}_{j_1} \cdots \bar{q}_{j_{N_c-1}}. \tag{2.6}$$

which we have called the "polyquark", which has to be taken into account in addition to the more conventional tetraquark/meson molecule. The other configurations that we consider are the classic $q\bar{q}$ conventional meson and the glueball gg. Let us once again emphasize that when we say $q\bar{q}$, we mean "$q\bar{q}$-like", so that we are also including states like $q\bar{q}g$, which according to the N_c counting, behaves as a $q\bar{q}$.

Normalization and mass in leading-N_c

Because of color-confinement, the states gg, $q\bar{q}$, $q\bar{q}g$, ggg provide a discrete spectrum. However, states with tetraquark composition $qq\bar{q}\bar{q}$ can fission into two mesons (OZI-superallowed decays) due to the lightness of the pion, that makes the $\pi\pi$ (or other Goldstone bosons) decay channel to always be open for decay. Therefore, they are expected to produce broad distortions of the density of states in the meson-meson continuum unless very specific dynamical circumstances occur. Finally, the polyquark configuration $q_1\bar{q}_1 \ldots q_{N_c-1}\bar{q}_{N_c-1}$ will fission to $N_c - 1$ "pions" (generally, lighter $q\bar{q}$ mesons).

Let us first advance the result of this section. The behaviors of the various configurations as the number of colors is varied towards the large N_c limit are collected in table 2.1, where we give the leading order of the mass and total width expansion in $1/N_c$. Of course, the behavior of the mass and width for the ordinary $q\bar{q}$ mesons and glueballs are already well known [96, 97] whereas it was already remarked that for tetraquarks there was "no zero width approximation" and that the mass of polyquark configuration should grow with N_c while being weakly bounded to mesons [230].

At large N_c the spectrum becomes, as expected, a set of isolated, narrow intrinsic resonances that interact weakly. Hybrid $q\bar{q}g$ configurations are not distinguishable by N_c alone

from conventional $q\bar{q}$ mesons. Lattice simulations and models find them in the vicinity of 1.6-1.8 GeV, so one can generically refer to the intrinsic part of the lightest mesons, for example in the σ wave function, as $q\bar{q}$.

To get started let us consider the long studied [96] conventional $q\bar{q}$ meson. Since $\langle q\bar{q}|q\bar{q}\rangle = 1$, and the quark and antiquark have to be in a color singlet configuration δ_{ij}, we have $\mathcal{N}^2\delta_{ij}\delta_{ij} = 1$, and since the sums run over $i = 1 \dots N_c$, $\mathcal{N} = \frac{1}{\sqrt{N_c}}$. Hence, the $q\bar{q}$ configuration becomes the obvious one (all non-color indices and arguments are suppressed):

$$|q\bar{q}\rangle = \frac{\delta_{ij}}{\sqrt{N_c}}|q_i\bar{q}_j\rangle \tag{2.7}$$

Much discussed are also hybrid mesons [231, 232, 233, 234], that in addition to a quark-antiquark pair, contain a transverse gluon in their wave function. Here we will consider them in connection to their N_c scaling. In particular, since now the quark and antiquark have to be in a color octet, and this is to be combined with the gluon to produce an overall color singlet, a compact way of expressing its wave function is through the adjoint Gell-Mann matrices. Noticing that:

$$T^a_{ij}T^a_{ji} = Tr(T^aT^a) = \frac{\delta_{aa}}{2} = \frac{N_c^2-1}{2}\ ,$$

the correctly normalized hybrid state for arbitrary N_c is:

$$|q\bar{q}g\rangle = \sqrt{\frac{2}{N_c^2-1}}T^a_{ij}|q_i\bar{q}_jg^a\rangle\ . \tag{2.8}$$

If one attempts to calculate the mass and width of these hybrid mesons, they yield the same result as the $q\bar{q}$ that will be studied below, and thus we will place it in the same generic large-N_c equivalence class of the $q\bar{q}$ meson

The glueball is a characteristic feature of non-Abelian gauge theories. In QCD, where the spectrum is gapped, one expects the few-body representation to be a good starting point [235, 236], and the positive parity pure-gauge glueballs have a wave function that starts with two gluons, that in a color singlet yield $|gg\rangle \propto \delta^{ab}$. Since $\delta^{aa} = N_c^2 - 1$, it is straightforward to show that:

$$|gg\rangle = \frac{\delta^{ab}}{\sqrt{N_c^2-1}}|g^ag^b\rangle\ . \tag{2.9}$$

Now we turn the to the very popular $q\bar{q}q\bar{q}$ tetraquark. Of course, various exotic color wave functions are possible, but it is obvious that they are all linear combinations of the two linearly independent:

$$|1\rangle = \frac{1}{N_c}\delta_{i_1j_1}\delta_{i_2j_2} \tag{2.10}$$

$$|2\rangle = \frac{1}{N_c}\delta_{i_1j_2}\delta_{i_2j_1} \tag{2.11}$$

$$\tag{2.12}$$

where i_1, i_2 represents the color index of the quark in the fundamental representation, and j_1, j_2 the color index of the antiquark in the conjugate fundamental representation. These two

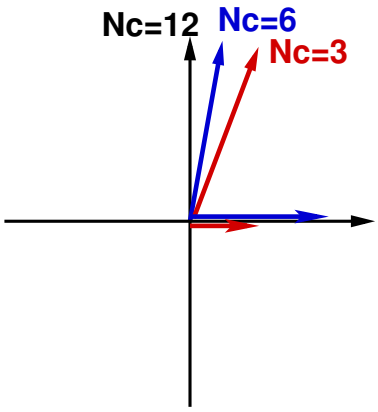

Figure 2.4: Angle between the $|2\rangle$ and $|1\rangle$ two-meson color wave functions, the last taken as the x-axis. For large N_c, the two-singlet (molecule-like) color configurations become an orthogonal basis of the two-dimensional space of $qq\bar{q}\bar{q}$ configurations. For any N_c they are not linearly dependent, hence, as far as color is concerned, all tetraquarks are linear combinations of meson-meson molecular states.

wave functions correspond to molecular configurations in which the quark-antiquark couple in pairs as would correspond to two color-singlet mesons.

In the large N_c limit, the two wave functions become orthogonal as depicted in figure 2.4. For finite N_c there is a small projection $\langle 1|2\rangle$ that is subleading in N_c, but the two wave functions still span the color space. Hence, all tetraquark configurations fission into two color-singlet mesons because the color wave functions have non-zero overlap with them [1]. Therefore, as far as color is concerned, all tetraquarks are linear combinations of molecule-molecule type states. This is true for all N_c, and can be seen easily because the combination of two quarks and two antiquarks can produce a color singlet only as a Young tableau of two columns, independently of the number of rows. Thus, although we denote it by $q\bar{q}q\bar{q}$, we actually mean "tetraquark/molecule".

The normalization is obviously the square of (2.7), so that one of the two linearly independent combinations becomes:

$$|qq\bar{q}\bar{q}\rangle = \frac{\delta_{ik}\delta_{jl}}{N_c}|q_i q_j \bar{q}_k \bar{q}_l\rangle \ . \tag{2.13}$$

The normalization of the polyquark extension of the tetraquark to an arbitrary number of colors is obtained by computing the overlap:

$$\mathcal{N}^2 = \langle 0|\bar{\mathbb{Q}}^a \mathbb{Q}_a|\bar{\mathbb{Q}}^b \mathbb{Q}_b|0\rangle \ . \tag{2.14}$$

where $\bar{\mathbb{Q}}^a \mathbb{Q}_a$ is given in eq. (2.6). Since the number of quarks and antiquarks is $2(N_c-1)$, the normalization will be different for different number of flavours. We will assume here for illustration that $N_f = 1$, whereas the case with two flavours is computed in Appendix D. One of the possible Feynman diagrams contributing to this overlap is represented in Fig. 2.5.

[1] Note also that a tetraquark scalar meson in its ground state has all relative orbital wave functions in an s-wave and therefore there is no centrifugal barrier holding the fission.

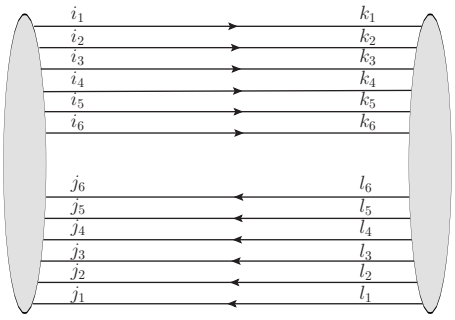

Figure 2.5: Polyquark normalization for the SU(7) case

Therefore, for $N_f = 1$, expanding eq. (2.14), we have:

$$\begin{aligned}\mathcal{N}_1^2 = \langle \mathbb{Q}\bar{\mathbb{Q}}|\mathbb{Q}\bar{\mathbb{Q}}\rangle \;\; &= \;\; \epsilon^{ai_1\cdots i_{N_c-1}}\epsilon^{aj_1\cdots j_{N_c-1}}\epsilon^{bk_1\cdots k_{N_c-1}}\epsilon^{bl_1\cdots l_{N_c-1}} \\ &\quad \times\langle q^{k_1}\bar{q}^{l_1}\cdots q^{k_{N_c-1}}\bar{q}^{l_{N_c-1}}|q^{i_1}\bar{q}^{j_1}\cdots q^{i_{N_c-1}}\bar{q}^{j_{N_c-1}}\rangle\ .\end{aligned} \tag{2.15}$$

Carrying out the Wick operator contractions we get

$$\mathcal{N}_1^2 = \epsilon^{ai_1\cdots i_{N_c-1}}\epsilon^{aj_1\cdots j_{N_c-1}}\epsilon^{bk_1\cdots k_{N_c-1}}\epsilon^{bl_1\cdots l_{N_c-1}}\epsilon^{ci_1\cdots i_{N_c-1}}\epsilon^{dk_1\cdots k_{N_c-1}}\epsilon^{dj_1\cdots j_{N_c-1}}\epsilon^{cl_1\cdots l_{N_c-1}}. \tag{2.16}$$

Employing now the relation

$$\epsilon^{ai_1\cdots i_{N_c-1}}\epsilon^{bi_1\cdots i_{N_c-1}} = (N_c-1)!\delta^{ab} \tag{2.17}$$

in eq. (2.16), we obtain

$$\mathcal{N}_1^2 = (N_c-1)\,!^4\delta^{ac}\delta^{ad}\delta^{bc}\delta^{bd} = N_c(N_c-1)!^4\ . \tag{2.18}$$

So that the polyquark normalization grows with N_c as:

$$\mathcal{N}_1 = \sqrt{N_c}(N_c-1)!^2. \tag{2.19}$$

As it is shown in Appendix D, the normalization for two flavours is:

$$\mathcal{N}_2 = \sqrt{N_c}(N_c-1)!((N_c-1)/2)!^2. \tag{2.20}$$

Using the Stirling approximation:

$$\log(N!) \simeq N\log N - N, \tag{2.21}$$

it can be seen that in large N_c, the two scaling laws are equivalent, so that the distinction between one and two flavors becomes idle in leading order.

The masses of all configurations that have a fixed number of constituents are of order $O(1)$ in leading N_c. This is a consequence of the QCD mass-gap that affects the leading order diagram in N_c (constituent counting) [97] and the stability of the N_c series. That is, the

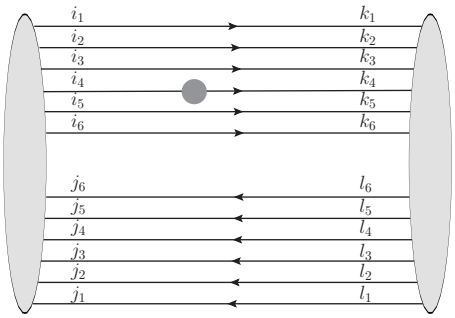

Figure 2.6: Polyquark self energy insertion, taking as example $N_c = 7$.

constituent mass is independent of N_c at leading order, and there are a fixed number of such masses and distinct interparticle couplings.

This rule of course does not apply to configurations with a variable number of particles. Thus it is well known that the mass of baryons grows with N_c, and the same behavior applies to our polyquark configuration, that has

$$M_{(N_c-1)q\bar{q}} \propto N_c \ . \tag{2.22}$$

This is in spite of the number of possible interactions growing factorially as argued by Witten [97]. These masses are reflected in the first row of table 2.1.

Coming to the mass of the polyquark, one would think that since the polyquark has $2(N_c - 1)$ constituents each of constant mass, its own mass scales as $M_P \propto N_c$. The interaction between different particles would seem to wreak havoc with this constituent N_c scaling, as each of the $2(N_c - 1)$ quarks or antiquarks could interact with any of the others yielding a scaling of order N_c^2 for two-body interactions, Fig. 2.6. But then iterated or multibody forces would yield still higher powers of N_c. Witten [97] recognized early on, in treating baryons, that this unreasonable combinatorial behavior is the one issue requiring dynamical insight overriding the blind N_c counting. Witten realized that in other many-body systems in nature (multielectron atoms, or multinucleon nuclei for example) a good zeroth order approximation is the Hartree-Fock mean field ansatz in which one individual particle can best be thought as interacting with the collectivity of all other particles, so that the interaction energy of the system also scales proportionally to N_c. We adopt this point of view and take for granted that:

$$M_P(N_c) \propto N_c \ . \tag{2.23}$$

Couplings between states

Let us start by considering the mixing between quark-antiquark configurations and the glueball. The relevant color matrix element is depicted in figure 2.7 and reads:

$$\left(\frac{1}{\sqrt{N_c}}\right) \times \left(\frac{T^a_{ij}}{\sqrt{N_c}} \frac{T^b_{ji}}{\sqrt{N_c}}\right) \times \left(\frac{\delta^{ab}}{\sqrt{N_c^2 - 1}}\right) \ .$$

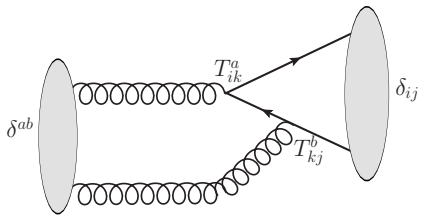

Figure 2.7: Feynman diagram showing the coupling between a pure glue configuration and a $q\bar{q}$ standard meson configuration.

The first and last factors respectively correspond to the $q\bar{q}$ and gg normalizations. The middle factor contains the coupling of the two gluons in the final state to the quark and antiquark in the initial state, with the corresponding color Gell-Mann matrix, and the $1/\sqrt{N_c}$ factor in the QCD coupling which, as we have seen in Section 1.4, is to be assigned to each vertex in perturbation theory [96]. Thus,

$$\langle q\bar{q}|gg\rangle \propto \frac{1}{\sqrt{N_c}}\,, \tag{2.24}$$

and we pass this result to the corresponding entries in table 2.2.

	$q\bar{q}$	$qq\bar{q}\bar{q}$	gg
$q\bar{q}$	$O(1)$	$O\left(\frac{1}{\sqrt{N_c}}\right)$	$O\left(\frac{1}{\sqrt{N_c}}\right)$
$qq\bar{q}\bar{q}$	$O\left(\frac{1}{\sqrt{N_c}}\right)$	$O(1)$	$O\left(\frac{1}{N_c}\right)$
gg	$O\left(\frac{1}{\sqrt{N_c}}\right)$	$O\left(\frac{1}{N_c}\right)$	$O(1)$

Table 2.2: We collect the couplings between configurations with fixed constituent number in leading order in the large N_c expansion. Note that the diagonal counts, of course, as the propagator (mass) and is of order 1.

Next let us illustrate in figure 2.8 the color computation of the matrix element for a transition between the glueball and two $q\bar{q}$ states (or tetraquark). This is of phenomenological relevance to compute glueball widths, through $G \to \pi\pi$ for example.

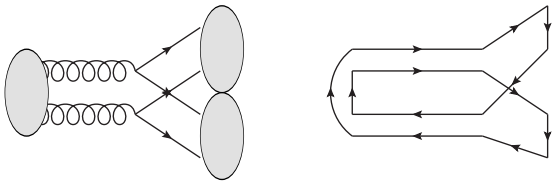

Figure 2.8: Left: the impulse diagram for the transition of a glueball to two pions already yields the leading-N_c behaviour of the entire amplitude as shown by t'Hooft. Right: color flow of the same diagram using the double-line notation discussed in Section 1.4. The line crossing reveals the $1/N_c$ suppression.

A way to establish the counting (left diagram in the figure) is to observe that the color-singlet two-gluon wave function, properly normalized, is $\frac{\delta_{ab}}{\sqrt{N_c^2-1}}$. Each of the two vertices

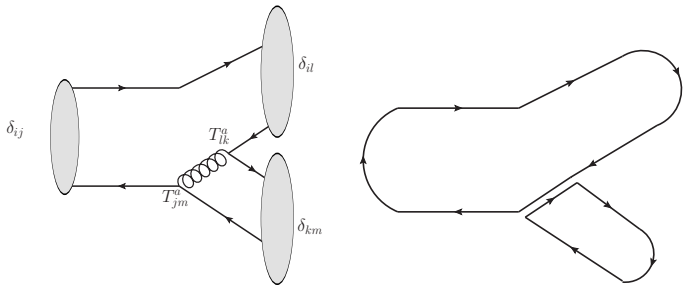

Figure 2.9: Feynman diagram exhibiting the coupling between the conventional $q\bar{q}$ configuration and the meson molecule (or tetraquark at fixed number of constituents), and its t'Hooft double-line equivalent.

carry $\frac{gT^a_{ij}}{\sqrt{N_c}}$ (this scaling of the color charge guarantees that higher-order diagrams scale in the same way under N_c). Finally, the pion wave functions in the final state combine a quark and antiquark to form a color singlet $\frac{\delta_{ij}}{\sqrt{N_c}}$.

The net result for the matrix element is $tr(T^aT^a)/(N_c^2\sqrt{N_c^2-1})$, suppressed as $1/N_c$,

$$\langle gg|qq\bar{q}\bar{q}\rangle \propto \frac{1}{N_c} \,. \tag{2.25}$$

This is reflected in table 2.2. In passing we note that the glueball width is proportional to the matrix element $G \to \pi\pi$ squared, and hence to $1/N_c^2$, so that the corresponding entry in table 2.1 follows.

Likewise the coupling between the $q\bar{q}$ and molecule-like $qq\bar{q}\bar{q}$ configurations, depicted in figure 2.9 can be extracted from a diagram in leading order perturbation theory, that contains already the correct N_c counting,

$$\left(\frac{\delta_{ij}}{\sqrt{N_c}}\right)\left(\frac{T^a_{jk}}{\sqrt{N_c}}\frac{T^a_{lm}}{\sqrt{N_c}}\right)\left(\frac{\delta_{il}\delta_{km}}{N_c}\right) \,, \tag{2.26}$$

where again the first factor is the $q\bar{q}$ bra, the last factor the $qq\bar{q}\bar{q}$ ket, and the middle factor corresponds to the gluon rung. The result is

$$\langle q\bar{q}|qq\bar{q}\bar{q}\rangle \propto \frac{1}{\sqrt{N_c}} \,, \tag{2.27}$$

that we again collect in table 2.2. Squaring we obtain the usual result for a meson's width $\Gamma \propto 1/N_c$, as written in table 2.1.

We now turn to the more difficult computations involving the polyquark. To avoid unnecessary detail, we have relegated again the $N_f = 2$ case to Appendix D. Let us study first the total decay width of the polyquark.

Total decay width of polyquark

The decay width of the polyquark is dominated, in large N_c, by its fission to a large number (of order N_c) of $q\bar{q}$-like states ("pions") not requiring the annihilation of valence $q\bar{q}$ pairs, as

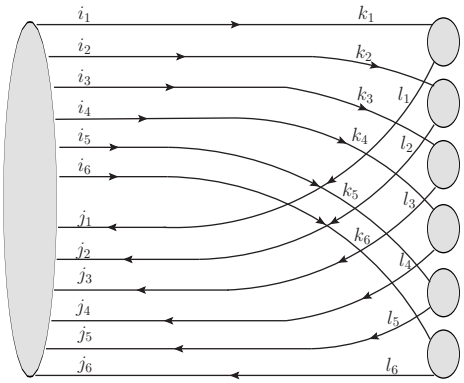

Figure 2.10: Characteristic fission diagram for the total polyquark width (for $N_c = 7$).

depicted in Fig. 2.10. This decay channel is open for arbitrary N_c as long as the pion remains a light quasi-Goldstone boson. Therefore the total width requires studying the matrix element:

$$\begin{aligned}\langle (q\bar{q}\,)^{N_c-1}|\mathrm{Q}\bar{\mathrm{Q}}\rangle &= \frac{\epsilon^{ai_1\cdots i_{N_c-1}}\epsilon^{aj_1\cdots j_{N_c-1}}}{\sqrt{N_c}(N_c-1)!^2}\frac{\delta^{k_1l_1}\ldots\delta^{k_{N_c-1}l_{N_c-1}}}{N_c^{(N_c-1)/2}} \\ &\quad \langle q^{k_1}\bar{q}^{\,l_1}\cdots q^{k_{N_c-1}}\bar{q}^{\,l_{N_c-1}}|q^{i_1}\bar{q}^{j_1}\cdots q^{i_{N_c-1}}\bar{q}^{j_{N_c-1}}\rangle.\end{aligned} \tag{2.28}$$

Making again all possible contractions:

$$\begin{aligned}\langle (q\bar{q}\,)^{N_c-1}|\mathrm{Q}\bar{\mathrm{Q}}\rangle &\propto \frac{\epsilon^{ai_1\cdots i_{N_c-1}}\epsilon^{aj_1\cdots j_{N_c-1}}}{\sqrt{N_c}(N_c-1)!^2}\frac{\delta^{k_1l_1}\ldots\delta^{k_{N_c-1}l_{N_c-1}}}{N_c^{(N_c-1)/2}} \\ &\quad \epsilon^{bi_1\cdots i_{N_c-1}}\epsilon^{ck_1\cdots k_{N_c-1}}\epsilon^{cj_1\cdots j_{N_c-1}}\epsilon^{bl_1\cdots l_{N_c-1}},\end{aligned} \tag{2.29}$$

and using again (2.17), we obtain:

$$\begin{aligned}\langle (q\bar{q}\,)^{N_c-1}|\mathrm{Q}\bar{\mathrm{Q}}\rangle &\propto \frac{(N_c-1)!^2\delta^{ab}\delta^{ac}}{\sqrt{N_c}(N_c-1)!^2}\frac{\delta^{k_1l_1}\ldots\delta^{k_{N_c-1}l_{N_c-1}}}{N_c^{(N_c-1)/2}}\epsilon^{ck_1\cdots k_{N_c-1}}\epsilon^{bl_1\cdots l_{N_c-1}} \\ &= \frac{N_c\,!}{N_c^{N_c/2}}.\end{aligned} \tag{2.30}$$

The growth of this equation is easily seen with the help of Stirling's approximation, given in eq. (2.21) to be, for large N_c:

$$g_{P\to(N_c-1)\pi} \propto N_c^{\frac{N_c}{2}}\ . \tag{2.31}$$

The coupling constant $g_{P\to(N_c-1)\pi}$ has energy-dimensions that depend on the number of colors. To ascertain this dimension we examine the total width of the polyquark; this is proportional to the square of the coupling times the appropriate phase space:

$$d\Gamma_{(N_c-1)\pi} = \frac{g_P^2}{2M_P(N_c)}\int \rho(M_P(N_c))\ , \tag{2.32}$$

having dimensions of energy. The phase space being integrated is:

$$\rho(E) = (2\pi)^4 \times \int \prod_{i=1}^{N_c-1} \frac{d^3\mathbf{p}_i}{2E_i(2\pi)^3} \delta\left(\sum E_i - E\right) \delta^{(3)}\left(\sum \mathbf{p}_i - \mathbf{P}\right) \tag{2.33}$$

(with $\mathbf{P} = 0$ for a particle decaying at rest as in Eq. (2.32)). This has energy-dimension E^{2N_c-6} (-4 from the energy-momentum conservation δ, the rest from the integration measure). Multiplying by E^{-1} from the flux normalization $1/M$ in Eq. (2.32) we get a mass-dimension for g_P given by:

$$\left[g_{P\to(N_c-1)\pi}\right] = E^{4-N_c} \ . \tag{2.34}$$

Armed with this result, we return to eq. (2.31). The color scaling of the coupling, including now the mass-dimension, is

$$g_P \propto c_g^{4-N_c} \frac{N_c!}{N_c^{N_c/2}} \ , \tag{2.35}$$

c_g being a constant with dimension of mass-energy.

We can then examine the color scaling of the total width. The maximum of the phase space occurs for momentum about equally spread out among all pions. Since both the number of pions and the total available energy, $M_P(N_c)$, are linearly growing with N_c, the momentum assigned to each pion is roughly constant. This yields an additional quantity with dimensions of energy, that we denote c_p. We find the scaling of the polyquark width to be

$$\Gamma_1 \propto \frac{N_c\,!^2}{N_c^{N_c}} \times c_p^{2(N_c-1)-4} c_g^{2(4-N_c)} \frac{1}{M_P} \tag{2.36}$$

or

$$\Gamma_1 \propto \frac{N_c\,!^2}{N_c^{N_c}} \frac{c_p^{-6} c_g^8}{M_P} \left(\left(\frac{c_p}{c_g}\right)^2\right)^{N_c} . \tag{2.37}$$

This can at last be expressed as

$$\Gamma_1 = c_1 \cdot c_2^{N_c} \frac{N_c\,!^2}{N_c^{N_c+1}}, \tag{2.38}$$

with c_1 an unspecified constant with dimension of energy (which is N_c independent), and c_2 a dimensionless constant (also N_c independent).

For $N_f = 2$, the result computed in Appendix D is:

$$\Gamma_2 \propto \frac{((N_c-1)/2)!^4 c_1 \cdot c_2^{N_c}}{N_c^{N_c+1}} \ . \tag{2.39}$$

Using the Stirling's approximation of eq. (2.21), we can see that both results are equivalent:

$$\Gamma_1 \sim \Gamma_2 \propto c_1 \cdot c_2^{N_c} \cdot N_c^{N_c-1} \ . \tag{2.40}$$

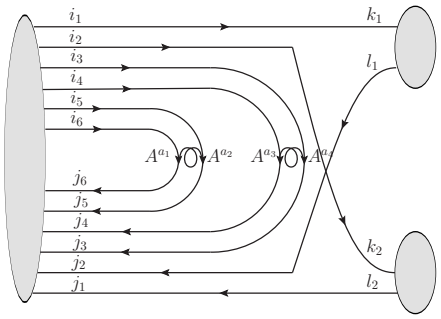

Figure 2.11: Polyquark meson-meson matrix element for the SU(7) case.

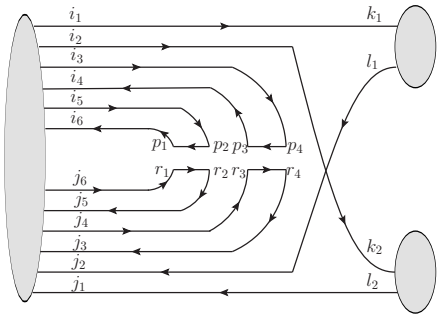

Figure 2.12: Polyquark-meson mixing (for SU(7)) in double-line notation. Quark and anti-quark arrows track color flow.

Polyquark and meson-molecule coupling

We now start with the off-diagonal couplings involving the polyquark to the other selected meson configurations. The first task is to obtain the polyquark-meson coupling, a characteristic contribution being shown in Fig. 2.11 for even $N_c - 1$ (for simplicity we limit ourselves to this case, and interpolate for odd $N_c - 1$). Therefore, we have to compute:

$$\begin{aligned}\langle (q\bar{q})^2 | \mathrm{Q}\bar{\mathrm{Q}} \rangle &= \frac{\epsilon^{ai_1\cdots i_{N_c-1}}\epsilon^{aj_1\cdots j_{N_c-1}}}{\sqrt{N_c}(N_c-1)!^2}\frac{\delta^{k_1 l_1}\delta^{k_2 l_2}}{N_c}\langle q^{k_1}q^{k_2}\bar{q}^{\,l_1}\bar{q}^{\,l_2}|\frac{H_I^{N_c-3}}{(N_c-3)!}|q^{i_1}\cdots q^{i_{N_c-1}}\bar{q}^{j_1}\cdots\bar{q}^{j_{N_c-1}}\rangle \\ &= \frac{\epsilon^{ai_1\cdots i_{N_c-1}}\epsilon^{aj_1\cdots j_{N_c-1}}}{\sqrt{N_c}(N_c-1)!^2}\frac{\delta^{k_1 l_1}\delta^{k_2 l_2}}{N_c}\langle q^{k_1}q^{k_2}\bar{q}^{\,l_1}\bar{q}^{\,l_2}|\frac{\mathcal{A}^{a_1}\cdots\mathcal{A}^{a_{N_c-3}}}{(N_c-3)!}|q^{i_1}\bar{q}^{j_1}\cdots q^{i_{N_c-1}}\bar{q}^{j_{N_c-1}}\rangle,\end{aligned} \tag{2.41}$$

where H_I is the interaction Hamiltonian and $\mathcal{A}^a = i\frac{g}{\sqrt{N_c}}A^a T^a_{ij}$ denotes the quark-gluon vertex.

To track the color flow between each ket-state quark and anti-quark and a bra-state quark, anti-quark or gluon, we redraw Fig. 2.11 using t'Hooft double line notation in Fig. 2.12. Choosing for example one quark in the ket, there are $N_c - 1$ ways to contract it (with one of the two final-state mesons, or with any of the $N_c - 3$ intermediate gluon vertices). The next quark chosen can be contracted in $N_c - 2$ different ways, and so on, and similarly one

contracts all antiquarks and collects the combinatorial factors. Antisymmetry under fermion exchange brings about two Levi-Civita tensors:

$$\begin{aligned}\langle(q\bar{q})^2|\mathrm{Q}\bar{\mathrm{Q}}\rangle \quad \propto \quad & \left(\frac{g^2}{N_c}\right)^{(N_c-3)/2} T^{a_1}_{p_1r_1}\cdots T^{a_{N_c-3}}_{p_{N_c-3}r_{N_c-3}} \frac{\epsilon^{ai_1\cdots i_{N_c-1}}\epsilon^{aj_1\cdots j_{N_c-1}}}{\sqrt{N_c}(N_c-1)!^2(N_c-3)!}\frac{\delta^{k_1l_1}\delta^{k_2l_2}}{N_c} \\ & \epsilon^{bi_1\cdots i_{N_c-1}}\epsilon^{bl_1l_2p_1\cdots p_{N_c-3}}\epsilon^{cj_1\cdots j_{N_c-1}}\epsilon^{ck_1k_2r_1\cdots r_{N_c-3}}\langle 0|A^{a_1}\cdots A^{a_{N_c-3}}|0\rangle,\end{aligned} \tag{2.42}$$

where we have kept track of color alone. Using again eq. (2.17) for both quark and anti-quark antysimmetryc tensors we get:

$$\begin{aligned}\langle(q\bar{q})^2|\mathrm{Q}\bar{\mathrm{Q}}\rangle \quad \propto \quad & \frac{\epsilon^{bk_1k_2p_1\cdots p_{N_c-3}}\epsilon^{bk_1k_2r_1\cdots r_{N_c-3}}}{\sqrt{N_c^3}(N_c-3)!} \\ \times \quad & \left(\frac{g^2}{N_c}\right)^{(N_c-3)/2} T^{a_1}_{p_1r_1}\cdots T^{a_{N_c-3}}_{p_{N_c-3}r_{N_c-3}}\langle 0|A^{a_1}\cdots A^{a_{N_c-3}}|0\rangle.\end{aligned} \tag{2.43}$$

To address the gluon combinatorics (line exchanges in t'Hooft notation), choose a field A^{a_i} and contract it with one of (N_c-4) others. The next one has only (N_c-6) possibilities and so on. Therefore, there are $(N_c-4)!!$ different ways to contract all the gluon vertices, resulting in:

$$\begin{aligned}\langle(q\bar{q})^2|\mathrm{Q}\bar{\mathrm{Q}}\rangle \quad \propto \quad & \frac{(N_c-4)!!\,\epsilon^{bk_1k_2p_1\cdots p_{N_c-3}}\epsilon^{bk_1k_2r_1\cdots r_{N_c-3}}}{\sqrt{N_c^3}(N_c-3)!} \\ & \left(\frac{g^2}{N_c}\right)^{(N_c-3)/2} T^{a_1}_{p_1r_1}T^{a_1}_{p_2r_2}\cdots T^{a_{N_c-3}/2}_{p_{N_c-4}r_{N_c-4}}T^{a_{N_c-3}/2}_{p_{N_c-3}r_{N_c-3}}.\end{aligned} \tag{2.44}$$

Next we reduce the Gell-Mann matrices. Summation over the Levi-Civita symbols yields $(N_c-1)!$ different permutations. Substituting:

$$T^a_{ij}T^a_{kl} = \frac{1}{2}\left(\delta_{il}\delta_{jk} - \frac{1}{N_c}\delta_{ij}\delta_{kl}\right), \tag{2.45}$$

there remain only $2^{(N_c-3)/2}$ non-vanishing terms coming from the $(N_c-3)/2$ gluon propagators, to name it

$$\left(\delta_{p_1r_2}\delta_{p_2r_1} - \frac{1}{N_c}\delta_{p_1r_1}\delta_{p_2r_2}\right)\cdots\left(\delta_{p_{N_c-4}r_{N_c-3}}\delta_{p_{N_c-3}r_{N_c-4}} - \frac{\delta_{p_{N_c-4}r_{N_c-4}}\delta_{p_{N_c-3}r_{N_c-3}}}{N_c}\right) \tag{2.46}$$

whose dominant contribution comes from $\delta_{p_1r_2}\delta_{p_2r_1}\cdots\delta_{p_{N_c-4}r_{N_c-3}}\delta_{p_{N_c-3}r_{N_c-4}}$ and yields

$$\begin{aligned}\frac{\epsilon^{bk_1k_2p_1\cdots p_{N_c-3}}\epsilon^{bk_1k_2p_2p_1\cdots p_{N_c-3}p_{N_c-4}}}{N_c^{N_c/2}(N_c-3)!}\left(\frac{g^2}{2}\right)^{(N_c-3)/2} &= \frac{(-1)^{(N_c-3)/2}N_c\,!}{N_c^{N_c/2}(N_c-3)!}\left(\frac{g^2}{2}\right)^{(N_c-3)/2} \\ &\sim \frac{(-1)^{(N_c-3)/2}}{N_c^{(N_c-6)/2}}\left(\frac{g^2}{2}\right)^{(N_c-3)/2}.\end{aligned} \tag{2.47}$$

However, this leading-N_c group of diagrams does not exhaust the dominant-N_c contribution because the nominally subleading diagrams are combinatorialy enhanced. In fact there are $(N_c-3)/2$ sub-leading terms of order $1/N_c$,

$$\frac{-1}{N_c}(\delta_{p_1r_1}\delta_{p_2r_2}\delta_{p_3r_4}\delta_{p_4r_3}\cdots\delta_{p_{N_c-4}r_{N_c-3}}\delta_{p_{N_c-3}r_{N_c-4}}+\cdots \\ \delta_{p_1r_2}\delta_{p_2r_1}\cdots\delta_{p_{N_c-4}r_{N_c-4}}\delta_{p_{N_c-3}r_{N_c-3}}), \tag{2.48}$$

(the sign here is opposite to the leading order contribution, but since there is one less fermion permutation, it will contribute with the same sign).

Likewise there will be $(N_c-3)(N_c-5)/4$ terms with $1/N_c^2$, again with the same sign; $(N_c-3)(N_c-5)(N_c-7)\,/\,8$ with $1/N_c^3$, $(N_c-3)(N_c-5)(N_c-7)(N_c-9)\,/\,2^4$ with $1/N_c^4$, etc. Finally, there will be $((N_c-3)(N_c-5)\cdots(N_c-3)/2)\,/2^{(N_c-3)/4}$ terms contributing with a $1/N_c^{(N_c-3)/4}$ weight. Summing all contributions we get

$$\begin{aligned}\langle(q\bar{q})^2|\mathrm{Q}\bar{\mathrm{Q}}\rangle &= \frac{(-1)^{(N_c-3)/2}N_c\,!(N_c-4)!!}{N_c^{N_c/2}(N_c-3)!}\frac{N_c-3}{4}\left(\frac{g}{2}\right)^{(N_c-3)} \\ &\sim \frac{(-1)^{(N_c-3)/2}N_c\,!!}{N_c^{(N_c-4)/2}}\left(\frac{g}{2}\right)^{(N_c-3)}\end{aligned} \tag{2.49}$$

The Stirling's approximation for the double factorial reads:

$$n!!\propto 2^n\left(\frac{n}{2}\right)!\sim 2^n\mathrm{e}^{\frac{\mathrm{n}}{2}(\log\frac{\mathrm{n}}{2}-1)}. \tag{2.50}$$

So applying this approximation to eq. (2.49), we get:

$$\langle(q\bar{q})^2|\mathrm{Q}\bar{\mathrm{Q}}\rangle\propto 2^{N_c}\mathrm{e}^{\frac{\mathrm{N_c}}{2}(\log\frac{\mathrm{N_c}}{2}-1)}\mathrm{e}^{-\frac{\mathrm{N_c}-4}{2}\log\frac{\mathrm{N_c}-4}{2}}\left(\frac{g}{2}\right)^{(N_c-3)}\sim g^{N_c}e^{-N_c/2}, \tag{2.51}$$

so the coupling to mesons vanishes with N_c. This result was conjectured by Witten [97] without providing any explicit calculation.

Polyquark and $\bar{q}q$ meson coupling

The simplest way to handle this computation is to assume that N_c is an even number (4,6,8,...). A leading order diagram for the polyquark-meson mixing is represented in Fig. 2.13. As familiar by now, higher order diagrams in perturbation theory will not change this counting.

Reading off that Feynman diagram we find that the coupling is given by

$$\begin{aligned}\langle q\bar{q}\,|\mathrm{Q}\bar{\mathrm{Q}}\rangle &= \frac{\epsilon^{ai_1\cdots i_{N_c-1}}\epsilon^{aj_1\cdots j_{N_c-1}}}{\sqrt{N_c}(N_c-1)!^2}\frac{\delta^{k_1l_1}}{\sqrt{N_c}}\langle q^{k_1}\bar{q}^{\,l_1}|\frac{H_I^{N_c-2}}{(N_c-2)!}|q^{i_1}\cdots q^{i_{N_c-1}}\bar{q}^{j_1}\cdots\bar{q}^{j_{N_c-1}}\rangle \\ &= \frac{\epsilon^{ai_1\cdots i_{N_c-1}}\epsilon^{aj_1\cdots j_{N_c-1}}}{\sqrt{N_c}(N_c-1)!^2}\frac{\delta^{k_1l_1}}{\sqrt{N_c}}\langle q^{k_1}\bar{q}^{\,l_1}|\frac{\mathcal{A}^{a_1}\cdots\mathcal{A}^{a_{N_c-2}}}{(N_c-2)!}|q^{i_1}\cdots q^{i_{N_c-1}}\bar{q}^{j_1}\cdots\bar{q}^{j_{N_c-1}}\rangle.\end{aligned} \tag{2.52}$$

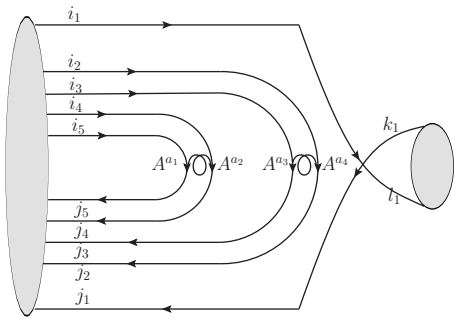

Figure 2.13: Polyquark $\bar{q}q$-meson matrix element for six colors.

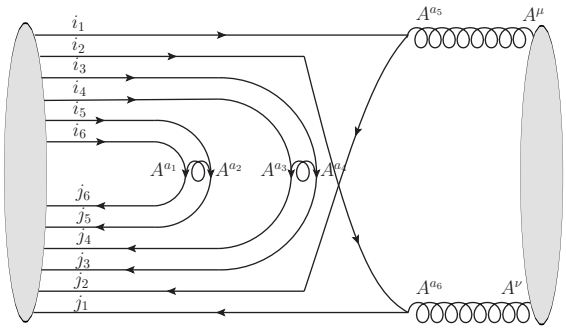

Figure 2.14: Polyquark gg matrix element for the SU(7) case.

Proceeding again as we did in subsection 2.2.6 we see that

$$\begin{aligned}
\langle q\bar{q}|\mathrm{Q}\bar{\mathrm{Q}}\rangle \quad &\propto \quad \frac{\epsilon^{ai_1\cdots i_{N_c-1}}\epsilon^{aj_1\cdots j_{N_c-1}}\delta^{k_1l_1}}{(N_c-1)!^3}\epsilon^{bi_1\cdots i_{N_c-1}}\epsilon^{bl_1p_1\cdots p_{N_c-2}}\epsilon^{cj_1\cdots j_{N_c-1}}\epsilon^{ck_1r_1\cdots r_{N_c-2}} \\
&\quad \times\left(\frac{g^2}{N_c}\right)^{(N_c-2)/2} T^{a_1}_{p_1r_1}\cdots T^{a_{N_c-2}}_{p_{N_c-2}r_{N_c-2}}\langle 0|A^{a_1}\cdots A^{a_{N_c-2}}|0\rangle \\
&\propto \quad \frac{(N_c-3)!!}{(N_c-1)!}\epsilon^{bk_1p_1\cdots p_{N_c-2}}\epsilon^{bk_1r_1\cdots r_{N_c-2}}\frac{g^2}{N_c}^{(N_c-2)/2} T^{a_1}_{p_1r_1}T^{a_1}_{p_2r_2}\cdots T^{a_{(N_c-2)/2}}_{p_{N_c-3}r_{N_c-3}}T^{a_{(N_c-2)/2}}_{p_{N_c-2}r_{N_c-2}} \\
&\sim \quad \frac{(-1)^{(N_c-2)/2}(N_c-1)\,!!}{N_c^{(N_c-4)/2}}\left(\frac{g}{2}\right)^{(N_c-2)}.
\end{aligned} \tag{2.53}$$

Polyquark and glueball coupling

The dominant diagram is the one given in Fig. 2.14, where we assume again that N_c-1 is an even number. Therefore, we have to calculate the matrix element

$$\begin{aligned}\langle gg|\mathrm{Q}\bar{\mathrm{Q}}\rangle &= \frac{\epsilon^{ai_1\cdots i_{N_c-1}}\epsilon^{aj_1\cdots j_{N_c-1}}}{\sqrt{N_c}(N_c-1)!^2}\frac{\delta^{\mu\nu}}{\sqrt{N_c^2-1}}\langle\mathcal{A}^\mu\mathcal{A}^\nu|\frac{H_I^{N_c-1}}{(N_c-1)!}|q^{i_1}\cdots q^{i_{N_c-1}}\bar{q}^{j_1}\cdots\bar{q}^{j_{N_c-1}}\rangle \\ &= \frac{\epsilon^{ai_1\cdots i_{N_c-1}}\epsilon^{aj_1\cdots j_{N_c-1}}}{\sqrt{N_c}(N_c-1)!^2}\frac{\delta^{\mu\nu}}{\sqrt{N_c^2-1}}\langle\mathcal{A}^\mu\mathcal{A}^\nu|\frac{\mathcal{A}^{a_1}\cdots\mathcal{A}^{a_{N_c-1}}}{(N_c-1)!}|q^{i_1}\cdots q^{i_{N_c-1}}\bar{q}^{j_1}\cdots\bar{q}^{j_{N_c-1}}\rangle.\end{aligned} \tag{2.54}$$

Making again all possible contractions produces

$$\begin{aligned}\langle gg|\mathrm{Q}\bar{\mathrm{Q}}\rangle &\propto \frac{\epsilon^{ai_1\cdots i_{N_c-1}}\epsilon^{aj_1\cdots j_{N_c-1}}}{\sqrt{N_c}(N_c-1)!^3}\frac{\delta^{\mu\nu}}{\sqrt{N_c^2-1}}\epsilon^{bi_1\cdots i_{N_c-1}}\epsilon^{bp_1\cdots p_{N_c-1}}\epsilon^{cj_1\cdots j_{N_c-1}}\epsilon^{cr_1\cdots r_{N_c-1}} \\ &\quad\times\left(\frac{g^2}{N_c}\right)^{(N_c-1)/2}T^{a_1}_{p_1r_1}\cdots T^{a_{N_c-1}}_{p_{N_c-1}r_{N_c-1}}\langle\mathcal{A}^\mu\mathcal{A}^\nu|A^{a_1}\cdots A^{a_{N_c-1}}|0\rangle \\ &\propto \frac{\epsilon^{ai_1\cdots i_{N_c-1}}\epsilon^{aj_1\cdots j_{N_c-1}}}{\sqrt{N_c}(N_c-1)!^3}\frac{\delta^{\mu\nu}}{\sqrt{N_c^2-1}}\epsilon^{bi_1\cdots i_{N_c-1}}\epsilon^{bk_1k_2p_1\cdots p_{N_c-3}}\epsilon^{cj_1\cdots j_{N_c-1}}\epsilon^{cl_1l_2r_1\cdots r_{N_c-3}} \\ &\quad(N_c-1)(N_c-2)\left(\frac{g^2}{N_c}\right)^{(N_c-1)/2}T^{a_1}_{p_1r_1}\cdots T^{a_{N_c-1}}_{p_{N_c-1}r_{N_c-1}}.\end{aligned} \tag{2.55}$$

that leads, following the same derivation as for the other matrix elements,

$$\begin{aligned}\langle gg|\mathrm{Q}\bar{\mathrm{Q}}\rangle &\sim \frac{(N_c-2)}{N_c^{N_c/2}(N_c-1)}\epsilon^{bp_1\cdots p_{N_c-1}}\epsilon^{br_1\cdots r_{N_c-1}}\times\left(\frac{g^2}{2}\right)^{(N_c-1)/2}T^{a_1}_{p_1r_1}\cdots T^{a_{N_c-1}}_{p_{N_c-1}r_{N_c-1}} \\ &\sim \frac{(-1)^{(N_c-1)/2}N_c}{N_c^{(N_c-2)/2}}\left(\frac{g}{2}\right)^{(N_c-1)}.\end{aligned} \tag{2.56}$$

The results for the $N_f = 1$ and $N_f = 2$ cases are collected in table 2.3, the latter being calculated in Appendix D.

Finally, it is worth remarking that this polyquark object is an exception to the rule that mesons are narrow in leading N_c. As remarked by Jaffe and Witten, this object fissions with a width that scales rapidly with N_c, as it can be seen in equation (2.38).

Summary

In this Section we have studied the large N_c behavior of masses, dominant decay channels and couplings of various meson quark-gluon components of standing interest. We have computed the $(N_c-1)q\bar{q}$ polyquark, and collected other results into a single, unified presentation.

We have addressed the cases of one and two flavors, that turn out to be equivalent in leading-N_c, and eschewed the spin discussion. If non-zero spin and an arbitrary number of

	$q\bar{q}$	gg	$qq\bar{q}\bar{q}$	$(N_c-1)\pi$
$N_f=1$	$(N_c-1)!!\left(\frac{c}{N_c}\right)^{(N_c-4)/2}$	$N_c!!\left(\frac{c}{N_c}\right)^{(N_c-2)/2}$	$N_c!!\left(\frac{c}{N_c}\right)^{(N_c-4)/2}$	$\frac{N_c!}{N_c^{N_c/2}}$
$N_f=2$	$(N_c-1)!!\left(\frac{c}{N_c}\right)^{(N_c-4)/2}$	$N_c!!\left(\frac{c}{N_c}\right)^{(N_c-2)/2}$	$N_c!!\left(\frac{c}{N_c}\right)^{(N_c-4)/2}$	$\frac{(N_c/2)^2!}{N_c^{N_c/2}}$

Table 2.3: Coupling matrix element of the $\mathbb{Q}^a\bar{\mathbb{Q}}^a$ polyquark (baryonium) to various other meson configurations with fixed particle number (from left to right conventional meson, glueball, tetraquark or two-mesons, and N_c-1 conventional mesons). We give results for one (first row) and two flavors (second row). Note that only the last entry (controlling the width) is slightly different for one flavor).

flavors was to be considered, one would need a more sophisticated approach than our brute-force evaluation in this work. The correct framework is the contracted spin-flavor symmetry of the large N_c limit [237], that should help organize more difficult calculations into a manageable form. This is beyond our present reach.

Our results can be found in tables 2.1,2.2,2.3 and should be useful for phenomenological N_c analysis of various meson configurations. In a nutshell, meson configurations (as is known) have an N_c-independent mass and falling width as function of N_c, excepting the baryonium-like configurations (that we dub polyquarks), that, as pointed out by Jaffe, become broad continua of increasing mass. We have contributed a calculation of the coupling of this polyquark to the other, more conventional, meson configurations.

None of these configurations reproduces by itself the expected behavior of the mass and width of the σ meson found in several of our group's works [211, 220, 238] in unitarized chiral perturbation theory. Thus, a study in which all these configurations appear mixed and where the mixing coefficients depend on N_c but are otherwise of natural order of magnitude seems appropriate. Such study is indeed the topic of the next Sections.

2.2.7 Publication: F. J. LLanes-Estrada, J.R. Pelaez, J. Ruiz de Elvira , *Fock space expansion of sigma meson in leading-Nc, Nucl. Phys.* Proc. Supl. 207-208 (2010)

Available online at www.sciencedirect.com
ScienceDirect
Nuclear Physics B (Proc. Suppl.) 207–208 (2010) 169–172
NUCLEAR PHYSICS B PROCEEDINGS SUPPLEMENTS
www.elsevier.com/locate/npbps

Fock space expansion of σ meson in leading-N_c

Felipe J. Llanes-Estrada *, Jose Ramón Peláez and Jacobo Ruiz de Elvira

Departamentos de Física Teórica I y II, Universidad Complutense de Madrid, 28040 Madrid, Spain.

Abstract

We examine the leading-N_c behavior of the masses and transition matrix elements of some low-lying, few-particle configurations in QCD. A truncation of the Fock space produces an effective, symmetric Hamiltonian that we diagonalize. The lowest eigenvalue is identified as the σ meson if the Hamiltonian is chosen to represent the scalar sector. As an application, the coefficients of the N_c powers are then fit to two-loop Unitarized SU(2) Chiral Perturbation Theory results for the σ mass and width as a function of the number of colors, and we show that those results can be accommodated using the QCD N_c dependence previously derived for matrix elements, without the need for unnatural parameters or fine tunings. Finally, we show a very preliminary good quality fit, estimating the proportion of tetraquark/molecule-like (dominant), $q\bar{q}$-like (subdominant) and exotic-like (marginal) configurations in the σ.

Keywords: Scalar mesons, Fock decomposition, UChPT, IAM, Large Nc

1. Motivation

A low-mass σ meson was introduced in 1955 [1] as an auxiliary device that has turned out to be very useful to explain the intermediate-distance attractive part in the nuclear potential. For long time debated, the mass and width of this meson (decaying almost always to $\pi\pi$, the only open strong decay channel) have been recently pinned down with very good precision employing different methods. The results of these analysis are in agreement with each other and some are shown in table 1.

Table 1: Precise determinations of the σ meson mass and half-width (in *MeV*).

M	$\Gamma/2$	Refs.
452(12)	260(15)	[2]
458(15)	262(15)	[3]
441(12)	272(12)	[4]

It behooves one to understand the composition of this meson in terms of the fundamental QCD degrees of freedom, quarks and gluons. Of current interest is the decomposition of states in terms of a Fock space expansion [5] and this we address in the present brief report. This expansion reads

$$|\sigma\rangle = \sum \int \left(\alpha_{q\bar{q}}|q\bar{q}\rangle + \alpha_{gg}|g\bar{g}\rangle + \alpha_{qq\bar{q}\bar{q}}|qq\bar{q}\bar{q}\rangle \ldots\right) \quad (1)$$

where the sum/integral signs remind us of spin, momentum and other degrees of freedom that, for simplicity, we will further omit in our notation; that is, we consider the summed amplitude over each Fock subspace

$$|\sigma\rangle = \alpha_{q\bar{q}}|q\bar{q}\rangle + \alpha_{gg}|g\bar{g}\rangle + \alpha_{qq\bar{q}\bar{q}}|qq\bar{q}\bar{q}\rangle \ldots \quad (2)$$

This expansion in terms of quarks and transverse gluons is well defined in Coulomb gauge QCD [6], that can be formulated without ghosts nor longitudinal gluons. At least for heavy mesons decaying to open-flavor channels, the intrinsic $q\bar{q}$ component can be identified in a model-independent way [7]. The setback of this full quantum-mechanical answer is that it is frame-dependent, presumably defined in the rest frame of the hadron [8]. This makes it less attractive for light hadrons where speeds can be large.

The $1/N_c$ expansion around $N_c = 3$ offers more limited information: it can only separate classes of equivalence of states whose mass and decays behave in the same way under N_c, but the information obtained is useful also for light quarks. Thus our states in Eq.(2) should be understood as $q\bar{q}$-like, $g\bar{g}$-like, etc... although for simplicity we are calling them $q\bar{q}$, $g\bar{g}$, etc...

2. Matrix elements in leading-N_c

We now consider what configurations may play an important role for the σ meson (and other light scalar mesons). First, the σ is a very broad resonance in $\pi\pi$ scattering, deep in the complex plane,

*Speaker

doi:10.1016/j.nuclphysbps.2010.10.044

so one can describe part of its nature as a pion-pion correlation (distortion of the density of states, or for brevity, 'molecule'), or equivalently as the leading-N_c color analysis is concerned, a tetraquark. Thus, although we denote it by $q\bar{q}q\bar{q}$, we actually mean "tetraquark/molecule".

Next, at some level one expects to find (and indeed finds as will be shown in figure 2 below) a $q\bar{q}$ component, that would correspond to the 1 GeV quark model's $^3P_0$ configuration.

Finally, one might expect more exotic configurations such as glueballs or baryonium-type multiquark correlations to also play a role.

We give the leading N_c behavior, N_c^β, of the mass and $\pi\pi$ width of these various configuration in table 2.

Table 2: Leading-N_c scaling of mass and width of various QCD Fock-states.

State	M	$\Gamma_{\pi\pi}$
$\pi\pi$, $q\bar{q}q\bar{q}$	$O(1)$	O(1)
$q\bar{q}$	$O(1)$	$O(1/N_c)$
gg	$O(1)$	$O(1/N_c^2)$
$(N_c-1)(q\bar{q})$	$O(N_c)$	$O(e^{-N_c})$

We illustrate the color computation of one of these matrix elements (the glueball to two pion transition $G \to \pi\pi$) in figure 1.

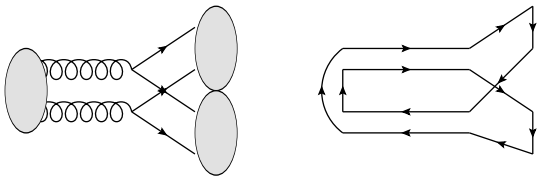

Figure 1: Left: the impulse diagram for the transition of a glueball to two pions already yields the leading-N_c behavior of the entire amplitude as shown by t'Hooft. Right: color flow of the same diagram. The line crossing reveals the $1/N_c$ suppression.

A way to establish the counting (left diagram in the figure) is to observe that the color-singlet two-gluon wavefunction, properly normalized, is $\frac{\delta_{ab}}{\sqrt{N_c^2-1}}$. Each of the two vertices carry $\frac{gT^a_{ij}}{\sqrt{N_c}}$ (this scaling of the color charge guarantees that higher-order diagrams scale in the same way under N_c). Finally, the pion wavefunctions in the final state combine a quark and antiquark to form a color singlet $\frac{\delta_{ij}}{\sqrt{N_c}}$.

The net result for the matrix element is $tr(T^aT^a)/(N_c^2\sqrt{N_c^2-1})$, suppressed as $1/N_c$. As the width is proportional to the matrix element $G \to \pi\pi$ squared, the corresponding entry in table 2 follows.

3. Effective Hamiltonian

We take one state from each class $q\bar{q}$, gg, $q\bar{q}q\bar{q}$ [1], to build a discrete 3×3 effective Hamiltonian H. We will not attempt to calculate this Hamiltonian from theory, but we factor the leading-N_c behavior of its matrix elements, known from a N_c analysis, and leave the pre-coefficients as free parameters. Diagonalization of H yields three eigenvalues. We identify the lowest one as the σ.

To describe the width, our three model states have to be coupled to the pion-pion continuum. For this we employ a Feshbach decomposition [17] in terms of a P subspace (our three discrete states) and a Q subspace (two free pions in an arbitrary relative momentum state). The full Hamiltonian in the total space

$$H = \begin{pmatrix} H_{PP} & H_{PQ} \\ H_{QP} & H_{QQ} \end{pmatrix} \tag{3}$$

is then restricted to the discrete P subspace via the resolvent in Q-space with appropriate boundary conditions

$$H^{eff}_{PP} = H_{PP} + H_{PQ}\frac{1}{E - H_{QQ} + i\epsilon}H_{QP}\ . \tag{4}$$

We actually do not need to calculate the integral over pion configurations in the rightmost term; all we need is to extract its leading-N_c behavior. The effective Hamiltonian is finally a symmetric (because of CP invariance), non-Hermitian (because of the Fock-space restriction) 3×3 complex matrix, that has therefore 12 free parameters in leading N_c (the exponents being known),

$$H_{ij} = h_{ij} \times N_c^{\beta_{ij}}\ . \tag{5}$$

The diagonal β are given in Table 2, but for brevity, all others – already calculated with the procedure explained above– will be given somewhere else. We express the lowest eigenvalue (now complex) in terms of these unspecified parameters h_{ij}.

4. Inverse Amplitude Method

We match our N_c results to a dispersive analysis, the well-established Inverse Amplitude Method (IAM) [9, 10]. The method proceeds by writing a dispersion relation for $G \equiv \frac{(t^{(2)})^2}{t}$ where t is the scalar, isoscalar pion-pion scattering amplitude and $t = t^{(2)} + t^{(4)} + t^{(6)}\ldots$ is its ChPT expansion. This reads

$$G(s) = G(0) + G'(0)s + \frac{1}{2}G''(0)s^2 + \frac{s^3}{\pi}\int_{RC} ds' \frac{\mathrm{Im}\,G(s')}{s'^3(s'-s)} + LC(G) + PC(G)$$

[1] For this analysis we discard the baryonium-like configuration, that will be reexamined in an upcoming work.

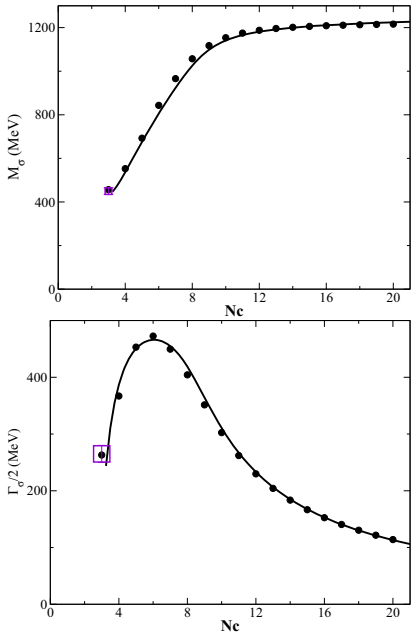

Figure 2: Mass (top) and width (bottom) of the σ meson in Unitarized Chiral Perturbation Theory (dots) as a function of the number of colors. The solid line is the fit to these data points in the three-state model that includes a molecule-like state, and two intrinsic $q\bar{q}$ and gg states. Squares (purple colored online) at $N_c = 3$ represent the precise dispersive determinations from table 1.

in terms of a left Mandelstam cut (LC), pole contributions (PC), due to the Adler zeroes of t and analyzed elsewhere [11], polynomial subtractions to assist convergence, and a dispersive integral over the right, unitarity cut. The two first terms in the first line are approximated in Chiral Perturbation Theory. Their contribution to the amplitude in the physical region with $E \geq 2m_\pi$ is very small since they lay well to the left of this threshold in the complex s-plane. The polynomic subtraction is represented exactly in the chiral expansion.

This leaves the dispersive integral on the second line. The nice feature about it is that, in the elastic region for $\pi\pi$ scattering, with $2m_K \geq E \geq 2m_\pi$, the imaginary part is exactly known, $\mathrm{Im}\, G = -\mathrm{Im}\, t_4$, and this formula provides a good approximation further up to $E \simeq 1.2$ GeV.

The dispersion relation can then be turned into simple algebraic expressions to the order desired, and while the approximation to order p^4 has been much exploited, we here employ the order p^6 in the expansion, that yields (not writing down the pole contributions for simplicity)

$$t \simeq \frac{t_2^2}{(t_2 - t_4 + t_4^2/t_2 - t_6)} \,. \qquad (6)$$

The poles (elastic resonances) in pion-pion scattering are thus simply obtained as zeroes of the denominator, and the σ mass and width extracted thereof. The dependence N_c dependence of the resonance parameters then obtained [12][13] by changing the chiral low energy parameters following their model independent ChPT/QCD description [14] (that follows from counting flavor traces). For this σ meson application we need only $f_\pi \to f_\pi \sqrt{\frac{N_c}{3}}$, $l_i \to l_i \frac{N_c}{3}$ for $i = 1 \ldots 4$ and $r_i \to r_i \left(\frac{N_c}{3}\right)^2$ for $i = 1 \ldots 6$. The values of the low energy constants at $N_c = 3$ are given in table 3.

l_1^r(x 10^3)	-5.4	r_1(x 10^4)	-0.6
l_2^r(x 10^3)	1.8	r_2(x 10^4)	1.5
l_3^r(x 10^3)	1.5	r_3(x 10^4)	-1.4
l_4^r(x 10^3)	9.0	r_4(x 10^4)	1.4
		r_5(x 10^4)	2.4
		r_6(x 10^4)	-0.6

Table 3: Two-loop IAM LECs employed, corresponding to the fit ρ as $\bar{q}q$ in [13]. We rely on $SU(2)$ chiral perturbation theory, while it is known that the subthreshold coupling of the σ to the closed $K\overline{K}$ channel is large [2]. A pure color analysis is blind to these flavor details, and for the time being the $K\overline{K}$ component must be understood as included in the (dominant) meson-meson component analyzed.

Figure 2 does not exceed $N_c \simeq 20$. The IAM is reliable near $N_c = 3$ where the resummation of s-channel rescattering effected by the IAM is the dominant physics, and the unitarity cut dominates the dispersion relation. Also a flavor singlet Goldstone boson is not necessary in the effective Lagrangian for modest N_c, as the axial anomaly is N_c suppressed. Our results should be understood as a *leading*-N_c expansion around $N_c = 3$, *never as* $N_c \to \infty$, see [18].

5. Results

The IAM results [13] for varying-N_c are displayed in figure 2. The mass M_σ initially increases towards 1 GeV with growing N_c, but then saturates to a more or less constant value after $N_c \simeq 8$. The half-width $\Gamma_\sigma/2$ also starts increasing with N_c, but around $N_c \simeq 6$, it decreases as it is expected for a $q\bar{q}$ meson. This behaviour has been interpreted [13] as a signal of the onset of the intrinsic, $q\bar{q}$ subdominant component of the σ meson and seems to be needed to ensure fulfillment of local duality [16]. The behavior of the width at lower N_c is characteristic of a molecule or tetraquark component.

It is plain from a comparison with table 1 that none of the intrinsic QCD states by itself can reproduce this behavior. One therefore needs to consider the mixing between different configurations.

Employing our 3×3 effective Hamiltonian, and varying N_c in the known manner, we fit the free pre-

coefficients h_{ij}. We restrict the fit to the parameter subspace yielding one light scalar only (in agreement with Unitarized Chiral Perturbation Theory), the other two being above 1.2 GeV, and we make no further statement about them since at that point they escape the reach of our method. We further examine naturality in the N_c pre-coefficients, in the sense that a coefficient of the known N_c powers is said to be natural if $h_{ij} \in (1/N_c, N_c)$.

This equation guarantees that the naive N_c counting works for the effective Hamiltonian. It could accidentally happen that one of the pre-coefficients of a subleading term was very large and the lowest orders in the $1/N_c$ expansion were therefore not a reliable approximation. Our naturality assumption means that we discard this case and believe the N_c counting *as is*.

Our very preliminary best fit is shown in figure 3, where we plot the probabilities $|\alpha|^2$ of finding one of our three model states in the lowest eigenvector.

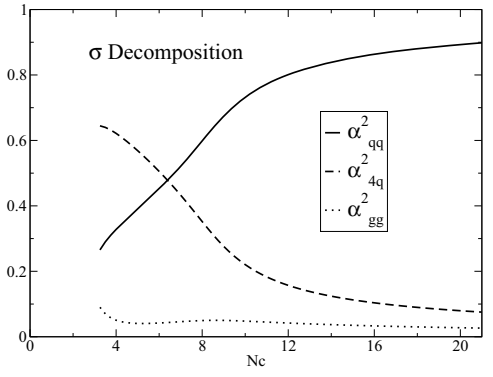

Figure 3: Fock space decomposition of the σ meson in a discrete model 3-state subspace, imposing naturality for the effective 3×3 Hamiltonian, whose pre-coefficients are obtained fitting leading-N_c to Unitarized Chiral Perturbation Theory. The dominant component behaves under N_c as a $q\bar{q}q\bar{q}$ through $N_c \simeq 6$, then the subdominant $q\bar{q}$-like takes over for larger N_c. The glueball-like component stays always at or below the 10% level.

The graph encodes all information that can be extracted from the N_c counting and naturality alone without increasing the model space. Given the large number of parameters in the minimization, we would be cautious about extending P beyond, say, four states.

It is rewarding that a good fit can be found (the solid line in figure 2) with such a simple model.

One could also inquire whether alternative fits that make the exotic (glueball) component dominant in the σ expansion could be found as some authors indicate that this might be the case [2]. This is ongoing work that will be reported in a follow-up publication.

A similar analysis could also be carried out for baryons and in fact, another problematic state in the low hadron spectrum, the $\Lambda(1405)$, is being examined [19].

Acknowledgements

We thank S. Narison for the invitation to the inspiring 2010 edition of this conference, and interesting discussions with R. Jaffe, J. A. Oller. Work supported by grants FPA2008-00592, FIS2008-01323, FIS2006-03438 (MICINN), U.Complutense/Banco Santander grant PR34/07-15875-BSCH and UCM-BSCH GR58/08 910309 and the EU-Research Infrastructure Integrating Activity "Study of Strongly Interacting Matter" (HadronPhysics2, Grant 227431) under the EU 7th Framework Programme.

References

[1] M. H. Johnson and E. Teller, Phys. Rev. **98** (1955) 783.
[2] R. Kaminski, G. Mennessier and S. Narison, Phys. Lett. B **680** (2009) 148
G. Mennessier, S. Narison and X. G. Wang, Phys. Lett. B **688** (2010) 59
[3] R. Garcia-Martin, R. Kaminski and J. R. Pelaez, Int. J. Mod. Phys. A **24** (2009) 590 F. J. Yndurain, R. Garcia-Martin and J. R. Pelaez, Phys. Rev. D **76** (2007) 074034
[4] I. Caprini, G. Colangelo and H. Leutwyler, Phys. Rev. Lett. **96** (2006) 132001
[5] A. H. Fariborz, R. Jora and J. Schechter, Phys. Rev. D **79** (2009) 074014 D. Black, Nucl. Phys. Proc. Suppl. **186** (2009) 275; E. van Beveren, D. V. Bugg, F. Kleefeld and G. Rupp, Phys. Lett. B **641** (2006) 265
[6] A. P. Szczepaniak and E. S. Swanson, Phys. Rev. D **65** (2002) 025012
[7] J. M. Torres-Rincon and F. J. Llanes-Estrada, Phys. Rev. Lett. **105** (2010) 022003
[8] M. G. Rocha, F. J. Llanes-Estrada, D. Schutte and S. V. Chavez, Eur. J. Phys. A **44** (2010) 411
[9] A. Dobado, M. J. Herrero and T. N. Truong, Phys. Lett. B **235** (1990) 134.
[10] A. Dobado and J. R. Pelaez, Phys. Rev. D **56** (1997) 3057
[11] A. Gomez Nicola, J. R. Pelaez and G. Rios, Phys. Rev. D **77** (2008) 056006
[12] J. R. Pelaez, Phys. Rev. Lett. **92** (2004) 102001
[13] J. R. Pelaez and G. Rios, Phys. Rev. Lett. **97** (2006) 242002
[14] J. Gasser and H. Leutwyler, Nucl. Phys. B **250**, 465 (1985).
[15] S. Peris and E. de Rafael, Phys. Lett. B **348**, 539 (1995).
[16] J. R. de Elvira, J. R. Pelaez, M. R. Pennington and D. J. Wilson, arXiv:1001.2746 [hep-ph].
[17] H. Feshbach, Ann. Phys. **19**, 287-313 (1962).
[18] J. R. Pelaez, arXiv:hep-ph/0509284. J. R. Pelaez and G. Rios, arXiv:0905.4689 [hep-ph]. J. Nieves and E.. Ruiz-Arriola, Phys. Rev. D **80** (2009) 045023. J. R. Pelaez, J. Nebreda and G. Rios, arXiv:1007.3461 [hep-ph].
[19] A. Hosaka, presentation at the workshop "QCD from the bound states perspective", Trento, 2-6 Aug. 2010.

2.2.8 Naturality and the σ meson composition

We have seen in the previous Section that there is a natural solution in order to explain the $f_0(500)$ behaviour from its composition in terms of quark and gluon states. In this Section, we want to study the constraints on the σ components that arise from its N_c behaviour and the assumption of naturality in the parameters of the Hamiltonian described in the previous Section.

Therefore, we consider again [240] a Fock expansion for the σ meson in terms of three QCD states, a tetraquark or $\pi\pi$-molecular state, an ordinary $\bar{q}q$ state and the glueball (actually, as we have seen in the previous two sections, they correspond to equivalent classes of states behaving the same as their representatives) , neglecting for simplicity the polyquark (that will only contribute increasing the tetraquark component [240]). Thus:

$$|\sigma\rangle = \alpha_1|\bar{q}q\bar{q}q\rangle + \alpha_2|\bar{q}q\rangle + \alpha_3|gg\rangle, \tag{2.57}$$

and we construct a symmetric and complex 3×3 Hamiltonian, whose diagonal elements, to leading order in $1/N_c$, are of the form:

$$H_{ii} = M_i + \frac{\Gamma_i}{2} = \mu\left(a_{ii} + iN_c^{\beta_i} b_{ii}\right), \tag{2.58}$$

where M_i and Γ_i would be the mass and width of the pure tetraquark/molecule, $\bar{q}q$ and glueball states if there was no mixing. In addition, the Hamiltonian off-diagonal elements are

$$H_{ij} = H_{ji} = \mu N_c^{\beta_{ij}}\left(a_{ij} + ib_{ij}\right). \tag{2.59}$$

Note that, for convenience we have extracted a dimensional constant μ, whose precise value is irrelevant, as well as the explicit N_c leading dependence of the Hamiltonian parameters. Thus, the "reduced Hamiltonian parameters" $h_{ij} = a_{ij}, b_{ij}$ are dimensionless and carry no N_c dependence. Since the powers β_i, β_{ij} are known integers that we have studied in Section 2.2.6, there are just 12 free reduced parameters in the Hamiltonian.

We expect all reduced parameters of the Hamiltonian to be of the same order of magnitude. Thus, we define a naturality function as the logarithm of the ratio between the largest and the smallest absolute value of these reduced coefficients, namely $\log |h_{ij}|_{max}/|h_{kl}|_{min}$. Other measures of naturality are also possible, but this is very simple and intuitive [240]. If this function was zero, all parameters would be equal, except possibly for a sign. If the absolute value of the largest parameter was ten times larger than the minimum, this function would be one. If it was a hundred times larger, it would be 2, etc... We have then fitted to the N_c behaviour of the σ meson, described in the publication of Section 2.2.7, minimizing simultaneously the naturality function. In addition, we will impose further constraints, namely, the lowest Hamiltonian eigenstate should be identified with the σ, and the other physical states should lie above 1.2 GeV, since they are not seen in the IAM below that energy. However, we allow one of the heavier states to be lighter than 1.2 GeV, if its width is also very large, satisfying the condition:

$$M_{phys_\alpha}^2 + \frac{\Gamma_{phys_\alpha}^2}{4} > \left(1.2\,\mathrm{GeV}\right)^2, \tag{2.60}$$

where with $phys_\alpha$, we label one of the physical states that appear once the Hamiltonian is diagonalized. This behaviour actually occurs for the tetraquark/two-pion state, which could

be interpreted as a real tetraquark or some continuum contribution or a mixture of both. We also do not consider physical states heavier that 2 GeV, since we think it would be rather unnatural that they have a large influence in σ at 500 MeV.

Thus, we have scanned the composition-space α_1^2, α_2^2, with the condition $\alpha_1^2 + \alpha_2^2 + \alpha_3^2 = 1$ by constraining the fits to lie within a particular area. In order to do that, we have divided the composition space in a 40×40 grid, and, within each grip element, we have used MINUIT to fit the N_c behavior while minimizing the naturality function. Given the large number of parameters, scanned the grid element with a sample of 1000 starting points, for a total of 1600000 fits, that took three days on a 76 core cluster.

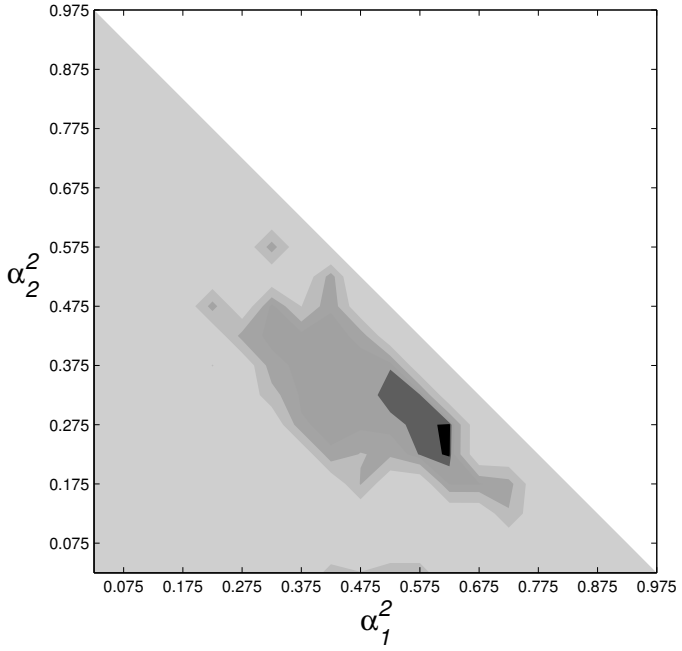

Figure 2.15: Composition space for the $f_0(500)$ meson.

In Fig. 2.15, we show the (α_1, α_2) space as a contour plot of the naturality function. The small dark area corresponds to fits that result in a naturality smaller than 0.85, which corresponds to a ratio of 7 or less between the largest and smallest absolute value of the coefficients. Actually our best fit lies in the area and corresponds to a composition of 60% tetraquark, 29% $\bar{q}q$ and 11% glueball, with the largest ratio between coefficients ~ 5. Very natural indeed. The darkest gray area corresponds to a naturality ≤ 1, which means that the ratio between the largest and the smallest absolute value of the coefficients is not larger than 10, which being conservative, may not be consider still very unnatural, and thus, we will use it to define our uncertainties. Beyond this point, we consider that the fits start being unnatural. In summary, we find a best fit with a 60% tetraquark, 29% $\bar{q}q$ and 11 % glueball. However, within the range $\alpha_1^2 \in [0.5, 0.65]$, $\alpha_2^2 \in [0.2, 0.37]$ and $\alpha_3^2 \in [0.1, 0.2]$, we are also able to find other natural fits, with relatives sizes of the parameters less than an order of magnitude.

For completeness, we have nevertheless provided in Fig. 2.15 more contours of naturality values. The next darkest gray area corresponds to a naturality up to 2, i.e. the ratio between

the maximum and minimum absolute values of the coefficients can be as large as 100. The next one bounds the region where the naturality function is smaller than 3, i.e. where we need some coefficients to be three orders of magnitude larger than another one. In these last areas it can be noticed that the increase in the naturality is very steep beyond 2. Actually, there are areas that would require ratios of parameters of many orders of magnitude. For instance, a glueball component larger than 20% is very disfavoured. A dominant glueball component ($\alpha_3^2 > 50\%$) would require cancellations of more than 4 orders of magnitude.

2.3 The role of the lightest scalar in the chiral symmetry restoration

2.3.1 Motivation

We have seen in Section 1.2.4 that the two-quark condensate $\langle \bar{q}q \rangle$ can be considered as the order parameter of the spontaneous chiral symmetry breaking since its non-zero value is a consequence of this spontaneous breaking and, as we have studied in Section 1.9, it is expected to vanish near the critical region. In addition, the scalar susceptibility describes the response of the QCD vacuum to any scalar field, and measures fluctuations of the quark condensate, showing a behaviour which grows dramatically close to the transition. In this Section, we want to study the role of the lightest scalar resonances, and in particular, the $f_0(500)$, in chiral symmetry restoration, which we achieve by analyzing their influence in the quark condensate and in the scalar susceptibility.

Note that the scalar susceptibility can be calculated as a quark mass derivative of the quark condensate or as the difference between the four-quark correlator and the square of the quark condensate. Thus, four-quark condensates occur naturally in the scalar susceptibility calculation. In principle, quark condensates of arbitrary order $\langle (\bar{q}q)^n \rangle$ are also built out of chiral non-invariant operators with vacuum quantum numbers and are also related to chiral symmetry restoration, so in principle, the four-quark condensate is another useful object to study the chiral transition. In addition, four-quark condensates are also of interest because they appear directly in QCD sum rules, through the operator product expansion (OPE) approach [258], where the factorization hypothesis is customarily made. This hypothesis states that four-quark condensates factorize into two-quark condensates squared $\langle (\bar{q}q)^2 \rangle \sim \langle \bar{q}q \rangle^2$ with the same quantum numbers. We wanted to check this hypothesis within the model independent ChPT approach. Furthermore, as we have seen in Section 2.2, we expect the $f_0(500)$ to be predominantly a tetraquark or molecular state, so studying the properties of four-quark condensates in chiral symmetry restoration is also of interest by itself. Note that the properties of quark condensates and susceptibilities are interesting not only in vacuum but also at finite temperature.

2.3.2 Outline of the results

With these motivations we have carried out the following research program. First, we study the properties of both the quark condensates and scalar susceptibilities at $T = 0$, within ChPT in a model independent way. As a by-product, we analyze the four-quark condensate and its factorization hypothesis. Finally, we include thermal effects in two different ways, using ChPT and the Virial approach with ChPT phase shifts. Both approaches are model independent at low temperatures, and can be derived from each other [196]. However, as we have seen in Section 1.3, within ChPT, partial-wave amplitudes do not reproduce resonances, so we cannot study, in particular, the effect of the $f_0(500)$ in the chiral transition. In order to make this analysis, we use the IAM combined with the virial approach, since, in this way, we can study and isolate the role of the resonances, ensuring that at low temperatures we are still reproducing the previous model independent result. Furthermore, we can study the

effect of non-resonant interactions, which are often neglected in different resonance hadron gas models, which, nevertheless, usually include the σ, $\rho(770)$, $\cdots$ etc as free states. Note that by Boltzman suppression, one expects the σ to be the most relevant.

Finally we also study the pseudoscalar susceptibility, which is another way to analyze chiral symmetry restoration by means of the degeneration of chiral partners.

Section 2.3.3 corresponds to results that we have already published, but, in addition, in Sections 2.3.4 and 2.3.5, we present further results that are not published yet, although part of them have already been made public as a preprint.

In the publication of Section 2.3.3, we analyze the properties of four-quark condensates and the scalar susceptibility in the meson sector using ChPT at T=0. As we have explained above, these results will be needed later, since the $T \neq 0$ calculations are very similar.

The main results obtained in this work are the following:

- We check in first place that the four-quark condensate can be expressed as the square of the two-quark condensate at leading (LO) and next to leading order (NLO), i.e. the factorization hypothesis holds.
- However, at next to next to leading order (NNLO), a term with a nontrivial spacetime dependence in the four-quark correlator yields a divergent four-quark condensate, whereas the $\bar{q}q$ condensate is finite. Despite the analysis of four-quark condensates was not the original object of study, this result is relevant by itself since it spoils the factorization hypothesis.
- We have checked that these factorization breaking terms are precisely those needed to provide finite and scale-independent scalar susceptibilities, for the light and strange sector, including the light-strange mixed one.
- However, we have also seen that the non-factorization terms vanish only in the chiral limit and that factorization holds formally in the $N_c \to \infty$ limit to any order in the chiral expansion.

In Section 2.3.4, we study the role of the $f_0(500)$ in chiral symmetry restorations, exploring additionally the properties of quark condensates and susceptibilities of the meson gas at low temperatures within ChPT. Thus, in this work we extend the previous analysis of publication 2.3.3 at finite temperature. We also use the virial approach to study chiral symmetry restoration, both using non-unitarized and unitarized interactions. The latter allow us to isolate the effect of the $f_0(500)$ resonance in the phase transition. The main results obtained in this section are:

- We first show that, as in the T=0 case studied in publication 2.3.3, the factorization hypothesis fails to NNLO in ChPT at finite temperature, preventing the use of four-quark condensates as order parameters since the factorization breaking terms diverge. Nevertheless, as it happened at $T = 0$, factorization holds at all orders formally in the large N_c limit.

- In the chiral limit, and contrary to the zero temperature case, for $T \neq 0$ the factorization breaking terms are finite and do not vanish. Thus, the chiral limit is the only case for which the four-quark condensate can be considered an order parameter. Actually, we have checked that it follows the same temperature melting behaviour as the two-quark condensate for the temperatures where ChPT is reliable. Note that chiral symmetry restoration takes place formally only in the chiral limit.

- We obtain next the scalar susceptibility within ChPT at finite temperature, obtaining a model independent result for its thermal behaviour at low temperatures. In its derivation, we also obtain the $SU(3)$ thermal quark condensates in ChPT including all the relevant meson interactions, thus extending to higher orders previous calculations of the condensate, which only considered free kaons and etas [196]. This allows for a model independent study of the relative size of such interactions at low temperatures.

- Next, we perform a detailed analysis of the scalar susceptibilities in the virial approach, with standard ChPT amplitudes, extending previous works in the literature and serving as a test of the robustness of the ChPT results, which together with their model independence makes them a useful prediction for temperatures well below the transition. Actually, within this regime, we already find that, for the pressure, the quark condensates and the scalar susceptibilities, a huge cancellation occurs between the $I = 0$ and $I = 2$ scalar channels.

- Furthermore, through the analysis of the unitarized interactions in the virial expansion, we have found that the effect of the $f_0(500)$ resonance is largely canceled with the $I = 2$ $J = 0$ partial wave contribution, leaving the $\rho(770)$ as the main contribution, which, nevertheless, is suppressed at low energies due to its angular momentum. As a consequence at very low energies, the interaction part of the virial coefficient is much smaller than naively expected from the size the individual scalar waves. This result is very relevant for those naive resonance hadron gas models where the σ is included as a free state, but the $I = 2$, $J = 0$ $\pi\pi$ interaction is ignored.

Finally, in Section 2.3.5 following similar methods in terms of four-quark correlators, we calculate the pseudoscalar susceptibility in ChPT at finite T to next to leading order. We will find that it scales as the quark condensate, as expected from general arguments, which implies chiral restoration via current degeneration. Notice that the light scalar susceptibility is roughly related to the inverse of the σ mass squared, since this is the state saturating the correlator, whereas the pseudoscalar one is dominated by the pion pole and hence is much better determined within ChPT, which describes correctly the pion dynamics at low energies and temperatures.

2.3.3 Publication: A. Gomez Nicola, J.R. Pelaez, J. Ruiz de Elvira *Non-factorization of four-quark condensates at low energies within Chiral Perturbation Theory, Phys. Rev.* D82 (2010) 074012

PHYSICAL REVIEW D **82,** 074012 (2010)

Nonfactorization of four-quark condensates at low energies within chiral perturbation theory

A. Gómez Nicola,* J. R. Peláez,† and J. Ruiz de Elvira‡

Departamento de Física Teórica II, Universidad Complutense, 28040 Madrid, Spain

(Received 24 May 2010; published 14 October 2010)

Four-quark correlators and the factorization hypothesis are analyzed in the meson sector within chiral perturbation theory. We define the four-quark condensate as $\lim_{x\to 0}\langle T(\bar{q}q)(x)(\bar{q}q)(0)\rangle$, which is equivalent to other definitions commonly used in the literature. Factorization of the four-quark condensate holds to leading and next to leading order. However, at next to next to leading order, a term with a nontrivial space-time dependence in the four-quark correlator yields a divergent four-quark condensate, whereas the two-quark condensate and the scalar susceptibility are finite. Such a nonfactorization term vanishes only in the chiral limit. We also comment on how factorization still holds in the large N_c limit, provided such a limit is taken before renormalization.

DOI: 10.1103/PhysRevD.82.074012 PACS numbers: 12.39.Fe, 11.15.Pg, 11.30.Rd

I. INTRODUCTION

Scalar condensates play a relevant role in QCD, since they are directly related to vacuum properties. The quark condensate $\langle\bar{q}q\rangle$ is a parameter deeply related to spontaneous chiral symmetry breaking and the description of low-energy QCD. In principle, quark condensates of arbitrary order $\langle(\bar{q}q)^n\rangle$ are also built out of chiral noninvariant operators with vacuum quantum numbers and are also related to chiral symmetry restoration. In addition, quark condensates appear directly in QCD sum rules, through the operator product expansion (OPE) approach [1], where the following hypothesis of factorization or vacuum saturation is customarily made:

$$\langle(\bar{q}q)^2\rangle = \left(1-\frac{1}{N}\right)\langle\bar{q}q\rangle^2. \tag{1}$$

Note that we have particularized to the case where the four-quark operator has the quantum numbers of the scalar, isoscalar, and colorless condensates that we are interested in. In addition, $N = 4N_cN_f$, where N_c and N_f denote the number of colors and flavors, respectively, and q is a Dirac spinor, flavor, and color vector. We remark that in the large-N_c limit factorization simply reduces to $\langle(\bar{q}q)^2\rangle = \langle\bar{q}q\rangle^2$. The second term in Eq. (1) comes from the contraction of indices (including color) between the first and second $\bar{q}q$ operators.

The use of the factorization hypothesis is a key point in order to estimate the size of higher order condensates in the OPE. However, its justification is still a matter of debate. It was shown in [2] that factorization implies that $\langle(\bar{q}q)^2\rangle$ becomes dependent on the QCD renormalization scale. This means that for QCD sum rules including six-dimensional operators, like $(\bar{q}q)^2$, one cannot write a renormalization-group (RG) invariant four-quark condensate, preventing RG improvements of such sum rules. This is not a problem when considering six-dimensional pure-gluon operators or quark operators with dimensions lower than six, like the RG-invariant $\bar{q}\mathcal{M}q$ with $\mathcal{M}$ the mass matrix. We will come back to this point in Sec. IV. The validity of vacuum saturation has also been questioned within the framework of finite-energy sum rules [3] and has been formally shown not to hold when dressed QCD vertices are considered [4].

In this work we will present a study of the scalar four-quark condensate within the framework of chiral perturbation theory (ChPT). Since ChPT relies only on symmetries and not on vacuum saturation or dominance assumptions, as in some of the approaches commented above, it will allow us to obtain low-energy model-independent results concerning the factorization hypothesis.

An important point concerns the definition of the quark condensate in terms of Green functions. In the chiral Lagrangian framework, one has access not to individual quark operators at a given space-time point x, but to the low-energy representation of the quark-antiquark operator $\bar{q}q(x)$, given by a functional derivative with respect to an external scalar source (see details in Sec. II). Therefore, a natural way to define the four-quark condensate is through the limit of the two-point function (four-quark correlator):

$$\langle(\bar{q}q)^2\rangle = \lim_{x\to 0}\langle T(\bar{q}q)(x)(\bar{q}q)(0)\rangle. \tag{2}$$

This is the definition that we will choose to work with here, where all the divergencies will be treated within the $\overline{\text{MS}}$ scheme in dimensional regularization, as it is customary in ChPT. However, from the comments above, it is not clear that the four-quark condensate itself has to be a scale-independent and finite object, which means that the $x \to 0$ limit is ill defined and other definitions in terms of Green functions could give different answers. Actually, Eq. (2) is not the usual $\overline{\text{MS}}$ definition when working, for instance, with four-quark vacuum expectation values in the

*gomez@fis.ucm.es
†jrpelaez@fis.ucm.es
‡jacobore@rect.ucm.es

context of electroweak penguin contributions [5,6], where the following prescription is used instead:

$$\langle(\bar{q}q)^2\rangle = \int d^D x \langle T(\bar{q}q)(x)(\bar{q}q)(0)\rangle \delta^{(D)}(x) = \int \frac{d^D Q}{(2\pi)^D} \Pi(Q^2), \quad (3)$$

where the integrals are defined in *Euclidean* space-time dimension D and $\Pi(Q^2)$ is the Fourier transform of the correlator $\langle T(\bar{q}q)(x)(\bar{q}q)(0)\rangle$. In the ChPT framework, we will show (details are given in Appendix B) that this definition gives the same result as that obtained when using the definition in Eq. (2), meaning that factorization is spoiled at next to next to leading order (NNLO), which questions seriously the validity of the factorization hypothesis, now from the point of view of the low-energy representation.

The four-quark two-point correlator, apart from defining the four-quark condensate, is also related to the chiral or scalar susceptibility, defined as $\chi = -\partial\langle\bar{q}q\rangle/\partial m_q$, which can be written also in terms of $\langle T(\bar{q}q)(x)(\bar{q}q)(0)\rangle$. The susceptibility is a crucial observable regarding chiral symmetry restoration, since it is associated with thermal fluctuations and tends to grow near the critical point [7]. For us, the susceptibility will serve as a crucial consistency check, since we can calculate it directly as a quark mass derivative or through the four-quark correlator, and both should coincide and be finite and scale independent.

Therefore, we will give the complete results in ChPT for the four-quark correlators and four-quark condensates in SU(2) and SU(3) up to NNLO, performing a consistency check by calculating the scalar susceptibility and showing the robustness of the result under different definitions of the vacuum four-quark expectation value. In addition, the discussion of factorization breaking necessarily implies the calculation and renormalization of the two-quark condensate also at NNLO, which we will perform explicitly here. We will also carry out the large-N_c analysis of the factorization breaking, which can also be performed from the low-energy representation and is formally relevant. These are the main results of this work.

The plan of the paper is the following: In Sec. II we present our calculation of the relevant four-quark correlators for two and three flavors. The details of the calculation are given for $N_f = 2$, for simplicity. The scalar susceptibility derived from the four-quark condensate is obtained in Sec. III. The factorization hypothesis is then examined in Sec. IV, whereas in Sec. V we discuss the large-N_c limit of our results, regarding factorization. In Sec. VI we present a brief summary and our conclusions. Finally, in Appendix A we provide the detailed mathematical expressions for the two-quark condensates to NNLO in ChPT and discuss in detail their renormalization, whereas in Appendix B we show the equivalence of our definition of the four-quark condensate with the usual one in the literature.

II. FOUR-QUARK CORRELATORS

Our main object of study will be the time-ordered four-quark correlator $\langle T(\bar{q}q)(x)(\bar{q}q)(0)\rangle$. We will follow the external source method and write this four-quark correlator as a second functional derivative of the QCD generating functional $Z_{\rm QCD}[s]$ with respect to the scalar source $s(x)$, which, in general, will be a matrix-valued function in flavor space and couples to the QCD Lagrangian as

$$Z_{\rm QCD}[s] = \int \mathcal{D}\bar{q}\mathcal{D}q \ldots \exp i \int d^4x \mathcal{L}_{\rm QCD}[\bar{q}, q, s(x), \ldots],$$
$$\mathcal{L}_{\rm QCD}[s] = \bar{q}(i\not{\partial} - s(x))q + \ldots, \quad (4)$$

where the rest of the Lagrangian terms and other fields, which are indicated by dots, are irrelevant for our purposes. A sum over N_f light flavors, N_c colors, and Dirac indices is assumed in $\bar{q}q$. The physical QCD Lagrangian and partition function correspond to setting $s(x) = \mathcal{M}$, the quark mass matrix, in the above equation.

We will consider the effective low-energy representation of $Z_{\rm QCD}[s]$ given by chiral perturbation theory [8], built from chiral symmetry invariance as an expansion in external momenta (derivatives) and meson masses:

$$Z_{\rm QCD}[s] \simeq Z_{\rm eff}[s] = \int \mathcal{D}\phi^a \exp i \int d^4x \mathcal{L}_{\rm eff}[\phi^a, s(x)],$$
$$\mathcal{L}_{\rm eff} = \mathcal{L}_2 + \mathcal{L}_4 + \mathcal{L}_6 \ldots, \quad (5)$$

where the subscript in the effective Lagrangian indicates the order in the derivative and mass expansion, formally $\mathcal{L}_k = \mathcal{O}(p^k)$ [$s = \mathcal{O}(p^2)$ in the standard ChPT power counting]. Note that ϕ^a denote the Nambu-Goldstone boson (NGB) fields, usually collected in the SU(N_f) matrix $U = \exp[i\lambda_a\phi^a/F]$, where λ_a are the Gell-Mann or Pauli matrices for $N_f = 3$ and $N_f = 2$, respectively, and F is the pion decay constant in the chiral limit. The Lagrangian $\mathcal{L}_2$ is the nonlinear sigma model:

$$\mathcal{L}_2 = \frac{F^2}{4} \mathrm{Tr}[\partial_\mu U^\dagger \partial^\mu U + \chi(U + U^\dagger)], \quad (6)$$

with $\chi = 2B_0 s(x)$. When $s(x) = \mathcal{M}$, the constants m_q, F, B_0 appearing in $\mathcal{L}_2$ are related to meson masses, decay constants, and the quark condensate. For simplicity, we will work in the isospin limit $m_u = m_d \equiv m$, so that, to lowest order in SU(2), $M_{0\pi}^2 = 2mB_0(1 + \mathcal{O}(p^2))$, $F_\pi = F(1 + \mathcal{O}(p^2))$, and $\langle\bar{q}q\rangle = B_0F(1 + \mathcal{O}(p^2))$. As usual, $M_{0\pi,0K,0\eta}$ stand for the leading order meson masses, in terms of which we will express our results. Their relation to the physical masses is given in Eqs. (A9) and (A10) in Appendix A. In addition, and for our purposes here, Weinberg's chiral power counting [9], on which chiral perturbation theory relies, can be equivalently accounted

for by keeping trace of inverse powers of F, which will be used extensively in this work.

The Lagrangians $\mathcal{L}_4$ and $\mathcal{L}_6$ are given in [8,10], respectively, where use has been made of different operator identities, partial integration, and the equations of motion to the relevant order. Those Lagrangians contain the so-called low-energy constants (LEC), multiplying each of the independent terms compatible with the symmetries. The $\mathcal{L}_4$ LEC receive different names depending on whether they multiply terms containing U fields or not, respectively, L_i and H_i in the SU(3) case. The terms without U fields are contact terms containing just external sources and no fields, but they are needed to absorb some divergences coming from loop diagrams using $\mathcal{L}_2$ vertices. The original SU(2) Lagrangians in [11] are written in terms of vector fields instead of matrix fields U as above, but they also use different names for the $\mathcal{L}_4$ low-energy constants—l_i and h_i in this case. However, it is possible to recast [12] these Lagrangians using matrix field notation, which we will use throughout this paper, and keep the same l_i, h_i low-energy constants. The relation between the SU(3) and SU(2) low-energy constants is given in [8,13,14].

This name differentiation for the $\mathcal{L}_6$ is not followed any longer [10]: All of them are called c_i in the SU(2) case and C_i in the SU(3) case. Note that the $\mathcal{O}(p^6)$ LEC contained in $\mathcal{L}_6$ absorb both two-loop divergences from $\mathcal{L}_2$ and one-loop divergences in diagrams with $\mathcal{L}_4$ vertices. All the details for renormalization of quark condensates up to the order we are considering here are given in Appendix A. We recall that the $\mathcal{L}_4$ Lagrangian in SU(3) also contains the Wess-Zumino-Witten (WZW) [15] anomalous term, accounting for anomalous NGB processes, whose coefficient is fixed by topology arguments and is proportional to the number of colors N_c.

A. Two flavors

For simplicity, we will discuss the full details of our approach in the simpler case $N_f = 2$. Thus we will denote by the subscript l the light quark correlator, and study $(\bar{q}q)_l \equiv \bar{u}u + \bar{d}d$. Note that we have defined the scalar source $s(x)$ as a matrix, but since for the physical partition function it corresponds to the mass matrix $\mathcal{M}$, which is diagonal, we are thus only interested in the diagonal elements of $s(x)$ and we can set the rest of the source terms to zero. In particular, for the two flavor case $\mathcal{M} = m\mathbb{1}_2$, and we can write $s(x) = s_0(x)\mathbb{1}_2$, so that

$$\langle \bar{q}q\rangle_l \equiv \frac{i}{Z_{\rm QCD}[m]}\frac{\delta Z_{\rm QCD}[s_0]}{\delta s_0(x)}\bigg|_{s_0=m} \simeq \frac{i}{Z_{\rm eff}[m]}\frac{\delta Z_{\rm eff}[s_0]}{\delta s_0(x)}\bigg|_{s_0=m} \equiv -\left\langle \frac{\delta \mathcal{L}_{\rm eff}[s_0]}{\delta s_0(x)}\right\rangle_{s_0=m}. \tag{7}$$

Following the same procedure, but now for the four light quark correlator, we get

$$\begin{aligned}\langle T(\bar{q}q)_l(x)(\bar{q}q)_l(0)\rangle &= -\frac{1}{Z_{\rm eff}[m]}\frac{\delta}{\delta s_0(x)}\frac{\delta}{\delta s_0(0)}Z_{\rm eff}[s_0]|_{s_0=m}\\ &= -i\left\langle T\frac{\delta^2\mathcal{L}_{\rm eff}[s_0(x)]}{\delta s_0(x)^2}\right\rangle_{s_0=m}\delta^{(D)}(x)\\ &\quad+\left\langle T\frac{\delta\mathcal{L}_{\rm eff}[s_0]}{\delta s_0(x)}\frac{\delta\mathcal{L}_{\rm eff}[s_0]}{\delta s_0(0)}\right\rangle_{s_0=m}.\end{aligned} \tag{8}$$

We will regularize all our expressions in dimensional regularization with $D = 4 - \epsilon$, and for that purpose, we keep the D dependence in the δ-function term above.

Now, from Eq. (8), and using the Lagrangians in [8,10], we obtain the following result:

$$\langle T(\bar{q}q)_l(x)(\bar{q}q)_l(0)\rangle_{\rm NLO} = 4B_0^2F^4\left\{1+\frac{4M_{0\pi}^2}{F^2}(l_3^r+h_1^r)-6\mu_\pi\right\}, \tag{9}$$

$$\begin{aligned}\langle T(\bar{q}q)_l(x)(\bar{q}q)_l(0)\rangle_{\rm NNLO} &= \langle T(\bar{q}q)_l(x)(\bar{q}q)_l(0)\rangle_{\rm NLO}\\ &+4B_0^2F^4\left[\frac{2M_{0\pi}^2}{F^2}(l_3^r+h_1^r)-3\mu_\pi\right]^2\\ &+8B_0^2F^4\left[-\frac{3}{2}\mu_\pi^2-\frac{3M_{0\pi}^2}{F^2}(\mu_\pi\nu_\pi+4l_3^r\mu_\pi)\right.\\ &\left.+\frac{3M_{0\pi}^4}{8F^4}(-16l_3^r\nu_\pi+\hat{c}_1^r)\right],\\ &+B_0^2[-8i(l_3+h_1)\delta^{(D)}(x)+K^{(2)}(x)],\end{aligned} \tag{10}$$

where the NNLO constants $\hat{c}_i$ are defined in Eq. (A3) and, as usual [8],

$$\begin{aligned}\mu_\pi &= \frac{M_{0\pi}^2}{32\pi^2F^2}\log\frac{M_{0\pi}^2}{\mu^2},\\ \nu_\pi &= F^2\frac{\partial\mu_{0\pi}}{\partial M_{0\pi}^2} = \frac{1}{32\pi^2}\left(1+\log\frac{M_{0\pi}^2}{\mu^2}\right).\end{aligned} \tag{11}$$

Note that we have defined $K^{(2)}(x)$ as the connected part of the four-pion correlator to leading order:

$$\begin{aligned}K^{(2)}(x) &= \langle T\phi^a(x)\phi_a(x)\phi^b(0)\phi_b(0)\rangle_{\rm LO}\\ &\quad-\langle T\phi^a(0)\phi_a(0)\rangle_{\rm LO}^2\\ &= 6G_\pi^2(x),\end{aligned} \tag{12}$$

$G_\pi(x)$ being the pion propagator to leading order, and the factor of $6 = 2(N_f^2 - 1)$ comes from the Wick contractions and is nothing but twice the number of NGB fields. The details of the renormalization and the dependence of the constants l_i^r, h_i^r, and $\hat{c}_i^r$ on the renormalization scale μ are given in Appendix A.

To understand the structure of the different contributions to Eqs. (9) and (10) it is useful to recall the general form of the SU(2) low-energy Lagrangian terms depending on the external scalar source. For our NNLO calculation, we will need to keep terms up to $\mathcal{O}(F^{-2})$. Let us then separate the terms in the Lagrangian [8,10], according to their s dependence after expanding the U in NGB fields:

$$\mathcal{L}_{\rm eff}[s_0] = \left(\mathcal{L}_2^{0\phi}F^2 + \mathcal{L}_2^{2\phi} + \frac{1}{F^2}\mathcal{L}_2^{4\phi} + \frac{1}{F^2}\mathcal{L}_4^{2\partial\phi}\right)s_0 + \left(\mathcal{L}_4^{0\phi} + \frac{1}{F^2}\mathcal{L}_4^{2\phi}\right)s_0^2 + \frac{1}{F^2}\mathcal{L}_6^{0\phi}s_0^3 + \frac{1}{F^2}\tilde{\mathcal{L}}_6^{0\phi}\partial_\mu s_0\partial^\mu s_0 + \mathcal{O}\left(\frac{1}{F^4}\right), \quad (13)$$

where we have also made explicit the leading $1/F^2$ dependence of each term. The superscripts "$n\phi$" indicate the number of NGB fields or field derivatives on each Lagrangian contribution. Note that, since $\mathcal{L}_k = \mathcal{O}(p^k)$ in derivatives or s powers [$s = \mathcal{O}(p^2)$], it counts at least as $\mathcal{O}(1/F^{k-4})$, but the $1/F^2$ order of each term grows when increasing the number of NGB fields, ϕ. We have represented the vertices arising from the different pieces of the Lagrangian above in the left column of Fig. 1. Note that all $\mathcal{L}_6$ terms in Eq. (13) have the 0ϕ superscript, because, to this order, they are simply constants. The constant $\mathcal{L}_6^{0\phi}$ term enters in $\langle\bar{q}q\rangle^2_{l,\rm NNLO}$ and ensures that one can renormalize the full result so that the quark condensate is finite and scale independent. The term containing $(\partial s_0)^2$ does not contribute to this order. The details as well as the explicit expression of the condensates up to NNLO are given in Appendix A.

Once the structure of the vertices arising from the Lagrangian equation (13) are understood, we represent diagrammatically in Fig. 1 the different contributions to $\langle T(\bar{q}q)(x)(\bar{q}q)(0)\rangle$. On each diagram, the horizontal dotted line represents space-time, where each quark-antiquark bilinear stands at separate points 0 and x. To LO and NLO—respectively, $\mathcal{O}(F^4)$ and $\mathcal{O}(F^2)$—all contributions are disconnected, as seen in diagrams (a), (b), and (c). The reason is that we can only use the $\mathcal{L}_2^{2\phi}$ term once, and therefore, the NGB line has to close upon itself—a tadpole. This gives diagram (b) in Fig. 1. To NNLO [$\mathcal{O}(F^0)$] we have all the possibilities shown in Fig. 1 in diagrams (d)–(j). If one of the vertices comes from $\mathcal{L}_4$ or $\mathcal{L}_6$, once more there is at most one NGB line and the resulting diagram is disconnected. Note that among these is the $\delta^{(D)}(x)$ term in Eq. (10) from diagram (h). With only $\mathcal{L}_2$ vertices, one has a diagram with a double tadpole in one of the vertices, leading to a LO propagator squared at the same point [diagram (d)], two vertices with one tadpole

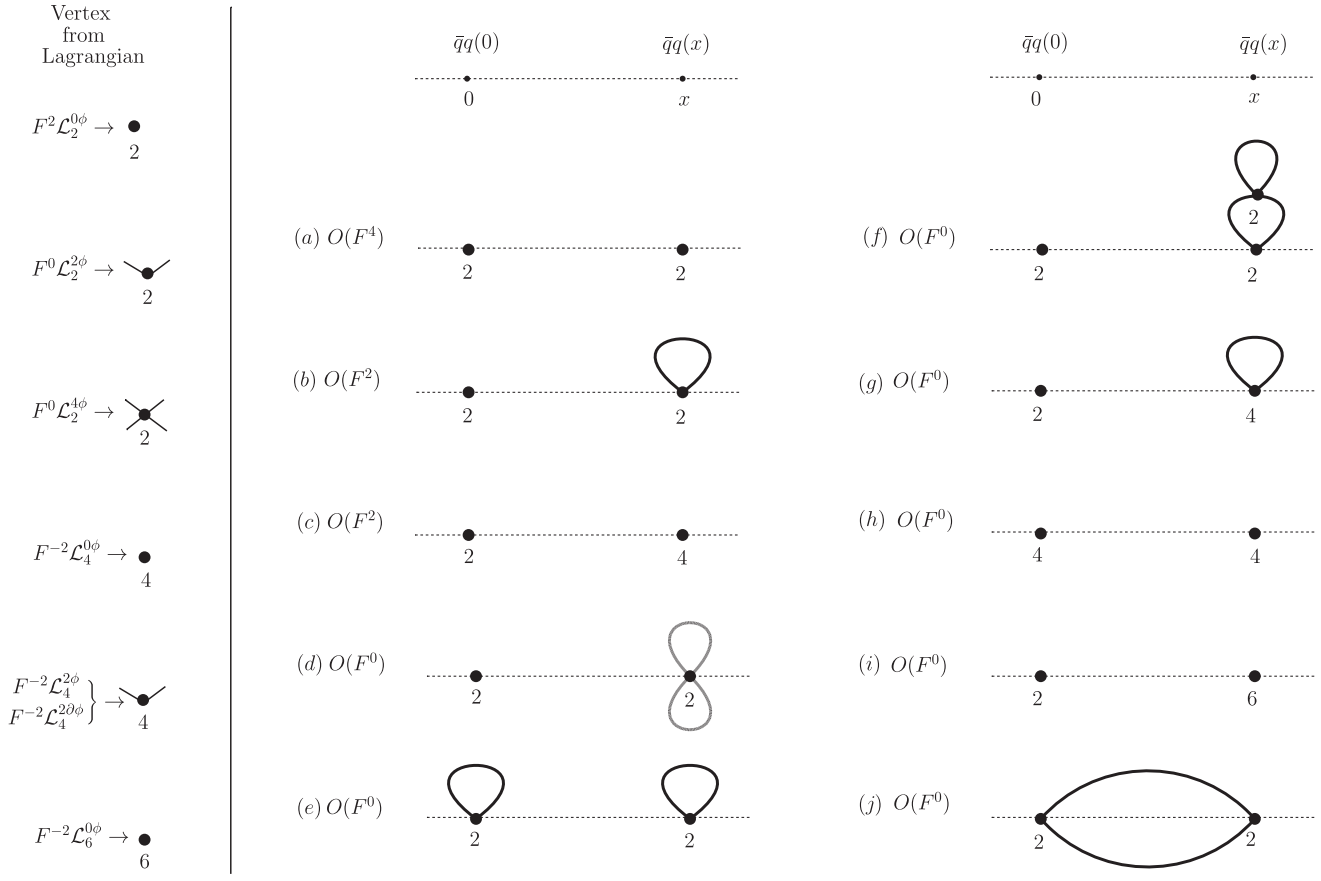

FIG. 1. In the left column we provide the diagrammatic representation of the vertices coming from the different terms of the Lagrangian in Eq. (13). The numbers attached to each vertex indicate the order of the Lagrangian. Diagrams (a) to (j) represent the different contributions to the four-quark correlator. The dotted horizontal line represents the space-time separation between 0 and x. Note that each NGB line decreases the order of the diagram by $1/F^2$. Diagram (j) is the first factorization-breaking term.

each [diagram (e)], a diagram like (b) but with the propagator renormalized to next to leading order (NLO) [diagram (f)], and another with two NGB lines on each vertex but joined to form a connected one-loop diagram, which is diagram (j). Actually, the latter is the only possible connected contribution to this order, and gives the $G^2(x)$ term in Eq. (12). This whole discussion of vertices and diagrams will be valid also for the SU(3) case discussed below.

Let us now turn to the factorization hypothesis and the relation between the four-quark correlation function and the two-quark condensate. We have collected in Appendix A all the two-quark condensate ChPT expressions up to NLO [given also in [11] for SU(2) and in [8] for SU(3)] and up to NNLO, which have been given explicitly in [16] for SU(3). Numerical estimations including NNLO corrections are given in [16,17]. In view of Eqs. (7), (A11), and (A12), it is easy to check that

$$\begin{aligned}\langle T(\bar{q}q)_l(x)(\bar{q}q)_l(0)\rangle_{\rm NLO} &= (\langle\bar{q}q\rangle_l^2)_{\rm NLO},\\ \langle T(\bar{q}q)_l(x)(\bar{q}q)_l(0)\rangle_{\rm NNLO} &= (\langle\bar{q}q\rangle_l^2)_{\rm NNLO}\\ &\quad + B_0^2[-8i(l_3+h_1)\delta^{(D)}(x) + K^{(2)}(x)].\end{aligned} \tag{14}$$

We see that all contributions from disconnected diagrams in Fig. 1, other than the $\delta^{(D)}$ term, can be absorbed in the two-quark condensate. Actually, up to NLO, we observe that $\langle T(\bar{q}q)_l(x)(\bar{q}q)_l(0)\rangle$ in Eq. (9) is constant and equal to the NLO of the quark condensate squared, which leads to factorization in the $N_c\to\infty$ limit (see Secs. IV and V). However, to NNLO the previous expression for $x=0$ contains the $G^2(0)$ divergent contribution, even after the quark condensate has been renormalized and the $\delta^{(D)}$ term regularized. We will show below that divergences cancel in physical quantities such as the scalar susceptibility, which is directly expressed in terms of observable quantities such as the free energy density. That is not the case for the four-quark condensate, which will remain divergent. Before analyzing these issues, let us extend the previous analysis to the SU(3) case.

B. Three flavors

In the SU(3) case, $\bar{q}q\equiv\bar{u}u+\bar{d}d+\bar{s}s$, $\mathcal{M}=\mathrm{diag}(m,m,m_s)$, $s(x)=\mathrm{diag}[s_0(x),s_0(x),s_s(x)]$, and

$$\langle\bar{q}q\rangle = -\left\langle\frac{\delta\mathcal{L}_{\rm eff}[s_0]}{\delta s_0(x)}+\frac{\delta\mathcal{L}_{\rm eff}[s_0,s_s]}{\delta s_s(x)}\right\rangle_{s=\mathcal{M}}, \tag{15}$$

$$\begin{aligned}&\langle T(\bar{q}q)(x)(\bar{q}q)(0)\rangle\\ &= -i\left\langle T\left(\frac{\delta}{\delta s_0(x)}+\frac{\delta}{\delta s_s(x)}\right)^2\mathcal{L}_{\rm eff}[s_0(x),s_s(x)]\right\rangle_{s=\mathcal{M}}\delta^{(D)}(x)\\ &\quad+\left\langle\left(\frac{\delta\mathcal{L}_{\rm eff}[s_0,s_s]}{\delta s_0(x)}+\frac{\delta\mathcal{L}_{\rm eff}[s_0,s_s]}{\delta s_s(x)}\right)\right.\\ &\quad\left.\times\left(\frac{\delta\mathcal{L}_{\rm eff}[s_0,s_s]}{\delta s_0(0)}+\frac{\delta\mathcal{L}_{\rm eff}[s_0,s_s]}{\delta s_s(0)}\right)\right\rangle_{s=\mathcal{M}}.\end{aligned} \tag{16}$$

The s-dependent terms in the SU(3) effective Lagrangian are now the generalization of Eq. (13) to include $s_s(x)$, so that we have crossed terms like s_0s_s, $s_0^2s_s$, and so on, but the general structure is the same. As in the SU(2) case, the derivative terms $(\partial s)^2$ do not contribute to $\langle T(\bar{q}q)(x)\times(\bar{q}q)(0)\rangle$, and thus only four $\mathcal{L}_6$ constant terms contribute to renormalization. As seen in Appendix A, they are proportional to the $\hat{C}_i$ LEC given in Eq. (A3). Since we already presented the detailed discussion for the SU(2) case in the previous section, for the sake of brevity we cast our SU(3) results for $\langle T(\bar{q}q)(x)(\bar{q}q)(0)\rangle$, which are much longer than before, directly in terms of the two-quark condensates, namely,

$$\begin{aligned}\langle T(\bar{q}q)(x)(\bar{q}q)(0)\rangle_{\rm NLO} &= (\langle\bar{q}q\rangle^2)_{\rm NLO},\\ \langle T(\bar{q}q)(x)(\bar{q}q)(0)\rangle_{\rm NNLO} &= (\langle\bar{q}q\rangle^2)_{\rm NNLO}\\ &\quad + B_0^2[-24i(12L_6+2L_8+H_2)\delta^{(D)}(x)+K(x)],\end{aligned} \tag{17}$$

where $K(x)$ is the extension of Eq. (12) to the SU(3) case:

$$\begin{aligned}K(x) &= \langle T\phi^a(x)\phi_a(x)\phi^b(0)\phi_b(0)\rangle_{\rm LO} - \langle T\phi^a(0)\phi_a(0)\rangle_{\rm LO}^2\\ &= 2[3G_\pi^2(x)+4G_K^2(x)+G_\eta^2(x)].\end{aligned} \tag{18}$$

The ChPT expressions for the four-quark condensates to NNLO given in Eqs. (14) and (17) (simplified in terms of the explicit expressions for $\langle\bar{q}q\rangle_{\rm NNLO}$, which are given in Appendix A) are among the main results of the present work.

Note that, as it happened in the SU(2) case, the contribution Eq. (18) stems from $2(N_f^2-1)$ NGB propagators, although this time they have different masses. Similarly, we can calculate separately the strange and nonstrange four-quark condensates, which also factorize up to NLO, whereas to NNLO we get

$$\begin{aligned}&\langle T(\bar{q}q)_l(x)(\bar{q}q)_l(0)\rangle\\ &= \langle\bar{q}q\rangle_{l,\mathrm{SU(3)}}^2 + B_0^2\left[-16i(8L_6+2L_8+H_2)\delta^{(D)}(x)\right.\\ &\quad\left.+6G_\pi^2(x)+2G_K^2(x)+\frac{2}{9}G_\eta^2(x)\right]+\mathcal{O}\left(\frac{1}{F^2}\right),\end{aligned} \tag{19}$$

$$\begin{aligned}&\langle T(\bar{s}s)(x)(\bar{s}s)(0)\rangle\\ &= \langle\bar{s}s\rangle^2 + B_0^2\left[-8i(4L_6+2L_8+H_2)\delta^{(D)}(x)\right.\\ &\quad\left.+2G_K^2(x)+\frac{8}{9}G_\eta^2(x)\right]+\mathcal{O}\left(\frac{1}{F^2}\right).\end{aligned} \tag{20}$$

Once again the explicit expressions for the renormalized $\langle\bar{q}q\rangle_{\rm NNLO}$ are given in Appendix A.

The $\langle T(\bar{q}q)(x)(\bar{s}s)(0)\rangle$ correlator has been calculated up to NNLO in [18,19] in terms of the basis of the solutions to the Muskhelishvili-Omnès equations.

We remark that the four-quark correlators to NNLO given in Eqs. (14) and (17) are key ingredients to define

the four-quark condensate and study the factorization hypothesis, as explained in the Introduction.

III. THE SCALAR SUSCEPTIBILITY

In this section we will provide a consistency check of our calculation by analyzing the chiral or scalar susceptibility to the first nontrivial order, which can be obtained either by differentiating the two-quark condensates or by integration of the four-quark ones. The susceptibility is defined in Euclidean space-time as

$$\chi_l \equiv -\frac{\partial}{\partial m}\langle \bar{q}q\rangle_l \tag{21}$$

and measures the condensate thermal fluctuations, growing dramatically near the chiral restoration, as confirmed by different lattice studies [7]. Therefore, let us consider the Euclidean (imaginary time $t = -i\tau$) version of Eqs. (4) and (5), replacing $i\int d^4x \to \int d\tau \int d^3\vec{x} \equiv \int_E d^4x$ and the $(-,-,-,-)$ metric in the Lagrangian. Recall that the finite temperature T case, which we will analyze elsewhere [20], would correspond to $\tau \in [0, \beta]$ with $\beta = 1/T$. In addition, in Eqs. (8) and (16) we have to replace $-i\delta^D(x) \to \delta(\tau)\delta^{(D-1)}(\vec{x}) \equiv \delta_E^D(x)$. With these replacements, we can now relate the susceptibility with the four-quark correlators in the nonstrange sector:

$$\begin{aligned}\chi_l &= \frac{1}{V_E}\frac{\partial^2}{\partial m^2}\log Z = \frac{1}{V_E}\left[\frac{1}{Z}\frac{\partial^2 Z}{\partial m^2} - \left(\frac{1}{Z}\frac{\partial Z}{\partial m}\right)^2\right] \\ &= \int_E d^Dx[\langle T(\bar{q}q)_l(x)(\bar{q}q)_l(0)\rangle - \langle \bar{q}q\rangle_l^2],\end{aligned} \tag{22}$$

where $V_E = \int_E d^Dx$ is the D-dimensional Euclidean volume and $Z = Z[s = \mathcal{M}] = e^{-zV_E}$ is the partition function, with z the free energy density.

The relation in Eq. (22) between χ_l and the four-point function allows us to check our previous results. From Eqs. (14) and (19), taking into account that

$$\int_E d^Dx[G_i(x)]^2 = -\frac{d}{dM_i^2}G_i(0), \tag{23}$$

and the expressions Eqs. (A1) and (A2), together with the renormalization of the LEC in Eqs. (A5) and (A6), we obtain, using the last integral in Eq. (22),

$$\chi_l^{\mathrm{SU}(2)} = B_0^2[8(l_3^r(\mu) + h_1^r(\mu)) - 12\nu_\pi] + \mathcal{O}\left(\frac{1}{F^2}\right), \tag{24}$$

$$\begin{aligned}\chi_l^{\mathrm{SU}(3)} = B_0^2\Big[&16(8L_6^r(\mu) + 2L_8^r(\mu) + H_2^r(\mu)) - 12\nu_\pi \\ &- 4\nu_K - \frac{4}{9}\nu_\eta\Big] + \mathcal{O}\left(\frac{1}{F^2}\right),\end{aligned} \tag{25}$$

with ν_i given in Eq. (A8).

This is the same result that we get by taking directly the mass derivative of the quark condensate to NLO in Eqs. (A11) and (A13) using the leading order relations between meson and quark masses [8]. This represents a check of consistency of our calculation of the four-quark condensates to NNLO. In addition, we have explicitly checked [using Eq. (A5)] that the susceptibilities above are finite and independent of the scale μ. Furthermore, with the conversion between the SU(2) and SU(3) LEC given in [8],

$$\begin{aligned}l_3^r(\mu) + h_1^r(\mu) = 2\Big(&8L_6^r(\mu) + 2L_8^r(\mu) + H_2^r(\mu) \\ &- \frac{1}{4}\nu_K - \frac{1}{36}\nu_\eta\Big),\end{aligned} \tag{26}$$

we end up with

$$\chi_l^{\mathrm{SU}(2)} = \chi_l^{\mathrm{SU}(3)}$$

which is also consistent since the SU(3) susceptibility is given by constant plus logarithmic terms in the $m_s \to \infty$ expansion, with no subleading terms in that expansion; therefore, the very same expression has to be exactly recovered by calculating directly in the SU(2) limit. Note also that the susceptibility to this order is independent of F.

Our result for the susceptibility is also consistent with a previous work [21], where only the leading infrared order in the chiral limit was calculated, namely, the $\log M_{0\pi}^2$ term inside the ν_π in Eq. (24). This is the expected behavior of the susceptibility from the $O(4)$ model universality class near the chiral limit and below the critical temperature, namely, $\chi \sim \log m$, with m the mass of the nonstrange quark [7,21].

We can follow the same procedure to obtain the strange quark susceptibility in terms of our strange four-quark correlation function:

$$\begin{aligned}\chi_s &\equiv -\frac{\partial}{\partial m_s}\langle \bar{s}s\rangle = \frac{1}{V_E}\frac{\partial^2}{\partial m_s^2}\log Z \\ &= \frac{1}{V_E}\left[\frac{1}{Z}\frac{\partial^2 Z}{\partial m_s^2} - \left(\frac{1}{Z}\frac{\partial Z}{\partial m_s}\right)^2\right] \\ &= \int_E d^4x[\langle T(\bar{s}s)(x)(\bar{s}s)(0)\rangle - \langle \bar{s}s\rangle^2],\end{aligned} \tag{27}$$

which, from Eq. (20), gives

$$\chi_s = B_0^2\left[8(4L_6^r + 2L_8^r + H_2^r) - 4\nu_K - \frac{16}{9}\nu_\eta\right]. \tag{28}$$

We have explicitly double checked this result by taking the derivative with respect to m_s of the NLO strange quark condensate in Eq. (A15). We remark that the results in Eqs. (24), (25), and (28) for the ChPT scalar susceptibilities have not been given elsewhere.

IV. NONFACTORIZATION

As explained in the Introduction, we define the four-quark condensate through Eq. (2), although in Appendix B we show that this is equivalent to the more usual definition

of Eq. (3). Therefore, by taking the $x \to 0$ limit in Eqs. (14) and (17), and despite the fact that $\delta^{(D)}(0)$ vanishes identically in dimensional regularization [22] (now we are not integrating over x as for the scalar susceptibility), there is still a term that clearly breaks factorization, as defined in Eq. (1). In particular, we get in SU(2), from Eq. (14),

$$\frac{\langle(\bar{q}q)^2\rangle}{\langle\bar{q}q\rangle^2} = 1 + \frac{6}{F^4}G_\pi^2(0) + \mathcal{O}\left(\frac{1}{F^6}\right), \tag{29}$$

whereas in SU(3) from Eq. (18), we find

$$\frac{\langle(\bar{q}q)^2\rangle}{\langle\bar{q}q\rangle^2} = 1 + \frac{2}{F^4}[3G_\pi^2(0) + 4G_K^2(0) + G_\eta^2(0)] + \mathcal{O}\left(\frac{1}{F^6}\right), \tag{30}$$

where the propagators $G_i(0)$ are given in dimensional regularization in Eq. (A1).

The nonfactorization terms above are divergent and independent of the LEC, once the two-quark condensate $\langle\bar{q}q\rangle$ has been rendered finite with the renormalization of the $\mathcal{O}(p^4)$ and $\mathcal{O}(p^6)$ LEC (see Appendix A). The renormalizability of $\langle\bar{q}q\rangle$ is of course consistent with the fact that $\bar{q}\mathcal{M}q$ is a QCD RG invariant. Therefore, our nonfactorization ChPT results in Eqs. (29) and (30) imply that the four-condensate is divergent, and hence the vacuum expectation value of $(\bar{q}q)^2$ does not admit a meaningful low-energy representation.

Our result is consistent with the one-loop QCD RG analysis in [2], where only one flavor is considered. In that paper it is shown that factorization is incompatible with the renormalization group. Their argument goes as follows: The operator $(\bar{q}q)^2$ mixes under renormalization with other four-quark operators, which can be chosen in combinations such that their vacuum expectation values would vanish if factorization holds. Then, assuming factorization for those other operators leads to the conclusion that $\langle(\bar{q}q)^2\rangle$ is divergent, which, in particular, means that it does not factorize in terms of $\langle\bar{q}q\rangle^2$ and that one cannot write any RG invariant made of four-quark operators.

Another interesting comment is that the factorization-breaking terms in Eqs. (29) and (30) vanish exactly in the chiral limit, since then all dimensionally regularized propagators $G_\pi(0) = G_K(0) = G_\eta(0) = 0$. In that case, we would be forced to examine the neglected NNNLO contributions in order to check the validity of factorization and the finiteness of the four-quark condensate. Recall that the arguments in [2] regarding four-quark operators actually hold for $m = 0$.

V. LARGE N_c

Let us now discuss the N_f and N_c dependence for the regularized expression, namely, before taking the $D = 4$ limit. As we have checked for the SU(2) and SU(3) cases, the $K(x)$ contributions to the connected four-field functions in Eqs. (12) and (18) are $\mathcal{O}(N_{\rm GB}) = \mathcal{O}(N_f^2)$, where $N_{\rm GB} = N_f^2 - 1$ is the number of Goldstone bosons. In addition, the N_c leading behavior of the different ChPT constants is well known [8] from the QCD $1/N_c$ expansion. In particular, $F^2 = \mathcal{O}(N_c)$. Therefore, the first term that breaks factorization in Eqs. (29) and (30) is $\mathcal{O}(N_f^2/N_c^2)$, which is rather different from the $1/(4N_fN_c)$ scaling suggested in Eq. (1). Unfortunately, we cannot say much more about the N_f behavior of higher order terms, which could change the global N_f behavior. Note that the N_f dependence of the quark correlators has been studied in detail in [23] with a different motivation.

In the following, we will easily deduce the $1/N_c$ behavior and, in particular, we can study the large N_c limit before renormalization. We will see that, in such a formal case, factorization holds for $N_c \to \infty$. First of all, contrary to Eq. (1), in Eqs. (29) and (30) there are no $\mathcal{O}(1/N_c)$ terms. These could have arisen from contributions of the type $L_iG(0)/F^4$, when L_i is $\mathcal{O}(N_c)$, that actually appear in the calculation. However, as we have said before, the whole L_i dependence of the four-quark condensate is exactly that of the two-quark condensate squared, and thus such terms do not break factorization. The same happens with the $\mathcal{O}(p^6)$ c_i LEC in Eq. (A3). Still, one could wonder if $\mathcal{O}(1/N_c)$ or larger N_c powers could arise from higher chiral orders that we have not calculated explicitly here.

Of course, as seen in Eqs. (29) and (30), these higher chiral orders count at least as $\mathcal{O}(1/F^6)$. Since $F^2 = \mathcal{O}(N_c)$, this already introduces a $1/N_c^3$ factor, but it is not the only one, since the LEC can carry their own N_c behavior. In particular, we recall that, according to the chiral power counting discussed in Sec. II, the $\mathcal{O}(1/F^n)$ contribution to the ratios in Eqs. (29) and (30) comes from connected diagrams with $n = 2(L+1) + \sum_d N_d(d-2)$, with L the number of loops and N_d the number of vertices from $\mathcal{L}_d = \mathcal{L}_2, \mathcal{L}_4, \ldots$. Note that a nonfactorizing term requires at least $L = 1$, the leading contribution being the connected one-loop diagram (j) in Fig. 1 with two $\mathcal{L}_2$ vertices. This diagram yields the factorization-breaking terms in Eqs. (29) and (30).

Now, the highest N_c scaling of the LEC from $\mathcal{L}_d$ is $\mathcal{O}(N_c^{(d-2)/2})$. The reason is that these LEC, when divided by F^{d-4}, should yield $\mathcal{O}(N_c)$ contributions at most, as expected from the large-N_c behavior of the low-energy generating functional [8]. This includes the WZW term, which is the anomalous part of $\mathcal{L}_4$ and is multiplied explicitly by N_c [15]. Although the WZW term does not depend on the quark mass, it could enter in this calculation through loop contributions. It is possible, of course, that some LEC do scale with a smaller N_c power. For instance, the L_1 to L_{10} appearing in $\mathcal{L}_4$ are known to scale as $\mathcal{O}(N_c)$, except L_4, L_6, and L_7, which scale as $\mathcal{O}(1)$. These are model-independent QCD predictions obtained in [8], with the exception of L_7, which was taken there as $O(N_c^2)$. This L_7 counting corresponds to integrating the η' as a heavy

particle but then considering $m_{\eta'}^2 \sim \mathcal{O}(1/N_c)$ and therefore a light particle. The consistent way of integrating the η' yields $L_7 \simeq \mathcal{O}(1)$ [24]. In summary, the L_i in $\mathcal{L}_4$ are $\mathcal{O}(N_c)$ at most, the c_i in $\mathcal{L}_6$ are $\mathcal{O}(N_c^2)$ at most, and so on.

Hence, if a diagram has N_d vertices from $\mathcal{L}_d$, they contribute, at most, with $N_d(d-2)/2$ powers of N_c. Summing over all the d, the scaling of the LEC that contribute to that diagram is given, at most, by $\sum_d N_d(d-2)/2$ powers of N_c. Taking into account that the $1/F^n$ factors behave as $\mathcal{O}(N_c^{-n/2})$, we conclude that the nonfactorization terms should be $\mathcal{O}(N_c^{\sum_d N_d(d-2)/2-(n/2)}) = \mathcal{O}(N_c^{-(L+1)})$ at most. But since we noted that nonfactorization terms require $L \geq 1$, then the largest factorization-breaking contribution is $\mathcal{O}(N_c^{-2})$, at most. Actually, this is the behavior of the nonfactorization correction we explicitly calculated in Eqs. (29) and (30). This $\mathcal{O}(N_c^{-2})$ counting of the factorization breaking, which we have formally showed here in the low-energy representation, confirms what had been suggested previously in the literature [25].

Finally, if we compare with the original QCD factorization hypothesis Eq. (1), we conclude that factorization of the four-quark condensate as the square of the two-quark condensate holds formally in the $N_c \to \infty$ limit. This is of course only a formal statement, since we have just seen that in the low-energy calculation the factorization-breaking terms diverge.

VI. CONCLUSIONS

In this work we have addressed the issue of the four-quark condensate factorization into the two-quark condensate squared, within the low-energy representation of those condensates provided by chiral perturbation theory.

Our main result is the formal model-independent proof of the nonvalidity of the factorization or vacuum saturation hypothesis for the low-energy sector of QCD. A detailed calculation of the NNLO two-quark and four-quark condensates for both two and three flavors shows that, to that order, factorization is broken by terms which cannot be rendered finite with the usual renormalization procedure, ensuring that the two-quark condensate is finite and scale independent. This breaking of the factorization assumption at low energies is then a model-independent result, since it relies only on the effective Lagrangian formalism, and is consistent with previous observations regarding the incompatibility of the factorization hypothesis with the QCD renormalization-group evolution. In addition, the very same nonfactorization term is obtained by using more conventional definitions of the quark condensate within the $\overline{\text{MS}}$ scheme in dimensional regularization. As a consistency check of our analysis, we have derived the light and strange susceptibilities from the calculated four-quark correlators, showing that they agree with a direct derivative with respect to the quark masses of the two-quark condensates. The explicit renormalized and scale-independent expressions for the ChPT NNLO susceptibilities are not given elsewhere, to our knowledge. Factorization holds formally in the $N_c \to \infty$ limit, as we have been able to show to any order in the chiral expansion, since the leading term that breaks factorization scales as $\mathcal{O}(1/N_c^2)$.

We believe that these results can be useful for workers in the field, in particular, concerning the OPE and sum-rule approach. A natural extension of this work is to consider finite temperature effects to see how they affect factorization and its connection with the chiral susceptibility, which in the thermal case plays a crucial role near chiral restoration [20].

ACKNOWLEDGMENTS

This work was partially supported by Spanish Ministerio de Educación y Ciencia Research Contracts No. FPA2008-00592, No. FIS2006-03438, and No. FIS2008-01323, and by U.Complutense/Banco Santander Grant No. UCM-BSCH GR58/08 910309. We acknowledge the support of the European Community-Research Infrastructure Integrating Activity "Study of Strongly Interacting Matter" (acronym HadronPhysics2, Grant Agreement No. 227431) under the Seventh Framework Programme of the EU.

APPENDIX A: QUARK CONDENSATES TO NNLO IN CHPT AND THEIR RENORMALIZATION

In this section we will give our NNLO results for the two-quark condensates. As explained in the text, the corresponding four-quark condensates cannot be obtained just by squaring these results, but one also has to add the nonfactorizing contributions described in Eqs. (14) and (17).

The free meson propagator in dimensional regularization is given by [8]

$$G_i(0) = 2M_{0i}^{D-2}\lambda, \tag{A1}$$

with

$$\lambda = \frac{\Gamma[1-\frac{D}{2}]}{2(4\pi)^{D/2}}, \tag{A2}$$

and $D = 4 - \epsilon$.

The SU(3) $\mathcal{L}_4$ ChPT Lagrangian is well known [8] and we do not reproduce it here. The relevant terms for the calculation of the condensates in the $\mathcal{O}(p^6)$ Lagrangian [10] are only those dependent on the quark masses to leading order in the Goldstone boson fields. Here, we will follow, for simplicity, a different notation than in [10] to denote the $\mathcal{L}_6$ low-energy constants involved in the mass terms:

$$\begin{aligned}\mathcal{L}_6^{m_q,\mathrm{SU}(2)} &= \frac{B_0^3}{F^2}\hat{c}_1 m^3,\\ \mathcal{L}_6^{m_q,\mathrm{SU}(3)} &= \frac{B_0^3}{F^2}(\hat{C}_1 m^3 + \hat{C}_2 m^2 m_s + \hat{C}_3 m m_s^2 + \hat{C}_4 m_s^3).\end{aligned} \tag{A3}$$

Recall that our $\hat{c}_i$ are linear combinations of the LEC considered in [10,26] whose precise form is not relevant here. Nevertheless, we still follow the convention in [26] for the renormalization of the $\mathcal{O}(p^4)$ and $\mathcal{O}(p^6)$ LEC in the $\overline{\text{MS}}$ scheme:

$$\begin{aligned}
l_i &= (c\mu)^{D-4}[l_i^r(\mu) + \gamma_i\Lambda],\\
h_i &= (c\mu)^{D-4}[h_i^r(\mu) + \delta_i\Lambda],\\
\hat{c}_i &= (c\mu)^{2(D-4)}[\hat{c}_i^r(\mu) - \hat{\gamma}_i^{(sq)}\Lambda^2 - (\hat{\gamma}_i^{(0)} + \hat{\gamma}_i^L(\mu))\Lambda],\\
L_i &= (c\mu)^{D-4}[L_i^r(\mu) + \Gamma_i\Lambda],\\
H_i &= (c\mu)^{D-4}[H_i^r(\mu) + \Gamma_i^H\Lambda],\\
\hat{C}_i &= (c\mu)^{2(D-4)}[\hat{C}_i^r(\mu) - \hat{\Gamma}_i^{(sq)}\Lambda^2 - (\hat{\Gamma}_i^{(0)} + \hat{\Gamma}_i^L(\mu))\Lambda],
\end{aligned} \tag{A4}$$

where μ is the renormalization scale, $\Lambda^{-1} = 16\pi^2(D-4)$, $\log c = -[\log(4\pi) - \gamma + 1]/2$, $\gamma = -\Gamma'[1]$, γ_i, δ_i, Γ_i, Γ_i^H, $\hat{\gamma}_i^{(sq)}$, $\hat{\Gamma}_i^{(sq)}$, $\hat{\gamma}_i^{(0)}$, and $\hat{\Gamma}_i^{(0)}$ are numerical coefficients, whereas $\hat{\gamma}_i^L$, $\hat{\Gamma}_i^L$ are linear combinations of the $L_i^r(\mu)$. The above expression for the $\hat{c}_i$ shows that these constants have to absorb both two-loop divergences with $\mathcal{L}_2$ vertices and one-loop ones with one $\mathcal{L}_4$ and one $\mathcal{L}_2$ vertex.

The renormalization of the L_i in Eq. (A4) coincides with that in [8] up to $\mathcal{O}(1)$ in the ϵ expansion:

$$L_i = L_i^r(\mu) + \Gamma_i\mu^{D-4}\lambda + \mathcal{O}(\epsilon), \tag{A5}$$

and so on for the H_i, whereas the l_i, h_i renormalizations coincide with [11] to that order. For the renormalization of the one-loop effective action, the $\mathcal{O}(\epsilon)$ in Eqs. (A4) and (A5) can be neglected. However, when two-loop diagrams are considered, as in our case here for the quark condensates [e.g., diagram (d) in Fig. 1] products of the form $L_iG(0)$ yield finite contributions that do not vanish in the $\epsilon \to 0^+$ limit. The $\mathcal{O}(\epsilon)$ has to also be kept in the expansion of λ in Eq. (A2) when expanding $G_i(0)$ in Eq. (A1) in $G_i(0)^2$ contributions.

As for the μ scale dependence, the L_i, l_i and the $\hat{C}_i$, $\hat{c}_i$ are scale independent so that the scale dependence of the $L_i^r(\mu)$, $l_i^r(\mu)$, $\hat{C}_i^r(\mu)$, $\hat{c}_i^r(\mu)$ is canceled with the explicit μ dependence appearing in Eq. (A4). This allows us to express all the logarithms of the masses in terms of $\log(M_i^2/\mu^2)$, so that the final result for the observables should be finite and scale independent.

We also recall that to the order we are calculating, the propagators are renormalized to NLO (tadpole corrections) and one has to include the wave-function and mass renormalization to that order. The renormalized masses are given in [8], while the explicit wave-function renormalization can be found, for instance, in [27]. We recall that we should now include up to $\mathcal{O}(\epsilon)$ in those tadpole corrections, for the reasons just explained.

With these renormalization conventions, we turn to the NNLO quark condensates. The Γ_i coefficients appearing in the calculation are [8]

$$\begin{aligned}
&\gamma_3 = -1/2, \qquad \delta_1 = 2, \qquad \Gamma_4 = 1/8,\\
&\Gamma_5 = 3/8, \qquad \Gamma_6 = 11/144, \qquad \Gamma_7 = 0,\\
&\Gamma_8 = 5/48, \qquad \Gamma_2^H = 5/24.
\end{aligned} \tag{A6}$$

Recall that in SU(3), L_6, L_8, and H_2 come explicitly from the $\mathcal{L}_4$ vertex contributions to the condensate and are therefore the only LEC appearing to NLO. The mass and wave-function renormalization introduce a dependence on L_4, L_5, and L_7 in the final result. L_7 only appears in the η mass renormalization. In the pure SU(2) case, only l_3 and h_1 enter in the calculation.

Once the above LEC renormalization is performed, we have checked that one can choose the $\hat{c}_i$ and $\hat{C}_i$ in Eq. (A3), renormalized through Eq. (A4), so that the final result for the two-quark condensates is finite and scale independent. We obtain

$$\begin{aligned}
&\hat{\gamma}_1^{(sq)} = 12, \qquad \hat{\gamma}_1^L = -48l_3^r, \qquad \hat{\Gamma}_1^{(sq)} = 896/81, \qquad \hat{\Gamma}_2^{(sq)} = 32/27, \qquad \hat{\Gamma}_3^{(sq)} = 64/9, \qquad \hat{\Gamma}_4^{(sq)} = 160/81,\\
&\hat{\Gamma}_1^L = \frac{32}{27}(444L_4^r + 191L_5^r - 6(148L_6^r + 4L_7^r + 65L_8^r)), \qquad \hat{\Gamma}_2^L = \frac{32}{9}(162L_4^r + 31L_5^r - 324L_6^r - 62L_8^r),\\
&\hat{\Gamma}_3^L = \frac{32}{9}(96L_4^r + 35L_5^r - 192L_6^r + 24L_7^r - 62L_8^r), \qquad \hat{\Gamma}_4^L = \frac{32}{27}(78L_4^r + 43L_5^r - 6(26L_6^r + 8L_7^r + 17L_8^r)),
\end{aligned} \tag{A7}$$

and all the linear terms $\hat{\gamma}_i^{(0)} = \hat{\Gamma}_i^{(0)} = 0$ for the above LEC.

For convenience and following the same notation as [8], we define

$$\begin{aligned}
\mu_i &= \frac{M_{0i}^2}{32\pi^2F^2}\log\frac{M_{0i}^2}{\mu^2},\\
\nu_i &= F^2\frac{\partial\mu_i}{\partial M_{0i}^2} = \frac{1}{32\pi^2}\left(1 + \log\frac{M_{0i}^2}{\mu^2}\right).
\end{aligned} \tag{A8}$$

In SU(2) the leading order pion mass is related to the physical one by

$$M_\pi^2 = M_{0\pi}^2\left(1 + \mu_\pi + \frac{4M_{0\pi}^2}{F^2}l_3^r\right), \tag{A9}$$

and in SU(3),

$$
\begin{aligned}
M_\pi^2 &= M_{0\pi}^2\Big[1+\mu_\pi-\frac{\mu_\eta}{3}+\frac{16M_{0K}^2}{F^2}(2L_6^r-L_4^r)+\frac{8M_{0\pi}^2}{F^2}(2L_6^r+2L_8^r-L_4^r-L_5^r)\Big],\\
M_K^2 &= M_{0K}^2\Big[1+\frac{2\mu_\eta}{3}+\frac{8M_{0\pi}^2}{F^2}(2L_6^r-L_4^r)+\frac{8M_{0K}^2}{F^2}(4L_6^r+2L_8^r-2L_4^r-L_5^r)\Big],\\
M_\eta^2 &= M_{0\eta}^2\Big[1+2\mu_K-\frac{4}{3}\mu_\eta+\frac{8M_{0\eta}^2}{F^2}(2L_8^r-L_5^r)+\frac{8}{F^2}(2M_{0K}^2+M_{0\pi}^2)(2L_6^r-L_4^r)\Big]\\
&\quad+M_{0\pi}^2\Big[-\mu_\pi+\frac{2}{3}\mu_K+\frac{1}{3}\mu_\eta\Big]+\frac{128}{9F^2}(M_{0K}^2-M_{0\pi}^2)^2(3L_7^r+L_8^r).
\end{aligned}
\tag{A10}
$$

The relation between the leading order pion decay constant and the physical one up to two loops is given in [28] for SU(2) and in [29] for SU(3).

The final expressions for the two-quark condensates, finite and scale independent, up to NNLO, that have been calculated previously in [16] for SU(3), are given by

$$
\langle\bar qq\rangle_{l,\mathrm{NLO}}^{\mathrm{SU}(2)}=-2B_0F^2\Big\{1+\frac{2M_{0\pi}^2}{F^2}(h_1^r+l_3^r)-3\mu_\pi\Big\},
\tag{A11}
$$

$$
\langle\bar qq\rangle_{l,\mathrm{NNLO}}^{\mathrm{SU}(2)}=\langle\bar qq\rangle_{l,\mathrm{NLO}}^{\mathrm{SU}(2)}-2B_0F^2\Big[-\frac{3}{2}\mu_\pi^2-\frac{3M_{0\pi}^2}{F^2}(\mu_\pi\nu_\pi+4l_3^r\mu_\pi)+\frac{3M_{0\pi}^4}{8F^4}(-16l_3^r\nu_\pi+\hat c_1^r)\Big],
\tag{A12}
$$

$$
\langle\bar qq\rangle_{l,\mathrm{NLO}}^{\mathrm{SU}(3)}=-2B_0F^2\Big\{1+\frac{4}{F^2}[(H_2^r+4L_6^r+2L_8^r)M_{0\pi}^2+8L_6^rM_{0K}^2]-3\mu_\pi-2\mu_K-\frac{1}{3}\mu_\eta\Big\},
\tag{A13}
$$

$$
\begin{aligned}
\langle\bar qq\rangle_{l,\mathrm{NNLO}}^{\mathrm{SU}(3)} &= \langle\bar qq\rangle_{l,\mathrm{NLO}}^{\mathrm{SU}(3)}-2B_0F^2\Big\{-\frac{3}{2}\mu_\pi^2+\frac{1}{18}\mu_\eta^2+\mu_\pi\mu_\eta-\frac{4}{3}\mu_K\mu_\eta+\frac{1}{F^2}\Big[-3M_{0\pi}^2\mu_\pi\nu_\pi+\frac{1}{3}M_{0\pi}^2\mu_\pi\nu_\eta\\
&\quad-\frac{8}{9}M_{0K}^2\mu_K\nu_\eta+M_{0\pi}^2\mu_\eta\nu_\pi-\frac{4}{3}M_{0K}^2\mu_\eta\nu_K+\frac{1}{27}(16M_{0K}^2-7M_{0\pi}^2)\mu_\eta\nu_\eta\Big]\\
&\quad+\frac{24}{F^2}\mu_\pi[(3L_4^r+2L_5^r-6L_6^r-4L_8^r)M_{0\pi}^2+2(L_4^r-2L_6^r)M_{0K}^2]\\
&\quad+\frac{16}{F^2}\mu_K[(L_4^r-2L_6^r)M_{0\pi}^2+2(3L_4^r+L_5^r-6L_6^r-2L_8^r)M_{0K}^2]\\
&\quad+\frac{8}{9F^2}\mu_\eta[(-3L_4^r-2L_5^r+6L_6^r-48L_7^r-12L_8^r)M_{0\pi}^2+2(15L_4^r+4L_5^r-30L_6^r+24L_7^r)M_{0K}^2]\\
&\quad+\frac{24M_{0\pi}^2}{F^4}\nu_\pi[(L_4^r+L_5^r-2L_6^r-2L_8^r)M_{0\pi}^2+2(L_4^r-2L_6^r)M_{0K}^2]\\
&\quad+\frac{16M_{0K}^2}{F^4}\nu_K[(L_4^r-2L_6^r)M_{0\pi}^2+(2L_4^r+L_5^r-4L_6^r-2L_8^r)M_{0K}^2]\\
&\quad+\frac{8}{27F^4}\nu_\eta[(-3L_4^r+L_5^r+6L_6^r-48L_7^r-18L_8^r)M_{0\pi}^4+2(3L_4^r-4L_5^r-6L_6^r+48L_7^r+24L_8^r)M_{0\pi}^2M_{0K}^2\\
&\quad+8(3L_4^r+2(L_5^r-3(L_6^r+L_7^r+L_8^r)))M_{0K}^4]\\
&\quad+\frac{1}{8F^4}[(3\hat C_1^r-2\hat C_2^r+\hat C_3^r)M_{0\pi}^4+4(\hat C_2^r-\hat C_3^r)M_{0\pi}^2M_{0K}^2+4\hat C_3^rM_{0K}^4]\Big\},
\end{aligned}
\tag{A14}
$$

$$
\langle\bar ss\rangle_{\mathrm{NLO}}=-B_0F^2\Big\{1+\frac{4}{F^2}[-(H_2^r-4L_6^r+2L_8^r)M_{0\pi}^2+2(H_2^r+4L_6^r+2L_8^r)M_{0K}^2]-4\mu_K-\frac{4}{3}\mu_\eta\Big\},
\tag{A15}
$$

$$\langle\bar{s}s\rangle_{\rm NNLO} = \langle\bar{s}s\rangle_{\rm NLO} - B_0F^2\Big\{\frac{8}{9}\mu_\eta^2 - \frac{8}{3}\mu_K\mu_\eta + \frac{1}{F^2}\Big[\frac{4}{3}M_{0\pi}^2\mu_\pi\nu_\eta - \frac{32}{9}M_{0K}^2\mu_K\nu_\eta - \frac{8}{3}M_{0K}^2\mu_\eta\nu_K + \frac{4}{27}(16M_{0K}^2 - 7M_{0\pi}^2)\mu_\eta\nu_\eta\Big] + \frac{48}{F^2}\mu_\pi(L_4^r - 2L_6^r)M_{0\pi}^2 + \frac{32}{F^2}\mu_K[(L_4^r - 2L_6^r)M_{0\pi}^2 + 2(2L_4^r + L_5^r - 4L_6^r - 2L_8^r)M_{0K}^2] + \frac{16}{9F^2}\mu_\eta[(3L_4^r - 4L_5^r - 6L_6^r + 48L_7^r + 24L_8^r)M_{0\pi}^2 + 8(3L_4^r + 2(L_5^r - 3(L_6^r + L_7^r + L_8^r)))M_{0K}^2] + \frac{32M_{0K}^2}{F^4}\nu_K[(L_4^r - 2L_6^r)M_{0\pi}^2 + (2L_4^r + L_5^r - 4L_6^r - 2L_8^r)M_{0K}^2] + \frac{32}{27F^4}\nu_\eta[(-3L_4^r + L_5^r + 6L_6^r - 48L_7^r - 18L_8^r)M_{0\pi}^4 + 2(3L_4^r - 4L_5^r - 6L_6^r + 48L_7^r + 24L_8^r)M_{0\pi}^2M_{0K}^2 + 8(3L_4^r + 2(L_5^r - 3(L_6^r + L_7^r + L_8^r)))M_{0K}^4] + \frac{1}{4F^4}[(\hat{C}_2^r - 2\hat{C}_3^r + 3\hat{C}_4^r)M_{0\pi}^4 + 4(\hat{C}_3^r - 3C_4^r)M_{0\pi}^2M_{0K}^2 + 12\hat{C}_4^rM_{0K}^4]\Big\}, \tag{A16}$$

where the Gell-Mann-Okubo relation $3M_{0\eta}^2 = 4M_{0K}^2 - M_{0\pi}^2$ for the SU(3) leading order masses has been used, and the renormalized L_i^r, l_i^r and $\hat{c}_i^r$, $\hat{C}_i^r$ constants depend on the scale μ as explained above.

APPENDIX B: FOUR-QUARK CONDENSATES IN THE USUAL $\overline{\rm MS}$ DEFINITION

Here we consider the definition in Eq. (3) of the four-quark condensate in Euclidean space. Let us restrict to SU(2) since it will become clear that the argument can be straightforwardly extended to the SU(3) case. The four-quark correlator to NNLO is given in Eq. (14), so that its Euclidean Fourier transform to this order is (see our Euclidean space-time conventions in Sec. III)

$$\Pi(Q^2) = (2\pi)^D\langle\bar{q}q\rangle^2\delta^{(D)}(Q) + 2B_0^2[4(l_3 + h_1) + 3J_\pi(Q^2)] \tag{B1}$$

with $Q^2 = \sum_{i=1}^D Q_i^2$ and

$$J_\pi(Q^2) = \int\frac{d^DK}{(2\pi)^D}G_\pi(K)G_\pi(K-Q), \tag{B2}$$

which is nothing but the one-loop integral appearing in pion-pion scattering, dimensionally regularized in [11]. Its divergent part is contained in $J_\pi(0) = -2M_\pi^{D-4}\lambda - 1/(16\pi^2)$, with λ defined in Eq. (A2), while $\bar{J}(Q^2) = J_\pi(Q^2) - J_\pi(0)$ is finite. Note also that $J_\pi(Q^2)$ defined in Euclidean space is real. The imaginary part in $\bar{J}_\pi$ giving the usual unitarity cut in scattering amplitudes arises when the analytical continuation of Q^2 to Minkowski space-time is performed, but here we should keep the Euclidean version, since we are following the prescription in Eq. (3) to perform the additional momentum integral.

Before proceeding to the calculation of the four-quark condensate, let us note that the divergent part of the J_π in Eq. (B1) cancels exactly with the LEC contribution since $l_3 + h_1 = l_3^r(\mu) + h_1^r(\mu) + (3/2)\mu^{D-4}\lambda$ [see Eqs. (A4) and (A6)]. Thus, $\Pi(Q^2)$ is finite and scale independent before integration in Q. This is actually a welcomed check, since the scalar susceptibility given in Eq. (22) can be written also as $\chi_l = \tilde{\Pi}(0)$ with $\tilde{\Pi}(Q^2) = \Pi(Q^2) - (2\pi)^D\langle\bar{q}q\rangle^2\delta^{(D)}(Q)$ and should be finite and scale independent.

However, we will immediately see that the additional integration in Q in Eq. (3) generates an extra divergence which cannot be removed, and in the end gives the same divergent factorization-breaking result as the definition in Eq. (2). For that purpose, let us follow the standard dimensional regularization procedure [22] and write

$$J_\pi(Q^2) = \frac{1}{(4\pi)^{D/2}}\int_0^1 dx\int_0^\infty d\lambda\lambda^{1-D/2}\times\exp\{-\lambda[M_\pi^2 + Q^2x(1-x)]\} \tag{B3}$$

which is valid within the domain $\mathrm{Re}[D] < 4$. Now, before performing the x and λ integrals above, we integrate over Q so that

$$\int\frac{d^DQ}{(2\pi)^D}J_\pi(Q^2) = \frac{1}{(4\pi)^D}\Big\{\int_0^1 dx[x(1-x)]^{-D/2}\Big\}\times\Big\{\int_0^\lambda d\lambda\lambda^{1-D}e^{-\lambda M_\pi^2}\Big\} = \frac{(M_\pi^2)^{D-2}}{(4\pi)^D}\Big[\Gamma\Big(1-\frac{D}{2}\Big)\Big]^2 = G_\pi^2(0), \tag{B4}$$

where the one-dimensional integrals are solved for $\mathrm{Re}[D] < 2$ and we have used standard properties of the Gamma function. Since the result is analytic in D, it can be extended to $D = 4 - \epsilon$ with $\epsilon \to 0^+$. Therefore, integrating in Eq. (B1) over Q according to Eq. (3), and taking into

account that $\int d^D Q/(2\pi)^D = \delta^{(D)}(0) = 0$, gives exactly the same divergent factorization-breaking result for the four-quark condensate as the one using the prescription of Eq. (2).

Another way to arrive at the same conclusion is to perform the change of variables $Q \to Q + K$ in the double D-integral $\int d^D Q \int d^D K$ in the region of D where it converges, which in this case is $\mathrm{Re}[D] < 2$, which follows by direct power counting in Q and K of the propagators in Eq. (B2) in the large Q^2 and K^2 Euclidean region.

It is clear that the same equivalence between the two definitions holds in the SU(3) case simply by considering J_K and J_η apart from J_π, since the results of the correlators in Eqs. (19) and (20) do not mix different meson species.

[1] M. A. Shifman, A. I. Vainshtein, and V. I. Zakharov, Nucl. Phys. **B147**, 385 (1979).
[2] S. Narison and R. Tarrach, Phys. Lett. **125B**, 217 (1983).
[3] R. A. Bertlmann, C. A. Dominguez, M. Loewe, M. Perrottet, and E. de Rafael, Z. Phys. C **39**, 231 (1988).
[4] H. s. Zong, D. k. He, F. y. Hou, and W. M. Sun, Int. J. Mod. Phys. A **23**, 1507 (2008).
[5] J. Bijnens, E. Gamiz, and J. Prades, J. High Energy Phys. 10 (2001) 009.
[6] V. Cirigliano, J. F. Donoghue, E. Golowich, and K. Maltman, Phys. Lett. B **555**, 71 (2003).
[7] F. Karsch (RBC-Bielefeld Collaboration), Nucl. Phys. **A820**, 99C (2009).
[8] J. Gasser and H. Leutwyler, Nucl. Phys. **B250**, 465 (1985).
[9] S. Weinberg, Physica A (Amsterdam) **96**, 327 (1979).
[10] J. Bijnens, G. Colangelo, and G. Ecker, J. High Energy Phys. 02 (1999) 020.
[11] J. Gasser and H. Leutwyler, Ann. Phys. (N.Y.) **158**, 142 (1984).
[12] S. Scherer, Adv. Nucl. Phys. **27**, 277 (2003).
[13] J. Gasser, C. Haefeli, M. A. Ivanov, and M. Schmid, Phys. Lett. B **652**, 21 (2007).
[14] J. Gasser, C. Haefeli, M. A. Ivanov, and M. Schmid, Phys. Lett. B **675**, 49 (2009).
[15] J. Wess and B. Zumino, Phys. Lett. **37B**, 95 (1971); E. Witten, Nucl. Phys. **B223**, 422 (1983).
[16] G. Amoros, J. Bijnens, and P. Talavera, Nucl. Phys. **B585**, 293 (2000); **B598**, 665(E) (2001).
[17] G. Amoros, J. Bijnens, and P. Talavera, Nucl. Phys. **B602**, 87 (2001).
[18] B. Moussallam, J. High Energy Phys. 08 (2000) 005.
[19] J. Bijnens, Prog. Part. Nucl. Phys. **58**, 521 (2007).
[20] A. Gómez Nicola, J. R. Peláez, and J. Ruiz de Elvira (work in progress).
[21] A. V. Smilga and J. J. M. Verbaarschot, Phys. Rev. D **54**, 1087 (1996).
[22] G. Leibbrandt, Rev. Mod. Phys. **47**, 849 (1975).
[23] S. Descotes-Genon, L. Girlanda, and J. Stern, J. High Energy Phys. 01 (2000) 041.
[24] S. Peris and E. de Rafael, Phys. Lett. B **348**, 539 (1995).
[25] B. L. Ioffe, Prog. Part. Nucl. Phys. **56**, 232 (2006).
[26] J. Bijnens, G. Colangelo, and G. Ecker, Ann. Phys. (N.Y.) **280**, 100 (2000).
[27] A. Gómez Nicola and J. R. Pelaez, Phys. Rev. D **65**, 054009 (2002).
[28] J. Bijnens, G. Colangelo, G. Ecker, J. Gasser, and M. E. Sainio, Nucl. Phys. **B508**, 263 (1997); **B517**, 639(E) (1998).
[29] G. Amoros, J. Bijnens, and P. Talavera, Nucl. Phys. **B568**, 319 (2000).

2.3.4 A. Gomez Nicola, J.R. Pelaez, J. Ruiz de Elvira *Scalar susceptibilities and four-quark condensates in the meson gas* arxiv:1210.7977

Scalar susceptibilities and four-quark condensates in the meson gas within Chiral Perturbation Theory

A. Gómez Nicola,* J.R. Peláez,† and J. Ruiz de Elvira‡
Departamento de Física Teórica II. Universidad Complutense. 28040 Madrid. Spain.

We analyze the properties of four-quark condensates and scalar susceptibilities in the meson gas, within finite temperature Chiral Perturbation Theory (ChPT). The breaking of the factorization hypothesis does not allow for a finite four-quark condensate and its use as an order parameter, except in the chiral limit. This is rigorously obtained within ChPT and is therefore a model-independent result. Factorization only holds formally in the large N_c limit and breaks up at finite temperature even in the chiral limit. Nevertheless, the factorization breaking terms are precisely those needed to yield a finite scalar susceptibility, deeply connected to chiral symmetry restoration. Actually, we provide the full result for the $SU(3)$ quark condensate to NNLO in ChPT, thus extending previous results to include kaon and eta interactions. This allows to check the effect of those corrections compared to previous approaches and the uncertainties due to low-energy constants. We provide a detailed analysis of scalar susceptibilities in the $SU(3)$ meson gas, including a comparison between the pure ChPT approach and the virial expansion, where the unitarization of pion scattering is crucial to achieve a more reliable prediction. Through the analysis of the interactions within this approach, we have found that the role of the σ resonance is largely canceled with the scalar isospin two channel interaction, leaving the $\rho(770)$ as the main contribution. Special attention is paid to the evolution towards chiral restoration, as well as to the comparison with recent lattice analysis.

PACS numbers: 11.10.Wx, 12.39.Fe, 11.30.Rd, 25.75.Nq

I. INTRODUCTION

Chiral symmetry restoration [1] is a very relevant ingredient in our present understanding of hadronic physics under extreme conditions of temperature and density and has been one of the main motivations for the development of the heavy-ion and nuclear matter experimental programs, which are still producing new results in facilities such as RHIC, CERN (ALICE) and FAIR. In parallel, the improvement of lattice data at finite temperature, performed by different groups [2–8], has contributed considerably to clarify the main properties of the chiral symmetry transition, which is believed to take place in the same range as the deconfinement one. Nowadays, there is a fair consistency between lattice simulations performed with different methods, pointing towards a crossover-like transition for $N_f = 3$ (2+1 flavors in the physical case), becoming of second order for $N_f = 2$ (in the $O(4)$ universality class) and first order in the degenerate case of three equal flavors. This behavior corresponds to vanishing baryon chemical potential and the transition temperature lies within the range $T_c \sim$ 150-175 MeV. It is important to remark that in the physical 2+1 case analyzed on the lattice, the transition being a crossover means that one should really talk about a transition range rather than a critical temperature, and that range can be established by looking at different order-like parameters, which can give different values for T_c. The chief parameters used in lattice analysis are the quark condensate and susceptibilities, defined as first derivatives of the quark condensates with respect to quark masses. Susceptibilities measure fluctuations of the associated order parameter and can be expressed in terms of current correlators. Thus, the scalar susceptibility, related to the quark condensate, is expected to grow faster just below the transition.

It is important to provide an accurate analytical description of the physics below the chiral transition, to compare with experimental data and to confront the lattice results in the continuum. On the one hand, a particularly useful approach has been the Hadron Resonance Gas (HRG), which has proven to be quite successful to describe thermodynamic quantities, i.e., those that can be derived directly from the free energy density, as compared to lattice data [8–10]. Within the usual HRG approach, the free contribution of all known physical hadron states to the partition function is considered. Models including resonance widths and hadron interactions improve the HRG approach description of hadron production experimental data [11, 12] and lattice results [13].

On the other hand, Chiral Perturbation Theory (ChPT) [14–16] allows to describe the low-temperature meson gas

*Electronic address: gomez@fis.ucm.es
†Electronic address: jrpelaez@fis.ucm.es
‡Electronic address: jacobore@rect.ucm.es

[17] in a model-independent and systematic way for $SU(N_f)_L \times SU(N_f)_R \to SU(N_f)_V$ symmetry breaking with $N_f = 2, 3$ light flavors. In particular, interactions can be included in the most general way compatible both with the underlying symmetries and with meson-meson scattering data. Although ChPT includes only the lightest degrees of freedom (π, K, η) and hence is limited to low and moderate temperatures, it provides model-independent results. In fact, in early studies of the partition function [17], extrapolations of the condensate and other quantities to the transition region give a qualitatively reasonable description of the relevant physics. In addition, there have been some relevant developments on the use of ChPT results in the description of the meson gas properties. For instance, it is known that the Inverse Amplitude Method [18–20], which is a dispersive method to unitarize ChPT without introducing spurious parameters, allows the generation of light meson resonances (the σ or $f_0(500)$, the $\rho(770)$, ...). Within that unitarized ChPT scheme, useful results have been developed for the temperature and density dependence of the lightest resonances and their connection to chiral restoration and chiral partner degeneration [21–23] as well as a phenomenologically successful description of transport coefficients [24]. It is particularly relevant to recall the virial expansion [17, 25–30] which allows to parametrize efficiently the effect of meson interactions in the partition function within a dilute gas description, valid below the transition. States of more energy are weighted by Boltzmann factors and then become more relevant as the system approaches the transition. Thus, in this approach, it is more important to include accurately the interaction of the lightest mesons, e.g. via unitarization, while the heavier ones can be added as free states. Actually, the HRG approach with just free states is nothing but the leading order in the virial expansion. An alternative approach, also within unitarized ChPT, is to take into account the temperature or density dependence of the phase shifts, which would make the σ resonance pole move towards the real axis precisely as a signature of chiral restoration [22, 23].

In this work we will explore some additional properties of the meson gas within the ChPT framework, regarding in particular quark condensates and susceptibilities. Our study will be deeply connected to the analysis of four-quark correlators of the type $\langle \mathcal{T}(\bar{q}q)(x)(\bar{q}q)(0)\rangle$ and the factorization hypothesis, thus extending our previous work at zero temperature [31]. This hypothesis states that four-quark condensates factorize into two-quark condensates squared $\langle(\bar{q}q)^2\rangle \sim \langle\bar{q}q\rangle^2$ with the same quantum numbers. We have shown in [31] that this hypothesis fails to next to next to leading order (NNLO) in ChPT. Here, we will show that the same holds at finite temperature, preventing the use of four-quark condensates as order parameters since the factorization breaking terms diverge. In the derivation we will in turn obtain the $SU(3)$ thermal quark condensate in ChPT including all the relevant meson interactions, which extends previous calculations of the condensate to this order which considered free kaons and etas [17]. The non-factorizing scalar four-quark correlator gives rise to the scalar susceptibility, allowing for a direct check of the calculation. Once the connection with factorization is established, we will perform a detailed analysis of the scalar susceptibilities in the virial approach, with and without including unitarized amplitudes, extending previous works in the literature and serving as a test of the robustness of the ChPT results, which together with their model independence makes them a useful prediction for low and moderate temperatures below the transition. In this respect, it is particularly relevant to note that unitarized ChPT is able to provide a relatively good description of the quark mass dependence of the resonant states obtained through unitarization [32–34], particularly robust in the case of the lightest scalar.

The paper is organized as follows. After fixing our notation and definitions (section II A), in section II B we present our calculation of the relevant four-quark correlators for two and three flavors at finite temperature. The details are given for $N_f = 3$. The factorization hypothesis is then examined in section II C, where we also comment on the large-N_c limit. In section II D we establish the connection with the scalar susceptibility. Different effects in the ChPT condensates and susceptibilities are discussed in section III, while section IV is devoted to the analysis within the virial approach, to compare with previous analysis and to study the role of interactions. We pay special attention to the comparison with lattice data (section V) and to study its behavior as the system approaches chiral restoration. In Appendix A we collect some of the $SU(2)$ results, while in Appendix B we provide the detailed expressions for the thermal quark condensates to NNLO in ChPT.

II. QCD CONDENSATES, SUSCEPTIBILITIES AND FOUR-QUARK CORRELATORS IN CHIRAL PERTURBATION THEORY

A. General definitions

Let us start from the QCD Euclidean Lagrangian including scalar sources:

$$\mathcal{L}_{QCD}[q, \bar{q}, s(x)] = \bar{q}\,(i\,\not{D} - s(x))\,q + \cdots\,, \tag{1}$$

where the rest of the Lagrangian indicated by dots is irrelevant for our purposes, the $(-,-,-,-)$ metric is used and a sum over N_f flavor, N_c colors and Dirac indices is implicit.

The physical QCD Lagrangian corresponds to setting $s(x) = \mathcal{M}$, the quark mass matrix. In the three flavor case $\mathcal{M}$=diag(m_u,m_d,m_s), where m_u, m_d and m_s correspond to the up, down and strange mass respectively. For simplicity, we will work in the isospin limit, so that $m_u = m_d = m$ and $s(x)$ =diag($s_0(x), s_0(x), s_s(x)$).

We will follow the external source method [16] to deal with the different two-quark ($\bar{q}q$) and four-quark ($\bar{q}q\bar{q}q$) correlators of interest. Consider first the quark condensates at finite temperature:

$$\langle \bar{q}q \rangle_T \equiv \langle \bar{u}u + \bar{d}d + \bar{s}s \rangle_T \equiv \frac{1}{Z_{QCD}[\mathcal{M}]} \int \mathcal{D}\bar{q}\mathcal{D}q \cdots \bar{q}q \exp \int_E d^4x \mathcal{L}_{QCD}[\bar{q}, q, s(x), \cdots], \tag{2}$$

where $Z_{\rm QCD}[\mathcal{M}]$ is the partition function. In the above equation $\int_E d^4x = \int_0^\beta d\tau \int d^3\vec{x}$ is the Euclidean (imaginary-time $t = -i\tau$) version of the Minkowski volume $i\int d^4x$, the averaging is performed over the thermal ensemble (an asymmetric box with imaginary time extension of $\beta = 1/T \ll L$ and $V = L^3$). The dots indicate the dependence on the rest of the QCD Lagrangian fields, not relevant for our purposes. Similar equations hold for the light condensate $\langle (\bar{q}q)_l \rangle_T \equiv \langle \bar{u}u + \bar{d}d \rangle_T$. Recall that the light sector (u, d) is the most relevant one concerning chiral symmetry restoration, mostly due to the heavier strange mass.

We consider the effective low-temperature representation given by Chiral Perturbation Theory (ChPT) [14–16] of the QCD generating functional, built from chiral symmetry invariance as an expansion in external momenta and quark masses:

$$\begin{aligned} Z_{QCD}[s] &\simeq Z_{eff}[s] = \int \mathcal{D}\phi^a \exp \int_E d^4x \mathcal{L}_{eff}[\phi^a, s(x)], \\ \mathcal{L}_{eff} &= \mathcal{L}_2 + \mathcal{L}_4 + \mathcal{L}_6 \ldots, \end{aligned} \tag{3}$$

We thus have:

$$\langle \bar{q}q \rangle_T = \frac{-1}{Z_{QCD}[\mathcal{M}]} \left(\frac{\delta}{\delta s_0(x)} + \frac{\delta}{\delta s_s(x)} \right) Z_{QCD}[s] \Big|_{s=\mathcal{M}} \simeq \frac{-1}{Z_{eff}[\mathcal{M}]} \left(\frac{\delta}{\delta s_0(x)} + \frac{\delta}{\delta s_s(x)} \right) Z_{eff}[s] \Big|_{s=\mathcal{M}}, \tag{4}$$

where $\mathcal{L}_{eff}$ is the most general one made out of pion, kaon and eta fields ϕ^a, that respects the QCD chiral symmetry breaking pattern. These particles are the QCD low-energy degrees of freedom since they are Nambu-Goldstone bosons (NGB) of the QCD spontaneous chiral symmetry breaking. The subscript in the effective Lagrangian indicates the order in the ChPT derivative and mass expansion $\mathcal{L} = \mathcal{O}(p^{2k})$ over a typical scale $\Lambda_\chi \sim 1$ GeV, and ϕ^a denote the NGB fields. Since the u, d, s quark masses are small compared with Λ_χ, they are introduced as perturbations, giving rise to the π, K and η masses, counted as $O(p^2)$. At each order, $\mathcal{L}_{eff}$ is the sum of all terms compatible with the symmetries, multiplied by chiral parameters, which absorb loop divergences order by order, yielding finite results. ChPT is thus the quantum effective field theory of QCD, and it allows for a systematic and model independent analysis of low-energy mesonic processes. The NGB fields are usually collected in the $SU(N_f)$ matrix $U = \exp[i\lambda_a\phi^a/F]$, where, in the $N_f = 3$ case, λ_a are the Gell-Mann matrices. The Lagrangian $\mathcal{L}_2$ is the non-linear sigma model:

$$\mathcal{L}_2 = \frac{F^2}{4} \mathrm{Tr} \left[\partial_\mu U^\dagger \partial^\mu U + \chi (U + U^\dagger) \right], \tag{5}$$

with $\chi = 2B_0 s(x)$, while F is the pion decay constant in the chiral limit. When $s(x) = \mathcal{M}$, the following lowest order SU(3) relations hold: $\langle \bar{q}q \rangle = -3B_0F^2$, $M_{0\pi}^2 = 2B_0 m$, $M_{0K}^2 = B_0(m + m_s)$ and $M_{0\eta}^2 = \frac{2}{3}B_0(m + 2m_s)$. The ChPT power counting can be formally traced in terms of the counting in $1/F^2$ and so we will do in the following. The Lagrangians $\mathcal{L}_4$ and $\mathcal{L}_6$ are given in [16] and [35] respectively, and contain the so-called low energy constants (LEC), L_i and H_i (the latter are contact terms without NGB fields) for $\mathcal{L}_4$ and C_i for $\mathcal{L}_6$.

The quark condensates (light and strange) can also be defined in terms of the free energy density z, which in the thermodynamic limit is given by:

$$z = -\lim_{V\to\infty} \frac{1}{\beta V} \log Z, \tag{6}$$

so that:

$$\langle (\bar{q}q)_l \rangle_T = \frac{\partial z}{\partial m}, \qquad \langle \bar{s}s \rangle_T = \frac{\partial z}{\partial m_s}, \qquad \langle \bar{q}q \rangle_T = \langle (\bar{q}q)_l \rangle_T + \langle \bar{s}s \rangle_T. \tag{7}$$

We turn now to the susceptibilities and their relation to four-quark correlators, which will play an important role in this work. Susceptibilities are defined as variations of the condensates with respect to the quark masses and are directly related to the thermal averages of four-quark operators measuring condensate fluctuations. Thus, the euclidean light scalar (or chiral) susceptibility is given by:

$$\begin{aligned}\chi_l(T) &= -\frac{\partial}{\partial m}\langle(\bar{q}q)_l\rangle_T = -\frac{\partial^2}{\partial m^2}z = \frac{1}{\beta V}\left[\frac{1}{Z[\mathcal{M}]}\frac{\partial^2}{\partial m^2}Z[\mathcal{M}] - \left(\frac{1}{Z[\mathcal{M}]}\frac{\partial}{\partial m}Z[\mathcal{M}]\right)^2\right] \\ &= \int_E d^4x\left[\langle\mathcal{T}(\bar{q}q)_l(x)(\bar{q}q)_l(0)\rangle_T - \langle(\bar{q}q)_l\rangle_T^2\right], \end{aligned} \tag{8}$$

which relates the light susceptibility (the most relevant one regarding chiral restoration) with the four-quark correlator of the light combination $(\bar{q}q)_l = \bar{u}u + \bar{d}d$:

$$\langle\mathcal{T}(\bar{q}q)_l(x)(\bar{q}q)_l(0)\rangle_T = \frac{1}{Z[\mathcal{M}]}\frac{\delta}{\delta s_0(x)}\frac{\delta}{\delta s_0(0)}Z[s]\Big|_{s=\mathcal{M}} \simeq \frac{1}{Z_{eff}[\mathcal{M}]}\frac{\delta}{\delta s_0(x)}\frac{\delta}{\delta s_0(0)}Z_{eff}[s]\Big|_{s=\mathcal{M}}, \tag{9}$$

where $\mathcal{T}$ denotes euclidean time ordering, and so on for the strange, light-strange and full $SU(3)$ susceptibilities:

$$\chi_s(T) = -\frac{\partial}{\partial m_s}\langle\bar{s}s\rangle_T = -\frac{\partial^2 z}{\partial^2 m_s} = \int_E d^4x\left[\langle\mathcal{T}(\bar{s}s)(x)(\bar{s}s)(0)\rangle_T - \langle\bar{s}s\rangle_T^2\right], \tag{10}$$

$$\chi_{ls}(T) = -\frac{\partial}{\partial m_s}\langle(\bar{q}q)_l\rangle_T = -\frac{\partial}{\partial m}\langle\bar{s}s\rangle_T = -\frac{\partial^2 z}{\partial m\partial m_s} = \int_E d^4x\left[\langle\mathcal{T}(\bar{q}q)_l(x)(\bar{s}s)(0)\rangle_T - \langle(\bar{q}q)_l\rangle_T\langle\bar{s}s\rangle_T\right], \tag{11}$$

$$\chi(T) = \chi_l(T) + 2\chi_{ls}(T) + \chi_s(T) = \int_E d^4x\left[\langle\mathcal{T}(\bar{q}q)(x)(\bar{q}q)(0)\rangle_T - \langle\bar{q}q\rangle_T^2\right]. \tag{12}$$

Note that, since the low-T representation of the free energy density is finite and independent of the low-energy renormalization scale μ [17] so are the quark condensates and susceptibilities, which can be expressed as mass derivatives of z. However, that is not the case of the four-quark condensates, which we define, for the different combinations of quark flavors, as:

$$\langle(\bar{q}q)_\alpha(\bar{q}q)_\beta\rangle_T = \lim_{x\to 0}\langle\mathcal{T}(\bar{q}q)_\alpha(x)(\bar{q}q)_\beta(0)\rangle_T, \tag{13}$$

where $(\bar{q}q)_\alpha$ stands for either $(\bar{q}q)_l$ or $(\bar{s}s)$. Actually, at $T = 0$ the low-energy representation of the four-quark condensates are divergent and scale-dependent, which is consistent with Renormalization Group (RG) analysis and holds also for other definitions of the four-quark condensates from the four-quark correlators, different from that in Eq. (13), as we showed in [31].

Our previous discussion will allow us to relate, in the finite-temperature case, susceptibilities to four-quark correlators, which in the next section will be calculated within ChPT. Susceptibilities can be calculated either directly as mass derivatives of the two-quark condensates, or from the four-quark correlators, as in Eq. (8), always yielding a finite and scale-independent result. Even though four quark-correlators are not strictly needed for the calculation of susceptibilities, we will nevertheless calculate them, since they are needed to test the factorization hypothesis in the thermal case, because we aim to determine their validity as order parameters, and because they allow for a direct consistency check of our susceptibility calculation.

B. ChPT thermal four-quark scalar correlators and condensates.

Here we will calculate the relevant four-quark scalar correlators, by taking the corresponding functional derivatives, as in Eq. (9), from the effective Lagrangian in Eq. (3) at a given order in ChPT. We also calculate the two-quark condensate Eq. (4) to the same order, to check the factorization hypothesis. We have:

$$\langle\bar{q}q\rangle_T = -\left\langle\frac{\delta\mathcal{L}_{eff}[s]}{\delta s_0(x)} + \frac{\delta\mathcal{L}_{eff}[s]}{\delta s_s(x)}\right\rangle_T\Bigg|_{s=\mathcal{M}}, \tag{14}$$

$$\langle \mathcal{T}(\bar{q}q)(x)(\bar{q}q)(0)\rangle_T = \left\langle \mathcal{T}\left(\frac{\delta}{\delta s_0(x)}+\frac{\delta}{\delta s_s(x)}\right)\left(\frac{\delta}{\delta s_0(0)}+\frac{\delta}{\delta s_s(0)}\right)\mathcal{L}_{eff}[s]\right\rangle_T\Big|_{s=\mathcal{M}}\delta(\tau)\delta^{(D-1)}(x) + \left\langle \mathcal{T}\left(\frac{\delta\mathcal{L}_{eff}[s]}{\delta s_0(x)}+\frac{\delta\mathcal{L}_{eff}[s]}{\delta s_s(x)}\right)\left(\frac{\delta\mathcal{L}_{eff}[s]}{\delta s_0(0)}+\frac{\delta\mathcal{L}_{eff}[s]}{\delta s_s(0)}\right)\right\rangle_T\Big|_{s=\mathcal{M}}. \quad (15)$$

All our results can be expressed in terms of the leading order (free) thermal meson propagators $G_i^T(x)$, with $i=\pi$, K, η. Using standard finite-temperature methods, one can separate the $T=0$ part. The divergent contribution is contained in the $x=0$ and $T=0$ part. We follow the notation of [17] for thermal functions:

$$G_i^T(0) = G_i(0)+g_1(M_i,T),$$
$$g_1(M,T) = \frac{1}{2\pi^2}\int_0^\infty dp\frac{p^2}{E_p}\frac{1}{e^{\beta E_p}-1}, \quad (16)$$

with $E_p=\sqrt{p^2+M^2}$ and $G_i(0)=M_{0i}^{D-2}\Gamma\left[1-D/2\right]/(4\pi)^{D/2}$, the $T=0$ divergent part in the dimensional regularization scheme, which we will use throughout this work. The renormalization of the LEC and the quark condensates up to NNLO in ChPT are the same as at $T=0$ and are discussed in detail in [31].

Now, from Eqs. (14) and (15), using the Lagrangians in [16] and [35], we obtain the following results:

$$\langle \mathcal{T}(\bar{q}q)(x)(\bar{q}q)(0)\rangle_{T,\,NLO} = \langle\bar{q}q\rangle^2_{T,NLO}, \quad (17)$$

$$\langle \mathcal{T}(\bar{q}q)(x)(\bar{q}q)(0)\rangle_{T,\,NNLO} = \langle\bar{q}q\rangle^2_{T,NNLO} + B_0^2\left[24(12L_6+2L_8+H_2)\delta(\tau)\delta^{(D-1)}(x)+K^T(x)\right], \quad (18)$$

where the NLO and NNLO are $\mathcal{O}(F^2)$ and $\mathcal{O}(F^2)+\mathcal{O}(F^0)$ in the ChPT counting respectively and $K^T(x)$ is the connected part of the four-meson correlator at leading order and finite temperature:

$$K^T(x) = \langle\mathcal{T}\phi^a(x)\phi_a(x)\phi^b(0)\phi_b(0)\rangle_{T,LO} - \langle\mathcal{T}\phi^a(0)\phi_a(0)\rangle^2_{T,LO} = 2\left(3G_\pi^T(x)^2+4G_K^T(x)^2+G_\eta^T(x)^2\right). \quad (19)$$

We have expressed our results as a function of the square of the thermal quark condensate $\langle\bar{q}q\rangle_T$, whose explicit expressions are given in Appendix B, Eqs. (B4)-(B7). As it happened in the $T=0$ case [31], up to NLO the four-quark correlator is just equal to the square of the quark condensate, but to NNLO the connected one-loop contribution breaks such equality. For a detailed diagrammatic description of the different terms contributing to the four-quark correlator, we refer to [31], since the diagrams are the same at $T\neq 0$.

At this point, it is important to remark that we provide the full ChPT $SU(3)$ result for the two-quark condensates to NNLO including all the relevant meson interactions. Previous works at finite temperature only included the kaon and eta (and other massive states such as nucleons) as free fields in the partition function [17], which is reasonable for heavier particles when $T << M_{K,\eta}$, since the heavy states are Boltzmann suppressed. Therefore, apart for the study of factorization, our complete NNLO calculation of the condensate will allow to test the effect of including in the diagrams contact interactions containing strange particles.

Similarly to the previous analysis, we calculate separately the light, strange and mixed four-quark correlators, which also factorize up to NLO in the product of the two-quark condensates, whereas up to NNLO we get:

$$\langle \mathcal{T}(\bar{q}q)_l(x)(\bar{q}q)_l(0)\rangle_T = \langle(\bar{q}q)_l\rangle^2_T + B_0^2\Big[16(8L_6+2L_8+H_2)\delta(\tau)\delta^{(D-1)}(x) + 6G_\pi^T(x)^2+2G_K^T(x)^2+\frac{2}{9}G_\eta^T(x)^2\Big]+\mathcal{O}\left(\frac{1}{F^2}\right), \quad (20)$$

$$\langle \mathcal{T}(\bar{s}s)(x)(\bar{s}s)(0)\rangle_T = \langle\bar{s}s\rangle^2_T + B_0^2\left[8(4L_6+2L_8+H_2)\delta(\tau)\delta^{(D-1)}(x)+2G_K^T(x)^2+\frac{8}{9}G_\eta^T(x)^2\right]+\mathcal{O}\left(\frac{1}{F^2}\right), \quad (21)$$

$$\langle \mathcal{T}(\bar{q}q)_l(x)(\bar{s}s)(0)\rangle_T = \langle(\bar{q}q)_l\rangle_T\langle\bar{s}s\rangle_T + B_0^2\left[64L_6\delta(\tau)\delta^{(D-1)}(x)+2G_K^T(x)^2+\frac{4}{9}G_\eta^T(x)^2\right]+\mathcal{O}\left(\frac{1}{F^2}\right). \quad (22)$$

C. Factorization breaking at finite temperature

As discussed in the introduction, scalar condensates play a relevant role in QCD, since they are directly related to vacuum properties. Attending only to their symmetry transformation properties, quark condensates of arbitrary

order $\langle(\bar{q}q)^n\rangle$ should behave similarly as the two-quark condensate under chiral restoration, since they transform as isoscalars and are built out of chiral non-invariant operators with the vacuum quantum numbers. Actually, it is well known that such quark condensates appear directly in QCD sum rules, through the Operator Product Expansion (OPE) approach [36]. In that framework, the following hypothesis of factorization or vacuum saturation is customarily made:

$$\langle(\bar{q}q)^2\rangle = \left(1 - \frac{1}{4N_cN_f}\right)\langle\bar{q}q\rangle^2, \tag{23}$$

and similarly for other condensates, which in the large-N_c limit simply reduces to $\langle(\bar{q}q)^2\rangle = \langle\bar{q}q\rangle^2$. The second term between brackets in Eq. (23) comes from the exchange of indices (including color) between the first and second $\bar{q}q$ operators.

The use of the factorization hypothesis has been a much debated tool in order to estimate the size of higher order condensates in the OPE. Let us remark that in [31] we have shown that factorization of the four-quark condensate does not hold within the model-independent QCD low-energy regime provided by ChPT, at $T = 0$. Actually, once the two-quark condensate is renormalized at a given order, factorization breaking terms are divergent and dependent on the low-energy scale. Therefore, the scalar four-quark condensate is not even a low-energy observable at $T = 0$. This factorization breaking is consistent with previous RG analysis [37]. Nevertheless, in [31] we found that factorization holds formally if the large N_c limit is taken before renormalization, since factorization breaking terms are $\mathcal{O}(N_c^{-2})$ suppressed.

In this paper we extend the analysis performed in [31] to the $T \neq 0$ case, since, among other reasons, this can shed light on the use of the four-quark condensate $\langle(\bar{q}q)^2\rangle_T$ as an order parameter of the chiral transition. In particular, in case factorization holds, the four-quark condensate should behave as an order parameter, melting at the same critical temperature as the two-quark condensate. We obtain readily the factorization properties of scalar four-quark condensates by setting $x \to 0$ in our results in section II B. It is clear then that, at finite temperature, factorization does not hold either. In fact, since $\delta^{(D-1)}(0)$ vanishes identically in dimensional regularization [38], we get from Eqs.(13) and (18):

$$\frac{\langle(\bar{q}q)^2\rangle_T}{\langle\bar{q}q\rangle_T{}^2} = 1 + \frac{2}{9F^4}\left(3G_\pi^T(0)^2 + 4G_K^T(0)^2 + G_\eta^T(0)^2\right) + \mathcal{O}(1/F^6). \tag{24}$$

We can calculate again the light, strange and mixed four-quark cases separately in $SU(3)$, namely:

$$\frac{\langle(\bar{q}q)_l^2\rangle_T}{\langle(\bar{q}q)_l\rangle_T{}^2} = 1 + \frac{1}{2F^4}\left(3G_\pi^T(0)^2 + G_K^T(0)^2 + \frac{1}{9}G_\eta^T(0)^2\right) + \mathcal{O}(1/F^6), \tag{25}$$

$$\frac{\langle(\bar{s}s)^2\rangle_T}{\langle\bar{s}s\rangle_T^2} = 1 + \frac{2}{F^4}\left(G_K^T(0)^2 + \frac{4}{9}G_\eta^T(0)^2\right) + \mathcal{O}(1/F^6), \tag{26}$$

$$\frac{\langle(\bar{q}q)_l\,(\bar{s}s)\rangle_T}{\langle(\bar{q}q)_l\rangle_T\langle ss\rangle_T} = 1 + \frac{1}{F^4}\left(G_K^T(0)^2 + \frac{2}{9}G_\eta^T(0)^2\right) + \mathcal{O}(1/F^6), \tag{27}$$

In view of these results, several remarks are in order: First, the factorization breaking terms at $T \neq 0$ are divergent and independent of the LEC, as for $T = 0$ [31], which was expected since the finite temperature result for the four-quark condensates to this order is just obtained by replacing $G_i(0) \to G_i^T(0)$. Since the quark NNLO condensates are rendered finite by the renormalization of the $\mathcal{O}(p^4)$ and $\mathcal{O}(p^6)$ LEC [31], this means that the four-condensate to this order is divergent, also at $T \neq 0$. Even subtracting the $T = 0$ factorization breaking term, the result is still divergent, since, from Eq. (16), there are terms in Eq. (24) proportional to $G_i(0)g_1(M_i, T)$. Recall that, as mentioned at the beginning of this section, the four-quark condensates cannot be expressed only in terms of mass derivatives of the free energy density, unlike the quark condensates.

Second, in the chiral limit, and contrary to the zero temperature case, for $T \neq 0$ the factorization breaking terms $G_i^T(0)$ in Eq. (24) are finite and do not vanish. Let us recall that in dimensional regularization the $T = 0$ propagators $G_i(0) = 0$ when $M_i = 0$, since they are proportional to M_i^2. However, the thermal part $g_1(M_i, T)$ is finite and non vanishing in the chiral limit. Thus, the chiral limit is the only case for which the four-quark condensate can be considered an order parameter. Actually, we have checked that $\langle(\bar{q}q)_l^2\rangle_T/\langle(\bar{q}q)_l^2\rangle_0$ follows the same temperature melting behavior as $\langle(\bar{q}q)_l\rangle_T/\langle(\bar{q}q)_l\rangle_0$ for the temperatures where ChPT is reliable. Note that chiral symmetry restoration takes place formally only in the chiral limit.

Third, for $T \neq 0$ factorization holds formally in the $N_c \to \infty$ limit, as it happened for the $T = 0$ case [31], since $F^2 = \mathcal{O}(N_c)$ and therefore factorization breaking terms are once again $\mathcal{O}(N_c^{-2})$ suppressed.

Partial results on the non-factorization of the thermal four quark condensates in certain approximations also exist in the literature. For instance, using the soft-pion and chiral limits it has been shown in [39] that if one assumes factorization at zero temperature, it will be spoiled by the lowest order thermal corrections. Our results support those in [39] since, on the one hand, we have proved factorization for $T = 0$ in the chiral limit, and, on the other hand, we have also found that factorization breaks due to $T \neq 0$ contributions.

In addition, an analysis of medium effects indicates that factorization is expected to be broken by $1/N_c^2$ suppressed contributions due to particles with the same quantum numbers as the operator under consideration [40]. Hence, we formally agree with [40], since the leading term in $1/N_c$ for the scalar four-quark condensate in the pure pion gas should factorize due to the absence of crossed terms $\langle\pi|\bar{q}q|0\rangle$. Nevertheless, by dropping these $1/N_c^2$ subleading breaking terms, some combinations of four-quark condensates, which include that in Eq.(25) above, have been proposed in [41] as order parameters. However, as we have just commented, even if these divergences are formally $1/N_c$ suppressed, the four-quark condensates in Eq.(25) are actually divergent. Therefore, for finite N_c, the use of the order parameters proposed in [41] would require checking the cancellation of the divergences in the combinations suggested in [41].

Thus, one of the main conclusions of the present work is that the four-quark condensates in Eqs.(24) to (27), cannot be used as order parameters of the chiral phase transition, because they are divergent. Their use in previous works is valid only formally for $N_c \to \infty$ or the chiral limit, but not in the physical case. We point out that a breaking of four-quark condensate factorization at finite temperature has been reported also in [42] within the framework of QCD sum rules.

D. Scalar susceptibilities within ChPT

We now turn to the ChPT evaluation of the different susceptibilities defined in section II A. As detailed in Eq. (8) and Eqs. (10) to (12), the scalar susceptibilities can be calculated either as a mass derivative of a quark condensate or from the corresponding four-quark correlators. Since we have available both the condensates (displayed in Appendix B) and the four-quark correlators given in section II B, we can obtain the ChPT susceptibilities in both ways, thus checking our results for the four-quark correlators. Recall that precisely the additional factorization-breaking like terms in the NNLO correlators in Eqs. (18) and (20)-(22) give nonzero susceptibilities of chiral order $\mathcal{O}(1)$. That order correspond to the derivatives of the NLO condensates in Appendix B, since the $\mathcal{O}(F^2)$ is mass independent. If we calculate the susceptibilities from the four-quark correlators, we check again that the $\mathcal{O}(F^2)$ vanishes (NLO correlators) while from the NNLO correlators, taking into account that

$$\int_T d^4x \left[G_i^T(x)\right]^2 = -\frac{d}{dM_i^2} G_i^T(0), \tag{28}$$

we readily obtain the different ChPT scalar susceptibilities to $\mathcal{O}(1)$ in the chiral power counting:

$$\begin{aligned}
\chi(T) &= B_0^2 \left[24\left(12L_6^r(\mu) + 2L_8^r(\mu) + H_2^r(\mu)\right) - 12\nu_\pi - 16\nu_K - 4\nu_\eta \right. \\
&+ \left. 6g_2(M_\pi, T) + 8g_2(M_K, T) + 2g_2(M_\eta, T)\right] + \mathcal{O}\left(\frac{1}{F^2}\right), \qquad (29) \\
\chi_l(T) &= B_0^2 \left[16\left(8L_6^r(\mu) + 2L_8^r(\mu) + H_2^r(\mu)\right) - 12\nu_\pi - 4\nu_K - \frac{4}{9}\nu_\eta \right. \\
&+ \left. 6g_2(M_\pi, T) + 2g_2(M_K, T) + \frac{2}{9}g_2(M_\eta, T)\right] + \mathcal{O}\left(\frac{1}{F^2}\right), \qquad (30) \\
\chi_s(T) &= B_0^2 \left[8\left(4L_6^r(\mu) + 2L_8^r(\mu) + H_2^r(\mu)\right) - 4\nu_K - \frac{16}{9}\nu_\eta + 2g_2(M_K, T) + \frac{8}{9}g_2(M_\eta, T)\right] + \mathcal{O}\left(\frac{1}{F^2}\right) \qquad (31) \\
\chi_{ls}(T) &= B_0^2 \left[64L_6^r(\mu) - 4\nu_K - \frac{8}{9}\nu_\eta + 2g_2(M_K, T) + \frac{4}{9}g_2(M_\eta, T)\right] + \mathcal{O}\left(\frac{1}{F^2}\right), \qquad (32)
\end{aligned}$$

with:

$$\begin{aligned}
\nu_i &= \frac{1}{32\pi^2}\left(1 + \log\frac{M_{0i}^2}{\mu^2}\right), \qquad (33) \\
g_2(M, T) &= -\frac{dg_1(M, T)}{dM^2} = \frac{1}{4\pi^2}\int_0^\infty dp \frac{1}{E_p}\frac{1}{e^{\beta E_p} - 1}. \qquad (34)
\end{aligned}$$

A further check is that the results for the different susceptibilities are finite and independent of the low-energy scale μ, unlike the four-quark condensates, with the same renormalization of the low-energy constants, provided in [31], which ensures that quark condensates are also finite and scale independent to that order.

Note that, in the $T \ll M_K$ regime, the thermal pion loops, i.e. $g_2(M_\pi, T)$, dominate over other particle thermal loop contributions, which are Boltzmann suppressed. An even more interesting regime is $M_K \gg T \gg M_\pi$, because it is related to the critical behavior [43]. Within our approach we cannot reach high temperatures but we can study the near chiral limit, where these functions behave as $g_2(M_\pi, T) \simeq T/(8\pi M_\pi)$. We will remark this expected linear behavior when we plot our results below.

Note that pion terms show up in the light susceptibility χ_l but not in the strange and mixed ones χ_s, χ_{ls} which are therefore subdominant compared to the light one at temperatures below the transition. We have explicitly checked that in the limit $m_s \to \infty$ ($M_{K,\eta} \to \infty$), the $SU(3)$ light susceptibility reduces to the $SU(2)$ result in Eq. (A5) in Appendix A, once the identification between $SU(2)$ l_i^r and L_i^r LEC is made, as given in [16].

The thermal scaling of the light susceptibility near the critical point $(m_{u,d}, T) \to (0^+, T_c)$ reveals important features about the nature of the phase transition and is the subject of detailed analysis in lattice simulations [7]. The leading pion mass dependence from Eq.(30) near the chiral limit is $\chi^{IR}_{l,T=0}/B_0^2 \sim -\frac{3}{8\pi^2}\log(M_\pi^2/\mu^2)$ and $(\chi_{l,T} - \chi_{l,T=0})^{IR}/B_0^2 \sim \frac{3T}{4\pi M_\pi}$ for $M_\pi \ll T \ll M_{K,\eta}$. This leading behavior was already found in [43]. In addition, our results for the light susceptibility are consistent with a recent and model-independent ChPT analysis [44] of the mass, temperature and flavor dependence of the light susceptibilities, where a separate analysis of the quark connected and disconnected contributions was provided.

After providing the analytic expressions for the susceptibilities, and addressing some formal aspects, let us discuss their phenomenology in connection with that of the quark condensate.

III. PHENOMENOLOGICAL RESULTS IN CHPT

A. Higher order meson interactions and the quark condensate

As we have stated in the previous section, we provide in this work for the first time the full NNLO ChPT SU(3) $\langle\bar{q}q\rangle_T$ results, which are model-independent and given in Appendix B (the SU(2) one is also given in that Appendix). This result includes all the meson-meson interactions for π, K, η up to that order. At NLO, only tadpole contributions proportional to $g_1(M_i, T)$ appear, which is equivalent to considering an ideal gas made of the mesonic components. Previous studies of the condensate [17] actually considered the contribution of the heavier K, η states as free, while keeping higher orders in pure pion interactions. Here we will extrapolate our results to the critical point and make an estimate of the effect of considering interactions involving those strange degrees of freedom, by comparing with the NLO and with the pure $SU(2)$ result in which kaons and eta have been decoupled.

In order to study the thermal effects it is customary to normalize the quark condensate to its $T = 0$ value and so we will do in what follows. An additional advantage of this normalization is that the ratio is QCD Renormalization Group (RG) independent, because the B_0 global factors cancel. Let us note that, to NLO no LEC appear in $\langle\bar{q}q\rangle_T/\langle\bar{q}q\rangle_0$. To NNLO, only the $\mathcal{O}(p^4)$ LEC do appear. For the ChPT plots that we will present next, we will use the $SU(3)$ set of L_i^r LEC from [45] and their error bands. An important remark is that, by definition, the H_2^r constant cannot be fixed by experimental meson data. This constant appears at NNLO and we estimate it as $H_2^r = 2L_8^r$ as suggested in [46] using scalar resonance saturation. In addition, as it is customary, at each given order we use $F = F_\pi(1 + \mathcal{O}(M_i^2/F^2))$, $M_{0i}^2 = M_i^2(1 + \mathcal{O}(M_i^2/F^2))$ [16] taking the physical values for F_π and M_i^2 and including the corrections in the next order.

Now, to comment on the relative size of different effects under discussion, we are going to extrapolate our results up to temperatures beyond the strict applicability limit of ChPT, typically estimated around $T = 150\,\text{MeV}$ [17]. The reason is that it is much easier to explain the changes due to different effects in the curves of the condensate ratios, by comparing the points where their corresponding extrapolation vanish. We will refer to this point as the "critical temperature", T_c, in the clear understanding that this is just for the sake of comparison between curves, since the particular value of this "extrapolated" temperature is just a very crude extrapolation and only the low temperature part is reliable and model independent. We will proceed similarly in section IV about the virial expansion.

In order to study the restoration of the spontaneously broken chiral symmetry it is customary to use the non-strange condensate. The reason not to include the thermal strange quark condensate is that it has a very slow decrease as T increases, because its evolution is dominated by the larger m_s mass, which is an explicit and not a spontaneous breaking. Thus, in the upper panel of Fig. 1 we show the thermal dependence of the normalized non-strange condensate within NLO and NNLO $SU(2)$ ChPT, which can be compared with the $SU(3)$ version in the lower panel. The gray bands surrounding the NNLO calculation cover the uncertainties in the LEC. We see that the NNLO correction is relatively small compared to the NLO one below T_c. The approximate temperature at which the $SU(2)$

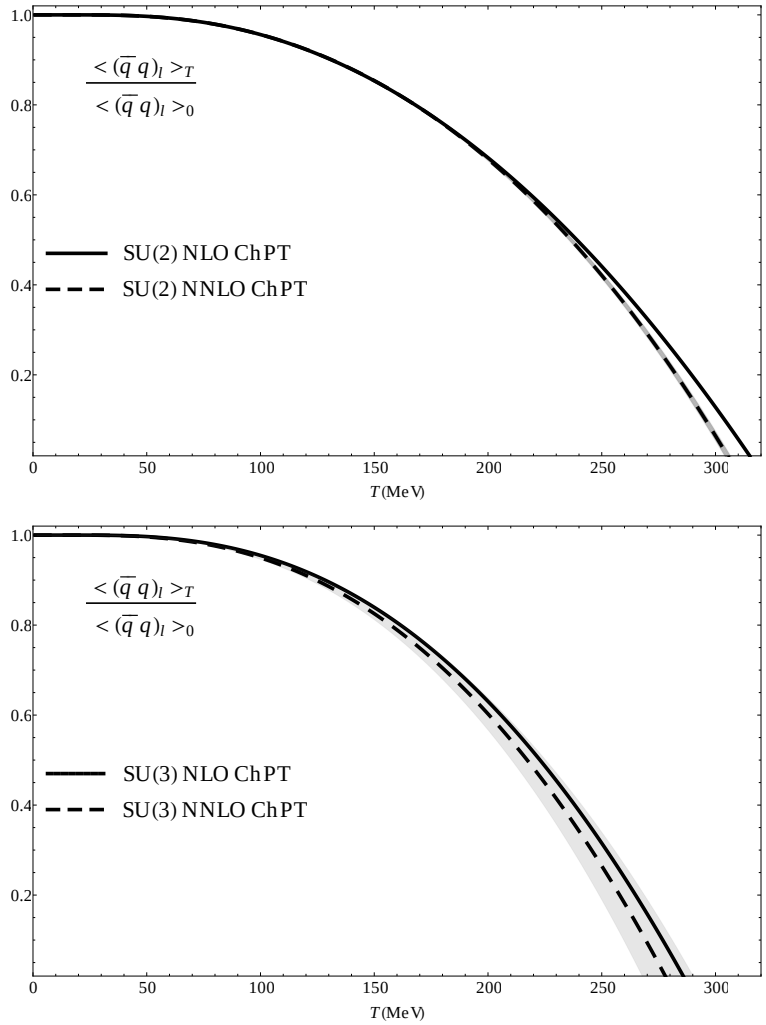

FIG. 1: Non-strange quark condensate in ChPT as a function of temperature in the different cases explained in the main text.

condensate vanishes is consistent with [17], when we compare to the same order of approximation, taking into account that we use a more recent set of LECs. The reduction in T_c from the $SU(2)$ to the $SU(3)$ case can be interpreted as a "paramagnetic" effect coming from the increase in entropy (and therefore disorder) due to the addition of the strange degrees of freedom to the system. To NLO, the reduction on T_c from $SU(2)$ to $SU(3)$ is of 30 MeV whereas at NNLO is of $28 \pm 12\,\mathrm{MeV}$. This is the behavior expected when adding more degrees of freedom as they become more relevant near the phase transition, and it actually provides a natural explanation to the smaller values of T_c obtained in approaches such as the HRG which take into account all the relevant (free) degrees of freedom. In the $SU(2)$ analysis we also observe a change in the value of T_c due to considering interacting pions (i.e., from NLO to NNLO) of about $\Delta T_c \sim -10\,\mathrm{MeV}$. However, the result is inconclusive for the $SU(3)$ case due to the uncertainties from the LEC dependence at NNLO.

B. ChPT susceptibility

We can also analyze the thermal evolution towards chiral restoration by studying the chiral susceptibility thermal dependence. In Fig. 2 we plot the ChPT $\chi_{l,T}$ result obtained for the $SU(2)$ and $SU(3)$ cases using Eqs. (30) and (A5), respectively, normalized to their $T = 0$ values and for the same set of parameters than the quark condensate in Fig. 1. Note that we plot the ratio of the thermal to $T = 0$ susceptibilities, which, once again, is QCD RG independent due to the cancellation of the B_0^2 factors. We do not expect our low-energy analysis to reproduce the dramatic growth just

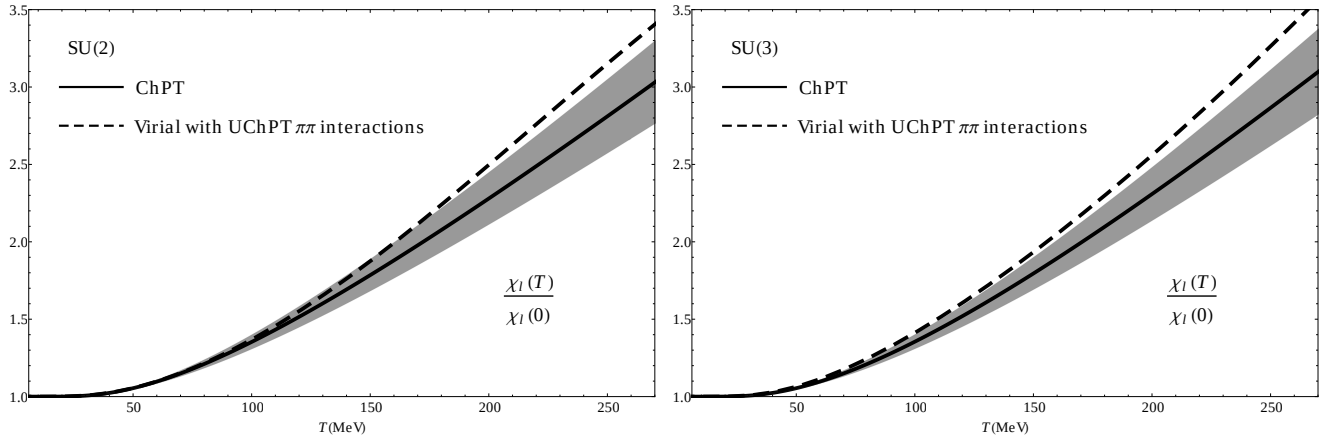

FIG. 2: Non-strange scalar susceptibility as a function of temperature for the $SU(2)$ and $SU(3)$ cases in ChPT at NNLO. The uncertainty bands, due to the in the LEC, have similar size for cases cases. The curves for the virial approach give a crude estimate of several sources of systematic uncertainties discussed in the text.

below the critical point for χ_l. As it also happens for the quark condensate, we expect only to reproduce reasonably the low T side of the critical curves. We will provide a quantitative comparison with lattice values in section V below. As we have discussed above, the temperature evolution is governed by the T-increasing functions g_2, so that, as we see in Fig. 2, the ChPT growth is roughly linear for temperatures high enough, according to the behavior in the chiral limit. In fact, although we have taken into account the full contribution of π, K, η loops in the $SU(3)$ massive case, the kaon and eta thermal contributions provide a weak dependence, so that the $SU(2)$ and $SU(3)$ curves are very similar to one another up to the critical point, unlike the "paramagnetic" shift for the case of the quark condensate. In fact, although in both cases the $SU(2)$ and $SU(3)$ differ by terms of order $e^{-M_{K,\eta}/T}$, the thermal dependence with $\tau = T/M_{K,\eta}$ is much softer in the susceptibility, since it comes from $g_2(M_{K,\eta}, T) \sim \sqrt{\tau} e^{-1/\tau}$, than in the condensate where $g_1(M_{K,\eta}, T) \sim T^2 (1/\sqrt{\tau}) e^{-1/\tau}$ for $\tau \ll 1$. Again, the strange quark susceptibility is not showed, χ_s/χ_0 being also increasing but remaining very close to unity for the range of temperatures showed in Fig. 2.

IV. THE VIRIAL APPROACH

In previous sections we have been able to estimate the effect of the uncertainties in the LEC. However, ChPT is a perturbative expansion that, when truncated, neglects higher order corrections and cannot reproduce resonances. This is a first motivation to use the virial expansion, because it allows for a simple implementation of unitarized ChPT, which includes the numerically relevant higher order effects. An additional motivation to use the virial approach is that the interaction part can be clearly identified and described realistically. Both features will allow us to establish a consistent comparison with our previous standard ChPT approach.

The virial expansion is a simple and successful approach already applied to describe many thermodynamical properties of dilute gases made of interacting pions [25, 26, 28] and other hadrons [17, 27, 29, 29, 30, 47]. For most thermal observables, it is enough to know the $T = 0$ scattering phase shifts of the particles that compose the gas. In principle these phase shifts could be taken from experiment avoiding any model dependence, so that it would not be necessary to go through the technicalities of finite temperature field theory. However, if one is interested in chiral symmetry restoration, and hence in scalar susceptibilities and quark condensates, one needs a model-independent theoretical description of the phase shifts in order to obtain their quark mass dependence, which cannot be obtained directly from experiment. Using directly one-loop ChPT for scattering lengths provides a remarkable description of the low energy hadronic interactions and should be accurate enough at very low temperatures [17]. However, for temperatures further away from the threshold region, a more precise description of the scattering is needed, which in particular takes into account the loss of unitarity, and the absence of resonances, in the pure ChPT expansion. For that purpose, we will make use of the so called unitarized ChPT, at the expense of loosing the systematic ordering of the effective approach.

The thermodynamics of a system of hadrons is encoded in the free energy density $z = \epsilon_0 - P$, where $\epsilon_0 = z^{T=0}$ and P is the pressure. In the present work, we are interested in a multi-component interacting relativistic gas made of pions, kaons and etas in thermal and chemical equilibrium, so the pressure only depends on temperature T. Thus,

the second order relativistic virial expansion of the pressure reads [17, 25, 26, 28]:

$$\beta P = \sum_i \left(B_i^{(1)} \xi_i + B_i^{(2)} \xi_i^2 + \sum_{j \geq i} B_{ij}^{\rm int} \xi_i \xi_j \right), \tag{35}$$

where $i = \pi, K, \eta$, the fugacities $\xi_i = e^{-\beta M_i}$, M_i is the mass of the i species and the B_i and B_{ij} are the virial coefficients for the gas. Expanding up to the second order in ξ_i means that we only consider binary interactions. The coefficients

$$B_i^{(n)} = \frac{g_i}{2\pi^2 n} \int_0^\infty dp\, p^2 e^{-n\beta(\sqrt{p^2+M_i^2}-M_i)}, \tag{36}$$

where the degeneracy is $g_i = 3, 4, 1$ for π, K, η respectively, correspond simply to the virial expansion for a free gas

$$\beta P_{\rm free} = -\sum_i \frac{g_i}{2\pi^2} \int_0^\infty dp\, p^2 \log\left[1 - e^{-\beta(\sqrt{p^2+M_i^2})}\right]. \tag{37}$$

The above free result is nothing but the HRG approach mentioned in the Introduction, when considering only the lightest hadrons π, K, η. Thus, the virial expansion provides naturally the corrections to the HRG due to interactions, which appear through the S-matrix. For the meson-meson interactions, relevant for this work, this can be recast in terms of the elastic scattering phase shifts [17, 25, 26, 28]. In this way, we can write

$$B_{ij}^{\rm int} = \frac{\xi_i^{-1}\xi_j^{-1}}{2\pi^3} \int_{M_i+M_j}^\infty dE\, E^2 K_1\left(E/T\right) \Delta_{ij}(E) \tag{38}$$

where K_1 is the first modified Bessel function and

$$\Delta_{ij}(E) = \sum_{I,J,S} (2I+1)(2J+1)\, \delta_{I,J,S}^{ij}(E), \tag{39}$$

where the $\delta_{I,J,S}^{ij}$ are the $ij \to ij$ elastic scattering phase shifts (chosen so that $\delta = 0$ at threshold $E_{th} = M_i + M_j$) of a state ij with quantum number I, J, S (isospin, angular momentum and strangeness), that we will explain below. The virial expansion breaks down typically where the dilute gas expansion does, for $T \sim 200 - 250$ MeV [28]. In that regime $\xi_\pi \gg \xi_K \sim \xi_\eta$ so that the density of higher mass states an their interactions are Boltzmann suppressed with respect to pions. Hence, for our purposes of estimating systematic uncertainties, the $ij = \pi K$ and $\pi\eta$ states can be neglected against the $\pi\pi$ interactions and we can drop the S index.

From Eq. (7) we can then express the quark condensate as:

$$\langle(\bar{q}q)_\alpha\rangle_T = \frac{\partial z}{\partial m_\alpha} = \langle 0|(\bar{q}q)_\alpha|0\rangle - \frac{\partial P}{\partial m_\alpha}, \tag{40}$$

with $\alpha = l, s$, $m_l = m$ and $\langle 0|(\bar{q}q)_\alpha|0\rangle = \langle(\bar{q}q)_\alpha\rangle_{T=0} = \partial\epsilon_0/\partial m_\alpha$. We emphasize again that in order to calculate Eq. (40) we need the dependence of $\delta(E)$ on the quark masses as well as the vacuum expectation value. For that information we turn to ChPT in order to translate Eq. (40) in terms of physical meson masses:

$$\langle(\bar{q}q)_\alpha\rangle_T = \langle 0|(\bar{q}q)_\alpha|0\rangle \left(1 + \sum_i \frac{c_i^\alpha}{2M_i F^2} \frac{\partial P}{\partial M_i}\right), \tag{41}$$

with:

$$c_i^\alpha = -F^2 \frac{\partial M_i^2}{\partial m_{q_\alpha}} \langle 0\,|(\bar{q}q)_\alpha|\,0\rangle^{-1}, \tag{42}$$

for which we will take the one-loop ChPT expressions from [16, 30]. Since they depend on the ChPT LEC, we take the same values as in previous sections, obtaining:

$$c_\pi^{\bar{q}q} = 1.02, \qquad c_K^{\bar{q}q} = 0.59, \qquad c_\eta^{\bar{q}q} = 0.52. \tag{43}$$

These numerical values are almost identical to those obtained in [30].

The behavior of the light and strange condensates within the virial expansion has been analyzed in detail for the meson gas in [26, 28–30] and also including baryon interactions in [47]. In this paper we are interested mostly in four-quark condensates and susceptibilities. The four-quark condensates, e.g Eq. (9), cannot be obtained directly from the pressure as mass derivatives and hence the virial approach cannot give further information about them. The susceptibilities, defined in section II A can be calculated taking one more mass derivative. Hence,

$$\chi_{\alpha\beta}(T) = -\frac{\partial^2 z}{\partial m_\alpha \partial m_\beta} = \chi_{\alpha\beta}(0) + \frac{\partial^2 P}{\partial m_\alpha \partial m_\beta}, \tag{44}$$

and again translating it in terms of meson masses:

$$\chi_{\alpha\beta}(T) = \chi_{\alpha\beta}(0)\left[1 + \frac{\langle 0|(\bar{q}q)_\alpha|0\rangle\langle 0|(\bar{q}q)_\beta|0\rangle}{4F^4\chi_{\alpha\beta}(0)}\sum_{i,j}\left(\frac{c_i^\alpha\, c_j^\beta}{M_i M_j}\frac{\partial^2 P}{\partial M_i \partial M_j} - \delta_{ij}\frac{c_j^\alpha c_j^\beta}{M_j^3}\frac{\partial P}{\partial M_j}\right)\right]. \tag{45}$$

By considering the ratios $\langle(\bar{q}q)_\alpha\rangle_T/\langle(\bar{q}q)_\alpha\rangle_0$ and $\chi_{\alpha\beta}(T)/\chi_{\alpha\beta}(0)$, we cancel the overall B_0 factors in the ChPT expressions for susceptibilities and condensates. These ratios are the quantities we will show in our plots. Note that, as it happened in the pure ChPT case, they are once again independent from the QCD renormalization group scale and can be expressed only in terms of meson parameters such as LEC, meson masses and decay constants. For these ratios we still need the values of $\langle 0|(\bar{q}q)_\alpha|0\rangle/B_0$, for which we will take the one-loop ChPT expressions from [16], and $\chi_{\alpha\beta}(0)/B_0^2$, which can be easily obtained from Eqs. (29) to (32) taking $g_1 = g_2 = 0$.

Recall also that the contribution to the susceptibility of the free part of the pressure Eq. (37) is precisely the same as the leading order ChPT results given in section II D, so that the size of the interaction contribution from Eqs. (38) and (39) is a measure not only of the convergence of the virial series but also of the robustness of the pure ChPT contribution.

Finally, in order to evaluate the interaction part of the virial coefficients, Eqs. (38) and (39), we need the theoretical description of the meson-meson elastic scattering phase shifts, which are nothing but the complex phase of each scattering partial wave t_{IJS}. These partial waves are obtained as the projection of the scattering amplitude in states of definite isospin I, angular momentum J and strangeness S. Let us remark that the unitarity of the S matrix implies that, for physical values of CM energy squared s, partial waves t_{IJ} for *elastic* meson-meson scattering should satisfy:

$$\mathrm{Im}\, t_{IJS} = \sigma|t_{IJS}|^2 \quad \Rightarrow \quad \mathrm{Im}\frac{1}{t_{IJS}} = -\sigma \quad \Rightarrow \quad t_{IJS} = \frac{1}{\mathrm{Re}\, t_{IJS}^{-1} - \mathrm{i}\sigma}, \tag{46}$$

where $\sigma = 2p/\sqrt{s}$, and p is the CM momenta of the two mesons. Note that unitarity implies

$$t_{IJS} = \frac{\sin\delta_{IJS}}{\sigma}e^{i\delta_{IJS}}, \tag{47}$$

where δ_{IJS} are the phase shifts needed in Eq. (39). The above equation leads to $|t_{IJ}| \leq 1/\sigma$, and a strong interaction is characterized precisely by the saturation of this unitarity bound.

In what follows we will first explain why the results for the susceptibility obtained combining standard ChPT with the virial expansion are very uncertain at very low temperatures due to a huge cancellation between the interactions in the scalar channels, and not reliable at moderate temperatures, since they do not describe data above typically 500 MeV. Later on we will explain how this can be solved using unitarized elastic ChPT, which provides a realistic description of data up to roughly 1 GeV.

A. ChPT Phase Shifts

Let us then start discussing the partial waves t_{IJS}, which are obtained within standard ChPT as an expansion in even powers of momenta and meson masses. Dropping for simplicity the IJS indices, we find: $t(s) = t_2(s) + t_4(s) + \cdots$ where $t_n(s) = O(p^n)$. Let us nevertheless recall that the ChPT series in only valid at low energies compared with $4\pi F \sim 1.2$ GeV, and in practice it is limited to scattering momenta of the order of 200-300 MeV above threshold, or about 400-500 MeV in energy. The reason is that, experimentally, for larger momenta several partial waves become resonant, a behavior that cannot be reproduced with a power expansion in energy.

The energy integrals that define the virial coefficients, Eq. (38), extend to infinity, where the low energy ChPT expansion is no longer valid. In principle, one may think that this is not a severe problem because, for the temperatures we are interested in, the very high energy region should be suppressed by the thermal Bessel functions in the virial coefficients. However, as already explained, in the interaction part of the virial coefficients, Eq.(38), the $\pi\pi$ scattering phase shifts appear through the combination

$$\Delta_{\pi\pi}(E) = \delta_{00}(E) + 5\delta_{20}(E) + 9\delta_{11}(E) + ... \tag{48}$$

where we have omitted waves with $J > 2$ because they are significantly smaller than those with $J \leq 1$ below 1 GeV, which is the region of interest for our calculations. It is now important to remark that, as we show in the top left panel of Fig. 3 there is huge cancellation between δ_{00} and $5\delta_{20}$. This cancellation was already observed for the scattering lengths in [17]. Using more recent determinations of the scattering lengths, we find $a_{00} + 5a_{20} = 0.002 \pm 0.009$ versus $a_{00} = 0.220 \pm 0.005$ from [48], or $a_{00} + 5a_{20} = 0.010 \pm 0.015$ versus $a_{00} = 0.220 \pm 0.008$ from [49], namely, a cancellation of more than one, possibly two, orders of magnitude. Note that the latter pair of numbers are just a data analysis that does not use ChPT.

As a consequence of that cancellation, the resulting $\Delta_{\pi\pi}$ is basically given by δ_{11} which at very low energies is extremely small. A similar cancellation also occurs both for the first and second mass derivatives of the phase shifts. Thus $\partial\Delta_{\pi\pi}/\partial M_\pi$ and $\partial^2\Delta_{\pi\pi}/\partial M_\pi^2$ are strongly dominated by the contribution from the vector channel, as we show in the left middle and left bottom panels of Fig.3. Let us nevertheless remark that the $J = 1$ wave is suppressed at low energies by a q^{2J} factor, and by itself yields a very small contribution to $\Delta_{\pi\pi}$ or its two first derivatives near threshold. Therefore, the model independent prediction of ChPT is that, at very low energies, the interaction part of the virial coefficient will be much smaller than naively expected from the size of each individual $J = 0$ wave. In other words, the results of the virial approach with standard ChPT interactions at very low temperature follow the free gas approximation much closer than naively expected.

Unfortunately, within ChPT we can state little more than the smallness of the interaction part of the virial coefficient at very low temperatures, because its value cannot be pinned down with numerical precision, since at very low energies what is left of $\Delta_{\pi\pi}$ after the cancellation is even smaller than the size of higher order corrections. Still, in the next section, we will try to estimate those higher order contributions by means of unitarized ChPT.

Nevertheless, one could think about providing ChPT results for moderate temperatures, say 100 or 150 MeV, where the bulk of the contribution to the integral extends beyond the threshold region and reaches, say, 500 MeV. However, in view of the left column in Fig.3, it is clear that this can be done for the pressure and its first derivative, i.e. for the condensate, because $\Delta_{\pi\pi}$ and $\partial\Delta_{\pi\pi}/\partial M_\pi$ are growing functions of the energy, and soon enough the δ_{11} becomes dominant and the large systematic uncertainties near threshold become less relevant. But this is not the case for $\partial^2\Delta_{\pi\pi}/\partial M_\pi^2$, which is needed for the susceptibility calculation. Actually, as seen in the left bottom panel of Fig.3, this second mass derivative is a decreasing function of the energy, so that the region nearby threshold, with its huge systematic uncertainties, continues to be dominant even for moderate temperatures, within ChPT calculations.

Of course, if we consider even higher temperatures we find the usual caveats for a standard ChPT calculation, but this time even more severe. First of all because due to the cancellation commented above, the dominant contribution comes from the δ_{11} channel, which is also suppressed near threshold, and we can only find a sizable contribution when this 11 channel becomes sufficiently large, but that only happens around the $\rho(770)$ resonance region. Unfortunately, whereas the ChPT description of the $(I, J) = (0, 0)$ channel is fairly good, at least qualitatively, up to energies as high as 700 MeV, the presence of the $\rho(770)$ resonance in the $(I, J) = (1, 1)$ channel is not reproduced even qualitatively.

Furthermore, the virial interaction coefficients in Eq. (38) are derived for an exactly unitary S matrix [25, 26], and this high energy thermal suppression quickly takes place for physical amplitudes respecting unitarity. But at this point we recall that ChPT scattering partial waves only satisfy unitarity perturbatively, i.e: $\mathrm{Im}\, t_2 = 0$, $\mathrm{Im}\, t_4 = \sigma t_2^2$,... and the unitarity constraint in Eq.(46) is badly violated pretty soon. Moreover, this violation grows fast with increasing momenta or in the vicinity of resonances. Hence, the contribution of ChPT is unphysically large due to the unitarity violation of the perturbative expansion and the contributions from the energy region $E > 1\,\mathrm{GeV}$, where any extrapolation is meaningless, become sizable already at temperatures of 150 MeV, for the ChPT virial calculation. In other words, for small temperatures, say formally $T \ll M_\pi$ the relevant momenta in the virial integrals are $p \sim \sqrt{M_\pi T}$ and hence the amplitudes are probed in the range $p \ll M_\pi$ where ChPT can be trusted. However, for $T \gtrsim M_\pi$ momenta are of the order of $2M_\pi$ or greater and the extrapolation of standard ChPT amplitudes does not describe meson scattering data.

Within one-loop ChPT, the correct low energy expansion of the non-unitarized phase shift is $\delta_{NU} \simeq \sigma(t_2 + \mathrm{Re}t_4)$, and gives a reasonable description of experimental data for very low energies with our choice of LEC. Then, for $E \gg M_\pi$, $\delta_{NU}(E) \sim E^4$, $\partial\delta_{NU}(E)/\partial M_\pi \sim E^2$, which produces additional powers of T in the interaction part compared to the free contribution, giving a large but unphysical weight to the higher energy contributions to the virial coefficients. Note in turn that by this same argument second derivative terms are subdominant in Eq. (45) with respect to the first derivatives. A rough estimation of the asymptotic behavior with T, say formally $T \gg M_\pi$, can be obtained by

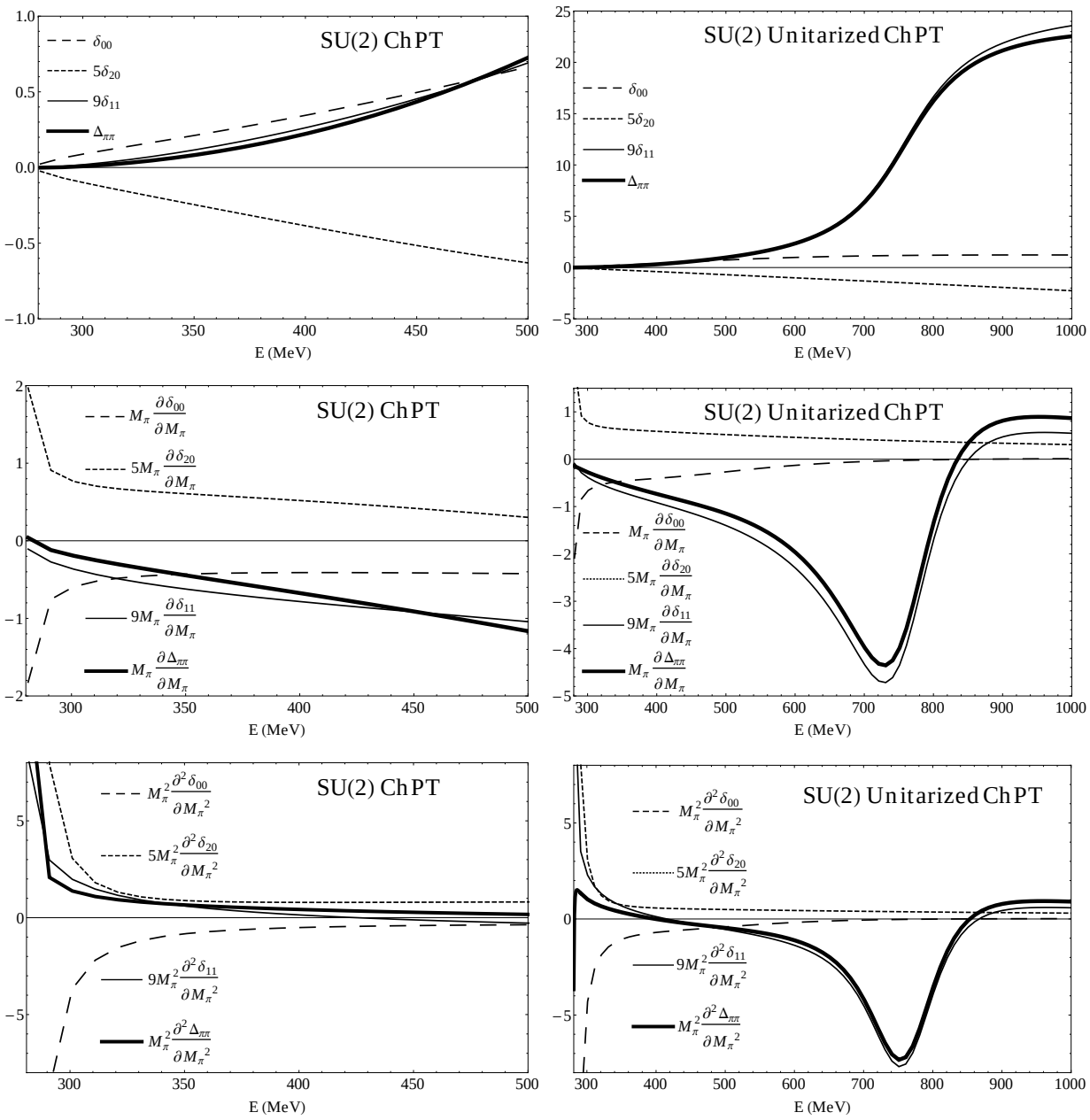

FIG. 3: From top to bottom, the $\pi\pi$ scattering phase shifts $(2I+1)\delta_{IJ}$ and their first and second mass derivatives compared to the combination $\Delta_{\pi\pi} = \delta_{00} + 5\delta_{20} + 9\delta_{11}$ and its mass derivatives. On the left column we plot the ChPT results and on the right one the unitarized ChPT calculations. Note the huge cancellation that occurs, in all graphs and irrespective of unitarization, between the $(I, J) = (0, 0)$ and $(2, 0)$ contributions. Hence, $\Delta_{\pi\pi}$ and its derivatives are dominated by the $(1, 1)$ contribution, with only a few exceptions around the threshold region where the $(1, 1)$ channel suffers an additional suppression.

looking at the $E \gg M_\pi$ behavior of the integrand in Eq. (38). The thermal function $x^2 K_1(x)$ weights the region $x \sim 1$ so that asymptotically we can just trade factors of E in the phase shifts by T, which also allows to compare the interaction part in Eq. (38) with the free contributions Eq. (36).

For all of these reasons, next we will make use of the so-called unitarized ChPT, which, under some reasonable approximations, combines ChPT at low energies with dispersion relations, and provides a realistic description of the data, reproducing the resonances relevant for this work, without introducing any spurious parameter other than those of ChPT. Of course, the price to pay is the loss of the systematic ChPT approach.

B. Unitarized interactions

In order to check the influence in the virial integrals of higher ChPT orders, the violation of unitarity and the lack of resonances, we will extend the ChPT amplitudes by means of unitarization, and in particular, we will use the elastic Inverse Amplitude Method (IAM) [18, 19] which provides a remarkably good description of the meson-meson scattering data up to roughly 1 GeV.

Unitarization methods provide amplitudes up to higher energies by using the fact implicit in Eq. (46), that *the imaginary part of the inverse amplitude is known exactly.* Naively, we can then impose the ChPT constraints to the real part of $\mathrm{Re}\, t^{-1} \simeq t_2^{-2}(t_2 + \mathrm{Re}\, t_4 + ...)$ to find that

$$t = \frac{1}{\mathrm{Re}t^{-1} - i\sigma} \simeq \frac{t_2}{1 - t_4/t_2}. \tag{49}$$

This is the one-channel IAM [18–20]. Although the use of the ChPT series in this naive derivation is only valid at low energies, the IAM can be derived also from a subtracted dispersion relation for the inverse amplitude, which justifies its extension to higher energies and even the complex plane. The details of the dispersive derivation can be found in [19, 20], but for our purposes here it is important to remark that the elastic cut is calculated exactly thanks to unitarity and the subtraction constants are calculated with ChPT, which is well justified since they correspond to evaluating the amplitude at very low energies. The IAM equation is valid at any energy as long as the left cut integral is well approximated by its low energy ChPT expansion, which is justified due to the subtractions, and as long as the energy where the amplitude is evaluated is sufficiently far from the inelastic region. Other terms due to so-called Adler zeros have also been shown explicitly to be negligible [20] in this region.

In summary, following a more rigorous derivation than the naive one above, the very same Eq. (49) is recovered not only at low energies, but for most of the elastic region. Remarkably, this simple equation is able to describe meson-meson scattering data enlarging considerably the energy applicability range [19], while still reproducing the ChPT series at low energies. In addition, the IAM generates [19] the poles in the second Riemann sheet associated with the resonances, from first principles like unitarity, analyticity and the QCD chiral symmetry breaking, without introducing these resonances by hand or any spurious parameter beyond the LEC of ChPT. Thus, the low-lying meson resonances are well described with this method, in very good agreement with the existing data. All these features can be reproduced with values of the ChPT parameters (LEC) that are fairly compatible with the values obtained within standard ChPT, despite being obtained from a fit to a much larger energy region. Nevertheless is important to point out that due to the nature of the IAM approach, the LEC needed to fit data and resonance poles with these unitarized amplitudes are only approximately those of ChPT. For this reason, we will use for the IAM phase shifts in the virial expansion the set of LEC obtained by fitting both scattering data and lattice results on meson masses, decay constants and scattering lengths. For the SU(3) case we take the values in [33] and for the SU(2) case from [34]. Note that we will only unitarize the pion-pion scattering amplitude since, as explained in previous sections and as it can be seen in our figures, this is the dominant contribution from meson interactions and, as we will see, correcting it with the IAM gives a considerably larger effect than including or not the kaon and eta interactions. Actually, and for the sake of simplicity, we will only consider two unitarized situations: either $SU(2)$ or $SU(3)$ but considering only free kaons and etas. With a lesser degree of rigor, the IAM can even be extended to the inelastic region [50] above 1 GeV, although that regime is not relevant for this work and the elastic formalism is enough for our purposes. Thus we prefer to rely on the most rigorous elastic formalism obtained from dispersion theory.

Thus, in the right column of Fig. 3 we show the $\pi\pi$ phase shifts and their derivatives which are obtained from our unitarized ChPT (UChPT) calculations. Once again we find a huge cancellation between the $(I, J) = (0, 0)$ and the $(2, 0)$ contributions. In the case of the phase and its first derivative, which have less uncertainty in the cancellation and also become very small at threshold, the effect of this cancellation uncertainty is very small in the virial integrals. But this is not the case for $\partial^2\Delta_{\pi\pi}/\partial M_\pi^2$, as can be noticed when comparing the lower left and right panels, where we see that there are large uncertainties near threshold due to the higher order effects. Note that the change on each individual wave due to unitarization is rather small, but a mere 10% change in the $(0, 0)$ channel produces a change of sign in the unitarized $\partial^2\Delta_{\pi\pi}/\partial M_\pi^2$. Hence, the interaction contribution to the susceptibilities is rather uncertain, but the overall uncertainty at very low energies is still small since the free contribution dominates by large.

Note also that, for the unitarized case, we now draw the phases up to 1 GeV in order to show the almost complete dominance of the $\rho(770)$ resonance contribution to $\Delta_{\pi\pi}$ and its derivatives above $E = 500\,\mathrm{MeV}$. The previously commented cancellation between the $(0, 0)$ and $(2, 0)$ contributions still persists at low energies, but deteriorates slightly above 500 MeV, where the $\rho(770)$ contributions simply dominates because it is much larger than the others. This $\rho(770)$ dominance is very relevant to asses the reliability of the UChPT results, since it has been recently shown that the $\rho(770)$ mass dependence obtained with the one-loop IAM is in fairly good agreement with the most recent lattice calculations [32].

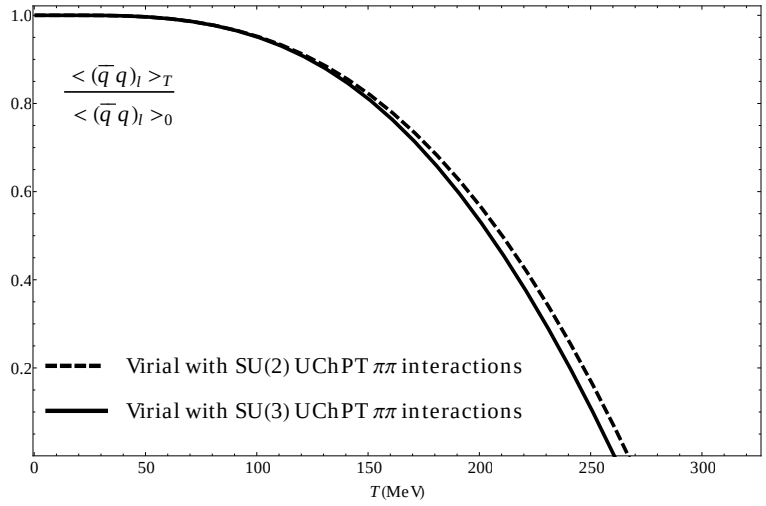

FIG. 4: Non-strange quark condensate as a function of temperature in the virial approach, using Unitarized interactions in SU(2) (dotted line)and in SU(3), only with pion-pion interaction and free kaons and etas (solid line)

If now recall the result that in the narrow width approximation a resonance exchange contributes to the partition function as the free resonance state would do [25], we conclude that the usual HRG with a free $\rho(770)$, is, according to our results, a fairly consistent approach to include the $\pi\pi$ interactions. In contrast, one might naively expect that the σ resonance, which is the nearest one to threshold and also has the quantum numbers of the vacuum, should provide the largest contribution to the susceptibility. However, and this is one of the remarkable results of this work, we have shown that in the threshold region it suffers a dramatic cancellation with the (I, J)=$(2, 0)$ interaction. Therefore including just the σ as a free state in a HRG without the $(2, 0)$ interaction, apart from ignoring the fact that the σ is by no means a narrow state, also neglects this very important cancellation.

Moreover, the unitarized partial waves have a much softer behavior for large energies, namely $t(E)$ behaves as a constant, giving rise to the asymptotic behavior $\delta_U(E) \sim$ constant, $\partial\delta_U(E)/\partial M_\pi \sim 1/E^2$. Thus, for the susceptibility in Eq. (45), the interaction part is suppressed with respect to the free one by inverse powers of T and the result is driven by the ChPT one. We have explicitly checked that the contributions to the integrals from energies higher than 1 GeV are very suppressed now, and barely affect our results, contrary to the non-unitarized case.

Thus, in Fig. 4 we plot the non-strange quark condensate using the virial approach with unitarized $\pi\pi$ interactions both within the SU(2) and SU(3) formalisms. The extrapolated melting temperatures are somewhat lower than those coming from standard NNLO ChPT calculations, already given in Fig. 1, particularly for the SU(2) case, this is partly explained, since as we have just discussed we are adding, in practice, the $\rho(770)$ as an additional degree of freedom. Note also that the paramagnetic decrease between the SU(2) and SU(3) cases is just of the order of 6 MeV, which is smaller than the one estimated with NNLO ChPT. Nevertheless this smaller difference is less reliable since it is not calculated with SU(2) LEC obtained from those of SU(3), since the unitarized phases are obtained by fitting to different sets of data in both cases.

Taking into account all the above considerations we have also plotted in Fig. 2 the chiral susceptibility with unitarized pion interactions. The results are similar to NNLO ChPT, and the difference provides the crude estimate of systematic uncertainties, giving rise to a quite consistent picture between ChPT and the virial approach.

V. COMPARISON WITH LATTICE

As explained in the introduction, the light scalar susceptibility is one of the main parameters analyzed in lattice simulations in order to identify its peak position as the transition point. A suitable quantity we can compare with is $\Delta(T) \equiv m^2 \left[\chi_l(T) - \chi_l(0)\right]/M_\pi^4 = \left[\chi_l(T) - \chi_l(0)\right]/(4B_0^2)$, which is given for instance in [6] for 2+1 $SU(3)$ flavor simulations with almost physical quark masses. By subtracting the $T = 0$ value, the lattice analysis of this quantity is free of ultraviolet divergences. Besides, $\Delta(T)$ obtained from the perturbative ChPT result in Eq. (30) is not only independent of B_0 but also of the LEC (in particular of H_2, which is subject to more uncertainty, as explained above). Thus, the ChPT result for $\Delta(T)$ depends only on meson masses and temperature. In the virial case, Eq. (45), there is no B_0 dependence but the result still depends on the LEC, through the $T = 0$ condensates, masses and phase shifts.

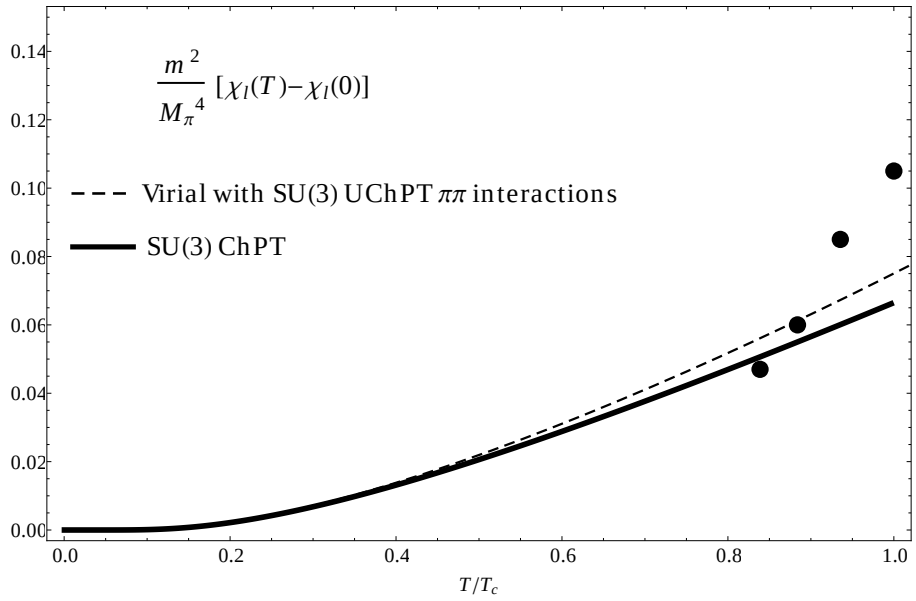

FIG. 5: Normalized relative non-strange scalar susceptibility in $SU(3)$ in terms of the relative temperature, in perturbative ChPT and in the unitarized virial approach. The points are lattice data taken from [6], where $T_c \simeq 155$ MeV.

As discussed previously, the lattice results predict a critical temperature considerably smaller than ChPT or virial extrapolations. This corresponds in part to the relevance of degrees of freedom of higher masses near T_c. Qualitatively, one expects that those degrees of freedom produce a "paramagnetic" reduction of T_c due to the increase of entropy. Thus, in order to establish a more appropriate comparison with lattice results, we will represent the results in terms of the reduced temperature T/T_c for each approach (ChPT, virial and lattice) which is a way to compensate for the number of degrees of freedom involved.

The results for $\Delta(T)$ are plotted in Fig. 5. At very low T, the curves remain close to one another. At high temperatures they grow roughly linear in T, up to the critical region. As stated before, this is a check of the robustness of both approaches, since the unitarized virial result is not only obtained within a different framework but it includes dependencies on the unitarization method and the LEC, thus giving an estimate of systematic uncertainties.

Compared to the lattice data, we see that the two lowest points available are rather well described with the ChPT or unitarized virial curves. This is reassuring, since ChPT is meant to provide the low T model-independent tail. Once the temperature is re-scaled to T_c we see that the agreement is rather good even up to $0.9T_c$, which is remarkable, given that ChPT captures only the qualitative features of the evolution towards chiral restoration but does not develop for instance a maximum, not even a sudden increase of $\Delta(T)$ near T_c. Actually, the lattice points reflect a clear departure from the ChPT prediction as they approach the critical point.

VI. CONCLUSIONS

We have analyzed several properties of the meson gas at low temperatures, regarding four-quark condensates and susceptibilities, within the ChPT and virial expansion approaches. Our analysis provides helpful results for understanding the behavior of the hadron gas formed after a relativistic heavy ion collision, below the chiral phase transition.

The factorization hypothesis for four-quark correlators does not hold in ChPT at finite temperature to NNLO in the chiral expansion. This is an extension of a previous $T = 0$ analysis and is a model independent result. In particular, it means that, in the physical case, the four-quark scalar condensate cannot be used as an order parameter for chiral restoration, since it contains divergent factorization breaking terms that cannot be renormalized. Nevertheless, there are two particular limits in which the four-quark condensate could be considered an order parameter, namely, the the large N_c limit, where factorization holds formally, and the chiral limit, where factorization is still broken, but, contrary to the $T = 0$ case, just by a finite contribution. Let us remark that the factorization breaking terms are precisely those needed to provide finite and scale-independent scalar susceptibilities for the light and strange sector, including the mixed one. We have provided explicit expressions for those susceptibilities in ChPT to leading order in

their chiral expansion. The most important one, regarding chiral restoration, is the light scalar susceptibility, which grows linearly in T at low temperatures.

In order to establish properly the previous factorization results, we have calculated the two-quark condensate in $SU(3)$ up to NNLO in ChPT, including meson interactions with strange degrees of freedom (πK, $\pi\eta$, $K\eta$ and so on). In particular, this allowed us to discuss the effect of those interactions in the crude determination of T_c from the extrapolated condensate. In addition, since the LEC of fourth order enter at that level, we have been able also to estimate the influence of the LEC in the ChPT determination of T_c. The net effect of strange interactions is about $\Delta T_c = 28 \pm 12$ MeV where the error comes from the LEC uncertainty.

An important part of our work has been devoted to the comparison of the ChPT approach with the virial or density expansion, especially for the light scalar susceptibility. We have shown that one should consider unitarized interactions when probing the low and moderate temperatures of interest for this work. Moreover, the unitarized virial curves remain close to the standard ChPT calculation, which is a reflection of the robustness of both approaches, at least at low and moderate T, and shows that the pion interactions are suppressed in thermal observables. This suppression is even larger than expected due to a huge cancellation between the scalar channels with isospin 0 and 2, which is already observed in the data below 1 GeV, but we have found also to occur for the first and second mass derivatives of the interactions. The existence of this cancellation implies that if the sigma particle, which dominates the scalar isoscalar channel near threshold is included alone as a free state, as in the usual hadron resonance gas approach, it can give large deviations from the model independent ChPT approach even at very low temperatures. As a consequence of this cancellation, the $\rho(770)$ dominates the interaction contribution starting at moderate temperatures of the order of 100 to 150 MeV, accelerating the melting of the condensate and the susceptibility growth.

The comparison with lattice data shows a remarkable agreement at those temperatures, when they are re-scaled with respect to the corresponding critical temperatures, i.e., compensating by the number of degrees of freedom involved in the calculation. When we compare between the $SU(2)$ and $SU(3)$ cases, we do not see a significant difference between considering free or interacting kaons and eta compared to the effect of unitarizing the interactions. In the standard virial treatment, where the phase shifts are considered at $T = 0$ and the thermal correction comes from the weight density functions, we have showed that the unitarized interactions decrease with inverse powers of T with respect to the free contribution.

Appendix A: SU(2) results

Here we collect, for completeness, the $SU(2)$ results for the four-quark correlator, factorization and scalar susceptibility.

For the four-quark correlator we get:

$$\langle \mathcal{T}(\bar{q}q)(x)(\bar{q}q)(0)\rangle_{T,\,NLO} = \langle \bar{q}q\rangle^2_{T,\,NLO}, \tag{A1}$$

$$\langle \mathcal{T}(\bar{q}q)(x)(\bar{q}q)(0)\rangle_{T,\,NNLO} = \langle \bar{q}q\rangle^2_{T,\,NNLO} + B_0^2\left[-8i(l_3+h_1)\delta^{(D)}(x) + K^T_{SU2}(x)\right], \tag{A2}$$

where we have defined $K^T_{SU2}(x)$ as the connected part of the four-pion correlator at leading order and finite temperature:

$$K^T_{SU2}(x) = \langle \mathcal{T}\phi^a(x)\phi_a(x)\phi^b(0)\phi_b(0)\rangle_{T,LO} - \langle \mathcal{T}\phi^a(0)\phi_a(0)\rangle^2_{T,LO} = 6G^T_\pi(x)^2. \tag{A3}$$

As it happened in $SU(3)$, to NLO the four-quark correlator can be expressed again as the square of the quark condensate, but not to NNLO where K^T_{SU2} breaks such factorization. As we did in the main text, we are giving Eqs. (A1) and (A2) simplified in terms of the explicit expression for $\langle \bar{q}q\rangle_{T,\,NNLO}$, which are given in Appendix B.

As for factorization, we have from Eq. (A2):

$$\frac{\langle (\bar{q}q)^2\rangle_T}{\langle \bar{q}q\rangle_T^{\,2}} = 1 + \frac{3}{2F^4}\left(G_\pi(0) + g_1(M_\pi, T)\right)^2, \tag{A4}$$

which is again divergent with the standard ChPT renormalization [31].

The $SU(2)$ susceptibility is given by:

$$\chi_l^{SU(2)}(T) \;=\; B_0^2\left[8\left(l_3^r(\mu) + h_1^r(\mu)\right) - 12\nu_\pi + 6g_2(M_\pi, T)\right] + \mathcal{O}\left(\frac{1}{F^2}\right), \tag{A5}$$

$$\tag{A6}$$

An important comment is that the renormalized $SU(2)$ LEC can be written in terms of the $SU(3)$ ones by performing formally an expansion for large strange quark mass in a given observable calculated in $SU(3)$ and comparing with the corresponding $SU(2)$ expression [16], although the numerical difference between them is small. In the $SU(2)$ case, the only two combinations of LEC appearing in the NNLO expression for $\langle\bar{q}q\rangle_T/\langle\bar{q}q\rangle_0$ are l_3^r and $l_3^r+h_1^r$, which can be readily expressed in terms of the $SU(3)$ LEC. Applying such LEC conversion in Eq. (A6) one gets directly the $SU(3)$ expression in Eq. (30) if the $g(M_{k,\eta},T)$ are neglected.

Appendix B: Finite temperature quark condensates to NNLO in ChPT

In this appendix we will provide the NNLO results for the two-quark condensates at finite temperature. As explained in the main text, the corresponding four-quark condensates cannot be obtained just by squaring these results, but one also has to add the factorization breaking contributions described in Eqs. (A2) and (18). The renormalization needed to render the quark condensates finite and scale independent is the same as for $T=0$. Therefore, for all the technical aspects concerning the conventions for the needed $\mathcal{L}_4$ and $\mathcal{L}_6$ LEC and their renormalization, we refer to [31].

For convenience we define:

$$\mu_i(T)=\frac{M_{0i}^2}{32\pi^2F^2}\log\frac{M_{0i}^2}{\mu^2}+\frac{g_1(M_i,T)}{2F^2},\qquad \nu_i(T)=F^2\frac{\partial\mu_i}{\partial M_{0i}^2}=\frac{1}{32\pi^2}\left(1+\log\frac{M_{0i}^2}{\mu^2}\right)-\frac{g_2(M_i,T)}{2}, \tag{B1}$$

where we denote, following the notation in [16], $\mu_i\equiv\mu_i(0)=\mu_i(g_1=0)$.

The final expressions for the two-quark condensates, finite and scale-independent, up to NNLO, at $T\neq 0$ are given by:

$$\langle(\bar{q}q)_l\rangle_{NLO}^{SU(2)}(T) = -2B_0F^2\left\{1+\frac{2M_{0\pi}^2}{F^2}\left(h_1^r+l_3^r\right)-3\mu_\pi(T)\right\}, \tag{B2}$$

$$\begin{aligned}\langle(\bar{q}q)_l\rangle_{NNLO}^{SU(2)}(T) &= \langle\bar{q}q\rangle_{l,NLO}^{SU(2)}-2B_0F^2\left[-\frac{3}{2}\mu_\pi^2(T)-\frac{3M_{0\pi}^2}{F^2}\left(\mu_\pi(T)\nu_\pi(T)+4l_3^r\mu_\pi(T)\right)\right.\\ &+ \left.\frac{3M_{0\pi}^4}{8F^4}\left(-16l_3^r\nu_\pi(T)+\hat{c}_1^r\right)\right],\end{aligned} \tag{B3}$$

$$\langle(\bar{q}q)_l\rangle_{NLO}^{SU(3)}(T) = -2B_0F^2\left\{1+\frac{4}{F^2}\left[\left(H_2^r+4L_6^r+2L_8^r\right)M_{0\pi}^2+8L_6^rM_{0K}^2\right]-3\mu_\pi(T)-2\mu_K(T)-\frac{1}{3}\mu_\eta(T)\right\}, \tag{B4}$$

$$\begin{aligned}\langle(\bar{q}q)_l\rangle_{NNLO}^{SU(3)}(T) &= \langle\bar{q}q\rangle_{l,NLO}^{SU(3)}-2B_0F^2\left\{-\frac{3}{2}\mu_\pi^2(T)+\frac{1}{18}\mu_\eta^2(T)+\mu_\pi(T)\mu_\eta(T)-\frac{4}{3}\mu_K(T)\mu_\eta(T)\right.\\ &+ \frac{1}{F^2}\left[-3M_{0\pi}^2\mu_\pi(T)\nu_\pi(T)+\frac{1}{3}M_{0\pi}^2\mu_\pi(T)\nu_\eta(T)-\frac{8}{9}M_{0K}^2\mu_K(T)\nu_\eta(T)\right.\\ &+ \left.M_{0\pi}^2\mu_\eta(T)\nu_\pi(T)-\frac{4}{3}M_{0K}^2\mu_\eta(T)\nu_K(T)+\frac{1}{27}\left(16M_{0K}^2-7M_{0\pi}^2\right)\mu_\eta(T)\nu_\eta(T)\right]\\ &+ \frac{24}{F^2}\mu_\pi(T)\left[\left(3L_4^r+2L_5^r-6L_6^r-4L_8^r\right)M_{0\pi}^2+2\left(L_4^r-2L_6^r\right)M_{0K}^2\right]\\ &+ \frac{16}{F^2}\mu_K(T)\left[\left(L_4^r-2L_6^r\right)M_{0\pi}^2+2\left(3L_4^r+L_5^r-6L_6^r-2L_8^r\right)M_{0K}^2\right]\\ &+ \frac{8}{9F^2}\mu_\eta(T)\left[\left(-3L_4^r-2L_5^r+6L_6^r-48L_7^r-12L_8^r\right)M_{0\pi}^2+2\left(15L_4^r+4L_5^r-30L_6^r+24L_7^r\right)M_{0K}^2\right]\\ &+ \frac{24M_{0\pi}^2}{F^4}\nu_\pi(T)\left[\left(L_4^r+L_5^r-2L_6^r-2L_8^r\right)M_{0\pi}^2+2\left(L_4^r-2L_6^r\right)M_{0K}^2\right]\\ &+ \frac{16M_{0K}^2}{F^4}\nu_K(T)\left[\left(L_4^r-2L_6^r\right)M_{0\pi}^2+\left(2L_4^r+L_5^r-4L_6^r-2L_8^r\right)M_{0K}^2\right]\\ &+ \frac{8}{27F^4}\nu_\eta(T)\left[\left(-3L_4^r+L_5^r+6L_6^r-48L_7^r-18L_8^r\right)M_{0\pi}^4+2\left(3L_4^r-4L_5^r-6L_6^r+48L_7^r+24L_8^r\right)M_{0\pi}^2M_{0K}^2\right.\\ &+ \left.8\left(3L_4^r+2(L_5^r-3(L_6^r+L_7^r+L_8^r))\right)M_{0K}^4\right]\\ &+ \left.\frac{1}{8F^4}\left[\left(3\hat{C}_1^r-2\hat{C}_2^r+\hat{C}_3^r\right)M_{0\pi}^4+4\left(\hat{C}_2^r-\hat{C}_3^r\right)M_{0\pi}^2M_{0K}^2+4\hat{C}_3^rM_{0K}^4\right]\right\},\end{aligned} \tag{B5}$$

$$\langle\bar{s}s\rangle_{NLO}(T) = -B_0F^2\left\{1+\frac{4}{F^2}\left[-\left(H_2^r-4L_6^r+2L_8^r\right)M_{0\pi}^2+2\left(H_2^r+4L_6^r+2L_8^r\right)M_{0K}^2\right]-4\mu_K(T)-\frac{4}{3}\mu_\eta(T)\right\}, \quad \text{(B6)}$$

$$\begin{aligned}
\langle\bar{s}s\rangle_{NNLO}(T) &= \langle\bar{s}s\rangle_{NLO} - B_0F^2\left\{\frac{8}{9}\mu_\eta^2(T)-\frac{8}{3}\mu_K(T)\mu_\eta(T)+\frac{1}{F^2}\left[\frac{4}{3}M_{0\pi}^2\mu_\pi(T)\nu_\eta(T)\right.\right.\\
&- \left.\frac{32}{9}M_{0K}^2\mu_K(T)\nu_\eta(T)-\frac{8}{3}M_{0K}^2\mu_\eta(T)\nu_K(T)+\frac{4}{27}\left(16M_{0K}^2-7M_{0\pi}^2\right)\mu_\eta(T)\nu_\eta(T)\right]\\
&+ \frac{48}{F^2}\mu_\pi(T)\left(L_4^r-2L_6^r\right)M_{0\pi}^2\\
&+ \frac{32}{F^2}\mu_K(T)\left[\left(L_4^r-2L_6^r\right)M_{0\pi}^2+2\left(2L_4^r+L_5^r-4L_6^r-2L_8^r\right)M_{0K}^2\right]\\
&+ \frac{16}{9F^2}\mu_\eta(T)\left[\left(3L_4^r-4L_5^r-6L_6^r+48L_7^r+24L_8^r\right)M_{0\pi}^2+8\left(3L_4^r+2(L_5^r-3(L_6^r+L_7^r+L_8^r))\right)M_{0K}^2\right]\\
&+ \frac{32M_{0K}^2}{F^4}\nu_K(T)\left[\left(L_4^r-2L_6^r\right)M_{0\pi}^2+\left(2L_4^r+L_5^r-4L_6^r-2L_8^r\right)M_{0K}^2\right]\\
&+ \frac{32}{27F^4}\nu_\eta(T)\left[\left(-3L_4^r+L_5^r+6L_6^r-48L_7^r-18L_8^r\right)M_{0\pi}^4+2\left(3L_4^r-4L_5^r-6L_6^r+48L_7^r+24L_8^r\right)M_{0\pi}^2M_{0K}^2\right.\\
&+ \left.8\left(3L_4^r+2(L_5^r-3(L_6^r+L_7^r+L_8^r))\right)M_{0K}^4\right]\\
&+ \left.\frac{1}{4F^4}\left[\left(\hat{C}_2^r-2\hat{C}_3^r+3\hat{C}_4^r\right)M_{0\pi}^4+4\left(\hat{C}_3^r-3C_4^r\right)M_{0\pi}^2M_{0K}^2+12\hat{C}_4^rM_{0K}^4\right]\right\}, \qquad \text{(B7)}
\end{aligned}$$

where the Gell-Mann-Okubo relation $3M_{0\eta}^2 = 4M_{0K}^2 - M_{0\pi}^2$ for the $SU(3)$ leading order masses has been used and the renormalized L_i^r, l_i^r and $\hat{c}_i^r, \hat{C}_i^r$ constants depend on the scale μ as explained in [31]. We recall that L_4 and L_5 appear because of the meson wave function and mass renormalization. In $SU(3)$, the constant L_7^r stems from the eta mass renormalization.

Acknowledgments

Work partially supported by the Spanish Research contracts FIS2008-01323 and FPA2011-27853-C02-02. We acknowledge the support of the European Community-Research Infrastructure Integrating Activity "Study of Strongly Interacting Matter" (acronym HadronPhysics2, Grant Agreement n. 227431) under the Seventh Framework Programme of EU.

[1] R.D.Pisarski and F.Wilczek, Phys. Rev. D **29**, 338 (1984).
[2] C. Bernard *et al.* [MILC Collaboration], Phys. Rev. D **71**, 034504 (2005).
[3] Y. Aoki, Z. Fodor, S. D. Katz and K. K. Szabo, Phys. Lett. B **643**, 46 (2006).
[4] Y. Aoki, G. Endrodi, Z. Fodor, S. D. Katz and K. K. Szabo, Nature **443**, 675 (2006).
[5] M. Cheng *et al.*, Phys. Rev. D **81**, 054504 (2010).
[6] Y. Aoki, S. Borsanyi, S. Durr, Z. Fodor, S. D. Katz, S. Krieg and K. K. Szabo, JHEP **0906**, 088 (2009).
[7] S. Ejiri *et al.*, Phys. Rev. D **80**, 094505 (2009).
[8] S. Borsanyi, Z. Fodor, C. Hoelbling, S. D. Katz, S. Krieg, C. Ratti and K. K. Szabo [Wuppertal-Budapest Collaboration], JHEP **1009**, 073 (2010).
[9] F. Karsch, K. Redlich and A. Tawfik, Eur. Phys. J. C **29**, 549 (2003).
[10] P. Huovinen and P. Petreczky, Nucl. Phys. A **837**, 26 (2010).
[11] A. Andronic, P. Braun-Munzinger and J. Stachel, Nucl. Phys. A **772**, 167 (2006).
[12] A. Andronic, P. Braun-Munzinger and J. Stachel, Phys. Lett. B **673**, 142 (2009) [Erratum-ibid. B **678**, 516 (2009)].
[13] A. Andronic, P. Braun-Munzinger, J. Stachel and M. Winn, arXiv:1201.0693 [nucl-th].
[14] S. Weinberg, Physica **A96**, 327 (1979).
[15] J. Gasser and H. Leutwyler, Annals Phys. **158**, 142 (1984).
[16] J. Gasser and H. Leutwyler, Nucl. Phys. B **250**, 465 (1985).
[17] P. Gerber and H. Leutwyler, Nucl. Phys. B **321**, 387 (1989).
[18] T. N. Truong, *Phys. Rev. Lett.* **61**, 2526 (1988). A. Dobado, M. J. Herrero and T. N. Truong, *Phys. Lett. B* **235**, 134 (1990).

[19] A. Dobado and J. R. Pelaez, *Phys. Rev. D* **47**, 4883 (1993). *Phys. Rev. D* **56**, 3057 (1997).
[20] A. Gomez Nicola, J. R. Pelaez and G. Rios, Phys. Rev. D **77**, 056006 (2008).
[21] A. Dobado, A. Gomez Nicola, F. J. Llanes-Estrada and J. R. Pelaez, Phys. Rev. C **66**, 055201 (2002).
[22] D. Fernandez-Fraile, A. Gomez Nicola and E. T. Herruzo, Phys. Rev. D **76**, 085020 (2007).
[23] D. Cabrera, D. Fernandez-Fraile and A. Gomez Nicola, Eur. Phys. J. C **61**, 879 (2009).
[24] D. Fernandez-Fraile and A. Gomez Nicola, Eur. Phys. J. C **62**, 37 (2009).
[25] R. Dashen, S. -K. Ma and H. J. Bernstein, Phys. Rev. **187**, 345 (1969).
[26] G. M. Welke, R. Venugopalan, M. Prakash, Phys. Lett. **B245**, 137-141 (1990); V. L. Eletsky, J. I. Kapusta, R. Venugopalan, Phys. Rev. **D48**, 4398-4407 (1993).
[27] A. Nyffeler, Z. Phys. C **60**, 159 (1993).
[28] A. Dobado, J. R. Pelaez, Phys. Rev. **D59**, 034004 (1999).
[29] R. Venugopalan, M. Prakash, Nucl. Phys. **A546**, 718-760 (1992).
[30] J. R. Pelaez, Phys. Rev. D **66**, 096007 (2002).
[31] A. Gomez Nicola, J. R. Pelaez and J. Ruiz de Elvira, Phys. Rev. D **82**, 074012 (2010).
[32] C. Hanhart, J. R. Pelaez and G. Rios, Phys. Rev. Lett. **100**, 152001 (2008). J. R. Pelaez and G. Rios, Phys. Rev. D **82**, 114002 (2010).
[33] J. Nebreda and J. R. Pelaez., Phys. Rev. D **81**, 054035 (2010).
[34] J. Nebreda, J. R. Pelaez and G. Rios, Phys. Rev. D **83**, 094011 (2011).
[35] J. Bijnens, G. Colangelo and G. Ecker, JHEP **9902**, 020 (1999).
[36] M. A. Shifman, A. I. Vainshtein and V. I. Zakharov, Nucl. Phys. B **147**, 385 (1979).
[37] S. Narison and R. Tarrach, Phys. Lett. B **125**, 217 (1983).
[38] G. Leibbrandt, Rev. Mod. Phys. **47**, 849 (1975).
[39] V. L. Eletsky, Phys. Lett. B **299**, 111 (1993).
[40] S. Leupold, Phys. Lett. B **616**, 203 (2005).
[41] S. Leupold, J. Phys. G **32**, 2199 (2006).
[42] M. B. Johnson and L. S. Kisslinger, Phys. Rev. D **61**, 074014 (2000).
[43] A. V. Smilga and J. J. M. Verbaarschot, Phys. Rev. D **54**, 1087 (1996).
[44] A. Gomez Nicola and R. Torres Andres, Phys. Rev. D **83**, 076005 (2011).
[45] G. Amoros, J. Bijnens and P. Talavera, Nucl. Phys. B **602**, 87 (2001).
[46] G. Ecker, J. Gasser, A. Pich and E. de Rafael, Nucl. Phys. B **321**, 311 (1989).
[47] R. Garcia Martin and J. R. Pelaez, Phys. Rev. D **74**, 096003 (2006).
[48] G. Colangelo, J. Gasser and H. Leutwyler, Nucl. Phys. B **603**, 125 (2001).
[49] R. Garcia-Martin, R. Kaminski, J. R. Pelaez, J. Ruiz de Elvira and F. J. Yndurain, Phys. Rev. D **83**, 074004 (2011).
[50] A. Gomez Nicola and J. R. Pelaez, Phys. Rev. D **65**, 054009 (2002).

2.3.5 Pseudoscalar susceptibilities within ChPT

In this Section, we are going to study chiral symmetry restoration through the degeneration of chiral partners. This brief review is just a summary of a future work [259].

As we have reviewed in Section 1.2.3, one of the main consequences of chiral symmetry breaking is the fact that the chiral partners have different masses. As we saw in that Section, if chiral symmetry would be conserved, states with same quantum numbers but opposite parity should have approximately the same mass. However it is not observed experimentally, as it can be seen by studying the vector and axial resonances. For example, the $\rho(770)$ has a mass of 770 MeV, whereas its chiral partner, the $a_1(1260)$, is nearly 500 MeV heavier. Nevertheless, it also occurs in the scalar-pseudoscalar sector. As it is given in eq. (1.35), the σ meson, which has the quark condensate quantum numbers, is the chiral partner of the pion in a O(4) representation, but the former is 300 MeV heavier that the latter. However, it is expected that, when chiral symmetry is restored, the currents corresponding to those mesons will become degenerate in mass. One way to analyze this degeneration is to study, together with the scalar susceptibility, the pseudoscalar susceptibility, since, as we will see, they can be related respectively with the sigma and pion propagator at zero momentum.

Following the external source method used in the previous two publications, and working for $N_f = 2$ and in the isospin limit, so m_u=m_d=m. we can define the pseudoscalar susceptibility as:

$$\chi_P^a = \frac{1}{\beta V}\frac{\partial^2}{\partial p_a^2}\log Z_{QCD}[m,p]\Big|_{p=0} = \int_E d^4x\langle T\bar{q}\gamma_5\frac{\tau^a}{2}q(x)\bar{q}\gamma_5\frac{\tau^a}{2}q(0)\rangle, \tag{2.61}$$

where $Z_{QCD}[p]$ is again the QCD generating functional, and p_a denotes a pseudoscalar source, whose coupling to $\mathcal{L}_{QCD}$ is given in eq. (1.50). Note that, as it can be obtained from eq. (1.34), the vacuum expectation value of $\bar{q}\gamma_5\tau^a q(x)$ vanishes.

In addition, the QCD axial current (1.24) is given by:

$$J_\mu^{5,a}(x) = \bar{q}\gamma_5\gamma_\mu\frac{\tau^a}{2}q(x), \tag{2.62}$$

and its divergence reads, classically:

$$\partial^\mu J_\mu^{5,a}(x) = m\bar{q}\gamma_5\frac{\tau^a}{2}q(x). \tag{2.63}$$

Therefore, eq. (2.63) implies that the pseudoscalar susceptibility is related to the correlator of the divergence of the axial current. Furthermore, using the PCAC relation given in eq. (1.32), we have, at leading order (LO), that:

$$\partial^\mu J_\mu^{5,a}(x) = FM_{0\pi}^2\phi^a(x), \tag{2.64}$$

where as in publications 2.3.3 and 2.3.4, $M_{0\pi}$ is the LO pion mass, F the LO pion decay constant and $\phi^a(x)$ is the pion field, Using then eqs. (2.61), (2.63) and (2.64), we can write the pseudoscalar susceptibility at LO as:

$$\chi_P^{a,LO} = \frac{F^2M_{0\pi}^4}{m^2}\int_E d^4x\langle T\phi^a(x)\phi^a(0)\rangle = \frac{F^2M_{0\pi}^4}{m^2}D_\pi(\mathbf{p}=0) = \frac{F^2M_{0\pi}^4}{m^2}\frac{1}{M_{0\pi}^2}, \tag{2.65}$$

where $D_\pi(\mathbf{p}=0)$ is the Euclidean free pion propagator at zero momentum. Using finally the Gell-Mann-Oakes-formula given in eq. (1.67), we obtain [260]:

$$\chi_P^{LO} = -\frac{\langle \bar{q}q \rangle}{m}, \tag{2.66}$$

which implies that the pseudoscalar susceptibility behaves at LO as the quark-condensate.

However, as we did in publication 2.3.4, we can also use the low-temperature representation of Z_{QCD} in order to calculate the pseudoscalar four-quark correlator and susceptibility within ChPT at low temperatures. Therefore, taking into account that:

$$Z_{QCD}[s,p] \simeq Z_{eff}[s,p] = \int \mathcal{D}\phi^a \exp \int_E d^4x \mathcal{L}_{eff}[\phi^a, s(x), p(x)], \tag{2.67}$$

where $\mathcal{L}_{eff}$ is the ChPT Lagrangian studied in Section 1.3, we can express the pseudoscalar four-quark correlator as:

$$\begin{aligned} \langle T\bar{q}(x)\gamma_5 \frac{\tau^a}{2} q(x) \bar{q}(0)\gamma_5 \frac{\tau^a}{2} q(0)\rangle &= \left\langle T \frac{\delta}{\delta p_a(x)} \frac{\delta}{\delta p_a(0)} \mathcal{L}_{\text{eff}}[p] \right\rangle \Big|_{p=0} \delta(x) \\ &+ \left\langle T \frac{\delta \mathcal{L}_{\text{eff}}}{\delta p_a(x)} \frac{\delta \mathcal{L}_{\text{eff}}}{\delta p_a(0)} \right\rangle \Big|_{p=0}, \end{aligned} \tag{2.68}$$

to obtain that the pseudoscalar susceptibility can be written at next to leading order as (NLO):

$$\chi_P^T = \frac{4B_0^2F^2}{M_{0\pi}^2} \left(1 + 2\frac{M_{0\pi}^2}{F^2}(l_3^r + h_1^r) - 3\frac{M_{0\pi}^2}{F^2}\mu_\pi(T) \right) \tag{2.69}$$

where:

$$\mu_\pi(T) = \frac{M_{0\pi}^2}{32\pi^2F^2} \log \frac{M_{0\pi}^2}{\mu^2} + \frac{g_1(M_\pi, T)}{2F^2} \tag{2.70}$$

As we did in publication 2.3.4, in order to study thermal effects, it is customary to normalize the pseudoscalar susceptibility to its $T=0$ value. In this way we have:

$$\frac{\chi_P^T}{\chi_p^{T=0}} = 1 - \frac{3}{2}\frac{g_1(M_\pi, T)}{F^2} = \frac{\langle \bar{q}q \rangle(T)}{\langle \bar{q}q \rangle(0)} \tag{2.71}$$

so at NLO the normalized pseudoscalar susceptibility behaves as the normalized quark condensate studied in publication 2.3.4. Therefore, as T increases the pseudoscalar susceptibility decreases indicating its critical behaviour, so it is expected χ_P^T vanishes near the critical region.

Using the linear sigma model, or any other model with a symmetry-breaking term proportional to the σ field [260], i.e:

$$\mathcal{L}_{\text{eff}}^{SB\sigma} \sim 2B_0Fs(x)\sigma(x), \tag{2.72}$$

we can express the quark condensate as:

$$\langle \bar{q}q \rangle = -2B_0F\langle \sigma \rangle, \tag{2.73}$$

In addition, the four-quark scalar correlator is given by:

$$\langle T\bar{q}q(x)\bar{q}q(0)\rangle = \frac{\delta}{\delta s(x)}\frac{\delta}{\delta s(0)}\log Z_{QCD}[s,0]\Big|_{s=m} = (2B_0F)^2\langle\sigma(x)\sigma(0)\rangle, \tag{2.74}$$

Then:

$$\langle T\bar{q}q(x)\bar{q}q\rangle - \langle\bar{q}q(0)\rangle^2 = (2B_0F)^2\left[\langle\sigma(x)\sigma(0)\rangle - \langle\sigma\rangle^2\right]. \tag{2.75}$$

Therefore, shifting the sigma field so that its new vacuum expectation value vanishes, i.e.:

$$\tilde{\sigma}(x) = \sigma(x) - \langle\sigma\rangle, \tag{2.76}$$

the scalar susceptibility can also be expressed at LO as the free propagator of the $\tilde{\sigma}$ meson:

$$\chi_S = \int_E d^4x\left[\langle T\bar{q}q(x)\bar{q}q(0)\rangle - \langle\bar{q}q\rangle^2\right] = 4F^2B_0^2D_\sigma(\mathbf{p}=0) = \frac{\langle\bar{q}q\rangle^2}{F^2}\frac{1}{M_\sigma^2}, \tag{2.77}$$

where $D_\sigma(\mathbf{p}=0)$ is the Euclidean free propagator of the σ meson at zero momentum, and M_σ is the $\tilde{\sigma}$ mass, consider as a free state in the Lagrangian. We can see then that eqs. (2.66) and (2.77) relate the pion and sigma propagators at zero momentum with the pseudoscalar and scalar susceptibilities.

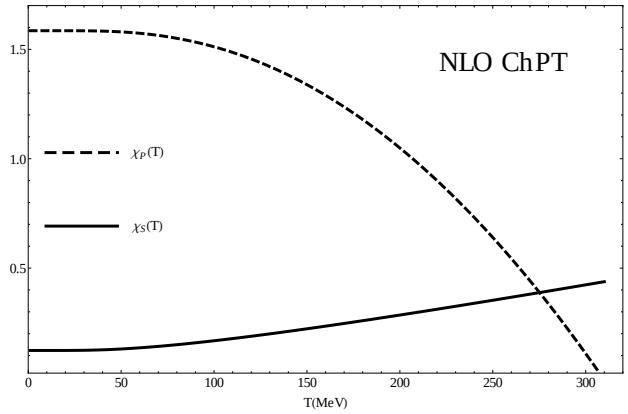

Figure 2.16: Pseudoscalar susceptibility and scalar susceptibility at NL0 within ChPT. We can see that the curves intersect at a temperature close to the melting temperature for the pseudoscalar susceptibility and quark condensates.

The pseudoscalar susceptibility behaves as the quark condensate and decreases with T, whereas the scalar susceptibility increases. Therefore, we can analyze the pion-sigma current degeneration by studying the thermal dependence of the scalar and pseudoscalar susceptibilities. In Fig. 2.16 we can see that both curves intersect at a temperature close to the melting temperature for the pseudoscalar susceptibility and quark condensate, which is another sign of chiral restoration from ChPT extrapolations. It reflects again that we cannot talk about a critical temperature but about a critical region where chiral symmetry restoration takes place.

Conclusions

Throughout this thesis we have studied the properties of $\pi\pi$-scattering and of the lightest scalar resonances appearing in it, the $f_0(500)$ and the $f_0(980)$. In addition, we have studied the role of the lightest scalar in the spontaneous chiral symmetry breaking, by studying the properties of higher quark-condensates configurations and of scalar susceptibilities. We can divide our main contributions in three different blocks.

In the first block, we have provided consistent, precise and model-independent parametrizations of $\pi\pi$-scattering and we have studied the properties of the poles associated with the two lightest scalars without strangeness. These have been obtained from fits to data constrained to satisfying once and twice-subtracted Roy equations. Actually, in this thesis, we have presented the derivation of the once-subtracted Roy equations, called GKPY equations, showing that they are much more precise in the resonance region given the same experimental input. To describe the scattering amplitudes, we have provided a set of simple parametrizations, which allow us to describe the whole energy range from threshold to ~ 20 GeV. These parametrizations, called Unconstrained Fit to Data (UFD), are obtained by fitting experimental data on partial waves below 1.42 GeV, and standard Regge fits above this energy. In particular, we have also made use of the final and very precise data on K_{l4} decays from NA48/2 [154], we have addressed several caveats suggested in the literature and included the isospin violation corrections proposed in [155].

Then, we have improved the central values of our fits requiring, besides fit to data, verification of forward dispersion relations up to 1.42 GeV, Roy and GKPY equations up to 1.1 GeV, and sum rules, obtaining a set of parametrizations that we have called Constrained Fit to Data (CFD). The central values in this CFD lie very well inside those of the UFD, but satisfying remarkably well all dispersion relations. The increased precision provided by the once-subtracted dispersion relations has required an improvement of the S0 wave parametrization to ensure a continuous matching between the low and intermediate energy parametrizations, and has favored the "dip-scenario" for the S0 inelasticity between 1000 and 1100 MeV, (Section 1.7). Using the CFD set as an input in different sum rules and the dispersion relations themselves, we have also provided a precise determination of phases in the elastic regime, threshold parameters and Adler zeros.

Finally, since the newly developed dispersive formalism is especially accurate in the resonance region, in this thesis we have been able to determine, in a model independent way, the

$f_0(500)$, $f_0(980)$ poles and couplings from data with no further theoretical input. As we have commented in previous Sections, both pole estimates have had a considerable impact in the substantial revision of the $f_0(500)$ and $f_0(980)$ properties in the 2012 edition of the Particle Data Group (PDG) Review of Particle Physics [11]. In particular, for the $f_0(500)$ resonance, our result has been used, among few others, by the PDG, in a major revision of their previous central value and uncertainty range for the σ mass and width, which as we showed in Fig. 1.4 was far too conservative, to the new one where all dispersive analysis results lie in.

In a second block, we have studied the nature of the lightest scalars using the $1/N_c$ expansion of QCD, which, as we have seen in Section 1.4, provides insight on their spectroscopic nature, together with other theoretical and phenomenological features as semi-local duality and spectral sum-rules. In order to parametrize the $\pi\pi$-scattering amplitude and to obtain the poles appearing in it, we have used the low energy effective theory of QCD, Chiral Perturbation Theory (ChPT), unitarized within two different approaches: the elastic Inverse Amplitude Method (IAM) and the N/D method.

The elastic IAM relies on the first principles of unitarity, analyticity and reproduces the ChPT expansion up to a desired order. As we have commented in Section 1.6.3, it is derived from a dispersion relation and only depends on the low energy constants (LECs) of ChPT, so there are no spurious parameters that could hide unknown dependencies on QCD parameters. The IAM generates poles on the second Riemann sheet without any assumption on their existence or nature. Thus, it is a very suitable tool to study the properties of these resonances and particularly their N_c scaling.

The N/D method (Section 1.6.2), can be used to describe the most general structure of an elastic partial wave amplitude when the unphysical cuts are neglected. These partial-wave amplitudes can be easily matched to the lowest order ChPT amplitudes and to the exchange of resonances in the s-channel. Therefore, the N/D method is a simple and useful tool to incorporate explicitly resonances satisfying exact unitarity on the right hand cut. Furthermore, it can be easily extended to coupled channels reproducing, consistently with experiment, the poles on the second Riemann sheet associated to the lightest resonances.

In addition, by including the leading $1/N_c$ behavior of the Lagrangian parameters, it is possible to study the $1/N_c$ behavior of the resonances generated with both methods, and compare it with the expected behaviors of different kinds of QCD states, namely $\bar{q}q$, tetraquarks or molecular states and glueballs.

On the one hand, it has been proposed in different models [211, 213, 214, 215, 216, 217, 218, 221] that the lightest scalars have a non-ordinary behaviour. On the other hand, vector resonances behave very well as a expected for $\bar{q}q$ states. As a consequence, vector and scalar resonances have different N_c behaviours [211]. However, any model where this happen is potentially in conflict with semi-local duality in $\pi\pi$-scattering, because as we have seen in Section 1.8.3, it requires a subtle cancellation between the $I = 0$ and $I = 1$ channels, which are dominated by the σ and $\rho(770)$ resonances respectively. If they behave differently at large N_c, this cancellation might be spoil in principle, and thus has to be checked explicitly.

In Section 2.2 of this thesis we have shown how unitarized ChPT avoids this possible conflict. In [211, 220], it was shown within the IAM, that for N_c not to far from the physical

number of colours, the $f_0(500)$ does not behave as a $\bar{q}q$ state, namely the mass and width increase as N_c increases. However, this behaviour is not uniquely fixed at larger N_c, since we have to choose a scale to start the N_c scaling. In practice we have checked that to $\mathcal{O}(p^4)$, several N_c behaviours are possible, which can be classified into two different classes: those where the σ moves far from the real, physical, axis, and those where it has a subdominant $\bar{q}q$-like component above 1 GeV and the σ pole turns back to the real axis for sufficiently large N_c. Actually, this last behaviour has been previously found as the most favours solution of the $\mathcal{O}(p^6)$ [220] . In this thesis, we have checked that within the IAM, for those cases in which the subdominant $\bar{q}q$ component of the σ does not emerge at large N_c, the required cancellation between the σ and the ρ resonances does not hold with N_c, and local duality fails. However, when this subleading component for the σ meson is included, this cancellation holds at all N_c and local duality is still satisfied when increasing the number of colours. Therefore, we conclude that in this approach, this subdominant $\bar{q}q$ component is essential if the scalar channel is to compensate the ρ $\bar{q}q$ contribution.

We have also studied that semi-local duality could also be satisfied in an N/D coupled channel approach within a $U(3)$ formalism. As we have reviewed in Section 1.4.3, the η' mass decreases with N_c, becoming in this regime the ninth NGB. In first place, and anticipated in [221], we have checked that the $f_0(500)$ is marginally coupled to the different η' channels, making it reasonable to neglect their contributions when studying the $f_0(500)$ dynamic. In agreement with the previous IAM results of [211, 220], the sigma pole moves initially deep in the complex plane as N_c increases, showing again a non-dominant $\bar{q}q$ behaviour. However, for higher N_c values, the σ poles bends in this case to the left of the s-complex plane, and thus, it does not contribute to cancel the $\rho(770)$ amplitude. However, we have shown within this approach, that there is also a $\bar{q}q$ subleading component with a mass around 1 GeV, this time in the $f_0(980)$ which, as in the IAM case, also compensate the $\rho(770)$ contribution. Nevertheless, here we need to include some "ad hoc" $1/N_c$ subleading components in the resonance behaviour (by fitting then to the appropriate behaviour to cancel the $I_t = 2$ $\pi\pi$-scattering channel), and we want to remark that the σ pole ends up in a very unphysical position, with $\mathrm{Re}\, s_{\mathrm{pole}} < 0$. It is important to remark that both within the N/D and the IAM formalisms, a $\bar{q}q$ state with a mass around 1 GeV is needed in order to satisfy semi-local duality.

We have also studied in this block the N_c behaviour of the mass, width and couplings, of different QCD quark and gluon configurations that could be constituent of the σ. We have checked that none of these states reproduces by itself the expected behaviour of the mass and width of the $f_0(500)$ found in [220], so it is concluded that the σ must be a mixture of different states. Finally, we have presented a model where a Fock decomposition of the σ in terms of QCD degrees of freedom is analyzed. By considering just three different QCD states, namely $\bar{q}q$, tetraquark or molecular state and the glueball, we have truncated the Fock space yielding a symmetric Hamiltonian which represents the lowest lying scalar sector. The lowest eigenvalue must be identified with the σ meson and the free coefficients of the Hamiltonian are fitted to the σ mass and width obtained in [220] as a function of N_c. From this fit we are able to estimate the proportion of each of these states in the σ meson, concluding that the molecular or tetraquark contributions is dominant at the physical number of colours, and giving a crude estimate of its composition.

Finally, in a third block we have analyzed the role or the $f_0(500)$ resonance in the chiral

symmetry restoration, by studying its influence in the quark condensate and in the scalar susceptibility. In order to do that, we have first studied these two observables at $T = 0$, within ChPT. The scalar susceptibility can be calculated in two ways: either as the quark mass derivative of the quark condensate, or as the difference between the four-quark correlator and the square of the quark condensate. When cross checking these two calculations, we came across an interesting and model independent result for the four-quark condensate, namely that the usual factorization hypothesis does not hold within next to next to leading order (NNLO) ChPT. This is a relevant result by itself because the four-quark condensate appears directly in QCD sum rules, through the operator product expansion, where it is usually assumed that the four-quark condensate factorizes as the square of the two-quark condensate. In particular, we have checked in this thesis that at next to leading order, the four-quark condensate factorizes, but at NNLO, a term with a nontrivial spacetime dependence yields a divergent four-quark condensate. This divergence vanishes, however, in the chiral limit, which is the regime where the spontaneous chiral symmetry formally takes place. Furthermore, we have shown that these NNLO factorization breaking terms are precisely those needed to yield a finite scalar susceptibility.

Following with our susceptibility calculation, at $T \neq 0$, we have used two different and model independent approaches, ChPT and the virial expansion. Within standard ChPT, we have simply calculated the four-quark condensate, this time at finite T, obtaining that it is divergent at NNLO, not only due to the pure $T = 0$ contribution. Nevertheless, it becomes finite either at large N_c or in the chiral limit, which strictly speaking is the only regime where it can be considered an order parameter of the spontaneous chiral symmetry restoration. In the case of the scalar susceptibility, we have studied its behaviour for low T, where we know that the ChPT expansion converges, obtaining that it grows linearly with T. Within the virial expansion, we have first studied non-unitarized ChPT interactions, because they provide model independent information although just limited to very low temperatures, showing strong cancellation between the scalar $I = 0$ and $I = 2$ partial waves. Finally, in order to study the role of the σ resonance, we have used the IAM. As we have seen in Section 1.6.3, this method is able to reproduce resonances, but recovering the chiral expansion at low energies. In this way we can isolate the role of the σ, ensuring that at low temperatures we still reproduce the previous model independent results. Using this approach, we have obtained that the contribution of the $f_0(500)$ to the quark-condensate and the scalar susceptibility is largely canceled by the $I = 2$ $J = 0$ amplitude, giving together a negligible contribution to both observables at low temperatures. Furthermore, at higher temperatures, the $\rho(770)$ contribution dominates the contribution of the pion interactions to the pressure, quark condensate and scalar susceptibility in a low temperature hadron gas. Therefore, our results invalidate the naive expectations of those hadron gas models that include the $f_0(500)$ alone, without taking into account the $I = 2$ scalar interactions, since the two of them cancel, and barely contribute to chiral symmetry restoration.

We think that these results have contributed to shed some light into the non–ordinary nature of the very controversial scalar mesons, and we hope they will also be useful as a guiding tool for future studies.

Derivation of Roy equations

In this appendix we show an explicit derivation of the Roy or twice subtracted dispersion relations for partial wave amplitudes introduced in this 1.7. We will follow the original Roy's article [169].

We begin from a twice subtracted general dispersion relation for an amplitude $T(s,t,u)$ describing a given $\pi\pi \to \pi\pi$ scattering process at fixed t, then, from eq. (1.131) we have:

$$T(s,t,u) = \alpha(t) + s\,\beta(t) + \frac{s^2}{\pi}\int_{4m_\pi^2}^{\infty} ds'\,\frac{\mathrm{Im}T(s',t,u')}{s'^2(s'-s)} + \frac{s^2}{\pi}\int_{-t}^{-\infty} ds'\,\frac{\mathrm{Im}T(s',t,u')}{s'^2(s'-s)}, \tag{A.1}$$

where $\alpha(t)$ and $\beta(t)$ are the subtraction constants. The first step is to rewrite the second integral, that is the integral over the left hand cut, as in integral over the right hand cut. Taking into account that $s = 4m_\pi^2 - t - u$ and $s' = 4m_\pi^2 - t - u'$, we can rewrite the kinematical coefficient which multiplies to the amplitude in the second integral as:

$$\begin{aligned}\frac{s^2}{s'^2(s'-s)} &= -\frac{u^2}{u'^2(u'-u)} - \left[\frac{1}{u'} + \frac{1}{4m_\pi^2 - t - u'} + \frac{4m_\pi^2 - t}{u'^2}\right] \\ &\quad -s\left[\frac{1}{(4m_\pi^2 - t - u')^2} - \frac{1}{u'^2}\right],\end{aligned} \tag{A.2}$$

so eq. (A.1) reads:

$$\begin{aligned}T(s,t,u) &= \alpha(t) + s\,\beta(t) + \frac{s^2}{\pi}\int_{4m_\pi^2}^{\infty} ds'\,\frac{\mathrm{Im}T(s',t,u')}{s'^2(s'-s)} + \frac{u^2}{\pi}\int_{-t}^{-\infty} du'\,\frac{\mathrm{Im}T(4m^2 - t - u',t,u')}{u'^2(u'-u)} \\ &\quad + \frac{1}{\pi}\int_{4m_\pi^2}^{\infty} du'\left[\frac{1}{u'} + \frac{1}{4m_\pi^2 - t - u'} + \frac{4m_\pi^2 - t}{u'^2}\right]\mathrm{Im}T(4m_\pi^2 - t - u',t,u') \\ &\quad + \frac{s}{\pi}\int_{4m_\pi^2}^{\infty} du'\left[\frac{1}{(4m_\pi^2 - t - u')^2} - \frac{1}{u'^2}\right]\mathrm{Im}T(4m_\pi^2 - t - u',t,u').\end{aligned} \tag{A.3}$$

Eq. (A.3) can be simplified considerably defining two new subtraction constants as:

$$\begin{aligned}\tilde{\alpha}(t) &= \alpha(t) + \frac{1}{\pi}\int_{4m_\pi^2}^{\infty} du'\left[\frac{1}{u'} + \frac{1}{4m_\pi^2 - t - u'} + \frac{4m_\pi^2 - t}{u'^2}\right]\mathrm{Im}T(4m_\pi^2 - t - u',t,u') \\ \tilde{\beta}(t) &= \beta(t) + \frac{1}{\pi}\int_{4m_\pi^2}^{\infty} du'\left[\frac{1}{(4m_\pi^2 - t - u')^2} - \frac{1}{u'^2}\right]\mathrm{Im}T(4m_\pi^2 - t - u',t,u').\end{aligned}$$

so:

$$T(s,t,u) = \tilde{\alpha}(t) + s\,\tilde{\beta}(t) \quad + \quad \frac{s^2}{\pi}\int_{4m_\pi^2}^{\infty} ds'\,\frac{\mathrm{Im}T(s',t,u')}{s'^2(s'-s)} \\ + \quad \frac{u^2}{\pi}\int_{4m_\pi^2}^{\infty} du'\,\frac{\mathrm{Im}T(4m^2-t-u',t,u')}{u'^2(u'-u)}, \tag{A.4}$$

However, for future convenience, we redefine the subtraction constants as:

$$\bar{\alpha}(t) = \tilde{\alpha}(t) + \frac{1}{2}(4m_\pi^2 - t)\tilde{\beta}(t) \tag{A.5}$$

$$\bar{\beta}(t) = \frac{1}{2}\tilde{\beta}(t) \tag{A.6}$$

Therefore, we can finally write eq. (A.1) as:

$$T(s,t,u) = \bar{\alpha}(t) + (s-u)\,\bar{\beta}(t) + \frac{s^2}{\pi}\int_{4m_\pi^2}^{\infty} ds'\,\frac{\mathrm{Im}T(s',t,4m_\pi^2-t-s')}{s'^2(s'-s)} \\ + \frac{u^2}{\pi}\int_{4m_\pi^2}^{\infty} du'\,\frac{\mathrm{Im}T(4m_\pi^2-t-u',t,u')}{u'^2(u'-u)}. \tag{A.7}$$

As remarked above, eq. (A.7) is valid for any $\pi\pi$-scattering amplitude this, and in particular for each isospin amplitude $T^I(s,t,u)$. As a consequence, and for convenience, we can gather the three dispersion relation for each isospin in the s-channel in a vector like formalism. Defining $\vec{T}(s,t,u)$ as the isovector amplitude with components (T^0,T^1,T^2), and $\vec{A}(t)$ and $\vec{B}(t)$ the isovector subtraction constants with components $(\bar{\alpha}^0,\bar{\alpha}^1,\bar{\alpha}^2)$ and $(\bar{\beta}^0,\bar{\beta}^1,\bar{\beta}^2)$. Therefore, following this convention, eq. (A.7) can be written as:

$$\vec{T}(s,t,u) = \vec{A}(t) + (s-u)\,\vec{B}(t) + \frac{s^2}{\pi}\int_{4m_\pi^2}^{\infty} ds'\,\frac{\mathrm{Im}\vec{T}(s',t,4m_\pi^2-t-s')}{s'^2(s'-s)} \\ + \frac{u^2}{\pi}\int_{4m_\pi^2}^{\infty} du'\,\frac{\mathrm{Im}\vec{T}(4m_\pi^2-t-u',t,u')}{u'^2(u'-u)}. \tag{A.8}$$

However, we can use the fact that $\pi\pi$-scattering amplitudes with definite isospin in each channel can be expressed through the crossing matrices of eq. (1.188) as:

$$\vec{T}(s,t,u) = C_{st}\,\vec{T}(t,s,u) = C_{su}\,\vec{T}(u,t,s) = C_{tu}\,\vec{T}(s,u,t). \tag{A.9}$$

Using the second equality in the second term of (A.8), we can thus rewrite this equation as:

$$\vec{T}(s,t,u) = \vec{A}(t) + (s-u)\vec{B}(t) + \frac{1}{\pi}\int_{4m_\pi^2}^{\infty}\frac{ds'}{s'^2}\left[\frac{s^2}{s'-s} + \frac{u^2}{s'-u}C_{su}\right]\mathrm{Im}\,\vec{T}(s',t,u'). \tag{A.10}$$

As we have seen in Sections 1.7 and 1.8, $\pi\pi$-scattering amplitudes with well defined isospin in t-channel have definite symmetry properties under $s \leftrightarrow u$ exchange. In particular, $T^{I_t=0}(s,t,u)$ and $T^{I_t=2}(s,t,u)$ are symmetric under such exchange, whereas $T^{I_t=1}(s,t,u)$ is

antisymmetric. In particular, since the subtraction constants $\vec{A}(t)$ and $\vec{B}(t)$ do not depended on s and u are symmetric under this interchange, so:

$$C_{st}A(t) = \vec{C}(t) = \begin{pmatrix} c^0(t) \\ 0 \\ c^2(t) \end{pmatrix} \tag{A.11}$$

$$C_{st}(s-u)B(t) = \vec{D}(t) = \begin{pmatrix} 0 \\ d(t) \\ 0 \end{pmatrix},$$

and since as we have seen in eq. (1.189) $C_{st}^2 = \mathbb{1}$, it is convenient recast the subtraction terms as:

$$\vec{A}(t) + (s-u)\vec{B}(t) = C_{st}[\vec{C}(t) + (s-u)\vec{D}(t)] \tag{A.12}$$

Therefore eq. A.10 reads:

$$\vec{T}(s,t,u) = C_{st}[\vec{C}(t) + (s-u)\vec{D}(t)] + \frac{1}{\pi}\int_{4m_\pi^2}^{\infty} \frac{ds'}{s'^2}\left[\frac{s^2}{s'-s} + \frac{u^2}{s'-u}C_{su}\right] \text{Im}\,\vec{T}(s',t,u'). \tag{A.13}$$

The next step is try extract relations between the subtraction constants and the amplitudes by evaluating them at chosen points. In particular, on the one hand, setting $s = 0$ in eq. (A.13), we have:

$$T(0,t,4m^2-t) = C_{st}[\vec{C}(t) + (t-4m_\pi^2)\vec{D}(t)] + \frac{1}{\pi}\int_{4m_\pi^2}^{\infty} \frac{ds'}{s'^2}\frac{(4m_\pi^2-t)^2}{s'-4m_\pi^2+t}C_{su}\text{Im}\,\vec{T}(s',t,u'), \tag{A.14}$$

on the other hand, for $T(t,0,4m^2-t)$, we can write:

$$\begin{aligned} T(t,0,4m^2-t) \;=\; & C_{st}[\vec{C}(0) + (2t-4m_\pi^2)\vec{D}(0)] \\ & + \frac{1}{\pi}\int_{4m_\pi^2}^{\infty} \frac{ds'}{s'^2}\left(\frac{t^2}{s'-t} + \frac{(4m_\pi^2-t)^2}{s'-4m_\pi^2+t}C_{su}\right)\text{Im}\,\vec{T}(s',0,u'). \end{aligned} \tag{A.15}$$

However, eqs. (A.14) and (A.15) are related since, $C_{st}\vec{T}(0,t,u') = \vec{T}(t,0,u')$. Furthermore, given the value of C_{tu} in eq. (1.189), we can see that: $C_{tu}\vec{C}(t) = \vec{C}(t)$ and $C_{tu}\vec{D}(t) = -\vec{D}(t)$. so, since $(1 \pm C_{tu})/2$ are orthogonal projectors, we have:

$$\frac{1+C_{tu}}{2}\vec{C}(t) = \vec{C}(t), \quad \frac{1+C_{tu}}{2}\vec{D}(t) = 0, \tag{A.16}$$

$$\frac{1-C_{tu}}{2}\vec{C}(t) = 0, \qquad \frac{1-C_{tu}}{2}\vec{D}(t) = \vec{D}(t), \tag{A.17}$$

which implies that the subtraction constants satisfy:

$$\vec{C}(t) = \frac{1+C_{tu}}{2}[\vec{C}(t) + (t-4m_\pi^2)\vec{D}(t)], \tag{A.18}$$

$$\vec{D}(t) = \frac{1-C_{tu}}{2}\frac{\vec{C}(t) + (t-4m_\pi^2)\vec{D}(t)}{t-4m_\pi^2}.$$

From the relation between eqs. (A.14) and (A.15), from eq. (A.18) and by using the product properties of the crossing matrices, namely, $C_{st}(1 \pm C_{tu})C_{st} = 1 \pm C_{su}$ and $(1 \pm C_{tu})C_{st}C_{su} = C_{st}(C_{su} \pm 1)$, we can write the dispersion relation given in eq. (A.13) as:

$$\begin{aligned}\vec{T}(s,t,u) = &\left(\frac{1+C_{su}}{2} + \frac{s-u}{t-4m_\pi^2}\frac{1-C_{su}}{2}\right)[\vec{C}(0) + (2t-4m_\pi^2)\vec{D}(0)] \\ &+ \int_{4m_\pi^2}^{\infty}\frac{ds'}{\pi s'^2}C_{st}\left(\frac{1+C_{tu}}{2} + \frac{s-u}{t-4m_\pi^2}\frac{1-C_{tu}}{2}\right) \\ &\times\left(\frac{t^2}{s'-t} + \frac{(4m_\pi^2-t)^2}{s'-4m_\pi^2+t}C_{su}\right)\mathrm{Im}\,\vec{T}(s',0,u') \\ &+ \int_{4m_\pi^2}^{\infty}\frac{ds'}{\pi s'^2}\left[\frac{s^2}{s'-s} + \frac{u^2}{s'-u}C_{su}\right. \\ &\left.-\frac{(4m_\pi^2-t)^2}{s'-4m_\pi^2+t}\left(\frac{C_{su}+1}{2} + \frac{s-u}{t-4m_\pi^2}\frac{C_{su}-1}{2}\right)\right]\mathrm{Im}\,\vec{T}(s',t,u').\end{aligned} \tag{A.19}$$

The integrals are now over the right hand cut of the s-channel, as we were looking for, but, however, we have still an unknown dependence on the subtraction constants. Nevertheless, at threshold, we have from eq. (A.15):

$$\vec{T}(4m_\pi^2,0,0) = C_{st}[\vec{C}(0) + 4m_\pi^2\vec{D}(0)] + \frac{1}{\pi}\int_{4m_\pi^2}^{\infty}\frac{ds'}{s'^2}\frac{16m_\pi^4}{s'-4m_\pi^2}\mathrm{Im}\,\vec{T}(s',0,u'), \tag{A.20}$$

so we can express $[\vec{C}(0) + 4m_\pi^2\vec{D}(0)]$ as a function of the amplitude at threshold and an integral over the right hand cut. Furthermore, from eq. (A.18), we have that:

$$\vec{C}(0) + (2t-4m_\pi^2)\vec{D}(0) = \left(\frac{1+C_{tu}}{2} + \frac{2t-4m_\pi^2}{4m_\pi^2}\frac{1-C_{tu}}{2}\right)\left[\vec{C}(0) + 4m_\pi^2\vec{D}(0)\right], \tag{A.21}$$

which implies that we have the following expression for the subtraction terms given in eq. (A.19):

$$\begin{aligned}&\left(\frac{1+C_{su}}{2} + \frac{s-u}{t-4m_\pi^2}\frac{1-C_{su}}{2}\right)\left(\frac{1+C_{tu}}{2} + \frac{2t-4m_\pi^2}{4m_\pi^2}\frac{1-C_{tu}}{2}\right)C_{st}\times \\ &\qquad\left\{\vec{T}(4m_\pi^2,0,0) - \int_{4m_\pi^2}^{\infty}\frac{1}{\pi s'^2}\frac{16m_\pi^4}{s'-4m_\pi^2}\mathrm{Im}\,\vec{T}(s',0,u)\right\}.\end{aligned}$$

The two first terms in bracket can be simplified as

$$\begin{aligned}&\left(\frac{1+C_{su}}{2} + \frac{s-u}{t-4m_\pi^2}\frac{1-C_{su}}{2}\right)\left(\frac{1+C_{tu}}{2} + \frac{2t-4m_\pi^2}{4m_\pi^2}\frac{1-C_{tu}}{2}\right)C_{st} = \\ &\qquad\left(\frac{1+C_{su}}{2} + \frac{s-u}{t-4m_\pi^2}\frac{1-C_{su}}{2}\right)C_{st}\left(\frac{1+C_{su}}{2} + \frac{2t-4m_\pi^2}{4m_\pi^2}\frac{1-C_{su}}{2}\right) = \\ &\qquad C_{st}\left(\frac{1+C_{tu}}{2} + \frac{s-u}{t-4m_\pi^2}\frac{1-C_{tu}}{2}\right)\left(\frac{1+C_{su}}{2} + \frac{2t-4m_\pi^2}{4m_\pi^2}\frac{1-C_{su}}{2}\right),\end{aligned} \tag{A.22}$$

and after working out the last bracket together with the integrand we can write it as:

$$\frac{16m_\pi^4}{s'-4m_\pi^2}\left(\frac{1+C_{su}}{2}+\frac{2t-4m_\pi^2}{4m_\pi^2}\frac{1-C_{su}}{2}\right)= \frac{1}{2}\frac{4m_\pi^2}{s'-4m_\pi^2}\left[4m_\pi^2+4m_\pi^2C_{su}+(2t-4m_\pi^2)+(-2t+4m_\pi^2)C_{su}\right]= \frac{4m_\pi^2t+4m_\pi^2(4m_\pi^2-t)C_{su}}{s'-4m_\pi^2},$$

Including all these simplification, we can write eq.(A.19) as:

$$\vec{T}(s,t,u)=\text{S.T.}+\int_{4m_\pi^2}^{\infty}ds'g_2(s,t;s')\text{Im}\,\vec{T}(s',0,u')+\int_{4m_\pi^2}^{\infty}ds'g_3(s,t;s')\text{Im}\,\vec{T}(s',t,u'), \quad (A.23)$$

with

$$\text{S.T.}=\left(\frac{1+C_{su}}{2}+\frac{s-u}{t-4m_\pi^2}\frac{1-C_{su}}{2}\right)\left(\frac{1+C_{tu}}{2}+\frac{2t-4m_\pi^2}{4m_\pi^2}\frac{1-C_{tu}}{2}\right)C_{st}\vec{T}(4m_\pi^2,0), \quad (A.24)$$

$$g_2(s,t;s')=C_{st}\left(\frac{1+C_{tu}}{2}+\frac{s-u}{t-4m_\pi^2}\frac{1-C_{tu}}{2}\right)\times \frac{1}{\pi s'^2}\left(\frac{t^2}{s'-t}+\frac{(4m_\pi^2-t)^2}{s'-4m_\pi^2+t}C_{su}-\frac{4m_\pi^2t+4m_\pi^2(4m_\pi^2-t)C_{su}}{s'-4m_\pi^2}\right) \quad (A.25)$$

and

$$g_3(s,t;s')=\frac{1}{\pi s'^2}\left[\frac{s^2}{s'-s}+\frac{u^2}{s'-u}C_{su}-\frac{(4m_\pi^2-t)^2}{s'-4m_\pi^2+t}\left(\frac{C_{su}+1}{2}+\frac{s-u}{t-4m_\pi^2}\frac{C_{su}-1}{2}\right)\right]. \quad (A.26)$$

The subtraction term S.T. still needs to be worked out. In order to do this we have to remember that the amplitude at threshold corresponds, apart from constant factors, to the scattering lengths of the process. This means that the $I=1$ component shall vanish, and we can make use of the fact that $C_{tu}\vec{T}(4m_\pi^2,0,0)=\vec{T}(4m_\pi^2,0.0)$ and $(1-C_{tu})\vec{T}(4m_\pi^2,0.0)=0$. We have:

$$\text{S.T.}=\left(\frac{1+C_{su}}{2}+\frac{s-u}{t-4m_\pi^2}\frac{1-C_{su}}{2}\right)\left(\frac{1+C_{tu}}{2}+\frac{2t-4m_\pi^2}{4m_\pi^2}\frac{1-C_{tu}}{2}\right)C_{st}\vec{T}(4m_\pi^2,0)= \left(-\frac{u+sC_{su}}{t-4m_\pi^2}\right)\frac{t+(4m_\pi^2-t)C_{tu}}{4m_\pi^2}C_{st}\vec{T}(4m_\pi^2,0)= \frac{1}{4m_\pi^2}\left[-\frac{u+sC_{su}}{t-4m_\pi^2}t+(u+sC_{su})C_{tu}\right]C_{st}\vec{T}(4m_\pi^2,0),$$

and rewriting u in terms of s and t,

$$\text{S.T.}=\frac{1}{4m_\pi^2}\left[-\frac{4m_\pi^2-t-s(1-C_{su})}{t-4m_\pi^2}t+(4m_\pi^2-t-s)C_{tu}+sC_{su}C_{tu}\right]C_{st}\vec{T}(4m_\pi^2,0)= \frac{1}{4m_\pi^2}\left[tC_{st}+\frac{st}{t-4m_\pi^2}(1-C_{su})C_{st}+(4m_\pi^2-t)C_{tu}C_{st}+s(C_{su}-1)C_{tu}C_{st}\right]\vec{T}(4m_\pi^2,0).$$

Now, $(1-C_{su})C_{st} = C_{st}(1-C_{tu})$, and the $st/(t-4m_\pi^2)$ does not contribute. The tC_{st} term is already in the form we want, to put the remaining terms in a simpler form we just substitute $\vec{T}(4m_\pi^2,0)$ by $C_{tu}\vec{T}(4m_\pi^2,0)$ in them, obtaining:

$$\text{S.T.} = \frac{1}{4m_\pi^2}\left[s(1-C_{su}) + tC_{st} - tC_{tu}C_{st} + 4m_\pi^2 C_{tu}C_{st}\right]\vec{T}(4m_\pi^2,0) = \frac{1}{4m_\pi^2}\left[s(1-C_{su}) + t(C_{st}-C_{su}) + 4m_\pi^2 C_{su}\right]\vec{T}(4m_\pi^2,0),$$

which is finally in the form given by Roy.

We can now project into partial-waves, to obtain

$$\begin{aligned}\text{Re}\,\vec{t}_J(s) &= \frac{1}{32\pi}\int_0^1 dx\, P_J(x)\vec{T}(s,t(x)) \\ &= \frac{1}{32\pi}\int_0^1 dx\, P_J(x)\ \text{S.T.} + \\ &\quad \sum_{J'}(2J'+1)\int_{4m_\pi^2}^\infty ds' \int_0^1 dx\, P_J(x)\left[g_2(s,t(x);s') + P_{J'}(x)g_3(s,t(x);s')\right]\text{Im}\,\vec{t}_{J'}(s')\end{aligned}$$

which can be rewritten as:

$$\text{Re}\,t_{IJ}(s) = ST_J^I(s) + \sum_I\sum_{J'}\int_{4m_\pi^2}^\infty ds' K_{JJ'}^{II'}(s',s)\text{Im}\,t_{I'J'}, \tag{A.27}$$

which is eq. (1.206).

The Sommerfeld-Watson transform

In this section we will derive the Regge high energy representation of scattering amplitudes given in eq. (1.214) and that we have used thorough in this thesis. A detailed derivation and analysis of Regge formulas can be found in [180, 181, 106, 107].

Regge Theory is based on the properties of the analytical continuation of the amplitudes to complex values of the angular momentum. Analogously to the s-channel partial wave series of eq. (1.132), it is possible to write a t-channel partial-wave series of spinless particles as:

$$T(s,t,u) = 16\pi N \sum_J (2J+1) P_J(z_t) t_J(t) \tag{B.1}$$

where in our case of interest, $\pi\pi$-scattering, we have:

$$z_t = 1 + \frac{2s}{t - 4m_\pi^2} \tag{B.2}$$

In order to perform the analytic continuation of the partial-wave series of eq. (B.1) to complex values of the angular momentum, one needs to express the total amplitude in a way that is explicitly J-dependent and which does not assume J to be an integer. That is, we need to regard J as a complex variable and introduce a partial-wave amplitude $t(J,t)$ that coincides with $t_J(t)$ at physical values of J. However this interpolation is not unique: it is always possible to add a function which is zero for physical values of J, so it is also needed to impose some conditions which makes this interpolation unique. The conditions imposed follow from the Carlson's theorem which states that if $f(z)$ is a function which satisfies:

1. $f(z)$ is analytic in Re$z > K$, where K is a real constant.
2. $f(z) < \exp(M|z|)$, where $M < \pi$ in Re $> K$.
3. $f(z) = 0$ at an infinite sequence of positive integer numbers then.

then, $f(z) = 0$. Therefore, if $t(J,t)$ is a function which satisfies the two first condition, then it is uniquely defined. However, the partial-wave amplitude:

$$t(J,t) = \frac{1}{32\pi} \int_{-1}^{1} dz_t P_J(z_t) T(s,t,u), \tag{B.3}$$

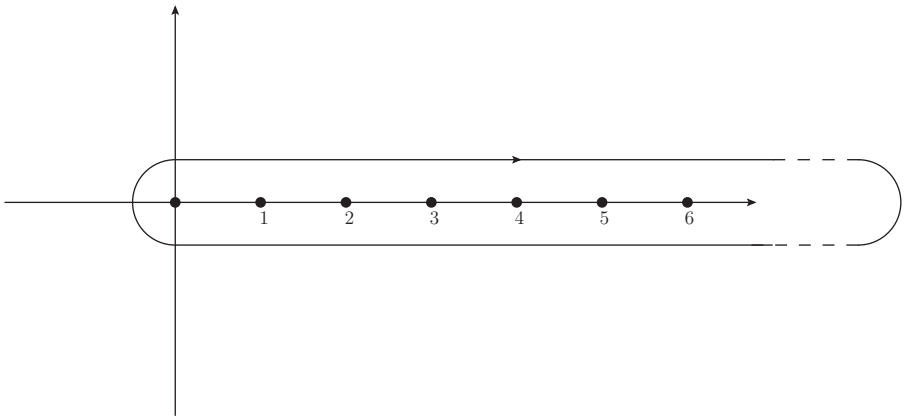

Figure B.1: An integration contour C in the complex J-plane surrounding the poles at integer values of J.

do not satisfy the Carlson's theorem since:

$$P_J(\cos\theta) \xrightarrow[J\to\infty]{} J^{1/2}\left(K_1 e^{iJ\theta} + K_2 e^{-iJ\theta}\right),$$

where K_1 and K_2 are constants and $|\cos\theta| < 1$, which implies that $t(J,t)$ does not satisfy the second condition.

Nevertheless we can avoid this problem by introducing the partial-wave amplitudes $t^{\pm}(J,t)$ defined as $t_J(t)$ for even and odd values of J respectively, i.e.

$$t^{+}(J,t) = t_J(t), \quad \text{for } J \text{ even}, \tag{B.4}$$
$$t^{-}(J,t) = t_J(t), \quad \text{for } J \text{ odd}. \tag{B.5}$$

Since $P_J(-z_t) = (-1)^J P_J(z_t)$, we can define the amplitudes:

$$T^{\pm}(s,t,u) = 8\pi N \sum_{l=0}^{\infty} (2J+1) t^{\pm}(J,t)\,(P_J(z_t) \pm P_J(-z_t)), \tag{B.6}$$

where $t^{\pm}(J,t)$ satisfy now the Carlson's theorem conditions [106] and:

$$T(s,t,u) = T^{+}(s,t,u) + T^{-}(s,t,u). \tag{B.7}$$

If we replace now the sum over the momentum J in eq. (B.1) by the contour integral over the path C of Fig. B.1, and we assume that $t^{\pm}(J,t)$ are analytic function of J throughout the right-hand half of the J-plane with only isolated poles, which has been proved order-by-order in perturbation theory, we can use Cauchy's theorem to rewrite the partial-wave series as:

$$T^{\pm}(s,t,u) = 8\pi N i \int_C dJ (2J+1) t^{\pm}(J,t) \frac{P_J(-z_t) \pm P_J(z_t)}{\sin(\pi J)}. \tag{B.8}$$

Now, if we replace the contour integral over C by that over C' and C'', showed in Fig. B.2, where C' consists of a line at $\mathrm{Re}J = -1/2$, and a semicircle which closes the path enclosing all the non-negative integers clockwise, since the partial-wave amplitudes $t^{\pm}(J,t)$ are uniquely

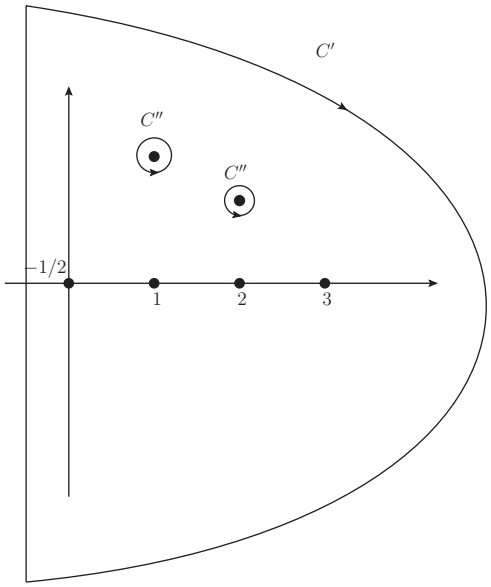

Figure B.2: Deformation of the contour C in Fig. B.1, to give the contour C' and C''.

chosen and they satisfy Carlson's theorem conditions, the contribution to the infinite semicircle is zero, and we obtain the result:

$$\begin{aligned} T^{\pm}(s,t,u) = \quad & 16\pi^2 \sum_i \frac{(2\alpha_i^{\pm}+1(t))\beta_i^{\pm}(t)}{sin(\pi\alpha_i^{\pm}(t))} \left(P_{\alpha_i^{\pm}(t)}(-z_t) \pm P_{\alpha_i^{\pm}(t)}(z_t)\right) \\ & +8\pi i \int_{-\frac{1}{2}-i\infty}^{-\frac{1}{2}+i\infty} dJ \frac{(2J+1)t^{\pm}(J,t)\,(P_J(-z_t) \pm P_J(z_t))}{\sin(\pi J)}, \end{aligned} \tag{B.9}$$

where $\alpha_i^{\pm}(t)$ are the positions of the poles in the J-plane and $\beta_i^{\pm}(t)$ their residues, and the sign $\pm$ corresponds to whether the pole occurs on the even or odd signature amplitude. These poles are called Regge poles.

The integral along $\mathrm{Re}J = -1/2$ is called background integral and it is chosen in similarity to non-relativistic scattering. In this regime, Regge [261] showed that the $t^{\pm}(J,t)$ partial-waves were meromorphic for $J > -1/2$ for a general class of potentials. However, in relativistic scattering, it was shown [262] that the background integral becomes as small as one wishes when it is pushed further to the left in the complex J-plane. Nevertheless, when doing that, the Regge representation of eq. (B.10) should include the contribution from all Regge poles, not just those whose trajectories satisfy $\mathrm{Re}\alpha_i^{\pm}(t) \geq -1/2$. We will assume then, that the background integral contribution in eq. (B.9) is negligible and that the sum is over all Regge poles.

Through this transform, known as Sommerfeld-Watson transform, we have converted the sums in eq. (B.1) into an integral, which enables us to continue the partial-wave expansion analytically from the physical t-region, $t > 4m^2$ and $s < 0$, to high energy s-channel scattering for which $t < 0$. Note that since the pole positions $\alpha_i^{\pm}(t)$ depend on t, each Regge pole generates a path in the J-plane as t varies along the real axis. This paths are the Regge trajectories of eq. (1.209) that we have studied in Section 1.8.1.

We can see from eq. (1.211) that at large s, t and z_t are both large and negative. Using the asymptotic behaviour of the Legendre polynomials for this limit, the amplitude $T^{\pm}(s,t,u)$ of eq. (B.9) have the leading behaviour:

$$\begin{aligned} T(s,t,u)^{\pm} &\sim -\pi \sum_i \beta_i^{\pm}(t) \frac{1 \pm e^{-i\pi\alpha_i^{\pm}(t)}}{\Gamma(\alpha_i^{\pm}(t)+1)\sin(\pi\alpha_i^{\pm}(t))} s^{\alpha_i^{\pm}}(t) \\ &\sim \sum_i \hat{\beta}_i^{\pm}(t)\Gamma(-\alpha_i^{\pm}(t))(1 \pm e^{-i\pi\alpha_i^{\pm}(t)})(s/s_0)^{\alpha_i^{\pm}}(t), \\ &\sim \sum_i \hat{\hat{\beta}}_i^{\pm}(t)(s/s_0)^{\alpha_i^{\pm}}(t) \end{aligned} \tag{B.10}$$

where s_0 is a fixed scale and $\hat{\beta}(t)$ and $\hat{\hat{\beta}}(t)$ are proportional to $\beta(t)$. This equation is the Regge representation of $T^{\pm}(s,t,u)$ of eq. (1.214), and it gives the behaviour of $T^{\pm}(s,t,u)$ for large s and small t. Using eq. (B.7), it also gives the leading behaviour of the transition amplitude $T(s,t,u)$.

One of the most relevant aspects of the Regge representation is related to the analysis of the poles of eq. (B.10). On the one hand the $\Gamma(-\alpha_i^{\pm})$ function have poles for value of t, such that $\alpha_i^{\pm}$ takes a non-negative integer value. On the other hand the factor $1 \pm e^{i\pi\alpha^{\pm}}$ vanishes for odd and even values of α^{+} and α^{-} respectively. Therefore, the even amplitude has poles at those values of t for which $\alpha_i^{+}(t)$ is a positive even integer, and the odd one has poles at the t values for which $\alpha_i^{-}(t)$ is a non-negative odd integer. These poles are the exchange of particles with spin $\alpha^{\pm}(t)$, whose mass is the corresponding value of $\sqrt{t}$. Thus, for each value of i in the sum of eq. (B.10), instead of exchanging a single particle of a given spin, we are exchanging a whole tower of resonances corresponding to the Regge trajectory.

Finite temperature field theory

In this appendix we derive the formulas obtained in 1.9.1. Further details can be found in [203, 204].

The thermal expectation value of a quantum field operator is based on the concept of partition function, which describes the statistical properties of a system in thermodynamic equilibrium and is defined as:

$$Z_\beta \equiv \mathrm{Tr}[\mathrm{e}^{-\beta\hat{H}}], \tag{C.1}$$

where $\beta = 1/T$, T is the temperature and $\hat{H}$ is the Hamiltonian operator of the system. Inserting a complete set of eigenvectors of $\hat{H}$, it is possible to evaluate the trace:

$$Z_\beta = \sum_n \mathrm{e}^{-\beta E_n}, \tag{C.2}$$

where E_n are the eigenvalues of $\hat{H}$. It is also possible to write the trace, by using a complete set of eigenvector of the position operator:

$$Z_\beta = \int dq \langle q|\mathrm{e}^{-\beta\hat{H}}|q\rangle, \tag{C.3}$$

where it is clear that $\mathrm{e}^{-\beta\hat{H}}$ can be interpreted formally as an evolution operator in imaginary time.

In this way, the thermal expectation value of the operator $\mathcal{O}(x)$ is given by:

$$\langle\mathcal{O}(x)\rangle_T \equiv \frac{1}{Z_\beta}\mathrm{Tr}[\mathcal{O}(x)\mathrm{e}^{\beta\hat{H}}]. \tag{C.4}$$

Therefore, the thermal propagator of a scalar field is defined as:

$$\begin{aligned} G(t-t',\mathbf{x}-\mathbf{y}) &\equiv \langle\hat{T}\left\{\hat{\phi}(t,\mathbf{x})\hat{\phi}(t',\mathbf{y})\right\}\rangle_T \\ &= \theta(t-t')G^{>}(t-t',\mathbf{x}-\mathbf{y}) \\ &+ \theta(t'-t)G^{<}(t-t',\mathbf{x}-\mathbf{y}), \end{aligned} \tag{C.5}$$

where $\hat{T}$ is the time-ordered operator, $\hat{\phi}(t,\mathbf{x}) = \mathrm{e}^{i\hat{H}t}\hat{\phi}(\mathbf{x})e^{-i\hat{H}t}$ is a scalar field defined in the interaction Heisenberg picture and

$$\begin{aligned} G^{>}(t,\mathbf{x}) &\equiv \langle\hat{\phi}(t,\mathbf{x})\hat{\phi}(0,\mathbf{0})\rangle_T, \\ G^{<}(t,\mathbf{x}) &\equiv \langle\hat{\phi}(0,\mathbf{0})\hat{\phi}(t,\mathbf{x})\rangle_T = G^{>}(-t,-\mathbf{x}). \end{aligned} \tag{C.6}$$

For short, we will write $G(t)$, $G^{>}(t)$ or $G^{<}(t)$ instead of $G(t,0)$, $G^{>}(t,0)$ and $G^{<}(t,0)$ respectively.

By inserting a complete set of eigenvectors of $\hat{H}$, one can express $G^{>}(t)$ as:

$$G^{>}(t) = \frac{1}{Z(\beta)} \sum_{n,m} \mathrm{e}^{-\beta E_n} \mathrm{e}^{-i(E_n - E_m)t} \left| \langle n|\hat{\phi}(\mathbf{x})|m\rangle \right|^2, \tag{C.7}$$

but it is only convergent if $G^{>}(t)$ is defined for:

$$-\beta \leq \mathrm{Im}(t) \leq 0, \tag{C.8}$$

while in the case of $G^{<}(t)$, it is only defined for:

$$\beta \geq \mathrm{Im}(t) \geq 0. \tag{C.9}$$

Using now the fact that $\mathrm{e}^{\beta\hat{H}}$ is an evolution operator defined in imaginary time:

$$\mathrm{e}^{-\beta\hat{H}} \hat{\phi}(t,\mathbf{x}) \mathrm{e}^{\beta\hat{H}} = \hat{\phi}(t + i\beta, \mathbf{x}), \tag{C.10}$$

and with the ciclicity of the trace it is possible to show that:

$$G^{>}(t,\mathbf{x}) = G^{<}(t + i\beta, \mathbf{x}), \tag{C.11}$$

The fourier transform of $G(t)^{>}$ and $G(t)^{<}$ is given by:

$$G^{>}(k_0) = \int_{-\infty}^{\infty} dt \mathrm{e}^{ik_0 t} G^{>}(t), \tag{C.12}$$

and

$$G^{<}(k_0) = \int_{-\infty}^{\infty} dt \mathrm{e}^{ik_0 t} G(t)^{<} = \int_{-\infty}^{\infty} dt \mathrm{e}^{ik_0 t} G^{>}(t - i\beta), \tag{C.13}$$

where the second equality follows from eq. (C.11), and implies that:

$$G^{<}(k_0) = G^{>}(-k_0) = \mathrm{e}^{-\beta k_0} G^{>}(k_0). \tag{C.14}$$

The spectral function is defined as:

$$\rho(k_0) = G^{>}(k_0) - G^{<}(k_0) = \int_{-\infty}^{\infty} dt \mathrm{e}^{ik_0 t} \langle [\phi(t,\mathbf{x}), \hat{\phi}(0,\mathbf{x})] \rangle_T, \tag{C.15}$$

but using eqs. (C.7) and (C.14), it can be expressed as:

$$\rho(k_0) = \frac{2\pi}{Z_\beta} \sum_{n,m} \mathrm{e}^{-\beta E_n} \left(\delta(k_0 + E_n - E_m) - \delta(k_0 + E_m - E_n) \right) \left| \langle n|\hat{\phi}(\mathbf{x})|m\rangle \right|^2, \tag{C.16}$$

which shows explicitly that the spectral function is an odd real function, i.e. $\delta(k_0) = -\delta(-k_0)$, and verifies the positivity condition: $\mathrm{sgn}(k_0)\rho(k_0) > 0$ Finally, in terms of the spectral function, the two-point functions $G^{>}(k_0)$ and $G^{<}(k_0)$ are defined as:

$$G^{>}(k_0) = (1 + n_B(k_0))\, \rho(K_0), \quad G^{<}(k_0) = n_B(K_0)\rho(K_0) \tag{C.17}$$

where $n_B(k_0)$ is the Bose-Einstein distribution:

$$n_B(k_0) = \frac{1}{\mathrm{e}^{\beta k_0} - 1}. \tag{C.18}$$

C.1 The Matsubara or imaginary-time Formalism

By analytical continuation from $t \to -i\tau$, we define the propagator of eq. (C.5) in imaginary time as:

$$\Delta(\tau, \mathbf{x}) = \langle \hat{T} \left\{ \hat{\phi}(\tau, \mathbf{x}) | \hat{\phi}(0, \mathbf{0}) \right\} \rangle, \tag{C.19}$$

where for short we write $\phi(\tau, \mathbf{x}) = \mathrm{e}^{\hat{H}\tau} \phi(\mathbf{x}) \mathrm{e}^{-\hat{H}\tau}$ instead of $\phi(i\tau, \mathbf{x})$ and $\Delta(\tau)$ instead of $\Delta(\tau, \mathbf{0})$. From the convergence conditions of eqs. (C.8) and (C.9), τ is defined in the interval $[-\beta, \beta]$ and $\hat{T}$ operates now in imaginary time:

$$\hat{T}\{\hat{\phi}(\tau_1, \mathbf{x}) \hat{\phi}(\tau_2, \mathbf{y})\} = \begin{cases} \hat{\phi}(\tau_1, \mathbf{x}) \hat{\phi}(\tau_2, \mathbf{y}), & \text{if } \tau_1 > \tau_2 \\ \hat{\phi}(\tau_2, \mathbf{y}) \hat{\phi}(\tau_1, \mathbf{x}), & \text{if } \tau_1 < \tau_2 \end{cases} \tag{C.20}$$

From eq (C.11), it is easy to check that this propagator verifies the periodicity property:

$$\Delta(\tau - \beta) = \Delta(\tau), \tag{C.21}$$

for any value of τ in the interval $[0, \beta]$. Due to this property, the Fourier transform of this propagator will be given by:

$$\Delta(iw_n) = \int_0^\infty d\tau \, \mathrm{e}^{iw_n \tau} \Delta(\tau), \tag{C.22}$$

where we have written $\Delta(iw_n)$ instead of $\Delta(w_n)$ for future convenience. The inverse formula of eq. (C.22) is

$$\Delta(\tau) = \frac{1}{\beta} \sum_n \mathrm{e}^{-iw_n \tau} \Delta(iw_n), \tag{C.23}$$

and implies, given the periodicity condition of eq. (C.21), that the frequencies w_n take the discrete values:

$$w_n = \frac{2\pi n}{\beta}, \qquad n \in \mathbb{Z} \tag{C.24}$$

which are called Matsubara frequencies. Choosing $\tau \in [0, \beta]$, we have $\Delta(\tau) = G^>(-i\tau)$, so using eqs. (C.22), (C.12) and the representation (C.17), $\Delta(iw_n)$ can be written as:

$$\Delta(iw_n) = -\int_{-\infty}^{\infty} \frac{dk_0}{2\pi} \frac{\rho(k_0)}{iw_n - k_0}, \tag{C.25}$$

and is known as Matsubara propagator. For the free-field case $\rho_F(k_0) = 2\pi \, \mathrm{sgn}(k_0) \delta(k_0^2 - E_k^2)$ so eq. (C.25) simplifies to:

$$\Delta_0(iw_n, \mathbf{k}) = \frac{1}{w_n^2 + E_K^2}, \tag{C.26}$$

where $E_k = \left(|\mathbf{k}|^2 + m^2\right)^{1/2}$, being m the mass of the scalar field.

We should now take a look at the quantization at finite temperature of the simplest field theory case: the neutral scalar field. In Minkowsky space, the corresponding Lagrangian density reads:

$$\mathcal{L} = \frac{1}{2} \partial_\mu \varphi(x) \partial^\mu \varphi(x) - \frac{1}{2} m^2 \varphi(x)^2 - \mathcal{V}(\varphi), \tag{C.27}$$

where $\varphi(x)$ is a real field, m is the mass of the corresponding scalar particles and $\mathcal{V}(\varphi)$ describes the interaction. From eq. (C.3), considering $e^{-\tau\hat{H}}$ as an evolution operator in imaginary-time with $\tau \in [0, \beta]$, this Lagrangian leads to the following action in an Euclidean space:

$$S_E(\beta) = \int_0^\beta d^4x \left(\frac{1}{2} \left(\partial_\mu \varphi(x)\right)^2 - \frac{1}{2} m^2 \varphi(x)^2 + \mathcal{V}(\varphi) \right), \tag{C.28}$$

where $x = (\tau, \mathbf{x})$, $\int_0^\beta d^4x = \int_0^\beta d\tau \int d^3x$ and $\left(\partial_\mu \varphi\right)^2 = (\partial_\tau \varphi)^2 + (\nabla \varphi)^2$. Proceeding as usual, the path-integral representation for the generating functional of n-point correlation functions, refs, is given by:

$$\begin{aligned} Z(\beta, j) &= \mathcal{N} \exp\left(- \int_0^\beta d^4z \mathcal{V}\left(\frac{\delta}{\delta j(z)} \right) \right) \\ &\quad \exp\left(\frac{1}{2} \int_0^\beta d^4x d^4y j(x) \Delta_0(x-y) j(y) \right), \end{aligned} \tag{C.29}$$

where $\mathcal{N}$ is a normalization constant. We can see that Eq. (C.29) is very similar to the generating functional in euclidean space at $T = 0$, but with the Feynman propagator replaced by the Matsubara propagator, $D_F \to \Delta_0$, and the integration range for the time variable that, in the imaginary time formalism, goes from 0 to β. Therefore, Feynmann rules in position space are the same in euclidean space at $T = 0$ and at finite T except for the aforementioned replacements. In momentum space, the Feynman rules are obtained by replacing:

$$D_F(\mathbf{p}, p_4) \to \Delta_0(i w_n, \mathbf{p}) \quad \int \frac{d^4p}{(2\pi)^4} \to T \sum_n \int \frac{d^3p}{(2\pi)^3}, \tag{C.30}$$

for propagator and integrals respectively, and the delta function corresponding to energy conservation in each vertex by a Kronecker delta involving the corresponding Matsubara frequencies: $\delta(\sum_i p_i^0) \to \beta \delta(\sum_i w_i)$.

$(N_c - 1)$ polyquark with two flavours

In this appendix we lift the assumption that the polyquark is composed of quarks of only one flavor. We now consider the necessary extension to two quark flavors, up and down. In this case the exotic wave function will be generated by:

$$\bar{\mathbb{Q}}^a \mathbb{Q}_a = \epsilon^{aj_i \cdots j_{N_c-1}} \epsilon_{ai_1 \cdots i_{N_c-1}} |u^{i_1} \cdots u^{i_{(N_c-1)/2}} d^{i_{(N_c+1)/2}} \cdots d^{i_{N_c-1}} \bar{u}_{j_1} \cdots \bar{u}_{j_{(N_c-1)/2}} \bar{d}_{j_{(N_c-1)/2}} \cdots \bar{d}_{j_{N_c-1}}\rangle. \tag{D.1}$$

and normalized by:

$$\begin{aligned} \mathcal{N}^2 = \langle \mathbb{Q}\bar{\mathbb{Q}} | \mathbb{Q}\bar{\mathbb{Q}} \rangle \quad &= \quad \epsilon^{ai_1 \cdots i_{N_c-1}} \epsilon^{aj_1 \cdots j_{N_c-1}} \epsilon^{bk_1 \cdots k_{N_c-1}} \epsilon^{bl_1 \cdots l_{N_c-1}} \\ &\quad \times \langle u^{k_1} \cdots u^{k_{(N_c-1)/2}} d^{k_{(N_c+1)/2}} \cdots d^{k_{N_c-1}} \bar{u}_{l_1} \cdots \bar{u}_{l_{(N_c-1)/2}} \bar{d}_{l_{(N_c-1)/2}} \cdots \bar{d}_{l_{N_c-1}}| \\ &\quad |u^{i_1} \cdots u^{i_{(N_c-1)/2}} d^{i_{(N_c+1)/2}} \cdots d^{i_{N_c-1}} \bar{u}_{j_1} \cdots \bar{u}_{j_{(N_c-1)/2}} \bar{d}_{j_{(N_c-1)/2}} \cdots \bar{d}_{j_{N_c-1}}\rangle. \end{aligned} \tag{D.2}$$

Of course, Wick contractions apply only to quarks of like flavour. Therefore we can no longer use a Levi-Civita tensor to express all possible antisymmetric combinations. The result is a cumbersome expression:

$$\begin{aligned} \mathcal{N}^2 \quad &\propto \quad \epsilon^{ai_1 \cdots i_{N_c-1}} \epsilon^{aj_1 \cdots j_{N_c-1}} \epsilon^{bk_1 \cdots k_{N_c-1}} \epsilon^{bl_1 \cdots l_{N_c-1}} \\ &\quad \times \left(\delta_{i_1 l_1} \cdots \delta_{i_{(N_c-1)/2} l_{(N_c-1)/2}} + \text{perm.}\right) \left(\delta_{i_{(N_c+1)/2} l_{(N_c+1)/2}} \cdots \delta_{i_{N_c-1} l_{N_c-1}} + \text{perm.}\right) \\ &\quad \times \left(\delta_{k_1 j_1} \cdots \delta_{k_{(N_c-1)/2} j_{(N_c-1)/2}} + \text{perm.}\right) \left(\delta_{k_{(N_c+1)/2} j_{(N_c+1)/2}} \cdots \delta_{k_{N_c-1} j_{N_c-1}} + \text{perm.}\right) \\ &\propto \quad \epsilon^{ai_1 \cdots i_{N_c-1}} \epsilon^{aj_1 \cdots j_{N_c-1}} \epsilon^{bk_1 \cdots k_{N_c-1}} \epsilon^{bl_1 \cdots l_{N_c-1}} \\ &\quad \left(\sum_{\alpha=1}^{((N_c-1)/2)!} (-1)^{\epsilon(\sigma_\alpha)} \delta_{i_1 l_{\sigma^\alpha_{i_1}}} \cdots \delta_{i_{(N_c-1)/2} l_{\sigma^\alpha_{i_{(N_c-1)/2}}}} \right) \left(\sum_{\beta=1}^{((N_c-1)/2)!} (-1)^{\epsilon(\sigma_\beta)} \delta_{i_{(N_c+1)/2} l_{\sigma^\beta_{i_{(N_c+1)/2}}}} \cdots \delta_{i_{N_c-1} l_{\sigma^\beta_{i_{N_c-1}}}} \right) \\ &\quad \left(\sum_{\gamma=1}^{((N_c-1)/2)!} (-1)^{\epsilon(\sigma_\gamma)} \delta_{k_1 j_{\sigma^\gamma_{k_1}}} \cdots \delta_{k_{(N_c-1)/2} j_{\sigma^\gamma_{k_{(N_c-1)/2}}}} \right) \left(\sum_{\rho=1}^{((N_c-1)/2)!} (-1)^{\epsilon(\sigma_\rho)} \delta_{k_{(N_c+1)/2} j_{\sigma^\rho_{k_{(N_c+1)/2}}}} \cdots \delta_{k_{N_c-1} j_{\sigma^\rho_{k_{N_c-1}}}} \right) \\ &\propto \quad \sum_{\alpha,\beta,\gamma,\rho}^{((N_c-1)/2)!} (-1)^{\epsilon(\sigma_\alpha)+\epsilon(\sigma_\beta)+\epsilon(\sigma_\gamma)+\epsilon(\sigma_\rho)} \epsilon^{aj_1 \cdots j_{N_c-1}} \epsilon^{bj_{\sigma^\gamma_{k_1}} \cdots j_{\sigma^\rho_{k_{N_c-1}}}} \epsilon^{bl_1 \cdots l_{N_c-1}} \epsilon^{al_{\sigma^\alpha_{i_1}} \cdots l_{\sigma^\beta_{i_{N_c-1}}}}. \end{aligned} \tag{D.3}$$

where α and β act on the first and last $(N_c-1)/2$ l indices, and γ and ρ on the first and last $(N_c-1)/2$ j indices. It is easy to check that for a given permutation γ and ρ,

$$\epsilon^{aj_1 \cdots j_{N_c-1}} \epsilon^{bj_{\sigma^\gamma_{k_1}} \cdots j_{\sigma^\rho_{k_{N_c-1}}}} = (-1)^{\epsilon(\sigma_\gamma)+\epsilon(\sigma_\rho)} \epsilon^{aj_1 \cdots j_{N_c-1}} \epsilon^{bj_1 \cdots j_{N_c-1}} = \delta_{ab}(N_c-1)! \tag{D.4}$$

where we have again used eq. (2.17). Besides, there are $(N_c-1)/2!$ different permutations for each permutation index. Taking all together we get:

$$\mathcal{N}^2 \propto \left(\frac{N_c-1}{2}\right)!^4 \delta_{ab}\delta_{ab}(N_c-1)!^2 N_c \left(\frac{N_c-1}{2}\right)!^4 (N_c-1)!^2 \tag{D.5}$$

Therefore:

$$\mathcal{N} = (N_c-1)!((N_c-1)/2)!^2\sqrt{N_c} \tag{D.6}$$

that yields basically the same scaling as the one-flavor case in equation (2.19).

The total width is dominated by the decay to $(N_c-1)/2$ $\pi^+\pi^-$ mesons or to (N_c-1) π^0. Let us explicitly show the scaling of the first matrix element.

$$\begin{aligned}\langle (u\bar{d}\,)^{(N_c-1)/2}(d\bar{u}\,)^{(N_c-1)/2}|\mathrm{Q}\bar{\mathrm{Q}}\rangle \;=\; & \frac{\epsilon^{ai_1\cdots i_{N_c-1}}\epsilon^{aj_1\cdots j_{N_c-1}}}{\sqrt{N_c}(N_c-1)!\,((N_c-1)/2)!^2}\frac{\delta^{k_1l_1}\ldots\delta^{k_{N_c-1}l_{N_c-1}}}{N_c^{(N_c-1)/2}} \\ & \langle u^{k_1}\ldots u^{k_{(N_c-1)/2}}\bar{d}^{\,l_1}\ldots\bar{d}^{\,l_{(N_c-1)/2}}d^{k_{(N_c+1)/2}}\ldots d^{k_{N_c-1}}\bar{u}^{\,l_{(N_c+1)/2}}\ldots\bar{u}^{\,l_{N_c-1}} \\ & |u^{i_1}\ldots u^{i_{(N_c-1)/2}}d^{i_{(N_c+1)/2}}\ldots d^{i_{N_c-1}}\bar{u}^{j_1}\ldots\bar{u}^{j_{(N_c-1)/2}}\bar{d}^{\,j_{(N_c+1)/2}}\bar{d}^{\,j_{N_c-1}}\rangle.\end{aligned} \tag{D.7}$$

Performing again the Wick contractions as we did for the normalization, we obtain:

$$\begin{aligned}\langle (u\bar{d}\,)^{(N_c-1)/2}(d\bar{u}\,)^{(N_c-1)/2}|\mathrm{Q}\bar{\mathrm{Q}}\rangle &\propto \frac{\epsilon^{ai_1\cdots i_{N_c-1}}\epsilon^{aj_1\cdots j_{N_c-1}}}{\sqrt{N_c}(N_c-1)!\,((N_c-1)/2)!^2}\frac{\delta^{k_1l_1}\ldots\delta^{k_{N_c-1}l_{N_c-1}}}{N_c^{(N_c-1)/2}} \\ \times\left(\sum_{\alpha=1}^{(N_c-1)/2!}(-1)^{\epsilon(\sigma_\alpha)}\delta_{i_1 l_{\sigma_i^\alpha}}\cdots\delta_{i_{(N_c-1)/2}l_{\sigma_{i_{(N_c-1)/2}}^\alpha}}\right)&\left(\sum_{\beta=1}^{(N_c-1)/2!}(-1)^{\epsilon(\sigma_\beta)}\delta_{i_{(N_c+1)/2}l_{\sigma_{i_{(N_c+1)/2}}^\beta}}\cdots\delta_{i_{N_c-1}l_{\sigma_{i_{N_c-1}}^\beta}}\right) \\ \times\left(\sum_{\gamma=1}^{(N_c-1)/2!}(-1)^{\epsilon(\sigma_\gamma)}\delta_{j_1 k_{\sigma_j^\gamma}}\cdots\delta_{j_{(N_c-1)/2}k_{\sigma_{j_{(N_c-1)/2}}^\gamma}}\right)&\left(\sum_{\rho=1}^{(N_c-1)/2!}(-1)^{\epsilon(\sigma_\rho)}\delta_{j_{(N_c+1)/2}k_{\sigma_{j_{(N_c+1)/2}}^\rho}}\cdots\delta_{j_{N_c-1}k_{\sigma_{j_{N_c-1}}^\rho}}\right) \\ &\propto \frac{1}{N_c^{N_c/2}(N_c-1)!\,((N_c-1)/2)!^2}\sum_{\alpha,\beta,\gamma,\rho}^{(N_c-1)/2!}(-1)^{\epsilon(\sigma_\alpha)+\epsilon(\sigma_\beta)+\epsilon(\sigma_\gamma)+\epsilon(\sigma_\rho)}\epsilon^{al_{\sigma_j^\gamma}\cdots l_{\sigma_{j_{N_c-1}}^\rho}}\epsilon^{al_{\sigma_i^\alpha}\cdots l_{\sigma_{i_{N_c-1}}^\beta}},\end{aligned}$$

and using again eq. (D.4):

$$\begin{aligned}\langle (u\bar{d}\,)^{(N_c-1)/2}(d\bar{u}\,)^{(N_c-1)/2}|\mathrm{Q}\bar{\mathrm{Q}}\rangle &\propto \frac{1}{N_c^{N_c/2}(N_c-1)!\,((N_c-1)/2)!^2}(N_c-1)!\left(\frac{N_c-1}{2}\right)!^4 \\ &\propto \frac{((N_c-1)/2)!^2}{N_c^{N_c/2}}.\end{aligned} \tag{D.8}$$

Therefore, the total width will be:

$$\Gamma_2 \propto \frac{((N_c-1)/2)!^4 c_1\cdot c_2^{N_c}}{N_c^{N_c+1}}\,. \tag{D.9}$$

where again c_1 is an unspecified constant with dimension of energy (N_c independent), and c_2 is a N_c dependent dimensionless constant.

Let us now study the coupling to a fixed $\pi^+\pi^-$ number, such as a molecule. It will be given by:

$$\begin{aligned}
\langle (u\bar{d})(d\bar{u})|\mathrm{Q}\bar{\mathrm{Q}}\rangle &= \tfrac{\epsilon^{ai_1\cdots i_{N_c-1}}\epsilon^{aj_1\cdots j_{N_c-1}}}{\sqrt{N_c}(N_c-1)!((N_c-1)/2)!^2}\tfrac{\delta^{k_1l_1}\delta^{k_2l_2}}{N_c}\times \\
&\langle u^{k_1}\bar{d}^{l_1}d^{k_2}\bar{u}^{l_2}|\tfrac{H_I^{N_c-3}}{(N_c-3)!}|u^{i_1}\cdots u^{(N_c-1)/2}d^{(N_c+1)/2}\cdots d^{N_c-1}\bar{u}^{j_{N_c-1}}\cdots\bar{u}^{(N_c-1)/2}\bar{d}^{(N_c+1)/2}\cdots\bar{d}^{j_{N_c-1}}\rangle \\
&= \tfrac{\epsilon^{ai_1\cdots i_{N_c-1}}\epsilon^{aj_1\cdots j_{N_c-1}}}{\sqrt{N_c}(N_c-1)!((N_c-1)/2)!^2}\tfrac{\delta^{k_1l_1}\delta^{k_2l_2}}{N_c}\times \\
&\langle u^{k_1}\bar{d}^{l_1}d^{k_2}\bar{u}^{l_2}|\tfrac{\mathcal{A}^{a_1}\cdots\mathcal{A}^{a_{N_c-3}}}{(N_c-3)!}|u^{i_1}\cdots u^{(N_c-1)/2}d^{(N_c+1)/2}\cdots d^{N_c-1}\bar{u}^{j_{N_c-1}}\cdots\bar{u}^{(N_c-1)/2}\bar{d}^{(N_c+1)/2}\cdots\bar{d}^{j_{N_c-1}}\rangle \\
&= \tfrac{\epsilon^{ai_1\cdots i_{N_c-1}}\epsilon^{aj_1\cdots j_{N_c-1}}}{\sqrt{N_c}(N_c-1)!((N_c-1)/2)!^2}\tfrac{\delta^{k_1l_1}\delta^{k_2l_2}}{N_c}\left(\tfrac{g^2}{N_c}\right)^{(N_c-3)/2}T^{a_1}_{p_1r_1}\cdots T^{a_{N_c-3}}_{p_{N_c-3}r_{N_c-3}} \\
&\langle u^{k_1}\bar{d}^{l_1}d^{k_2}\bar{u}^{l_2}|\tfrac{A^{a_1}\cdots A^{a_{N_c-3}}}{(N_c-3)!}|u^{i_1}\cdots u^{(N_c-1)/2}d^{(N_c+1)/2}\cdots d^{N_c-1}\bar{u}^{j_{N_c-1}}\cdots\bar{u}^{(N_c-1)/2}\bar{d}^{(N_c+1)/2}\cdots\bar{d}^{j_{N_c-1}}\rangle,
\end{aligned} \tag{D.10}$$

where again H_I is the interaction Hamiltonian and $\mathcal{A}^a = i\frac{g}{\sqrt{N_c}}A^aT^a_{ij}$ the gluon vertex. To perform the Wick contractions we again keep track of flavor. Each of the quarks in the final mesons can be contracted with one of $(N_c-1)/2$ different quarks in the initial state ket. This gives a combinatoric $(N_c-1)/2^4$ factor, and results in:

$$\begin{aligned}
\langle (u\bar{d})(d\bar{u})|\mathrm{Q}\bar{\mathrm{Q}}\rangle \quad\propto\quad & \frac{\epsilon^{ai_1\cdots i_{N_c-1}}\epsilon^{aj_1\cdots j_{N_c-1}}}{\sqrt{N_c}(N_c-1)!\,((N_c-1)/2)!^2}\frac{\delta^{k_1l_1}\delta^{k_2l_2}}{N_c}\left(\frac{g^2}{N_c}\right)^{(N_c-3)/2}\frac{T^{a_1}_{p_1r_1}\cdots T^{a_{N_c-3}}_{p_{N_c-3}r_{N_c-3}}}{(N_c-3)!} \\
& \times\left(\frac{N_c-1}{2}\right)^4\delta_{i_{(N_c-1)/2}l_2}\delta_{i_{N_c-1}l_1}\delta_{j_{(N_c-1)/2}k_1}\delta_{j_{N_c-1}k_2} \\
& \times\sum_{\alpha=1}^{(N_c-3)!}\sum_{\beta,\gamma=1}^{(N_c-3)/2!}\Bigg((-1)^{\epsilon(\alpha)+\epsilon(\beta)+\epsilon(\gamma)}\delta_{i_1p_{\sigma^\alpha_{i_1}}}\cdots\delta_{i_{(N_c-3)/2}p_{\sigma^\alpha_{i_{(N_c-3)/2}}}} \\
& \delta_{i_{(N_c+1)/2}p_{\sigma^\alpha_{i_{(N_c+1)/2}}}}\cdots\delta_{i_{N_c-2}p_{\sigma^\alpha_{i_{N_c-2}}}}\delta_{j_{\sigma^\beta_{i_1}}r_{\sigma^\alpha_{i_1}}}\cdots\delta_{j_{\sigma^\beta_{i_{(N_c-3)/2}}}r_{\sigma^\alpha_{i_{(N_c-3)/2}}}} \\
& \delta_{j_{\sigma^\gamma_{i_{(N_c+1)/2}}}p_{\sigma^\alpha_{i_{(N_c+1)/2}}}}\cdots\delta_{j_{\sigma^\gamma_{i_{N_c-2}}}p_{\sigma^\alpha_{i_{N_c-2}}}}\Bigg)\langle 0|A^{a_1}\cdots A^{a_{N_c-3}}|0\rangle \\
\propto\quad & \frac{1}{N_c^{3/2}(N_c-1)!\,((N_c-1)/2)!^2}\left(\frac{g^2}{N_c}\right)^{(N_c-3)/2}\frac{T^{a_1}_{p_1r_1}\cdots T^{a_{N_c-3}}_{p_{N_c-3}r_{N_c-3}}}{(N_c-3)!}. \\
& \times\left(\frac{N_c-1}{2}\right)^4\left(\frac{N_c-3}{2}\right)!^2(N_c-3)!\,\epsilon^{ak_1k_2p1\cdots p_{N_c-3}}\epsilon^{ak_1k_2r_1\cdots r_{N_c-3}}\langle 0|A^{a_1}\cdots A^{a_{N_c-3}}|0\rangle \\
\sim\quad & \frac{g^{N_c-3}}{4N_c^{N_c/2}}\frac{T^{a_1}_{p_1r_1}\cdots T^{a_{N_c-3}}_{p_{N_c-3}r_{N_c-3}}}{(N_c-3)!}\epsilon^{ak_1k_2p1\cdots p_{N_c-3}}\epsilon^{ak_1k_2r_1\cdots r_{N_c-3}}\langle 0|A^{a_1}\cdots A^{a_{N_c-3}}|0\rangle.
\end{aligned} \tag{D.11}$$

Finally we have to contract the gluon lines. Using the same arguments than in the one-flavour

case and eq. (2.45), we have:

$$\begin{aligned}\langle(u\bar{d})(d\bar{u})|\mathrm{Q}\bar{\mathrm{Q}}\rangle &\sim \left(\frac{g^2}{2}\right)^{(N_c-3)/2}\frac{(N_c-4)!!}{4N_c^{N_c/2}(N_c-3)!}\epsilon^{ak_1k_2p1\cdots p_{N_c-3}}\epsilon^{ak_1k_2r_1\cdots r_{N_c-3}} \\ &\times\left(\delta_{p_1r_2}\delta_{p_2r_1}-\frac{1}{N_c}\delta_{p_1r_1}\delta_{p_2r_2}\right)\cdots\left(\delta_{p_{N_c-4}r_{N_c-3}}\delta_{p_{N_c-3}r_{N_c-4}}-\frac{1}{N_c}\delta_{p_{N_c-4}r_{N_c-4}}\delta_{p_{N_c-3}r_{N_c-3}}\right) \\ &\sim \frac{(-1)^{(N_c-3)/2}(N_c-4)!!N_c!(N_c-3)}{N_c^{N_c/2}(N_c-3)!}\left(\frac{g^2}{2}\right)^{(N_c-3)/2}\sim\frac{(-1)^{(N_c-3)/2}N_c!!}{N_c^{(N_c-4)/2}}\left(\frac{g}{2}\right)^{(N_c-3)},\end{aligned} \tag{D.12}$$

which is the same as eq. (2.49) for only one flavour.

Turning to the next matrix element, the glueball coupling to the polyquark with two flavors is given by:

$$\begin{aligned}\langle gg|\mathrm{Q}\bar{\mathrm{Q}}\rangle &= \frac{\epsilon^{ai_1\cdots i_{N_c-1}}\epsilon^{aj_1\cdots j_{N_c-1}}}{\sqrt{N_c}(N_c-1)!((N_c-1)/2)!^2}\frac{\delta^{\mu\nu}}{\sqrt{N_c^2-1}}\langle\mathcal{A}^\mu\mathcal{A}^\nu|\frac{H_I^{N_c-1}}{(N_c-1)!}|u^{i_1}\cdots d^{i_{N_c-1}}\bar{u}^{j_1}\cdots\bar{d}^{j_{N_c-1}}\rangle \\ &= \frac{\epsilon^{ai_1\cdots i_{N_c-1}}\epsilon^{aj_1\cdots j_{N_c-1}}}{\sqrt{N_c}(N_c-1)!^2}\frac{\delta^{\mu\nu}}{\sqrt{N_c^2-1}}\langle\mathcal{A}^\mu\mathcal{A}^\nu|\frac{\mathcal{A}^{a_1}\cdots\mathcal{A}^{a_{N_c-1}}}{(N_c-1)!}|u^{i_1}\cdots d^{i_{N_c-1}}\bar{u}^{j_1}\cdots\bar{d}^{j_{N_c-1}}\rangle \\ &= \frac{\epsilon^{ai_1\cdots i_{N_c-1}}\epsilon^{aj_1\cdots j_{N_c-1}}}{\sqrt{N_c}(N_c-1)!((N_c-1)/2)!^2}\frac{\delta^{\mu\nu}}{\sqrt{N_c^2-1}}\left(\frac{g^2}{N_c}\right)^{(N_c-1)/2}T^{a_1}_{p_1r_1}T^{a_1}_{p_1r_1}\cdots T^{a_{N_c-1}}_{p_{N_c-1}r_{N_c-1}} \\ &\times\langle\mathcal{A}^\mu\mathcal{A}^\nu|\frac{A^{a_1}\cdots A^{a_{N_c-1}}}{(N_c-1)!}|u^{i_1}\cdots u^{(N_c-1)/2}d^{(N_c+1)/2}\cdots d^{N_c-1}\bar{u}^{j_{N_c-1}}\cdots\bar{u}^{(N_c-1)/2}\bar{d}^{(N_c+1)/2}\cdots\bar{d}^{j_{N_c-1}}\rangle.\end{aligned}$$

Performing the Wick contractions as customary by now:

$$\begin{aligned}\langle gg|\mathrm{Q}\bar{\mathrm{Q}}\rangle &\propto \frac{\epsilon^{ai_1\cdots i_{N_c-1}}\epsilon^{aj_1\cdots j_{N_c-1}}}{\sqrt{N_c}(N_c-1)!((N_c-1)/2)!^2}\frac{\delta^{\mu\nu}}{\sqrt{N_c^2-1}} \\ &\left(\frac{N_c-1}{2}\right)^4\times\sum_{\alpha=1}^{(N_c-1)!}\sum_{\beta,\gamma=1}^{(N_c-1)/2!}\Big((-1)^{\epsilon(\alpha)+\epsilon(\beta)+\epsilon(\gamma)}\delta_{i_1p_{\sigma^\alpha_{i_1}}}\cdots\delta_{i_{(N_c-1)/2}p_{\sigma^\alpha_{i_{(N_c-1)/2}}}} \\ &\delta_{i_{(N_c+1)/2}p_{\sigma^\alpha_{i_{(N_c+1)/2}}}}\cdots\delta_{i_{N_c-2}p_{\sigma^\alpha_{i_{N_c-2}}}}\delta_{j_{\sigma^\beta_{i_1}}r_{\sigma^\alpha_{i_1}}}\cdots\delta_{j_{\sigma^\beta_{i_{(N_c-1)/2}}}r_{\sigma^\alpha_{i_{(N_c-1)/2}}}} \\ &\delta_{j_{\sigma^\gamma_{i_{(N_c+1)/2}}}p_{\sigma^\alpha_{i_{(N_c+1)/2}}}}\cdots\delta_{j_{\sigma^\gamma_{i_{N_c-1}}}p_{\sigma^\alpha_{i_{N_c-1}}}}\Big) \\ &\times\left(\frac{g^2}{N_c}\right)^{(N_c-1)/2}\frac{T^{a_1}_{p_1r_1}T^{a_1}_{p_1r_1}\cdots T^{a_{N_c-1}}_{p_{N_c-1}r_{N_c-1}}}{(N_c-1)!}\langle\mathcal{A}^\mu\mathcal{A}^\nu|A^{a_1}\cdots A^{a_{N_c-1}}|0\rangle \\ &\propto \frac{1}{\sqrt{N_c}(N_c-1)!((N_c-1)/2)!^2}\frac{\delta^{\mu\nu}}{\sqrt{N_c^2-1}} \\ &\times\left(\frac{N_c-1}{2}\right)!^2(N_c-1)!\epsilon^{ap_1\cdots p_{N_c-1}}\epsilon^{ar_1\cdots r_{N_c-1}} \\ &\times\left(\frac{g^2}{N_c}\right)^{(N_c-1)/2}\frac{T^{a_1}_{p_1r_1}T^{a_1}_{p_1r_1}\cdots T^{a_{N_c-1}}_{p_{N_c-1}r_{N_c-1}}}{(N_c-1)!}\langle\mathcal{A}^\mu\mathcal{A}^\nu|A^{a_1}\cdots A^{a_{N_c-1}}|0\rangle \\ &\sim \frac{(-1)^{(N_c-1)/2}}{\sqrt{N_c}\sqrt{N_c^2-1}N_c^{(N_c-1)}}(N_c-1)(N_c-2)!!N_c^2\left(\frac{g}{2}\right)^{(N_c-1)/2}.\end{aligned} \tag{D.13, D.14}$$

So that finally:

$$\langle gg|\mathrm{Q}\bar{\mathrm{Q}}\rangle \propto\sim \frac{(-1)^{(N_c-1)/2}N_c!!}{N_c^{(N_c-2)/2}}\left(\frac{g}{2}\right)^{(N_c-1)/2}, \tag{D.15}$$

which is again the same result than in the one flavour case, eq. (2.56).

Repeating again the same procedure, whose steps we do not detail now, we obtain the 0^+ $q\bar{q}$ meson and polyquark coupling as given by:

$$\langle\frac{u\bar{u}+d\bar{d}}{\sqrt{2}}|\mathrm{Q}\bar{\mathrm{Q}}\rangle \quad\sim\quad \frac{(-1)^{(N_c-2)/2}(N_c-1)\,!!}{N_c^{(N_c-4)/2}}\left(\frac{g}{2}\right)^{(N_c-2)} .$$

Since the results of this appendix closely parallel those of Section 2.2.6, we do not further complicate the calculation by including the spin counting. This should not change the leading N_c scaling, but the combinatorics would now be rather unmanageable.

Resumen en español

Introducción y objetivos

Los mesones escalares más ligeros juegan un papel fundamental en Física Hadrónica y Nuclear. Particularmente, el más ligero de estos estados, el mesón $f_0(500)$ o σ, es en gran medida responsable de la parte atractiva de la interacción nucleón–nucleón [1]. Además, los mesones escalares-isoescalares tienen los números cuánticos del vacío, por lo que también son importantes en la ruptura espontánea de la simetría quiral en la Cromodinámica Cuántica (QCD en sus siglas en inglés). Asimismo, esta ruptura, aunque con importantes diferencias, es similar al mecanismo de Higgs en la ruptura electro-débil del modelo Estándar [2, 3, 4]. Otro aspecto relevante para esta discusión está relacionado con el hecho de que QCD, al ser una teoría construida a partir de una invariancia gauge no abeliana, predice la existencia de los glueballs. Puesto que el glueball más ligero tiene los números cuánticos de los mesones escalares, es de esperar que se mezcle con ellos. Finalmente, también es interesante entender por qué los escalares más ligeros, contrariamente a los mesones vectoriales, contribuyen tan poco a la saturación de los parámetros de la teoría de baja energía de QCD [5, 6].

A pesar de su importancia en muchos y diferentes campos de la física hadrónica y nuclear, la naturaleza de los mesones escalares más ligeros es todavía un tema de debate, como se puede ver, por ejemplo, en la "Nota sobre mesones escalares" en [10, 11]. Esto se debe al hecho de que hay muchos estados escalares en la región por debajo de 2 GeV, muchos de los cuales son muy anchos, lo que da lugar a solapamientos que hacen difícil su identificación experimental. Además, se encuentran distorsionados por un fondo destructivo y por los intercambios de resonancias en canales cruzados, lo que hace que su estudio espectroscópico no éste aún nada claro. Adicionalmente se cree que los mesones escalares más ligeros no tienen la naturaleza ordinaria $\bar{q}q$, y muchas posibilidades sobre su composición han sido discutidas en la literatura, tales como que son moleculas de mesones, tetraquarks, glueballs o una mezcla de algunos de estos estados [12, 13, 14, 15, 16, 17, 18, 19, 20, 21, 22, 23, 24].

Particularmente, las propiedades e incluso la existencia del meson σ, han sido durante muchos años un problema en profunda discusión. Esto puede ser ilustrado por el hecho de que el "Grupo de Datos de las Partículas" (PDG en sus siglas en inglés), sólo incluyó la σ en la edición de 1996 de su Resumen de Física de Partículas, casi unos 40 años después de haber sido propuesta en [1]. Además, en el periodo que va desde 1996 a 2010, su masa fue estimada en la región entre 400-1200 MeV, y su anchura entre 600-1200 MeV [10]. Sin embargo, análisis

recientes y de gran precisión han desencadenado una revisión sustancial de esta resonancia en la última edición del PDG; la estimación de su masa ha cambiado a la región entre 400-550 MeV, y la de su anchura a la región entre 400-700 MeV [11].

Por tanto, en esta tesis vamos a estudiar las propiedades y naturaleza de las resonancias escalares más ligeras que aparecen en el scattering de piones. A pesar de que QCD está bien establecida como la teoría que describe las interacciones fuertes, a baja energía su constante de acoplamiento se hace muy grande, lo que implica que no podemos usar QCD para estudiar las interacciones de los mesones ligeros. Por consiguiente, utilizaremos otros métodos a la hora de abordar este problema. En primer lugar, usaremos relaciones de dispersión, que conectan la amplitud de scattering de un determinado proceso y para una energía determinada, con una integral sobre todo el rango de energía, dando resultados precisos e información, incluso allí donde no hay datos experimentales o donde éstos son imprecisos. En segundo lugar, utilizaremos la Teoría de Perturbaciones Quiral (ChPT en sus siglas en inglés), que es la teoría efectiva a baja energía de QCD [7, 8, 9]. ChPT es consecuencia de la ruptura espontánea de la simetría quiral y sus grados de libertad relevantes, son los bosones de Goldstone de dicha ruptura, mesones pseudo-escalares cuya masa está separada del resto de resonancias por una diferencia de varios cientos de MeV.

Podemos dividir los resultados obtenidos en esta tesis en tres bloques diferentes. En el primer bloque, hemos usado técnicas dispersivas para parametrizar de una forma precisa e independiente del modelo, la amplitud del scattering de piones. Por medio de este procedimiento hemos sido capaces de obtener la posición del polo y el acoplamiento a dos piones de las resonancias $f_0(500)$ y $f_0(980)$. En el segundo bloque, usaremos ChPT, unitarizada con el Método de la Amplitud Inversa (IAM en sus siglas en inglés) y el método N/D, para generar polos asociados a las resonancias más ligeras. Usaremos el primer enfoque ya que, siendo consecuencia de una relación de dispersión, no introduce ningún parámetro espurio, lo que hace que sea muy apropiado para estudiar la naturaleza de las resonancias generadas. Usaremos el segundo por su sencillez y facilidad con la que es posible incorporar resonancias directamente en el Lagrangiano. Ambos métodos de unitarización serán usados conjuntamente con la expansión $1/N_c$ de QCD y con otras herramientas fenomenológicas como son la dualidad semi-local o las reglas de suma espectrales. Estos métodos nos permitirán estudiar y constreñir la naturaleza de estas resonancias. Finalmente, en el tercer bloque, analizaremos el papel e influencia del mesón σ en la restauración de la simetría quiral de QCD, combinando ChPT con el formalismo de temperatura finita y la aproximación del virial. A continuación estudiaremos detenidamente cada uno de estos bloques.

Resultados y aportaciones fundamentales

Propiedades de los escalares más ligeros a partir de un análisis dispersivo del scattering de piones.

Motivación

Una determinación a baja energía de la amplitud de scattering de piones es relevante para el estudio de ChPT, la masa de los quarks y el condensado quiral. Además, su análisis a energías intermedias es importante para estudiar las propiedades del controvertido mesón σ, así como de la resonancia $f_0(980)$, cuyo análisis es el objetivo principal de esta tesis. Los desfasajes e inelasticidades del scattering de piones también son importantes para muchos otros procesos hadrónicos donde el estado final está formado por dos o más piones. Estos procesos hadrónicos son actualmente objeto de un intenso análisis tanto teórico como experimental. Sin embargo, la información experimental de la que disponemos sobre el scattering de piones está formada por conjuntos de datos que son conflictivos en la zona de energía intermedia y, durante muchos años, muy escasos en la interesante zona cercana al umbral. Esta situación ha hecho que haya sido difícil obtener resultados concluyentes sobre el scattering de piones a baja energía o, incluso, en la zona de la resonancia σ. Sin embargo, en los últimos años, se ha renovado el interés por este proceso. Ésto es debido desde el punto de vista experimental, a los últimos resultados, que han sido obtenidos con gran precisión de la desintegración de kaones y que están relacionados con el scattering de piones a baja energía. Pero también, desde el punto de vista teórico, debido al uso de técnicas dispersivas, utilizadas en ocasiones conjuntamente con ChPT [179, 49, 146, 147, 50, 148, 149]. De igual modo hay actualmente, un amplio esfuerzo a nivel mundial en el estudio experimental de la desintegración de mesones pesados como, por ejemplo, la Φ, D o B en estados finales de piones.

El formalismo dispersivo es independiente del modelo, sólo esta basado en propiedades de analiticidad y simetría de crossing, y relaciona la amplitud de scattering a una energía determinada, con una integral sobre todo el rango de energía, lo que aumenta la precisión y proporciona información de la amplitud para energías donde los datos son imprecisos o, incluso, en el plano complejo. Además, las parametrizaciones utilizadas para describir los datos experimentales, resultan irrelevantes una vez que éstas son incluidas en las integrales, relacionando, a su vez, diferentes canales de scattering entre ellos.

En una serie de trabajos [146, 147, 148, 149], el grupo de Madrid-Cracovia ha usado este enfoque dispersivo para construir la amplitud del scattering de piones incorporando analiticidad, unitariedad y simetría de crossing, usando como punto de inicio un conjunto de expresiones simples, con las que se parametrizan los datos experimentales disponibles. Estos trabajos comparten una metodología común. En primer lugar, se dan parametrizaciones sencillas en las que la amplitud de cada onda parcial se ajusta indepedientemente a los datos correspondientes. Estas parametrizaciones se confrontan entonces con relaciones de dispersión y, en el caso de que éstas se satisfagan razonablemente, son usadas como punto de partida para los Ajustes Constreñidos de los Datos (CFD en sus siglas en inglés), en el que las relaciones de dispersión se imponen como constricciones adicionales al ajuste de los datos experimen-

tales. De esta forma, las paramatrizaciones así obtenidas son una descripción consistente de la amplitud del scattering de piones.

Particularmente, en el último de estos trabajos antes mencionado, los autores completaron y mejoraron los ajustes de los datos experimentales obtenidos en los dos trabajos previos, incluyendo los más recientes de NA48/2 en esa fecha [154], al igual que otros datos creíbles de la desintegración K_{l4} [153, 140, 209]. A continuación, los autores repitieron los ajustes incluyendo como constricciones añadidas, relaciones de dispersión hacia adelante (FDR en sus siglas en inglés), ecuaciones de Roy por debajo del umbral de kaones y reglas de suma. Estas amplitudes de scattering constreñidas verificaban de forma muy precisa las FDR, las reglas de suma y especialmente las ecuaciones de Roy, en la que los parámetros de ajuste habían cambiado muy poco con respecto a los datos obtenidos en el ajuste exclusivo a los datos experimentales. Por lo tanto, estas parametrizaciones mejoradas, procuraban una representacion creíble de la amplitud del scattering de piones con la que era posible analizar diferentes relaciones físicas.

Sin embargo, desde la publicación de este último trabajo, ha aparecido una publicación [155] que analiza el hecho de que los experimentos sobre desintegraciones de kaones introducen correciones de isospín mayores de las esperadas. Además, en [210] se sugirió que el punto de matching entre la zona de baja energía y energía intermedia en la parametrización de la onda S0 del grupo Madrid-Cracovia, introducía una discontinuidad en la derivada del desfasaje en el punto de matching, lo que podría ser una fuente importante de errores.

Finalmente, la situación de las propiedades de la resonancia $f_0(500)$ invitaba a un análisis más profundo.

Resumen de los resultados

Los resultados de esta sección han sido publicados en dos artículos de investigación que se incluyen en las secciones 2.1.3 and 2.1.4.

En la publicación de la sección 2.1.3, continuamos el análisis previo con el fin de actualizar los resultados experimentales, incluyendo los últimos datos de NA48/2, que tienen en cuenta las correcciones de violación de isospín propuestas en [155], así como para mejorar la parametrización de la zona de energía intermedia de la onda S0, imponiendo una derivada continua en el punto de matching. Además, en esta tesis hemos probado que, era posible obtener ecuaciones de dispersión parecidas a las ecuaciones de Roy, pero sólo una sustracción, las llamadas ecuaciones GKPY. La propiedad más relevante de estas ecuaciones, es que las incertidumbres crecen muy lentamente al aumentar la energía, debido al hecho de que, contrariamente a las ecuaciones de Roy, los términos de sustracción son constantes y, por tanto, las incertidumbres que introducen no crecen con la energía. Ésto implica que estas nuevas ecuaciones de dispersión son muy convenientes para constreñir las amplitudes del scattering de piones en la zona de energía intermedia, permitiendo mejorar la parametrización de la onda S0 en esta controvertida zona. Finalmente, también hemos extendido el rango de energía en el que aplicamos tanto las ecuaciones de Roy como las ecuaciones GKPY. Hasta ahora estas ecuaciones eran usadas para constreñir las amplitudes hasta $\sqrt{s} \sim 932$ MeV por

el grupo de Madrid-Cracovia, y hasta 800 MeV en [49], mientras que en nuestro trabajo son utilzadas hasta $\sqrt{s} \sim 1.1$ GeV, lo que nos permite describir correctamente la zona de la resonancia $f_0(980)$, cerca del umbral de kaones. Los principales resultados obtenidos en esta publicación son:

- Obtenemos y presentamos las ecuaciones GKPY, proporcionando todos los núcleos y estudiando minuciosamente su comportamiento cerca del umbral. Además, también estudiamos y comparamos cómo se propagan las incertidumbres en las ecuaciones de Roy y GKPY, concluyendo que las ecuaciones de Roy son más precisas para estudiar la zona de baja energía, mientras que las ecuaciones de GKPY proporcionan mejores resultados en la zona $\sqrt{s} > 500 MeV$. También extendemos el análisis de estas ecuaciones hasta 1.1 GeV, para mejorar la descripción que hacemos de la zona correspondiente a la resonancia $f_0(980)$.

- Obtenemos un conjunto de parametrizaciones por medio de Ajustes no Constreñidos a los Datos (UFD en sus siglas en inglés) para las ondas S0, S2, P, D0, D2 y F, así como de la zona de alta energía, resolviendo las dudas e incertidumbres sobre los datos experimentales de la literatura. Particularmente, mejoramos la parametrización de la onda S0 en la zona de energía intermedia, imponiendo una derivada continua en el punto de matching.

- A continuación, imponemos las ecuaciones de Roy y GKPY, las FDR y las reglas de suma a las parametrizaciones previas UFD. Como resultado, obtenemos parametrizaciones consistentes y fáciles de implementar, que satisfacen bien todas las relaciones de dispersión dentro de sus errores, de forma uniforme en todo el rango de energía. Estos nuevos fits son llamados Ajustes Constreñidos de Datos (CFD en sus siglas en inglés). Para obtener estos nuevos ajustes, los parámetros de la onda S0 en la zona de energía intermedia cambian alrededor de 0.8 desviaciones estándar con respecto a los parámetros del UFD.

- Hemos obtenido, usando reglas de suma, valores precisos y compatibles con determinaciones previas tanto experimentales como teóricas [179, 49], de las longitudes y pendientes de scattering de las ondas S, P, D y F.

- Obtenemos la posición de los ceros de Adler de las ondas S0 y S2, usando las ecuaciones de Roy y de GKPY, en concordancia con las predicciones obtenidas usando ChPT.

- El uso de las ecuaciones de GKPY, nos permite mostrar que la solución a la inelasticidad de piones que muestra una brusca caída, o solución dip, se encuentra claramente favorecida con respecto a la solución que no la muestra.

En la publicación de la sección 2.1.4 usamos las ecuaciones de Roy y GKPY obtenidas en la publicación previa, para realizar una extrapolación analítica al plano complejo de las ondas parciales de la amplitud del scattering de piones de una forma independiente del modelo. Ésto nos prermite buscar en la segunda hoja de Riemann los polos asociados a resonancias en dicha onda parcial. Los resultados obtenidos puedes ser resumidos como sigue:

- Determinamos de una forma precisa e independiente del modelo, los polos de las resonancias $f_0(500)$, $f_0(980)$ y $\rho(770)$ sin usar ninguna suposición teórica por medio de las ecuaciones de Roy y GKPY.
- Los polos obtenidos utilizando ambos conjuntos de ecuaciones, son compatibles entre sí. Sin embargo, el resultado obtenido con las ecuaciones de GKPY, tiene incertidumbres menores y lo consideramos nuestro mejor resultado.
- También obtenemos para cada una de estas resonancias, sus acoplamientos a dos piones obtenidos a partir del residuo del polo.

Como hemos comentado anteriormente, los resultados obtenidos para los polos de las resonancias $f_0(500)$ y $f_0(989)$ han sido usados por el PDG para realizar una importante revisión de las estimaciones de la masa y anchura de ambas resonancias [11].

Naturaleza de las resonancias escalares más ligeras.

Motivación

La expansión de $1/N_c$ es una aproximación análitica a QCD en todo su rango de energía, que proporciona una definición clara de los estados $\bar{q}q$. Por otra parte, la dependencia con el número de colores de las constantes de baja energía de ChPT es bien conocida. Además, las técnicas de unitarización mencionadas anteriormente, nos permiten reproducir o incluir explícitamente resonancias en la teoría. En particular, el IAM genera resonancias que no están inicialmente en el Lagrangiano satisfaciendo unitariedad en la zona elástica de la amplitud de scattering, y respetando la expansión de ChPT a baja energía. Todo ello sin introducir ningún parámetro espurio o dependencia desconocida. Por otro lado, el IAM elástico también se puede generalizar a canales acoplados, implementando unitariedad en todos ellos. A pesar de que esta generalización del IAM no puede ser obtenida a partir de una relación de dispersión, permite obtener polos asociados a las resonancias: $f_0(980)$, $a_0(980)$, $K^\star(892)$ y κ.

En [211] se obtuvo, usando el IAM con canales acoplados y la expansión $1/N_c$, que las resonancias vectoriales generadas se comportaban de una manera muy próxima a como cabría esperar de estados $\bar{q}q$, mientras que en el caso de las resonancias escalares, esta interpretación estaba muy desfavorecida. En la Fig. D.1, se muestra la evolución con N_c de la masa M y anchura Γ de las resonancias vectoriales $\rho(770)$ y $K^\star(892)$ y de las escalares $f_0(500)$ y κ, definidas a partir de la posición de su polo, $\sqrt{s_{\rm polo}} = M - i\Gamma/2$. Las cantidades representadas están normalizadas a sus valores para $N_c = 3$, de forma que puedan ser comparados con el comportamiento esperado para un estado $\bar{q}q$, $M/M_{N_c=3} = 1$ y $\Gamma/\Gamma_{N_c=3} = 3/N_c$. Las bandas grises de la figura corresponden a la incertidumbre en la escala de renormalización en la que se aplica la expansión $1/N_c$, que es escogida en el intervalo $\mu \sim 0.5 - 1$ GeV. Se puede ver perfectamente en esta figura, que los vectores siguen sorprendentemente bien el comportamiento en la expansión del número de colores de los estados $\bar{q}q$. Sin embargo, el comportamiento de los escalares σ y κ es muy diferente, pues tanto su masa como su anchura crecen con N_c. Otros resultados en la literatura [213, 214, 215, 216, 217, 218] también han encontrado que cerca de $N_c = 3$, el comportamiento de la σ no es el esperado de un estado $\bar{q}q$.

Es importante recalcar que la principal conclusión de este resultado es que los escalares no se comportan predominantemente como estados $\bar{q}q$. Sin embargo, en [212] se demostró que el comportamiento del polo de la σ con N_c sólo era robusto cerca de $N_c = 3$, y que fuera de esta región, era posible encontrar resultados cualitativamente diferentes. La principal fuente de incertidumbre de este hecho, es la elección de la escala de renormalización en la que se aplica el escaleo con N_c. Cómo se puede ver en la Fig. D.2, esta incertidumbre es suficiente para cambiar el comportamiento del polo de ls σ para valores de N_c grandes, incluso cuando se parte exactamente del mismo conjunto de LECs para $N_c = 3$. De hecho, sólo cuando μ es escogida entre 0.5 y 1 GeV, el polo de la resonancia $\rho(770)$ se comporta como lo haría un estado $\bar{q}q$. Sin embargo, dentro de esta banda de incertidumbre, el polo de la σ obtenido con el IAM a un loop, puede moverse alejándose del eje real, o acercándose a él, pero con una masa menor de la inicial o, incluso por debajo del umbral de dos piones. Además, el IAM no se puede utilizar para valores de N_c muy grandes, porque la teoría se vuelve debílmente interactuante, e, intuitivamente, la unitarización pierde su sentido. Más detalles de este hecho se pueden encontrar en [219].

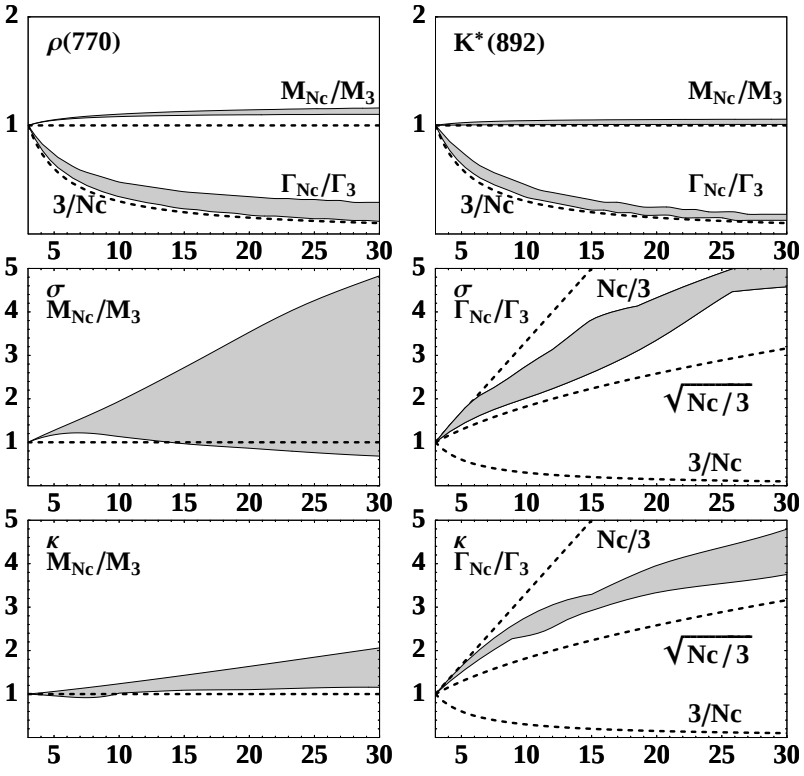

Figure D.1: $1/N_c$ dependence found in [143], of the $\rho(770)$, $K^*(892)$, σ and κ poles positions defined as $\sqrt{s_{pole}} = M - i\Gamma/2$, normalized to their $N_c = 3$ values. The dashed lines show different N_c scaling laws, and the gray areas cover the uncertainty in $\mu = 0.5 - 1$ GeV.

En [220], los autores extendieron el análisis previo a dos loops. El mejor ajuste de este resultado a $O(p^6)$ era compatible con el resultado a $O(p^4)$ para valores de pequeños N_c, pues la σ seguía sin ser predominantemente un estado $\bar{q}q$. Sin embargo, al aumentar el número de colores, en esta solución aparecía de forma natural una componente subdominante de este

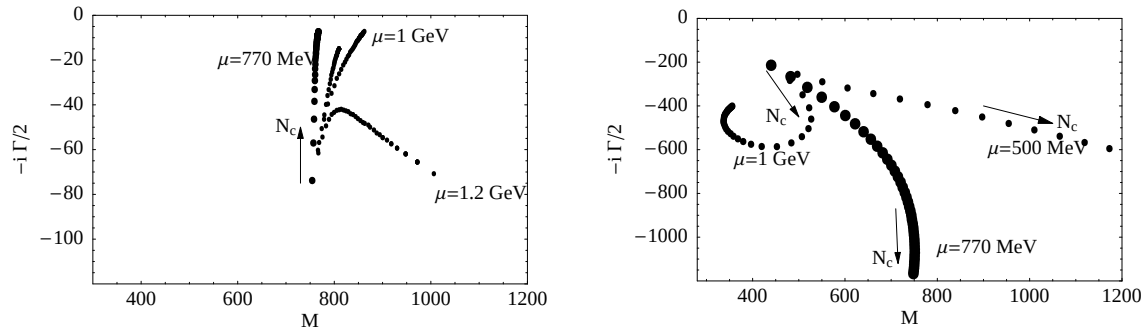

Figure D.2: $1/N_c$ behaviour versus the renormalization scale choice from [212]. Left panel: The ρ pole tends to the real axis if 0.5 GeV < μ < 1 GeV, but not for μ = 1.2 GeV. Right panel: The sigma pole behaviour changes dramatically when μ changes from 0.5 to 1 GeV.

estado con una masa por encima de 1 GeV. Como podemos ver en la Fig. D.3, el polo de la resonancia $f_0(500)$ se aleja del eje real en la región que va entre 400-600 MeV. Sin embargo, éste acaba volviendo al eje real por encima de 1 GeV cuando N_c es aproximadamente mayor de 10. Esto ocurre de forma bastante natural para el cálculo a 2 loops, pero esta solución también estaba escondida en parte del espacio de parámetros del resultado a 1 loop. De hecho, hemos comprobado en esta tesis que este resultado realmente ocurre a un loop. Este comportamiento indica que, mientras que para $N_c = 3$ la σ no es predominantemente un estado $\bar{q}q$, puede tener una componente subdominante, pero siempre originada con una masa por encima de 1 GeV. Sim embargo, como hemos puntualizado anteriormente, el hecho de tener que elegir la escala en la que se inicia la expansión con N_c, implica que, aunque este resultado está naturalmente favorecido, el resto de comportamientos posibles dentro de la banda de incertidumbre mostrada en la Fig. D.1 no pueden ser excluídos.

Dada la situación que acabamos de describir, la motivación para nuestro trabajo ha sido la siguiente: en primer lugar, queríamos encontrar restricciones adicionales a la dependencia con N_c de los escalares más ligeros, con la finalidad de clarificar su comportamiento y naturaleza. En segundo lugar, queríamos estudiar si el comportamiento con N_c encontrado para el escalar más ligero, la resonancia σ, podía ser interpretado de forma natural a partir de su composición en términos de estados hechos explícitamente de quarks y gluones, a partir de la expansión de $1/N_c$ de QCD. Finalmente, queríamos estudiar si la naturalidad permitía desechar otras posibles composiciones.

Resumen de los resultados

Los resultados de esta sección han sido publicados en tres artículos de investigación que presentamos en las secciones 2.2.3, 2.2.4 y 2.2.5. Resultados aún preliminares, también han sido publicados en el proceeding de una conferencia, 2.2.7. Finalmente, también presentamos resultados aún sin publicar en las secciones 2.2.6 y 2.2.8.

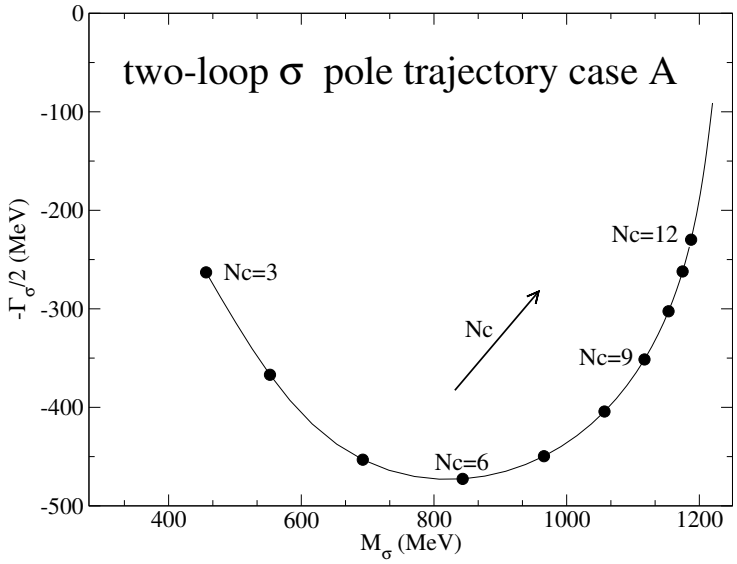

Figure D.3: $1/N_c$ dependence found in [220] for the $f_0(500)$ pole. The mass and width start increasing as N_c increases. However, for $N_c = 6 \sim 8$, the pole trajectory turns around moving back towards the real axis above 1 GeV.

En las publicaciones de las secciones 2.2.3, 2.2.4 y 2.2.5, analizamos la relación que hay entre la naturaleza del mesón σ y la dualidad semi-local. La dualidad semi-local permite constreñir las amplitudes de scattering a baja energía, y por consiguiente, la naturaleza de las resonancia que aparecen en éstas. Particularmente, la amplitud del scattering de piones con isospín $I = 2$ en onda s, es una amplitud exótica, en la que ninguna resonancia contribuye. Puesto que los intercambios de Regge en canal t estan relacionados (son duales) a los intercambios de resonancias en canal s, la ausencia de resonancias intercambiadas en el canal escalar con $I = 2$ en el scattering de piones, implica que la amplitud de scattering con I=2 definido en canal t, tiene que estar suprimida con respecto a las amplitudes de aquellos canales donde sí hay resonancias intercambiadas. Esta amplitud de scattering con isospín definido en canal t, se puede expresar como una combinación de amplitudes en canal s:

$$T^{I_t=2}(s,t,u) = \frac{1}{3}T^{I_s=0}(s,t,u) - \frac{1}{2}T^{I_s=1}(s,t,u) + \frac{1}{6}T^{I_s=2}(s,t,u). \tag{D.16}$$

Puesto que la amplitud $T^{I_s=2}$ es repulsiva y muy pequeña, la dualidad semi-local implica una cancelación muy fuerte entre las amplitudes $T^{I_s=0}$ y $T^{I_s=1}$, que están saturadas respectivamente a bajas energías por las resonancias $f_0(500)$ y $\rho(770)$. Por consiguiente, la dualidad semi-local requiere que la contribución de ambas resonancias se anule en media, para que el intercambio de Regge de $I = 2$ en el canal t siga estando suprimido. Esta cancelación debe ocurrir además para todo valor de N_c. Por lo tanto, todo modelo en el que la resonancia σ y $\rho(770)$ se comporten con N_c de manera distinta, no garantiza la cancelación de estas resonancias para todo N_c y por consiguiente está potencialmente en conflicto con la dualidad semi-local. En las publicaciones de las secciones 2.2.3, 2.2.4 y 2.2.5, mostramos cómo ChPT unitarizada con el IAM o con el método N/D resuelve este conflicto.

Los resultados principales obtenidos en la publicación de la sección 2.2.3 pueden ser resumidos como sigue:

- En primer lugar, comprobamos que la dualidad semi-local se satisface correctamente para $N_c = 3$ usando datos experimentales. Para ello, comparamos las predicciones obtenidas usando teoría de Regge por un lado, y por otro con las parametrizaciones de la amplitud del scattering de piones de [149]. Incluyendo las ondas S, P y D, o sólo las ondas S y P, analizamos cómo están dominadas las integrales por las ondas parciales más pequeñas.

- Mostramos que los parámetros de Regge, ajustados a partir del comportamiento a alta energía del scattering de nucleones y del scattering pion-nucleón, nos permiten obtener correctamente las longitudes de scattering de las ondas P y D a través de sus representaciones de Froissart-Gribov.

- Habiendo confirmado que la dualidad semi-local entre resonancias e intercambios de Regge se satisface para $N_c = 3$, usamos el IAM para describir las amplitudes. Comprobamos que el IAM satisface dualidad semi-local para $N_c = 3$, lo que nos permite estudiar este fenómeno cuando incrementamos N_c.

- Como ya se anticipó en [212], encontramos que para $O(p^4)$, las incertidumbres derivadas de la elección de la escala de renormalización en la que se fija el escaleo con N_c, lleva a diferentes comportamientos para el polo de resonancia σ cuando N_c se aleja de 3. Se obtienen resultados que van del representado en la Fig. D.3, a aquellos en las que la σ se aleja del eje real, o en los que la σ se mueve hacía al eje real pero con una masa por debajo del umbral de piones.

- Comprobamos que para aquellos comportamientos en los que la $f_0(500)$ se aleja del eje real, o se mueve hacía el corte izquierdo, es decir, en los que no aparece un estado $\bar{q}q$ por encima de 1 GeV que sobrevive a gran N_c, la cancelación entre la σ y la $\rho(770)$ no se produce, dando lugar a un conflicto con la dualidad semi-local. Demostramos pues, que, para satisfacer la dualidad semi-local, el polo de la σ no puede desaparecer completamente en el plano complejo, lo que de hecho ocurre para la mayor parte del espacio de parámetros de los cálculos unitarizados a un loop.

- Sin embargo, cuando la σ introduce una componente subdominante $\bar{q}q$ con una masa por encima de 1 GeV, como la que hemos represetado en la Fig. D.3, la dualidad semi-local se satisface para todo N_c.

- Finalmente, comprobamos que estos resultados son consistentes, aún cuando se incluyen resonancias más pesadas como por ejemplo la $f_0(980)$ o la $f_2(1270)$.

En las publicaciones de las secciones 2.2.4 y 2.2.5, abordamos de nuevo el problema de la naturaleza de la σ estudiando el papel que juegan las resonancias más ligeras en la dualidad semi-local y en las reglas de suma espectrales. Para ello utilizamos ChPT en un formalismo de U(3), usando por tanto, no sólo los pseudo-bosones de Goldstone: π, K y η, sino también utilizando la η'. Además, en vez de utilizar las contribuciones a un loop, introducimos explícitamente el intercambio de resonancias a tree level, asumiendo que las constantes de baja energía están saturadas por las resonancias más ligeras. También utilizaremos el método no perturbativo N/D, para unitarizar las amplitudes de scattering de diferentes mesones y los intercambios de las resonancias a tree level. Una de las principales motivaciones para utilizar

este formalismo es discutir la expansión de N_c, puesto que la η' se convierte en el noveno bosón de Goldstone al incrementar N_c. A la hora de obtener este resultado, asumiremos que el comportamiento con N_c de las constantes de acoplamiento de las resonancias es $\mathcal{O}(\sqrt{N_c})$, que las masas de las resonancias son $\mathcal{O}(\sqrt{1})$, y que las constantes de sustracción que aparecen al unitarizar las interacciones son $\mathcal{O}(\sqrt{1})$.

Los principales puntos de discusión de estas dos publicaciones son:

- En primer lugar ajustamos los parámetros libres de la teoría utilizando una gran cantidad de datos experimentales, consistentes en desfasajes e inelasticidades de los procesos de scattering $\pi\pi \to \pi\pi(K\bar{K})$ y $\pi K \to \pi K$ para diferentes valores de isospín y momento angular.

- A partir de los ajustes previos, obtenemos en la segunda hoja de Riemann de las amplitudes de scattering unitarizadas, polos asociados a siete resonancias escalares y tres vectoriales, especificamente, los polos: $f_0(500)$, $f_0(980)$, $f_0(1370)$, $K_0(800)$, $K_0(1430)$, $a_0(980)$, $a_0(1450)$, $\rho(770)$, $K(892)$ y $\phi(1020)$. Las masas y anchuras de estas resonancias se ajustan bien a los valores recogidos en el PDG. Además, también calculamos los acoplamientos de estas resonancias a diferentes pares de pseudo-bosones de Goldstone. Es importante hacer notar que la $f_0(500)$ se acopla de una manera muy marginal a los canales de la η y de la η', lo que indica que esta resonancia apenas está afectada por la dinámica de estos dos pseudo-bosones de Goldstone.

- Al estudiar el canal de $I = 2$ definido en el canal t, confirmamos de nuevo los resultados obtenidos en la publicación de la sección 1.8.3: la dualidad semi-local también se satisface para el $N_c = 3$ en este formalismo.

- Al incrementar N_c, somos capaces de satisfacer la dualidad semi-local cuando se imponen ad hoc los comportamientos subdominantes con N_c de las resonancias escalares y vectoriales. Como ya se encontró en [221] utilizando este formalismo, la resonancia $f_0(500)$ se adentra en el plano complejo alejándose del eje real, por lo que la fuerza necesaria para cancelar la contribución de la resonancia $\rho(770)$, que, como hemos visto anteriormente, es necesaria para satisfacer la dualidad semi-local, viene en este caso del singlete escalar, que para $N_c = 3$ es sólo una parte subdominante de la $f_0(980)$, pero que, para valores mayores de N_c, se convierte en la componente dominante. Esta es la fuente crucial necesaria para cancelar la contribución de la $\rho(770)$, y por consiguiente, para satisfacer la dualidad semi-local cuando aumenta N_c.

- En importante hacer notar que, tanto en este trabajo como en el anterior realizado usando el IAM, es una componente $\bar{q}q$ con una masa alrededor de 1 GeV, la que compensa la contribución de la $\rho(770)$. Esta componente $\bar{q}q$, subdominante para ambas resonancias en $N_c = 3$, se convierte en dominante cuando aumenta N_c. Por consiguiente, mientras que la solución obtenida en ambos análisis es similar, la forma de llegar a ella es diferente.

- Finalmente, estudiamos otra forma de constreñir las propiedades de las resonancias ligeras, como es el uso de las reglas de suma espectrales, que se satisfacen en el límite

quiral [222, 223]. En particular, calculamos las regla de suma espectral escalar y pseudoescalar, que se obtienen a partir de los factores de forma apropiados, unitarizados usando el método N/D. A partir de los parámetros obtenidos en el ajuste previo, concluímos que estas reglas de suma se satisfacen en el límite quiral con una violación de sólo un 10%.

En la Sección 2.2.6, estudiamos la dependencia con el número de colores de los acoplamientos de varios tipos de estados, que corresponden a diferentes estructuras de mesones representado en términos de quarks y gluones. La expansión N_c de estos acoplamientos es de interés porque investigaciones actuales se dedican a entender la composición de los hadrones en términos de su representación fundamental en los grados de libertad de QCD. Para estudiar una posible expansión de Fock de los componentes de la controvertida resonancia σ, estudiamos los acoplamientos, masas y anchuras de diferentes estados de QCD compatibles con los números cuánticos de la σ, específicamente: $\bar{q}q$, $(\bar{q}q)^2$, $\bar{q}\bar{q}qq$, y el glueball, donde el segundo estado denota el estado tetraquark o molecular, y el tercero al tetraquark exótico, también denomiado polyquark. En este trabajo encontramos que ninguno de estos estados tiene el comportamiento con N_c encontrado en [220], por lo que esperamos que la resonancia σ sea una mezcla de diferentes estados.

En la publicación de la sección 2.2.7, presentamos resultados preliminares sobre una posible descomposición de Fock de la σ en términos de tres estados de QCD, el mesón ordinario $\bar{q}q$, la molécula $\pi\pi$ o estado tetraquark y el glueball:

$$|\sigma\rangle = \alpha|\bar{q}q\rangle + \beta|(\bar{q}q)^2\rangle + \gamma|gg\rangle, \tag{D.17}$$

donde los coeficientes α, β y γ son en principio dependientes de N_c. Los principales puntos de discusión:

- A la hora de obtener el valor de estos coeficientes, construimos un Hamiltoniano efectivo 3×3, que asumimos representa al sector escalar más ligero, y factorizamos el comportamiento dominante con N_c de los elementos de esta matriz, que es conocido gracias al estudio realizado en la sección previa. Al diagonalizar este Hamiltoniano, obtenemos tres estados, identificando el más ligero de ellos como el mesón σ.
- Los coeficientes de las diferentes potencias de N_c de los elementos de matriz del Hamiltoniano se ajustan a continuación al comportamiento para la masa y anchura de la sigma con el número de colores obtenido en [220].
- Sin embargo, dado el gran número de parámetros, imponemos que deben ser naturales. A partir de este ajuste, podemos obtener entonces el comportamiento con N_c de los coeficientes dados en la ecuación (D.17), y por consiguiente, la composición de la σ para $N_c = 3$.
- En los resultados preliminares presentados en la sección 2.2.7, obtenemos que el mesón σ está compuesto para $N_c = 3$ por alrededor de un 65% de tetraquark o estado molecular, un 25% de $\bar{q}q$ y sólo un 10% de glueball. Sin embargo, cuando incrementa N_c, esta composición cambia. Para $N_c = 8$ la componente $\bar{q}q$ es más importante que la componente molecular. Para $N_c = 20$ la σ es predominantemente un estado $\bar{q}q$ con sólo un

10% de tetraquark y una contribucción despreciable de glueball. Es evidente que estos resultados son ligeramente dependientes de la forma en que imponemos la condición de naturalidad, pero esta estimación puede ser considerada como un resultado bastante aproximado. Es importante recalcar que este resultado se obtiene a partir de coeficientes del Hamiltoniano naturales.

- Cuando imponemos una contribución dominante para el glueball o el estado $\bar{q}q$, ésto implica una falta considerable de naturalidad en los parámetros de Hamiltoniano.

Finalmente, en la seccion 2.2.8, estudiamos si hay otras soluciones naturales a este problema. Para ello analizamos cómo la condición de naturalidad restringe la posible composición del escalar más ligero.

El papel de la resonancia más ligera en la restauración de la simetría quiral.

Motivación

El condensado de dos quarks $\langle \bar{q}q \rangle$ puede considerarse como el parámetro de orden de la ruptura espontánea de la simetría quiral, pues su valor no nulo es una consecuencia de esta ruptura, y es de esperar que se anule cerca de la región crítica. Además, la susceptibilidad escalar describe la respuesta del vacío de QCD a cualquier campo escalar, y por tanto, mide las fluctuaciones del condensado de quarks, mostrando un comportamiento que crece considerablemente cerca de la transición crítica. En esta sección, queremos estudiar el papel de la resonancias escalares más ligeras, y en particular, el de la resonancia $f_0(500)$, en la restauración de la simetría quiral, lo cual conseguiremos estudiando su papel en el condensado de quarks y en la susceptibilidad escalar.

La susceptibilidad escalar puede ser calculada como la derivada del condensado de quarks con respecto a la masa de éstos o, como la diferencia entre el correlador de cuatro quarks y el cuadrado de condesado de dos quarks. De esta forma, los condensados de cuatro quarks aparecen naturalmente en el cálculo de la susceptibilidad escalar. En principio, condensados de orden arbitrario $\langle (\bar{q}q)^n \rangle$ pueden ser también construidos a partir de operadores que no son invariantes bajo transformaciones quirales, pero que tienen los números cuánticos del vacío, por lo que son también objetos útiles para estudiar la restauración de la simetría quiral. Además, los condesados de cuatro quarks también son relevantes en física hadrónica porque aparecen directamente en la reglas de suma de QCD, por medio de la expansión de producto de operadores (OPE en sus siglas en inglés) [258], en la que suele aceptarse la hipótesis de factorización, que asume que el condensado de cuatro quarks factoriza en el cuadrado del condensado de dos $\langle (\bar{q}q)^2 \rangle \sim \langle \bar{q}q \rangle^2$. En esta sección también queremos comprobar esta hipótesis usando ChPT. Además, como hemos visto en la sección anterior, esperamos que la resonancia $f_0(500)$ esté formada predominantemente por un tetraquark o estado molecular, por lo que estudiar las propiedades de los condensados de cuatro quarks es interesante por sí mismo. Es importante hacer notar que, para logar nuestro objetivo, hemos de estudiar las propiedades del condensado de quark y de la susceptibilidad escalar no sólo a temperatura cero, sino también a temperatura finita.

Resumen de los resultados

Con estas motivaciones procedemos a realizar el siguiente programa de investigación. En primer lugar, estudiamos las propiedades del condensado de quarks y la susceptibilidad escalar a temperatura cero, usando ChPT que, como hemos dicho, es un formalismo independiente del modelo. Como resultado derivado del cálculo de la susceptibilidad, hemos analizado también el condensado de cuatro quarks y la hipótesis de factorización. Finalmente, incluimos efectos térmicos de dos maneras diferentes, usando ChPT y la aproximación del virial intoduciendo los desfasajes obtenidos usando ChPT. Ambos formalismos son independientes del modelo a bajas temperaturas y pueden ser obtenidos el uno del otro [196]. Sin embargo, los desfasajes calculados usando ChPT, no reproducen las resonancias que aparecen en las amplitudes de scattering, por lo que no podemos estudiar, en particular, el efecto de la resonancia $f_0(500)$ en la transición quiral. Para poder realizar este análisis, usamos el IAM combinado con la aproximación del virial, pues, de esta forma, vamos a poder estudiar y aislar el papel de la resonancias, pero comprobando que a bajas temperaturas, todavía reproducimos los resultados anteriores independientes del modelo. Además, de esta forma, podemos estudiar los efectos no resonantes que, muchas veces, son despreciados en modelos de gases de resonancias que, sin embargo, sí incluyen la σ, $\rho(770)$ $\cdots$ etc. como estados libres. Es importante hacer notar que, debido a la supresión Bolzmann, es de esperar que la σ juege el papel más relevante en las interacciones. Finalmente, también estudiamos en esta sección la suceptibilidad pseudo-escalar, que es otra manera de analizar la restauración de la simetría quiral por medio de la degeneración de parejas quirales.

En la publicación de la seccion 2.3.3, analizamos las propiedades de los condensados de cuatro quarks y de la susceptibilidad escalar en ChPT a temperatura cero. Como hemos dicho anteriormente, estos resultados serán necesarios para realizar los cálculos a temperatura finita. Los principales resultados obtenidos en esta sección son:

- Comprobamos en primer lugar que el condensado de cuatro quarks puede expresarse como el cuadrado del condensado de dos al orden dominante (LO en sus siglas en inglés) y al siguiente orden dominante (NLO en sus siglas en inglés), es decir, la hipótesis de factorización se satisface a estos órdenes.

- Sin embargo, al tercer orden dominante (NNLO en sus siglas en inglés), un término con una dependencia espacio-temporal no trivial en el correlador de cuatro quarks, da lugar a un condensado divergente, mientras que el de dos, sigue siendo finito a ese mismo orden. A pesar de que el estudio de los condensados de cuatro quarks no era el motivo original de estudio, este resultado es relevante por sí mismo, pues contradice la hipótesis de factorización.

- A continuación comprobamos que los términos que rompen la hipótesis de factorización, son precisamente los necesarios para obtener una suceptibilidad escalar finita e independiente de la escala, para el caso ligero, el extraño, y el mixto ligero-extraño.

- Finalmente, vemos cómo los términos que rompen la factorización se anulan en el límite quiral, al igual que formalmente cuando se toma el límite $N_c \to \infty$. Ésto se da a cualquier orden en la expansión quiral.

En la sección 2.3.4, estudiamos el papel de la resonancia $f_0(500)$ en la restauración de la simetría quiral, explorando propiedades adicionales de los condensados de quarks y de la susceptibilidad escalar a temperatura finita usando ChPT. Por consiguiente, en este trabajo extendemos el análisis de la sección previa a bajas temperaturas. También usamos la aproximación del virial para estudiar la restauración de la simetría quiral usando, tanto interacciones unitarizadas, como no unitarizadas. Las últimas, nos permiten aislar el efecto y papel de la resonancia $f_0(500)$ en la transición de fase. Los principales resultados en esta sección son:

- En primer lugar mostramos que, al igual que en el caso a temperatura cero, la hipótesis de factorización no se cumple a NNLO en ChPT a temperatura finita, lo que implica que no es adecuado usar los condensados de cuatro quarks como parámetros de orden de la restauración de la simetría quiral, puesto que los términos que rompen la factorización son divergentes. Sin embargo, al igual que ocurría a temperatura cero, la factorización sí tiene lugar en el límite $N_c \to \infty$.

- En el límite quiral, y contrariamente al caso de temperatura cero, a temperatura finita los términos que rompen la factorización son finitos y no se anulan. Por consiguiente, el límite quiral es el único caso en el que el condesado de cuatro quarks puede considerarse un parámetro de orden. De hecho, comprobamos que se funde siguiendo el mismo comportamiento que el condensado de dos quarks para las temperaturas en las que ChPT es, aún, una expansión válida. Es importante hacer notar que, es en este límite, en el que la restauración de la simetría quiral tiene lugar formalmente.

- A continuación, obtenemos la susceptibilidad escalar en ChPT a temperatura finita. En la derivación de ésta, también obtenemos en ChPT el condensado térmico de dos quarks en SU(3) a NNLO. Este resultado no ha sido obtenido previamente en la literatura a este orden, y es, por tanto, una extensión a órdenes superiores de trabajos anteriores, en los que sólo se introducían a ese orden, kaones y etas libres [196]. Ésto nos permite obtener de forma independiente del modelo, el tamaño relativo de las interacciones a bajas temperaturas.

- A continuación, realizamos un análisis detallado de la susceptibilidad escalar usando la aproximación del virial con amplitudes obtenidas en ChPT, extendiendo resultados previos y estudiando su robustez. Debido a que la aproximación del virial es independiente del modelo, ésto nos permite hacer predicciones para temperaturas por debajo de la crítica. De hecho, en este régimen, encontramos que, tanto para la presión como para el condensado y la susceptibilidad escalar, hay una gran cancelación entre los canales de isospín 0 y de isospín 2.

- Estudiando las interacciones unitarizadas en la aproximación del virial, hemos encontrado que el efecto de la la resonancia $f_0(500)$, está casi completamente cancelado por el canal escalar de $I = 2$, dejando a la resonancia $\rho(770)$, como la principal contribución. Esta resonancia, se encuentra, sin embargo, suprimida a bajas energías debido a su momento angular. Por tanto, en este régimen, la parte de interacción de los coeficientes del virial es mucho más pequeña de lo que en principio cabría esperar a partir del tamaño de cada una de las ondas por separado. Este resultado es de gran importancia para todos los modelos que consideran gases de hadrones libres, y en los que la resonancia σ es incluida mientras que el canal $I = 2$, $J = 0$ es ignorado.

Por último, en la sección 2.3.5, siguiendo el mismo procedimiento anterior de utilizar correladores de cuatro quarks, calculamos la suceptibilidad pseudo-escalar en ChPT a temperatura finita y a NLO. Encontramos que ésta evoluciona como el condensado de dos quarks, tal y como cabía de esperar a partir de argumentos generales relacionados con el álgebra de corrientes. Ésto nos permite realizar un estudio de la restauración de la simetría quiral a partir de la degeneración de compañeros quirales. La susceptibildad escalar se puede aproximar al cuadrado del inverso de la masa de la resonancia σ, pues es el estado que satura el correlador escalar en un modelo O(4). La suceptibilidad pseudo-escalar está dominada por el polo del pión y, por tanto, está mucho mejor determinado en ChPT.

Conclusiones

A lo largo de esta tesis hemos estudiado las propiedades del scattering de piones y de las resonancias más ligeras que aparecen en este proceso, es decir, la resonancia $f_0(500)$ y $f_0(980)$. Además, hemos analizado el papel de la resonancia escalar más ligera en la ruptura espontanea de la simetría quiral, estudiando el comportamiento de configuraciones de orden superior de condensados de quarks y la susceptibilidad escalar. Podemos dividir nuestras contribuciones principales en tres bloques diferentes.

En el primer bloque, hemos obtenido parametrizaciones consistentes, precisas e independientes del modelo, de los polos asociados con las dos resonancias escalares más ligeras sin extrañeza. Estas resonancias han sido obtenidas a partir de ajustes de datos experimentales, pero también imponiendo que satisfagan ecuaciones de Roy una o dos veces sustraidas. De hecho, en esta tesis hemos presentado la obtención de las ecuaciones de Roy con una sola sustracción, que hemos denominado ecuaciones GKPY, mostrando que dan resultados mucho más precisos en la región de las resonancias a partir de los mismos inputs teóricos. Para describir las amplitudes de scattering, hemos obtenido un conjunto de parametrizaciones simples que nos permiten describir todo el rango de energía desde el umbral hasta 20 GeV. Estas parametrizaciones que denominamos Ajustes no Constreñidas de Datos (UFD en sus siglas en inglés), son obtenidas ajustando a los datos experimentales de las ondas parciales hasta una energía de 1.42 GeV, y a datos de amplitudes de Regge por encima de esta energía. En particular, hemos hecho uso de los últimos resultados de desintegraciones de K_{l4} obtenidos por la colaboración NA48/2 [154], que son muy precisos. También hemos resuelto varias incertidumbres de la literatura e incluido la violación de isospín propuesta en [155].

A continuación, hemos mejorado los valores centrales de nuestros ajustes imponiendo, a parte del ajuste de datos, la satisfacción de relaciones de dispersión hacía delante hasta 1.42 GeV, ecuaciones de Roy y GKPY hasta 1.1 GeV, y reglas de suma, obteniendo de esta forma, un conjunto de parametrizaciones que hemos denomiado Ajustes Constreñidos de Datos (CFD en sus siglas en inglés). Los valores centrales de las parametrizaciones CFD se encuentran dentro de los valores de la UFD, pero satisfacen también todas las relaciones de dispersión mencionadas anteriormente. El incremento de la precisión que introducen las ecuaciones GKPY requiere la mejora de la parametrización de la onda S0, a la que imponemos una derivada continua en el punto de matching entre la zona de baja energía y energía intermedia. Además, estas ecuaciones favorecen la solución de un "dip" en la inelasticidad de la onda S0

en la región entre 1000 y 1100 MeV. Usando el conjuto CFD como input en diferentes reglas de suma y en las propias relaciones de dispersión, obtenemos determinaciones precisas de los desfasajes en la zona elástica, de los parámetros umbrales y de los ceros de Adler.

Finalmente, y puesto que el formalismo dispersivo que hemos utilizado es especialmente preciso en la zona de las resonancias, hemos sido capaces de determinar en esta tesis de una manera independiente del modelo, los polos de la $f_0(500)$ y $f_0(980)$ y sus acoplamientos a dos piones, sólo a partir de los datos y sin usar ningún input teórico. Como ya hemos visto en la sección anterior, los resultados obtenidos de ambos polos han tenido un gran impacto en la revisión que el Grupo de Datos de Partículas (PDG en sus siglas en inglés) ha realizado en su último resumen de física de partículas [11].

En un segundo bloque, hemos estudiado la naturaleza de las resonancias escalares más ligeras usando la expansión $1/N_c$ de QCD, que proporciona una manera de analizar su naturaleza espectroscópica, así como otras herramientras teóricas y fenomenológicas como son la dualidad semi-local, o las reglas de suma espectrales. Para parametrizar la amplitud de scattering de piones, y para obtener los polos que aparecen en este proceso, hemos usado la teoría de baja energía de QCD, llamada Teoría de Perturbaciones Quiral (ChPT), unitarizada con dos formalismos diferentes: el Método de la Amplitud Inversa elástico (IAM en sus siglas en inglés), y el método N/D.

El IAM elástico está basado en primeros principios como son la unitariedad y la analiticidad, reproduciendo a su vez la expansión de ChPT a un orden determinado. El IAM se obtiene a partir de una relación de dispersión y sólo depende de las contantes de baja energía (LECs en sus sigla en inglés) de ChPT, por lo que no introduce ningún parámetro espurio que pueda esconder dependencias desconocidas de los parámetros de QCD. El IAM permite generar polos en la segunda hoja de Riemann sin realizar ninguna suposición sobre su existencia o naturaleza. Por consiguiente, es un método muy apropiado para estudiar las propiedades de estas resonancias y, particularmente, su dependencia con el número de colores.

El método N/D puede usarse para describir la estructura más general de una onda parcial elástica cuando los cortes no físicos son despreciados. Las amplitudes de estas ondas parciales se pueden ajustar a las amplitudes de ChPT al orden más bajo y al intercambio de resonancias en canal s. Por tanto, el método N/D es una herramienta simple con la que es posible incorporar directamente resonancias en el Lagrangiano, pero satisfaciendo unitariedad en el corte derecho. Además se puede extender fácilmente a canales acoplados, reproduciendo polos en la segunda hoja de Riemann asociados a las resonancias más ligeras, cuyas determinaciones son consistentes con los experimentos.

Adicionalmente, incluyendo la dependencia al orden dominante con N_c de los parámetros del Lagrangiano, es posible estudiar la expansión $1/N_c$ de las resonancias generadas usando ambos formalismos, y compararlos con el comportamiento esperado de diferentes estados de QCD.

Por un lado, se ha propuesto en muchos modelos [211, 213, 214, 215, 216, 217, 218, 221] que las resonancias escalares más ligeras no tienen el comportamiento esperado de un estado $\bar{q}q$. Por otro lado, las resonancias vectoriales sí se comportan como cabría esperar de estos estados. En consecuencia, las resonancias vectoriales y escalares tienen un comportamiento diferente

con N_c [211]. Sin embargo, cualquier modelo en el que ésto ocurre esta potencialmente en conflicto con la dualidad semi-local en el scattering de piones, pues ésta requiere una sutil cancelación entre los canales $I = 0$ e $I = 1$, que están dominados a bajas energías por la σ y la $\rho(770)$ respectivamente. Si estas resonancias se comportan de manera diferente con N_c, esta cancelación puede verse afectada en un principio, teniendo que ser comprobado este hecho explícitamente.

En la sección 2.2 de esta tesis hemos demostrado como ChPT unitarizada evita este posible conflicto. En [211, 220], se mostró usando el IAM, que para N_c cercano a 3, la $f_0(500)$ no se comportaba como un estado $\bar{q}q$, es decir, su masa y su anchura se incrementaban al incrementar N_c. Sin embargo, este comportamiento no está fijado de una manera única cuando N_c se hace más grande, pues hemos de elegir la escala en la que comenzar la expansión de N_c. En esta tesis hemos comprobado que a $\mathcal{O}(p^4)$ son posibles varios comportamientos con N_c, pero que pueden ser sin embargo clasificados en dos formas diferentes: aquellos que poseen una componente $\bar{q}q$ subdominante con una masa por encima de 1 GeV, y en los que por lo tanto, la σ vuelve al eje real para N_c suficientemente grande o aquellos en los que se aleja del eje real. De hecho el primer comportamiento es el más favorecido para la mayor parte del espacio de parámetros en cálculos a $\mathcal{O}(p^6)$ [220]. En esta tesis hemos comprobado que para aquellos casos en los que la σ no muestra una componente subdominante $\bar{q}q$ al incrementar N_c, la dualidad semi-local falla. Sin embargo, cuando esta componente sí aparece con una masa alrededor de 1 GeV, la dualidad semi-local aún se satisface al incrementar N_c. Por tanto, concluimos que, en este formalismo, esta componente es esencial a la hora de compensar la contribución $\bar{q}q$ de la $\rho(770)$.

También hemos comprobado que la dualidad semi-local se satisface usando el método N/D con canales acoplados en un formalismo U(3). Como hemos comentado anterioremente, la masa de la η' decrece con N_c, llegando a ser en este régimen el noveno pseudo-bosón de Goldstone. En primer lugar, como ya fue anticipado en [221], vemos como la σ apenas se acopla a los diferentes canales de la η', haciendo que sea por tanto razonable despreciarla al estudiar la dinámica de la σ. De acuerdo con los resultados obtenidos usando el IAM, en este formalismo la σ también se aleja del eje real para N_c cercano a tres, evidenciando una vez más que esta resonancia no es predominantemente un estado $\bar{q}q$. Sin embargo, cuando incrementamos N_c, el polo de la σ gira a la izquierda del plano complejo, y por tanto no cancela la contribución de la $\rho(770)$. En este formalismo hay una componente subdominante $\bar{q}q$ con una masa alrededor de 1 GeV esta vez en la resonancia $f_0(980)$, que, como en el caso del IAM, compensa la contribución de la $\rho(770)$. No obstante es neceario imponer ad hoc comportamientos subdominantes de las resonancias en N_c. Por otro lado, el polo de la resonancia σ va a parar a una región en la que es muy complicado hacer suposiciones físicas sobre su naturaleza.

También hemos estudiado en este bloque el comportamiento con N_c de las masas, anchuras y acoplamientos de diferentes configuraciones de QCD hechas de quarks y gluones que podrían ser constituyentes de la σ. Hemos comprobado que ninguno de estos estados reproduce por si mismo el comportamiento de la masa y anchura de la σ encontrado en [220], concluyendo por tanto que ésta tiene que ser una mezcla de algunos de estos estados. Finalmente, hemos presentado un modelo en el que se analiza una descomposición de la σ en términos de grados de libertad de QCD. Considerando sólo tres estados, el $\bar{q}q$, el molecular

o tetraquark y el glueball, truncamos el espacio de Fock, dando lugar a un Hamiltoniano simétrico que representa el sector escalar. El autovalor más ligero se identifica entonces con la σ, y los coeficientes libres del Hamiltoniano se ajustan a la masa y anchura de la σ obtenida en [220] como función de N_c. A partir de este ajuste, somos capaces de estimar la proporción de estos estados en el mesón σ, concluyendo que el estado molecular o tetraquark es la contribución dominante en $N_c = 3$.

Finalmente, en el tercer bloque hemos analizado el papel de la resonancia $f_0(500)$ en la restauración de la simetría quiral, estudiando su influencia en el condensado de quarks y en la suceptibilidad escalar. Para hacer esto, hemos estudiado en primer lugar ambos observables a temperatura cero usando ChPT. La susceptibilidad escalar puede ser obtenida de dos maneras diferentes: como la derivada del condesado de quarks respecto a la masa de estos, o como la diferencia entre el correlador de cuatro quarks y el cuadrado del condensado de dos. A la hora de comprobar los resultados obtenidos con ambas definiciones, llegamos a un resultado interesante e independiente del modelo para el condensado de cuatro quarks; el hecho de que la hipótesis de factorización no se satisface en ChPT al tercer orden dominante (NNLO en sus siglas en inglés). Este resultado es relevante por si mismo pues el condensado de cuatro quarks aparece directamente en las reglas de suma de QCD, por medio de la expansión del producto de operadores, donde se suele asumir la hipótesis de factorización. De hecho, hemos demostrado en esta tesis que los términos que rompen la factorización a NNLO son divergentes, y provienen de un término con una dependencia espacio-temporal no trivial. Estos términos divergentes, se anulan, sin embargo, en el límite quiral, que es el régimen en el que la restauración de la simetría quiral tiene lugar formalmente. Además, hemos comprobado que éstos son precisamente los necesarios para obtener una susceptibilidad escalar finita e independiente de la escala.

Volviendo al cálculo de la susceptibilidad escalar, a temperatura finita, hemos usado dos métodos diferentes e independientes del modelo, ChPT y la aproximación del virial. Usando ChPT, hemos calculado el condensado de cuatro quarks a temperatura finita, obteniendo que también es divergente a NNLO, no sólo debido a la contribución de temperatura cero. Sin embargo, éste se vuelve finito tanto en la expansión de $1/N_c$ como en el límite quiral. En el caso de la susceptibilidad escalar, hemos estudiado su comportamiento a bajas temperaturas, donde sabemos que la expansión de ChPT converge, obteniendo que crece linealmente con la temperatura. Usando la aproximación del virial, hemos estudiado en primer lugar las interacciones no unitarizadas obtenidas con ChPT, pues son independientes del modelo, aunque sólo dan información a muy bajas temperaturas. Este cálculo nos permite comprobar una importante cancelación entre los canales escalares con $I = 0$ e $I = 2$. Finalmente, para estudiar el papel de las resonancias hemos usado el IAM. Como hemos comentado anteriormente, este método permite reproducir las resonancias que aparecen en el scattering de piones a bajas energías pero recuperando la expansión quiral. De esta forma, podemos aislar el efecto de la resonancia σ, asegurando que a bajas temperaturas aún reproducimos los resultados previos independientes del modelo. Usando este formalismo, hemos obtenido que la contribución de la resonancia σ en el condensado de quarks y en la susceptibilidad escalar está cancelada casi totalmente por el canal escalar con $I = 2$, dando lugar conjuntamente a una contribución despreciable en ambos observables. Además, a temperaturas más altas la interacción está dominada por la $\rho(770)$. Por tanto, estos resultados invalidan aquéllos de los modelos que

incluyen la σ sin tener en cuenta el canal escalar $I = 2$.

Creemos que estos resultados han contribuido a aportar cierta luz en la naturaleza de los mesones escalares, y esperamos que sirva de herramienta para futuros estudios.

Bibliography

[1] M. Johnson and E. Teller, *Classical Field Theory of Nuclear Forces*, *Phys. Rev.* **98** (1955) 783–787.

[2] A. Dobado and J. R. Pelaez, *On The Equivalence theorem in the chiral perturbation theory description of the symmetry breaking sector of the standard model*, Nucl. Phys. B **425**, 110 (1994) [Erratum-ibid. B **434**, 475 (1995)] [hep-ph/9401202].

[3] A. Dobado and J. R. Pelaez, *The Equivalence theorem for chiral lagrangians*, Phys. Lett. B **329** (1994) 469 [Addendum-ibid. B **335** (1994) 554] [hep-ph/9404239].

[4] A. Dobado, M. J. Herrero, J. R. Pelaez, E. Ruiz Morales and M. T. Urdiales, *Learning about the strongly interacting symmetry breaking sector at LHC*, Phys. Lett. B **352**, 400 (1995) [hep-ph/9502309].

[5] G. Ecker, J. Gasser, A. Pich, and E. de Rafael, *The Role of Resonances in Chiral Perturbation Theory*, *Nucl. Phys.* **B321** (1989) 311.

[6] J. F. Donoghue, C. Ramirez and G. Valencia, *The Spectrum of QCD and Chiral Lagrangians of the Strong and Weak Interactions*, Phys. Rev. D **39**, 1947 (1989).

[7] S. Weinberg, *Phenomenological Lagrangians*, *Physica* **A96** (1979) 327.

[8] J. Gasser and H. Leutwyler, *Chiral Perturbation Theory to One Loop*, *Annals Phys.* **158** (1984) 142.

[9] J. Gasser and H. Leutwyler, *Chiral Perturbation Theory: Expansions in the Mass of the Strange Quark*, *Nucl. Phys.* **B250** (1985) 465.

[10] C. Amsler *et al.* [Particle Data Group Collaboration], *Review of Particle Physics*, Phys. Lett. B **667**, 1 (2008).

[11] J. Beringer *et al.* [Particle Data Group Collaboration], *Review of Particle Physics (RPP)*, Phys. Rev. D **86**, 010001 (2012).

[12] R. L. Jaffe, *Multi-Quark Hadrons. 1. The Phenomenology of (2 Quark 2 anti-Quark) Mesons*, *Phys. Rev.* **D15** (1977) 267.

[13] R. L. Jaffe, *Multi-Quark Hadrons. 2. Methods*, *Phys. Rev.* **D15** (1977) 281.

[14] R. Jaffe and F. Low, *The Connection Between Quark Model Eigenstates and Low-Energy Scattering*, *Phys. Rev.* **D19** (1979) 2105–2118.

[15] J. D. Weinstein and N. Isgur, *Do Multi-Quark Hadrons Exist?*, *Phys. Rev. Lett.* **48** (1982) 659.

[16] J. D. Weinstein and N. Isgur, *The q q anti-q anti-q System in a Potential Model*, *Phys. Rev.* **D27** (1983) 588.

[17] J. D. Weinstein and N. Isgur, *K anti-K Molecules*, *Phys. Rev.* **D41** (1990) 2236.

[18] G. Janssen, B. Pearce, K. Holinde, and J. Speth, *On the structure of the scalar mesons f0 (975) and a0 (980)*, *Phys. Rev.* **D52** (1995) 2690–2700, [nucl-th/9411021].

[19] N. Achasov and V. Gubin, *Search for the scalar a0 and f0 mesons in the reactions e+ e- —> gamma pi0 pi0 (eta)*, *Phys. Rev.* **D56** (1997) 4084–4097, [hep-ph/9703367].

[20] P. Minkowski and W. Ochs, *Identification of the glueballs and the scalar meson nonet of lowest mass*, *Eur. Phys. J.* **C9** (1999) 283–312, [hep-ph/9811518].

[21] E. van Beveren and G. Rupp, *Modified Breit-Wigner formula for mesonic resonances describing OZI decays of confined q anti-q states and the light scalar mesons*, *Eur. Phys. J.* **C22** (2001) 493–501, [hep-ex/0106077].

[22] J. Vijande, A. Valcarce, F. Fernandez, and B. Silvestre-Brac, *Nature of the light scalar mesons*, *Phys. Rev.* **D72** (2005) 034025, [hep-ph/0508142].

[23] T. Hyodo, D. Jido, and T. Kunihiro, *Nature of the σ meson as revealed by its softening process*, *Nucl. Phys.* **A848** (2010) 341–365, [arXiv:1007.1718].

[24] R. Kaminski, G. Mennessier, and S. Narison, *Gluonium nature of the sigma/f(0)(600) from its coupling to K anti-K*, *Phys. Lett.* **B680** (2009) 148–153, [arXiv:0904.2555].

[25] Y. Ne'eman, *Derivation of strong interactions from a gauge invariance*, *Nucl. Phys.* **26**, 222 (1961).

[26] M. Gell-Mann, *Symmetries of baryons and mesons*, Phys. Rev. **125**, 1067 (1962).

[27] M. Gell-Mann, *A Schematic Model of Baryons and Mesons*, Phys. Lett. **8**, 214 (1964).

[28] G. Zweig, *An Su(3) Model For Strong Interaction Symmetry And Its Breaking. 2.'* CERN-TH-412.

[29] V. E. Barnes, P. L. Connolly, D. J. Crennell, B. B. Culwick, W. C. Delaney, W. B. Fowler, P. E. Hagerty and E. L. Hart *et al.*, *Observation of a Hyperon with Strangeness -3*, Phys. Rev. Lett. **12**, 204 (1964).

[30] J. E. Augustin *et al.* [SLAC-SP-017 Collaboration], *Discovery of a Narrow Resonance in e+ e- Annihilation*, Phys. Rev. Lett. **33**, 1406 (1974).

[31] S. W. Herb, D. C. Hom, L. M. Lederman, J. C. Sens, H. D. Snyder, J. K. Yoh, J. A. Appel and B. C. Brown *et al.*, *Observation of a Dimuon Resonance at 9.5-GeV in 400-GeV Proton-Nucleus Collisions*, Phys. Rev. Lett. **39**, 252 (1977).

[32] S. Abachi *et al.* [D0 Collaboration], *Search for high mass top quark production in $p\bar{p}$ collisions at $\sqrt{s} = 1.8$ TeV*, Phys. Rev. Lett. **74**, 2422 (1995) [hep-ex/9411001].

[33] N. A. Tornqvist, *Understanding the scalar meson q anti-q nonet*, Z. Phys. C **68**, 647 (1995) [hep-ph/9504372].

[34] F. E. Close and N. A. Tornqvist, *Scalar mesons above and below 1-GeV*, J. Phys. G **28**, R249 (2002) [hep-ph/0204205].

[35] C. J. Morningstar and M. J. Peardon, *The Glueball spectrum from an anisotropic lattice study*, *Phys. Rev.* **D60** (1999) 034509, [hep-lat/9901004].

[36] A. Vaccarino and D. Weingarten, *Glueball mass predictions of the valence approximation to lattice QCD*, *Phys. Rev.* **D60** (1999) 114501, [hep-lat/9910007].

[37] Y. Chen, A. Alexandru, S. Dong, T. Draper, I. Horvath, *et. al.*, *Glueball spectrum and matrix elements on anisotropic lattices*, *Phys.Rev.* **D73** (2006) 014516, [hep-lat/0510074].

[38] C. Amsler and F. E. Close, *Evidence for a a scalar glueball*, *Phys. Lett.* **B353** (1995) 385–390, [hep-ph/9505219].

[39] J. Sexton, A. Vaccarino, and D. Weingarten, *Numerical evidence for the observation of a scalar glueball*, *Phys. Rev. Lett.* **75** (1995) 4563–4566, [hep-lat/9510022].

[40] D. Bugg, M. J. Peardon, and B. Zou, *The Glueball spectrum*, *Phys. Lett.* **B486** (2000) 49–53, [hep-ph/0006179].

[41] M. Albaladejo and J. Oller, *Identification of a Scalar Glueball*, *Phys.Rev.Lett.* **101** (2008) 252002, [arXiv:0801.4929].

[42] Y. Nambu and G. Jona-Lasinio, *Dynamical Model of Elementary Particles Based on an Analogy with Superconductivity. 1.*, Phys. Rev. **122** (1961) 345.

[43] Y. Nambu and G. Jona-Lasinio, *Dynamical Model Of Elementary Particles Based On An Analogy With Superconductivity. II*, Phys. Rev. **124**, 246 (1961).

[44] V. Chaloupka *et al.* [Particle Data Group Collaboration], *Review Of Particle Properties. Particle Data Group*, Phys. Lett. B **50**, 1 (1974).

[45] T. G. Trippe *et al.* [Particle Data Group Collaboration], *Review of Particle Properties. Particle Data Group*, Rev. Mod. Phys. **48**, S1 (1976) [Erratum-ibid. **48**, 497 (1976)].

[46] L. Montanet *et al.* [Particle Data Group Collaboration], *Review of particle properties. Particle Data Group*, Phys. Rev. D **50**, 1173 (1994).

[47] R. M. Barnett *et al.* [Particle Data Group Collaboration], *Review of particle physics. Particle Data Group*, Phys. Rev. D **54**, 1 (1996).

[48] K. Hagiwara *et al.* [Particle Data Group Collaboration], *Review of particle physics. Particle Data Group*, Phys. Rev. D **66**, 010001 (2002).

[49] G. Colangelo, J. Gasser, and H. Leutwyler, *pi pi scattering*, *Nucl. Phys.* **B603** (2001) 125–179, [hep-ph/0103088].

[50] I. Caprini, G. Colangelo and H. Leutwyler, *Mass and width of the lowest resonance in QCD*, Phys. Rev. Lett. **96**, 132001 (2006) [hep-ph/0512364].

[51] B. Moussallam, *Couplings of light I=0 scalar mesons to simple operators in the complex plane*, Eur. Phys. J. C **71**, 1814 (2011) [arXiv:1110.6074 [hep-ph]].

[52] K. Abe *et al.* [SLD Collaboration], *Measurement of alpha-s (M(Z)**2) from hadronic event observables at the Z0 resonance*, Phys. Rev. D **51**, 962 (1995) [hep-ex/9501003].

[53] D. J. Gross and F. Wilczek, *Ultraviolet Behavior of Nonabelian Gauge Theories*, Phys. Rev. Lett. **30**, 1343 (1973).

[54] D. J. Gross and F. Wilczek, *Asymptotically Free Gauge Theories. 1*, Phys. Rev. D **8**, 3633 (1973).

[55] H. D. Politzer, *Reliable Perturbative Results for Strong Interactions?*, Phys. Rev. Lett. **30**, 1346 (1973).

[56] S. L. Adler and W. A. Bardeen, *Absence of higher order corrections in the anomalous axial vector divergence equation*, Phys. Rev. **182**, 1517 (1969).

[57] W. A. Bardeen, *Anomalous Ward identities in spinor field theories*, Phys. Rev. **184**, 1848 (1969).

[58] K. Fujikawa, *Path Integral for Gauge Theories with Fermions*, Phys. Rev. D **21**, 2848 (1980) [Erratum-ibid. D **22**, 1499 (1980)].

[59] R. D. Peccei and J. Sola, *A Phenomenological Analysis Of The Weinberg Sum Rules And Of The Pi+ Pi0 Mass Difference*, Nucl. Phys. B **281**, 1 (1987).

[60] C. A. Dominguez and J. Sola, *Determination of quark and gluon condensates from tau lepton decay data*, Z. Phys. C **40**, 63 (1988).

[61] C. Vafa and E. Witten, *Restrictions on Symmetry Breaking in Vector-Like Gauge Theories*, Nucl. Phys. B **234**, 173 (1984).

[62] Y. Nambu, *Axial vector current conservation in weak interactions*, *Phys. Rev. Lett.* **4** (1960) 380–382.

[63] Y. Nambu and G. Jona-Lasinio, *Dynamical Model of Elementary Particles Based on an Analogy with Superconductivity. I.*, *Phys. Rev.* **122** (1961) 345–358.

[64] Y. Nambu and G. Jona-Lasinio, *Dynamical model of elementary particles based on an analogy with superconductivity. II.*, *Phys. Rev.* **124** (1961) 246–254.

[65] J. Goldstone, *Field Theories with Superconductor Solutions*, *Nuovo Cim.* **19** (1961) 154–164.

[66] J. Goldstone, A. Salam, and S. Weinberg, *Broken Symmetries*, *Phys. Rev.* **127** (1962) 965–970.

[67] G. Colangelo, J. Gasser and H. Leutwyler, *The Quark condensate from K(e4) decays*, Phys. Rev. Lett. **86**, 5008 (2001) [hep-ph/0103063].

[68] R. Williams, C. S. Fischer and M. R. Pennington, *Anti-q q condensate for light quarks beyond the chiral limit*, Phys. Lett. B **645**, 167 (2007) [hep-ph/0612061].

[69] S. Scherer, *Introduction to chiral perturbation theory*, *Adv.Nucl.Phys.* **27** (2003) 277, [hep-ph/0210398]. To be edited by J.W. Negele and E. Vogt.

[70] A. Pich, *Chiral perturbation theory*, *Rept.Prog.Phys.* **58** (1995) 563–610, [hep-ph/9502366].

[71] B. Kubis, *An Introduction to chiral perturbation theory*, hep-ph/0703274.

[72] H. Leutwyler, *Chiral dynamics*, hep-ph/0008124. Contribution to the Festschrift in honor of B.L. Ioffe.

[73] A. Dobado, A. Gomez-Nicola, A. L. Maroto, and J. Pelaez, *Effective lagrangians for the standard model*, . See the BOOKS subfile under the following call number: QC174.45:D6:1997.

[74] U. G. Meissner, *Recent developments in chiral perturbation theory*, *Rept.Prog.Phys.* **56** (1993) 903–996, [hep-ph/9302247].

[75] S. Weinberg, *Nonlinear realizations of chiral symmetry*, Phys. Rev. **166**, 1568 (1968).

[76] S. R. Coleman, J. Wess and B. Zumino, *Structure of phenomenological Lagrangians. 1.*, Phys. Rev. **177**, 2239 (1969).

[77] C. G. Callan, Jr., S. R. Coleman, J. Wess and B. Zumino, *Structure of phenomenological Lagrangians. 2.*, Phys. Rev. **177**, 2247 (1969).

[78] H. Leutwyler, in Perspectives in the Standard Model, Proceedings of the 1991 Advanced Theoretical Study Institute in Elementary Particle Physics, Boulder, Colorado, 2 - 28 June, 1991, edited by R. K. Ellis, C. T. Hill, and J. D. Lykken (World Scientific, Singapore, 1992) .

[79] M. Gell-Mann, Caltech Report CTSL-20 (1961)

[80] S. Okubo, *Note on unitary symmetry in strong interactions*, Prog. Theor. Phys. **27**, 949 (1962).

[81] G. Colangelo, S. Durr, A. Juttner, L. Lellouch, H. Leutwyler, *et. al.*, *Review of lattice results concerning low energy particle physics*, *Eur. Phys. J.* **C71** (2011) 1695, [arXiv:1011.4408].

[82] N. Fuchs, H. Sazdjian, and J. Stern, *How to probe the scale of (anti-q q) in chiral perturbation theory*, *Phys.Lett.* **B269** (1991) 183–188.

[83] J. Stern, H. Sazdjian, and N. Fuchs, *What pi - pi scattering tells us about chiral perturbation theory*, *Phys.Rev.* **D47** (1993) 3814–3838, [hep-ph/9301244].

[84] M. Knecht, H. Sazdjian, J. Stern, and N. Fuchs, *A Possible experimental determination of M(s) / M(u) + M(d) decays*, *Phys.Lett.* **B313** (1993) 229–233, [hep-ph/9305332].

[85] M. Knecht, B. Moussallam, and J. Stern, *The Reaction gamma gamma —> pi0 pi0 in generalized chiral perturbation theory*, *Nucl.Phys.* **B429** (1994) 125–152, [hep-ph/9402318].

[86] M. Gell-Mann, R. J. Oakes and B. Renner, *Behavior of current divergences under SU(3) x SU(3)*, Phys. Rev. **175**, 2195 (1968).

[87] D. Espriu, E. de Rafael, and J. Taron, *The QCD effective action at long distances*, *Nucl. Phys.* **B345** (1990) 22–56.

[88] L. Girlanda, M. Knecht, B. Moussallam, and J. Stern, *Comment on the prediction of two loop standard chiral perturbation theory for low-energy pi pi scattering*, *Phys. Lett.* **B409** (1997) 461–468, [hep-ph/9703448].

[89] G. Amoros, J. Bijnens, and P. Talavera, *Low-energy constants from K(lepton-4) form-factors*, *Phys. Lett.* **B480** (2000) 71–76, [hep-ph/9912398].

[90] F. J. Llanes-Estrada and P. De A. Bicudo, *Quark Schwinger-Dyson evaluation of the l1, l2 coefficients in the chiral Lagrangian*, *Phys. Rev.* **D68** (2003) 094014, [hep-ph/0306146].

[91] S. Descotes-Genon and B. Moussallam, *The K*0 (800) scalar resonance from Roy-Steiner representations of pi K scattering*, *Eur. Phys. J.* **C48** (2006) 553, [hep-ph/0607133].

[92] J. Bijnens, G. Colangelo and G. Ecker, *The Mesonic chiral Lagrangian of order p**6*, JHEP **9902**, 020 (1999) [hep-ph/9902437].

[93] J. Bijnens, G. Colangelo and G. Ecker, *Renormalization of chiral perturbation theory to order p**6*, Annals Phys. **280**, 100 (2000)

[94] G. 't Hooft, *Computation of the Quantum Effects Due to a Four-Dimensional Pseudoparticle*, Phys. Rev. D **14**, 3432 (1976) [Erratum-ibid. D **18**, 2199 (1978)].

[95] G. 't Hooft, *How Instantons Solve the U(1) Problem*, Phys. Rept. **142**, 357 (1986).

[96] G. 't Hooft, *A Planar Diagram Theory for Strong Interactions*, *Nucl. Phys.* **B72** (1974) 461.

[97] E. Witten, *Baryons in the 1/n Expansion*, Nucl. Phys. **B160** (1979) 57.

[98] S. R. Coleman and E. Witten, *Chiral Symmetry Breakdown in Large N Chromodynamics*, Phys. Rev. Lett. **45**, 100 (1980).

[99] G. Veneziano, *Goldstone Mechanism From Gluon Dynamics*, Phys. Lett. B **95**, 90 (1980).

[100] C. Rosenzweig, J. Schechter and C. G. Trahern, *Is the Effective Lagrangian for QCD a Sigma Model?*, Phys. Rev. D **21**, 3388 (1980).

[101] P. Di Vecchia and G. Veneziano, *Chiral Dynamics in the Large n Limit*, Nucl. Phys. B **171**, 253 (1980).

[102] E. Witten, *Large N Chiral Dynamics*, *Annals Phys.* **128** (1980) 363.

[103] E. Witten, *Current Algebra Theorems for the U(1) Goldstone Boson*, Nucl. Phys. B **156**, 269 (1979).

[104] A. V. Manohar, *Large N QCD*, hep-ph/9802419. From 'Probing the Standard Model of Particle Interactions', F. David & R. Gupta eds.

[105] J.F.Donoghue, E.Golowich and B.R.Holstein, *Dynamics of the Standard Model*, Cambridge University Press 1992.

[106] A. D. Martin and T. D. Spearman, *Elementary particle theory*. North-Holland Pub. Co., 1970.

[107] S. Donnachie, G. Dosch, P. Landshoff and O. Nachtmann, *Pomeron Physics and QCD*. Cambridge University Press, 2002.

[108] S. Mandelstam, *Determination of the pion - nucleon scattering amplitude from dispersion relations and unitarity. General theory*, Phys. Rev. **112**, 1344 (1958).

[109] S. Mandelstam, *Analytic properties of transition amplitudes in perturbation theory*, Phys. Rev. **115**, 1741 (1959).

[110] G. Ecker, J. Gasser, H. Leutwyler, A. Pich and E. de Rafael, *Chiral Lagrangians for Massive Spin 1 Fields*, Phys. Lett. B **223**, 425 (1989).

[111] V. Bernard, N. Kaiser and U. G. Meissner, *Chiral perturbation theory in the presence of resonances: Application to pi pi and pi K scattering*, Nucl. Phys. B **364**, 283 (1991).

[112] M. Harada, F. Sannino and J. Schechter, *Simple description of pi pi scattering to 1-GeV*, Phys. Rev. D **54**, 1991 (1996) [hep-ph/9511335].

[113] J. Oller and E. Oset, *N/D description of two meson amplitudes and chiral symmetry*, *Phys.Rev.* **D60** (1999) 074023, [hep-ph/9809337].

[114] M. Jamin, J. A. Oller and A. Pich, *S wave K pi scattering in chiral perturbation theory with resonances*, Nucl. Phys. B **587**, 331 (2000) [hep-ph/0006045].

[115] S. N. Gupta, *Quantum Electrodynamics*, London 1977, 226p

[116] N. Kaiser, P. B. Siegel and W. Weise, *Chiral dynamics and the low-energy kaon - nucleon interaction*, Nucl. Phys. A **594**, 325 (1995) [nucl-th/9505043].

[117] J. Oller and E. Oset, *Chiral symmetry amplitudes in the S wave isoscalar and isovector channels and the sigma, f0(980), a0(980) scalar mesons*, *Nucl. Phys.* **A620** (1997) 438–456, [hep-ph/9702314].

[118] J. A. Oller, E. Oset and J. R. Pelaez, *Nonperturbative approach to effective chiral Lagrangians and meson interactions*, Phys. Rev. Lett. **80**, 3452 (1998) [hep-ph/9803242].

[119] E. Oset and A. Ramos, *Nonperturbative chiral approach to s wave anti-K N interactions*, Nucl. Phys. A **635**, 99 (1998) [nucl-th/9711022].

[120] J. A. Oller, E. Oset and J. R. Pelaez, *Meson meson interaction in a nonperturbative chiral approach*, Phys. Rev. D **59**, 074001 (1999) [Erratum-ibid. D **60**, 099906 (1999)] [Erratum-ibid. D **75**, 099903 (2007)] [hep-ph/9804209].

[121] J. Nieves and E. Ruiz Arriola, *Bethe-Salpeter approach for meson meson scattering in chiral perturbation theory*, *Phys. Lett.* **B455** (1999) 30–38, [nucl-th/9807035].

[122] J. Nieves and E. Ruiz Arriola, *Bethe-Salpeter approach for unitarized chiral perturbation theory*, Nucl. Phys. A **679**, 57 (2000) [hep-ph/9907469].

[123] J. Nieves and E. Ruiz Arriola, *Bethe-Salpeter approach for the P(33) elastic pion-nucleon scattering in heavy baryon chiral perturbation theory*, Phys. Rev. D **63**, 076001 (2001) [hep-ph/0008034].

[124] T. N. Truong, *Chiral Perturbation Theory and Final State Theorem*, *Phys. Rev. Lett.* **61** (1988) 2526. Revised version.

[125] T. N. Truong, *Remarks on the unitarization methods*, Phys. Rev. Lett. **67**, 2260 (1991).

[126] A. Dobado, M. J. Herrero, and T. N. Truong, *Unitarized Chiral Perturbation Theory for Elastic Pion-Pion Scattering*, *Phys. Lett.* **B235** (1990) 134.

[127] A. Dobado and J. Pelaez, *A Global fit of pi pi and pi K elastic scattering in ChPT with dispersion relations*, *Phys. Rev.* **D47** (1993) 4883–4888, [hep-ph/9301276].

[128] A. Dobado and J. Pelaez, *The Inverse amplitude method in chiral perturbation theory*, *Phys. Rev.* **D56** (1997) 3057–3073, [hep-ph/9604416].

[129] A. Gomez Nicola, J. R. Pelaez and G. Rios, *The Inverse Amplitude Method and Adler Zeros*, Phys. Rev. D **77**, 056006 (2008) [arXiv:0712.2763 [hep-ph]].

[130] J. Nieves, M. Pavon Valderrama, and E. Ruiz Arriola, *The Inverse amplitude method in pi pi scattering in chiral perturbation theory to two loops*, *Phys. Rev.* **D65** (2002) 036002, [hep-ph/0109077].

[131] A. Dobado and J. R. Pelaez, *Chiral perturbation theory and the f(2)(1270) resonance*, Phys. Rev. D **65**, 077502 (2002) [hep-ph/0111140].

[132] C. Hanhart, J. R. Pelaez and G. Rios, *Quark mass dependence of the rho and sigma from dispersion relations and Chiral Perturbation Theory*, Phys. Rev. Lett. **100**, 152001 (2008) [arXiv:0801.2871 [hep-ph]].

[133] S. Protopopescu, M. Alston-Garnjost, A. Barbaro-Galtieri, S. M. Flatte, J. Friedman, *et. al.*, *Pi pi Partial Wave Analysis from Reactions pi+ p —> pi+ pi- Delta++ and pi+ p —> K+ K- Delta++ at 7.1-GeV/c*, *Phys. Rev.* **D7** (1973) 1279.

[134] N. Durusoy, M. Baubillier, R. George, M. Goldberg, A. Touchard, *et. al.*, *Study of the i=2 pi pi scattering from the reaction pi- d —> pi- pi- p(s) p at 9.0 gev/c*, *Phys. Lett.* **B45** (1973) 517–520.

[135] M. Losty, V. Chaloupka, A. Ferrando, L. Montanet, E. Paul, *et. al.*, *A Study of pi- pi- scattering from pi- p interactions at 3.93-GeV/c*, *Nucl. Phys.* **B69** (1974) 185–204.

[136] B. Hyams, C. Jones, P. Weilhammer, W. Blum, H. Dietl, G. Grayer, W. Koch and E. Lorenz *et al.*, *pi pi Phase Shift Analysis from 600-MeV to 1900-MeV*, Nucl. Phys. B **64**, 134 (1973) [AIP Conf. Proc. **13**, 206 (1973)].

[137] G. Grayer, B. Hyams, C. Jones, P. Schlein, P. Weilhammer, *et. al.*, *High Statistics Study of the Reaction pi- p –> pi- pi+ n: Apparatus, Method of Analysis, and General Features of Results at 17-GeV/c*, *Nucl. Phys.* **B75** (1974) 189.

[138] P. Estabrooks and A. D. Martin, *pi pi Phase Shift Analysis Below the K anti-K Threshold*, *Nucl. Phys.* **B79** (1974) 301.

[139] W. Hoogland, S. Peters, G. Grayer, B. Hyams, P. Weilhammer, *et. al.*, *Measurement and Analysis of the pi+ pi+ System Produced at Small Momentum Transfer in the Reaction pi+ p —> pi+ pi+ n at 12.5-GeV*, *Nucl. Phys.* **B126** (1977) 109.

[140] **BNL-E865 Collaboration** Collaboration, S. Pislak *et. al.*, *A New measurement of K+(e4) decay and the s wave pi pi scattering length a0(0)*, *Phys. Rev. Lett.* **87** (2001) 221801, [hep-ex/0106071].

[141] **NA48/2 Collaboration** Collaboration, J. Batley *et. al.*, *New high statistics measurement of K(e4) decay form factors and pi pi scattering phase shifts*, *Eur. Phys. J.* **C54** (2008) 411–423.

[142] A. Gomez Nicola and J. Pelaez, *Meson meson scattering within one loop chiral perturbation theory and its unitarization*, *Phys. Rev.* **D65** (2002) 054009, [hep-ph/0109056].

[143] J. Pelaez, *Light scalars as tetraquarks or two-meson states from large N(c) and unitarized chiral perturbation theory*, *Mod. Phys. Lett.* **A19** (2004) 2879–2894, [hep-ph/0411107].

[144] A. Gomez Nicola, F. J. Llanes-Estrada, and J. R. Pelaez, *Finite temperature pion scattering to one-loop in chiral perturbation theory*, *Phys. Lett.* **B550** (2002) 55–64, [hep-ph/0203134].

[145] S. L. Adler, *Consistency conditions on the strong interactions implied by a partially conserved axial-vector current. II*, Phys. Rev. **139**, B1638 (1965).

[146] J. R. Pelaez and F. J. Yndurain, *On the precision of chiral dispersive calculations of pi pi scattering*, Phys. Rev. D **68**, 074005 (2003) [hep-ph/0304067].

[147] J. R. Pelaez and F. J. Yndurain, *The Pion-pion scattering amplitude*, Phys. Rev. D **71**, 074016 (2005) [hep-ph/0411334].

[148] R. Kaminski, J. R. Pelaez and F. J. Yndurain, *The pion-pion scattering amplitude. II. Improved analysis above bar K anti-K threshold*, Phys. Rev. D **74**, 014001 (2006) [Erratum-ibid. D **74**, 079903 (2006)] [hep-ph/0603170].

[149] R. Kaminski, J. R. Pelaez and F. J. Yndurain, *The Pion-pion scattering amplitude. III. Improving the analysis with forward dispersion relations and Roy equations*, Phys. Rev. D **77**, 054015 (2008) [arXiv:0710.1150 [hep-ph]].

[150] R. Kaminski and L. Lesniak, *Threshold parameters of the K anti-K and pi pi scalar - isoscalar interactions*, Phys. Rev. C **51**, 2264 (1995).

[151] B. Hyams, C. Jones, P. Weilhammer, W. Blum, H. Dietl, G. Grayer, W. Koch and E. Lorenz *et al.*, *A Study of All the pi pi Phase Shift Solutions in the Mass Region 1.0-GeV to 1.8-GeV from pi- p –> pi- pi+ n at 17.2-GeV*, Nucl. Phys. B **100**, 205 (1975).

[152] N. Cabibbo and A. Maksymowicz, *Angular Correlations in Ke-4 Decays and Determination of Low-Energy pi-pi Phase Shifts*, Phys. Rev. **137**, B438 (1965) [Erratum-ibid. **168**, 1926 (1968)].

[153] L. Rosselet, P. Extermann, J. Fischer, O. Guisan, R. Mermod, R. Sachot, A. M. Diamant-Berger and P. Bloch *et al.*, *Experimental Study of 30,000 K(e4) Decays*, Phys. Rev. D **15**, 574 (1977).

[154] J. R. Batley *et al.* [NA48-2 Collaboration], *Precise tests of low energy QCD from K(e4)decay properties*, Eur. Phys. J. C **70**, 635 (2010).

[155] G. Colangelo, J. Gasser and A. Rusetsky, *Isospin breaking in K(l4) decays*, Eur. Phys. J. C **59**, 777 (2009) [arXiv:0811.0775 [hep-ph]].

[156] D. H. Cohen, T. Ferbel, P. Slattery and B. Werner, *Study Of Pi Pi Scattering In The Isotopic Spin-2 Channel*, Phys. Rev. D **7**, 661 (1973).

[157] W. Wetzel, K. Freudenreich, F. X. Gentit, P. Muhlemann, W. Beusch, A. Birman, D. Websdale and P. Astbury *et al.*, *A Study of pi pi –> K anti-K Using an Experiment on pi- p –> K0(s) K0(s) n at 8.9-GeV/c*, Nucl. Phys. B **115**, 208 (1976).

[158] A. Etkin, K. J. Foley, R. S. Longacre, W. A. Love, T. W. Morris, S. Ozaki, E. D. Platner and V. A. Polychronakos *et al.*, *Evidence For Two New 0++ Mesons And A Possible Scalar Decuplet*, Phys. Rev. D **25**, 2446 (1982).

[159] K. L. Au, D. Morgan and M. R. Pennington, *Meson Dynamics Beyond the Quark Model: A Study of Final State Interactions*, Phys. Rev. D **35**, 1633 (1987).

[160] D. Morgan and M. R. Pennington, *New data on the K anti-K threshold region and the nature of the f0 (S*)*, Phys. Rev. D **48**, 1185 (1993).

[161] B. S. Zou and D. V. Bugg, *Is f0 (975) a narrow resonance?*, Phys. Rev. D **48**, 3948 (1993).

[162] D. V. Bugg, *Reconciling phi radiative decays with other data for a0(980), fo(980), pi pi —> KK and pi pi —> eta eta*, Eur. Phys. J. C **47**, 45 (2006) [hep-ex/0603023].

[163] J. R. Pelaez and F. J. Yndurain, *Regge analysis of pion pion (and pion kaon) scattering for energy s**1/2 > 1.4-GeV*, Phys. Rev. D **69**, 114001 (2004) [hep-ph/0312187].

[164] P. B. Johnson *et al.* [Notre Dame-Purdue-SLAC Collaboration], *COMPILATION OF pi- p DATA AT 4-GeV/c: BACKWARD RESONANCE PRODUCTION AND pi pi SCATTERING*, Phys. Rev. **176**, 1651 (1968).

[165] W. J. Robertson, W. D. Walker and J. L. Davis, *High-energy pi pi collisions*, Phys. Rev. D **7**, 2554 (1973).

[166] J. Hanlon, A. Brody, R. Engelmann, T. Kafka, H. Wahl, A. A. Seidl, W. S. Toothacker and J. C. Van der Velde *et al.*, *The Inclusive Reactions p n —> p X and pi+ n —> p X at 100-GeV/c*, Phys. Rev. Lett. **37**, 967 (1976).

[167] H. Abramowicz, M. Gorski, G. Sinapius, A. Wroblewski, A. Zieminski, H. J. Lubatti, K. Moriyasu and C. D. Rees *et al.*, *STUDY OF pi- pi- SCATTERING IN pi- n INTERACTIONS AT HIGH-ENERGIES*, Nucl. Phys. B **166**, 62 (1980).

[168] F. P. Palou, J. L. Sanchez Gomez and F. J. Yndurain, *Low-Energy Parameters for Scattering of Pions and Kaons*, Z. Phys. A **274**, 161 (1975).

[169] S. M. Roy, *Exact integral equation for pion pion scattering involving only physical region partial waves*, Phys. Lett. B **36**, 353 (1971).

[170] M. R. Pennington and S. D. Protopopescu, *Pi pi scattering amplitude in the low-energy region*, Phys. Rev. D **7**, 1429 (1973).

[171] M. R. Pennington and S. D. Protopopescu, *How roy's equations resolve the up-down ambiguity and reproduce the s* resonance*, Phys. Rev. D **7**, 2591 (1973).

[172] J. L. Basdevant, C. D. Froggatt and J. L. Petersen, *Construction of Phenomenological pi pi Amplitudes*, Nucl. Phys. B **72**, 413 (1974).

[173] J. L. Basdevant, C. D. Froggatt and J. L. Petersen, *Pi pi phenomenology below 1100 mev*, Phys. Lett. B **41**, 178 (1972).

[174] J. L. Basdevant, C. D. Froggatt and J. L. Petersen, *Role of crossing and the rho meson in low energy pi pi amplitudes*, Phys. Lett. B **41**, 173 (1972).

[175] C. D. Froggatt and J. L. Petersen, *Phase-Shift Analysis of pi+ pi- Scattering Between 1.1-GeV and 1.8-GeV Based on Fixed Momentum Transfer Analyticity*, Nucl. Phys. B **91**, 454 (1975) [Erratum-ibid. B **104**, 186 (1976)].

[176] C. D. Froggatt and J. L. Petersen, *Phase Shift Analysis of pi+ pi- Scattering Between 1.0-GeV and 1.8-GeV Based on Fixed Momentum Transfer Analyticity. 2.*, Nucl. Phys. B **129**, 89 (1977).

[177] R. Kaminski, L. Lesniak and K. Rybicki, *A Joint analysis of the S wave in the pi+pi- and pi0pi0 data*, Eur. Phys. J. direct C **4**, 4 (2002) [hep-ph/0109268].

[178] S. Descotes-Genon, N. H. Fuchs, L. Girlanda and J. Stern, *Analysis and interpretation of new low-energy pi pi scattering data*, Eur. Phys. J. C **24**, 469 (2002) [hep-ph/0112088].

[179] B. Ananthanarayan, G. Colangelo, J. Gasser and H. Leutwyler, *Roy equation analysis of pi pi scattering*, Phys. Rept. **353**, 207 (2001) [hep-ph/0005297].

[180] V. D. Barger, D. B. Cline. Phenomenological theories of high energy scattering, W.A. Benjamin 1969

[181] P. D. B. Collins, *An Introduction to Regge Theory and High-Energy Physics*, Cambridge 1977, 445p

[182] G. F. Chew and S. C. Frautschi, *Principle Of Equivalence For All Strongly Interacting Particles Within The S Matrix Framework*, Phys. Rev. Lett. **7**, 394 (1961).

[183] G. F. Chew and S. C. Frautschi, *Regge Trajectories And The Principle Of Maximum Strength For Strong Interactions*, Phys. Rev. Lett. **8**, 41 (1962).

[184] K. Igi and S. Matsuda, *New Sum Rules and Singularities in the Complex J Plane*, Phys. Rev. Lett. **18**, 625 (1967).

[185] R. Dolen, D. Horn and C. Schmid, *Prediction of Regge Parameters of rho Poles from Low-Energy pi N Data*, Phys. Rev. Lett. **19**, 402 (1967).

[186] R.D.Pisarski and F.Wilczek, Phys. Rev. D **29**, 338 (1984).

[187] C. Bernard *et al.* [MILC Collaboration], *QCD thermodynamics with three flavors of improved staggered quarks*, Phys. Rev. D **71**, 034504 (2005).

[188] Y. Aoki, Z. Fodor, S. D. Katz and K. K. Szabo, *The QCD transition temperature: Results with physical masses in the continuum limit*, Phys. Lett. B **643**, 46 (2006).

[189] Y. Aoki, G. Endrodi, Z. Fodor, S. D. Katz and K. K. Szabo, *The order of the quantum chromodynamics transition predicted by the standard model of particle physics*, Nature **443**, 675 (2006).

[190] M. Cheng *et al.*, *Equation of State for physical quark masses*, Phys. Rev. D **81**, 054504 (2010).

[191] Y. Aoki, S. Borsanyi, S. Durr, Z. Fodor, S. D. Katz, S. Krieg and K. K. Szabo, *The QCD transition temperature: results with physical masses in the continuum limit II*, JHEP **0906**, 088 (2009).

[192] S. Ejiri *et al.*, *On the magnetic equation of state in (2+1)-flavor QCD*, Phys. Rev. D **80**, 094505 (2009).

[193] S. Borsanyi, Z. Fodor, C. Hoelbling, S. D. Katz, S. Krieg, C. Ratti and K. K. Szabo [Wuppertal-Budapest Collaboration], *Is there still any Tc mystery in lattice QCD? Results with physical masses in the continuum limit III*, JHEP **1009**, 073 (2010).

[194] T. Hatsuda and T. Kunihiro, *Fluctuation Effects In Hot Quark Matter: Precursors Of Chiral Transition At Finite Temperature*, Phys. Rev. Lett. **55**, (1985) 158.

[195] G. Chanfray and M. Ericson, *Critical fluctuations of the quark density in nuclei*, Eur. Phys. J. A **16**, 291 (2003).

[196] P. Gerber and H. Leutwyler, *Hadrons Below the Chiral Phase Transition*, Nucl. Phys. B **321**, 387 (1989).

[197] F. Karsch, K. Redlich and A. Tawfik, *Hadron resonance mass spectrum and lattice QCD thermodynamics*, Eur. Phys. J. C **29**, 549 (2003).

[198] P. Huovinen and P. Petreczky, *QCD Equation of State and Hadron Resonance Gas*, Nucl. Phys. A **837**, 26 (2010).

[199] A. Dobado, A. Gomez Nicola, F. J. Llanes-Estrada and J. R. Pelaez, *Thermal rho and sigma mesons from chiral symmetry and unitarity*, Phys. Rev. C **66**, 055201 (2002).

[200] D. Fernandez-Fraile, A. Gomez Nicola and E. T. Herruzo, *Pion scattering poles and chiral symmetry restoration*, Phys. Rev. D **76**, 085020 (2007).

[201] D. Cabrera, D. Fernandez-Fraile and A. Gomez Nicola, *Chiral Symmetry and light resonances in hot and dense matter*, Eur. Phys. J. C **61**, 879 (2009).

[202] D. Fernandez-Fraile and A. Gomez Nicola, *Transport coefficients and resonances for a meson gas in Chiral Perturbation Theory*, Eur. Phys. J. C **62**, 37 (2009).

[203] J. I. Kapusta, *Finite Temperature Field Theory*,

[204] M. Le Bellac, *Thermal field theory* Cambdrige university press, (1995).

[205] R. Dashen, S. -K. Ma and H. J. Bernstein, *S Matrix formulation of statistical mechanics*, Phys. Rev. **187**, 345 (1969).

[206] G. M. Welke, R. Venugopalan, M. Prakash, *The Speed of sound in an interacting pion gas*, Phys. Lett. **B245**, 137-141 (1990);

V. L. Eletsky, J. I. Kapusta, R. Venugopalan, *Screening mass from chiral perturbation theory, virial expansion and the lattice*, Phys. Rev. **D48**, 4398-4407 (1993).

[207] A. Dobado, J. R. Pelaez, *Chiral symmetry and the pion gas virial expansion*, Phys. Rev. **D59**, 034004 (1999).

[208] R. Venugopalan, M. Prakash, *Thermal properties of interacting hadrons*, Nucl. Phys. **A546**, 718-760 (1992).

[209] A. Aloisio *et al.* [KLOE Collaboration], *Measurement of Gamma(K(S) —> pi+ pi- (gamma)) / Gamma(K(S) —> pi0 pi0)*, Phys. Lett. B **538**, 21 (2002) [hep-ex/0204024].

[210] H. Leutwyler, *On the dispersion theory of pi pi scattering*, AIP Conf. Proc. **892**, 58 (2007) [hep-ph/0612111].

[211] J. R. Pelaez, *On the Nature of light scalar mesons from their large N(c) behavior*, *Phys. Rev. Lett.* **92** (2004) 102001, [hep-ph/0309292].

[212] J. R. Pelaez, *Comments on the large N(c) behavior of light scalars*, hep-ph/0509284.

[213] J. Nieves and E. Arriola, *Properties of the rho and sigma Mesons from Unitary Chiral Dynamics*, *Phys. Rev.* **D80** (2009) 045023, [arXiv:0904.4344].

[214] J. Nieves and E. Ruiz Arriola, *Meson Resonances at large N(C): Complex Poles versus Breit-Wigner Masses*, *Phys.Lett.* **B679** (2009) 449–453, [arXiv:0904.4590].

[215] M. Uehara, *A Unitarized chiral approach to f(0)(980) and a(0)(980) states and nature of light scalar resonances*, hep-ph/0404221.

[216] T. Hyodo, D. Jido, and T. Kunihiro, *Nature of the σ meson as revealed by its softening process*, *Nucl. Phys.* **A848** (2010) 341–365, [arXiv:1007.1718].

[217] T. Kojo and D. Jido, *Sigma meson in pole-dominated QCD sum rules*, *Phys.Rev.* **D78** (2008) 114005, [arXiv:0802.2372].

[218] T. Kojo and D. Jido, *Dynamical study of bare sigma pole with 1/N(c) classifications*, arXiv:0807.2364.

[219] J. R. Pelaez, J. Nebreda and G. Rios, Prog. Theor. Phys. Suppl. **186**, 113 (2010) [arXiv:1007.3461 [hep-ph]].

[220] J. R. Pelaez and G. Rios, *Nature of the f0(600) from its N(c) dependence at two loops in unitarized Chiral Perturbation Theory*, Phys. Rev. Lett. **97**, 242002 (2006) [hep-ph/0610397].

[221] Z.-H. Guo and J. Oller, *Resonances from meson-meson scattering in U(3) CHPT*, *Phys. Rev.* **D84** (2011) 034005, [arXiv:1104.2849].

[222] C. W. Bernard, A. Duncan, J. LoSecco and S. Weinberg, *Exact Spectral Function Sum Rules*, Phys. Rev. D **12**, 792 (1975).

[223] J. Bijnens, E. Gamiz and J. Prades, *Matching the electroweak penguins Q(7), Q(8) and spectral correlators*, JHEP **0110**, 009 (2001) [hep-ph/0108240].

[224] M. Ishida, *Possible classification of the chiral scalar sigma nonet*, Prog. Theor. Phys. **101**, 661 (1999) [hep-ph/9902260].

[225] A. P. Szczepaniak and E. S. Swanson, *Coulomb gauge QCD, confinement, and the constituent representation*, Phys. Rev. D **65**, 025012 (2002) [hep-ph/0107078].

[226] J. M. Torres-Rincon and F. J. Llanes-Estrada, *Heavy Quark Fluorescence*, Phys. Rev. Lett. **105**, 022003 (2010) [arXiv:1003.5989 [hep-ph]].

[227] M. G. Rocha, F. J. Llanes-Estrada, D. Schutte and S. V. Chavez, *Boost operators in Coulomb-gauge QCD: The Pion form factor and Fock expansions in phi radiative decays*, Eur. J. Phys. A **44**, 411 (2010) [arXiv:0910.1448 [hep-ph]].

[228] R. L. Jaffe, *Q**2 anti-Q**2 Resonances in the Baryon - anti-Baryon System*, Phys. Rev. D **17**, 1444 (1978).

[229] R. L. Jaffe, *Extraordinary Hadrons*, In *Stanford 1977, Proceedings, Summer Institute On Particle Physics*, Stanford 1977, 351-369

[230] R. L. Jaffe, Proceedings of the Intl. Symposium on Lepton and Photon Interactions at High Energies. Physikalisches Institut, University of Bonn (1981) . ISBN: 3-9800625-0-3

[231] N. Isgur, R. Kokoski and J. E. Paton, *Gluonic Excitations of Mesons: Why They Are Missing and Where to Find Them*, Phys. Rev. Lett. **54**, 869 (1985).

[232] F. Iddir, S. Safir and O. Pene, *Do 1- c anti-c g hybrid meson exist, do they mix with charmonium?*, Phys. Lett. B **433**, 125 (1998) [hep-ph/9803470].

[233] F. J. Llanes-Estrada and S. R. Cotanch, *Many body Coulomb gauge exotic and charmed hybrids*, Phys. Lett. B **504**, 15 (2001) [hep-ph/0008337].

[234] C. Semay, F. Buisseret and B. Silvestre-Brac, *Towers of hybrid mesons*, Phys. Rev. D **79**, 094020 (2009) [arXiv:0812.3291 [hep-ph]].

[235] A. P. Szczepaniak and E. S. Swanson, *The Low lying glueball spectrum*, Phys. Lett. B **577**, 61 (2003) [hep-ph/0308268].

[236] C. McNeile, *Lattice status of gluonia/glueballs*, Nucl. Phys. Proc. Suppl. **186**, 264 (2009) [arXiv:0809.2561 [hep-lat]].

[237] R. F. Dashen, E. E. Jenkins and A. V. Manohar, *Spin flavor structure of large N(c) baryons*, Phys. Rev. D **51**, 3697 (1995) [hep-ph/9411234].

[238] J. Ruiz de Elvira, J. R. Pelaez, M. R. Pennington and D. J. Wilson, *Chiral Perturbation Theory, the* $1/N_c$ *expansion and Regge behaviour determine the structure of the lightest scalar meson*, Phys. Rev. D **84**, 096006 (2011) [arXiv:1009.6204 [hep-ph]].

[239] A. Gomez Nicola, J. R. Pelaez and J. Ruiz de Elvira, *Non-factorization of four-quark condensates at low energies within Chiral Perturbation Theory*, Phys. Rev. D **82**, 074012 (2010).

[240] F. J. Llanes-Estrada, J. R. Pelaez and J. Ruiz de Elvira, in preparation.

[241] M. A. Shifman, A. I. Vainshtein and V. I. Zakharov, *QCD And Resonance Physics. Sum Rules*, Nucl. Phys. B **147**, 385 (1979).

[242] S. Narison and R. Tarrach, *Higher Dimensional Renormalization Group Invariant Vacuum Condensates In Quantum Chromodynamics*, Phys. Lett. B **125**, 217 (1983).

[243] V. L. Eletsky, *Four quark condensates at T not = 0*, Phys. Lett. B **299**, 111 (1993).

[244] S. Leupold, *Factorization and non-factorization of in-medium four-quark condensates*, Phys. Lett. B **616**, 203 (2005).

[245] S. Leupold, *Four-quark condensates and chiral symmetry restoration in a resonance gas model*, J. Phys. G **32**, 2199 (2006).

[246] G. Leibbrandt, *Introduction To The Technique Of Dimensional Regularization*, Rev. Mod. Phys. **47**, 849 (1975).

[247] M. B. Johnson and L. S. Kisslinger, *Light quark mesons and four quark condensates at finite temperature*, Phys. Rev. D **61**, 074014 (2000).

[248] A. V. Smilga and J. J. M. Verbaarschot, *Scalar susceptibility in QCD and the multiflavor Schwinger model*, Phys. Rev. D **54**, 1087 (1996).

[249] A. Gomez Nicola and R. Torres Andres, *Isospin Breaking and chiral symmetry restoration*, Phys. Rev. D **83**, 076005 (2011).

[250] G. Amoros, J. Bijnens and P. Talavera, *QCD isospin breaking in meson masses, decay constants and quark mass ratios*, Nucl. Phys. B **602**, 87 (2001).

[251] J. R. Pelaez, *The SU(2) and SU(3) chiral phase transitions within chiral perturbation theory*, Phys. Rev. D **66**, 096007 (2002)

[252] R. Garcia Martin and J. R. Pelaez, *Chiral condensate thermal evolution at finite baryon chemical potential within Chiral Perturbation Theory*, Phys. Rev. D **74**, 096003 (2006).

[253] J. Nebreda and J. R. Pelaez., *Strange and non-strange quark mass dependence of elastic light resonances from SU(3) Unitarized Chiral Perturbation Theory to one loop*, Phys. Rev. D **81**, 054035 (2010).

[254] J. Nebreda, J. R. Pelaez and G. Rios, *Chiral extrapolation of pion-pion scattering phase shifts within standard and unitarized Chiral Perturbation Theory*, Phys. Rev. D **83**, 094011 (2011).

[255] R. Garcia-Martin, R. Kaminski, J. R. Pelaez and J. Ruiz de Elvira, *Precise determination of the f0(600) and f0(980) pole parameters from a dispersive data analysis*, Phys. Rev. Lett. **107**, 072001 (2011)

[256] J. Bijnens, G. Colangelo, G. Ecker, J. Gasser and M. E. Sainio, *Pion pion scattering at low energy*, Nucl. Phys. B **508** (1997) 263 [Erratum-ibid. B **517** (1998) 639]

[257] G. Amoros, J. Bijnens and P. Talavera, *Two-point functions at two loops in three flavour chiral perturbation theory*, Nucl. Phys. B **568** (2000) 319.

[258] M. A. Shifman, A. I. Vainshtein and V. I. Zakharov, *QCD and Resonance Physics. Sum Rules*, Nucl. Phys. B **147**, 385 (1979).

[259] A. G. Nicola, J. Ruiz de Elvira, R. Torres, in preparation.

[260] G. Chanfray and M. Ericson, Eur. Phys. J. A **16**, 291 (2003) [nucl-th/0106069].

[261] T. Regge, *Introduction to complex orbital momenta*, Nuovo Cim. **14**, 951 (1959).

[262] S. Mandelstam, *Quantum electrodynamics without potentials*, Annals Phys. **19**, 1 (1962).